Dissertation zur Erlangung des Doktorgrades
der Fakultät für Chemie und Pharmazie
der Ludwig-Maximilians-Universität München

Molecular Machines Based on Hemithioindigo

Nicolai Nanook Bach
aus
Mannheim, Deutschland

2023

Erklärung

Diese Dissertation wurde im Sinne von § 7 der Promotionsordnung vom 28. November 2011 von Herrn Prof. Dr. Henry Dube betreut.

Eidesstattliche Versicherung

Diese Dissertation wurde eigenständig und ohne unerlaubte Hilfe erarbeitet.

München, 09.02.2023 ……..

Nicolai Nanook Bach

Dissertation eingereicht am:	09.02.2023
1. Gutachter:	Prof. Dr. Henry Dube
2. Gutachter:	Prof. Dr. Konstantin Karaghiosoff
Mündliche Prüfung am:	23.03.2023

Danksagung

Allen voran möchte ich mich bei meinem Doktorvater *Professor Dr. Henry Dube* bedanken. Danke für die Gelegenheit zur Promotion in deiner Gruppe, die spannenden und herausfordernden Themen (high risk – high gain), den kreativen Freiraum und deinen unerschöpflichen Strom an Ideen.

Ein herzlicher Dank geht an *Professor Dr. Konstantin Karaghiosoff* für die Übernahme des Zweitgutachtens.

Ebenfalls danke ich den weiteren Mitgliedern der Prüfungskommission: *Professor Dr. Jürgen Schatz*, *Professor Dr. Franz Bracher*, *Professor Dr. Anne Schütz* und *Dr. Armin Ofial*.

Nun die eigentlichen Stars dieser Danksagung: alle Mitglieder des Awesome AK Dube – *past and present*. Ihr macht diesen Arbeitskreis so einmalig! Einige möchte ich nochmal besonders hervorheben. Danke an *Moni*, *Kerstin* (wer hätte gedacht, dass wir mal fast gleichzeitig verteidigen!), *Ludwig*, *Tom* (mein Mittelbench-Buddy), *Esteban* (Wer ist Stefan?), *Aaron*, *Ed*, *Chris*, *Benni & Laura* (zu dritt haben wir mitten in der Corona Pandemie den großen Schritt von München nach Erlangen gemacht), *Max S.*, *Fabien* und *Lilli*. Ich freue mich über die Freundschaften, die über das Labor hinaus entstanden sind! Ein besonderer shout-out geht an die Münchner Boulderizer Crew, die mich in der Masterarbeit in ihre Reihen aufgenommen hat. Danke auch an die Kochrunde in ihren verschiedenen Formen. Mal kein Gluten, keine Laktose, keine Tomaten, keine Gurken, kein Fisch, kein Fleisch oder kein Ofen (sad) – mal nur zu dritt oder zu acht – trotzdem haben wir es immer wieder geschafft und es gab einige Highlights zum Mittag.

Ein besonderer Dank geht auch an alle fleißigen Korrekturleser für ihre Zeit und ihre hilfreichen Kommentare zu dieser Arbeit: *Dr. Pronay Biswas*, *Verena Josef*, *Laura Köttner, Fabien Kohl*, *Dr. Ani Özcelik*, *Benjamin Regen-Pregizer*, *Lilli Reißenweber*, *Maximilian Sacherer*, *Manuel Valentin* und *Max Zitzmann*.

Danke außerdem an *Verena* für ihre Mitarbeit, als es darum ging das Threading-Projekt zur Publikation zu bringen.

Bedanken möchte ich mich auch bei meinen Praktikanten und Masterstudenten: *Matthias Fischer*, *Veronika Fuchs*, *Sebastian König* und *Sven Waldmannstetter* – ihr habt hervorragende Arbeit geleistet!

Ohne sie geht nichts – vielen Dank an die zentrale Versorgung, Werkstätten und Analytikabteilungen der LMU und FAU. Besonders hervorheben möchte ich die NMR-Abteilungen: *Dr. David Stephenson*, *Claudia Ober*, *Brigitte Breitenstein* (alle LMU) sowie *Dr. Harald Maid* und *Christian Placht* (FAU). Danke für unzählige gemessene Spektren, den Input, die Neugierde und natürlich die Bereitschaft, bei −105 °C eine Glasfaser im Spektrometer zu versenken. Danke an *Dr. Peter Mayer* (LMU) und *Dr. Frank Hampel* (FAU) für die Messung und Lösung von Kristallstrukturen. Bedanken möchte ich mich auch beim Organisations- und Geräteteam aus dem 4. Stock: *Dr. Frank Hampel*, *Dr. Alexander Scherer* und *Pamela Hampel*.

Ein großes Dankeschön geht an *Aki Naritomi* vom Sprachenzentrum der LMU für den fantastischen Japanisch-Unterricht. ありがとうございました。

Das Wichtigste kommt zum Schluss: der größte Dank gebührt meinen Eltern. Danke für eure immerwährende und bedingungslose Unterstützung. Ohne euch wäre ich nicht so weit gekommen.

List of Publications

Parts of this thesis have been published:

"Active Mechanical Threading by a Molecular Motor", N. N. Bach, V. Josef, H. Maid, H. Dube, *Angew. Chem. Int. Ed.* **2022**, *61*, e202201882; *Angew. Chem.* **2022**, *134*, e202201882.

Parts of this thesis have been presented at a scientific conference:

Poster "Visible Light Powered Molecular Threading", N. N. Bach, V. Josef, H. Maid, H. Dube, *28th PhotoIUPAC* **2022**, Amsterdam.

Other publications not part of this thesis:

"Azotriptycenes: Photoswitchable Molecular Brakes", W. J. Stockerl, L. Reißenweber, A. Gerwien, N. N. Bach, S. Thumser, P. Mayer, R. M. Gschwind, H. Dube, *Chem. Eur. J.* **2023**, e202302267.

"Steric Effects on the Thermal Processes of Hemithioindigo Based Molecular Motor Rotation", L. A. Huber, S. Thumser, K. Grill, D. Voßiek, N. N. Bach, P. Mayer, H. Dube, *Chem. Eur. J.* **2021**, *27*, 10758.

Publications of work conducted prior to this thesis:

"Dibenzochrysene enables tightly controlled docking and stabilizes photoexcited states in dual-pore covalent organic frameworks", N. Keller, T. Sick, N. N. Bach, A. Koszalkowski, J. M. Rotter, D. D. Medina, T. Bein, *Nanoscale* **2019**, *11*, 23338-23345.

"Switching on and off Interlayer Correlations and Porosity in 2D Covalent Organic Frameworks", T. Sick, J. M. Rotter, S. Reuter, S. Kandambeth, N. N. Bach, M. Döblinger, J. Merz, T. Clark, T. B. Marder, T. Bein, D. D. Medina, *J. Am. Chem. Soc.* **2019**, *141*, 12570-12581.

Contributions

Matthias Fischer	First-time synthesis of **96** and initial investigations of photophysical and electrochemical properties.
Dr. Frank Hampel	X-Ray crystal structure analysis of compounds annotated[§]
Verena Josef	*pss* and IR data of **1** and **2**.
Dr. Peter Mayer	X-Ray crystal structure analysis of compounds annotated[§]
Dr. Robert Mayer	Cyclic voltammetry measurements of **96**.
Dr. Stefan Thumser	Introduction into *Gaussian16* and *MacroModel*, advice on quantum chemical calculations and troubleshooting.
Sven Waldmannstetter	2D NMR data of **58**, **81** and **82**, attempted macrocyclization of **82** with **83**.

Abbreviations

Å	angstrom(s)
Abs	absorption
Ac	acetyl
APhos	(4-(*N*,*N*-dimethylamino)phenyl)di-*tert*-butyl phosphine
APPI	atmospheric pressure photoionization
aq.	aqueous (solution)
Ar	aryl
a.u.	arbitrary unit(s)
Bn	benzyl
Bu	butyl
Boc	*tert*-butoxycarbonyl
B3LYP	3-parameter hybrid *Becke* exchange/*Lee–Yang–Parr* correlation functional
calc.	calculated
CD	circular dichroism
COSY	correlation spectroscopy
δ	chemical shift
DASA	donor-acceptor Stenhouse adduct
DavePhos	2-dicyclohexylphosphino-2'-(*N*,*N*-dimethylamino)biphenyl
dba	dibenzylideneacetone
DBU	1,8-diazabicyclo[5.4.0]undec-7-ene
DEPTq	distortionless enhancement by polarization transfer including the detection of quaternary nuclei
DFT	density functional theory
DIPA	diisopropylamine
DMAc	*N*,*N*-dimethylacetamide
DME	1,2-dimethoxyethane
DMF	*N*,*N*-dimethylformamide
DMSO	dimethyl sulfoxide
dppf	1,1'-ferrocenediyl-*bis*(diphenylphosphine)
D3	D3 version of *Grimme's* dispersion
D3BJ	D3 version of *Grimme's* dispersion with *Becke-Johnson* damping

ε	molar absorption coefficient
ECD	electronic circular dichroism
EDCI	1-ethyl-3-(3-dimethylaminopropyl)carbodiimide hydrochloride
EI	electron ionization
equiv.	equivalent(s)
ESI	electrospray ionization
ESPT	excited state proton transfer
Et	ethyl
Fc	ferrocene
Fmoc	fluorenylmethoxycarbonyl
GPC	gel permeation chromatography
h	*Planck* constant
Hex	hexane
HMBC	heteronuclear multiple bond correlation
HPLC	high-performance liquid chromatography
HRMS	high-resolution mass spectrometry
HSQC	heteronuclear single quantum correlation
HTI	hemithioindigo
i-	*iso*-
IR	infrared (spectroscopy)
J	coupling constant
JackiePhos	2-[*bis*[3,5-*bis*(trifluoromethyl)phenyl]phosphino]-3,6-dimethoxy-2',4',6'-triisopropyl-1,1'-biphenyl
k_B	*Boltzmann* constant
λ	wavelength
LED	light emitting diode
M	mol L^{-1}
µ	micro
Me	methyl
MMFF94	*Merck* molecular force field 94
MOM	methoxymethyl ether
m.p.	melting point
MS	mass spectrometry

M062X	M06 hybrid meta exchange-correlation functional with double nonlocal exchange
mdeg	millidegrees (unit of CD)
m/*z*	mass-to-charge ratio
v	frequency
$\tilde{\nu}$	wave number
n. d.	not determined
NMR	nuclear magnetic resonance
NOE(SY)	nuclear *Overhauser* effect (spectroscopy)
norm.	normalized
PCM	polarizable continuum model using the integral equation formalism variant
Pd G2	2nd generation palladium precatalyst
Pd G3	3rd generation palladium precatalyst
PEG	polyethylene glycol
PEPPSI-iPr	[1,3-*bis*(2,6-diisopropylphenyl)imidazol-2-ylidene](3-chloropyridyl)palladium(II) dichloride
Ph	phenyl
Φ	quantum yield
ppm	parts per million
Pr	propyl
pss	photostationary state
quant.	quantitative
R	gas constant
ref.	reference
R_f	retention factor
RockPhos	2-di(*tert*-butyl)phosphino-2',4',6'-triisopropyl-3-methoxy-6-methylbiphenyl
ROE(SY)	rotating frame *Overhauser* effect (spectroscopy)
RP-LC	reverse phase liquid chromatography
RuPhos	2-dicyclohexylphosphino-2',6'-diisopropoxybiphenyl
SFC	supercritical fluid chromatography
sSPhos	sodium 2'-dicyclohexylphosphino-2,6-dimethoxy-1,1'-biphenyl-3-sulfonate hydrate

T	temperature
t-	*tert*-
$TBABF_4$	tetrabutylammonium tetrafluoroborate
TBAF	tetrabutylammonium fluoride
$TBAPF_6$	tetrabutylammonium hexafluorophosphate
TBS	*tert*-butyldimethylsilyl
TBTA	*tris*[(1-benzyl-1*H*-1,2,3-triazol-4-yl)methyl]amine
tBuBrettPhos	2-(di-*tert*-butylphosphino)-2',4',6'-triisopropyl-3,6-dimethoxy-1,1'-biphenyl
TD-DFT	time-dependent density functional theory
TEG	tetraethylene glycol
TFA	trifluoroacetic acid
TfOH	triflic acid
THF	tetrahydrofuran
THI	thermal helix inversion
TIPS	triisopropylsilyl
TLC	thin layer chromatography
TS	transition state
UHP LED	ultra-high power light emitting diode
UV	ultraviolet
Vis	visible
v:v	volume to volume ratio
wt	weight
XPhos	2-dicyclohexylphosphino-2',4',6'-triisopropylbiphenyl
1,2-DCE	1,2-dichloroethane
4-DMAP	4-dimethylaminopyridine
°C	degree Celsius

Table of Contents

1 Summary

"Living matter avoids the decay to equilibrium."

Erwin Schrödinger[1]

"There's plenty of room at the bottom."

Richard P. Feynman[2]

These two quotes are often referenced in the context of molecular motors and machinery, as they illustrate two of the most intriguing aspects of this field of research. To start with, molecular motors can be used to continuously drive a system away from chemical equilibrium thus performing useful work. Furthermore, they operate on the nanoscale, inspiring visions of miniaturized factories and precise control over matter at the molecular level. Research in the field of artificial molecular machines and motors is highly dynamic and the pioneering work of *Jean-Pierre Sauvage*,[3] *Sir Fraser Stoddart*[4] and *Ben Feringa*[5] was highlighted by the jointly awarded Nobel Prize in Chemistry 2016 "for the design and synthesis of molecular machines".[6]

To date, a large variety of artificial molecular motors has been reported. However, making actual use of motor rotation remains challenging. To this end, motors need to be integrated into more complex machinery to allow them to perform useful tasks.[7] As part of this thesis, novel macrocyclic motors based on the hemithioindigo (HTI) scaffold were designed, synthesized and studied. Conceptually, the light-driven motor rotation is coupled to the translation of a flexible linear chain through the macrocyclic ring. A generalized representation, as well as molecular structures of compounds **1** and **2** are shown in Figure 1. Both systems, **1** and **2**, were studied through a combination of spectroscopic techniques (variable temperature NMR, UV/Vis, ECD) and quantum chemical calculations.[8] It was found that molecule **1** undergoes unidirectional rotation around the central double bond upon photoirradiation and follows the established four-step mechanism of HTI motor rotation.[9] All four isomeric states could be observed in low-temperature NMR photoirradiation experiments. Molecule **2**, on the other hand, was found to act as a directional switch, with the bulky tetraphenylmethane stopper group blocking the linear chain from passing through the ring. From these results, it could be concluded that active mechanical threading driven by motor rotation occurs for molecule **1**. In combination with theoretical calculations of ECD

spectra and low-temperature ECD experiments, the threading step could be identified as the thermal helix inversion from (*Z,S,M*/*Z,R,P*)-**1** to (*Z,S,P*/*Z,R,M*)-**1**.

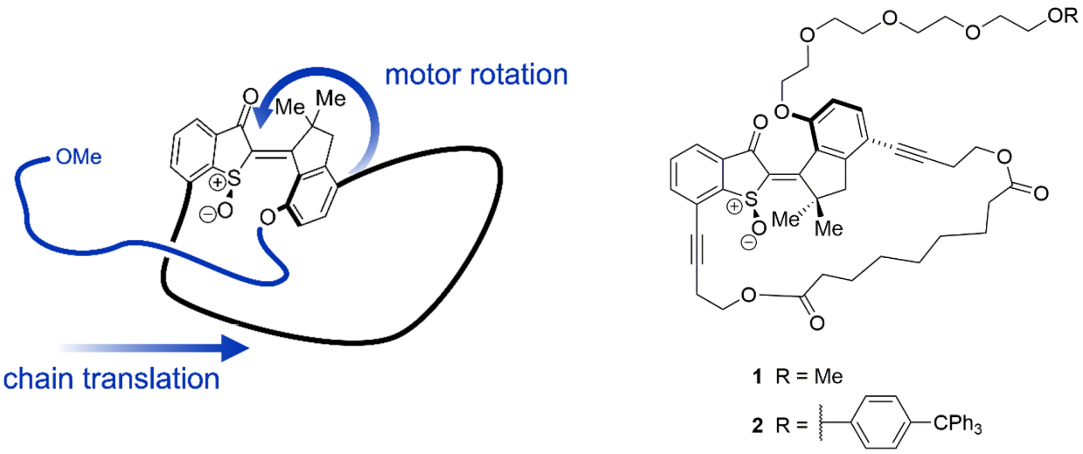

Figure 1 *left:* Schematic representation of the mechanical threading concept: A macrocyclic motor based on HTI is equipped with a flexible tetraethylene glycol chain on the indanone fragment. Light-driven rotation of the motor core results in a translational motion of the chain through the ring. *right:* Molecular structures of compounds **1** and **2**, that were synthesized and investigated as part of this thesis. Molecule **1** shows mechanical threading behavior, whereas threading is blocked for derivative **2** bearing a bulky stopper group. Only the (*E,S,P*)-configured enantiomer is depicted for clarity.

The synthetic approach developed for this project is modular and enables the combination of different chain and macrocycle building blocks. A schematic overview of derivatives synthesized as part of this thesis is shown in Figure 2. Additionally, approaches to other macrocyclic photoresponsive systems, e.g. a ferrocenophane-HTI hybrid, as well as towards a prospective hydrogen bond controlled molecular motor are reported. In conclusion, the approaches presented in this thesis might inspire new concepts of integrated molecular machinery for functional systems.

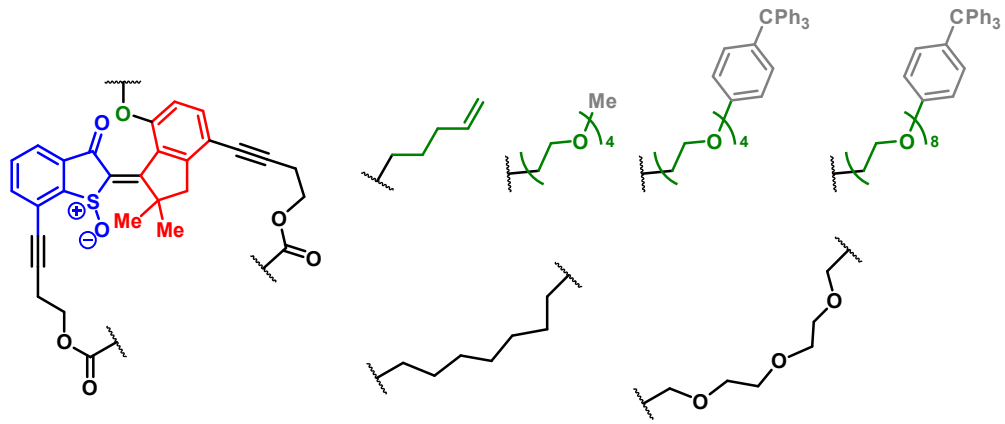

Figure 2 Schematic overview of building blocks for the synthesis of potential macrocyclic HTI motors.

2 Introduction

Molecular machines are "systems where a stimulus triggers the controlled, relatively large amplitude (or directional) motion of one molecular or submolecular component relative to another that can potentially result in a net task being performed".[10] Molecular motors and switches can both be considered subclasses of molecular machines, but an important distinction has to be made: Much like macroscopic motors, molecular motors convert energy into directional motion and are able to perform mechanical work. Molecular switches can also perform work on their environment, but all mechanical actuation is undone once they return to their initial state. In contrast, molecular motors return to their initial state *via* a different pathway, meaning that the mechanical work performed is not undone. This, in principle, allows molecular motors to be used to *continuously* drive a coupled system away from thermodynamic equilibrium.[10-13] Biological molecular machines are essential to living organisms and exist in immense variety.[14-15] Prominent examples include F_1-ATPase,[16] RNA polymerase,[17] kinesins and myosins.[18] The following introduction will focus solely on artificial molecular machines.

2.1 Photoswitches

The phenomenon of reversible change of color upon light irradiation is known as *photochromism*.[19] The earliest scientific description of photochromism was given by *Fritzsche* in 1867, who observed the loss of orange color when a solution of tetracene was exposed to sunlight.[20] Upon heating, the orange color was restored and tetracene was recovered. This could later be ascribed to the reversible formation of endoperoxide **3**.[21]

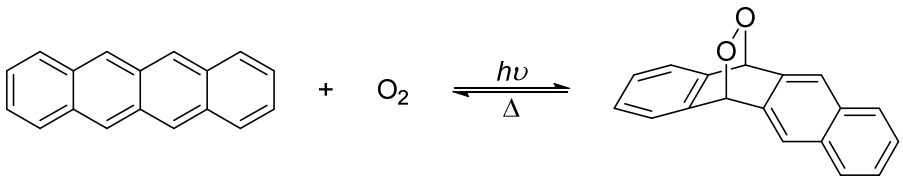

tetracene **3**

Scheme 1 Photoinduced reversible formation of endoperoxide **3** from tetracene, the photochromic reaction observed by *Fritzsche*.[21]

In the following, a slightly narrowed definition of photoswitches will be used: Photoswitches are molecules which undergo photoinduced unimolecular reversible transformation between two or more isomeric states. Some fundamental properties and concepts will be discussed

on generalized model switch system **I**/**II**. Model photoswitch **I** can undergo reversible photoisomerization to **II** and thermal or photoinduced back isomerization to **I**.

$$\mathrm{I} \underset{h\upsilon_2 \text{ or } \Delta}{\overset{h\upsilon_1}{\rightleftharpoons}} \mathrm{II}$$

An idealized absorption spectrum is shown in Figure 3a. The absorption maxima of **I** and **II** are marked as $\lambda_{max,I}$ and $\lambda_{max,II}$ respectively. The absorption maximum of **II** is shifted bathochromically to longer wavelengths ("redshifted"), which corresponds to positive photochromism.[22] At the isosbestic point λ_{iso} both isomers have exactly the same molar absorption. This is an intrinsic property of photoswitches of this type and the experimental observation of isosbestic points can be evidence of two interconverting species. The corresponding simplified energy scheme is given in Figure 3b. **I** is the thermodynamically stable isomer, whereas **II** is the metastable isomer. The *Gibbs* free energy difference ΔG dictates the isomer distribution in thermodynamic equilibrium according to the relation

$$\Delta G = -RT \ln K$$

The free activation energy $\Delta G^{\ddagger}_{II \rightarrow I}$ for thermal back isomerization is a measure for kinetic lability of the metastable state. If the activation barrier is sufficiently high, the metastable state can be kinetically trapped, with the lifetime depending on the barrier height and the temperature of the system. As the metastable isomer **II** is reached *via* photoexcitation to the excited state, photoswitches are systems that can be driven away from thermodynamic equilibrium.[23]

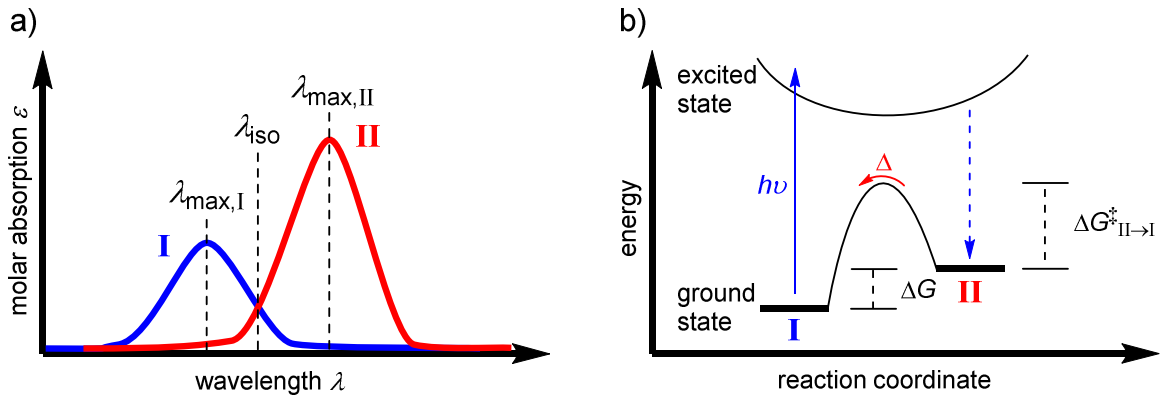

Figure 3 **a)** Idealized absorption spectra of model photoswitch system **I**/**II**. The respective absorption maxima $\lambda_{max,I}$ and $\lambda_{max,II}$ as well as the isosbestic point λ_{iso} are indicated by dotted lines. **b)** Simplified energy scheme for photoswitch system **I**/**II**. Only the "forward" photoreaction is depicted for clarity. The thermal reaction from **II** to **I** is depicted by the red arrow.

In Figure 4, different examples for isomeric distributions of model photoswitch **I**/**II** are shown. In thermodynamic equilibrium (Figure 4a), only stable isomer **I** is populated under

the condition that ΔG is sufficiently large. In photoequilibrium, the isomer composition is independent of ΔG. Instead, a *photostationary state* (*pss*) is established. The isomer composition of the *pss* depends on two factors: One is the difference in absorption of both isomers at the excitation wavelength and the other is the photoisomerization quantum yield Φ. The quantum yield $\Phi_{I\rightarrow II}$ is the number of **I**→**II** isomerization events divided by the total amount of photons absorbed by **I** and can be considered a measure of switching efficiency.[19] Upon irradiation at $\lambda_{max,I}$, where absorption of **II** is negligible, **I** will be fully converted to **II** and the isomer distribution depicted in Figure 4b will be established. At λ_{iso}, absorption is identical for both isomers and the *pss* composition at this wavelength is determined only by the quantum yields for both switching directions. Assuming identical values for $\Phi_{I\rightarrow II}$ and $\Phi_{II\rightarrow I}$, this will result in a 50:50 distribution of **I**:**II**, as shown in Figure 4c.

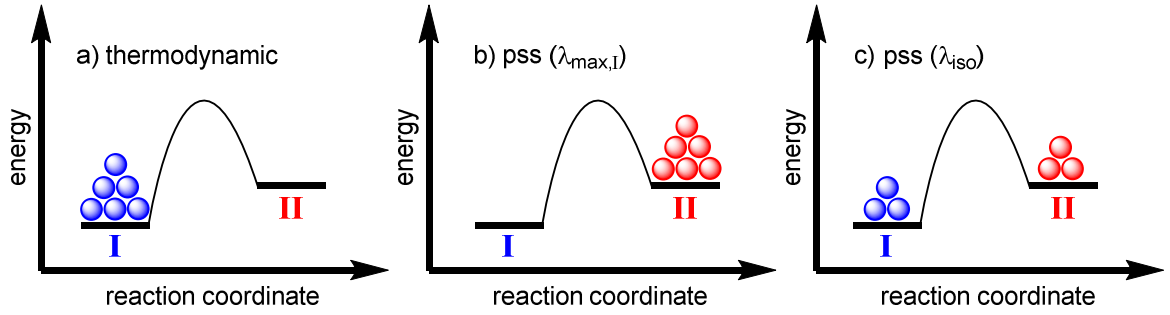

Figure 4 Different isomer compositions of stationary states that can be obtained for model system **I**/**II**. **a)** Thermodynamic equilibrium **b)** *pss* for irradiation at $\lambda_{max,I}$ **c)** *pss* for irradiation at λ_{iso} (assuming $\Phi_{I\rightarrow II} = \Phi_{II\rightarrow I}$).

To date, a vast number of photoswitches has been reported. Some of the most prominent classes of photoswitches are shown in Figure 5 and are discussed shortly in the following. Stilbenes[24], azobenzenes[25-26], diazocines[27] as well as hydrazones[28] all undergo *E*/*Z*-isomerization of the central double bond upon photoirradiation.

Spiropyrans[29-30] can undergo photoisomerization between the closed-ring spiropyran and the open merocyanine form. The closed form is typically colorless, while the merocyanine form is strongly colored. In addition, there is often a significant change in polarity and some spiropyrans are potent photoacids.[31]

Diarylethenes, pioneered by *Irie*,[32-33] are among the most thoroughly studied photoswitches. The photoisomerization mechanism of diarylethenes is a $6\,\pi$ electrocyclization, resulting in small geometric but drastic electronic changes. The open (aromatic) form is typically colorless, while the closed (fully conjugated but non-aromatic) form is strongly colored.

Norbornadienes[34-35] undergo a [2+2] cycloaddition upon photoexcitation, yielding strained quadricyclanes. Depending on the substitution pattern the resulting quadricyclane structures can be high in energy due to strain but kinetically inert at the same time, making them interesting candidates for molecular solar thermal energy storage applications.[36]

Finally, donor-acceptor Stenhouse adducts (DASA)[37] are molecules that contain an amine donor unit and a barbiturate or meldrum's acid derived acceptor unit connected by three conjugated double bonds. DASAs show photoinduced *E*/*Z*-isomerization of the central double bond, followed by cyclization to a bicyclic zwitter-ionic isomer.[38]

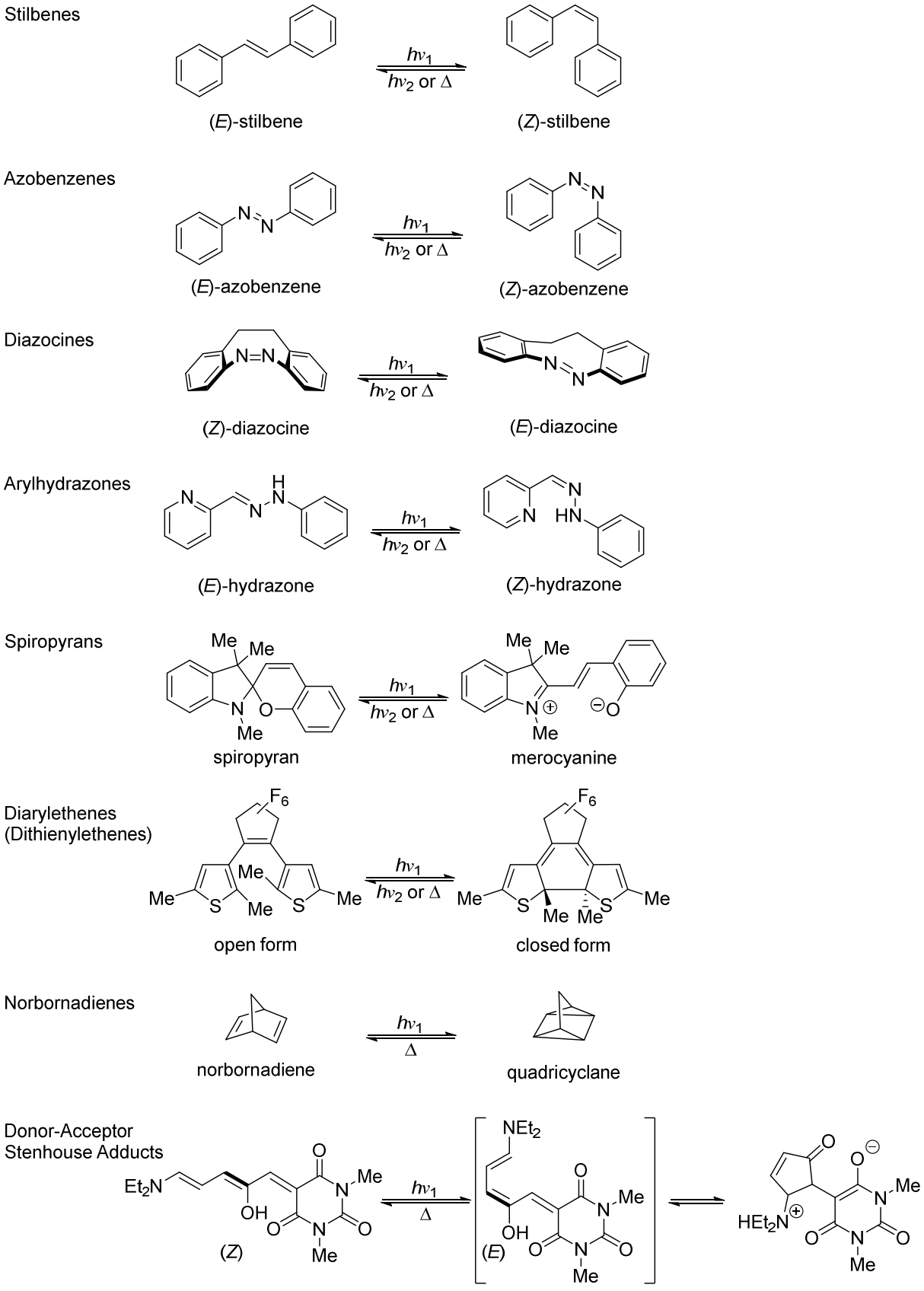

Figure 5 Overview of different classes of photoswitches and their isomers. The core structural motif or representative examples are shown; the thermodynamically stable form is shown on the left.[28, 38-39]

2.1.1 Indigoid Photoswitches

Indigoid photoswitches[40] are derived from the parent dye indigo (see Figure 6a). Indigo itself is one of the most iconic dyes, known for its characteristic blue color, and has been used by humans for over 4000 years.[41] Its chemical constitution was elucidated in 1883 by *Adolf von Baeyer*,[42] who also devised a number of synthetic routes to indigo and who was awarded the Nobel Prize in Chemistry in 1905 "in recognition of his services in the advancement of organic chemistry and the chemical industry, through his work on organic dyes and hydroaromatic compounds".[43] However, due to excited state proton transfer (ESPT) providing an efficient de-excitation pathway, indigo is not a photoswitch.[44] When aromatic or aliphatic residues are introduced on the nitrogen atoms, ESPT is no longer possible and *E*/*Z*-photoisomerization of the central double bond can be observed.[45-46]

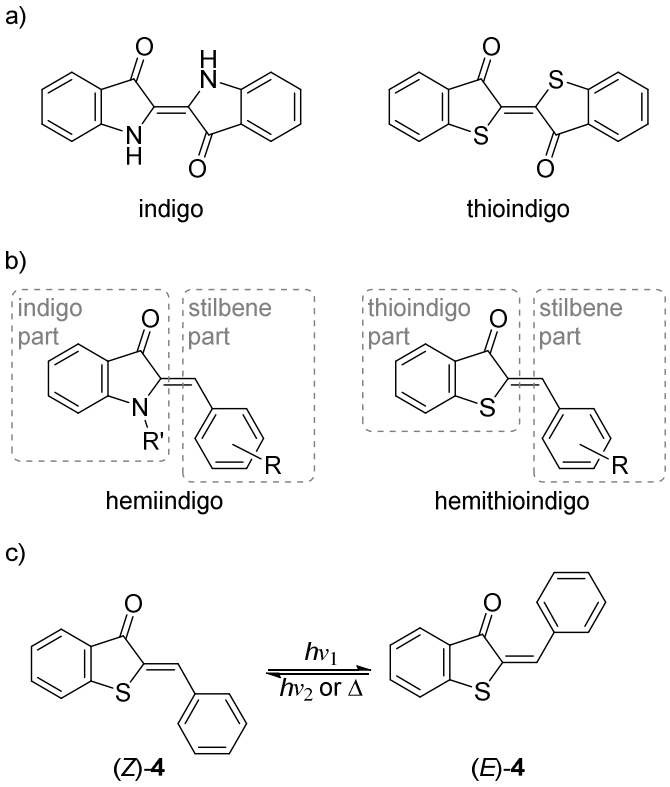

Figure 6 Indigo and indigoid molecules. a) Molecular structures of indigo and thioindigo. b) Generalized structures of hemi-indigoids. c) Double bond isomerization of HTI **4**.

Hemiindigos and hemithioindigos are formally obtained by combining half a (thio)indigo with half a stilbene (see Figure 6b). Hemiindigos with strong donors on the stilbene fragment[47-48] combine pronounced photochromism and red-shifted absorption, near quantitative switching in both directions and long thermal half-lives (up to 3400 years at 25 °C)[48], making them attractive candidates for switching applications, e.g. in the field of

photopharmacology.[49-50] Recently, a method to synthesize highly substituted hemiindigos (e.g. **5** in Figure 7) was reported by *Dube* and coworkers.[51] In 2021, the same group also reported on alkylated indirubins (e.g. **6** in Figure 7), a structural isomer of indigo.[52] The reported indirubins can be switched using red light for both switching directions and their photochemistry can additionally be controlled through supramolecular interactions with *Schreiner's* thiourea catalyst.

Hemithioindigos[53] are a class of structurally diverse and versatile switches. They were first described by *Friedländer* in 1906[54] and their photochromic properties were reported by *Mostoslavskii* in 1961.[53, 55] A number of synthetic protocols has been devised, enabling a high degree of functionalization.[53-54, 56-59] HTIs undergo *E*/*Z*-isomerization of the central double bond upon excitation with visible light. Typically, the *Z*-isomer is the thermodynamically stable isomer, while the *E*-isomer is metastable and its absorption maximum is shifted bathochromically. For unsubstituted HTI **4**, the absorption maxima in the visible region are at 433 nm for (*Z*)**-4** and 457 nm for (*E*)**-4** in CH_2Cl_2.[53] The free activation energy for thermal *E* to *Z* double bond isomerization is $\Delta G^{\ddagger} = 31$ kcal mol.[53] Depending on the solvent as well as the substituents, photoswitching behavior and thermal stability can be tuned.[60-63] The introduction of heterocycles (*e.g.* imidazole derivative **7** in Figure 7) which can form intramolecular hydrogen bonds in the *E*-isomer results in beneficial properties, such as redshifted absorption, near-quantitative photoswitching and high quantum yields for both switching directions.[64-65] An example for a highly-functionalized HTI derivative is **8**, reported by *Gerwien* et al. in 2022.[66] In addition to *E*/*Z*-configuration of the central double bond, introduction of axial chirality *via* two substituted phenyl residues results in a total of $2^3 = 8$ possible isomers, which can undergo sequential interconversion.

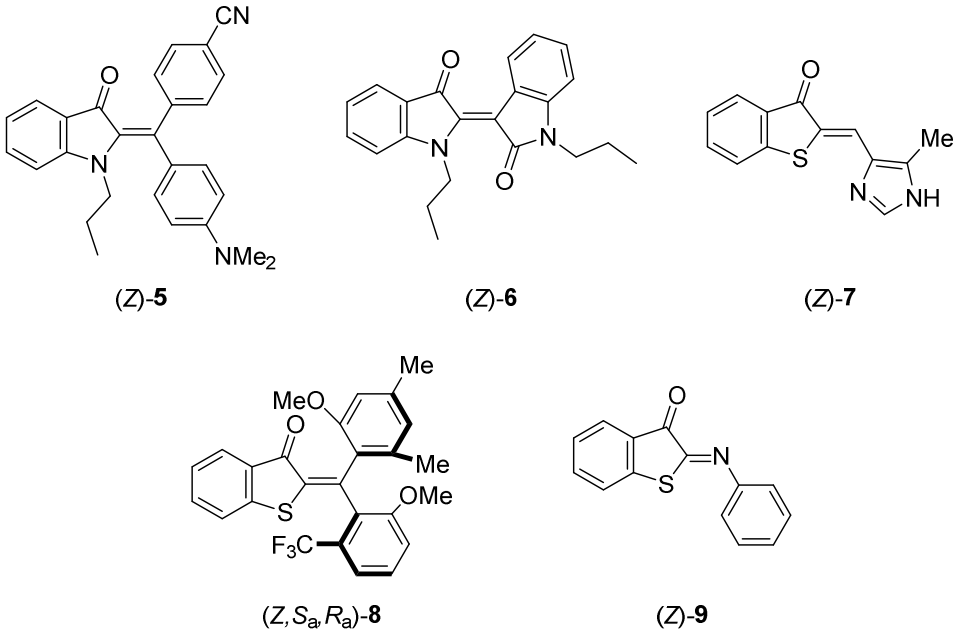

Figure 7 Recent examples of novel indigoid photoswitches: highly substituted hemiindigo **5**,[51] alkylated indirubin **6**,[52] heterocyclic HTI **7**,[65] eight-state HTI photoswitch **8**[66] and phenylimino indolinone **9**.[67]

HTI derivatives have been investigated with regard to photopharmacological applications and photoswitchable antimitotics,[68-69] ion channels,[70] inhibitors,[71] and amino acids[72] based on HTI have been reported. Furthermore, HTIs have been integrated into photoswitchable molecular tweezers[73-75] and have been used in light-controlled host-guest encapsulation.[76] HTIs as molecular motors will be discussed separately.

2.2 Molecular Motors

When discussing rotary molecular motors, one part of the molecule is usually termed the "rotor", which is assumed to be rotating *versus* the "stator". If the stator is not fixed in space, e.g. by attachment to a surface, this distinction becomes somewhat arbitrary but is a useful visual aid for emphasizing the rotational movement nevertheless. In the following, rotor and stator fragments will be highlighted in chemical structure diagrams (see e.g. Figure 9).

2.2.1 Chemically Fueled Molecular Motors

One of the first artificial molecules undergoing directional rotation was reported by *Kelly* and coworkers in 1999.[77] The molecular setup and rotation sequence of the chemically fueled[78] rotor are depicted in Figure 8. Compound **10** consists of an amino-triptycene connected to a helicene unit *via* a single bond at the bridgehead carbon atom. Reaction of **10** with phosgene results in the formation of isocyanate **11**. Clockwise rotation of the triptycene brings the isocyanate group in close proximity to the primary alcohol (rotamer **12**) and through an intramolecular reaction urethane **13** is formed. Subsequent clockwise rotation of the triptycene unit to thermodynamically stable isomer **14** occurs at ambient temperature. Finally, the amine functionality is restored by reduction of the urethane and compound **15** is obtained. With regard to initial isomer **15**, the triptycene unit has undergone directional (clockwise) rotation by 120°, formally powered by the consumption of phosgene.

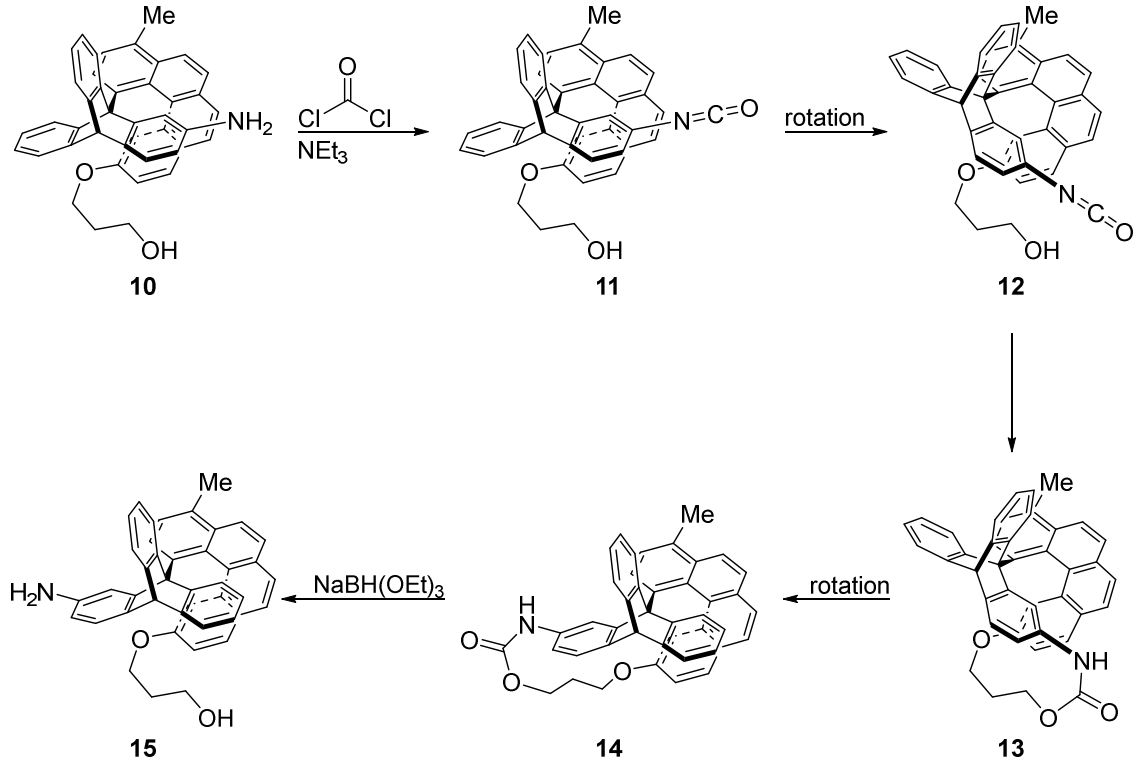

Figure 8 Chemically fueled system undergoing unidirectional rotation reported by *Kelly* and coworkers.[77] In total, the triptycene unit is rotated clockwise by 120° with regard to the helicene unit.

Further chemically driven rotary motors haven been developed, e.g. by *Feringa* and coworkers.[79-80] An example for such a system is shown in Figure 9. It is based on an axially chiral biaryl unit with an additional chirality center (molecule **16**). Sequential and selective protection and deprotection of the hydroxyl functions in *ortho*-position to the biaryl axis results in reversible lactone formation. The molecule is designed in such a way, that the initially formed lactone (shown in brackets) is unstable and undergoes complete thermal isomerization to the stable state, resulting in fully unidirectional rotation.

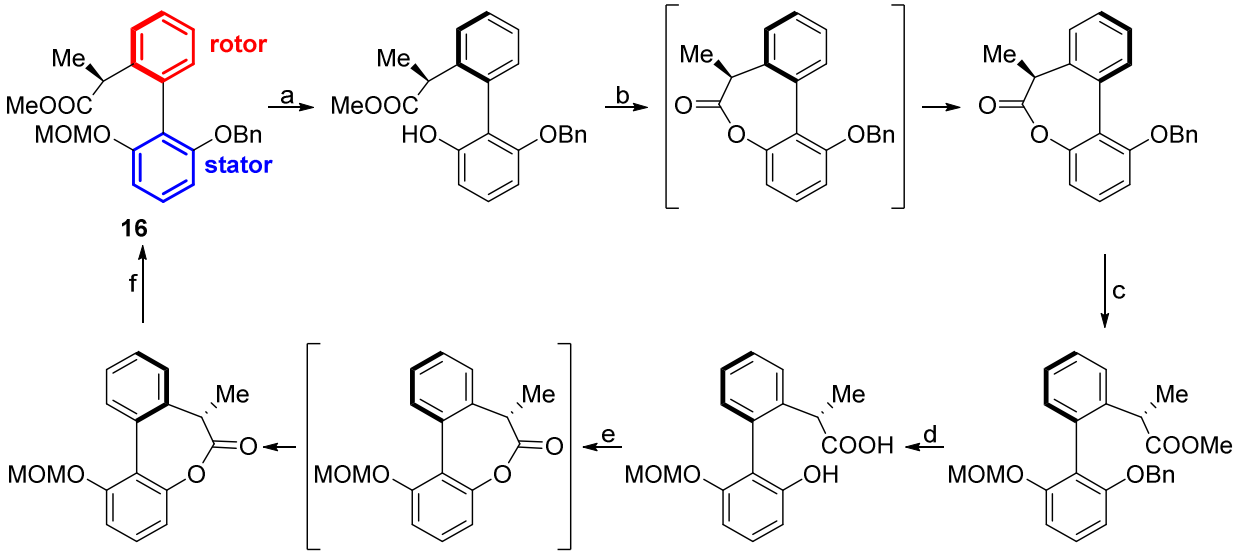

Figure 9 Chemically driven molecular motor **16** undergoing fully unidirectional 360° rotation around the biaryl axis reported by the group of *Feringa*.[79] Conditions: **a)** HCl, MeOH, then aq. NaOH **b)** EDCI, NEt_3, CH_2Cl_2 **c)** NaOMe, MeOH/THF, 0 °C, then NaH,, MOMCl, DMF, 0 °C **d)** Pd/C, H_2, then aq. NaOH **e)** EDCI, NEt_3, CH_2Cl_2 **f)** NaOMe, then BnBr, DMF.

The motors discussed so far have in common that they can be considered *energy ratchet* motors.[12] A conceptually different chemically fueled rotary motor was characterized by *Leigh* and coworkers.[81] The chemical structure of catenane **17**, as well as a cartoon representation, is given in Figure 10. The setup consists of a macrocyclic receptor (highlighted in blue) and a mechanically interlocked second macrocycle containing two fumaramide binding sites (highlighted in green). The two otherwise identical binding sites are made distinguishable by deuteration of one of the sites. Next to the fumaramide "stations" there are bulky Fmoc stopper groups (highlighted in red), which can be detached and reattached by chemical reactions.

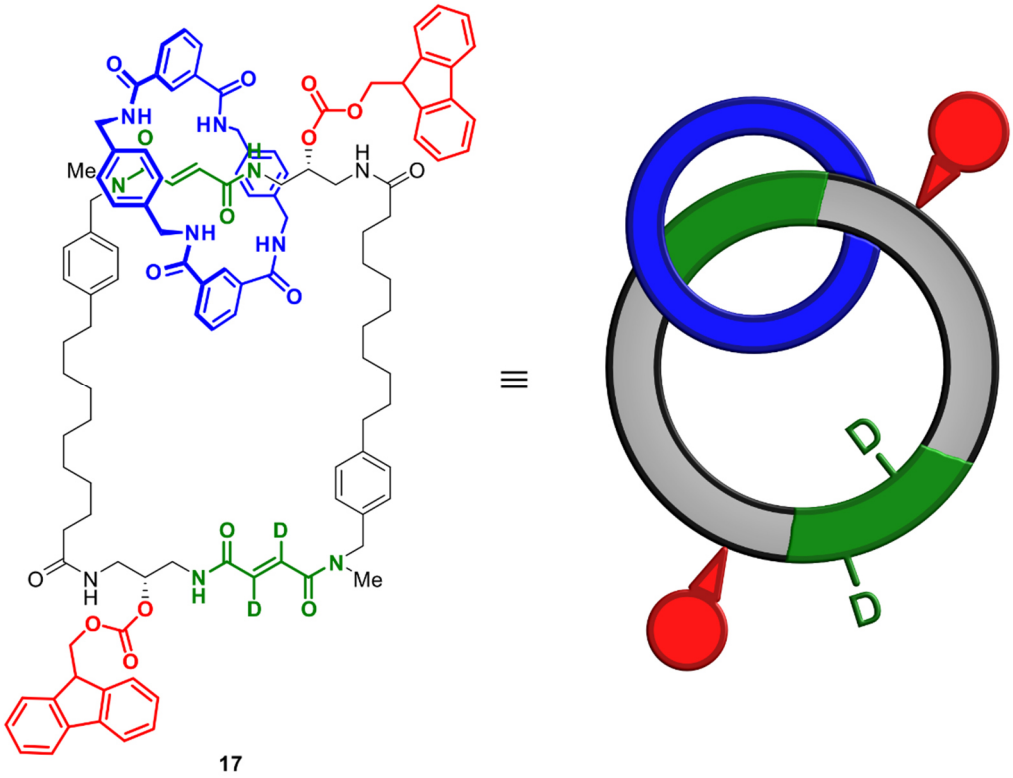

Figure 10 Catenane-based molecular motor **17** reported by *Leigh* and coworkers.[81] See Figure 11 for mechanism of operation. *Adapted with permission of Springer Nature from* M. R. Wilson et al., "An autonomous chemically fuelled small-molecule motor", *Nature* **2016**, *534*, 235-240; *© 2016, Springer Nature Limited.*

The mechanism of motor operation is depicted in Figure 11 and will be described in the following. The macrocyclic receptor can bind to either of the two fumaramide binding sites. As long as both Fmoc "blocking groups" are present, the receptor is restricted to one of the respective half-spaces. Once one of the two Fmoc groups is detached, the receptor can freely shuttle back and forth between the two binding sites. The rate of blocking group detachment is independent of the receptor's position. The rate of blocking group attachment, however, is *larger*, when the receptor is *far* from the blocking site. Therefore, it is more likely for the receptor to be trapped in the *other* half-space, once a new blocking group is attached. As depicted in Figure 11, this continuous process of chemically fueled attachment and detachment of blocking groups results in a net unidirectional movement of the macrocyclic receptor along the second ring. This type of mechanism, with the kinetic barriers depending on the receptor position, is also known as *information ratchet*.[81-84]

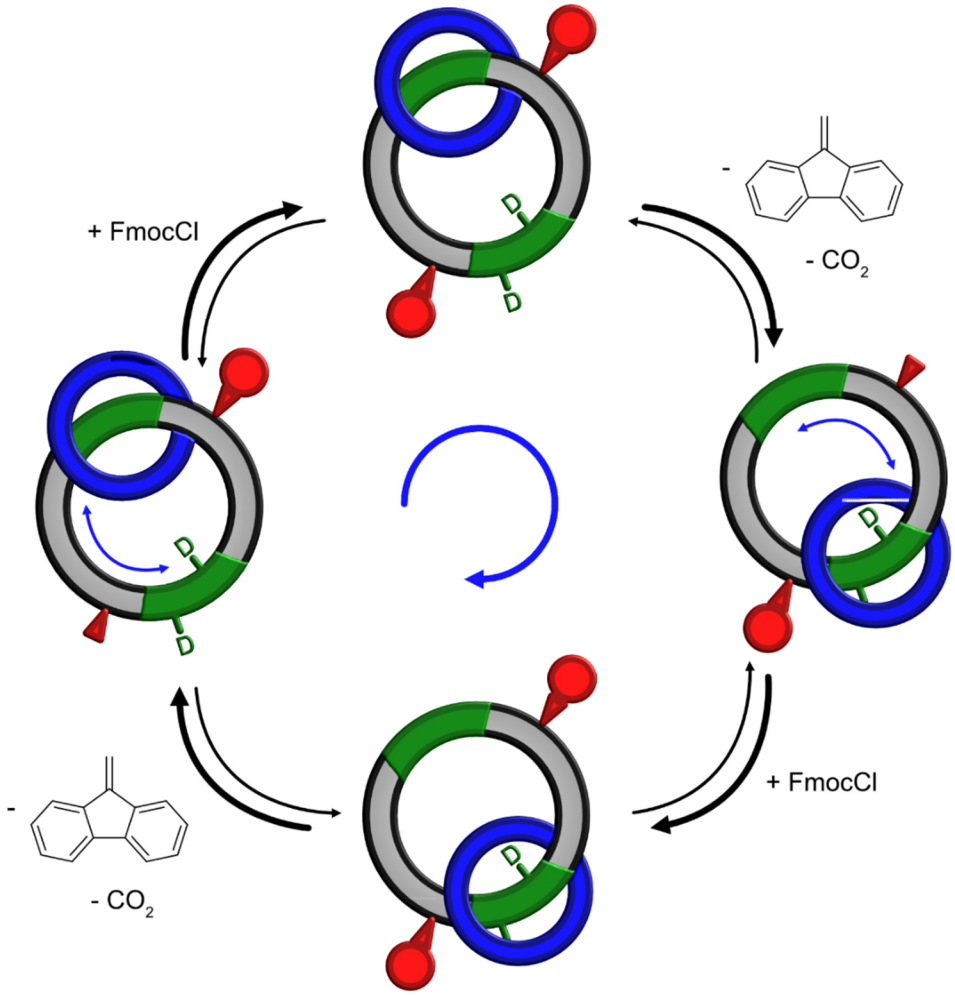

Figure 11 Information ratchet mechanism of molecular motor **17**.[81] The macrocyclic receptor (blue ring) can bind to either of the binding sites (green) and shuttle back and forth between them, once (at least) one of the blocking groups (red) is detached. When both blocking groups are installed, the macrocyclic receptor is restricted to one of the two half-spaces. Net directionality of the ring motion arises from the kinetics of blocking group attachment and detachment: When the macrocyclic receptor is close to a blocking site, the rate of blocking group attachment is decreased, compared to when the ring is further away (at the other binding site). The rate of blocking group detachment stays the same, independent of the position of the macrocyclic receptor. Full conditions of motor operation (not depicted for clarity): CH_2Cl_2 is used as solvent, $KHCO_3$ is added and a bulky pyridine catalyst is used for Fmoc activation. FmocCl as blocking group source is added continuously. NEt_3, which is necessary for Fmoc detachment, is added after some time delay. *Adapted with permission of Springer Nature, from* M. R. Wilson et al., "An autonomous chemically fuelled small-molecule motor", *Nature* **2016**, *534*, 235-240; *© 2016, Springer Nature Limited.*

2.2.2 Light-powered Molecular Motors

Compared to motors powered by chemical fuels, light-powered motors[85-87] offer some attractive advantages: There is no need to continuously provide reactants and no waste byproducts are formed. Instead, light as energy source can be provided with high spatial and temporal control. The first artificial light-driven rotary molecular motor **18** was reported by *Feringa* and coworkers in 1999 (see Figure 12 for molecular structure).[88]

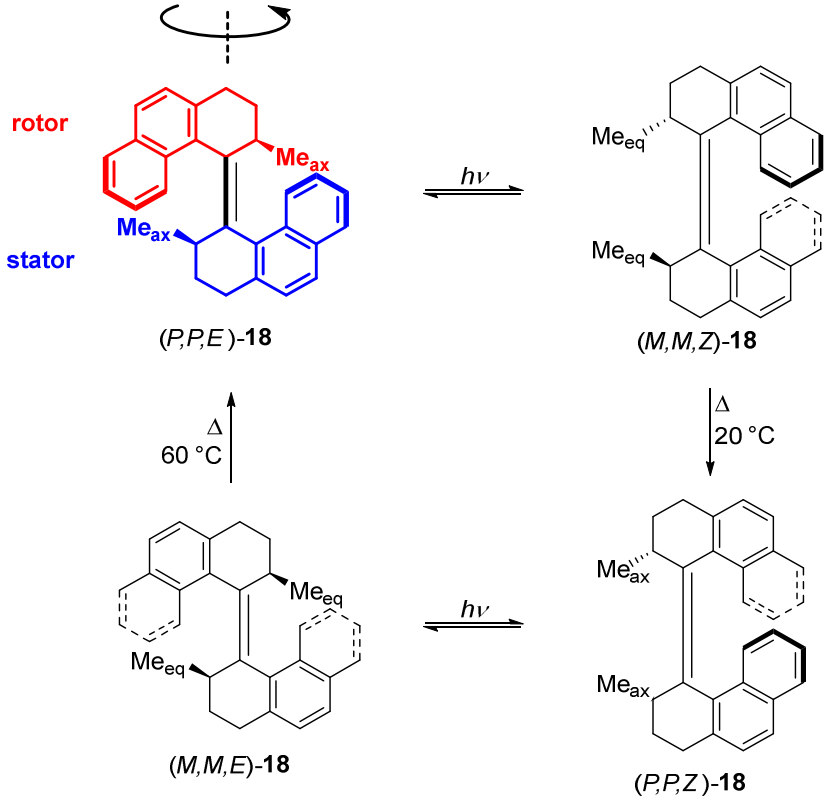

Figure 12 *Feringa*'s first-generation light-driven rotary molecular motor based on an overcrowded alkene.[88] There are four diastereoisomers of motor **18**, which can be interconverted in a step-wise manner, resulting in unidirectional rotation around the central double bond.

The overcrowded alkene **18** undergoes a four step rotational motion following an energy ratchet mechanism: Starting from stable (*P*,*P*,*E*)**-18**, photoisomerization of the central double bond results in (*M*,*M*,*Z*)**-18**. This isomer is thermodynamically metastable due to unfavorable steric interactions and undergoes a thermal helix inversion (THI) process to stable (*P*,*P*,*Z*)**-18**. Photoirradiation of this isomer again results in double bond isomerization, giving metastable (*M*,*M*,*E*)**-18**. Subsequent THI results in the recovery of initial isomer (*P*,*P*,*E*)**-18**. In total, this constitutes a unidirectional 360° rotation around the central double bond. Following the development of this "first generation" motor with two stereocenters, second generation (one stereocenter)[89] and third generation (one pseudo-asymmetric

center)[90] have been reported (see Figure 13). Another light-driven molecular motor framework, based on chiral imines, was reported by the group of *Lehn*.[91] It should be noted, that these motors are typically driven by high-energy and potentially damaging UV light. This has some drawbacks, e.g. for biomedical applications. Therefore, significant effort has been dedicated to shifting the absorption wavelength of light-driven molecular motors into the visible region of the electromagnetic spectrum. Strategies include the use of sensitizers for energy transfer[92] or the introduction of donor-acceptor ("push-pull")[93-94] systems.

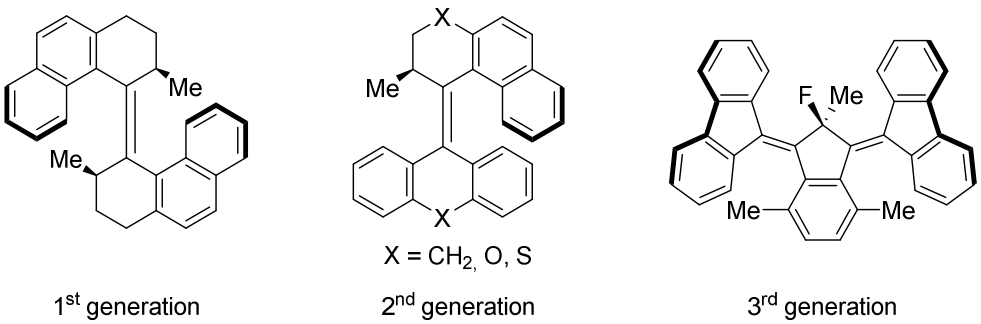

Figure 13 Examples for first, second and third generation overcrowded alkene molecular motors from the group of *Feringa*.[87]

2.2.2.1 Light-powered Molecular Motors Based on the HTI Scaffold

In 2015, *Dube* and coworkers reported on novel molecular motor **19**, which is based on the HTI scaffold and powered by visible light (up to 500 nm).[95] There are a number of modifications to the HTI core structure, which are essential for motor functionality. First of all, by oxidation to the sulfoxide, a stable stereocenter (*R* or *S*) is introduced. The stilbene fragment is conformationally restricted through ring-fusion and steric crowding induces helical twisting (*M* or *P*). As a result, there are eight possible isomers, which can be grouped as four sets of enantiomers. The molecular structures of the (*S*)-configured isomers, namely (*Z*,*S*,*P*)-, (*Z*,*S*,*M*)-, (*E*,*S*,*P*)- and (*E*,*S*,*M*)-**19**, are shown in Figure 14.

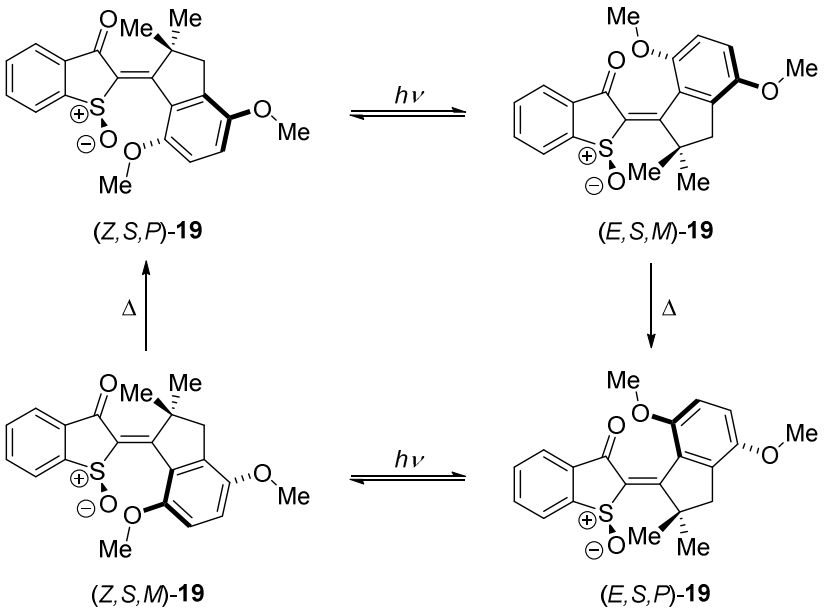

Figure 14 Visible light-driven rotary molecular motor **19** by *Dube* et al., based on an HTI structure.[95] In analogy to *Feringa's* first generation motor, there are four diastereoisomers undergoing sequential interconversion, resulting in unidirectional rotation around the central double bond.

Similarly to *Feringa's* overcrowded alkene motors, directional rotation of the motor is governed by a combination of photoisomerization of the central double bond and thermal helix inversion steps. Starting from thermodynamically stable (*Z*,*S*,*P*)**-19** (**A-19**), photoirradiation yields (*E*,*S*,*M*)**-19** (**B-19**). Due to unfavorable steric interactions, (*E*,*S*,*M*)-**19** is metastable and undergoes rapid THI to stable (*E*,*S*,*P*)**-19** (**C-19**). As (*E*,*S*,*M*)**-19** is 3.0 kcal mol^{-1} higher in energy than (*E*,*S*,*P*)**-19** (theoretical description at DFT MPW1K/6-31+G(d,p) level)[95], full conversion is obtained upon THI. The activation barrier for this process is very low (12.9 kcal mol^{-1} at ambient temperature)[9] and low-temperature (−90 °C) NMR experiments are necessary to monitor THI progress. Subsequent photo-induced double bond isomerization yields (*Z*,*S*,*M*)**-19** (**D-19**), which again is a metastable isomer. A final THI step results in recovery of the initial (*Z*,*S*,*P*)-configuration (**A-19**) and completes a 360° rotational cycle around the central double bond. The activation barrier for this second THI was found to be even lower, rendering observation of metastable (*Z*,*S*,*M*)-**19** by NMR impossible at −90 °C. A full summary of the qualitative ground state energy profile is given in Figure 15. Motor unidirectionality is determined by the helix inversion steps, which function as thermal ratcheting steps.

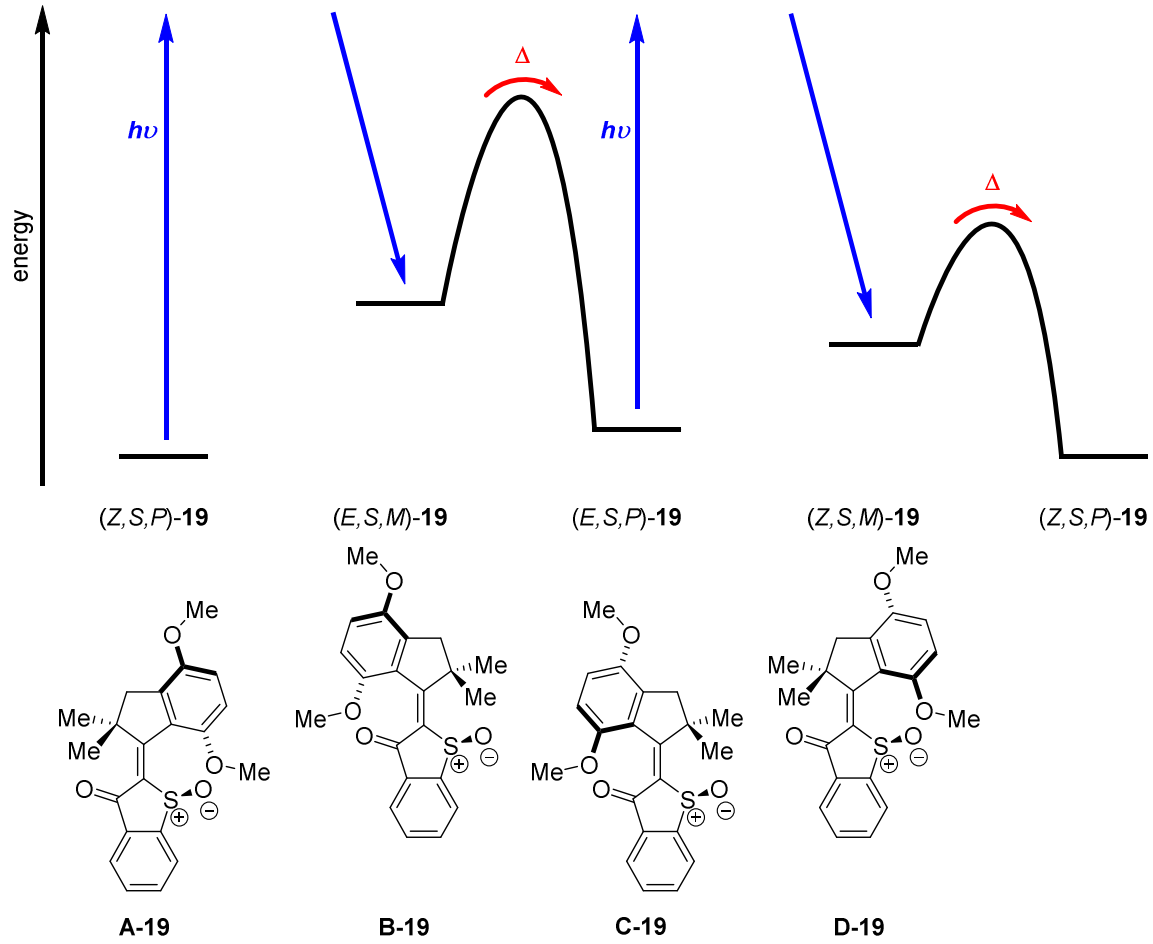

Figure 15 Qualitative ground state energy profile of HTI molecular motor **19**.[9, 95]

In a follow-up investigation on derivative **20** bearing a bulky *iso*-propyl group, which significantly slowed down THI, (*Z*,*S*,*M*)**-20** could be observed at −105 °C, thus directly confirming motor unidirectionality.[96] For a more detailed study on steric effects on hemithioindigo motor-rotation see also ref. [97]. Further light-driven motors based on HTI include a motor undergoing eight-shaped unidirectional motion,[98] a photon-only motor,[99] and a potentially ultrafast motor incorporating a pyridine moiety.[100]

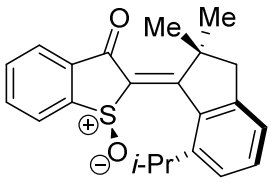

Scheme 2 Molecular structure of molecular motor **20**, that has a significantly decreased speed of rotation compared to HTI motor **19**.[96]

Key advantages of HTI molecular motors include the small size of the motor core motif, the high variety of possible functionalization options and the use of visible light to drive motor rotation. This makes HTI motors promising candidates for incorporation into molecular machinery and a number of examples will be discussed in the following sections.

2.3 Integrated Molecular Machinery and Coupled Motion

Several strategies exist for making use of or amplifying molecular motor motion in order to perform useful work.[101] One approach is the immobilization of motors, e.g. on surfaces[102-105], in polymers[106-107] or in frameworks such as metal organic frameworks (MOFs)[108] and covalent organic frameworks (COFs)[109]. Another approach is the doping of liquid crystalline materials with molecular motors. A prominent example was reported by *Feringa* and coworkers,[110] where UV-light irradiation of a liquid-crystalline film doped with 1 wt-% motor resulted in rotation of a microscale glass rod. A third approach is the self-assembly of responsive materials containing molecular motors, harnessing their collective motion e.g. in artificial "muscles".[111-112] Another attractive strategy is the coupling of molecular motions by integration of molecular switches and motors into sophisticated molecular machinery.[113-114] A number of examples will be discussed in more detail in the following section.

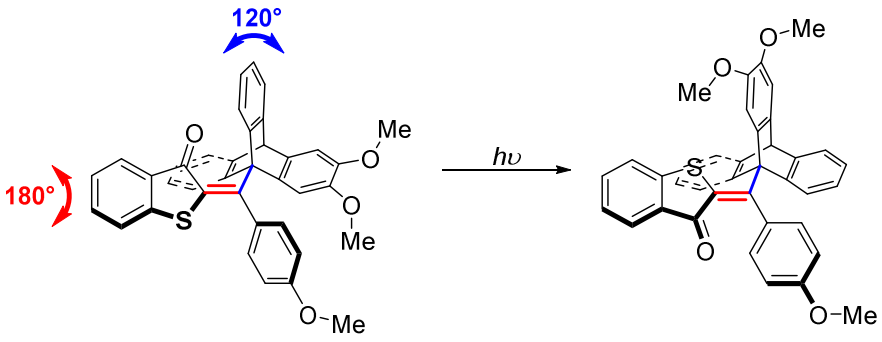

Figure 16 Photogearing system from the group of *Dube*.[115] Simultaneous double bond isomerization and triptycene rotation occur upon photoirradiation.

One possibility to couple motion at the molecular level is through intermeshing of different rotators, resulting in molecular gears.[116] Typically, in gearing systems motion is activated thermally resulting in non-directional Brownian motion. A conceptually novel "photogear" was described by *Dube* and coworkers.[115] The photogearing system **21** depicted in Figure 16 consists of an HTI photoswitch bearing a triptycene rotor and an anisole substituent. The

thioindigo part and the triptycene rotor are oriented in an arrangement resembling a 2:3 bevel gear. Photoirradiation of (*E*)-**21** with 420 nm light results in simultaneous double bond isomerization (180° rotation) and triptycene rotation (120° rotation). This way, two distinct molecular motions could be coupled and driven by light energy.

Another – highly versatile – approach to coupling molecular motion is the use of macrocycles and mechanically interlocked molecules, such as rotaxanes and catenanes.[117] Rotaxanes consist of a macrocyclic ring threaded onto a linear axle. Bulky stopper groups on both ends prevent de-threading of the ring. Catenanes are formally derived from rotaxanes by connecting both ends of the linear thread, resulting in two chain-like interlocked rings.

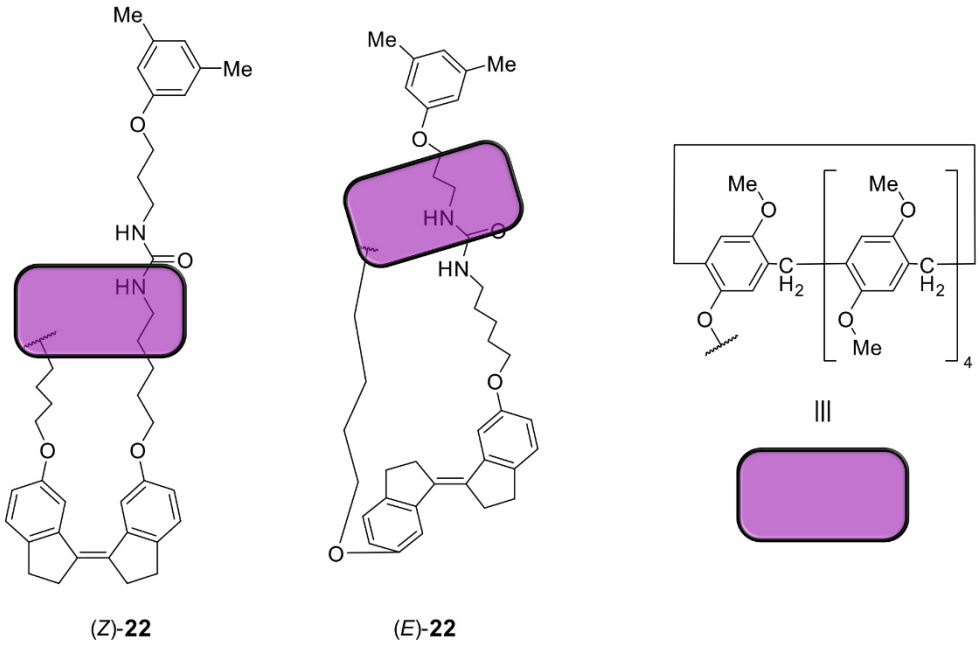

Figure 17 Rotaxane-like molecular machine **22** incorporating a stiff stilbene photoswitch as actuator.[118] *Adapted with permission of Royal Society of Chemistry, from* Y. Wang et al., "A light-driven molecular machine based on stiff stilbene" *Chem. Commun.* **2018**, *54*, 7991-7994 © *2018; permission conveyed through Copyright Clearance Center, Inc.*

An instructive example for such a molecular architecture was reported on by *Boulatov* and coworkers.[118] Molecular machine **22** (see Figure 17) consists of a stiff stilbene photoswitch as a stopper group in a rotaxane-like assembly. One half of the stiff stilbene is covalently linked to the rotaxane axle (containing a urea unit), while the other half is covalently linked to the rotaxane "wheel" (a pillar[5]arene). In this setup, the stiff stilbene serves both as a stopper group and as a photoactuator. Photoisomerization of the central double bond results

in translation of the "wheel" along the axis by 1.1 nm.[118] However, as this device is based on a switch, all mechanical work is undone on back-isomerization.

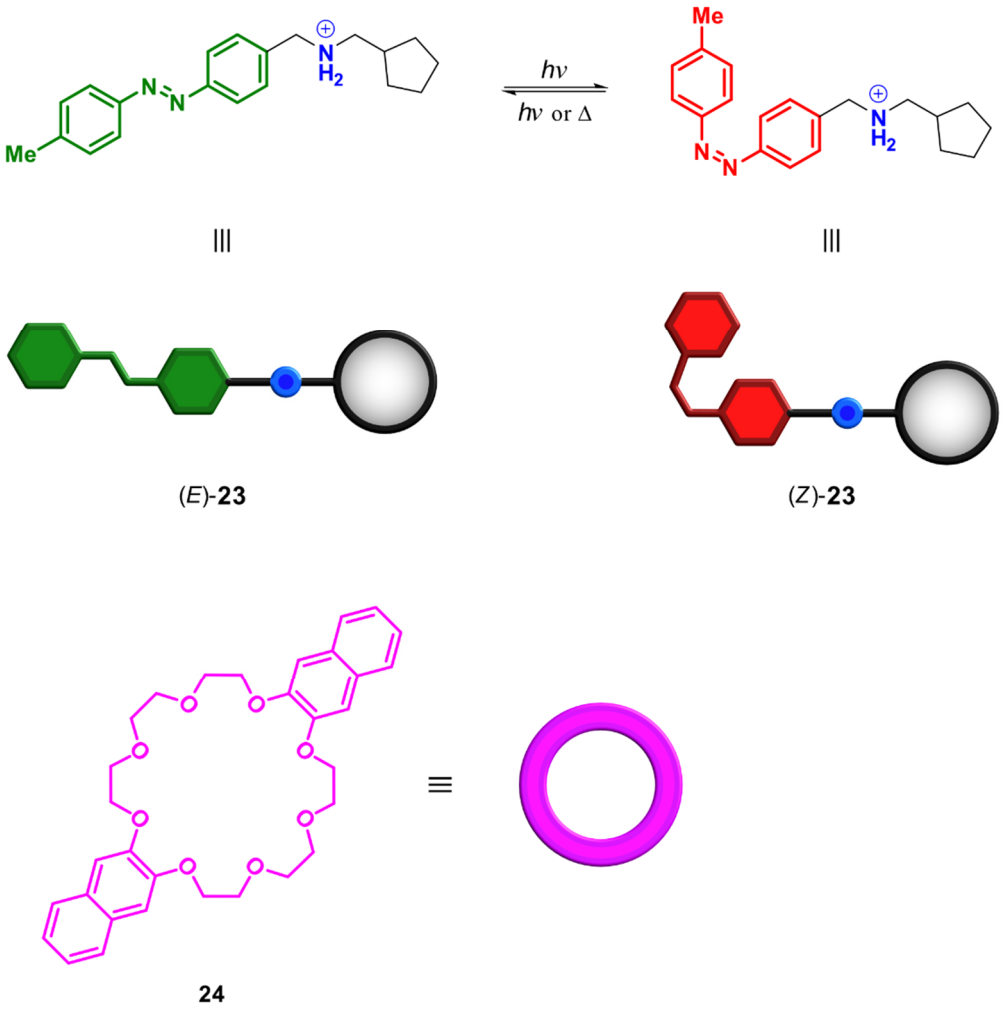

Figure 18 Molecular structures and cartoon representation of the components of a directional threading system reported by *Credi* and coworkers.[119] *Adapted with permission of Springer Nature, from* G. Ragazzon et al., "Light-powered autonomous and directional molecular motion of a dissipative self-assembling system", *Nat. Nanotechnol.* **2015**, *10*, 70-75. *© 2014, Springer Nature Limited.*

A switch-based system capable of inducing *directional* motion was designed by *Credi* and coworkers.[119] It consists of azobenzene-capped axle **23** with an ammonium binding site and crown ether **24**. How this system can be employed for directional threading is depicted in Figure 19. When the axle is in *E*-configuration threading and de-threading of the macrocycle will preferentially occur *via* the azobenzene-terminus. When the axle is in *Z*-configuration, the activation barrier for threading and de-threading *via* the azobenzene terminus is

significantly increased due to steric bulk. Instead, threading and de-threading will now proceed *via* the cyclopentyl-terminus preferentially. A full cycle of operation starts with free (*E*)-**23** and **24**. Macrocycle **24** will thread onto the axle *via* the azobenzene-terminus and bind to the ammonium-site, reaching the thermodynamically stable complex [**24**⊃(*E*)-**23**]. Photoisomerization to [**24**⊃(*Z*)-**23**] results in destabilization of the supramolecular complex and (partial) de-threading of **24** *via* the cyclopentyl terminus. Finally, thermal or photo-isomerization will regenerate (*E*)-**23**, completing a full cycle of machine operation. In total, this corresponds to a net directional threading of macrocycle **24** along the axle.

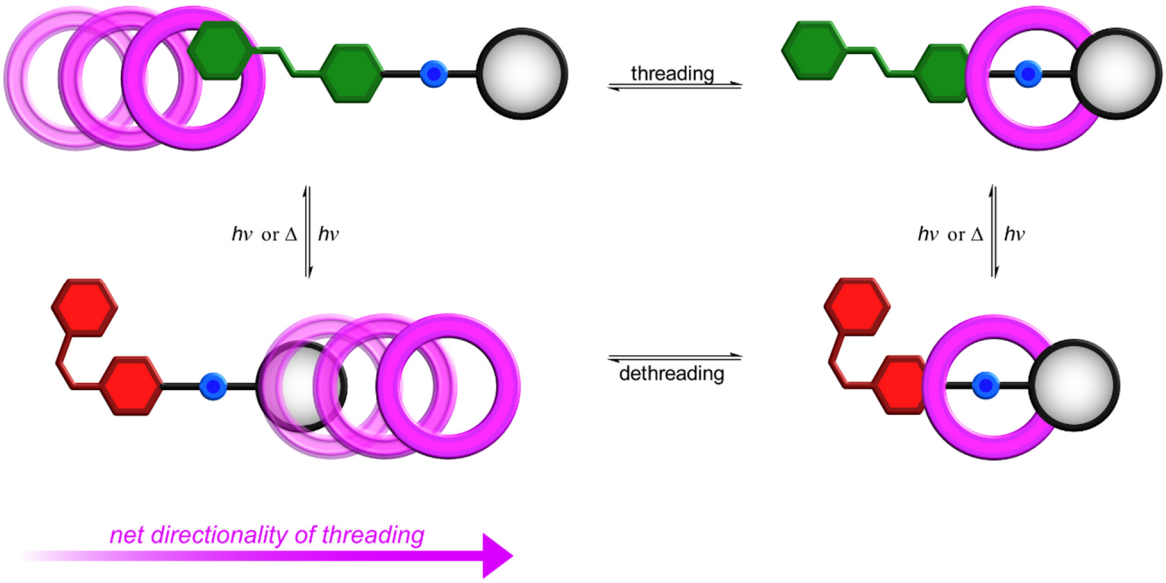

Figure 19 Cartoon representation of the directional threading process reported by *Credi* et al.[119] *Adapted with permission of Springer Nature from* G. Ragazzon et al., "Light-powered autonomous and directional molecular motion of a dissipative self-assembling system", *Nat. Nanotechnol.* **2015**, *10*, 70-75. *© 2014, Springer Nature Limited.*

A number of systems incorporating molecular motors into macrocycles or mechanically interlocked molecules has been reported and a selection will be discussed in the following. Molecular motor **25**, equipped with a "self-complexing lock", was described by *Feringa* and *Qu*.[120] It consists of a second generation overcrowded alkene motor, with the stator incorporated into a dibenzo-24-crown-8 ether and the rotor bearing a linear amine chain. Upon protonation of the amine group, complexation of the ammonium ion by the crown ether results in a "locked" state, inhibiting rotation of the molecular motor. Deprotonation with a base will liberate the amine from the crown ether and light-driven rotation of the molecular motor is possible again.

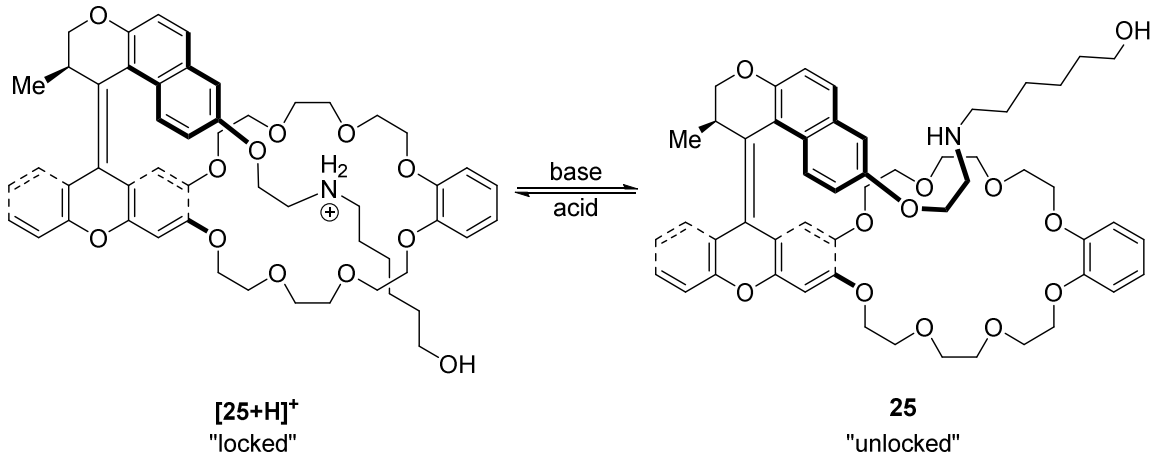

Figure 20 Molecular motor **25** with a "self-complexing lock" reported by *Qu* and *Feringa*.[120]

Qu, *Feringa* and coworkers[121] also reported on similar system **26**, again consisting of a motor-rotaxane hybrid (see Figure 21 for molecular structure). In this case, the linear axle is significantly longer and contains two binding sites (a triazolium and an amide group) with different affinities for the crown ether receptor. Upon light-driven rotation of the motor, the crown ether macrocycle will move back and forth along the rotaxane axis, shuttling between the higher-affinity triazolium and the lower-affinity amide unit. Figuratively, the motor has to continuously work against the restoring "pull" on the rotaxane axle.

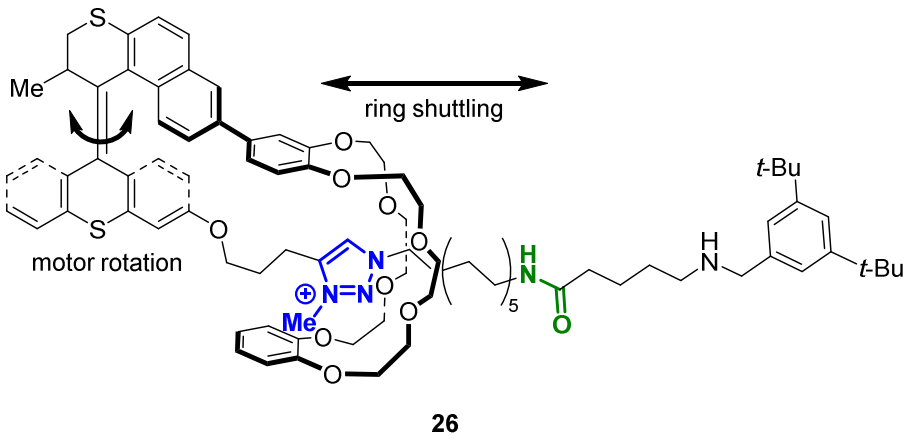

Figure 21 Rotaxane system **26** investigated by *Qu* and coworkers.[121] Upon light-fueled motor rotation, the crown ether receptor unit is shuttled back and forth between a triazolium (blue) and an amide (green) binding site.

A different concept of unidirectional motor motion transmission was realized by the *Dube* group.[122-123] In these HTI-based molecular machines, one of which is depicted in Figure 22, the stator fragment is equipped with a "receiver" or "follower" biaryl unit, which is connected to the rotor fragment *via* a flexible ethylene glycol chain. Light-driven unidirectional rotation around the central double bond simultaneously drives inversion of

biaryl axial chirality, drastically accelerating rotation around the biaryl axis compared to non-cyclic "open" analogues.

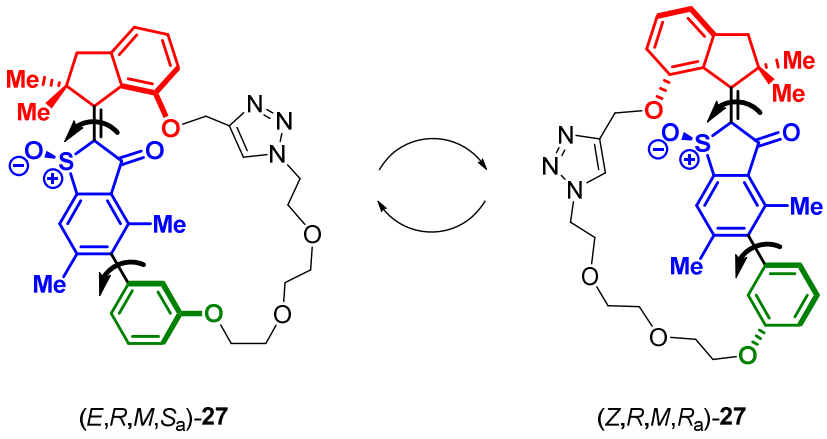

(*E*,*R*,*M*,S_a)-**27** (*Z*,*R*,*M*,R_a)-**27**

Figure 22 Integrated molecular machine **27** from *Dube* and coworkers,[123] consisting of an HTI-derived molecular motor in a macrocycle, with the stator highlighted in blue and the rotor highlighted in red. The unidirectional rotation of the motor is transferred to a remote biaryl "receiver" unit (green), resulting in accelerated and directional inversion of axial chirality.

The group of *Giuseppone* reported molecular "whirligig" **28**. Structurally similar motors have been incorporated into polymer gels by the same group, showing macroscopic contraction of the gel as visible proof of molecular motor work performed. The molecular structure of whirligig **28** is shown in Figure 23. A second generation overcrowded alkene motor is incorporated into two macrocycles in such a way, that rotation of the motor results in crossing of the two strands. Repeated rotation around the central double bond will increase the number of crossings with every turn, giving more and more coiled-up structures. It is important to note, that such behavior could not be observed when using a simple two state photoswitch. As shown in Figure 23c, light energy is used to continuously push the system energetically "uphill". Once the light is switched off, the molecule can relax along the ground state reaction coordinate to thermodynamic equilibrium (starting structure **28**) by rotation in the opposite direction, thus releasing the energy stored in the entanglement.

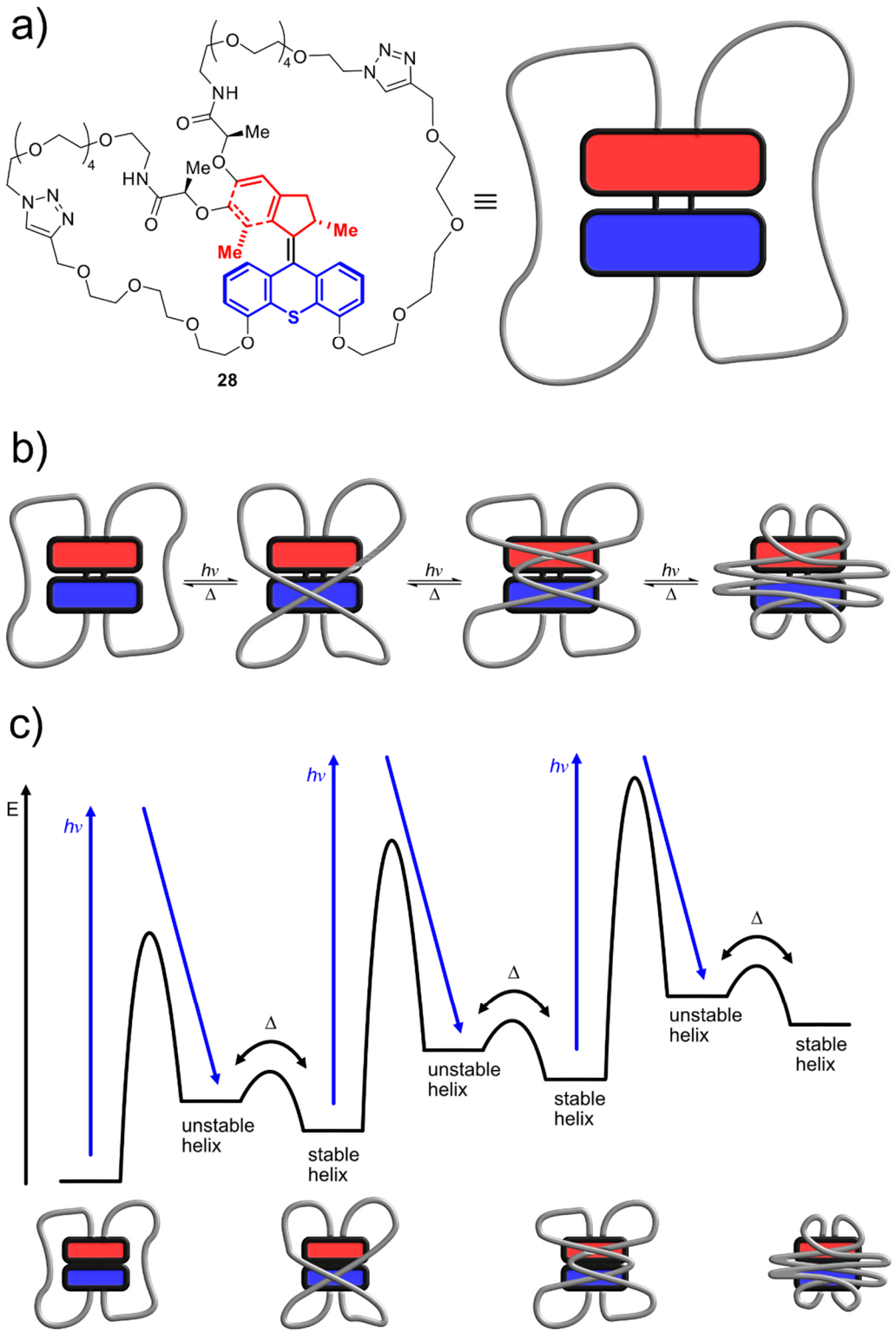

Figure 23 Molecular "whirligig" **28** from the group of *Giuseppone*.[124] **a)** Molecular structure and cartoon representation with the rotor highlighted in red and the stator highlighted in blue. **b)** Light-driven unidirectional rotation of the motor core leads to stepwise coiling up of the macrocycles. **c)** Qualitative energy diagram of the "winding-up" process. *Adapted with permission from* C. Gao et al., "Light-Driven Molecular Whirligig", *J. Am. Chem. Soc.* **2022**, *144*, 9845-9852; *© 2022, American Chemical Society.*

A structurally similar system was reported by *Kathan* and coworkers (**29**, see Figure 24).[125] Again, a second generation overcrowded alkene motor is incorporated into two macrocycles. The macrocycles both contain one imine function each, additionally enabling dynamic imine exchange reactions. Similarly to **28**, the number of crossings and the energy stored in the system increase with each rotation around the central double bond. The strain can be released by nucleophilic attack on the imine bonds and subsequent "reshuffling" of the imine bonds to thermodynamic equilibrium.

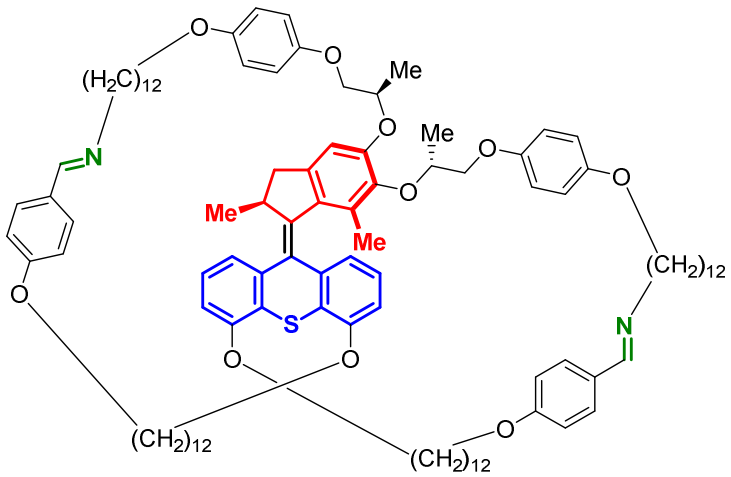

29

Figure 24 Molecular motor system **29** reported by *Kathan* et al.[126] The molecular motor fragments are highlighted in blue (stator) and red (rotor). Rotor and stator are connected by two linear chains, resulting in a double macrocyclic structure, similar to the one reported in ref. [124]. Both macrocycles contain one imine bond each (highlighted in green) that can undergo dynamic covalent chemistry reactions.

Further notable examples of integrated machinery and coupled motion include the locked synchronous motion of a naphthalene unit attached to a molecular motor,[127] motor-crown-ether hybrids for guest recognition,[128] and rocking[129] or oscillatory[130] motion in molecular motors.

3 Molecular Motors in Macrocyclic Systems

In the following sections, synthetic efforts towards a number of macrocyclic motor systems will be discussed. Three general structural concepts were investigated. A schematic representation of each assembly is given at the beginning of the respective chapter. All systems incorporate a molecular motor based on HTI in a macrocycle. They differ in the attachment points of the macrocyclic ring as well as additional stopper groups or flexible chains. The specific setups as well as the synthetic steps undertaken are discussed in detail in the following.

3.1 Synthetic Approach 1

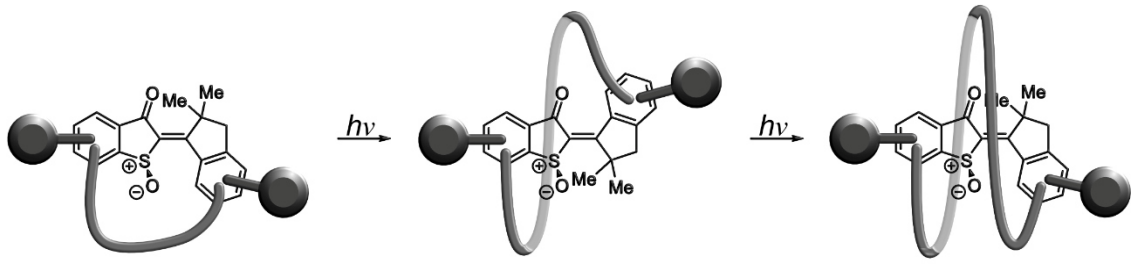

Figure 25 Schematic representation of a molecular machine "winding up" a linear chain powered by light energy. The central core is based on an HTI sulfoxide motor embedded in a macrocyclic setup with bulky stopper groups preventing "slipping" (i.e. unproductive steps in which the system returns to the initial state *via* the chain passing over the HTI axle instead of winding-up) of the wound up chain.

In Figure 25, a schematic representation of a molecular motor system capable of "winding up" a molecular chain is given. An HTI sulfoxide, based on the established molecular motor **19**, is incorporated into a macrocycle in such a way, that unidirectional rotation of the motor results in a helical structure around the central double bond. Bulky stopper groups are introduced on both halves of the molecule in near-colinear orientation to the double bond in order to prevent "slipping" (i.e. passing over the HTI axle) of the chain.

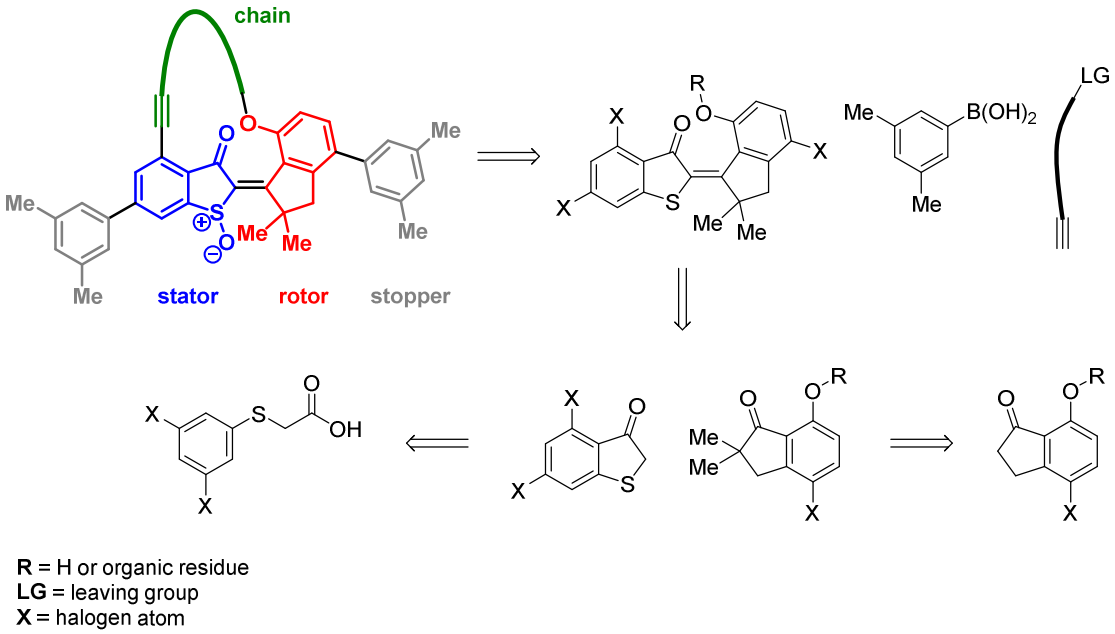

Scheme 3 Retrosynthetic analysis of a potential HTI based motor capable of "winding up" a chain around the motor's central double bond. A three-fold halogenated HTI core is devised, enabling the introduction of stopper and linker groups *via* cross coupling reactions. The bulky stopper groups are positioned almost in parallel to the central double bond so the resulting arrangement resembles a dumbbell. The attachment points for the chain are chosen to give a perpendicular orientation of the chain with respect to the central axle.

A more detailed structural depiction of the prospective molecular machine is shown in Scheme 3. The central HTI motif was envisioned to be accessible *via* an established aldol condensation reaction between benzothiophenone and indanone building blocks.[73, 104, 122-123] The building blocks were chosen based on considerations of synthetic availability and attachment points for stopper groups and linkers. The orientation of the macrocycle chain attachment points should be perpendicular to the central double bond. Therefore, attachment in *ortho* position to either the sulfur or carbonyl substituent of the thioindigo fragment was desired. On the indanone fragment, the chain should be attached via an ether linkage in *ortho* position to the double bond attachment. This mode of connection has the added benefit of close structural and electronic similarity to the original motor motif, which is substituted with a methoxy group in this position, without adding significant changes to the synthesis or building blocks. The methoxy group is of fundamental importance for the pronounced helicity of the HTI sulfoxide system and closely connected to the motor operating mechanism (thermal ratcheting steps). The attachment points for the bulky stopper groups are positioned in *para* position to the carbonyl attachment on the thioindigo fragment and in *para* position to the alkoxy group on the indanone fragment, resulting in an almost collinear

arrangement with regard to the central double bond. Halogen atoms are placed in those positions, as they allow for the use of broad and versatile cross coupling chemistry.

4,6-Dichlorobenzothiophenone **31** was prepared in two steps starting from 3,5-dichloro thiophenol (see Scheme 4).[104] Nucleophilic substitution on bromoacetic acid gave the corresponding phenyl thioacetic acid **30** in good yield. **30** was then converted to the acid chloride using oxalyl chloride and catalytic amounts of DMF. Subsequent intramolecular FRIEDEL-CRAFTS acylation catalyzed by $AlCl_3$ gave benzothiophenone **31** in very good yield (87%).

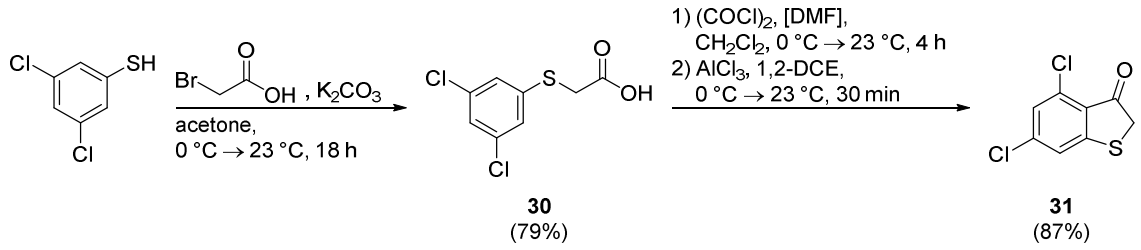

Scheme 4 Synthesis of dichlorinated benzothiophenone **31** starting from 3,5-dichloro thiophenol.[104] Nucleophilic substitution on bromoacetic acid followed by an intramolecular FRIEDEL-CRAFTS acylation gave **31**.

Methylation of 4-bromo-7-hydroxy-1-indanone with iodomethane and sodium hydride in THF gave methylated indanone **32** in low yield (31%). Unexpectedly, the hydroxyl function was not methylated (see Scheme 5). This might be due to hydrogen bonding interactions to the neighboring carbonyl, which prevent deprotonation of the phenolic OH-group. It was found, that using DMF as a solvent, potassium carbonate as a base and iodomethane as electrophile, **32** could be transformed into the corresponding methyl aryl ether **33**.

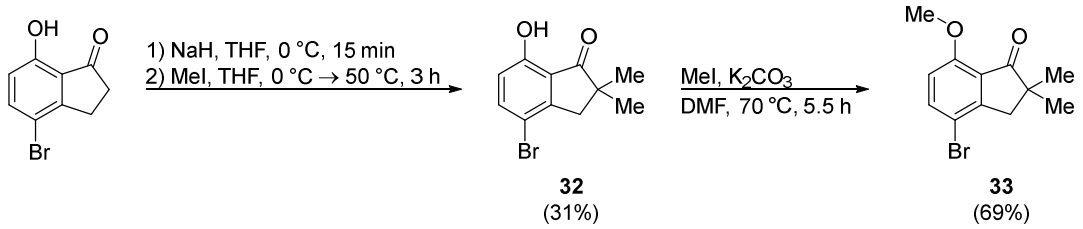

Scheme 5 Methylation of 4-bromo-7-hydroxy-indan-1-one with iodomethane in THF afforded **32** in 31% yield. Subsequent methylation with iodomethane in DMF gave **33** in 69% yield.

With indanone **32** and benzothiophenone **31** at hand, the condensation to give the corresponding HTI was attempted following an established procedure with BCl_3 as LEWIS acid.[104, 122-123] However, no formation of the desired condensation product **34** was observed

(see Scheme 6). As this might be due to the presence of a phenolic hydroxy group on the indanone fragment, methylated analogue **33** was used in the following.

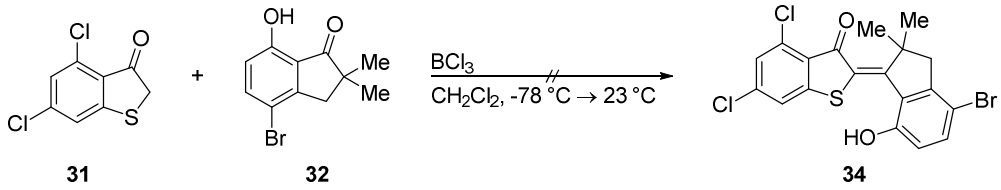

Scheme 6 Attempted condensation of benzothiophenone **31** with indanone **32**. No formation of the desired product **34** was observed.

Indanone **33** could be obtained by methylation of commercially available 4-bromo-7-methoxy-1-indanone with iodomethane and sodium hydride in THF in 67% yield (see Scheme 7).

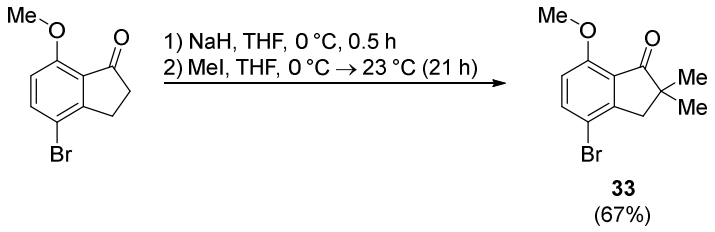

Scheme 7 Synthesis of dimethylated indanone **33** by methylation of 4-bromo-7-methoy-indan-1-one.

Next, the condensation of benzothiophenone **31** and indanone **33** was performed (see Scheme 8). It was found, that the reaction time and the number of equivalents of BCl_3 had an impact on the products formed. When 1.1 equiv. of BCl_3 were used and the reaction time was kept short (15 min), the methoxy group was left intact and **35** was obtained in 41% yield. When additional 1.8 equiv. of BCl_3 were added to the reaction mixture after the initial condensation and the mixture was stirred at 0 °C for 2.5 h, the aryl methyl ether was cleaved and hydroxy substituted HTI **34** could be isolated in 15% yield. This is to be expected, as BCl_3 and especially BBr_3 are known to cleave aryl methyl ethers to the corresponding phenols.[131-132] At a later stage, the hydroxy function should serve as an attachment point for a chain or linker group. As the synthesis and isolation of **35** proceeded more smoothly and with higher yields than that of **34**, it was decided to first functionalize the methoxy derivative and to then cleave it later in the synthesis.

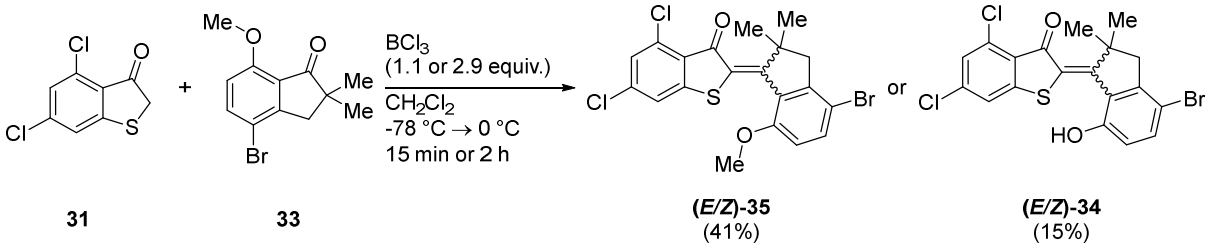

31 **33** **(*E*/*Z*)-35** (41%) **(*E*/*Z*)-34** (15%)

Scheme 8 Synthesis of HTIs **34** and **35** by BCl_3 mediated condensation of benzothiophenone **31** and indanone **33**. Product formation depends on the amount of BCl_3 and the reaction time. Using 1.1 equivalents of BCl_3, **35** was obtained in 41% yield after 15 min reaction time. When a total of 2.9 equivalents of BCl_3 was employed and the reaction time was 2 h, **34** was obtained in 15% yield.

There are three halogen atoms on HTI **35**, which should be able to undergo palladium catalyzed cross coupling reactions. As they differ in their element (bromine vs. chlorine) and their environment, in an initial screening of cross coupling conditions, possible differences in reactivity were investigated. 3,5-dimethylphenylboronic acid served as a coupling partner and model compound for bulky stopper groups. Table 1 gives a summary of the conditions investigated for the SUZUKI cross coupling reaction of HTI **35** and 3,5-dimethylphenylboronic acid. All possible cross coupling products **A**-**E** are listed in Table 1. The desired target structure is a specific regioisomer of **C**, with $R^1 = R^3 = Ar$ and $R^2 = Cl$.

Table 1 Conditions tested for SUZUKI cross coupling of HTI **35** with 3,5-dimethylphenylboronic acid. All reactions were performed on microscale (approx. 10 µmol) in 1.5 mL glass vials. 1 equiv. of **35**, 2 equiv. of boronic acid and 3 equiv. of base were used, as well as approx. 0.1 equiv. of palladium catalyst and 0.2 equiv. of ligand where applicable. After a simple reaction workup, crude mixtures were analyzed by MS and products identified based on MS.

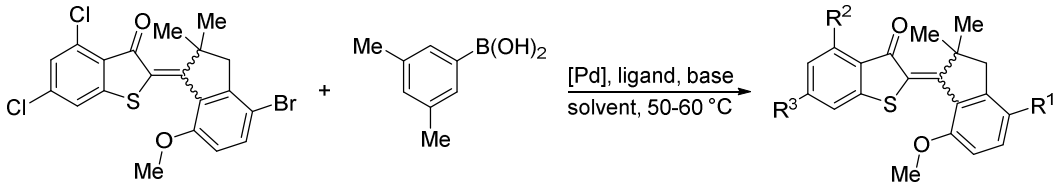

(*E*/*Z*)-35

A R^1=Ar, R^2=R^3=Cl
B R^1=Br, R^2=Ar, R^3=Cl
or R^1=Br, R^2=Cl, R^3=Ar
C R^1=Ar, R^2=Ar R^3=Cl
or R^1=Ar, R^2=Cl, R^3=Ar
D R^1=Br, R^2=R^3=Ar
E R^1=R^2=R^3=Ar

Entry	[Pd]	Ligand	Base	Solvent	Result (MS)
1	$Pd(PPh_3)_4$	-	K_2CO_3	1,2-DME (0.1 M)	**A, B**
2	Pd_2dba_3	XPhos	K_2CO_3	1,2-DME (0.1 M)	**A, B, C, D, E**
3	Pd_2dba_3	APhos	K_2CO_3	1,2-DME (0.1 M)	**A, C**
4	$Pd(PPh_3)_4$	-	K_2CO_3	1,4-dioxane:H_2O (4:1) (0.05 M)	**A, C**
5	sSPhos Pd G2	-	K_3PO_4	1,4-dioxane:H_2O (4:1) (0.05 M)	**C, E**
6	RuPhos Pd G3	-	K_3PO_4	1,4-dioxane:H_2O (4:1) (0.05 M)	**E**
7	RockPhos Pd G3	-	K_3PO_4	1,4-dioxane:H_2O (4:1) (0.05 M)	**C**
8	DavePhos Pd G3	-	K_3PO_4	1,4-dioxane:H_2O (4:1) (0.05 M)	**A, C, E**
9 *65°C	$Pd(PPh_3)_4$	-	K_3PO_4	1,4-dioxane:H_2O (4:1) (0.07 M)	**A, B, C, D, E**

In all cases, cross coupling products could be identified by mass spectrometry. However, there was mostly a mix of mono-, di- and sometimes tri-substituted coupling products and no clear preference for one substitution pattern was evident. This was further complicated by the impossibility of differentiating the two chlorine positions based on mass spectroscopy

results alone. In order to reduce the number of possible coupling products, indanone **36** was prepared (see Scheme 9). **36** was obtained by SUZUKI cross coupling of indanone **33** with 3,5-dimethylphenylboronic acid in excellent yield (95%).

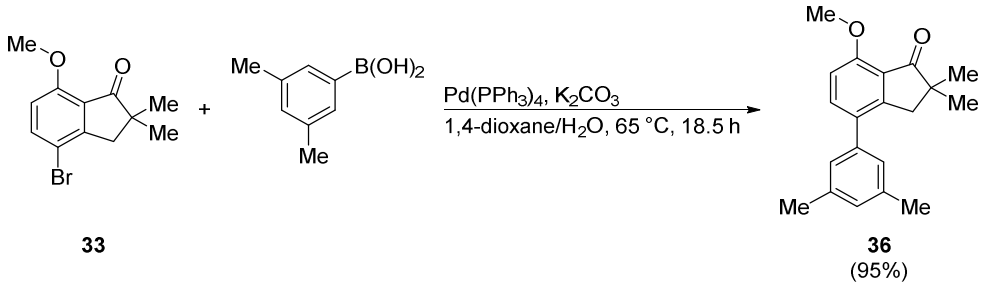

33 **36** (95%)

Scheme 9 Synthesis of indanone **36** by SUZUKI cross coupling of indanone **33** with 3,5-dimethylphenylboronic acid.

As shown in Scheme 10, indanone **36** underwent BCl_3 mediated condensation with benzothiophenone **31** to give HTI **37** in acceptable yield (36%).

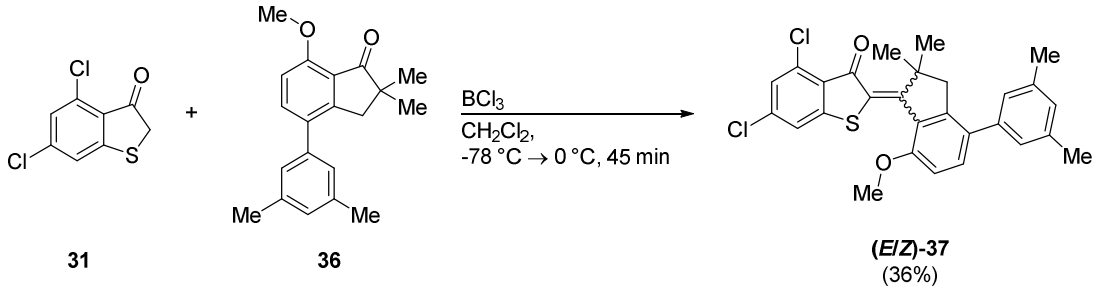

31 **36** **(*E*/*Z*)-37** (36%)

Scheme 10 Synthesis of HTI **37** by BCl_3 mediated condensation of benzothiophenone **31** and **36**.

HTI **37** was then used as a substrate in a number of different attempted cross coupling reactions. Table 2 gives a summary of the conditions investigated for the SUZUKI cross coupling reaction of HTI **37** and 3,5-dimethylphenylboronic acid. All possible cross coupling products **A**-**C** are listed in Table 2. The desired target structure is **B**, with R^1 = Ar and R^2 = Cl.

Table 2 Conditions investigated for the SUZUKI cross coupling of **37** with 3,5-dimethylphenylboronic acid. 1.1 equiv. of boronic acid, 2.0 equiv. of base and 0.1 equiv. of palladium catalyst were used. The concentration was approx. 0.05 M and the reaction was performed under N_2-atmosphere. Reaction products were assigned based on MS results.

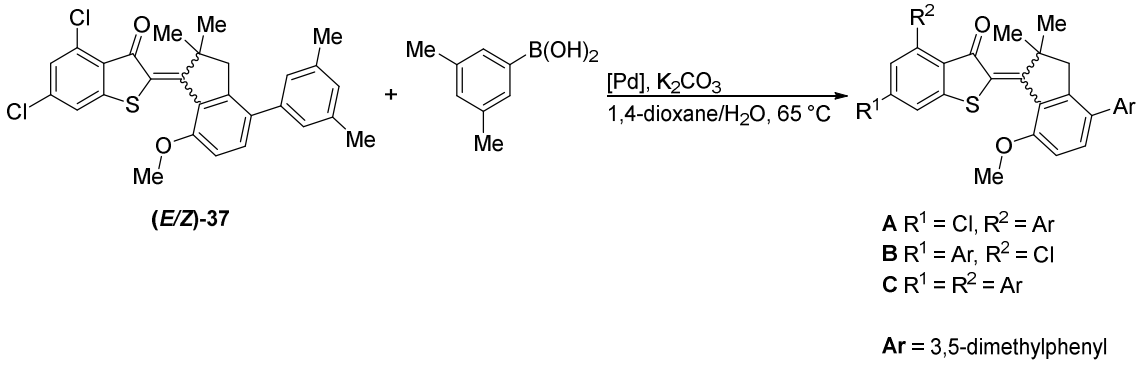

Entry	[Pd]	Result (MS)
1	$Pd(PPh_3)_4$	**A** and / or **B**
2	XPhos Pd G2	**A** and / or **B**, **C**

In the case of Entry 1 in Table 2, purification by column chromatography was not successful. A complex mixture of starting material (*E*/*Z*-mixture), as well as **A** and **B** (both *E*/*Z*-mixtures) was obtained as judged by ^{1}H NMR. No regioselectivity was observed. Entry 2: With the use of XPhos Pd G 2, the reactivity was increased and the mass of two-fold coupling product **C** could be identified by HRMS. As only 1.1 equiv. of boronic acid were used, there is clearly no regioselectivity or even selectivity of mono- versus disubstitution in this case.

In an analogous fashion, dichlorinated HTI **39**, a regioisomer of **37**, was prepared (see Scheme 11).

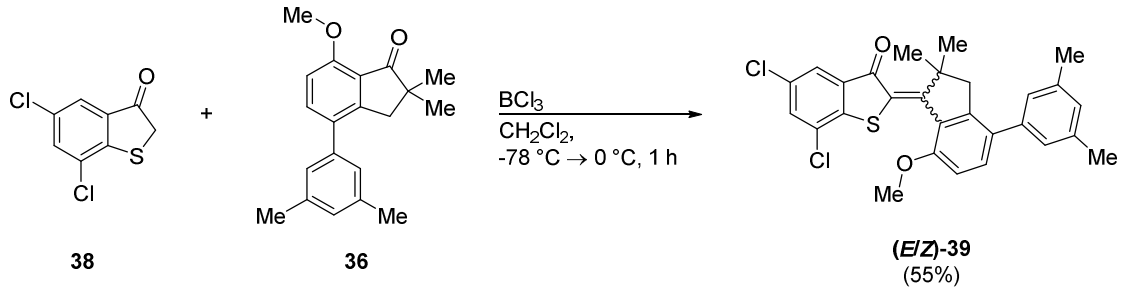

Scheme 11 Synthesis of dichlorinated HTI **39** by BCl_3 mediated condensation of benzothiophenone **38** and indanone **36**.

Again, the SUZUKI cross coupling reaction of HTI **39** with 3,5-dimethylphenylboronic acid was attempted. Two conditions were tested (see Table 3). Similar to previous experiments, no clear preference for one of the possible reaction products was observed. Combined with the difficult separation of products, this route was deemed not practical and not pursued any further.

Table 3 Conditions tested for the SUZUKI cross coupling reaction of HTI **39** with 3,5-dimethylphenylboronic acid on microscale. 1 equiv. of boronic acid, 2 equiv. of base and 0.1 equiv. of palladium catalyst were used. The concentration was approx. 0.1 M and the reaction was performed under N_2-atmosphere.

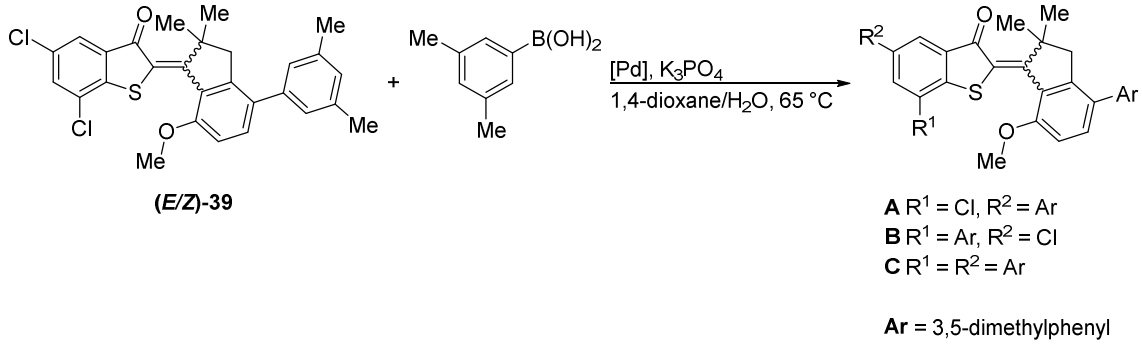

(*E*/*Z*)-39

A R^1 = Cl, R^2 = Ar
B R^1 = Ar, R^2 = Cl
C R^1 = R^2 = Ar

Ar = 3,5-dimethylphenyl

Entry	[Pd]	Result (MS)
1	$Pd(PPh_3)_4$	**A** and / or **B**
2	XPhos Pd G2	**A** and / or **B**, **C**

3.2 Synthetic Approach 2

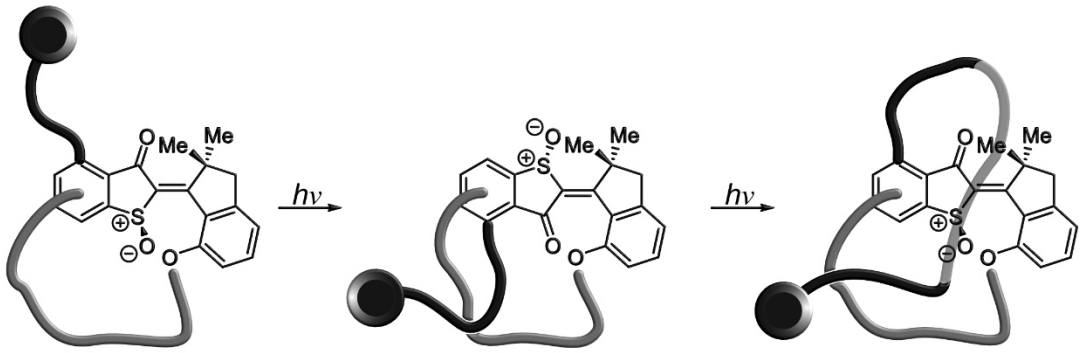

Figure 26 Schematic representation of a macrocyclic system based on a previously reported molecular setup. An HTI based molecular motor core is incorporated into a macrocyclic structure and a chain terminated by a bulky stopper group is installed on the thioindigo fragment. The chain is attached on the thioindigo fragment in a such way, that a perpendicular orientation to the central double bond is achieved.

As the initial setup posed a number of challenges, mostly due to low selectivity of the attempted cross coupling reactions in combination with difficult separation of products, a new approach was devised. An established macrocyclic HTI structure[122] was taken as a starting point (see Scheme 12). A schematic representation of the proposed setup is given in Figure 26. Again, the macrocyclic ring is attached to the indanone fragment *via* an ether linkage in *ortho* position to the double bond attachment site. On the thioindigo fragment, the macrocyclic ring is attached in a co-linear orientation with regard to the central double bond. An additional chain, terminated by a bulky stopper group, is introduced on the thioindigo fragment in perpendicular orientation to the central double bond. It is assumed, that this arrangement results in threading of the linear chain through the macrocycle and helical winding of the chain around the central double bond upon unidirectional rotation of the motor core. Due to the arrangement of the individual parts, no additional stopper groups are necessary to prevent chain "slipping" events, thus potentially reducing the number of synthetic steps. A more detailed structural description of the proposed system is given in Scheme 12.

Key steps in the synthesis of the previously reported macrocyclic system are the attachment of an ethylene glycol chain *via* copper catalyzed azide-alkyne click chemistry, followed by an intramolecular SUZUKI cross coupling reaction to close the macrocycle. The established route was modified by the introduction of a second halogen atom on the thioindigo fragment for later functionalization.

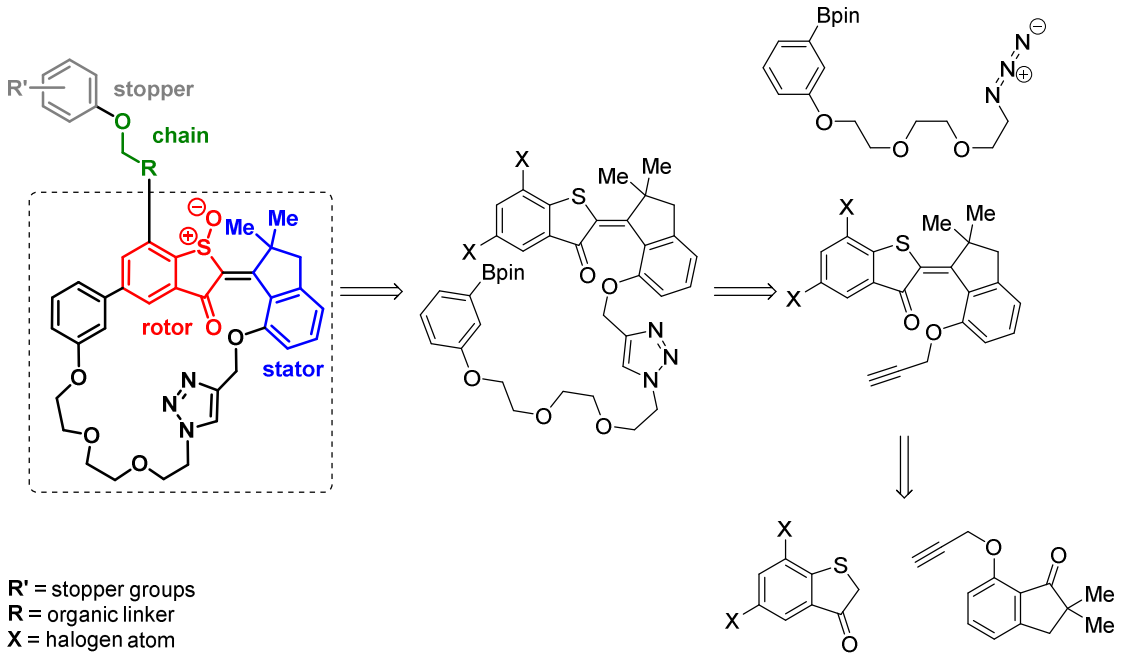

Scheme 12 Simplified retrosynthetic analysis of a potential macrocyclic threading system based on a previously reported HTI motor setup. The established structural motif is marked by a dashed box. An ethylene glycol chain, terminated by an arylboronic ester, is introduced *via* azide-alkyne cycloaddition. The macrocycle is then formed by an intramolecular SUZUKI cross coupling reaction. A second halogen atom on the thioindigo fragment enables the installation of a linear chain *via* cross coupling reactions.

2,4-Dichlorobenzothiophenone **38** was prepared in two steps starting from 2,4-dichloro thiophenol. Nucleophilic substitution on bromoacetic acid gave the corresponding phenyl thioacetic acid **40** in near quantitative yield. **40** was then converted to the acid chloride using thionyl chloride. Subsequent intramolecular FRIEDEL-CRAFTS acylation catalyzed by $AlCl_3$ gave benzothiophenone **38** in excellent yield (94%).

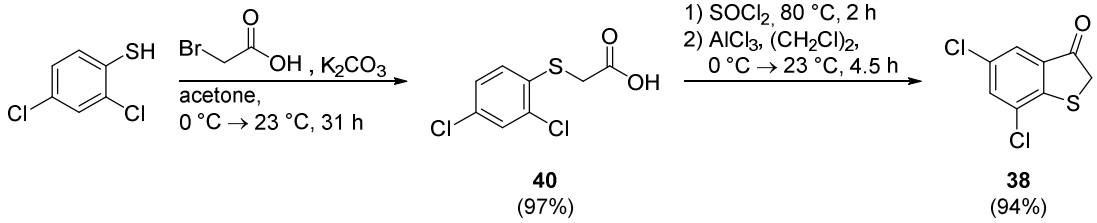

Scheme 13 Synthesis of dichlorinated benzothiophenone **38** starting from 2,4-dichloro thiophenol. Nucleophilic substitution on bromoacetic acid followed by an intramolecular FRIEDEL-CRAFTS acylation gave **38** in 94% yield.

It would be attractive to install the chain or a synthetic "handle" (a short linker with an attachment point for later functionalization) on the benzothiophenone prior to condensation in order to circumvent selectivity issues due to the presence of two chlorine atoms later in

the synthesis. Therefore, the STILLE coupling of allyltributylstannane with benzothiophenone **38** was investigated. With the successful installation of an allyl moiety in the 2-position, this could serve as an attachment point for a longer chain *via* olefin metathesis. Table 4 gives an overview over the conditions tested for the STILLE cross coupling reaction of **38** with allyltributylstannane.

Table 4 Conditions tested for STILLE cross coupling of benzothiophenone **38** with allyltributylstannane. Reactions were performed on microscale in 1.5 mL glass vials. 1.2 equiv. of allyltributylstannane and two equiv. of CsF were used. A small amount of CuI (tip of a glass pipette) was added as indicated. 0.1 equiv. of palladium catalyst were used and 0.2 equiv. of ligand (where applicable). The concentration was 0.15 M for entries 1–6 and 0.12 M for entries 7–12. Product identification is based on MS analysis.

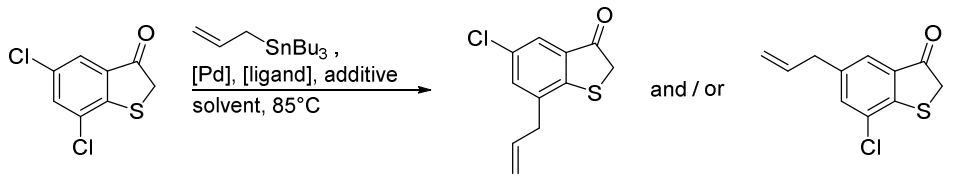

38 **A** **B**

Entry	[Pd]	Ligand	Additive	Solvent	Product (MS)
1	$Pd(PPh_3)_4$	-	CuI, CsF	DMF	-
2	$Pd(dppf)Cl_2$	-	CuI, CsF	1,4-dioxane	-
3	PEPPSI-iPr	-	CuI, CsF	1,4-dioxane	-
4	RockPhos Pd G3	-	CuI, CsF	1,4-dioxane	-
5	JackiePhos Pd G3	-	CuI, CsF	PhMe	-
6	RuPhos Pd G3	-	CsF	PhMe	**A** and / or **B**
7	$Pd(PPh_3)_4$	-	CsF	1,4-dioxane	-
8	PEPPSI-iPr	-	CsF	1,4-dioxane	-
9	Pd_2dba_3	tBuBrettPhos	CsF	1,4-dioxane	-
10	Pd_2dba_3	CPhos	CsF	PhMe	**A** and / or **B**
11	PEPPSI-iPr	-	CsF	PhMe	
12	$Pd(PPh_3)_4$	-	CsF	PhMe	

As the regioselectivity cannot be determined based on mass spectrometry alone, the coupling reaction was repeated on larger scale (see Scheme 14 for conditions). **41** could be obtained in a mixture with carbazole (which is liberated by the palladium precatalyst). COSY NMR

(Figure 27) analysis showed correlations between both aromatic protons and the aliphatic protons of the allyl moiety. From this, structure **41** with the allyl moiety in 4-position was concluded as the most plausible regioisomer.

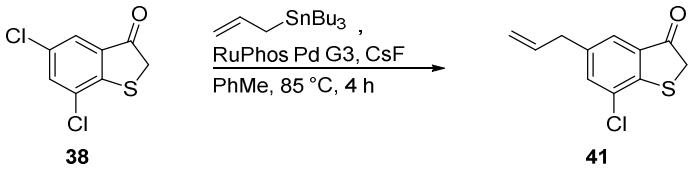

38 **41**

Scheme 14 STILLE coupling of **38** and allyltributylstannane on larger scale. Compound **41** was assigned as the depicted regioisomer based on correlations observed in COSY NMR.

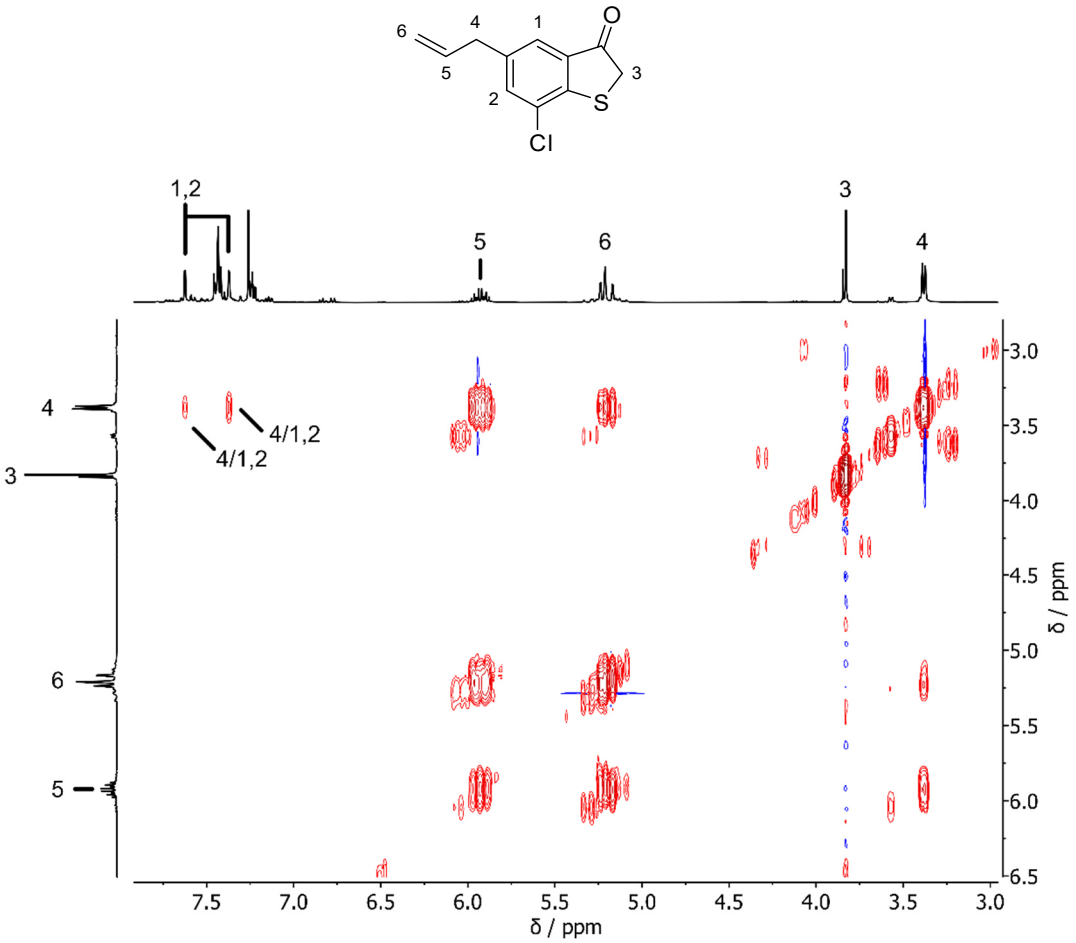

Figure 27 Excerpt from ^{1}H COSY NMR (400 MHz, $CDCl_3$, 20 °C) of **41** (with carbazole impurity). The highlighted correlations between aliphatic proton 4 and aromatic protons 1 and 2 support assignment to this regioisomer.

As STILLE coupling did not produce the desired regioisomer, the synthesis was continued with 2,4-dichloro benzothiophenone **38** and the selectivity was to be addressed at a later stage. Indanone **43** was prepared in two steps starting from 7-hydroxy-1-indanone (see Scheme 15).[122] Alkylation with propargyl bromide in DMF with potassium carbonate as a base gave indanone **42** in very good yield (89%). After subsequent methylation with iodomethane and sodium hydride in THF, indanone **43** was obtained in 78% yield.

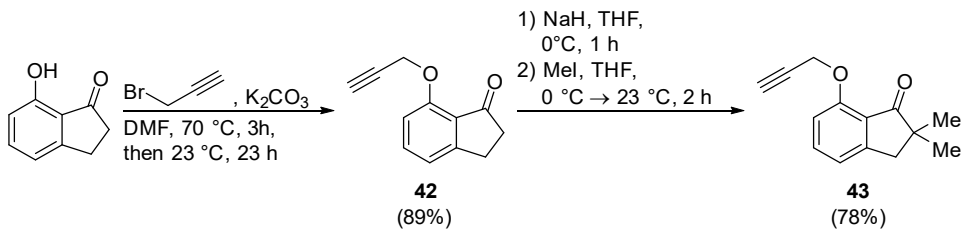

Scheme 15 Synthesis of indanone **43** starting from 7-hydroxy-1-indanone.[122]

Benzothiophenone **38** and indanone **43** underwent BCl_3 mediated condensation to give HTI **44** in 53% yield (see Scheme 16).

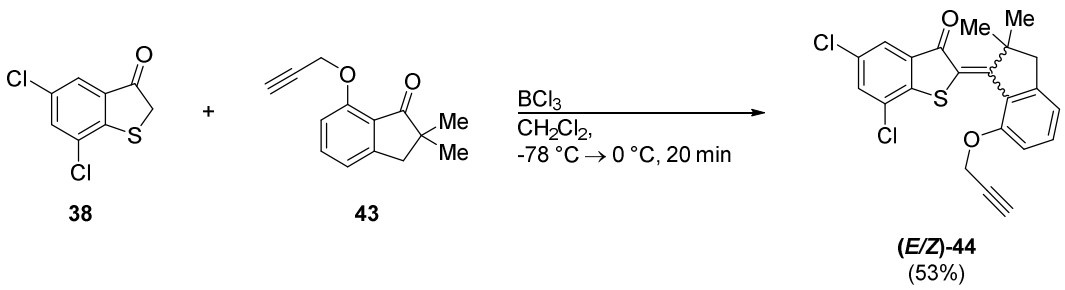

Scheme 16 Synthesis of HTI **44** by BCl_3 mediated condensation of benzothiophenone **38** with indanone **43**.

In the following synthetic step, HTI **44** was subjected to a copper catalyzed azide-alkyne "click" reaction with linker unit **45**. Using the conditions reported in literature,[122] after purification by column chromatography HTI **46** was obtained as a mixture containing both boronic acid pinacol ester as well as hydrolyzed boronic acid.

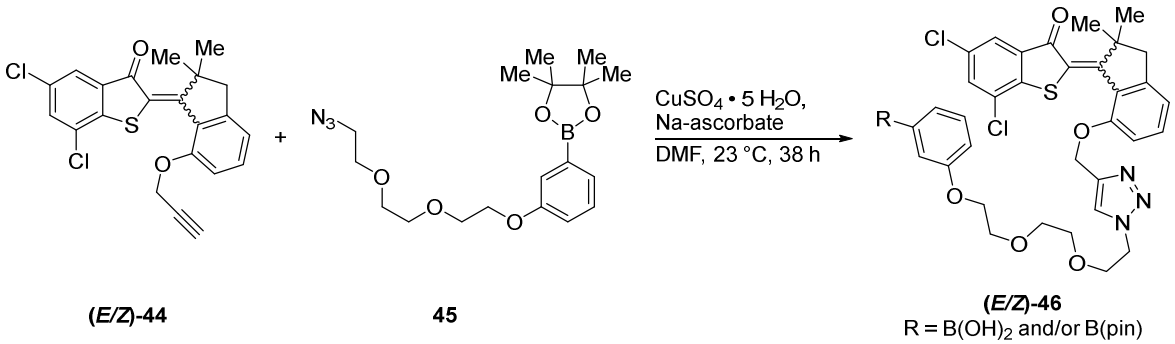

Scheme 17 Copper catalyzed azide alkyne click reaction of HTI **44** with azide **45** furnished **46** as a mixture of pinacol ester and hydrolyzed boronic acid.

The mixture of boronic acid and boronic acid pinacol ester was used in the following without further purification and characterization. With the boronic acid at hand, the intramolecular SUZUKI cross coupling was attempted. Table 5 gives an overview of the conditions tested for the macrocyclization reaction. In all cases monitoring by TLC showed a highly diverse mixture of reaction products. In the case of entries 4-6 in Table 5, the desired product mass could be found in mass spectrometry analysis. However, based on this analysis alone, it was not possible to identify the actual regioisomer obtained. Due to the challenging separation of reaction products, the synthetic route was deemed not practical and therefore not pursued any further.

Table 5 Conditions tested for the intramolecular SUZUKI cross coupling reaction of HTI **46**. Reactions were performed with 25 mg of starting material (approx. 32 µmol) at 0.01 M concentration. 0.1 equiv. of catalyst and 2.5-3.0 equiv. of base were used.

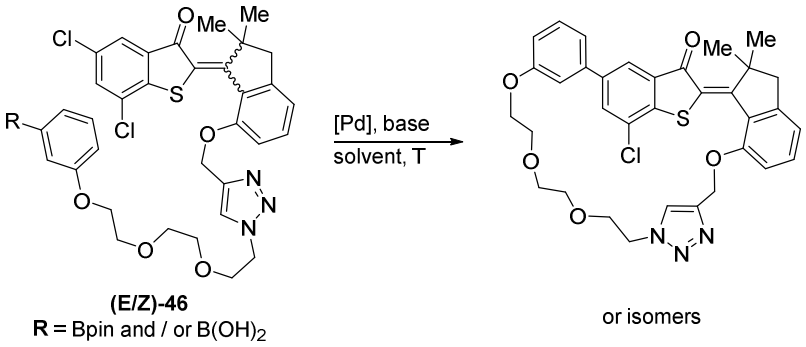

Entry	[Pd]	base	solvent	T	Product
1	XPhos Pd G2	K_3PO_4	1,4-dioxane:H_2O (4:1)	50 °C	-
2	$Pd(PPh_3)_4$	K_3PO_4	1,4-dioxane:H_2O (4:1)	50 °C	-
3	RuPhos Pd G3	K_3PO_4	PhMe:H_2O (9:1)	50 °C	-
4	RuPhos Pd G3	K_2CO_3	DMF (wet)	80 °C	MS found
5	XPhos Pd G2	K_3PO4	DMAc:H_2O (9:1)	65 °C	MS found
6	$[P(t\text{-Bu})_3PdI]_2$	K_3PO_4	DMAc:H_2O (9:1)	65 °C	MS found

3.3 Synthetic Approach 3

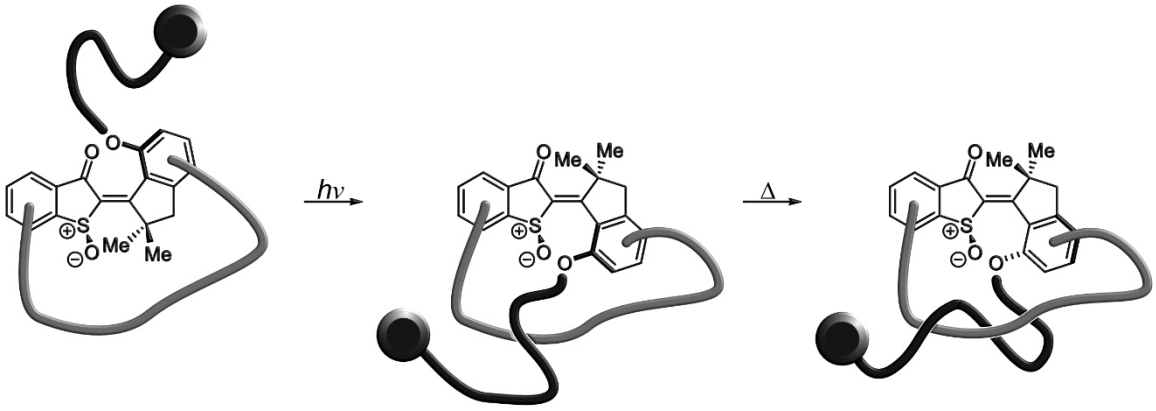

Figure 28 Schematic representation of a molecular machine based on HTI, which is able to produce threaded structures by harnessing the unidirectional motor rotation. The HTI molecular motor is embedded in a macrocyclic system and a flexible chain is attached to the indanone fragment. The attachment points are chosen in such a way, that the rotational movement of the motor is transformed into a translational movement of the chain through the ring.

In a third synthesis attempt, a new strategy was devised based around the attachment of a chain on the indanone fragment. The retrosynthesis is depicted in Scheme 18. Starting from simple mono-brominated benzothiophenone and indanone building blocks, a dibrominated HTI is obtained. This HTI is either substituted with a hydroxy group or an organic linker moiety, which allow for the attachment of a chain. Handles for the macrocyclization are introduced via SONOGASHIRA cross coupling (simultaneously on both bromine sites, so no selectivity issues are expected). Finally, the macrocycle is closed via twofold esterification and the HTI is oxidized to the sulfoxide.

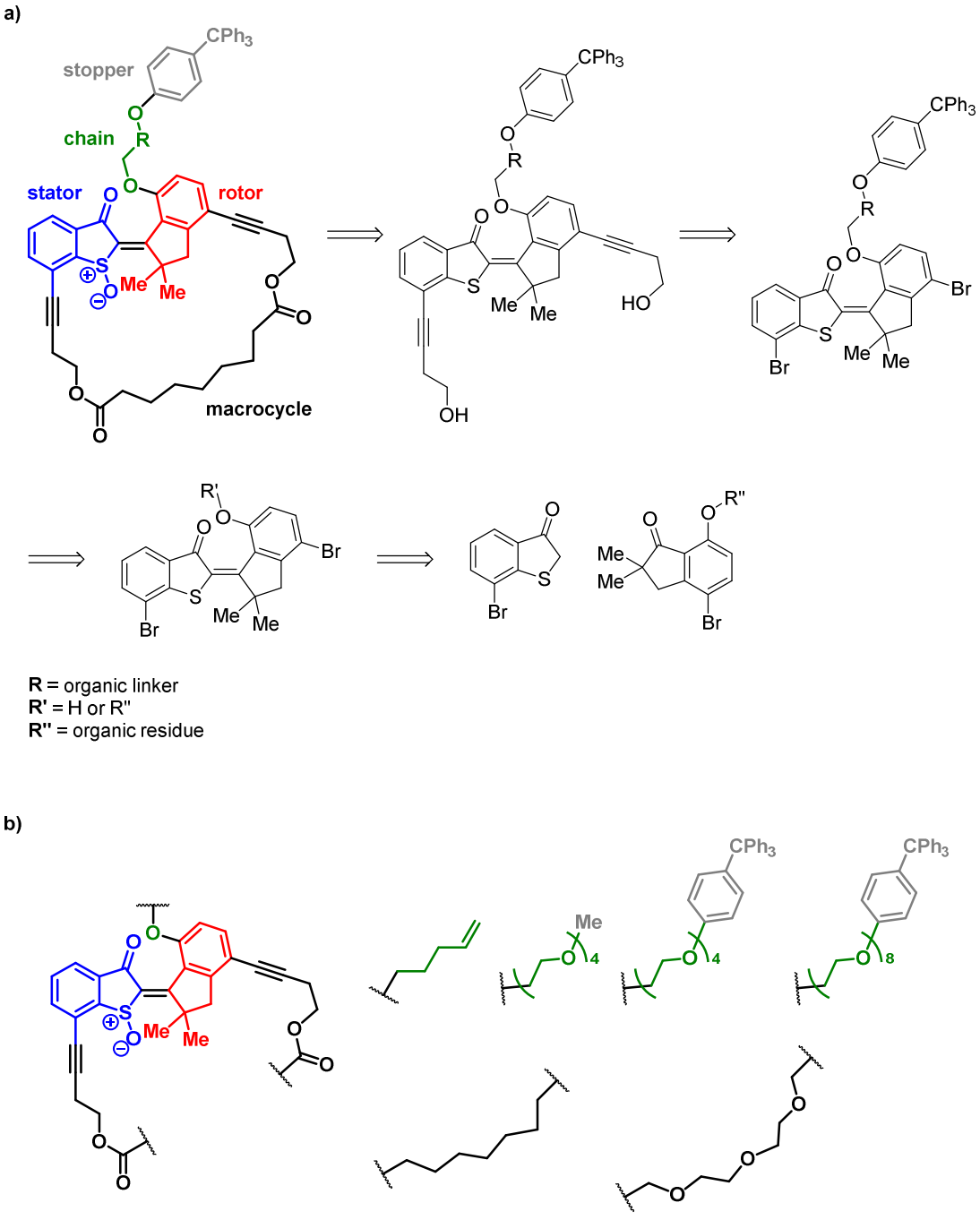

R = organic linker
R' = H or R''
R'' = organic residue

Scheme 18 **a)** Retrosynthetic analysis of a macrocyclic system incorporating an HTI based molecular motor unit as well as a chain terminated by a bulky stopper group. Starting from brominated benzothiophenone and indanone building blocks, the central HTI fragment is obtained. A linear chain is introduced on the indanone fragment, connected *via* ether linkage. Finally, two primary alcohol "handles" are installed and the macrocycle is closed by twofold esterification. Oxidation to the sulfoxide then gives the corresponding motor candidate. **b)** Schematic overview of the different chain, stopper and macrocycle fragments that were incorporated in various synthesis attempts.

The reasoning behind the chain setup was the following: First, a bulky stopper group was necessary to lock possible threaded structures in a rotaxane-like conformation. Tetraphenylmethanes are rather large and of near spherical shape making them good stopper candidates. 4-Tritylphenol is commercially available and can easily be functionalized by etherification. Second, the chain itself should be flexible, so an oligo ethylene glycol chain (tetraethylene glycol, TEG) was chosen. Finally, the chain needs to be connected to the motor unit. Olefin metathesis was envisioned as an attractive means of introducing a variety of chains and stoppers at a late stage in the synthesis. A terminal olefin was therefore needed on the stoppered chain unit, as well as on the indanone building block.

Indanone **48** bearing a pentenyl ether was synthesized as building block. It was accessible starting from commercially available 4-bromo-7-hydroxy-1-indanone (see Scheme 19). First, etherification with 5-bromo-1-pentene using potassium carbonate as base in DMF afforded indanone **47** in excellent yield. In the next step, indanone **48** was obtained in 63% yield by methylation with iodomethane and sodium hydride in THF.

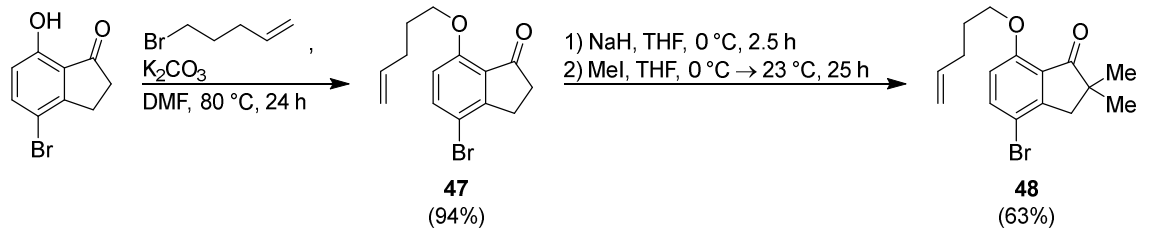

Scheme 19 Synthesis of indanone **48** starting from 4-bromo-7-methoxy-indan-1-one. *O*-alkylation followed by methylation afforded **48**.

Brominated benzothiophenone **50** was prepared starting from 2-bromo thiophenol following an established synthesis route.[73] Nucleophilic substitution on bromoacetic acid gave the corresponding phenyl thioacetic acid **49** in good yield. **49** was then converted to the acid chloride using thionyl chloride under reflux. Subsequent intramolecular FRIEDEL-CRAFTS acylation catalyzed by $AlCl_3$ gave benzothiophenone **50** in near quantitative yield (see Scheme 20).

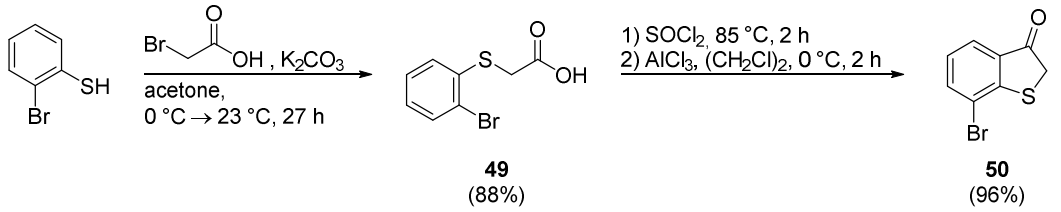

49
(88%)

50
(96%)

Scheme 20 Synthesis of brominated benzothiophenone **50** starting from 2-bromo thiophenol. Nucleophilic substitution on bromoacetic acid followed by an intramolecular FRIEDEL-CRAFTS acylation gave **50**.

Condensation of benzothiophenone **50** and indanone **48** with BCl_3 as LEWIS acid gave HTI **51** in 35% yield (Scheme 21).

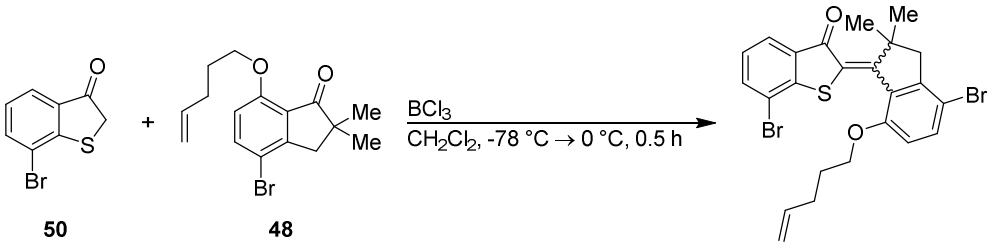

50 **48**

(*E*/*Z*)-51
(35%)

Scheme 21 Synthesis of HTI **51** by BCl_3 mediated condensation of benzothiophenone **50** with indanone **48**.

In the next step, 3-butyn-1-ol was introduced on both the indanone and thioindigo fragments *via* a twofold SONOGASHIRA cross coupling reaction. XPhos Pd G2 with copper iodide in 1,4-dioxane:DIPA (1:1) was found to be a suitable catalytic system for the rather electron rich substrate **51**. Satisfyingly, diol **52** was obtained in good yield (73%). The macrocycle was formed in a twofold esterification with azelaic acid dichloride using 4-DMAP as activating agent. The reaction proceeded under mild conditions and high dilution, giving macrocycle **53** in 54% yield. In the final step, **53** was oxidized using sodium perborate in acetic acid, giving sulfoxide motor candidate **54** in 70% yield. The synthetic steps and conditions starting from **51** are shown in Scheme 22.

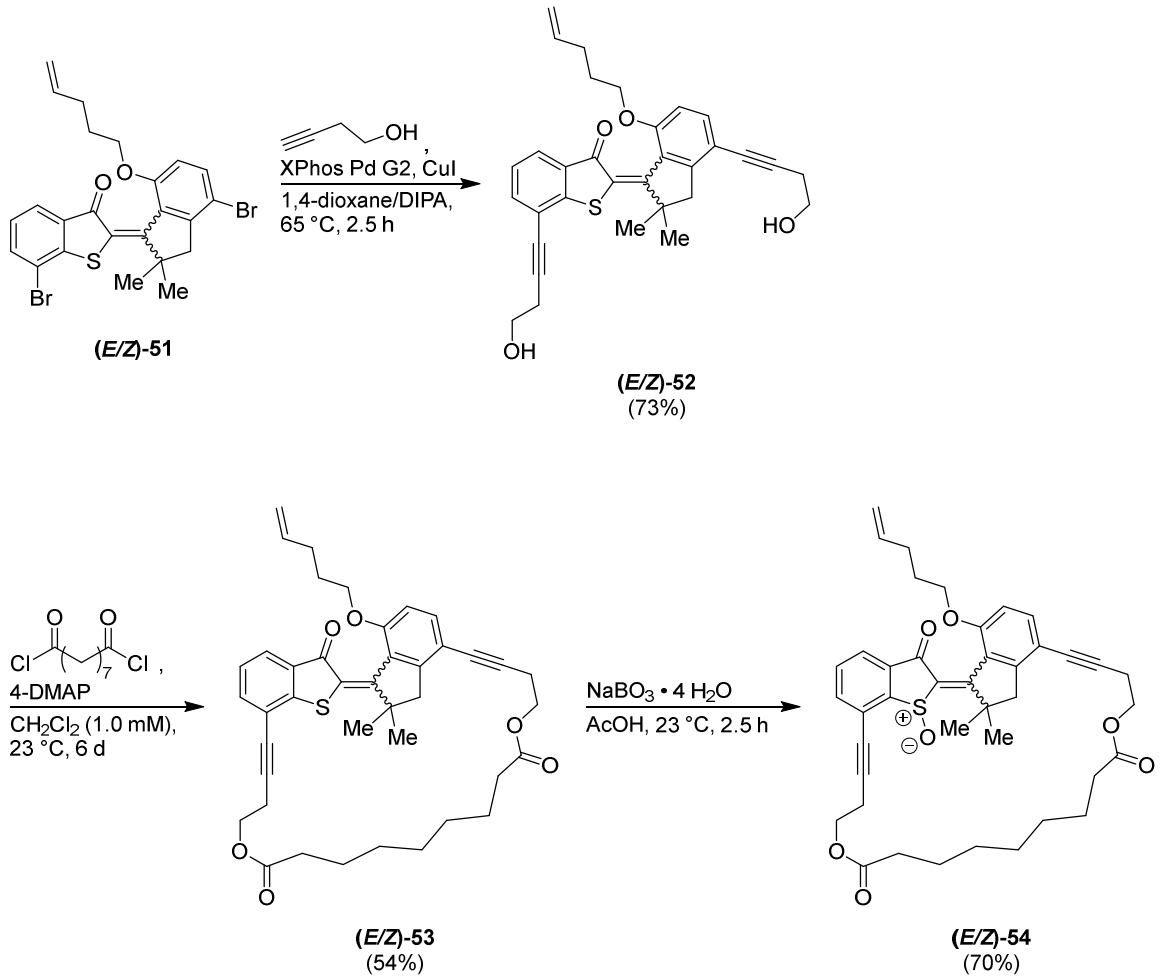

Scheme 22 Synthesis of macrocyclic motor candidate **54** starting from HTI **51**. In the first step, two hydroxy handles were installed via SONOGASHIRA cross coupling with 3-butyn-1-ol. Next, the macrocycle was formed by esterification with azelaic acid dichloride under high dilution conditions. In the final step, oxidation with sodium perborate yielded motor candidate **54**.

Stoppered chain **55** was accessible by etherification of tritylphenol with tetraethylene glycol monotosylate.[133] The olefinic residue was successfully installed by alkylation with 5-bromo-1-pentene with sodium hydride in THF in 51% yield (see Scheme 23).

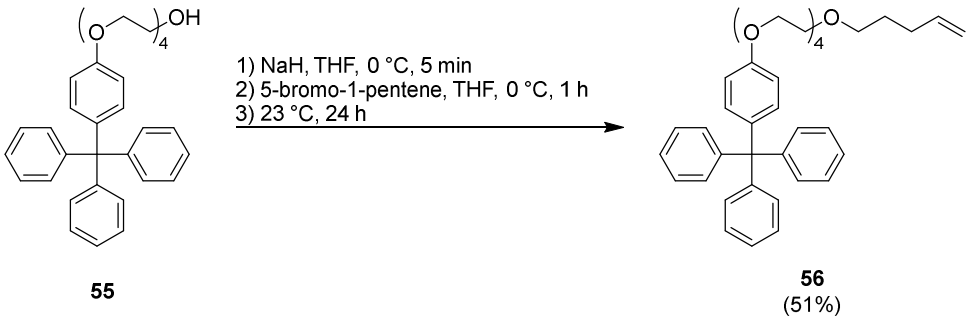

55 **56** (51%)

Scheme 23 Synthesis of stoppered ethylene glycol chain **56** by alkylation of **55** with 5-bromo-1-pentene.

In order to test the feasibility of the metathesis approach, a number of model reactions were performed. First, HTI **51** successfully underwent olefin cross metathesis with 5-bromo-1-pentene using the second generation HOVEYDA-GRUBBS catalyst in chlorobenzene (see Scheme 24). The hetero-coupling product **57** was obtained in 32% yield.

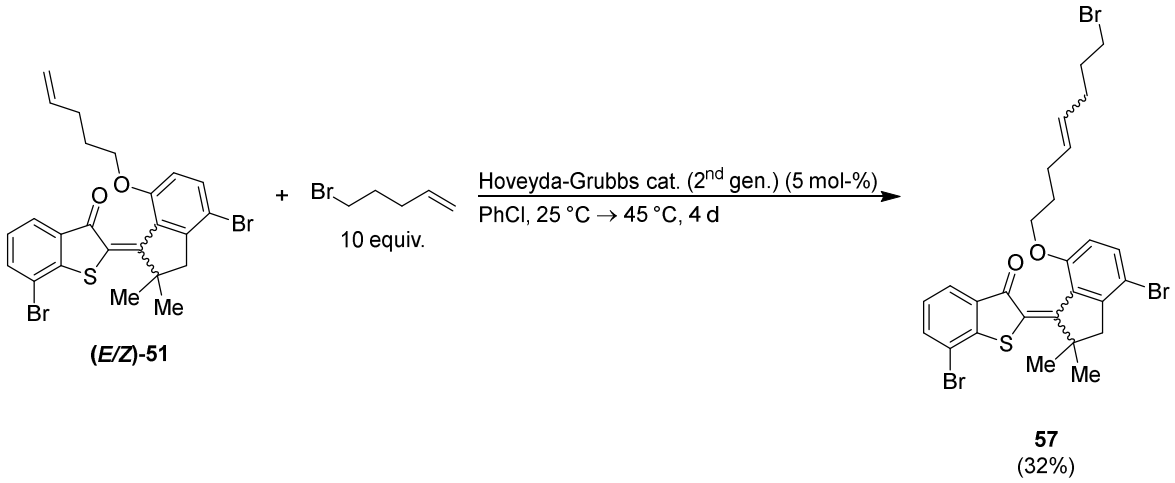

(*E*/*Z*)-51 **57** (32%)

Scheme 24 Successful cross metathesis on HTI **51**. In order to increase the yield of hetero-coupling product **57**, the readily available bromopentene was used in excess.

Having confirmed the ability of HTI **51** to undergo cross metathesis, the olefin metathesis of **51** with stoppered chain **56** was attempted next using the previously established conditions (see Scheme 25). As the mass of the desired product could be identified by HRMS, the next step was olefin metathesis attempts on motor candidate **54**.

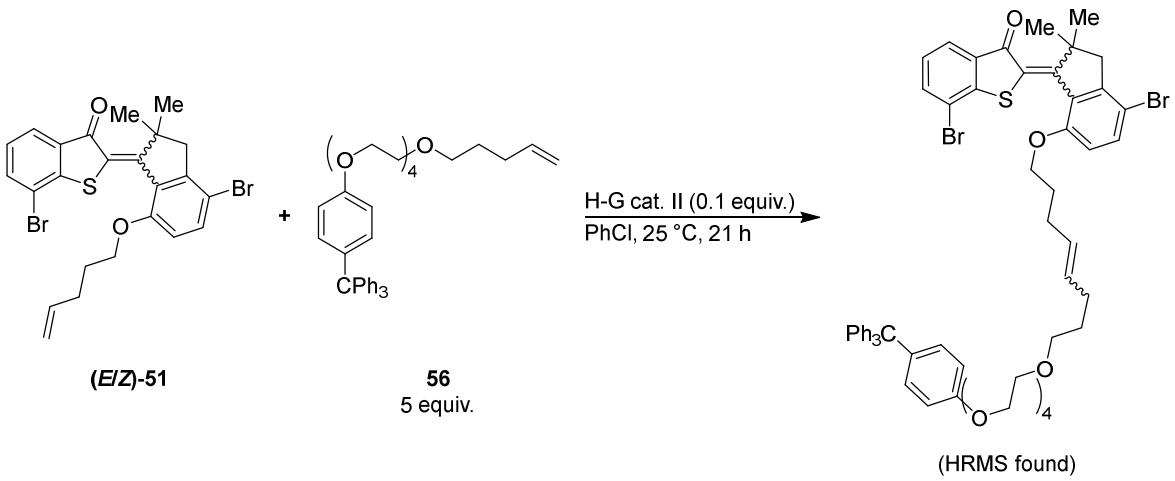

Scheme 25 Cross metathesis test reaction with **51** and **56** on microscale. The product mass was identified by HRMS.

When HTI **54** was treated with 5-bromo-1-pentene in chlorobenzene in the presence of the second generation HOVEYDA-GRUBBS catalyst, no desired product could be isolated. Instead the mass corresponding to the enyne metathesis[134] product depicted in Scheme 26 could be identified by HRMS. As the alkyne bonds are an integral part of the macrocyclic structure, another way of linking chain and motor fragment had to be found.

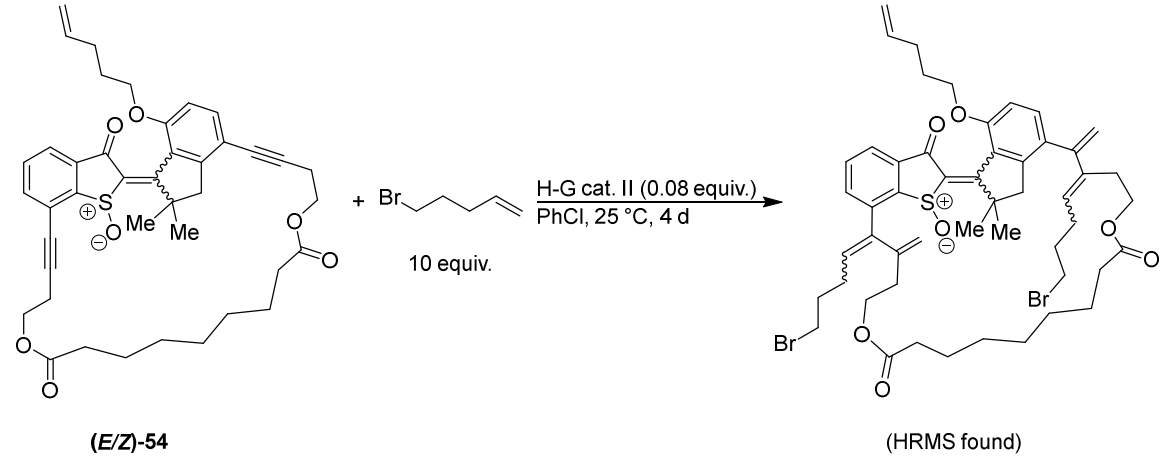

Scheme 26 Attempted cross metathesis of motor **54** and 5-bromo-1-pentene did not afford the desired alkyl chain extension. Instead, the mass of the depicted enyne-metathesis product was identified by HRMS.

BCl_3 mediated aldol condensation of benzothiophenone **50** and indanone **33** afforded HTI **58** in 64% yield. In a one-pot approach, condensation of benzothiophenone **50** and indanone **33**, followed by *in situ* demethylation with BBr_3 gave HTI **59** in 82% yield. (see Scheme 27).

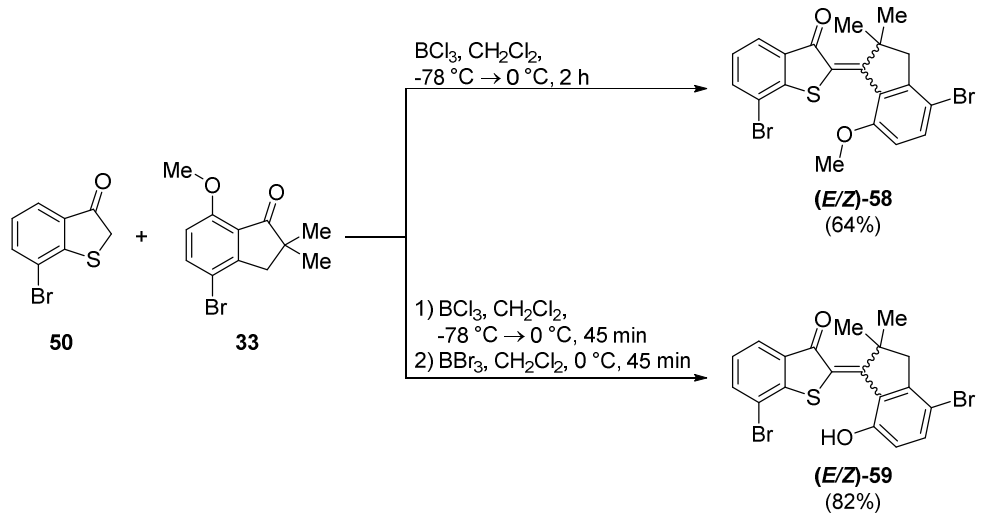

Scheme 27 Synthesis of HTIs **58** and **59** by BCl_3 mediated condensation of benzothiophenone **50** and indanone **33** and – in the case of **59** – subsequent demethylation with BBr_3.

The stoppered chain fragment **55** was transformed into the corresponding tosylate **60**, as shown in Scheme 28.

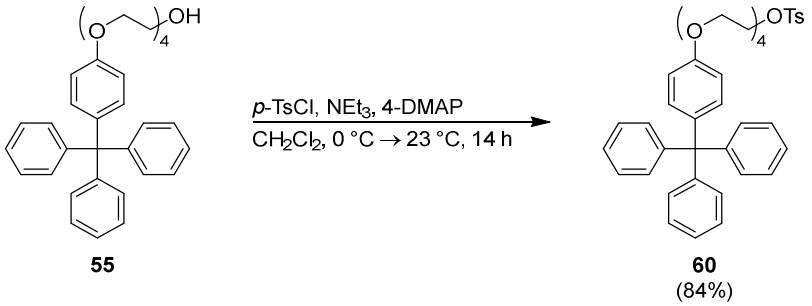

Scheme 28 Synthesis of tosylated ethylene glycol chain **60** bearing a tetraphenylmethane stopper group.

In the next synthetic step, the stoppered chain fragment was introduced by alkylation of the phenol moiety with tosylate **60** and potassium carbonate in DMF, giving HTI **61** in 36% yield. The separation of unreacted chain fragment was challenging and could not be fully achieved by column chromatography on silica at this stage. However, continuing without further purification did not hamper the following synthetic step.

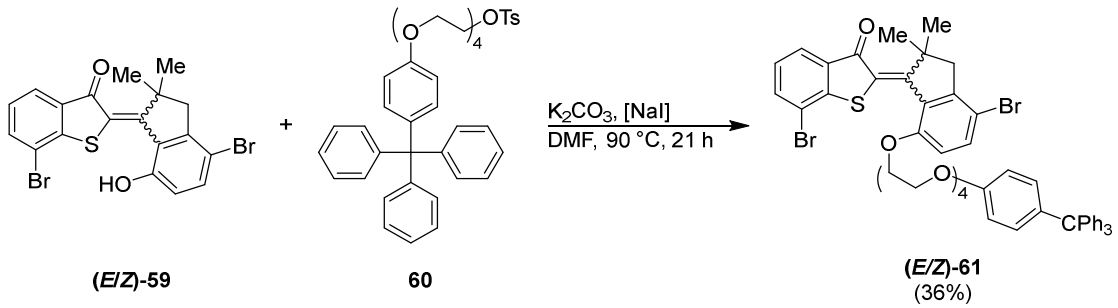

(*E*/*Z*)-59 **60** **(*E*/*Z*)-61** (36%)

Scheme 29 Alkylation of HTI **59** with tosylated compound **60** gave HTI **61** in low to moderate yield.

In the following, the analogous synthetic steps as for HTI **54** were performed on **61**. SONOGASHIRA cross coupling with 3-butyn-1-ol proceeded with good yield (75%) and gave diol **62**, which could be easily separated from residual linker **60** by column chromatography. **62** was then subjected to macrocyclization with azelaic dichloride, resulting in macrocycle **63** in 40% yield. Finally, oxidation of **63** with sodium perborate in acetic acid gave motor candidate **2** in 63% yield. In compound **2**, all the fragments (macrocyclic motor, chain, stopper) are assembled in the desired fashion. The synthetic steps and conditions starting from compound **61** are shown in Scheme 30.

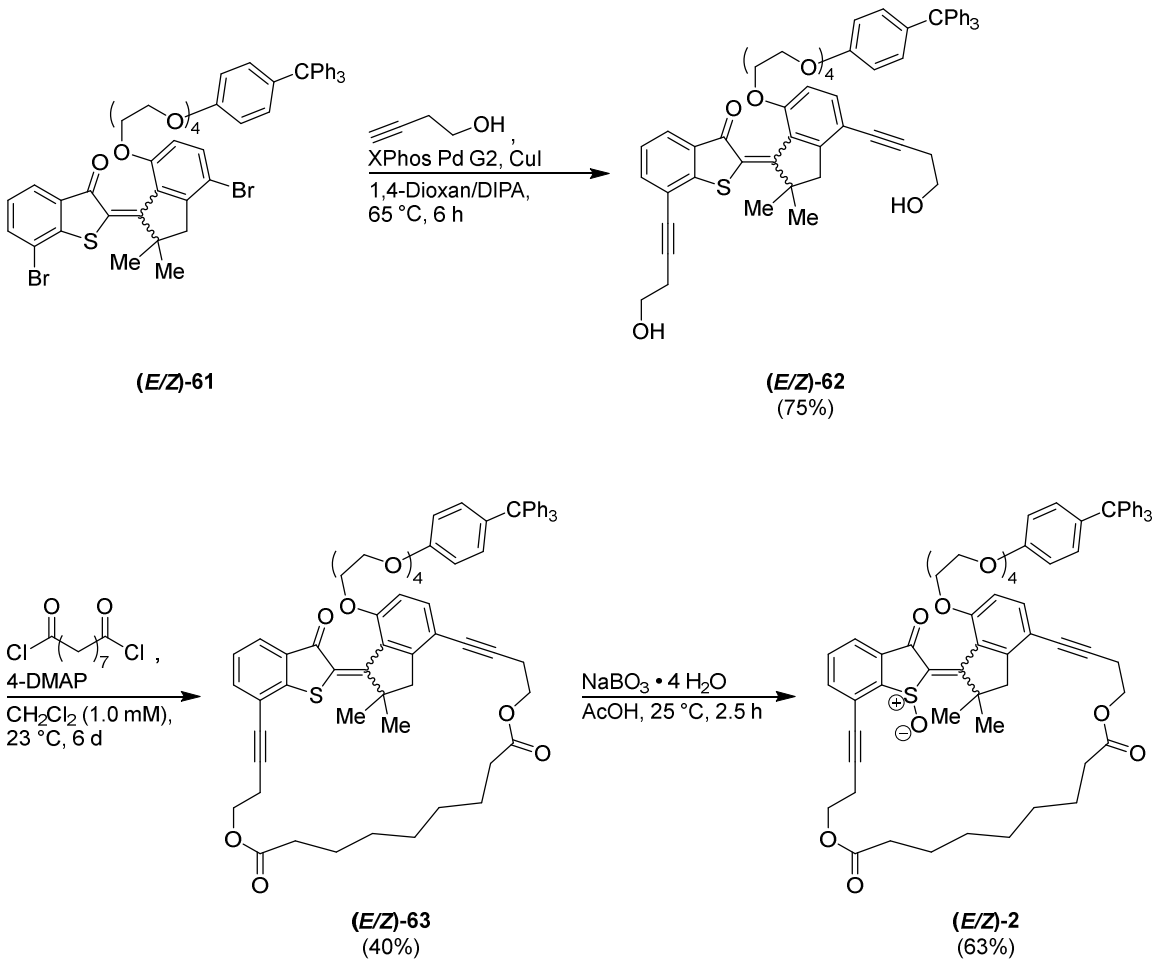

Scheme 30 Synthesis of motor candidate **2** starting from **61**. In the first step, two hydroxy handles were installed via SONOGASHIRA cross coupling with 3-butyn-1-ol. Next, the macrocycle was formed by esterification with azelaic acid dichloride under high dilution conditions. In the final step, oxidation with sodium perborate yielded motor candidate **2**.

In another variation of the setup, an analogue without bulky stopper group was prepared. The tetraethylene glycol chain was terminated by a methoxy group, which was envisioned to allow continuous threading of the chain through the ring upon motor rotation. Phenol **59** was alkylated with tosylate **65**, giving HTI **66** in low to moderate yield (see Scheme 31). Again, purification was challenging, as **65** could not easily be separated from the desired product.

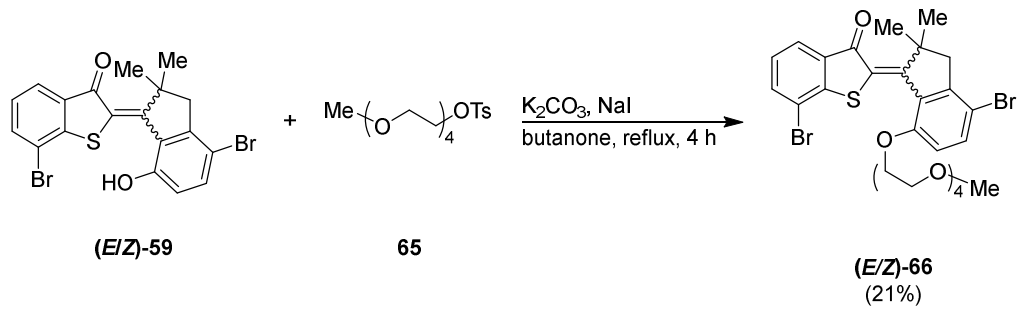

Scheme 31 Alkylation of HTI **59** with tosylate **65** afforded HTI **61** in 21% yield.

Once more, the following synthetic steps proceeded in an analogous fashion to the previous examples (see Scheme 32). SONOGASHIRA cross coupling of **66** with 3-buty-1-ol gave diol **67** in good yield (82%). After macrocyclization with azelaic acid dichloride, **68** was obtained in 36% yield. Finally, oxidation with sodium perborate in acetic acid afforded macrocyclic motor candidate **1** in excellent yield (91%).

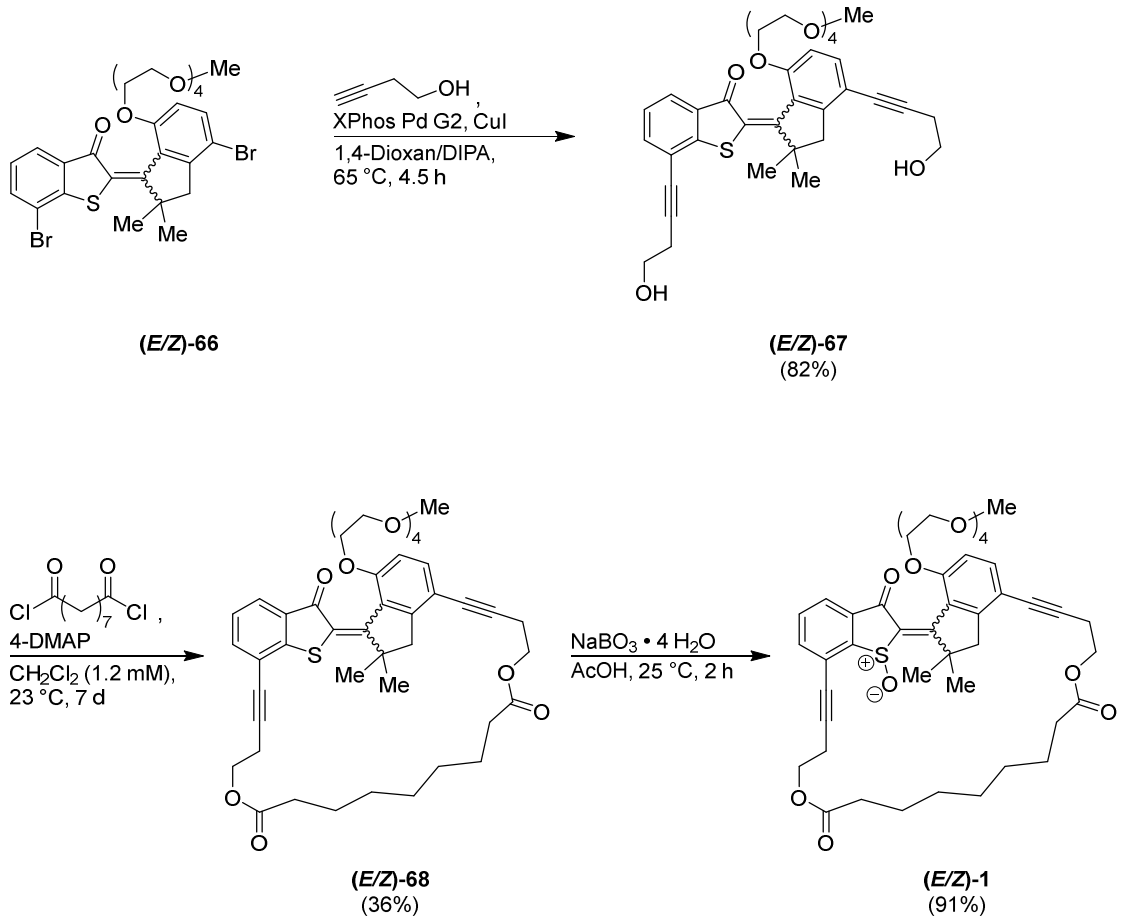

Scheme 32 Synthesis of macrocyclic motor **1** starting from HTI **66**. SONOGASHIRA cross coupling with 3-butyn-1-ol gave diol **67**, which then underwent macrocyclization with azelaic acid dichloride to **68** under high dilution conditions. In the final step, **68** was oxidized with sodium perborate in acetic acid to give motor **1**.

3.3.1 Further Modifications

As the synthesis approach is modular, the individual fragments can be varied rather easily and a number of additional variation approaches is reported in this chapter.

In the following example, the macrocycle was formed with a different chain based on an oligo ethylene glycol (see Scheme 33). Macrocyclization to form **69** proceeded with moderate yield compared to previous attempts. Finally, oxidation of **69** with sodium perborate in acetic acid gave trace amounts of motor candidate **70**.

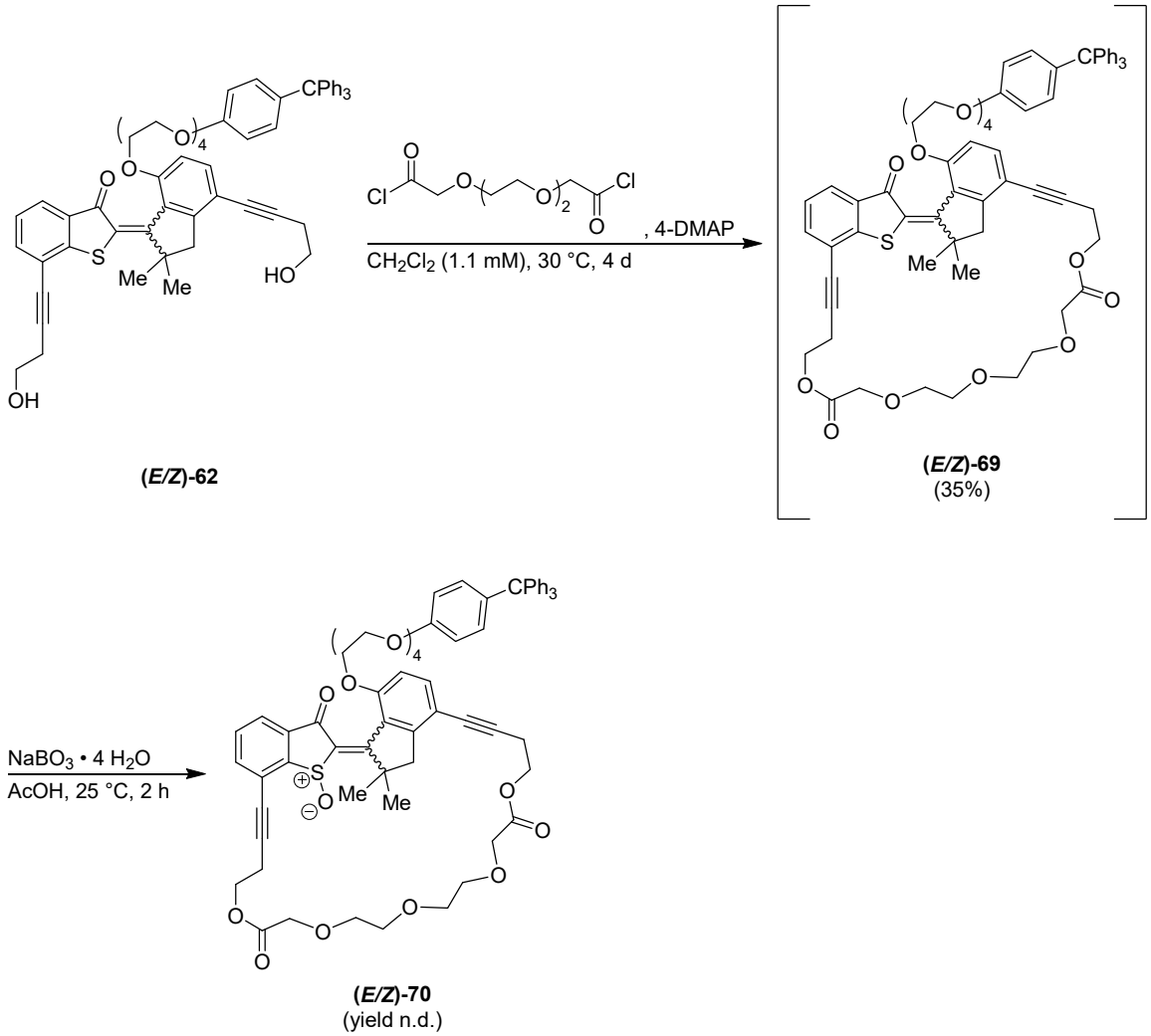

Scheme 33 Synthesis of macrocyclic HTI derivative **70** incorporating an ethylene glycol chain in the macrocycle. Diol **62** underwent macrocyclization with 3,6,9-trioxaundecanedioic acid dichloride under high dilution conditions to give compound **69** in low yield. Oxidation of **69** with sodium perborate in acetic acid gave **70** in trace amounts.

A longer chain analogue of **61** was prepared by the alkylation of HTI **59** with stoppered PEG_8-tosylate **71**. HTI **72** was obtained in 55% yield (see Scheme 34).

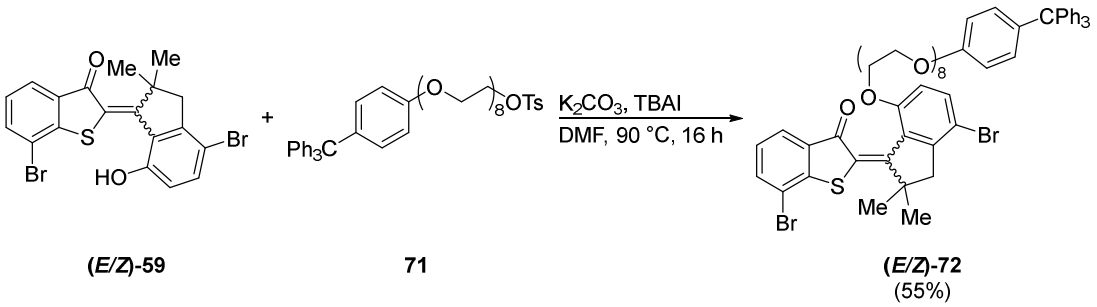

(*E*/*Z*)-59 **71** **(*E*/*Z*)-72** (55%)

Scheme 34 Synthesis of HTI **72** substituted with a longer PEG_8-chain by alkylation of HTI **59** with tosylate **71**.

Subsequent SONOGASHIRA cross coupling of **72** with 3-butyn-1-ol using the established conditions gave diol **73** in 56% yield. Macrocyclization of **73** with 3,6,9-trioxaundecanedioic acid dichloride to give **74** proceeded with a very low yield of 7%. The oxidation product **75** could only be obtained in traces upon treatment of **74** with sodium perborate in acetic acid (see Scheme 35). Molecular structures of **74** and **75** were tentatively assigned based on HRMS, ^{1}H NMR and UV/Vis and were not fully characterized.

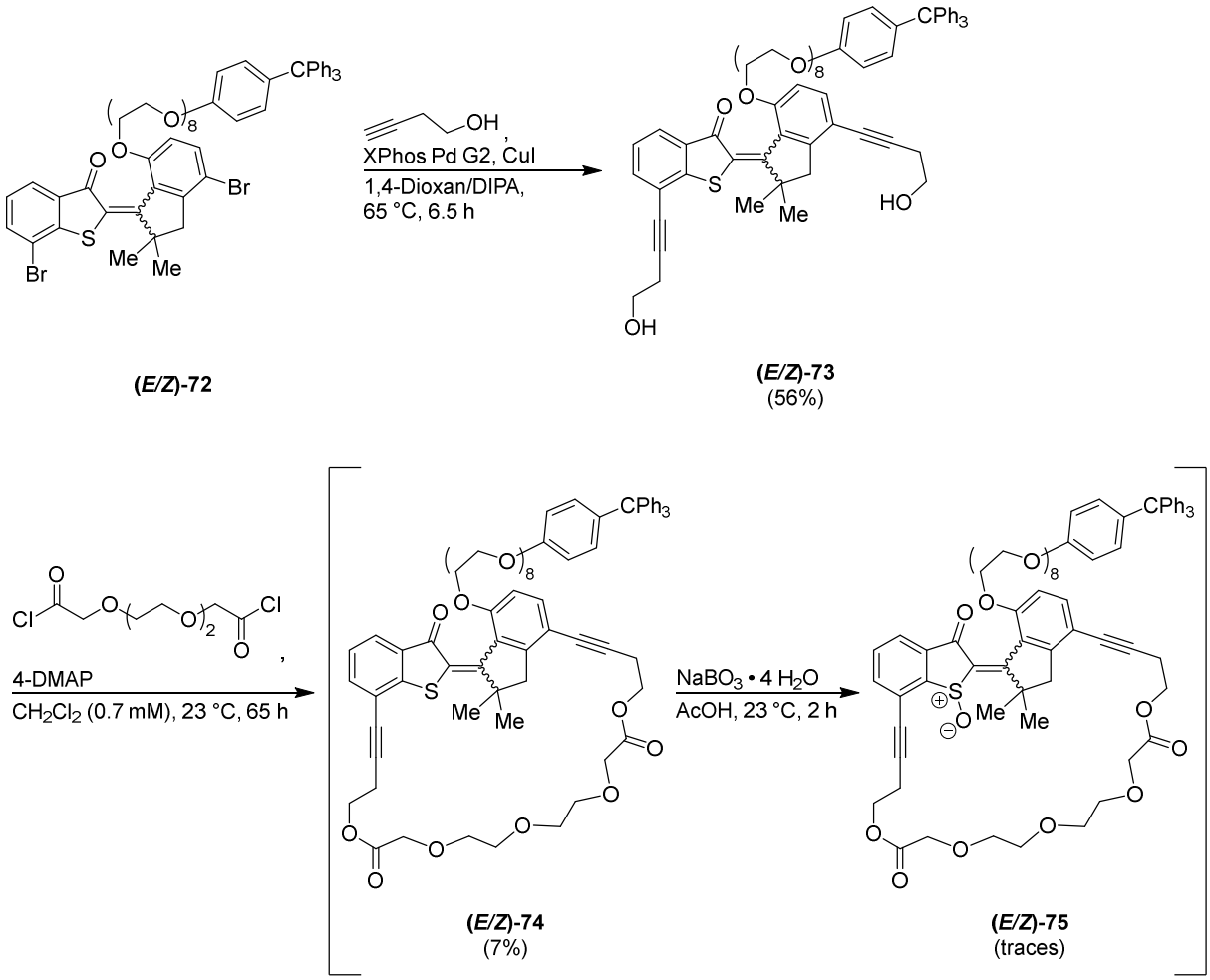

Scheme 35 Synthesis towards a potentially more flexible macrocyclic HTI motor derivative **75**.

An even longer PEG_{20}-chain was to be integrated into the motor setup. A commercial building block, N_3-PEG_{20}-OH was identified as suitable starting material for this task. First, the tritylphenol stopper group was modified with an alkyne handle by the introduction of a propargyl unit. Alkylation of tritylphenol with propargyl bromide and potassium carbonate in acetone gave **76** in 64% yield. The copper catalyzed azide-alkyne click reaction of **76** and N_3-PEG_{20}-OH proceeded smoothly to **77** with 86% yield. Subsequent tosylation of **77** gave **78** in very good yield (93%). The full synthetic sequence is shown in Scheme 36.

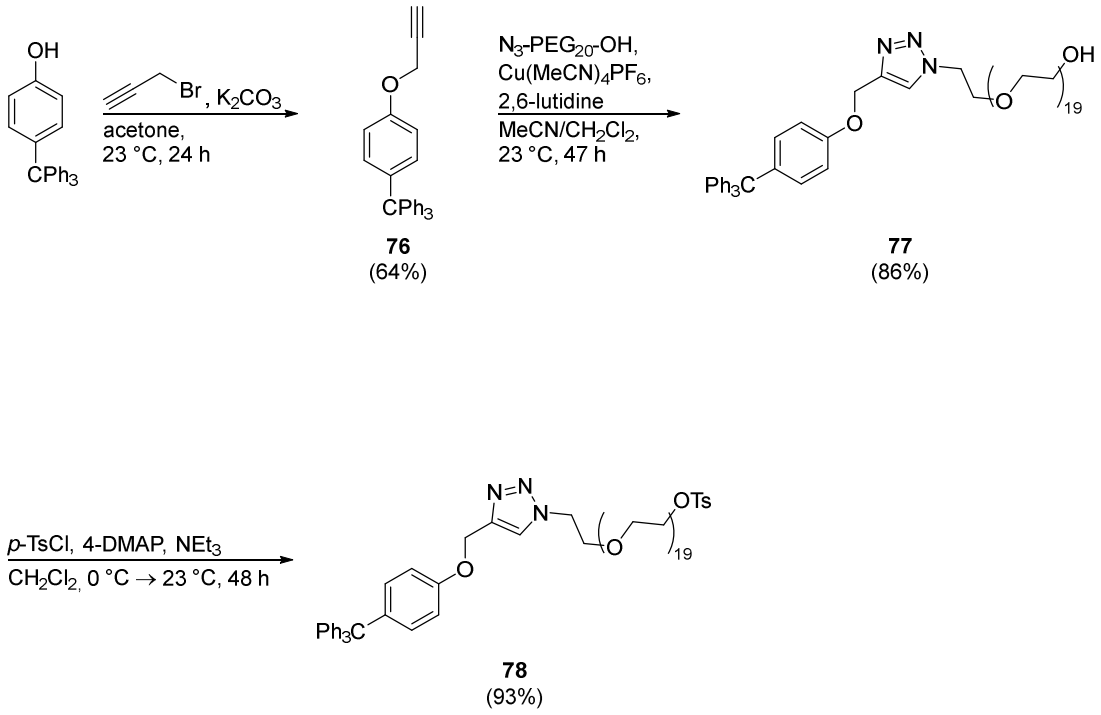

Scheme 36 Synthesis of significantly longer stoppered chain building block **78**. Commercially available monodisperse N_3-PEG_{20}-OH underwent a copper catalyzed azide alkyne click reaction with **76** to give **77**. Subsequent tosylation afforded **78** in very good yield.

In the next step, alkylation of HTI **59** with tosylate **77** was attempted. However, the separation of the PEG-chain building block from the desired product **79** was not possible with standard normal phase chromatographic techniques, as well as RP-LC and GPC.

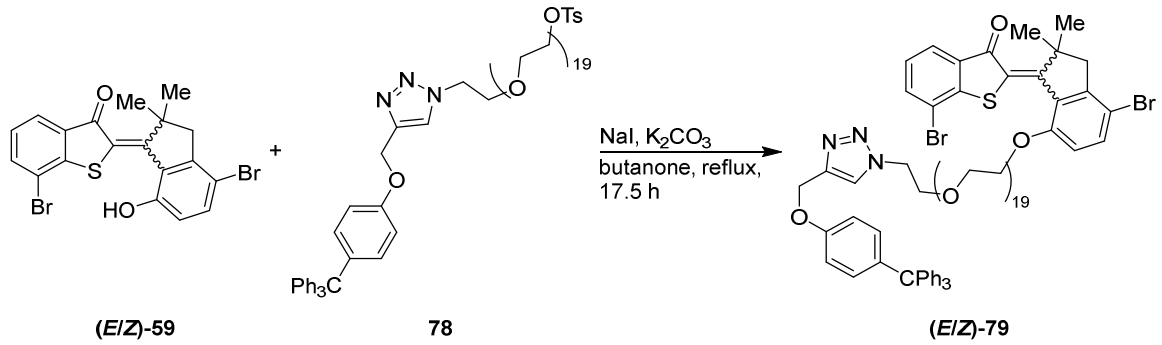

Scheme 37 Synthesis of PEGylated HTI **79**. The successful synthesis of **79** was indicated by HRMS and ^{1}H NMR. However, **78** could not be separated from the product by conventional chromatographic methods.

As, judging from TLC, HRMS and ^{1}H NMR, **79** could successfully be prepared, the next synthetic step was attempted without isolation of **79**. For previous derivatives, the change in polarity upon introduction of two butynol moieties greatly facilitated the purification process. Therefore, HTI **79** was reacted with 3-butyn-1-ol in a SONOGASHIRA cross coupling

reaction (see Scheme 38). Diol **80** could possibly be obtained, as judged by HRMS, but isolation and conclusive identification of the compound was not achieved as the substitution had no significant impact on the purification process.

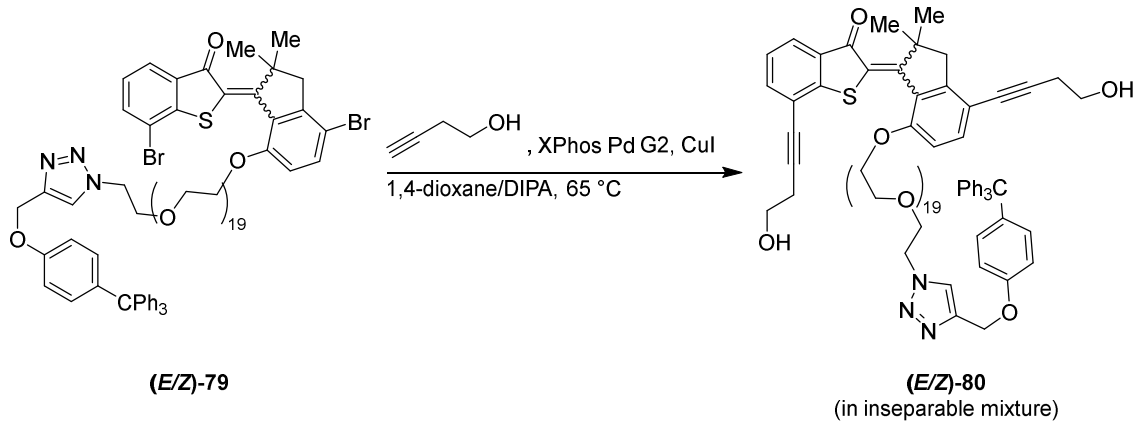

Scheme 38 SONOGASHIRA cross coupling of **79** (mixture with **78**) with 3-butyn-1-ol. Again, the product was obtained in an inseparable mixture with other PEG_{20}-compounds.

As macrocycle functionalities or linkages other than ester bonds may be desirable, an approach based on the copper catalyzed azide-alkyne click reaction (pioneered by *Meldal*[135] and *Sharpless*[136]) was investigated. Terminal alkynes were introduced as "handles" on both the thioindigo and indanone fragments and then connected *via* twofold click reaction with a PEG-diazide. Starting from HTI **58**, two TIPS-acetylene moieties were introduced via SONOGASHIRA cross coupling reaction, giving **81** in 76% yield. Subsequent desilylation with TBAF in THF gave **82** in quant. yield.

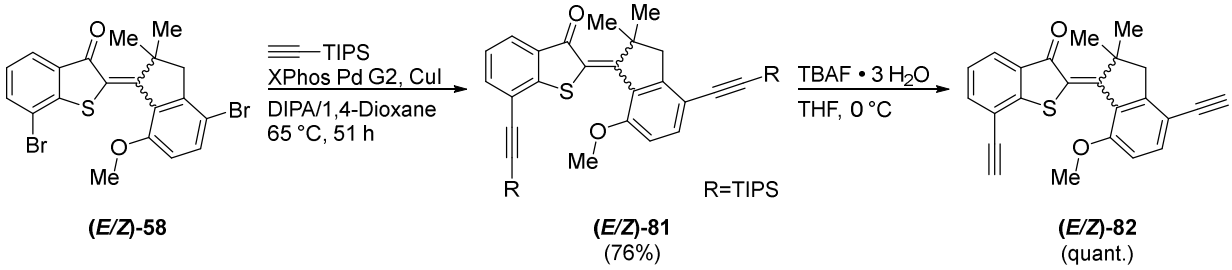

Scheme 39 Synthesis of bis-alkyne **82** starting from **58** *via* SONOGASHIRA cross coupling with TIPS-acetylene and subsequent deprotection with TBAF.

In an initial attempt at the macrocyclization with diazide **83**, the mono-click product depicted in Scheme 40 was obtained and identified by *Sven Waldmannstetter*.

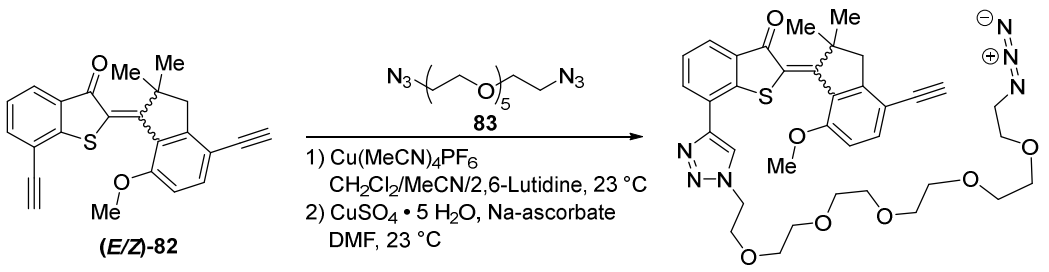

Scheme 40 Initial attempt at the synthesis of macrocycle **84**, which furnished the depicted mono-click product instead.

This observation might be explained in the following way: Upon triazole formation on the thioindigo fragment, a chelating ligand for copper ions is formed, with sulfur, oxygen and nitrogen atoms participating in the complexation of copper ions. As copper ions are used in catalytic amounts, the availability of copper ions is drastically reduced and the reaction does not proceed any further.

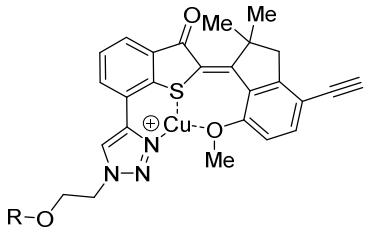

Scheme 41 Proposed mode of copper ion complexation by the mono-click intermediate. As a result, no more free copper ions are available for the catalytic process.

In order to circumvent this problem, in another attempt the ligand TBTA, which is known to increase activity and availability of copper ions in click reactions,[137] was added to the reaction mixture. Macrocycle **84** could successfully be isolated after purification by SFC in 3% yield (see Scheme 42). Further experiments are necessary to increase the yield, with an obvious starting point being the stoichiometric use of copper ions and ligands such as TBTA. However, these early results demonstrate the feasibility of using "double" click reactions for the formation of HTI-incorporating macrocycles.

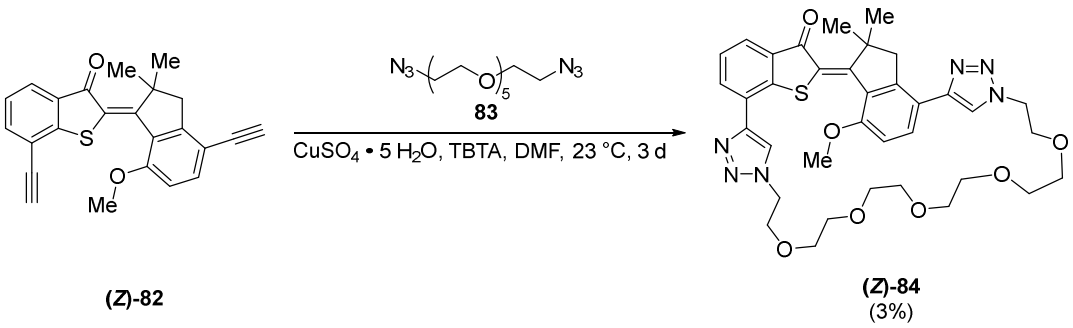

Scheme 42 Successful synthesis of macrocycle **84** using modified conditions. TBTA was added in order to increase copper reactivity and availability.

Building on the macrocycle synthesis *via* click reactions discussed above, the synthesis route could potentially be modified in order to incorporate an amine "handle" into the system. In initial attempts, Boc-protected ethylamine was introduced by alkylation of HTI **59** with Boc-protected 2-bromoethylamine in a microwave reaction. As judged by HRMS and ^{1}H NMR, alkylation product **85** could be obtained in 38% yield and was used directly in the next synthetic step without full characterization. After subsequent SONOGASHIRA cross coupling reaction with TIPS-acetylene, successful transformation to **86** was indicated by HRMS, but **86** could not be isolated from a mixture with inseparable side products. The optimization of reaction conditions as well as desilylation, followed by the copper catalyzed click reaction and finally deprotection of the amine remain as future work (see Scheme 43).

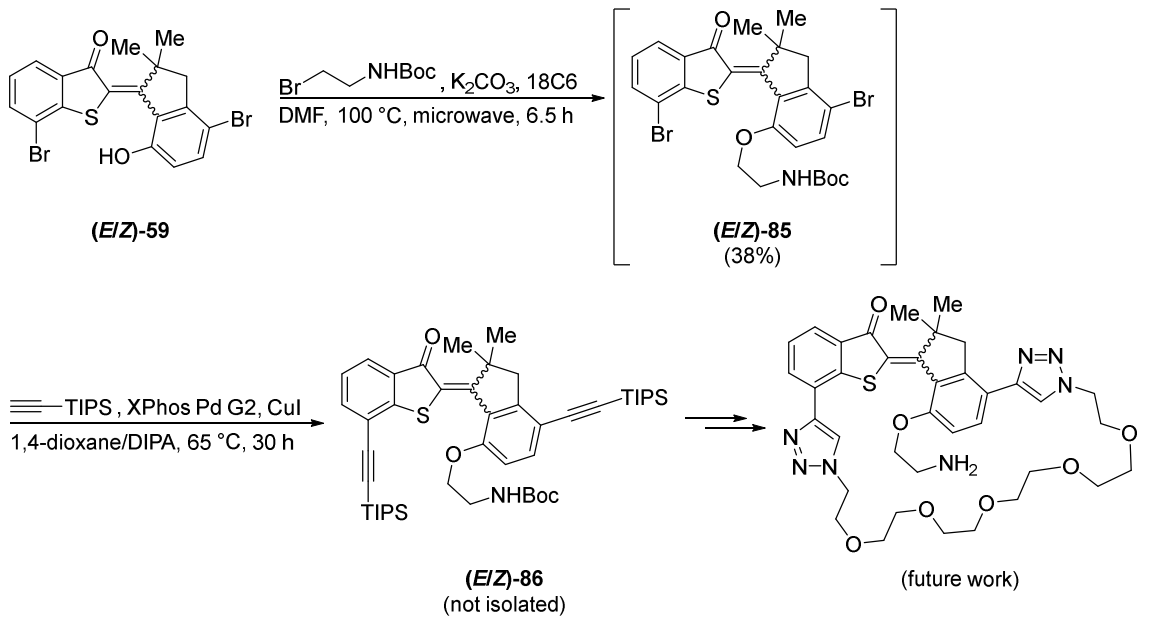

Scheme 43 Synthesis towards a macrocyclic HTI incorporating an amine handle. Microwave assisted alkylation of **59** with Boc-protected 2-bromoethylamine gave **85** in 38% yield, which was used in the next step without full characterization. Subsequent SONOGASHIRA cross coupling afforded an inseparable mixture. **86** was identified based on HRMS. Future work includes desilylation of the alkyne handles, followed by copper catalyzed azide alkyne click macrocyclization and finally deprotection of the amine functional group.

3.4 Analysis of Macrocyclic Motor Systems

The following chapters are in part based on work that has been published[8] under Creative Commons License "Attribution 4.0 International" (CC BY 4.0)[138] as
"Active Mechanical Threading by a Molecular Motor", N. N. Bach, V. Josef, H. Maid, H. Dube, *Angew. Chem. Int. Ed.* **2022**, *61*, e202201882; *Angew. Chem.* **2022**, *134*, e202201882.

In the following, **ABCD** identifiers will be used for isomers of **1** and **2** in accordance with the sequence introduced in the Introduction: **A** for (*Z,S,P/Z,R,M*), **B** for (*E,S,M/E,R,P*), **C** for (*E,S,P/E,R,M*) and **D** for (*Z,S,M/Z,R,P*) isomers.

3.4.1 Conformational Analysis of Macrocycle 1

A low-quality crystal structure of racemic **C-1** could be obtained, confirming (*E*,*S*,*P*/*E*,*R*,*M*)-configuration of this isomer. The structure is depicted in Figure 29.

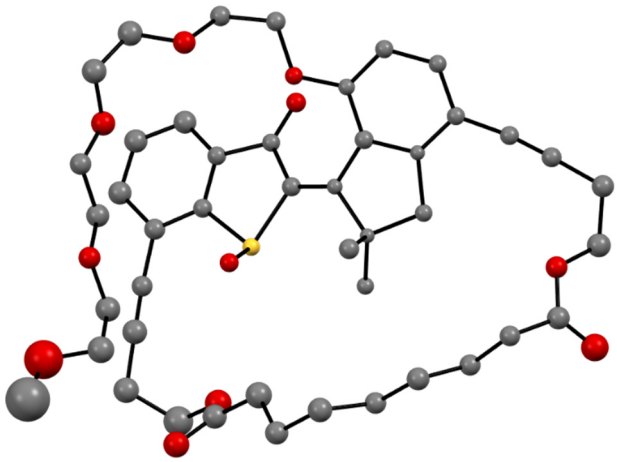

Figure 29 Structure of racemic **C-1** in the crystalline state. Only the (*S*)-configured enantiomer is shown and hydrogen atoms are omitted for clarity. *Note:* X-ray crystal structure analysis was performed by *Dr. Peter Mayer*.

3.4.1.1 Conformational Analysis of 1 in Solution

Conformational analysis of stable isomers **A-1** and **C-1** as well as metastable isomer **D-1** was performed by solution NMR spectroscopy. The ^{1}H and ^{13}C NMR spectra, as well as the assignment of signals to the respective molecular structure are reproduced in the following section.

For **C-1**, the NOESY spectrum (see Figure 33) shows cross peaks between proton 1 on the thioindigo fragment with protons 20, 21 and 22 on the tetraethylene glycol chain, thus confirming (*E*)-configuration of the central double bond. Additional evidence for (*E*)-configuration comes from the cross peaks between methyl group 14' on the indanone part with methylene group 33 in the aliphatic ring, as well as the cross peaks between protons 12 and 12' on the indanone fragment with methylene group 39 in the aliphatic ring (see Figure 34). Further information on the molecular configuration can be obtained from the HMBC spectrum by applying the *Karplus* relation to the $^{3}J_{H,C}$ coupling between protons 12/12' and carbon atoms 14/14'. If the dihedral angle between the coupling partners is close to 90°, the coupling constant is close to zero and no correlation is observed in the HMBC spectrum. Indeed, there is one of the four potential correlations that is not observed (marked by a green arrow in Figure 35). Analysis of the theoretically obtained minimum geometry shows, that the dihedral angle between proton 12 and carbon atom 14' is −86.5° and the signals were assigned accordingly.

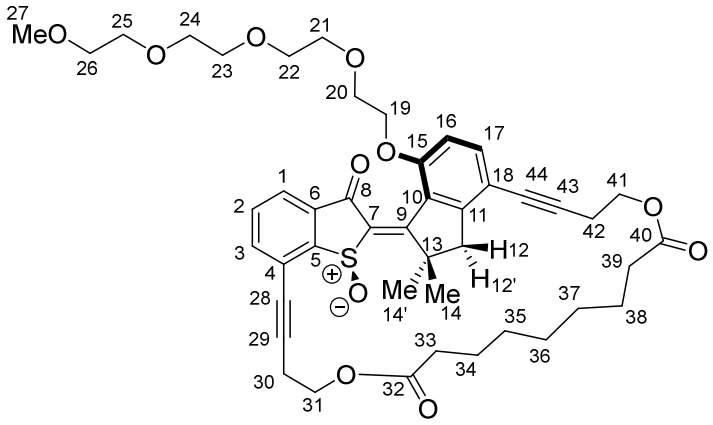

Figure 30 Chemical structure of **C-1** and the numbering used in the following. Only the (*S*)-configured isomer is shown for clarity.

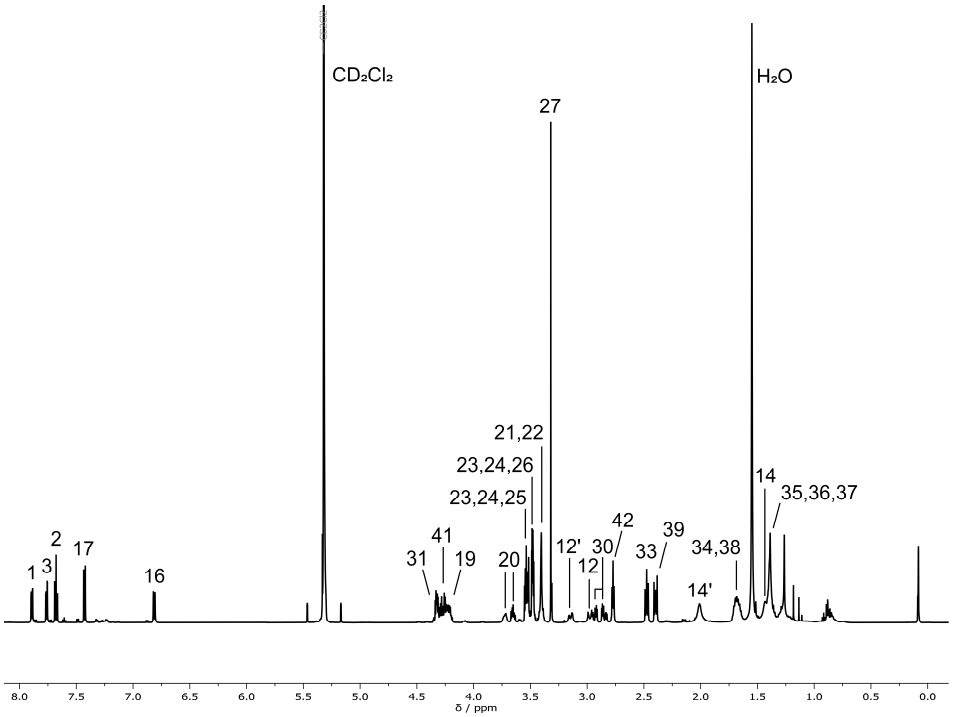

Figure 31 ^{1}H NMR (600 MHz, CD_2Cl_2, 25 °C) of racemic **C-1** and assignment of proton signals to the molecular structure. Residual small signals belong to small amounts of isomer **A-1**. *Adapted from the supporting information to ref.* [8].

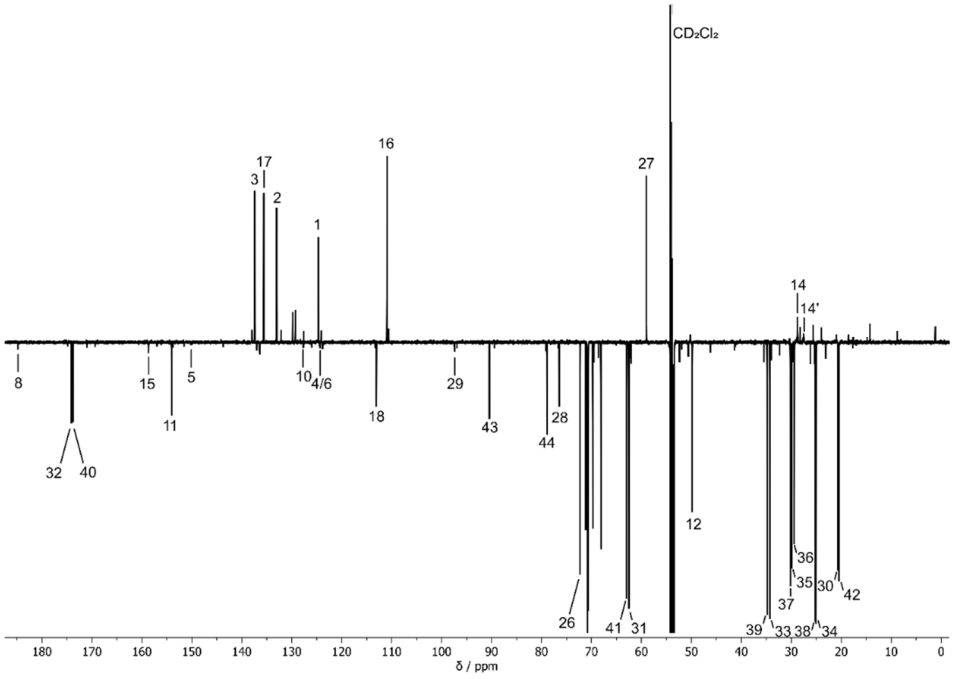

Figure 32 DEPTq NMR (600 MHz, CD_2Cl_2, 25 °C) of racemic **C-1** and assignment of the signals to the molecular structure. Residual small signals belong to small amounts of isomer **A-1**. *Adapted from the supporting information to ref.* [8].

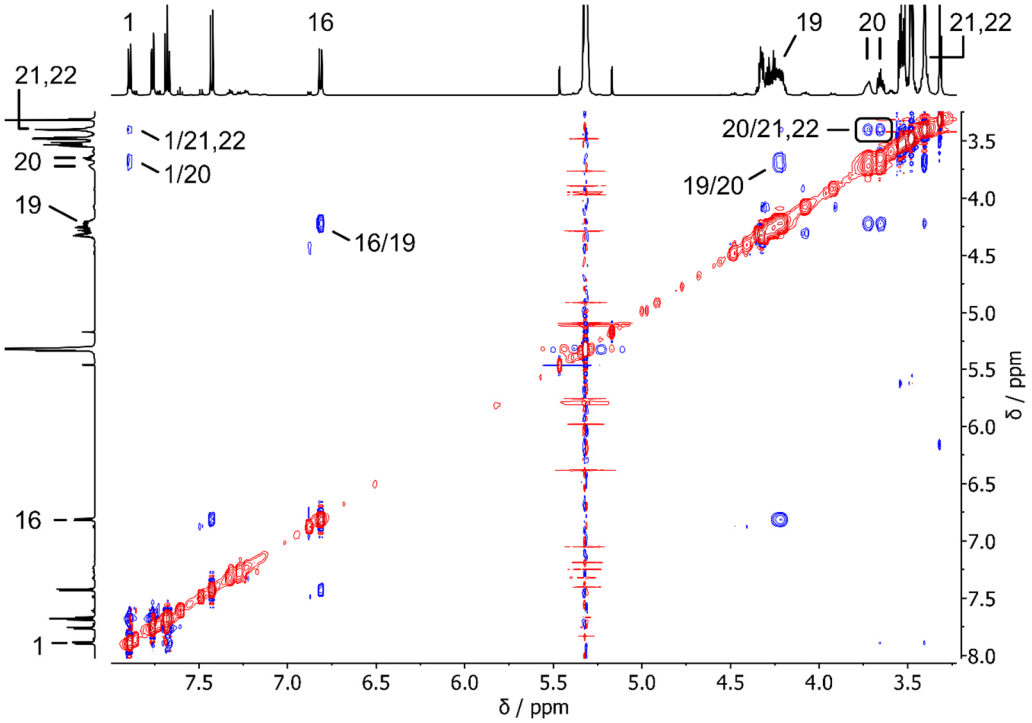

Figure 33 Excerpt from NOESY (600 MHz, CD_2Cl_2, 25 °C) spectrum of **C-1**. Cross signals between protons 1 (thioindigo fragment) and 20, 21 and 22 (tetraethylene glycol chain) confirm (*E*)-configuration.

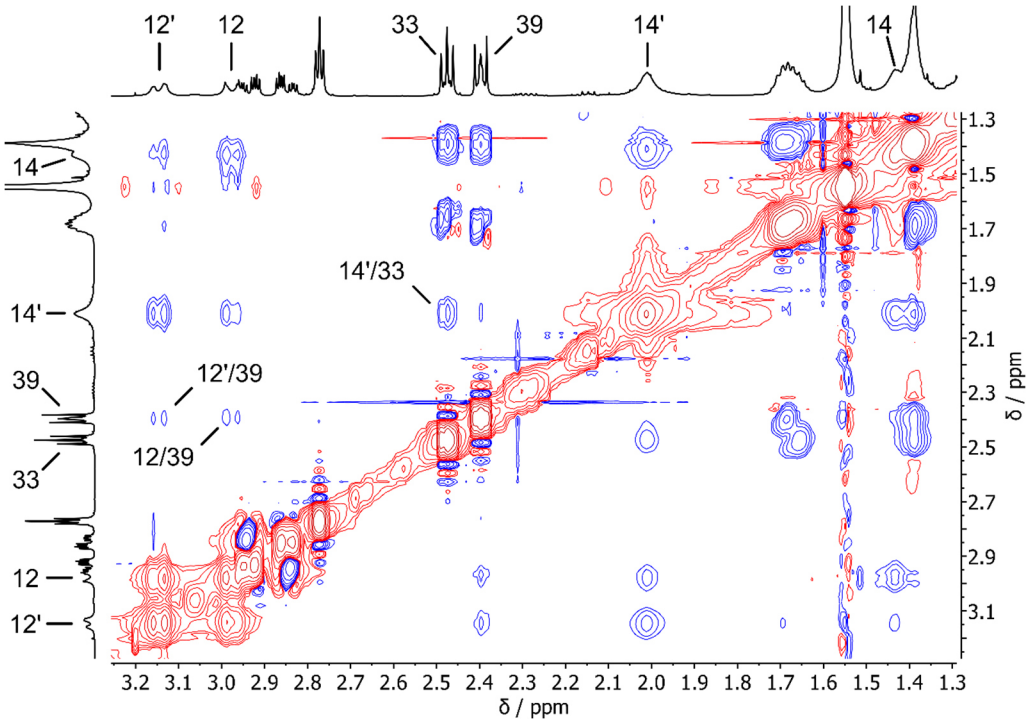

Figure 34 Excerpt from NOESY (600 MHz, CD_2Cl_2, 25 °C) spectrum of **C-1**. Cross signals between methyl group protons 14' (indanone fragment) and methylene group protons 33 (aliphatic macrocycle ring), as well as between protons 12/12' (indanone fragment) and methylene group protons 39 (aliphatic macrocycle ring) confirm (*E*)-configuration.

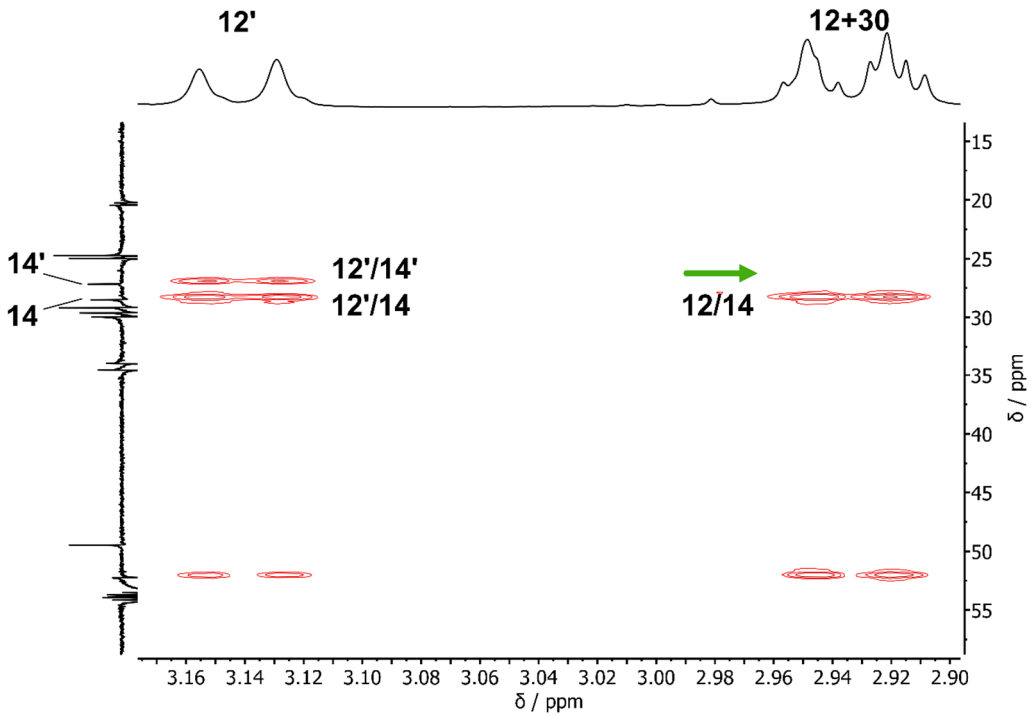

Figure 35 Excerpt from HMBC (600 MHz, CD_2Cl_2, 0 °C) spectrum of **C-1**. There is no correlation between the signals of protons 12 and 14' (green arrow) due to the torsional angle being close to 90°. The spectrum was recorded at 0 °C, as these correlations could not be observed at ambient temperature. *Adapted from the supporting information to ref.* [8].

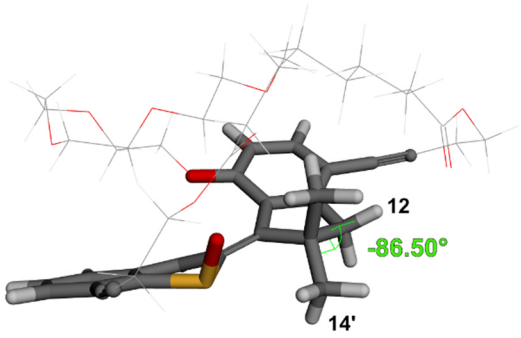

Figure 36 Lowest energy geometry obtained for **C-1** at the B3LYP-D3BJ/6-311G(d,p) PCM (CH_2Cl_2) level of theory. The torsional angle between protons 12 and 14' is close to 90°. The HTI core structure is highlighted for clarity. *Adapted from the supporting information to ref.* [8].

For **A-1**, the NOESY spectrum shows cross peaks between proton 1 on the thioindigo fragment and methyl group 14’ on the indanone fragment, confirming (*Z*)-configuration of the central double bond (see Figure 40). Additional evidence for (*Z*)-configuration comes from the cross peaks between aromatic proton 16 on the indanone part with methylene groups 33 and 34 in the aliphatic ring. Further information on the molecular configuration can be obtained from the HMBC spectrum by applying the *Karplus* relation to the $^{3}J_{H,C}$ coupling between protons 12/12’ and carbon atoms 14/14’. If the dihedral angle between the coupling partners is close to 90°, the coupling constant is close to zero and no correlation is observed in the HMBC spectrum. Indeed, there is one of the four potential correlations that is not observed (marked by a green arrow in Figure 41). Analysis of the theoretically obtained minimum geometry shows, that the dihedral angle between proton 12 and carbon atom 14’ is −89.55° and the signals were assigned accordingly.

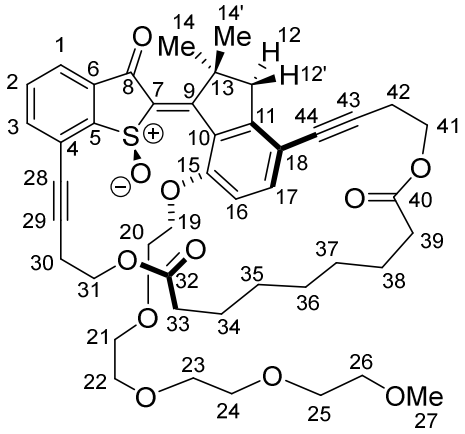

Figure 37 Chemical structure of **A-1** and the numbering used in the following. Only the (*S*)-configured isomer is shown for clarity.

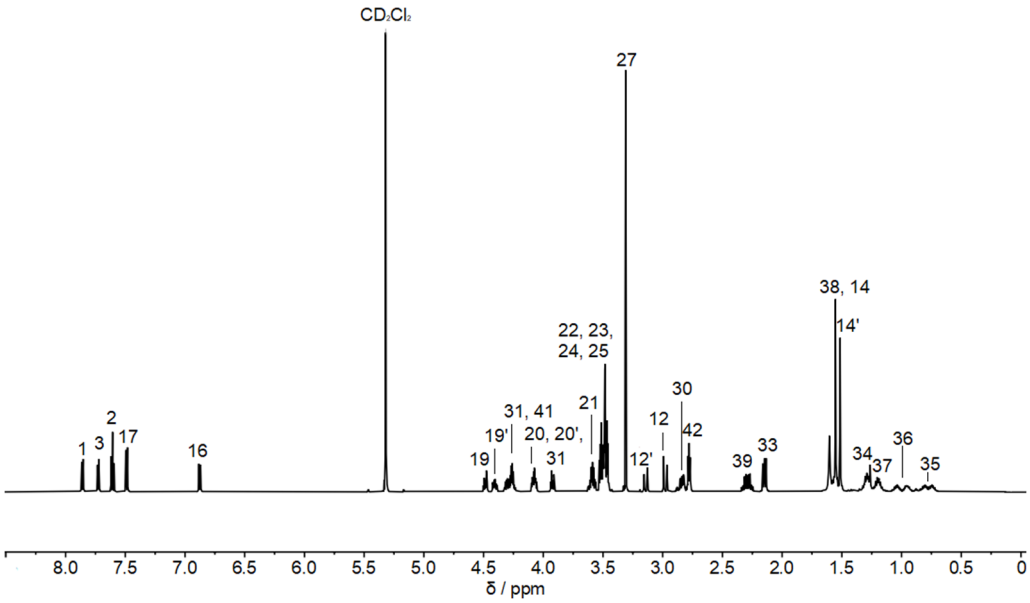

Figure 38 ^{1}H NMR (601 MHz, CD_2Cl_2, 10 °C) spectrum of racemic **A-1** and assignments of the signals to the molecular structure. *Adapted from the supporting information to ref.* [8].

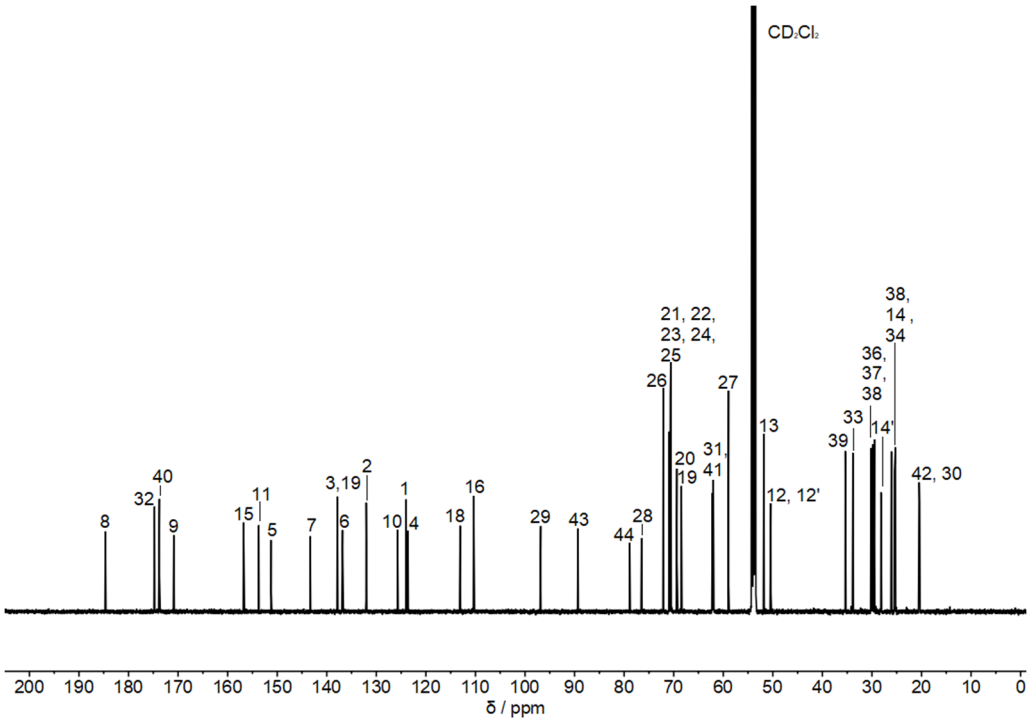

Figure 39 ^{13}C NMR (151 MHz, CD_2Cl_2, 10 °C) spectrum of racemic **A-1** and assignments of the signals to the molecular structure. *Adapted from the supporting information to ref.* [8].

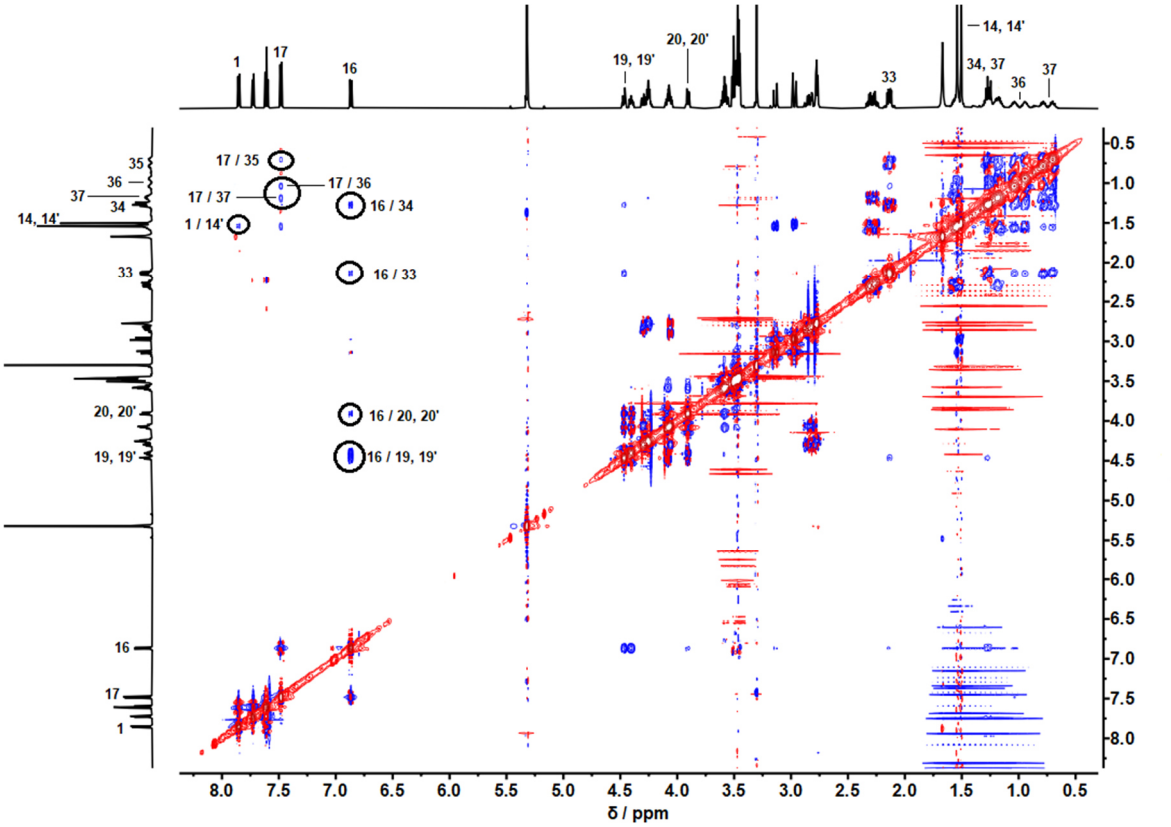

Figure 40 NOESY NMR (601 MHz, CD_2Cl_2, 10 °C) spectrum of racemic **A-1**. (*Z*)-configuration is evidenced by the cross signal of indanone fragment proton 16 with the aliphatic ring protons 33 and 34, as well as cross signal of thioindigo fragment proton 1 with protons 14'. *Adapted from the supporting information to ref.* [8].

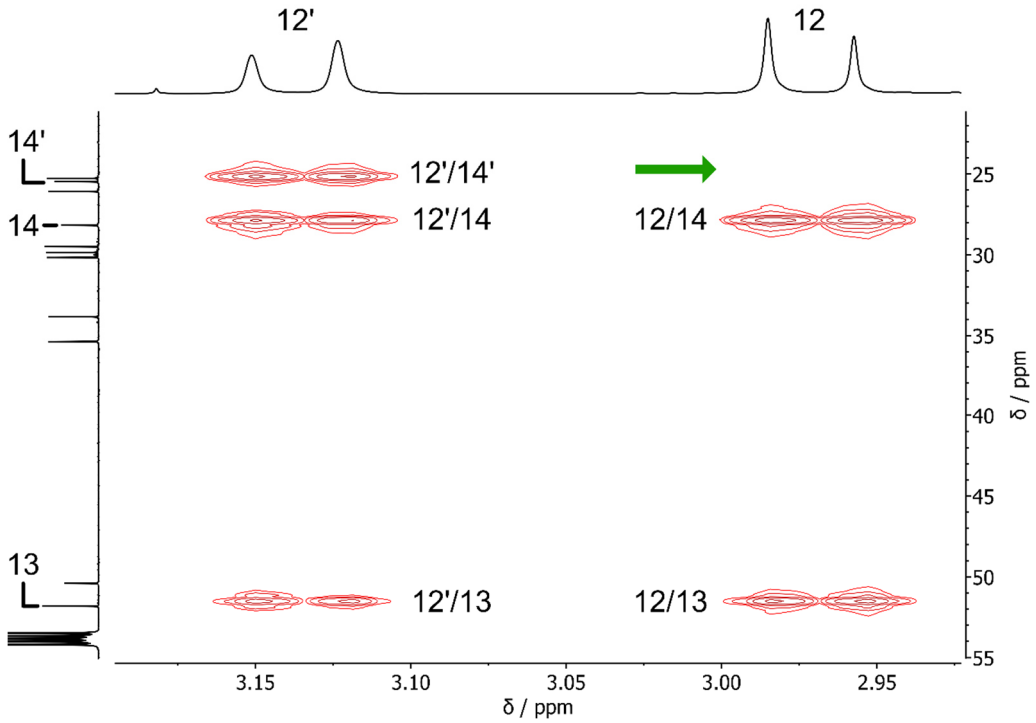

Figure 41 Excerpt from HMBC NMR (601 MHz, CD_2Cl_2, 10 °C) spectrum of racemic **A-1**. There is no correlation observed between proton 12 and carbon atom 14' (marked by a green arrow) due to the torsional angle being close to 90°.

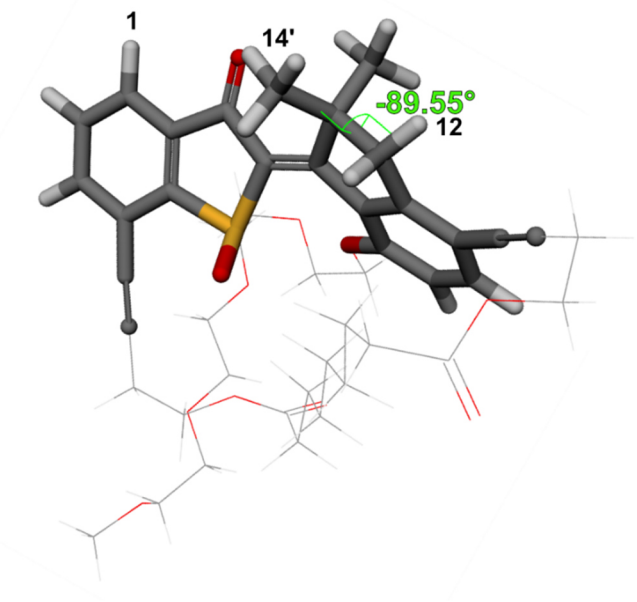

Figure 42 Minimum geometry obtained for **A-1** at the B3LYP-D3BJ/6-311G(d,p) PCM (CH_2Cl_2) level of theory. The HTI core structure is highlighted for clarity. The torsional angle between proton 12 and carbon atom 14' is very close to 90°, which is in agreement with the observed HMBC pattern. *Adapted from the supporting information to ref.* [8].

Isomer **D-1** could be accumulated by *in situ* irradiation of an NMR sample of **C-1** in CD_2Cl_2 with 450 light at −80 °C. As the isomer is metastable, it was characterized at the same temperature. ^{1}H (Figure 44) and ^{13}C DEPTq NMR (Figure 45) spectra, as well as signal assignments to the molecular structure are shown below. In order to assess the double bond configuration, a number of 1D NOE experiments was performed. 1D NOE was chosen over NOESY due to the higher sensitivity in combination with shorter measuring times, as the NMR spectrometer can be kept at such low temperatures only for limited time periods. Upon irradiation of proton 1 on the thioindigo fragment, an NOE signal was observed for protons 14 on the indanone fragment, confirming (*Z*)-configuration of the central double bond (see Figure 46). Additional evidence comes from the through-space coupling observed between proton 16 on the indanone part with methylene group protons 33 in the aliphatic macrocycle ring (shown in Figure 47).

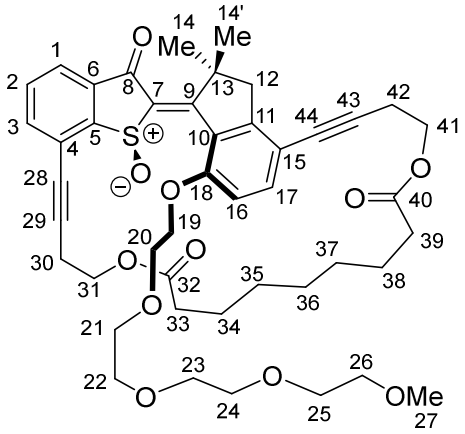

Figure 43 Molecular structure of **D-1**. Only the (*S*)-configured enantiomer is shown for clarity.

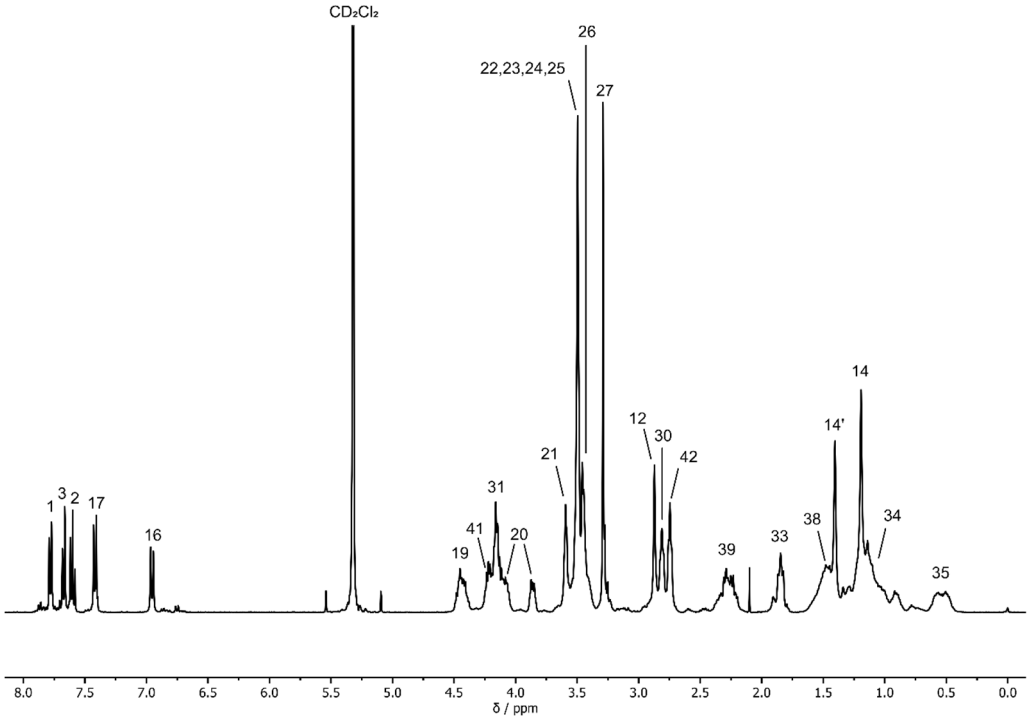

Figure 44 ^{1}H NMR (400 MHz, CD_2Cl_2, −80 °C) spectrum of a solution enriched in racemic **D-1** and assignments of the signals to the molecular structure. For preparation, a sample of pure racemic **C-1** in CD_2Cl_2 was irradiated in situ with 450 nm light at −80 °C until **C-1** was almost completely converted to **D-1**. *Adapted from the supporting information to ref.* [8].

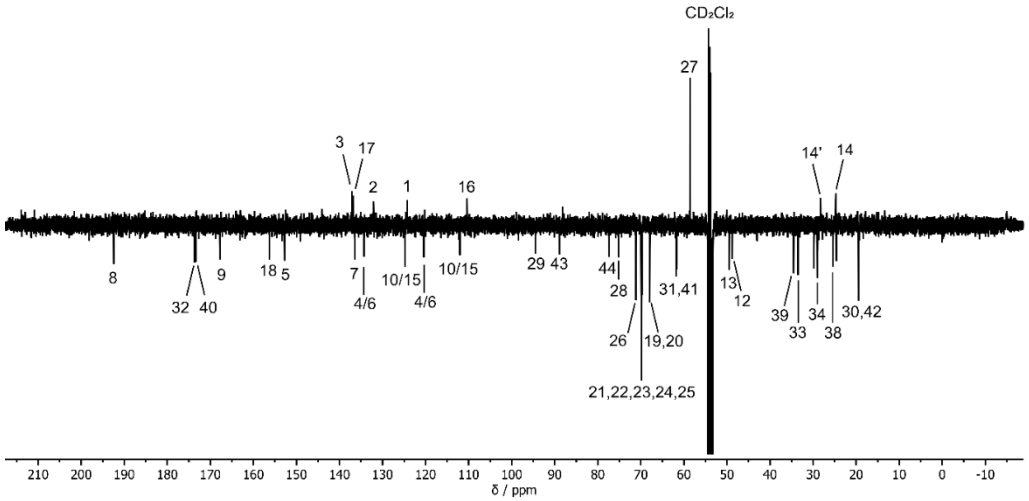

Figure 45 DEPTq NMR (400 MHz, CD_2Cl_2, −80 °C) spectrum of a solution enriched in **D-1** and assignment of the signals to the molecular structure. *Adapted from the supporting information to ref.* [8].

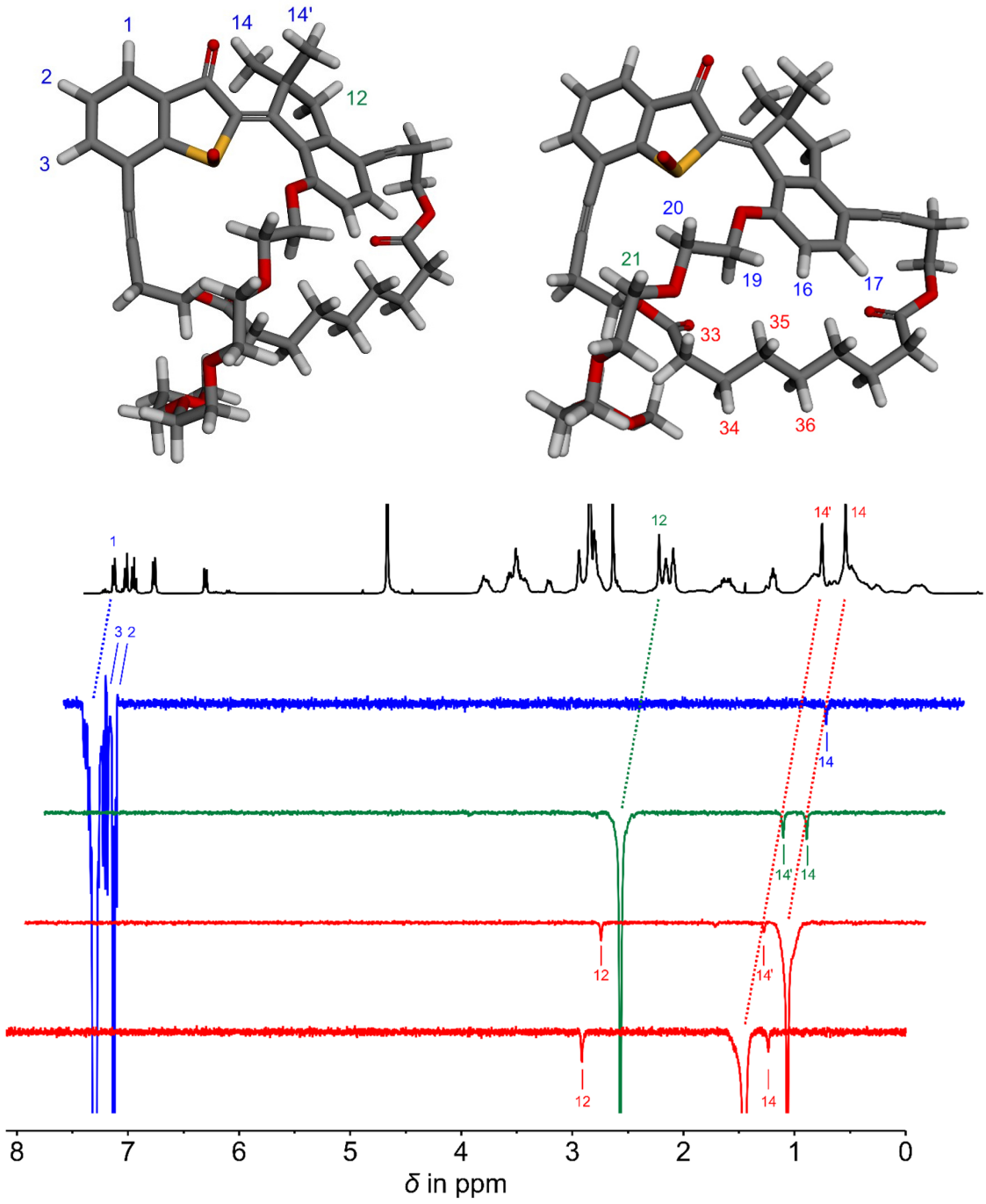

Figure 46 *top:* Global minimum structure of **D-1** as calculated on the B3LYP-D3BJ/6-311G(d,p) PCM (CH_2Cl_2) level of theory depicted in two different viewing angles with indicative protons labelled. *bottom:* ^1H (black) and 1D NOE (colored) NMR (400 MHz, CD_2Cl_2, −80 °C) spectra of a solution enriched in racemic **D-1**. Dotted lines indicate which proton signal was irradiated in the NOE experiment. The (*Z*)-configuration is evidenced by the through-space coupling between proton 1 of the thioindigo fragment and methyl group 14 as predicted by theory. *Adapted from the supporting information to ref.* [8].

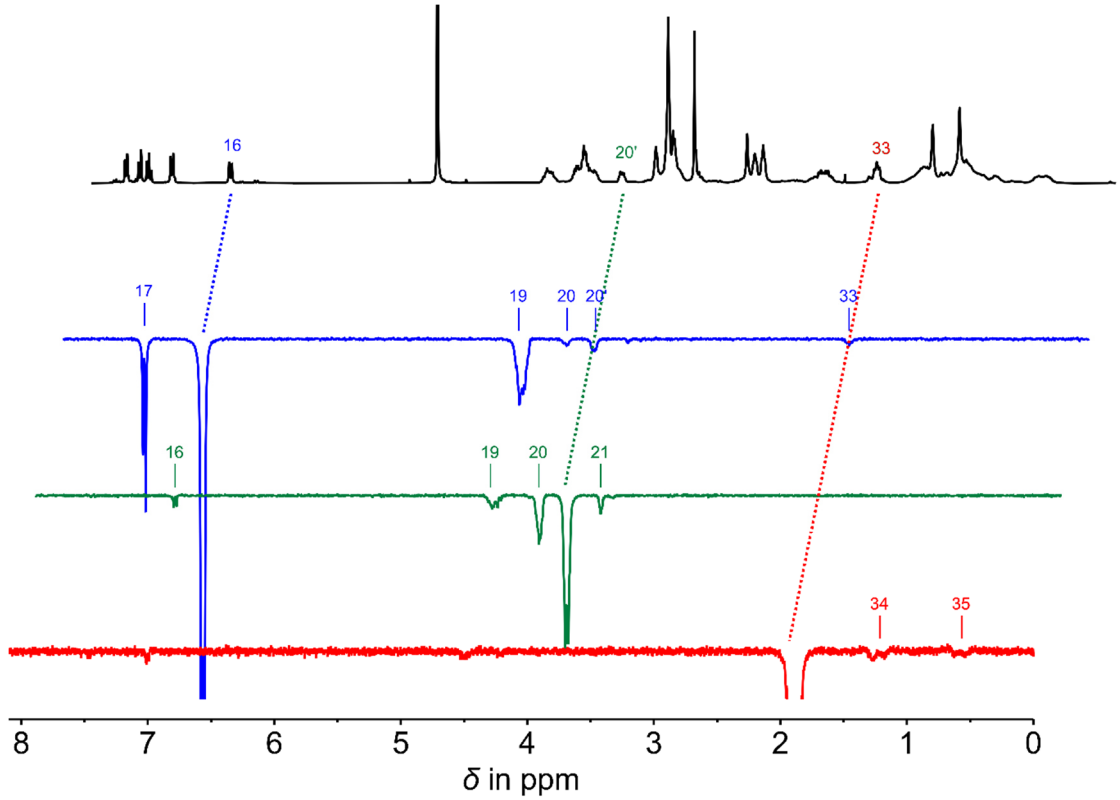

Figure 47 ^{1}H (black) and 1D NOE (colored) NMR (400 MHz, CD_2Cl_2, −80 °C) spectra of a solution enriched in racemic **D-1**. Dotted lines indicate, which proton signal was irradiated in the NOE experiment. (*Z*)-configuration is evidenced by the through-space coupling between proton 16 of the indanone fragment and aliphatic ring protons 33. For assignments of indicated signals to the theoretically obtained geometry see Figure 46 (top). *Adapted from the supporting information to ref.* [8].

3.4.2 Conformational Analysis of **2** in Solution

Conformational analysis of stable isomers **A-2** and **C-2** as well as metastable isomer **D-2** was performed by solution NMR spectroscopy. The ^{1}H and ^{13}C NMR spectra, as well as the assignment of signals to the respective molecular structure are reproduced in the following section.

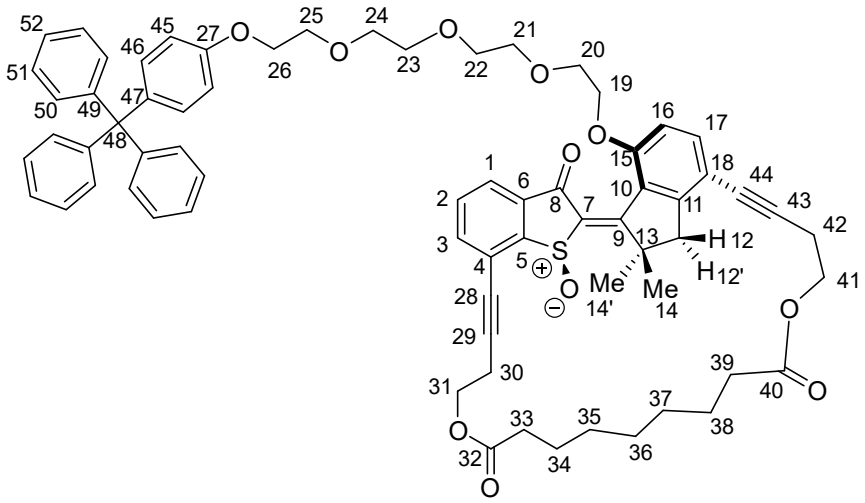

Figure 48 Structure formula of **C-2** and numbering used in the following. Only the (*S*)-configured isomer is shown for clarity.

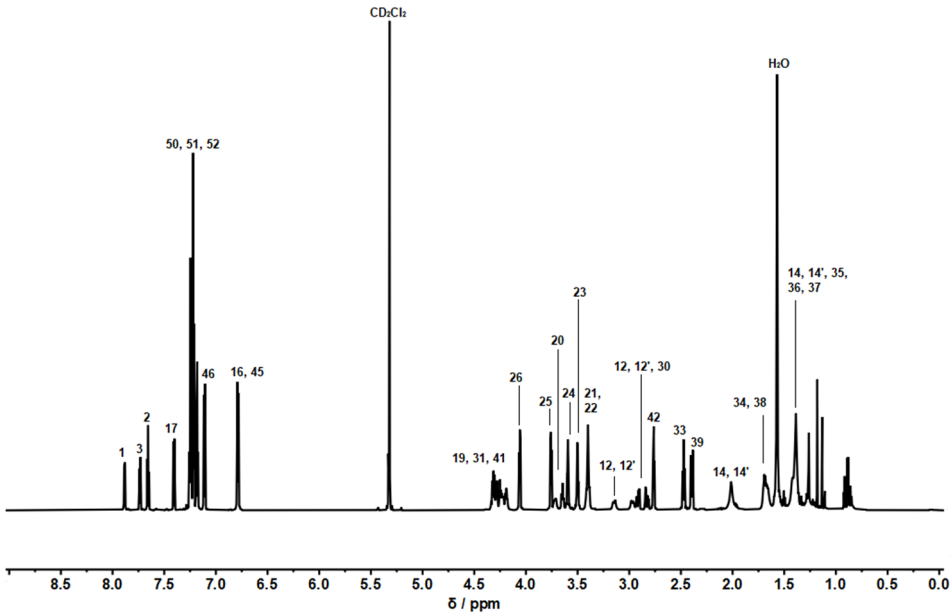

Figure 49 ^{1}H NMR (800 MHz, CD_2Cl_2, 25 °C) spectrum of racemic **C-2** with assignments to the molecular structure. *Adapted from the supporting information to ref.* [8].

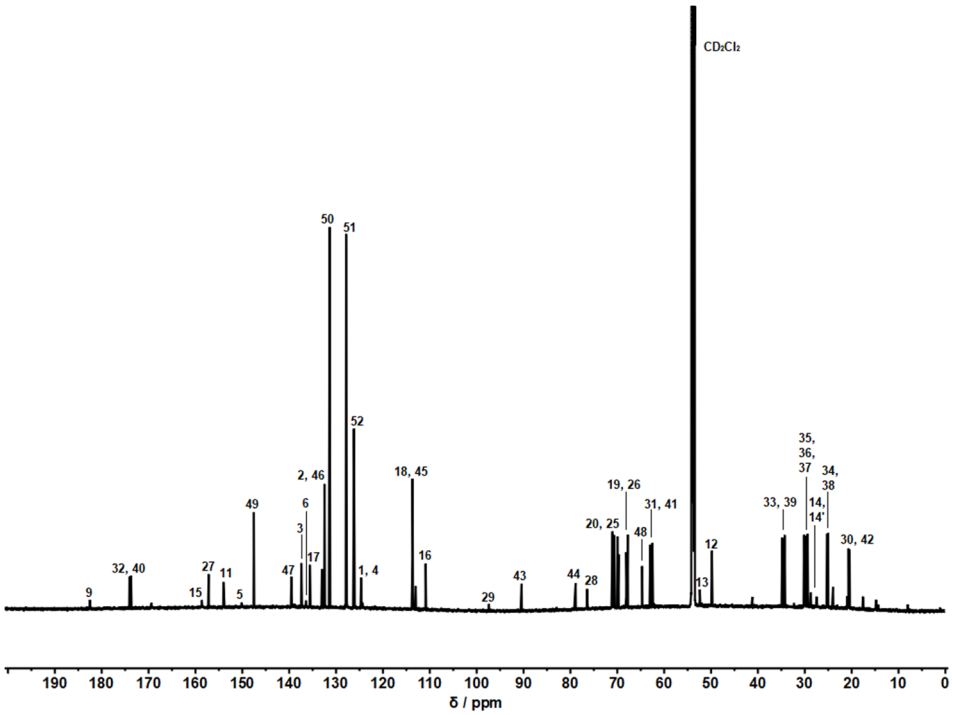

Figure 50 ^{13}C NMR (201 MHz, CD_2Cl_2, 25 °C) spectrum of racemic **C-2** and assignments of signals to the molecular structure. *Adapted from the supporting information to ref.* [8].

For compound **A-2**, ^{1}H and ^{13}C NMR assignments are repoduced from ref. [8] in the following.

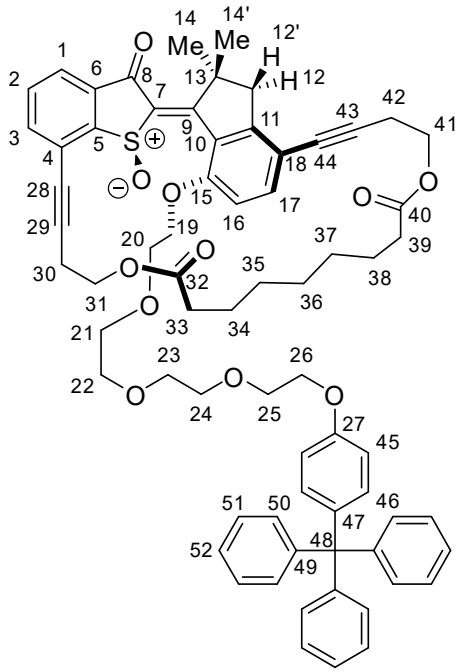

Figure 51 Structure diagram of **A-2** and the numbering used in the following. Only the (*S*)-configured isomer is shown for clarity.

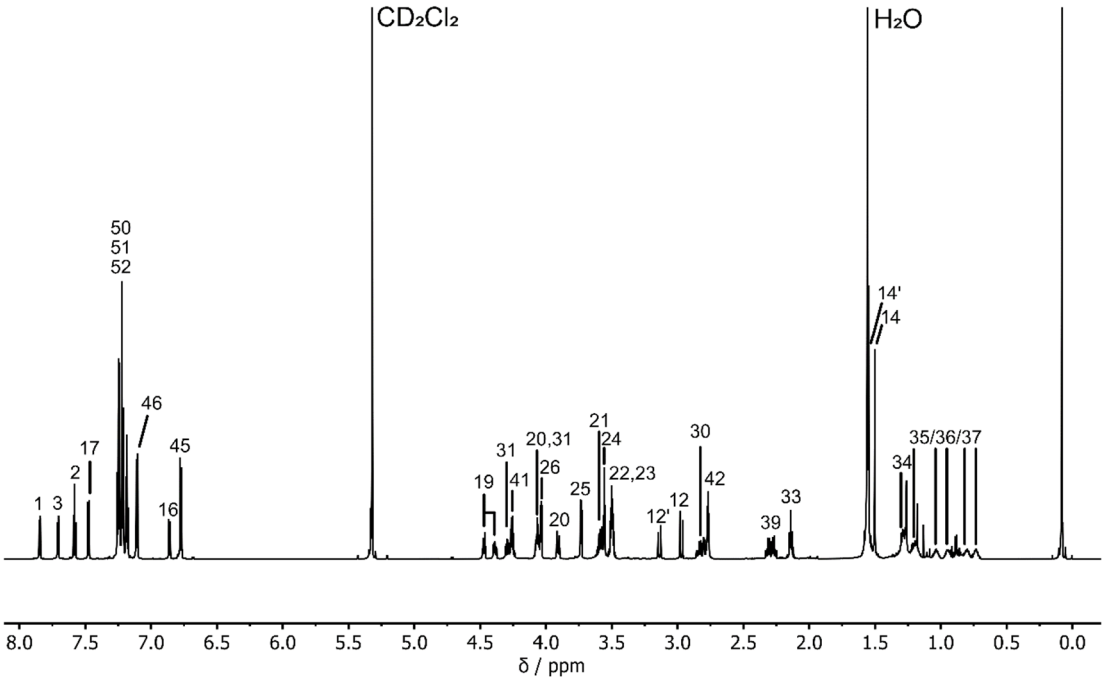

Figure 52 ^{1}H NMR Spectrum (800 MHz, CD_2Cl_2, 25 °C) of racemic **A-2** with assignments of the signals to the molecular structure. *Adapted from the supporting information to ref.* [8].

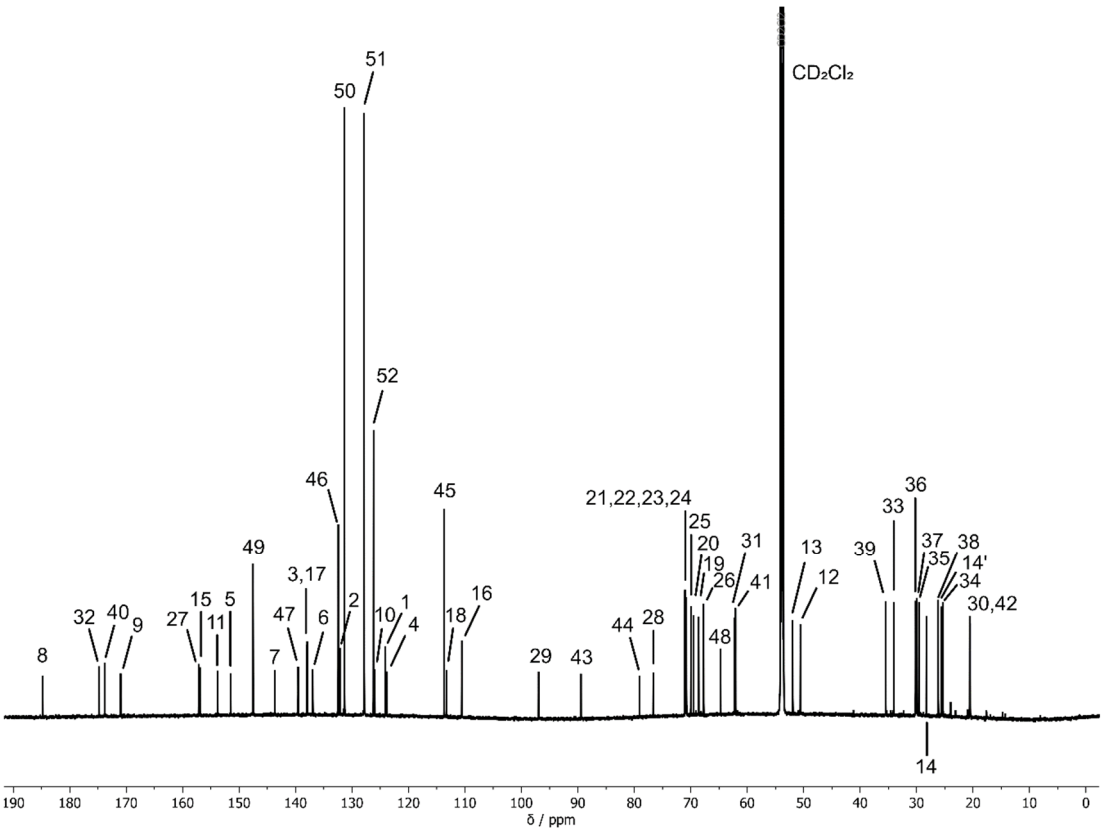

Figure 53 ^{13}C NMR spectrum (201 MHz, CD_2Cl_2, 25 °C) of racemic **A-2** with assignments of the signals to the molecular structure. *Adapted from the supporting information to ref.* [8].

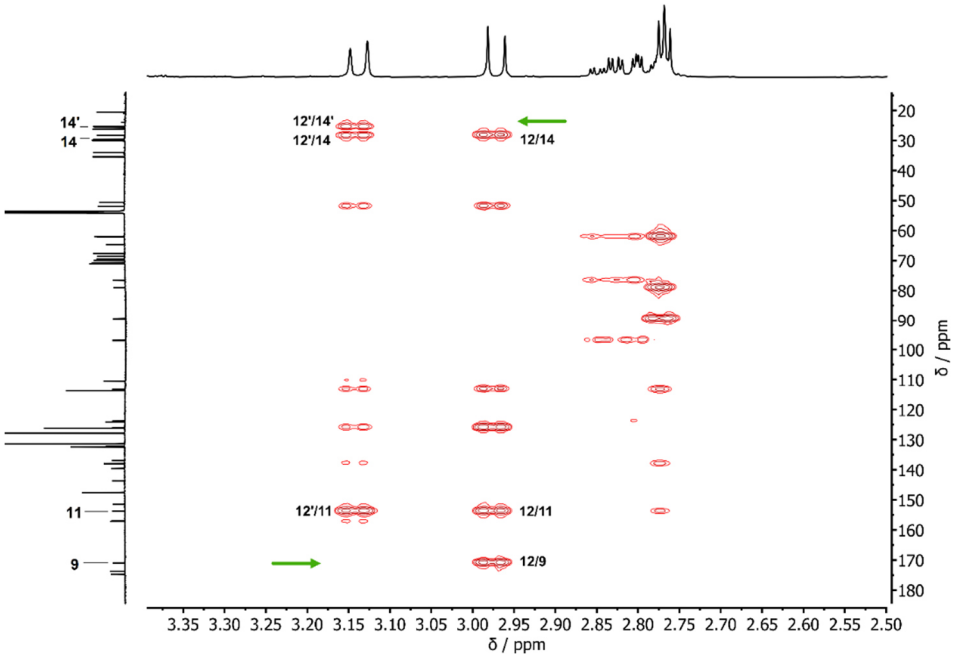

Figure 54 Section of the HMBC (800 MHz, CD_2Cl_2, 25 °C) spectrum of racemic **A-2**. The correlations between proton 12 and carbon atom 14', as well as proton 12' and carbon atom 9, disappear due to the torsional angle being close to 90°. *Adapted from the supporting information to ref.* [8].

Isomer **D-2** could be accumulated by external irradiation of an NMR sample of **C-2** in CD_2Cl_2 with 450 nm light at 23 °C. It was then characterized by NMR spectroscopy at 0 °C (the lower temperature was necessary, as some HMBC correlations could not be observed at 25 °C). ^{1}H and ^{13}C NMR spectra as well as signal assignments to the molecular structure are given in the following. In order to assess the configuration of the central double bond, 1D ROE experiments were performed. The observed through-space coupling of proton 1 on the thioindigo fragment with methyl group protons 14 on the indanone fragment confirms (*Z*)-configuration of the double bond. As no ROE is observed between proton 1 and methyl group 14' protons, methyl group 14 must be closer to the thioindigo fragment. Further information on the molecular configuration can be obtained from the HMBC spectrum by applying the *Karplus* relation to the $^{3}J_{H,C}$ coupling between protons 12/12' and carbon atoms 14/14'. If the dihedral angle between the coupling partners is close to 90°, the coupling constant is close to zero and no correlation is observed in the HMBC spectrum. Indeed, there is one of the four potential correlations that is not observed (marked by a green arrow in Figure 59). Analysis of the theoretically obtained minimum geometry for **D-1** (assuming that the HTI core geometry is very similar for both **D-1** and **D-2**) shows, that the dihedral angle between proton 12' and carbon atom 14 is 91.53° and the signals were assigned accordingly.

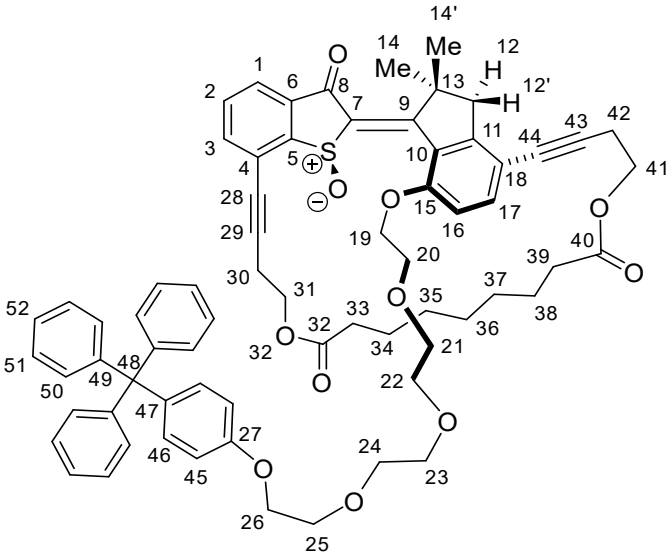

Figure 55 Structure diagram of **D-2** and the numbering used in the following. Only the (*S*)-configured isomer is shown for clarity.

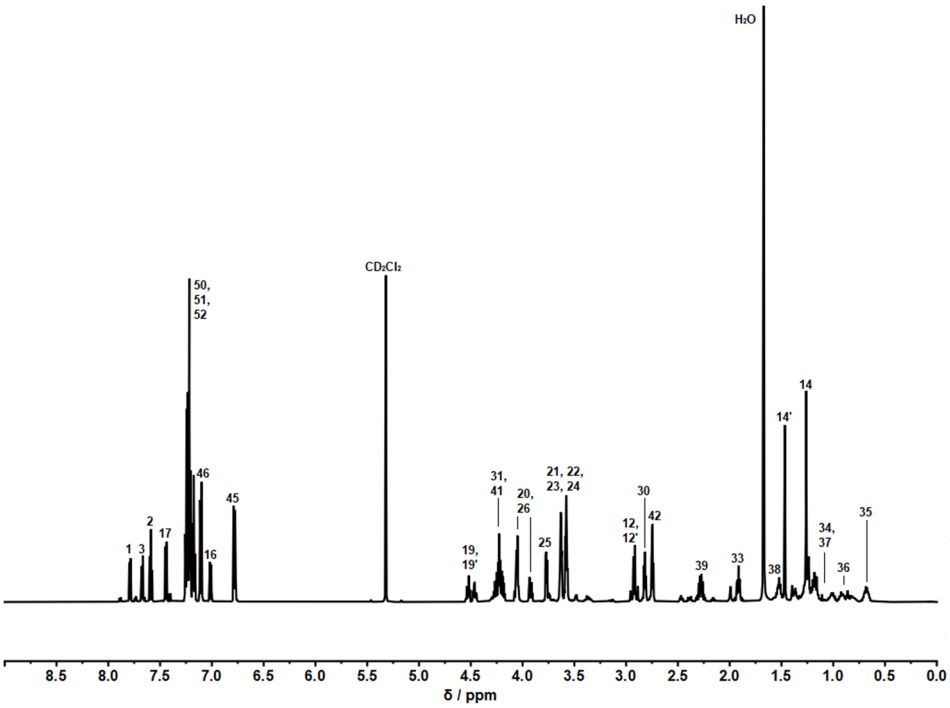

Figure 56 ^{1}H NMR (601 MHz, CD_2Cl_2, 0 °C) spectrum of a mixture enriched in racemic **D-2** and assignments of the signals to the molecular structure. **D-2** was accumulated by external irradiation of a solution of racemic **C-2** in CD_2Cl_2 with 450 nm light at 23 °C. *Adapted from the supporting information to ref.* [8].

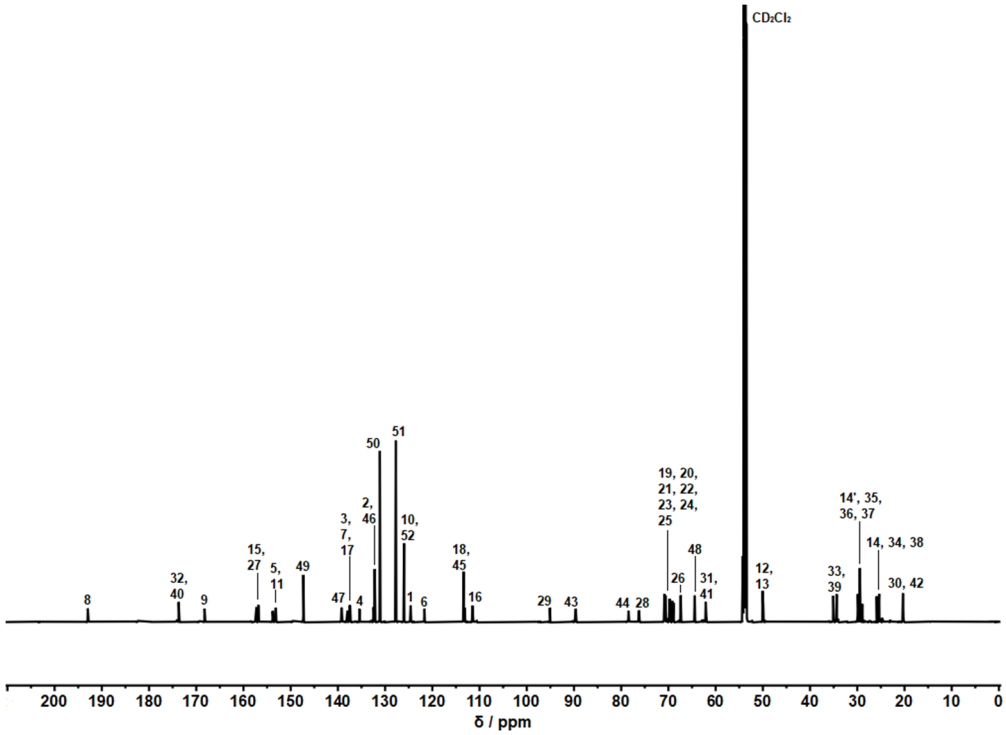

Figure 57 ^{13}C NMR (151 MHz, CD_2Cl_2, 0 °C) spectrum of a solution enriched in racemic **D-2** and assignments of the signals to the molecular structure. *Adapted from the supporting information to ref.* [8].

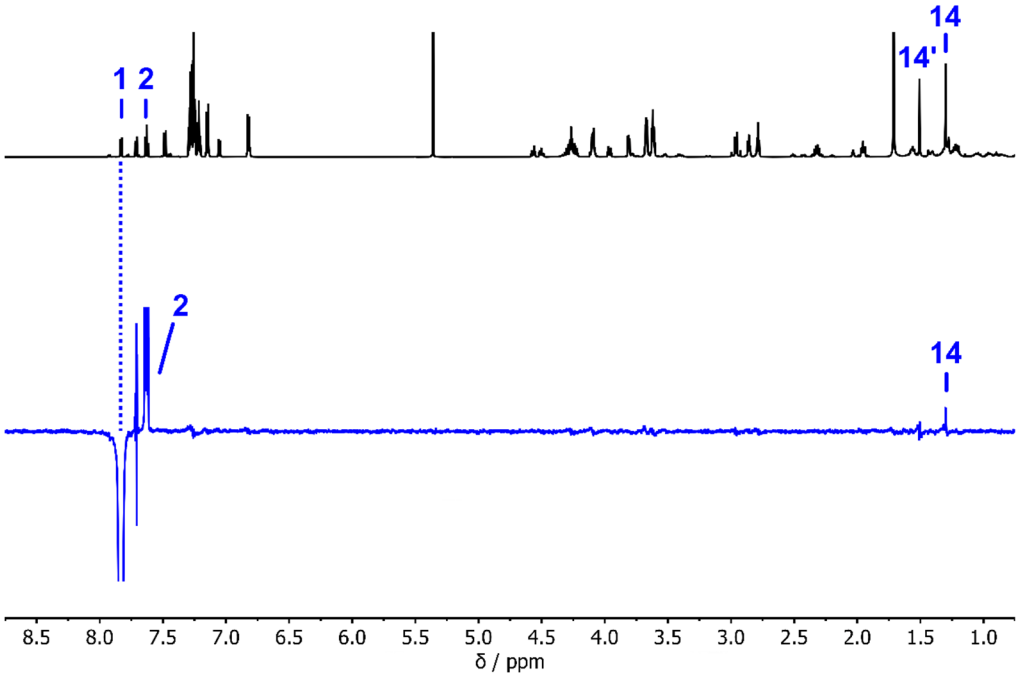

Figure 58 ^{1}H (black) and 1D ROE (blue) NMR (600 MHz, CD_2Cl_2, 0 °C) spectra of a solution enriched in racemic **D-2**. The dotted line indicates, which proton signal was irradiated in the ROE experiment. The observed coupling between aromatic proton 1 (on the thioindigo fragment) with methyl group 14 (on the indanone fragment) confirms (*Z*)-configuration of the central double bond. Stacked spectra are clipped vertically for clarity.

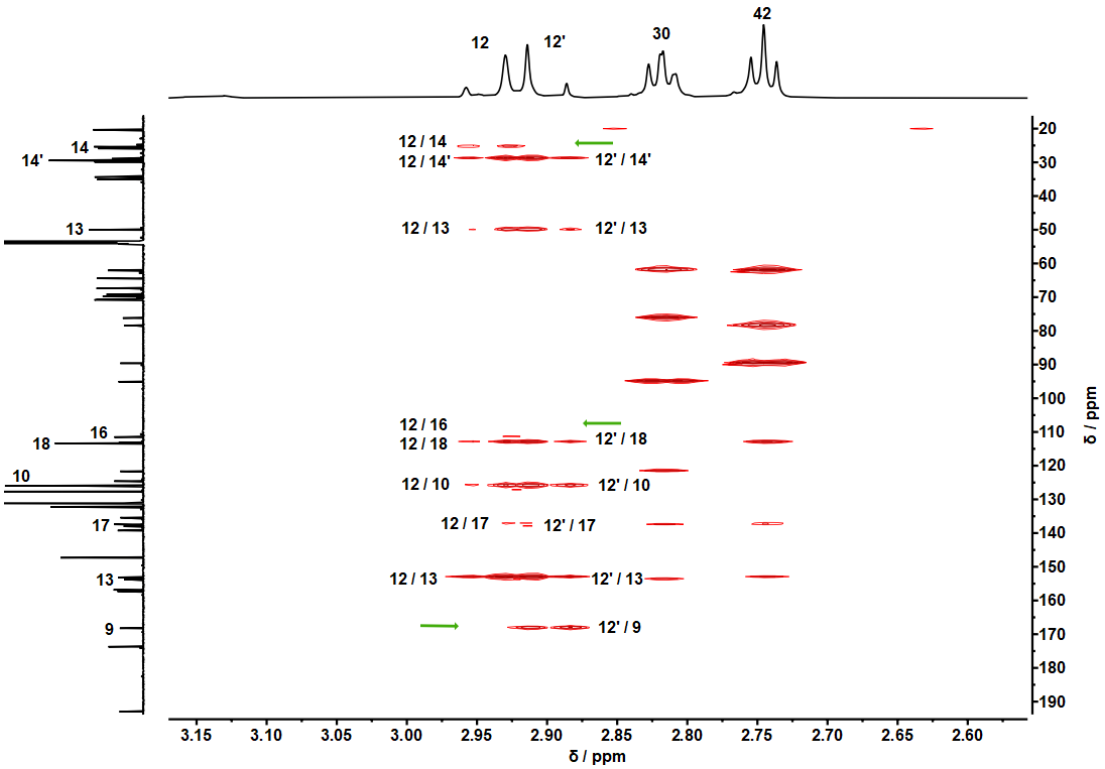

Figure 59 HMBC NMR (601 MHz, CD_2Cl_2, 0 °C) of a solution enriched in **D-2**. No correlation between proton 12' and carbon atom 14 is observed due to the torsional angle being close to 90°. *Adapted from the supporting information to ref.* [8].

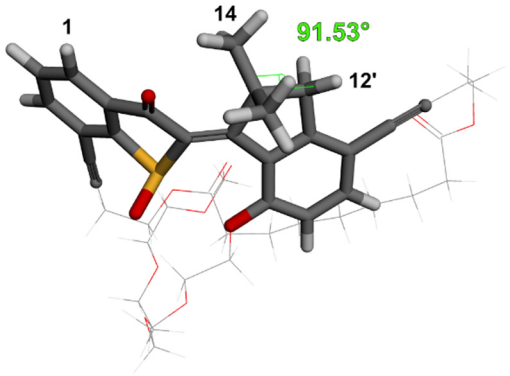

Figure 60 Minimum geometry obtained for **D-1** at the B3LYP-D3BJ/6-311G(d,p) PCM (CH_2Cl_2) level of theory. The HTI core structure is highlighted for clarity and the numbering of some atoms of interest is given. The torsional angle between proton 12' and carbon atom 14 is close to 90°. Assuming a similar structure of the HTI core of **D-2**, this is in agreement with the observed HMBC pattern.

3.4.3 Comparison of ^{1}H NMR Spectra

When directly comparing ^{1}H NMR spectra of the respective **A**-,**C**- and **D**-isomers of compounds **1** and **2**, a striking similarity between the corresponding isomer pairs is found (see Figure 61 and Figure 62). This suggests a close similarity in molecular geometry.

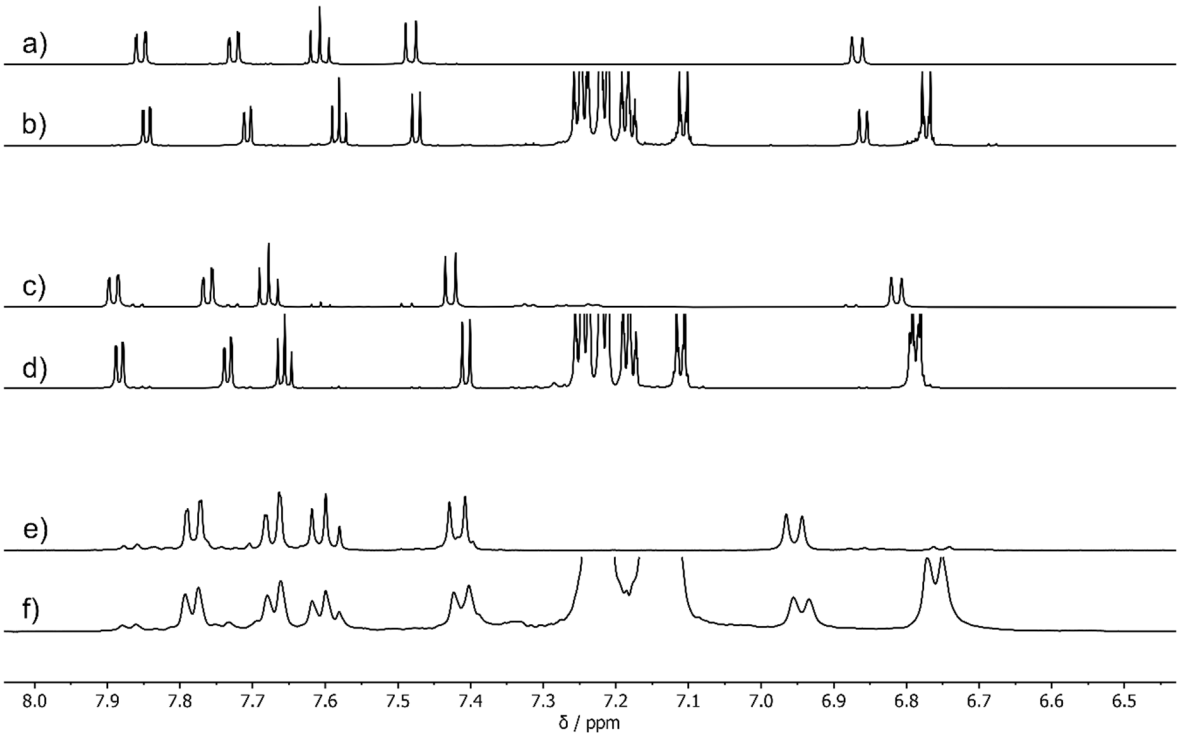

Figure 61 Comparison of the aromatic region of ^{1}H NMR (CD_2Cl_2) spectra of **a) A-1** (600 MHz, 10 °C), **b) A-2** (800 MHz, 25 °C), **c) C-1** (600 MHz, 25 °C), **d) C-2** (800 MHz, 25 °C), **e) D-1** (400 MHz, −80 °C), **f) D-2** (400 MHz, −80 °C). Respective chemical shifts are very similar, suggesting high structural similarity of the isomeric pairs. Spectra are clipped vertically for clarity.

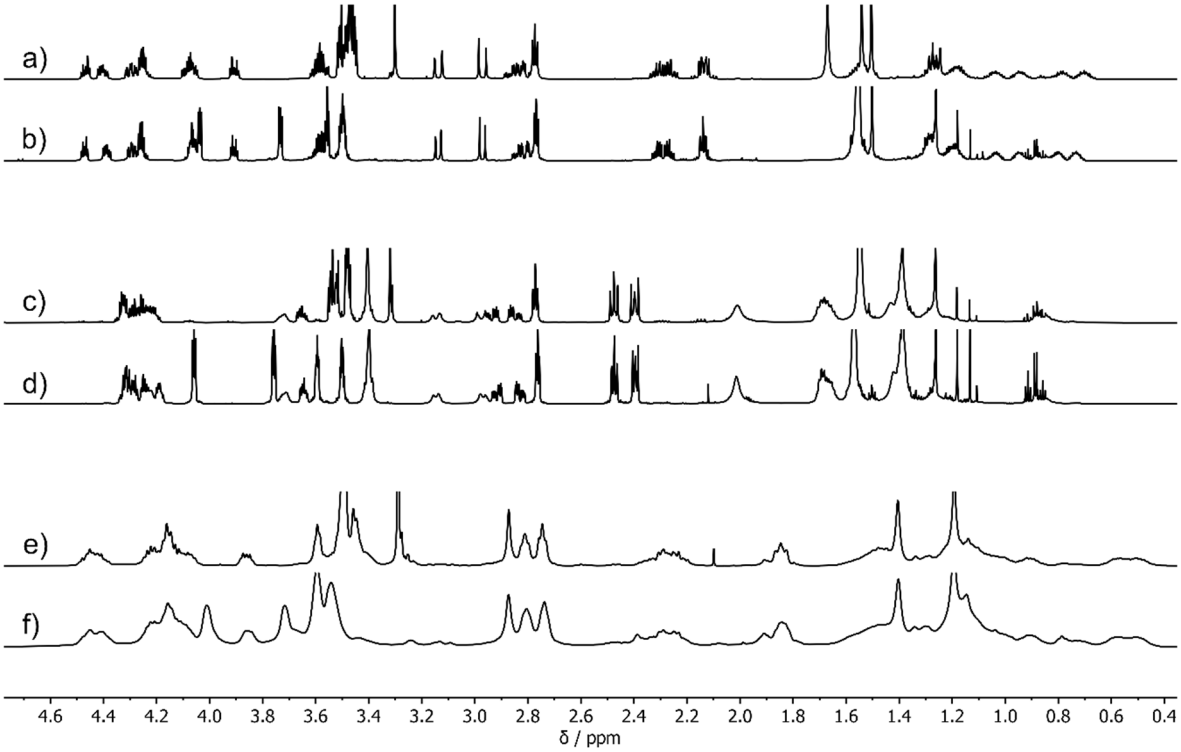

Figure 62 Comparison of the aliphatic region of ^{1}H NMR (CD_2Cl_2) spectra of **a) A-1** (600 MHz, 10 °C), **b) A-2** (800 MHz, 25 °C), **c) C-1** (600 MHz, 25 °C), **d) C-2** (800 MHz, 25 °C), **e) D-1** (400 MHz, −80 °C), **f) D-2** (400 MHz, −80 °C). Respective chemical shifts are very similar, suggesting high structural similarity of the isomeric pairs. Spectra are clipped vertically for clarity.

3.5 UV/Vis Absorption and Photoswitching Experiments

UV/Vis absorption spectra were measured for both stable isomers **A-1**/**A-2** and **C-1**/**C-2** in CH_2Cl_2 at 23 °C. The absorption characteristics are similar to previously reported HTI molecular motors.[9, 95] Both **A**-isomers show an absorption maximum at 343 nm, the **C**-isomers at 345 nm with a shoulder extending to approx. 365 nm (see Figure 63 and Figure 66 for spectra).

Upon irradiation of a sample of pure racemic **A-2** in CH_2Cl_2 with 405 nm light at 23 °C **C-2** was formed, which then underwent photoisomerization to **D-2** with 450 nm light. It was then possible to alternate between the *pss* at 405 nm and 450 nm using light of the respective wavelength. When starting from pure racemic **C-2** in CH_2Cl_2, a similar behavior was observed. Irradiation with 450 nm light at 23 °C resulted in the accumulation of **D-2**, whereas photoisomerization to **C-2** was observed upon irradiation with 405 nm light.

The UV/Vis absorption spectra of **A-1** and **C-1** in CH_2Cl_2 (see Figure 66) show similar characteristics compared to **A-2** and **C-2** respectively. However, upon photoirradiation at 23 °C only interconversion between the two isomers was observed and the *pss* composition was independent of the starting isomer. When using 410 nm light, a *pss* enriched in **C-1** was obtained. When 490 nm light was used, the **A-2** isomer was enriched in the *pss*.

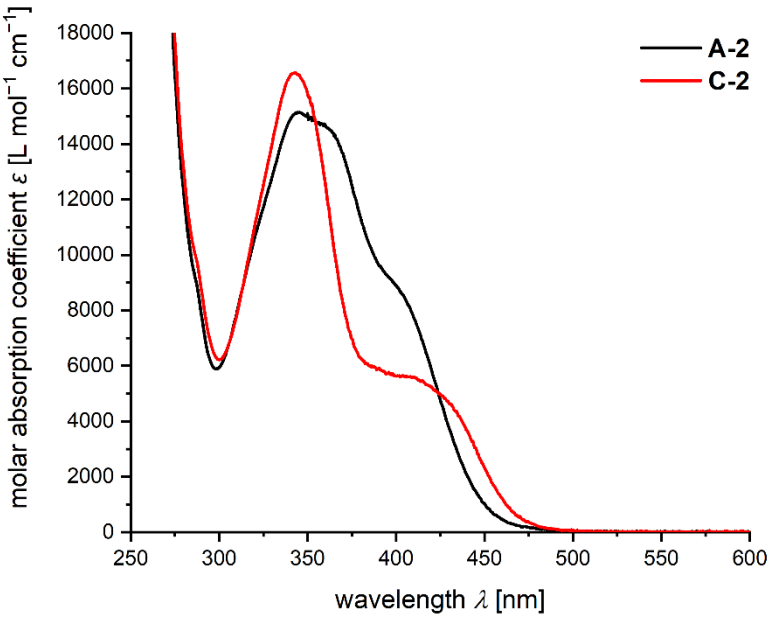

Figure 63 Molar absorption coefficients of racemic **A-2** (black spectrum) and racemic **C-2** (red spectrum) in CH_2Cl_2. *Adapted from the supporting information to ref.* [8].

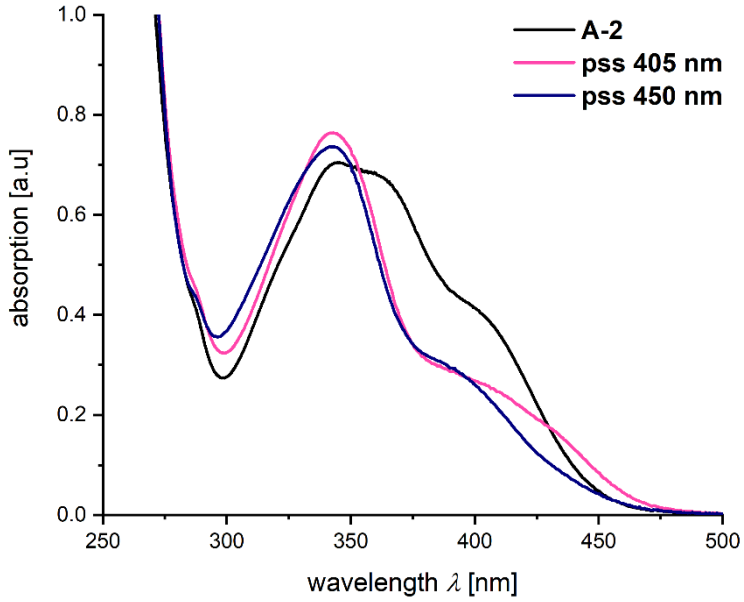

Figure 64 Absorption spectra recorded during photoisomerization of **A-2** in CH_2Cl_2 at 23 °C. A sample of racemic **A-2** (black spectrum) was irradiated with 405 nm light (pink spectrum), followed by irradiation with 450 nm light (blue spectrum). Irradiation of **A-2** with 405 nm light lead to formation of **C-2** (*via* transient **B-2**), which subsequently photoisomerized to **D-2**. At 450 nm irradiation strong accumulation of isomer **D-2** took place (blue spectrum). *Adapted from the supporting information to ref.* [8].

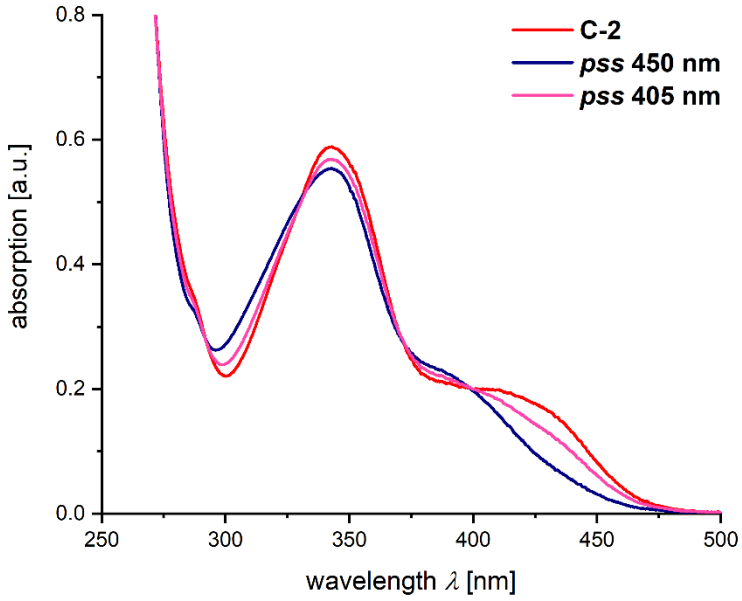

Figure 65 Absorption spectra recorded during photoisomerization of **C-2** in CH_2Cl_2 at 23 °C. A sample of racemic **C-2** (red spectrum) was irradiated with 450 nm light (blue spectrum), followed by irradiation with 405 nm light (pink spectrum). Irradiation of **C-2** with 450 nm light lead to strong accumulation of **D-2** (blue spectrum), which photoisomerized back to **C-2** at shorter irradiation wavelengths (405 nm in this case, pink spectrum). Isosbestic points were observed at 291 nm, 332 nm, 372 nm and 399 nm. *Adapted from the supporting information to ref.* [8].

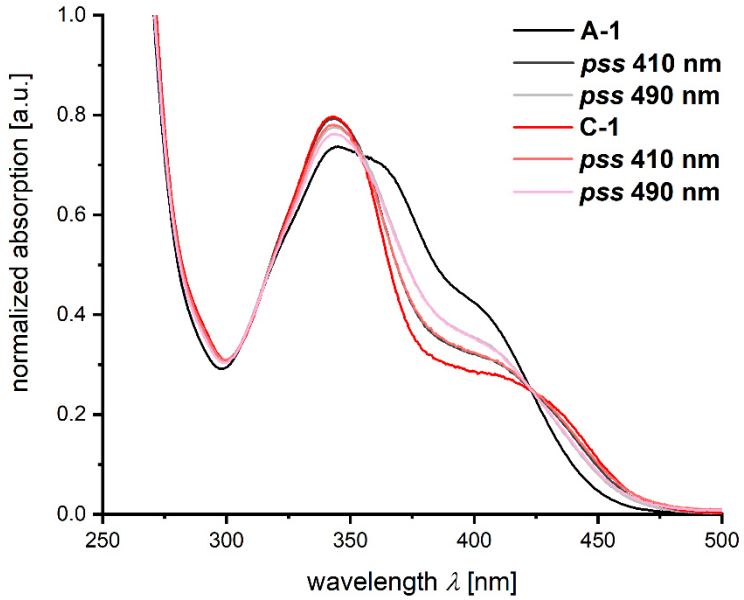

Figure 66 Absorption spectra of racemic **A-1** (black spectrum) and racemic **C-1** (red spectrum), as well as spectra recorded after reaching the *pss* at 410 nm or 490 nm irradiation. All spectra were recorded in CH_2Cl_2 and were normalized with respect to the isosbestic point at 423 nm. A second isosbestic point was found at 355 nm. Starting irradiations from either isomer **A-1** or **C-1**, the same *pss* spectra were obtained. *Adapted from the supporting information to ref.* [8].

3.5.1 *pss* Composition of 1 and 2

Table 6 Isomer composition of **1** in the *pss* at different irradiation wavelengths λ, as determined by ^{1}H NMR (400 MHz, CD_2Cl_2, 23 °C). *Note*: Data were acquired by *Verena Josef*.

λ	**A-1**	**C-1**
nm	%	%
405	24	76
420	30	70
430	33	67
450	49	51
470	58	42
490	63	37
505	59	41
515	51	49

Table 7 Isomer composition of **2** in the *pss* at different irradiation wavelengths λ, as determined by ^{1}H NMR (400 MHz, CD_2Cl_2, 23 °C). *Note*: Data were acquired by *Verena Josef*.

λ	**A-2**	**C-2**	**D-2**
nm	%	%	%
405	5	68	27
420	4	54	42
430	3	45	52
450	3	19	78
470	0	7	93
490	0	6	94
505	0	4	96

3.6 Thermal Double Bond Isomerization of 1 and 2

With the double bond configuration successfully assigned, the thermal double bond isomerization could then be investigated. To this end, an NMR sample of compound **1** (mixture of **A**- and **C**-isomers) in $(CDCl_2)_2$ was kept at 80 °C in the dark. ^{1}H NMR spectra (at 25 °C) were measured in irregular time intervals to monitor the isomerization progress. Indicative excerpts from the ^{1}H NMR spectra are shown in Figure 67a. The first order rate constants can then be obtained from the respective decay kinetics.

The isomerization is a reversible process and, as **A-1** and **C-1** are close in energy, an equilibrium between the two species will be established. This process can be described using the following equation:

$$\ln\left(\frac{[\mathbf{C\text{-}1}]_0 - [\mathbf{C\text{-}1}]_{eq}}{[\mathbf{C\text{-}1}]_t - [\mathbf{C\text{-}1}]_{eq}}\right) = (k_{\text{A-1}\rightarrow\text{C-1}} + k_{\text{C-1}\rightarrow\text{A-1}})t = mt \qquad \text{(Equation 1)}$$

with

$[\mathbf{C\text{-}1}]_0$ = initial concentration of **C-1**

$[\mathbf{C\text{-}1}]_{eq}$ = concentration of the decaying **C-1** isomer at equilibrium

$[\mathbf{C\text{-}1}]_t$ = concentration of the decaying **C-1** isomer at a particular point in time

$k_{\text{A-1}\rightarrow\text{C-1}}$ = rate constant of **A-1** to **C-1** isomerization

$k_{\text{C-1}\rightarrow\text{A-1}}$ = rate constant of **C-1** to **A-1** isomerization

m = slope

t = elapsed time

The slope m can be obtained from the ln-plot (see Equation 1) of **C-1** to **A-1** isomerization. The law of mass action is taken into account in the following Equation 2:

$$\frac{[\mathbf{A\text{-}1}]_{eq}}{[\mathbf{C\text{-}1}]_{eq}} = \frac{k_{C\rightarrow A}}{k_{A\rightarrow C}} \qquad \text{(Equation 2)}$$

with

$[\mathbf{A\text{-}1}]_{eq}$ = concentration of **A-1** at equilibrium

$[\mathbf{C\text{-}1}]_{eq}$ = concentration of **C-1** at equilibrium

By substituting the relation $k_{\text{A-1}\rightarrow\text{C-1}} + k_{\text{C-1}\rightarrow\text{A-1}} = m$ from Equation 1 in Equation 2 and solving for $k_{\text{A-1}\rightarrow\text{C-1}}$ and $k_{\text{C-1}\rightarrow\text{A-1}}$ respectively, the following Equations are obtained:

$$k_{\text{A-1}\rightarrow\text{C-1}} = \frac{m}{1 + \frac{[\mathbf{A\text{-}1}]_{eq}}{[\mathbf{C\text{-}1}]_{eq}}} \qquad \text{(Equation 3)}$$

$$k_{\text{C-1}\rightarrow\text{A-1}} = \frac{m}{1 + \frac{[\mathbf{C\text{-}1}]_{eq}}{[\mathbf{A\text{-}1}]_{eq}}} \qquad \text{(Equation 4)}$$

Using Equation 3 and Equation 4, the rate constants can be obtained from the slope *m* of the ln-plot. The *Eyring* equation (Equation 5) relates a reaction's rate constant with the *Gibbs* energy of activation $\Delta G^{\ddagger}$.

$$k = \frac{k_B T}{h}\, e^{-\frac{\Delta G^{\ddagger}}{RT}} \qquad \text{(Equation 5)}$$

with

k_B = *Boltzmann* constant (1.381×10^{-23} J K^{-1})

T = temperature in K

h = *Planck* constant (6.626×10^{-34} J s)

R = universal gas constant (8.314 J mol^{-1}K^{-1})

k = rate constant for the respective isomerization direction ($k_{\text{A-1}\rightarrow\text{C-1}}$ or $k_{\text{C-1}\rightarrow\text{A-1}}$)

The rearranged equation (Equation 6) can be used to directly calculate the *Gibbs* energies of activation $\Delta G^{\ddagger}$ for the thermal double bond isomerization processes from the respective rate constants.

$$\Delta G^{\ddagger} = -RT \ln\left(\frac{kh}{k_B T}\right) \qquad \text{(Equation 6)}$$

The free enthalpy difference ΔG between isomers **A-1** and **C-1** can be calculated from the isomeric ratio at equilibrium according to Equation 7:

$$\Delta G = -RT \ln K = -RT \ln \frac{[\mathbf{C\text{-}1}]_{eq}}{[\mathbf{A\text{-}1}]_{eq}} \qquad \text{(Equation 7)}$$

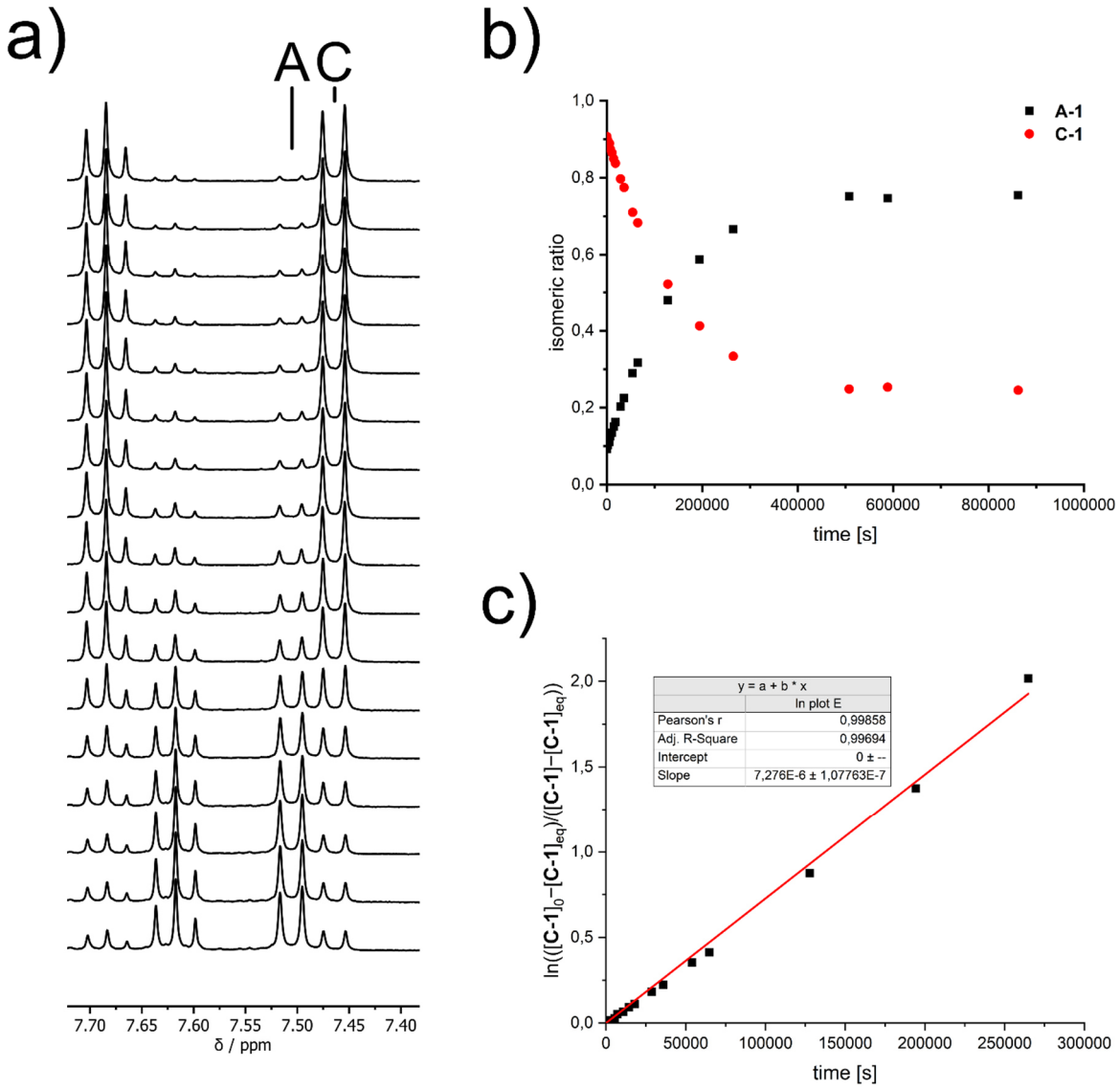

Figure 67 Kinetic analysis of thermal **C-1** to **A-1** double bond isomerization at 80 °C in $(CDCl_2)_2$. **a)** Excerpt of the aromatic region of ^{1}H NMR (400 MHz, 25 °C, $(CDCl_2)_2$) spectra recorded in irregular intervals during double bond isomerization of **C-1**. Proton signals that were used for integration are indicated. **b)** Isomeric ratios of **A-1** and **C-1** changing over time. After heating the mixture at 80 °C for extended time, a constant equilibrium ratio of 75% **A-1** and 25% **C-1** was reached. **c)** First order kinetic analysis taking into account the dynamic equilibrium gives a linear relation. The slope *m* of the linear fit is 7.3×10^{-6} s^{-1}, which can be used to calculate the rate constants for both isomerization directions. The corresponding *Gibbs* energies of activation $\Delta G^{\ddagger}$ are 30.0 kcal mol^{-1} for **A-1** to **C-1** and 29.2 kcal mol^{-1} for **C-1** to **A-1** thermal double bond isomerization at 80 °C. *Adapted from the supporting information to ref.* [8].

The slope *m* of the linear fit for the thermal **C-1** to **A-1** conversion is 7.3×10^{-6} s^{-1}, which contains the rate constants for both forward and backward isomerization. The corresponding

Gibbs energies of activation $\Delta G^{\ddagger}$ are 30.0 kcal mol^{-1} for **A-1** to **C-1** isomerization, and 29.2 kcal mol^{-1} for **C-1** to **A-1** isomerization at 80 °C in $(CDCl_2)_2$.

In thermal equilibrium the isomeric ratio is 75% **A-1** and 25% **C-1**, which corresponds to a free enthalpy difference $\Delta G = 0.8$ kcal mol^{-1} at 80 °C, with **A-1** being the thermodynamically more stable isomer.

Kinetic analysis of the analogous thermal **C-2** to **A-2** isomerization at 80 °C in $(CDCl_2)_2$ was performed in the same way. However, there was a short "lag" or induction period at the start of the kinetic analysis and the resulting graph had a slightly sigmoidal shape (see Figure 68). Therefore, three independent repeat experiments were performed (Figure 69 – Figure 71). In all cases, a similar behavior was observed. The resulting rate constants and activation energies, as well as the averaged values, are listed in Table 8.

The average slope *m* of the linear fit for the thermal **C-2** to **A-2** isomerization at 80 °C is 6.9×10^{-5} s^{-1}. This contains the rate constants for both forward and backward isomerization. The corresponding *Gibbs* energies of activation $\Delta G^{\ddagger}$ are 28.4 kcal mol^{-1} for **A-2** to **C-2** isomerization, and 27.7 kcal mol^{-1} for **C-2** to **A-2** isomerization at 80 °C. The thermal isomerization process was significantly slowed down in the last two repeat experiments. This seems to be related to the residual water content in the sample, as a slow-down was observed for samples with high water content (due to extended storage times in the freezer). An acceleration of the isomerization was observed when the water content decreased over the course of the heating experiment.

In thermal equilibrium the isomer ratio is 74% **A-2** and 26% **C-2**, which corresponds to a free enthalpy difference $\Delta G = 0.8$ kcal mol^{-1} at 80 °C, with **A-2** being the thermodynamically more stable isomer.

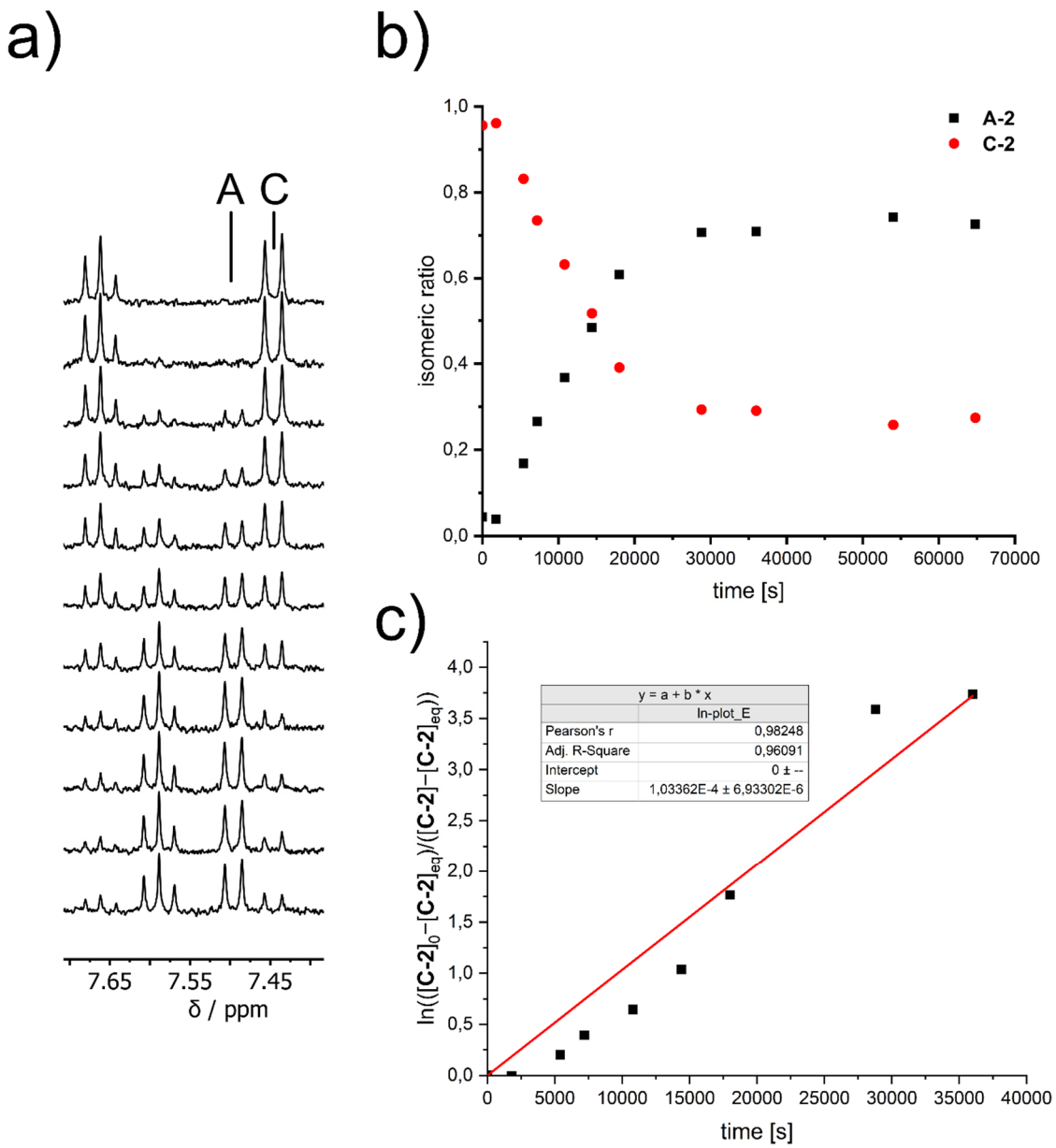

Figure 68 Kinetic analysis of thermal **C-2** to **A-2** double bond isomerization at 80 °C in $(CDCl_2)_2$. **a)** Excerpt of the aromatic region of ^{1}H NMR (400 MHz, 25 °C, $(CDCl_2)_2$) spectra recorded in irregular intervals during double bond isomerization of **C-2**. Proton signals that were used for integration are indicated. **b)** Isomeric ratios of **A-2** and **C-2** changing over time. After heating the mixture at 80 °C for extended time, a constant equilibrium ratio of 73% **A-2** and 27% **C-2** was reached. **c)** First order kinetic analysis taking into account the dynamic equilibrium gives a linear relation. The slope *m* of the linear fit is 1.0×10^{-4} s^{-1}. The corresponding *Gibbs* energies of activation $\Delta G^{\ddagger}$ are 28.1 kcal mol^{-1} for **A-2** to **C-2** and 27.4 kcal mol^{-1} for **C-2** to **A-2** thermal double bond isomerization at 80 °C. *Adapted from the supporting information to ref.* [8].

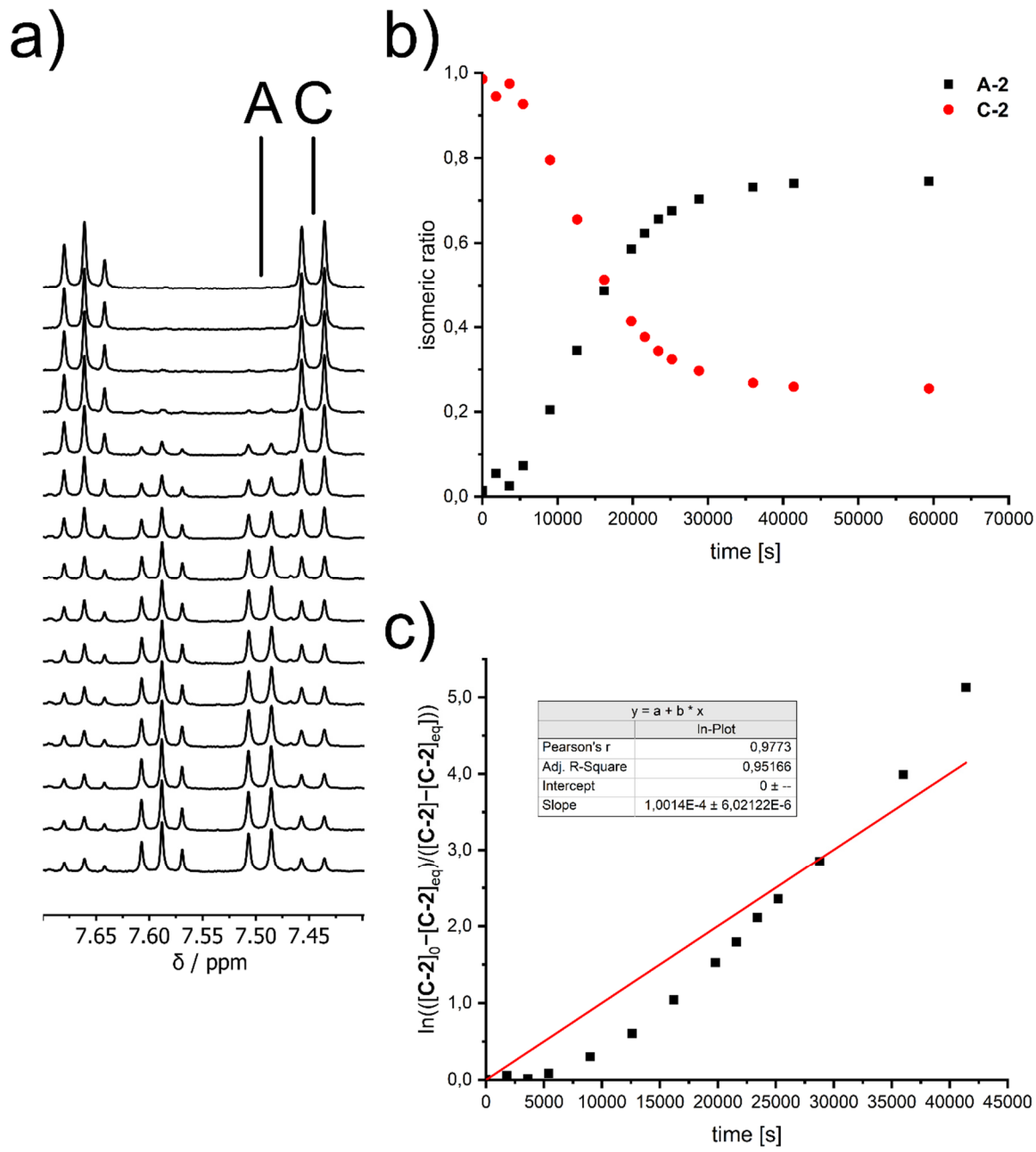

Figure 69 Repeat experiment of thermal **C-2** to **A-2** double bond isomerization at 80 °C in $(CDCl_2)_2$ and kinetic analysis. a) Excerpt of the aromatic region of ^{1}H NMR (400 MHz, 23 °C, $(CDCl_2)_2$) spectra recorded in irregular intervals during double bond isomerization of **C-2**. Proton signals that were used for integration are indicated. b) Isomeric ratios of **A-2** and **C-2** changing over time. After heating the mixture at 80 °C for extended time, a constant equilibrium ratio of 75% **A-2** and 25% **C-2** was reached. c) First order kinetic analysis taking into account the dynamic equilibrium gives a linear relation. The slope *m* of the linear fit is 1.0×10^{-4} s^{-1}. The corresponding *Gibbs* energies of activation $\Delta G^{\ddagger}$ are 28.2 kcal mol^{-1} for **A-2** to **C-2** and 27.4 kcal mol^{-1} for **C-2** to **A-2** thermal double bond isomerization at 80 °C. *Adapted from the supporting information to ref.* [8].

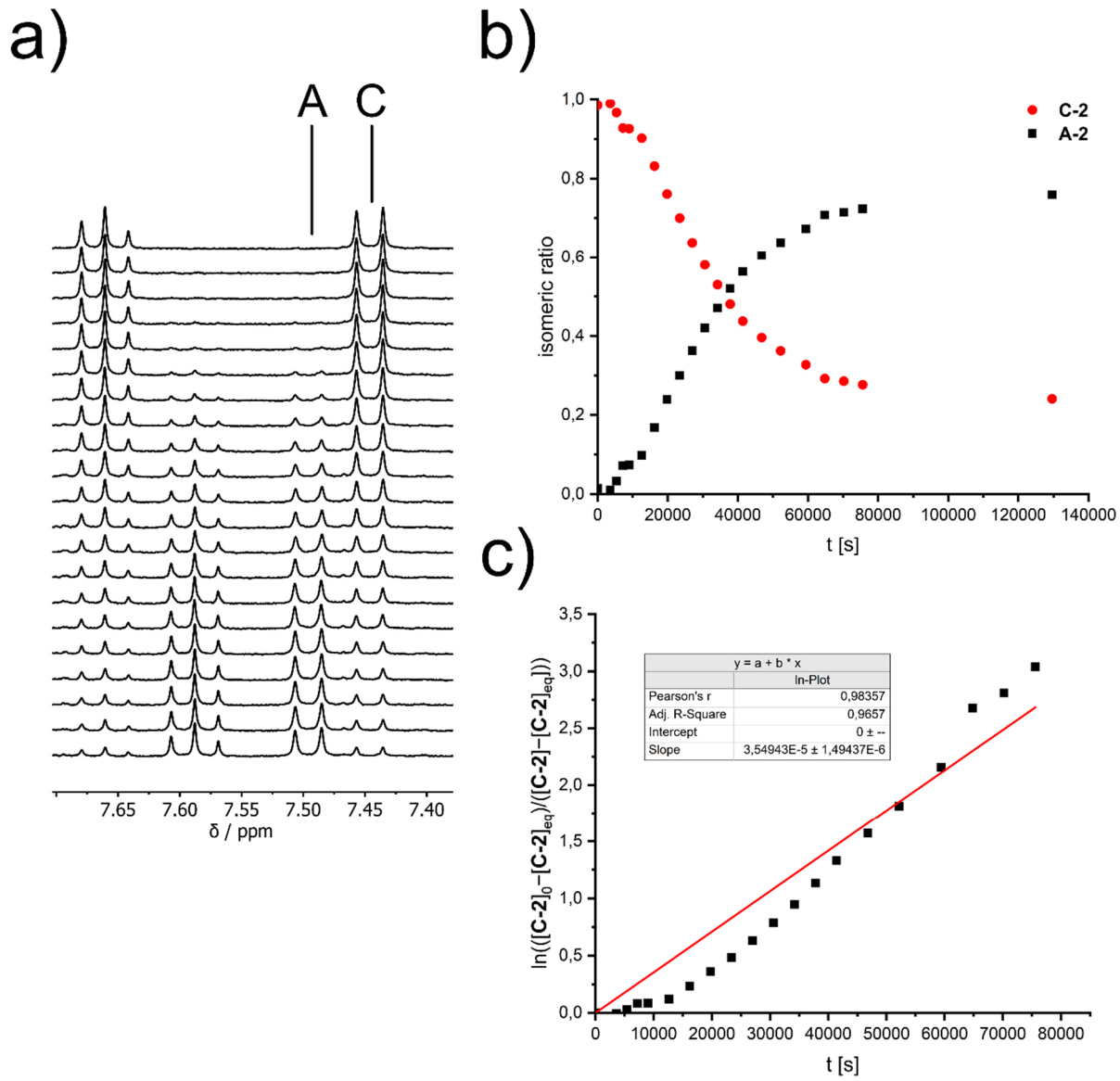

Figure 70 Repeat experiment of thermal **C-2** to **A-2** double bond isomerization at 80 °C in $(CDCl_2)_2$ and kinetic analysis. a) Excerpt of the aromatic region of ^{1}H NMR (400 MHz, 23 °C, $(CDCl_2)_2$) spectra recorded in irregular intervals during double bond isomerization of **C-2**. Proton signals that were used for integration are indicated. b) Isomeric ratios of **A-2** and **C-2** changing over time. After heating the mixture at 80 °C for extended time, a constant equilibrium ratio of 74% **A-2** and 26% **C-2** was reached. c) First order kinetic analysis taking into account the dynamic equilibrium gives a linear relation. The slope *m* of the linear fit is 3.5×10^{-5} s^{-1}. The corresponding *Gibbs* energies of activation $\Delta G^{\ddagger}$ are 28.9 kcal mol^{-1} for **A-2** to **C-2** and 28.2 kcal mol^{-1} for **C-2** to **A-2** thermal double bond isomerization at 80 °C. *Adapted from the supporting information to ref.* [8].

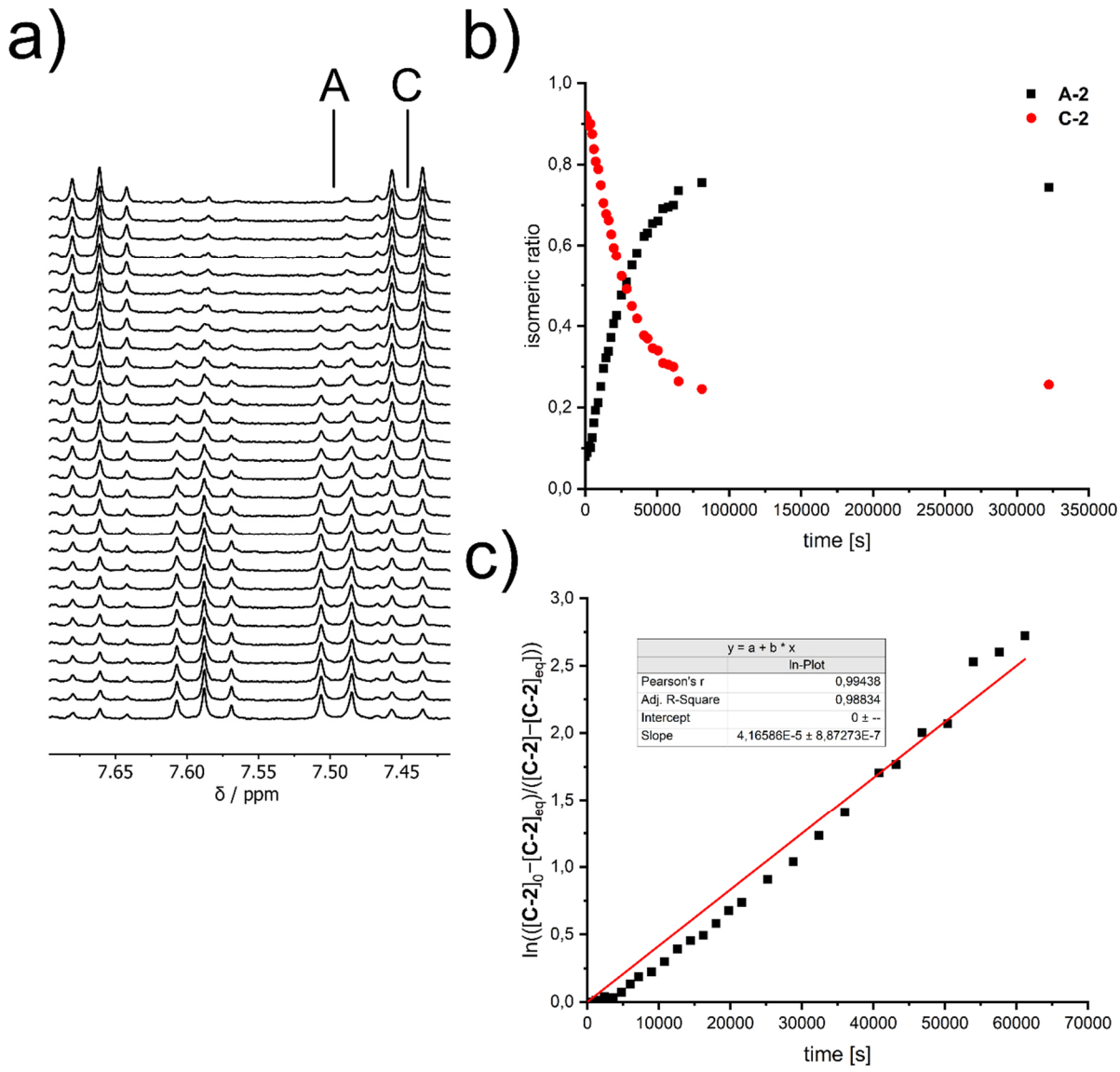

Figure 71 Repeat experiment of thermal **C-2** to **A-2** double bond isomerization at 80 °C in $(CDCl_2)_2$ and kinetic analysis. a) Excerpt of the aromatic region of ^{1}H NMR (400 MHz, 23 °C, $(CDCl_2)_2$) spectra recorded in irregular intervals during double bond isomerization of **C-2**. Proton signals that were used for integration are indicated. b) Isomeric ratios of **A-2** and **C-2** changing over time. After heating the mixture at 80 °C for extended time, a constant equilibrium ratio of 74% **A-2** and 26% **C-2** was reached. c) First order kinetic analysis taking into account the dynamic equilibrium gives a linear relation. The slope *m* of the linear fit is 4.2×10^{-5} s^{-1}. The corresponding *Gibbs* energies of activation $\Delta G^{\ddagger}$ are 28.8 kcal mol^{-1} for **A-2** to **C-2** and 28.0 kcal mol^{-1} for **C-2** to **A-2** thermal double bond isomerization at 80 °C. *Adapted from the supporting information to ref.* [8].

Table 8 Summary of results obtained from **C-2** to **A-2** isomerization experiments in $(CDCl_2)_2$ at 80 °C. *Adapted from the supporting information to ref.* [8]..

Entry	Slope m / s^{-1}	Equilibrium ratio **A-2**:**C-2**	ΔG / kcal mol^{-1}	$\Delta G^{\ddagger}$ A→C / kcal mol^{-1}	$\Delta G^{\ddagger}$ C→A / kcal mol^{-1}
1	1.0×10^{-4}	73:27	0.7	28.1	27.4
2	1.0×10^{-4}	75:25	0.8	28.2	27.4
3	3.5×10^{-5}	74:26	0.8	28.9	28.2
4	4.2×10^{-5}	74:26	0.8	28.8	28.0
average	6.9×10^{-5}	74:26	(0.8±0.1)	(28.4±0.4)	(27.7±0.4)

3.7 Motor Function Elucidation of 1

3.7.1 Comparison Between Ambient and Low Temperature ^{1}H NMR Spectra

Variable temperature NMR experiments were performed on **A-1** and **C-1** in order to observe possible changes in the chemical shift of certain signals. The resulting spectra are shown in Figure 72 and Figure 73. Upon stepwise cooling, a significant broadening of aliphatic signals and, to a lesser degree, of aromatic signals was observed. However, there was no significant change in chemical shifts, making it easy to compare ambient temperature and low-temperature spectra.

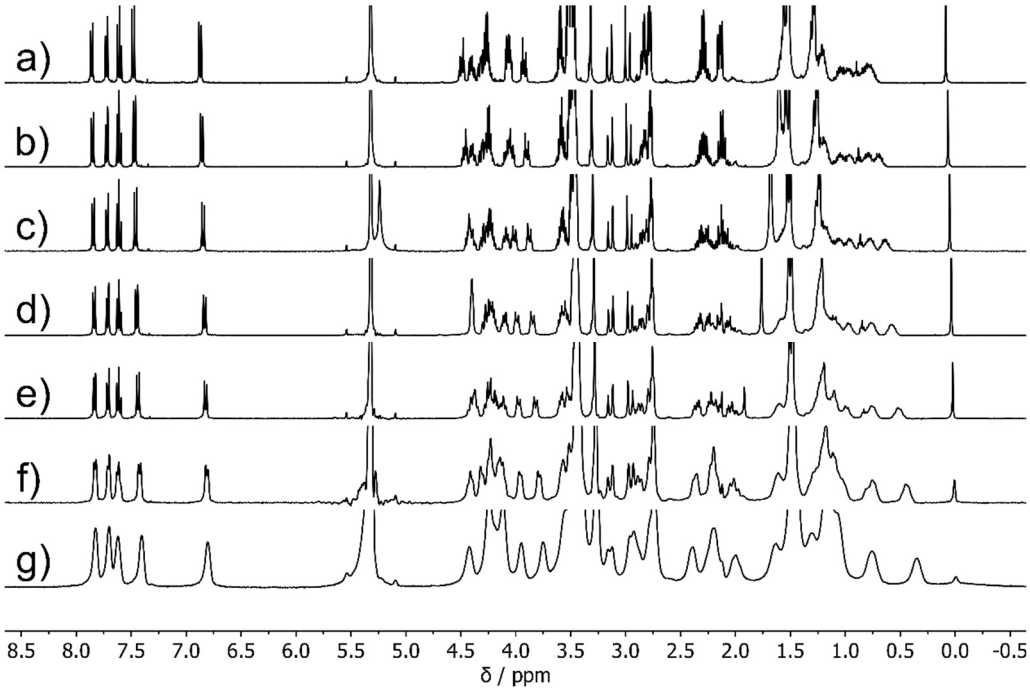

Figure 72 Variable temperature ^{1}H NMR (400 MHz, CD_2Cl_2:CS_2, 4:1) spectra of a solution of racemic **A-1** acquired at **a)** 25 °C **b)** 0 °C **c)** −20 °C **d)** −40 °C **e)** −60 °C **f)** −80 °C **g)** −105 °C. Spectra are clipped vertically for clarity. *Adapted from the supporting information to ref.* [8].

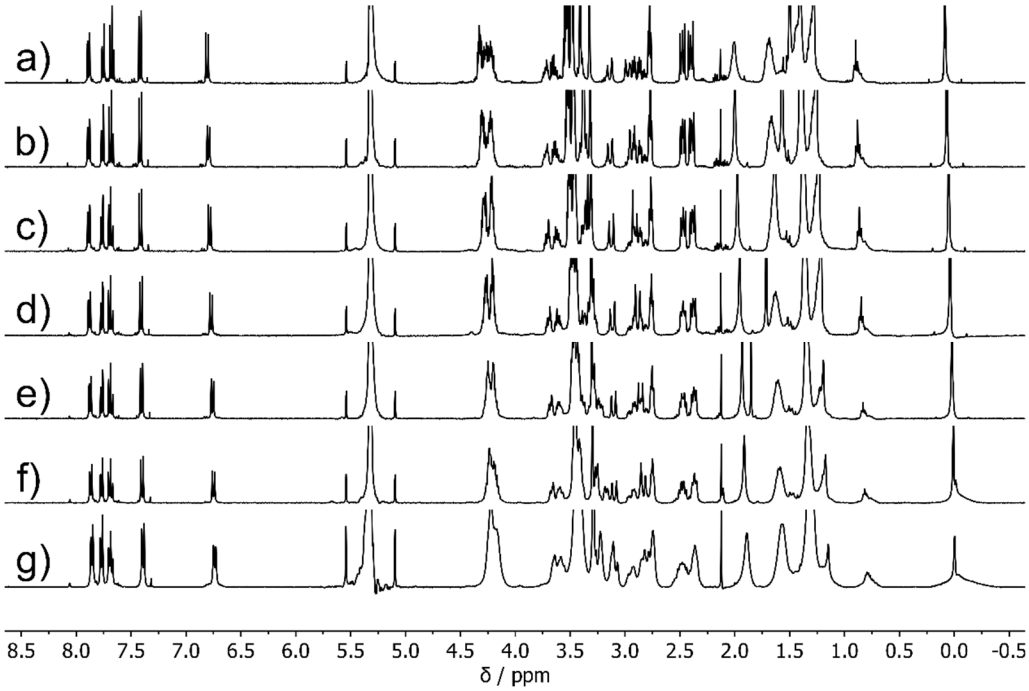

Figure 73 Variable temperature ^{1}H NMR (400 MHz, CD_2Cl_2:CS_2, 4:1) spectra of a solution of racemic **C-1** acquired at **a)** 25 °C **b)** 0 °C **c)** −20 °C **d)** −40 °C **e)** −60 °C **f)** −80 °C **g)** −105 °C. Spectra are clipped vertically for clarity. *Adapted from the supporting information to ref.* [8].

3.7.2 Irradiation of Isomer A-1

In order to investigate potential rotation unidirectionality, irradiation experiments at low temperature were performed inside an NMR spectrometer. This allowed to monitor the formation of photoproducts while at the same time providing structural and quantitative information. This method is especially valuable for the observation of photogenerated metastable intermediates, which undergo fast thermal helix inversion to the respective stable isomers.[95-96] First, a sample of racemic **A-1** in CD_2Cl_2:CS_2 (4:1) was cooled to −105 °C. The sample was then irradiated with 405 nm light *via* a glass fiber coupled to an LED and ^{1}H NMR spectra were recorded in regular time intervals (see Figure 74). Over time, the evolution of a new set of signals was observed and assigned to the **B-1** isomer. The sample was then removed from the spectrometer, allowed to warm to ambient temperature and cooled to −105 °C again. Another ^{1}H NMR spectrum was measured, showing the **B-1** signals had disappeared, while a new set of signals corresponding to the **C-1** isomer had appeared proportionally (see also Figure 79). This observation is in agreement with a thermal isomerization step from **B-1** to **C-1**.

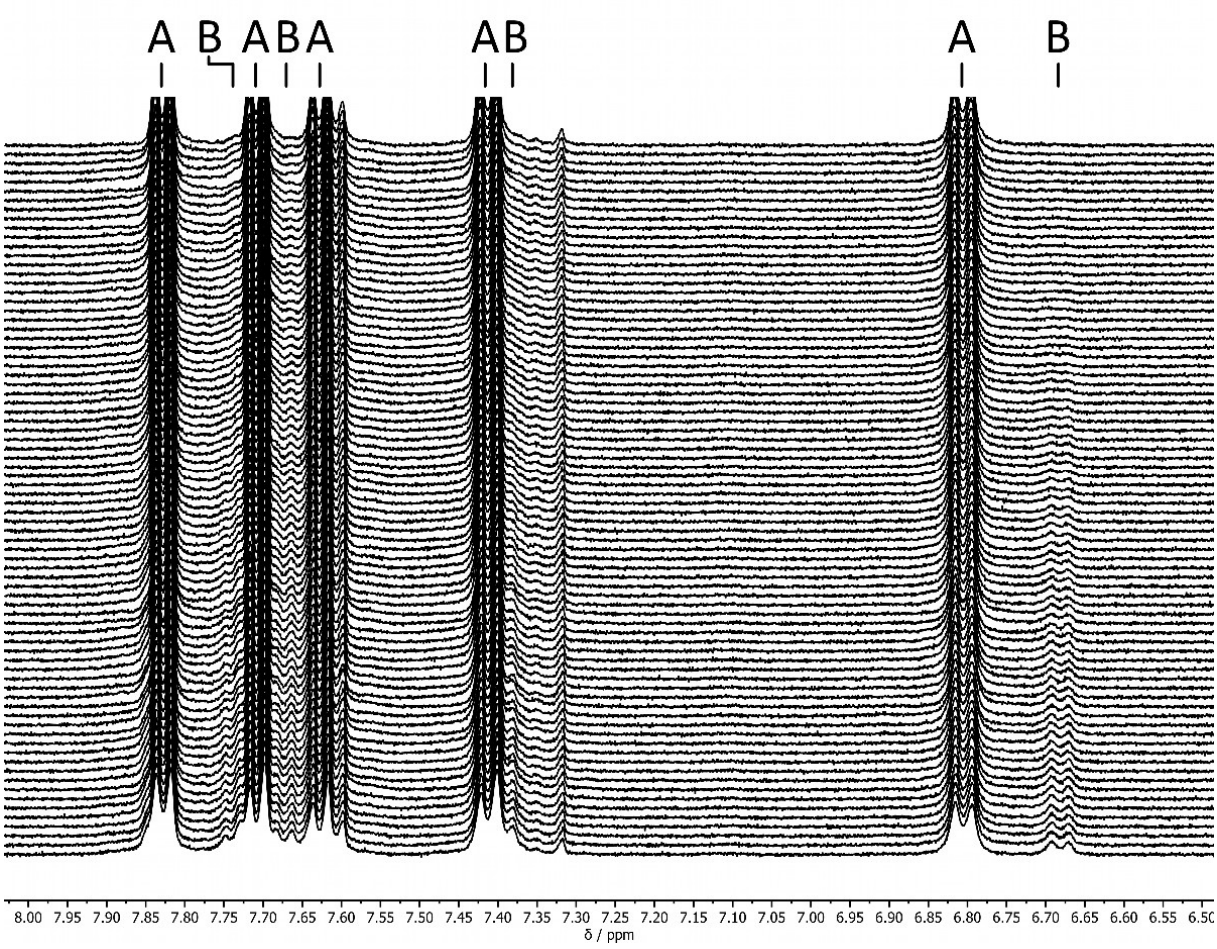

Figure 74 ^{1}H NMR (400 MHz, CD_2Cl_2:CS_2 4:1, −105 °C) spectra acquired during high power *in situ* LED irradiation (405 nm) starting from racemic **A-1** (top spectrum). Spectra were recorded in 25 s intervals. A new set of signals assigned to the **B-1** isomer emerged with increasing irradiation time. *Adapted from the supporting information to ref.* [8].

3.7.3 Thermal Conversion of B-1 at Low Temperatures

A sample of racemic **A-1** in CD_2Cl_2:CS_2 (4:1) was enriched in **B-1** by *in situ* irradiation with 405 nm light at –105 °C inside an NMR spectrometer. After the *pss* had been reached, the temperature was increased to –80 °C and ^{1}H NMR spectra were recorded in regular time intervals to monitor the thermal isomerization progress in the dark.

Assuming a first order irreversible process, the kinetics of thermal helix isomerization from **B-1** to **C-1** can be described by the following equation:

$$\mathbf{B\text{-}1} \xrightarrow{k} \mathbf{C\text{-}1} \qquad \text{(Equation 8)}$$

with k being the rate constant. The rate law is

$$\frac{d[\mathbf{B\text{-}1}]}{dt} = -k[\mathbf{B\text{-}1}] \qquad \text{(Equation 9)}$$

Integration of Equation S9 gives

$$\ln[\mathbf{B\text{-}1}] = -kt + \ln[\mathbf{B\text{-}1}]_0 \qquad \text{(Equation 10)}$$

and can be written as

$$\ln\left(\frac{[\mathbf{B\text{-}1}]_0}{[\mathbf{B\text{-}1}]}\right) = kt \qquad \text{(Equation 11)}$$

with $[\mathbf{B\text{-}1}]_0$ being the initial concentration of **B-1** and [**B-1**] being the concentration of **B-1** at time t. By plotting $\ln([\mathbf{B\text{-}1}]_0/[\mathbf{B\text{-}1}])$ versus the time t, the rate constant k can be obtained as the slope of the linear fit. The *Gibbs* energy of activation $\Delta G^{\ddagger}$ for the thermal helix inversion can be calculated from the rate constant using the rearranged *Eyring* equation (see Equation 6).

The half-life $\tau_{1/2}$ of a first order reaction can be expressed as

$$\tau_{1/2} = \frac{\ln 2}{k} \qquad \text{(Equation 12)}$$

The first order rate constant for the thermal decay of **B-1** is $k_{\text{B-1}\rightarrow\text{C-1}} = 4.2 \times 10^{-4}\ \text{s}^{-1}$ at −80 °C. Using Equation 6 and Equation 12, this corresponds to a *Gibbs* energy of activation $\Delta G^{\ddagger} = 14.1\ \text{kcal mol}^{-1}$ and a half-life of 28 min at −80 °C, respectively.

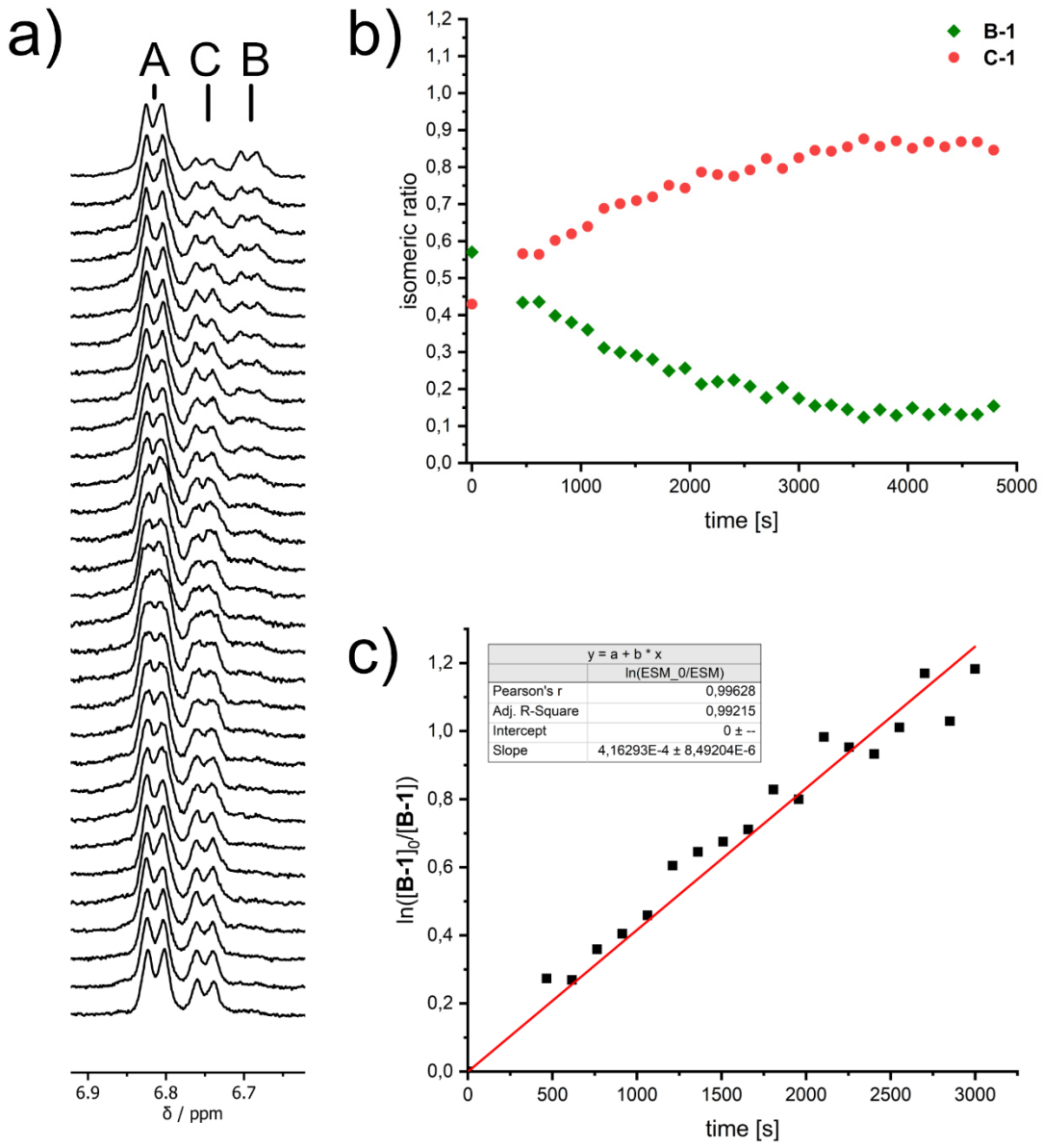

Figure 75 Kinetic analysis of the thermal **B-1** to **C-1** isomerization process at −80 °C. **a)** Indicative region of ^{1}H NMR (400 MHz, CD_2Cl_2:CS_2 4:1, −80 °C) spectra recorded during thermal decay of **B-1** in the dark. Starting from racemic **A-1**, **B-1** was accumulated by *in situ* irradiation with 405 nm at −105 °C. The thermal decay of the metastable **B-1** isomer was monitored at −80 °C in the dark (starting from the top spectrum). The time difference between the top spectrum and the second spectrum is 7:46 min. The following spectra were recorded in 2:29 min intervals. **b)** Thermal decay of **B-1** in the dark at −80°C over time. Isomeric ratios were obtained by integration of indicative ^{1}H NMR signals. **c)** ln plot of thermal **B-1** decay at −80°C in the dark. The slope is 4.2×10^{-4} s^{-1}, which corresponds to a *Gibbs* energy of activation $\Delta G^{\ddagger} = 14.1$ kcal mol^{-1} for the **B-1**- to **C-1** helix inversion at −80°C. Small amounts of **C-1** are already present in the first spectrum, as the isomerization process started during the warming-up to −80 °C and the time necessary for setting of instrument parameters. *Adapted from the supporting information to ref.* [8].

3.7.4 Irradiation of Isomer C-1

In an analogous experiment, a sample of racemic **C-1** in CD_2Cl_2:CS_2 (4:1) was cooled to −105 °C inside an NMR spectrometer. The sample was irradiated with 450 nm light *via* a glass fiber coupled to an LED and ^{1}H NMR spectra were recorded in regular time intervals. Over time, the **C-1** signal set disappeared and the simultaneous appearance of a new set of signals, assigned to the **D-1** isomer, was observed. Near quantitative conversion of **C-1** to **D-1** was achieved. Again, the sample was removed from the spectrometer, allowed to warm to ambient temperature and cooled to −105 °C again. Another ^{1}H NMR spectrum was measured, showing full conversion of **D-1** to **A-1**. This is in agreement with a thermal helix isomerization step and formally closes the motor rotation cycle (see Figure 79 for full motor rotation step sequence).

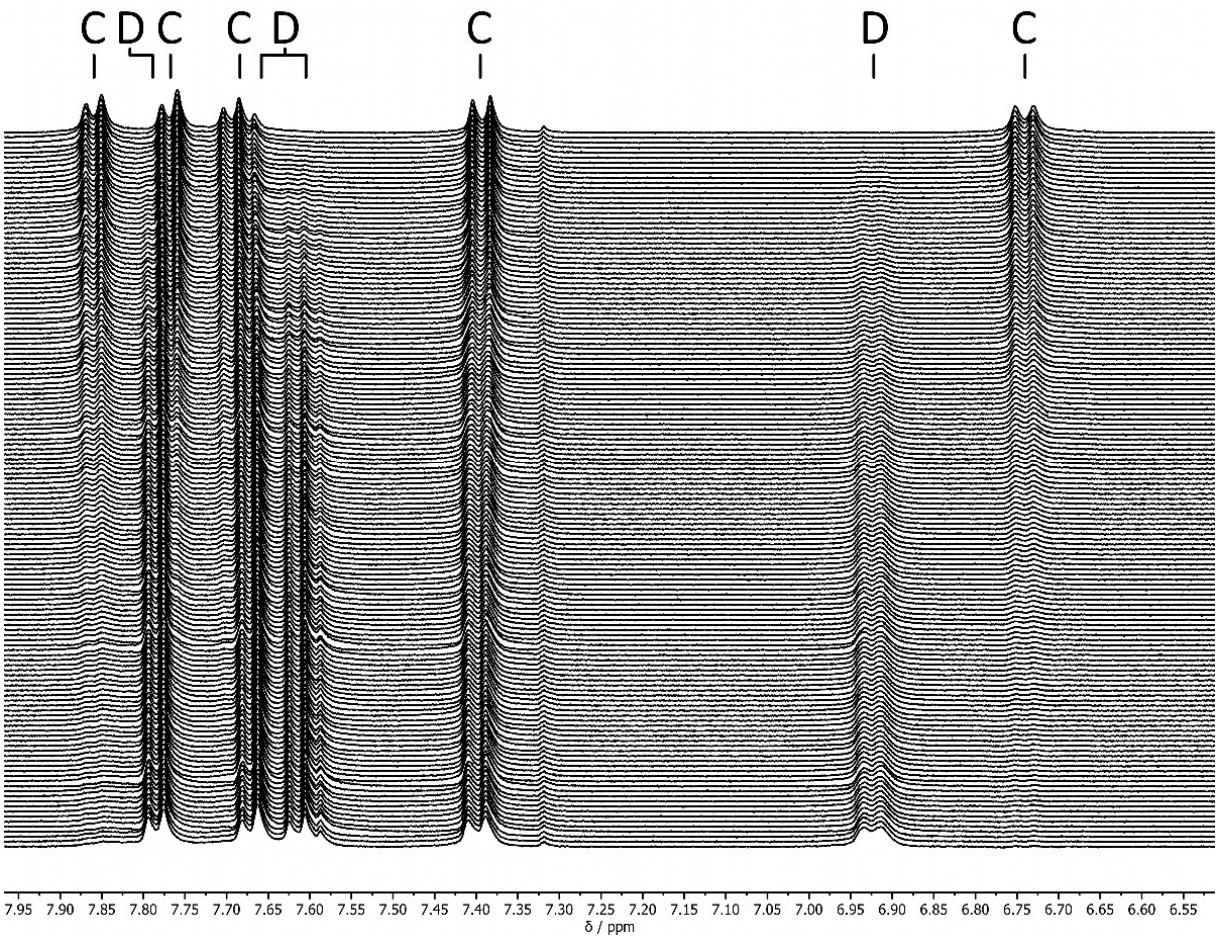

Figure 76 ^{1}H NMR (400 MHz, CD_2Cl_2:CS_2 4:1, −105 °C) spectra acquired during high power *in situ* LED irradiation (450 nm) starting from racemic **C-1** (top spectrum). Spectra were recorded in 35 s intervals. A new set of signals assigned to the **D-1** isomer emerged with increasing irradiation time. *Adapted from the supporting information to ref.* [8].

3.7.5 Thermal Conversion of D-1 at Low Temperatures

A sample of racemic **C-1** in CD_2Cl_2 was enriched in **D-1** by *in situ* irradiation with 450 nm light at –80 °C inside an NMR spectrometer. After the *pss* had been reached, the temperature was increased to –50 °C and ^{1}H NMR spectra were recorded in regular time intervals to monitor the thermal isomerization progress in the dark.

Assuming a first order irreversible process for the thermal helix inversion from **D-1** to **A-1**, the kinetics can be analyzed in an analogous way as described above for the thermal **B-1** to **C-1** isomerization. The rate constant for the thermal decay of **D-1** can be obtained from the linear plot and is $k_{\text{D-1}\rightarrow\text{A-1}} = 2.6 \times 10{-}4\ \text{s}^{-1}$. Using Equation 6 and Equation 12, this equals a *Gibbs* energy of activation $\Delta G^{\ddagger} = 16.6$ kcal mol^{-1} and a thermal half-life of 44 min for the **D-1** to **A-1** helix inversion at −50 °C, respectively.

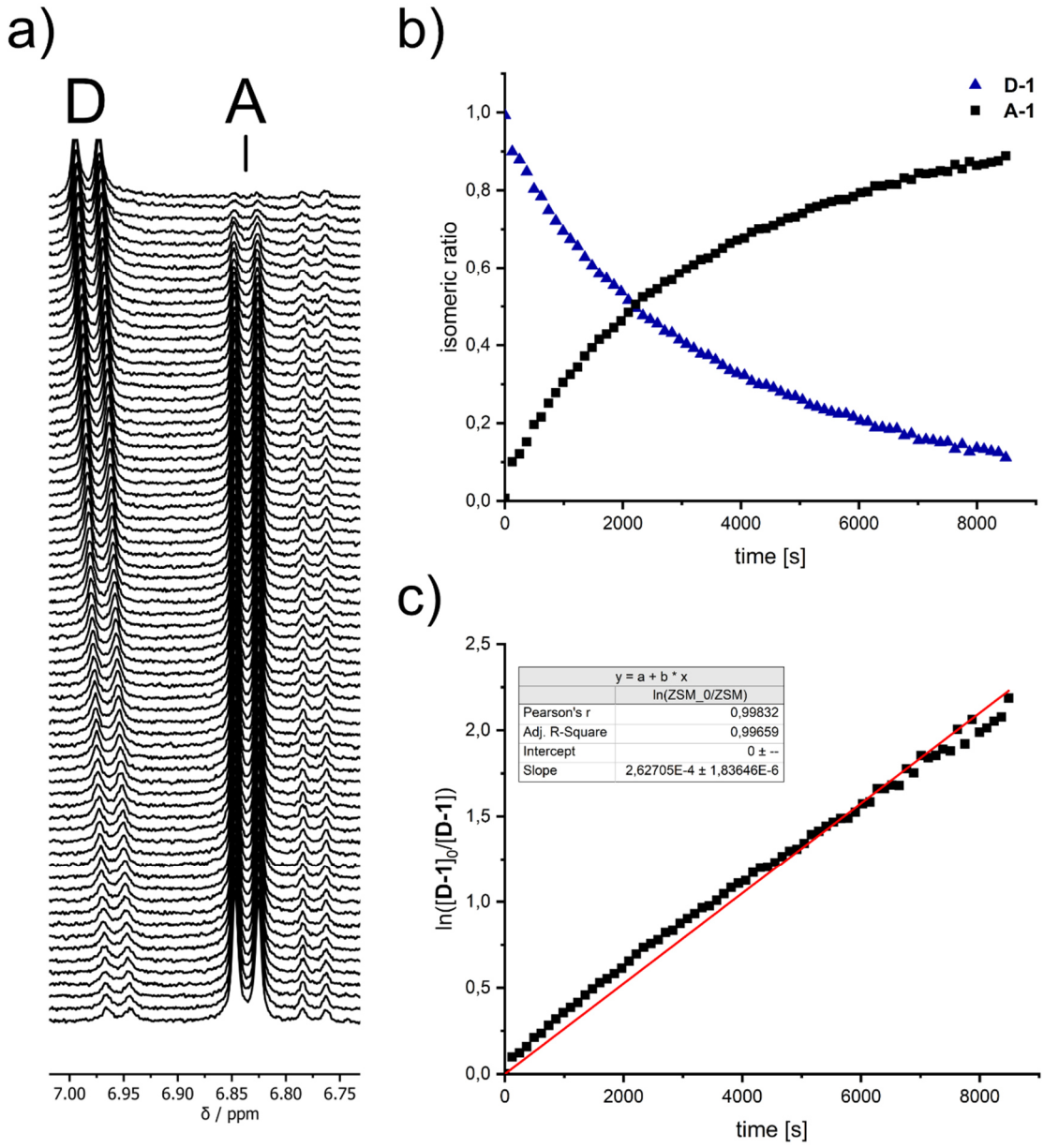

Figure 77 Kinetic analysis of the thermal **D-1** to **A-1** isomerization process at −50 °C. **a)** Excerpt from ^{1}H NMR spectra (400 MHz, CD_2Cl_2, −50°C) recorded during thermal isomerization of **D-1** to **A-1** at −50°C in the dark (top to bottom). The spectra were recorded in intervals of 123 s. The signal at approx. 6.78 ppm is due to a small amount of aromatic impurity. **b)** Thermal decay of **D-1** at −50°C in the dark. Isomeric ratios were determined by integration of indicative ^{1}H NMR signals. **c)** ln plot of thermal **D-1** decay at −50°C in the dark. The slope is 2.6×10^{-4} s^{-1}, which corresponds to a *Gibbs* energy of activation $\Delta G^{\ddagger} = 16.6$ kcal mol^{-1} for the **D-1**- to **A-1** thermal helix inversion. *Adapted from the supporting information to ref.* [8].

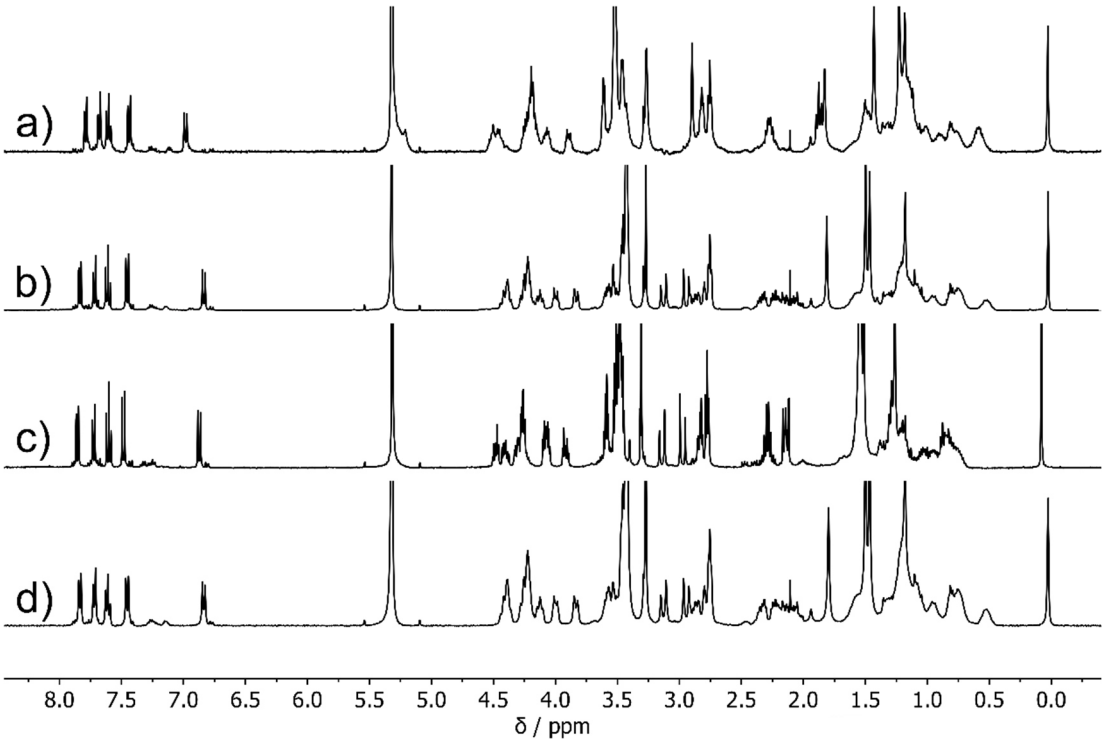

Figure 78 Thermal isomerization of **D-1** at low temperature (^{1}H NMR, 400 MHz, CD_2Cl_2). In order to discern, whether **A-1** is the direct thermal product of **D-1** isomerization, the thermal isomerization of **D-1** at −50 °C was observed until completion. The sample was then warmed to 25 °C, to allow for hypothetic further isomerization processes. In the final step, the sample was re-cooled to −50 °C. Differences in chemical shifts before and after the annealing step would indicate an additional intermediate in the process of **D-1** to **A-1** isomerization. **a)** Solution enriched in **D-1**, prior to thermal decay at −50 °C in the dark. **b)** Isomer **D-1** is fully converted to **A-1** after 215 min at −50 °C. **c)** The same solution after warming to 25 °C. **d)** After re-cooling of the solution to −50 °C. No shift of signals is noticeable between b) and d), confirming that **D-1** is thermally converted to **A-1** without any observable intermediate at −50 °C. Spectra are clipped vertically for clarity. *Adapted from the supporting information to ref.* [8].

3.7.6 Sequence of Motor Operation Steps

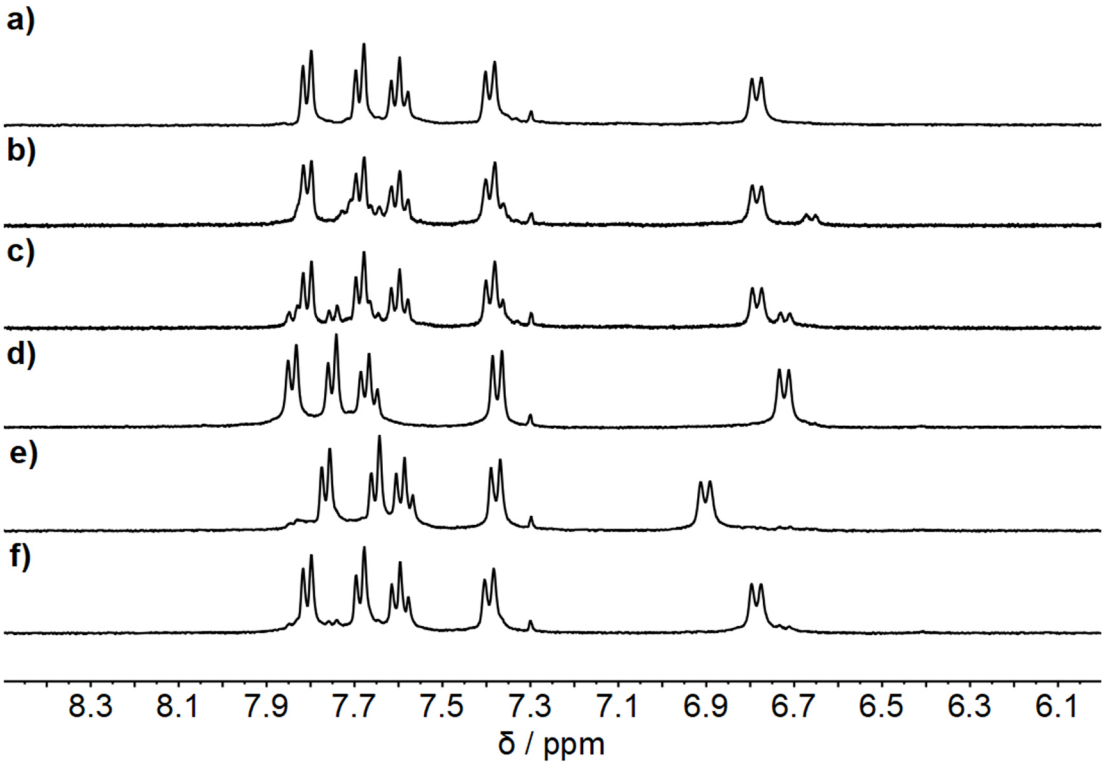

Figure 79 ^{1}H NMR spectra (400 MHz, −105 °C, CD_2Cl_2:CS_2 4:1) recorded during low-temperature irradiation experiments of motor **1**; only the aromatic region is shown for clarity. **a)** Pure racemic **A-1**. **b)** *pss* (74% **A-1**, 26% **B-1**) reached after *in situ* irradiation of **A-1** with 405 nm light. A new set of signals attributed to **B-1** appeared. **c)** After thermal annealing to 23 °C in the dark, **B-1** disappeared and the proportional appearance of **C-1** was observed. **d)** Pure racemic **C-1**. **e)** *pss* (95% **D-1**, 5% **C-1**) reached after *in situ* irradiation of **C-1** with 450 nm light. A new set of signals appeared, which is attributed to **D-1**. **f)** After thermal annealing at 23 °C in the dark **D-1** fully converted to **A-1**. *Adapted from the supporting information to ref.* [8].

3.8 Switching Behavior of HTI 2

3.8.1 Photoswitching

In order to investigate possible motor rotation of compound **2**, low temperature ^{1}H NMR experiments were performed. However, when a sample of **A-2** in CD_2Cl_2 was irradiated with 405 nm or 450 nm light at −80 °C, no change in NMR signals was observed. When the temperature was raised to −30 °C, the formation of a set of signals corresponding to **C-2** was observed upon irradiation with 405 nm light. Assuming a similar barrier for thermal helix inversion (compared to **B-1**), the expected metastable **B-2** intermediate cannot be observed at −30 °C. Instead, photogenerated **B-2** is likely rapidly converted to stable **C-2** *via* thermal helix inversion. After substantial accumulation of **C-2**, the sample was irradiated with 450 nm light. The signals associated with **C-2** decreased and the formation of a new set of signals, assigned to **D-2** was observed. Upon warming the sample to 23 °C, no noticeable decay of the **D-2** signals took place. As **D-2** was found to be kinetically inert at ambient temperature, an additional irradiation experiment was performed at 23 °C. A sample of pure racemic **A-2** in CD_2Cl_2 was irradiated externally with 405 nm light and ^{1}H NMR spectra were measured in irregular intervals. Over the course of the irradiation experiment, the formation of **C-2** was observed (see Figure 80). After some time, **D-2** started to form in small amounts. When **A-2** was completely consumed, the sample was irradiated with 450 nm light. A *pss* enriched in **D-2** (and containing small amounts of **C-2**) was obtained, but no **A-2** could be regenerated.

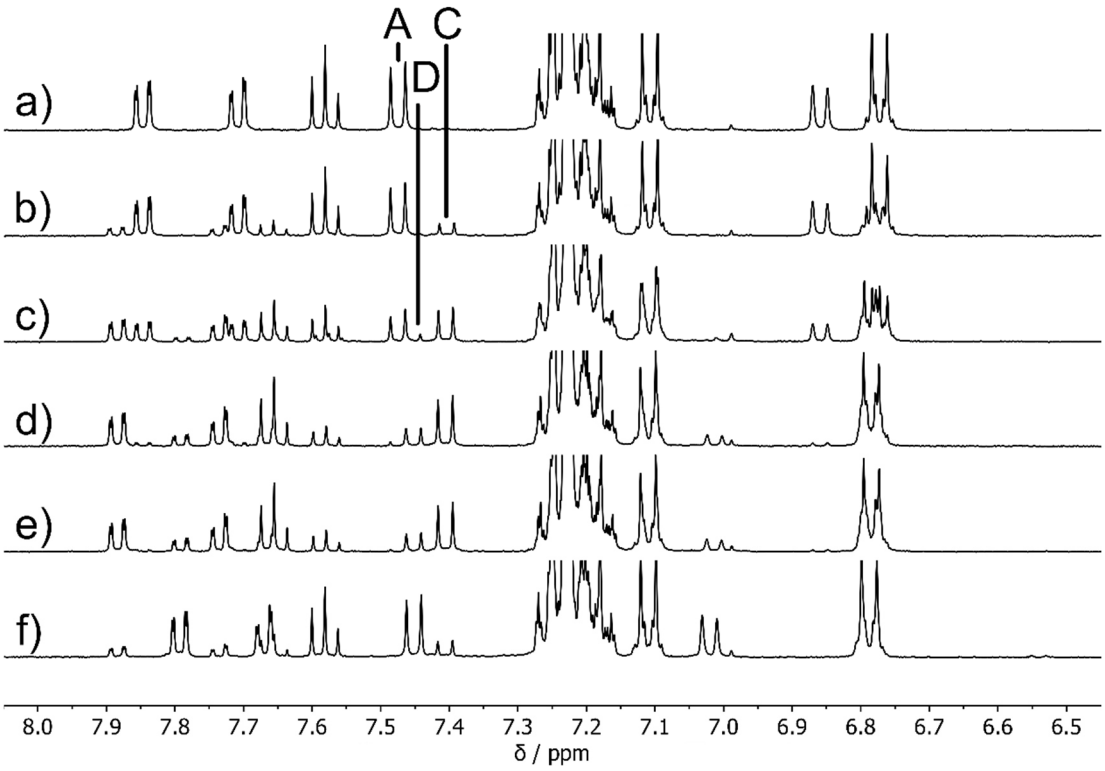

Figure 80 ^{1}H-NMR (400 MHz, CD_2Cl_2, 25 °C) spectra; only the aromatic region is shown and spectra are clipped vertically for clarity. **a)** Racemic **A-2**. **b-e)** Spectra recorded during external irradiation with 405 nm light. **A-2** was completely converted to **C-2** and after 20 min of irradiation a *pss* composed of 71% **C-2** and 29% **D-2** was established. **f)** After 5 min of external irradiation with 450 nm light, **D-2** could be accumulated and the isomer ratio was 76% **D-2** and 24% **C-2**. *Note*: Data were acquired by *Verena Josef*.

To ensure comparability between spectra of **D-1** and **D-2**, a sample enriched in **D-2** in CD_2Cl_2 was prepared and ^{1}H NMR spectra at various temperatures were recorded (see Figure 81). Upon cooling, broadening of aliphatic signals was observed, but only negligible changes in chemical shifts occurred.

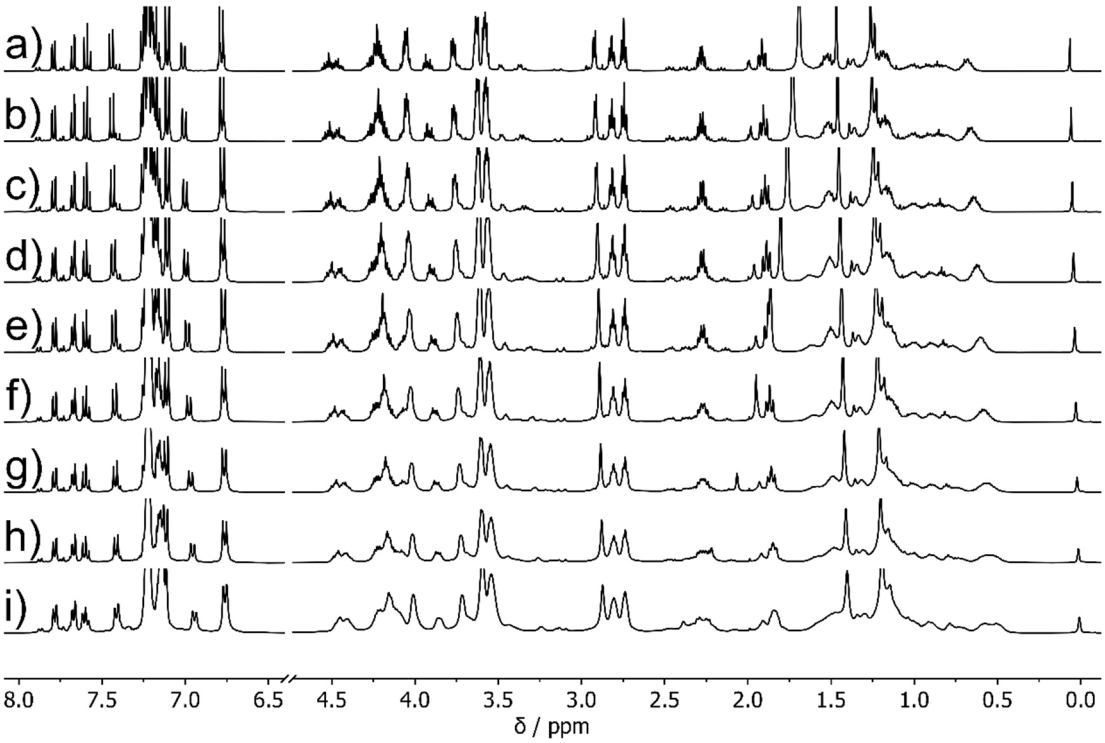

Figure 81 Variable temperature ^{1}H NMR (400 MHz, CD_2Cl_2) spectra of a solution enriched in racemic **D-2** acquired at **a)** 0 °C, **b)** −10 °C, **c)** −20 °C, **d)** −30 °C, **e)** −40 °C, **f)** −50 °C, **g)** −60 °C, **h)** −70 °C and **i)** −80 °C. Spectra are clipped vertically for clarity.

3.8.2 Thermal Conversion of D-2 at Elevated Temperature

As no thermal isomerization of **D-2** was observed at neither low nor ambient temperatures, an experiment at elevated temperature was performed. To this end, a sample of racemic **C-2** in CD_2Cl_2 was irradiated with 490 nm light (this wavelength was also found suitable for accumulation of **D-2**) until the sample was enriched in **D-2**. The solvent was then removed *in vacuo* and exchanged for $(CDCl_2)_2$, which is of similar polarity[139] but has a significantly higher boiling point than CD_2Cl_2. The sample was transferred to an amberized NMR tube and kept at 65 °C for one week. ^{1}H NMR spectra were recorded in irregular time intervals to monitor the isomerization progress.

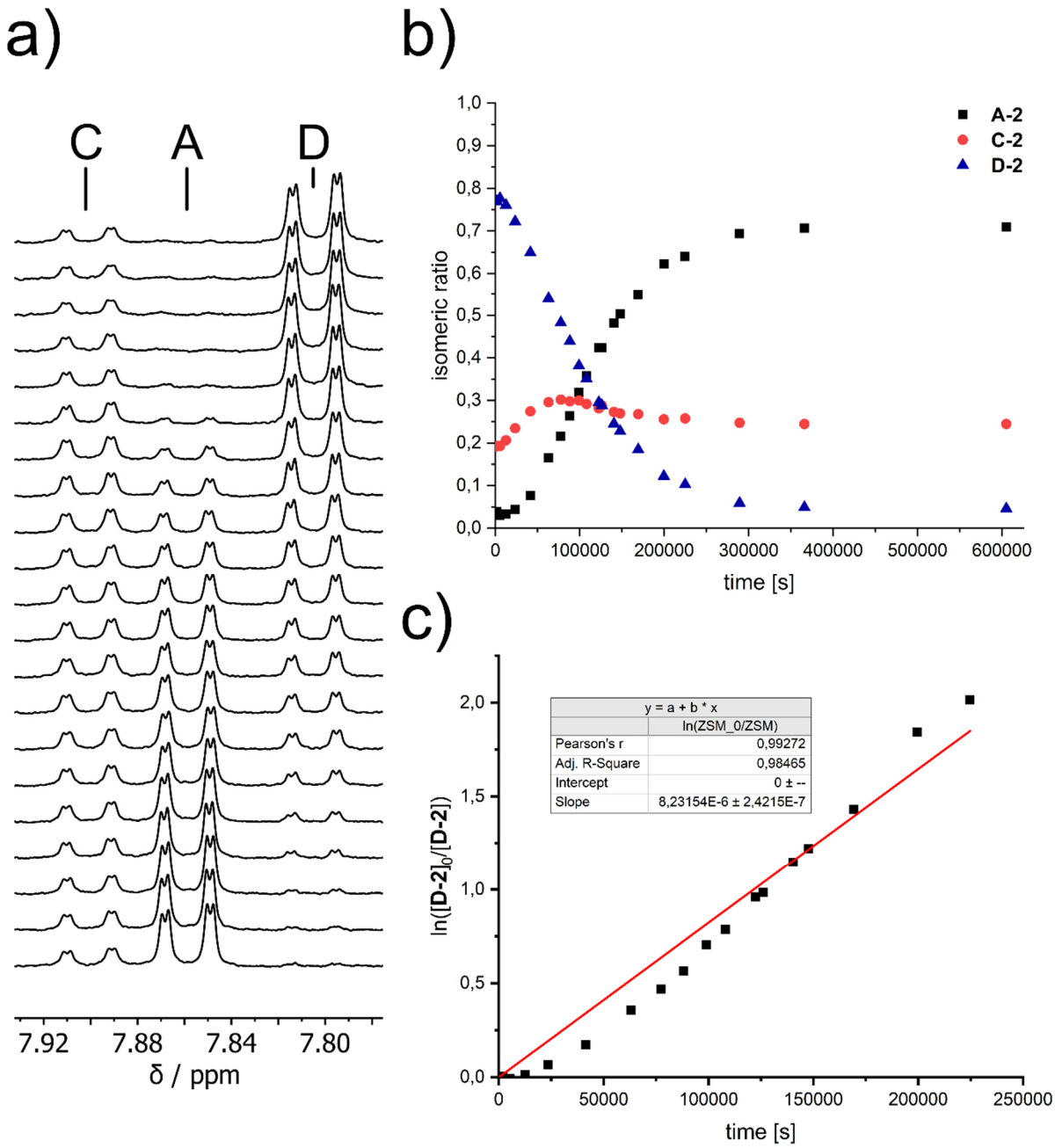

Figure 82 Kinetic analysis of thermal **D-2** isomerization at 65 °C in $(CDCl_2)_2$ in the dark. **a)** Indicative ^{1}H NMR (400 MHz, $(CDCl_2)_2$, 25 °C) signals that were used for determination of isomeric ratios. **b)** Changing isomeric ratios over time obtained by integration of indicative ^{1}H NMR signals. **c)** First order kinetic analysis of the thermal decay of isomer **D-2**. The slope of the linear fit is 8.2×10^{-6} s^{-1}. *Adapted from the supporting information to ref.* [8].

As can be seen in Figure 82b, upon heating there is near-full conversion of **D-2** to **C-2** and **A-2**. Upon closer inspection of the kinetic trace it is apparent that **C-2** is initially formed faster until a maximum ratio of 30% **C-2** before eventually reaching an equilibrium of 26%

C-2 and 74% **A-2**. This observation suggests a first order decay of **D-2** to **C-2**, coupled to a follow-up equilibrium between **C-2** and **A-2**.

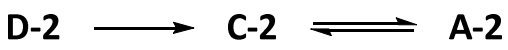

Again, the rate constant k can be obtained as the slope of a linear fit in combination with Equation 11 (replacing **B-1** with **D-2** in that equation). The rate constant is $k_{\text{D-2}\rightarrow\text{C-2}} = 8.2 \times 10^{-6}\ \text{s}^{-1}$, corresponding to a *Gibbs* energy of activation $\Delta G^{\ddagger} = 27.7\ \text{kcal mol}^{-1}$ for the thermal **D-2** to **C-2** double bond isomerization at 65 °C in $(CDCl_2)_2$.

As three species are interconverting in this process, the rate constants for the **C-2** to **A-2** isomerization cannot be extracted with the methods used above. To gain further insight, the isomerization kinetics were simulated based on the experimental data, using the parameter estimation task integrated in the *COPASI 4.34*[140] software package. The 'Evolutionary Programming' method was used, with the number of generations set to 2000 and the population size set to 200. Three species (**A-2**, **C-2**, **D-2**) were defined and the initial concentrations were set to 0 (**A-2**), 0.2 (**C-2**) and 0.8 (**D-2**) mol L^{-1} respectively. In the first iteration, all species were considered to be in dynamic equilibrium with each other. Reactions that did not contribute significantly ($k < 1.0 \times 10^{-11}\ \text{s}^{-1}$ for the first iteration, $k < 1.0 \times 10^{-6}\ \text{s}^{-1}$ for the second iteration) were removed from the model. After a total of three iterations, the following model was obtained:

D-2 → **C-2** (mass action irreversible)

C-2 ⇌ **A-2** (mass action reversible)

With the corresponding rate constants

$$k_{\text{D-2}\rightarrow\text{C-2}} = 7.8 \times 10^{-6}\ \text{s}^{-1}$$

$$k_{\text{C-2}\rightarrow\text{A-2}} = 1.6 \times 10^{-5}\ \text{s}^{-1}$$

$$k_{\text{A-2}\rightarrow\text{C-2}} = 4.8 \times 10^{-6}\ \text{s}^{-1}$$

The *Gibbs* energies of activation $\Delta G^{\ddagger}$ at 65 °C are obtained from the rate constants as described above.

D-2 to **C-2**: $\Delta G^{\ddagger} = 27.7\ \text{kcal mol}^{-1}$

C-2 to **A-2**: $\Delta G^{\ddagger} = 27.3\ \text{kcal mol}^{-1}$

A-2 to **C-2**: $\Delta G^{\ddagger} = 28.1\ \text{kcal mol}^{-1}$

The values obtained from the simulation are in agreement with the experimentally determined ones (**D-2** to **C-2**, as well as **C-2**/**A-2** interconversion) and a plot combining

experimentally obtained data and simulated fit is given in Figure 83. The activation barriers for the double bond isomerization processes are quite similar. As a consequence, the barrier for a possible **D-2** to **A'-2** isomerization (**A'-2** being a threaded state analogous to **A'-1**) must be significantly higher than 28 kcal mol^{-1} and / or **A'-2** must be very unstable, resulting in virtually no population of this state.

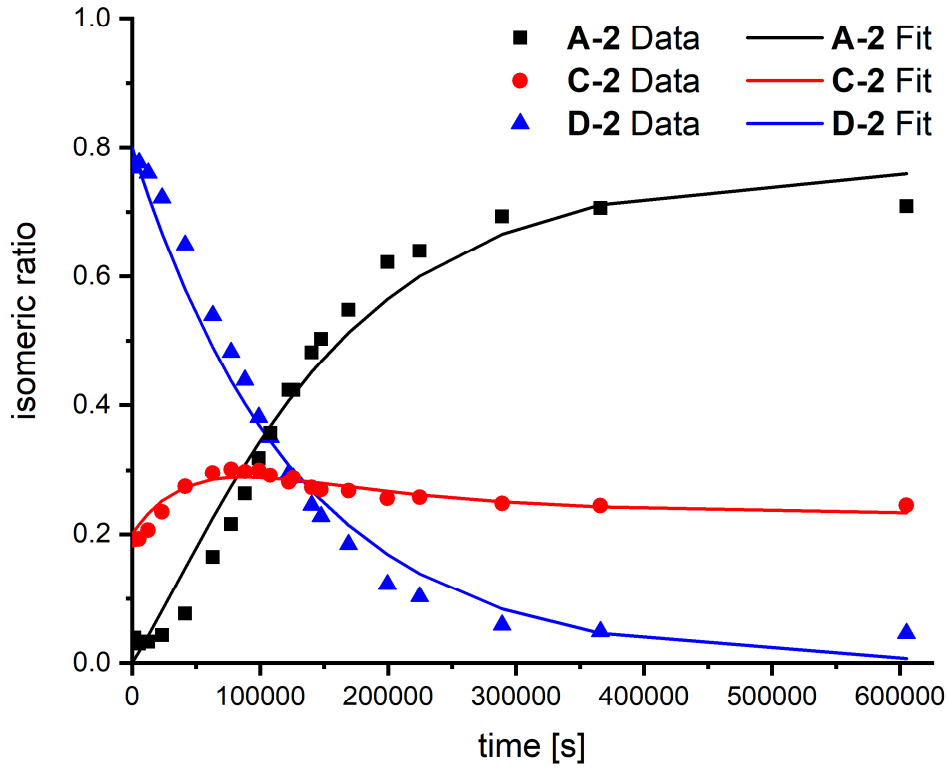

Figure 83 Kinetic analysis of thermal **D-2** isomerization at 65 °C in $(CDCl_2)_2$ in the dark. A plot of the isomeric ratios over time is shown. Experimental data (obtained from ^1H NMR integration) is plotted as symbols, the fit obtained from *COPASI* is plotted as lines. The model is based on an irreversible conversion of **D-2** to **C-2** and an equilibrium between **C-2** and **A-2**. *Adapted from the supporting information to ref.* [8].

3.9 Separation of Enantiomers

Based on NMR analysis it was possible to assign (*Z*)- and (*E*)-configuration of the central double bond. As only a low-quality crystal structure could be obtained, other methods had to be used for unambiguous determination of the helical chirality and absolute configuration. ECD is a powerful method, that has previously been successfully used to assign stereoconfiguration of individual HTI motor isomers.[95-96, 122-123] In order to measure ECD spectra, chiral resolution of (*R*)- and (*S*)-configured enantiomers is essential. This was achieved by chiral HPLC using *Chiralpak IC* and *ID* stationary phases. It was possible to isolate enantiomer pairs of all compounds investigated here (**A-1**, **A-2**, **C-1** and **C-2**). HPLC chromatograms are depicted in the following Figures. All enantiomer pairs showed matching ^{1}H NMR and UV/Vis spectra, confirming the assignment.

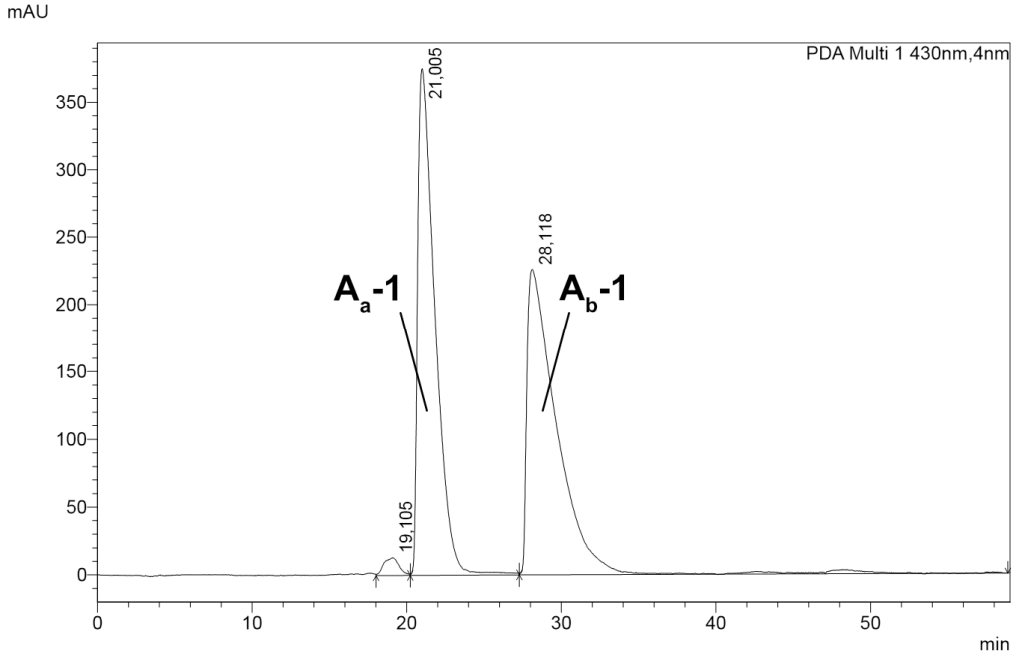

Figure 84 Chromatogram of the chiral resolution of **A-1** by chiral HPLC on a *Daicel Chiralpak ID* semi-preparative column eluting with *i*-PrOH:*n*-hexane 60:40 at 30 °C and a flow rate of 4.5 mL/min. Retention times are approx. 21 min for **A$_a$-1** and 28 min for **A$_b$-1**. The chromatogram was recorded at 430 nm. *Adapted from the supporting information to ref.* [8].

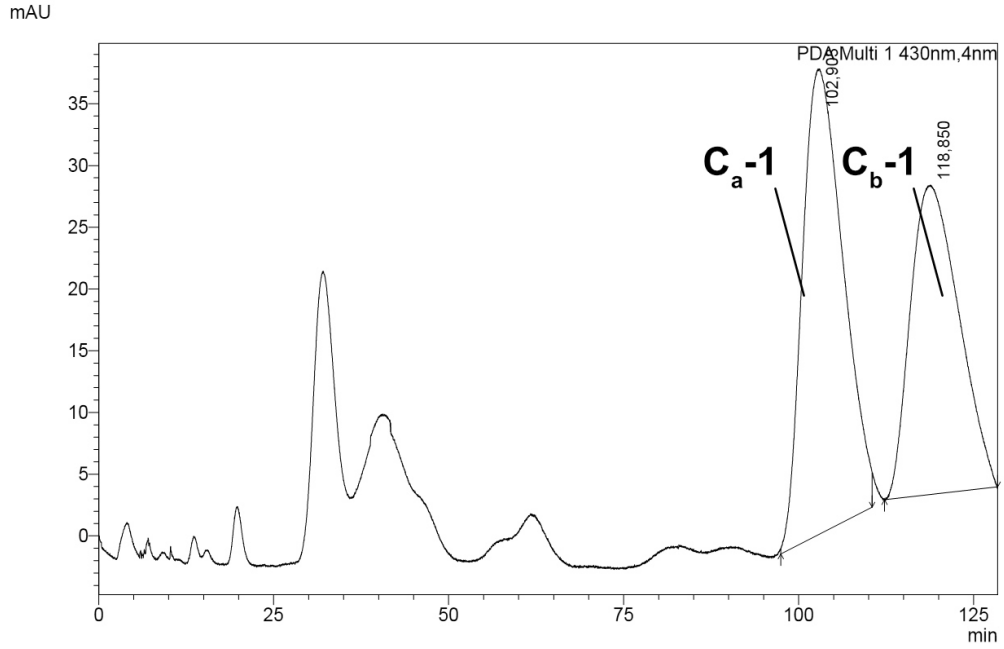

Figure 85 Chromatogram of the chiral resolution of **C-1** by chiral HPLC on a *Daicel Chiralpak IC* semi-preparative column eluting with *i*-PrOH (100%) at 30 °C and a flow rate of 2.8 mL/min. Retention times are approx. 103 min for **C$_a$-1** and 118 min for **C$_b$-1**. The chromatogram was recorded at 430 nm. *Adapted from the supporting information to ref.* [8].

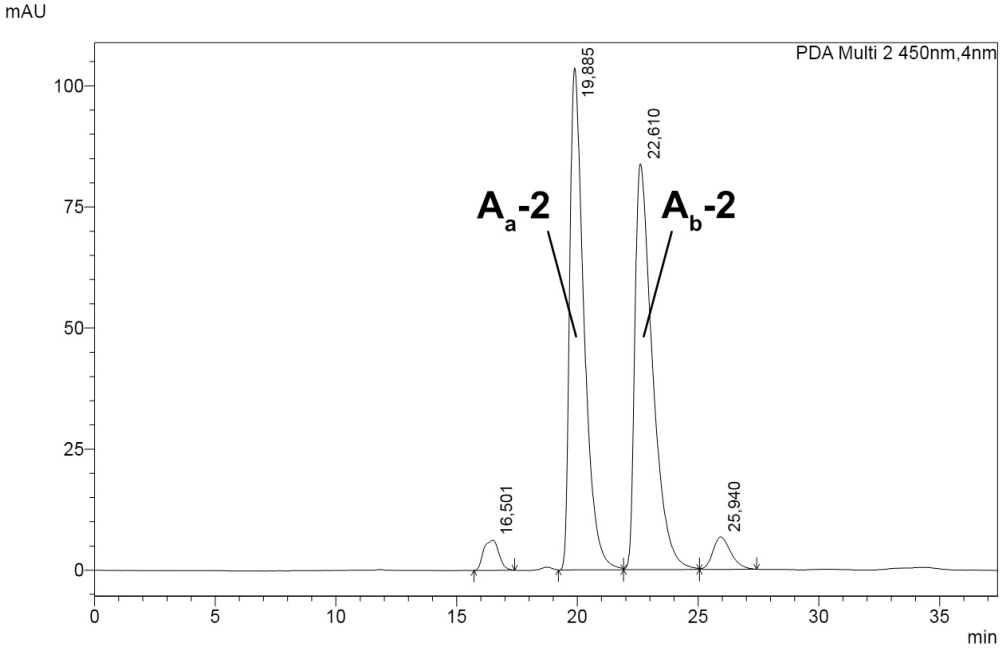

Figure 86 Chromatogram of the chiral resolution of **A-2** by chiral HPLC on a *Daicel Chiralpak IC* semi-preparative column eluting with EtOAc:*n*-heptane 25:75 at 30 °C and a flow rate of 2 mL/min. Retention times are approx. 20 min for **A$_a$-2** and 23 min for **A$_b$-2**. The chromatogram was recorded at 450 nm. *Adapted from the supporting information to ref.* [8].

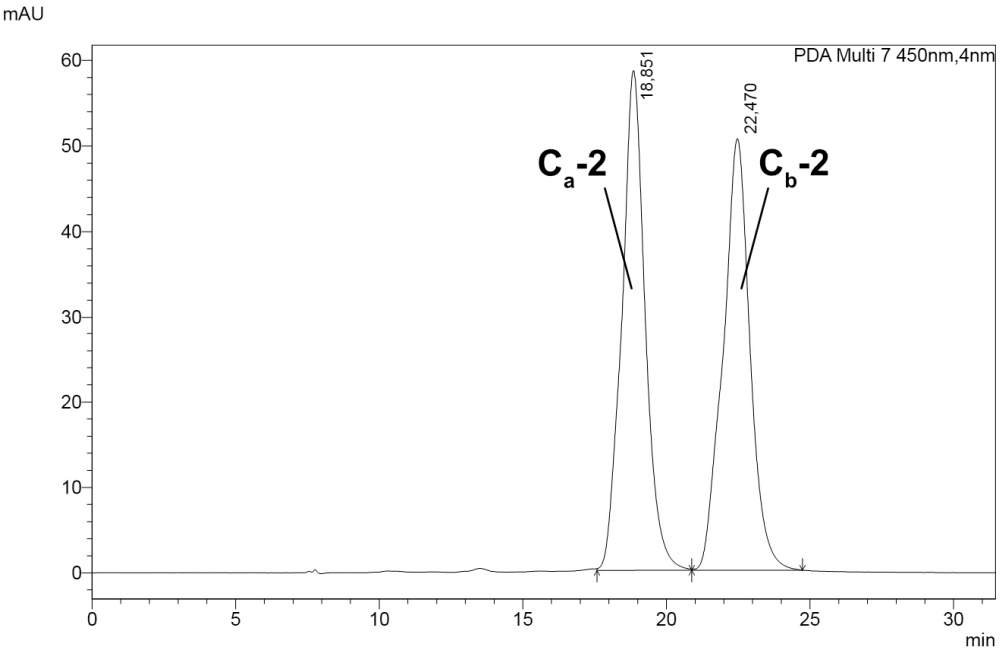

Figure 87 Chromatogram of the chiral resolution of **C-2** by chiral HPLC on a *Daicel Chiralpak IC* semi-preparative column eluting with EtOAc:*n*-heptane 40:60 at 30 °C and a flow rate of 2 mL/min. Retention times are approx. 19 min for **C$_a$-2** and 22 min for **C$_b$-2**. The chromatogram was recorded at 450 nm. *Adapted from the supporting information to ref.* [8].

3.10 ECD Spectra

With the enantiomers successfully separated, ECD spectra were measured next. In all cases, the ECD spectra of the isolated pairs were mirror images relative to one another, confirming them to be of opposite stereochemistry. Again, there is a striking similarity in spectra for **A-1** to **A-2** and **C-1** to **C-2**. As the chiral information is localized on the HTI chromophore, it is plausible to assume a high similarity in geometry of the respective motor cores.

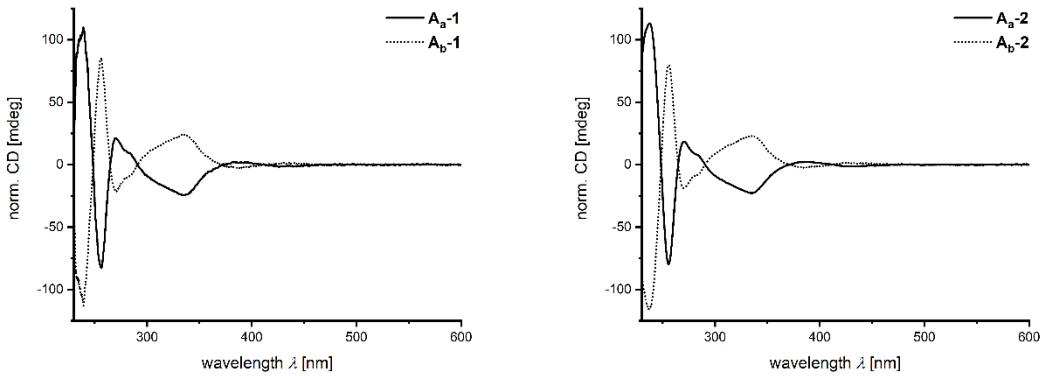

Figure 88 Normalized ECD spectra of chirally resolved **A-1** (left, 23 °C) and **A-2** (right, 25 °C) in CH_2Cl_2 solution. Subscript **a** and **b** denote the respective HPLC fraction (see Figure 84). *Adapted from the supporting information to ref.* [8].

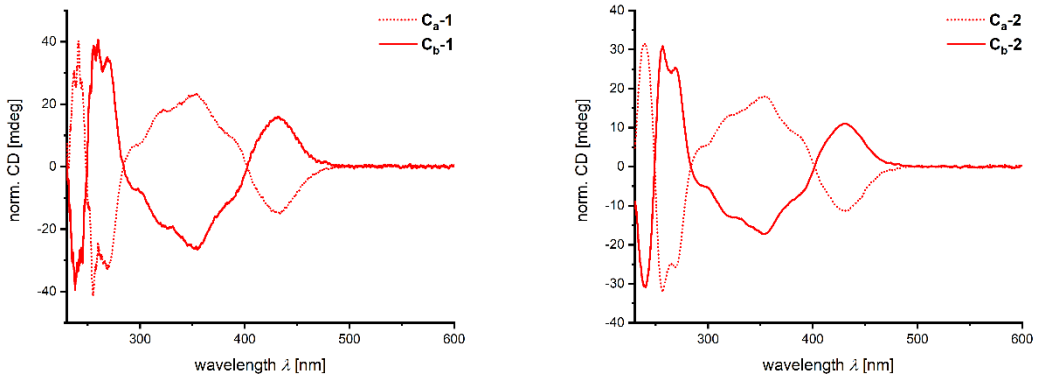

Figure 89 Normalized ECD spectra of chirally resolved **C-1** (left, 23 °C) and C-2 (right, 25 °C) in CH_2Cl_2 solution. Subscript **a** and **b** denote the respective HPLC fraction (see Figure 85). *Adapted from the supporting information to ref.* [8].

3.10.1 Experimentally Determined *g*-Factors

g-Factors are obtained by division of CD signal by absorption at the same wavelength. They are independent of concentration and thus allow for better comparability between different compounds. Again, the respective spectra prove to be mirror images of each other and the similarity between **A-1** and **A-2**, as well as **C-1** and **C-2** is confirmed once more.

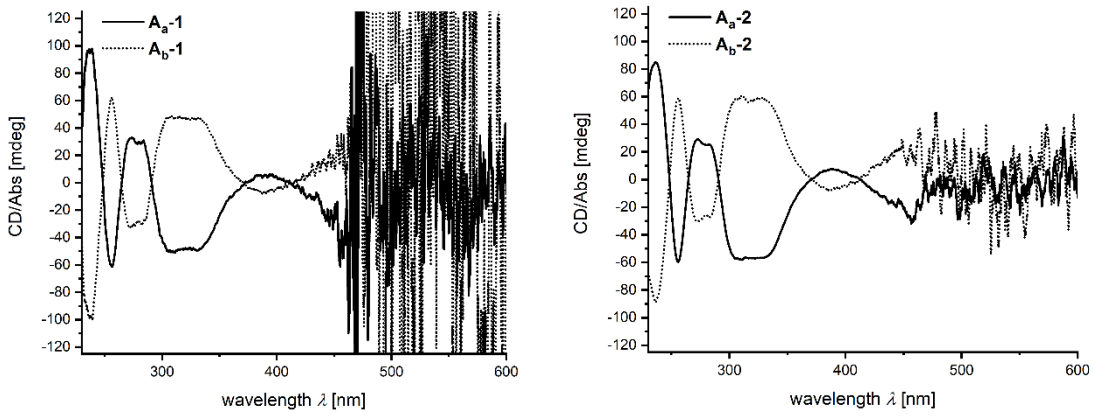

Figure 90 *g*-Factors for enantiomers of **A-1** (left, 23 °C) and **A-2** (right, 25 °C) in CH_2Cl_2 solution obtained by division of the CD in mdeg by the absorption of the sample. Subscript **a** and **b** denote the respective HPLC fraction (see Figure 84). *Adapted from the supporting information to ref.* [8].

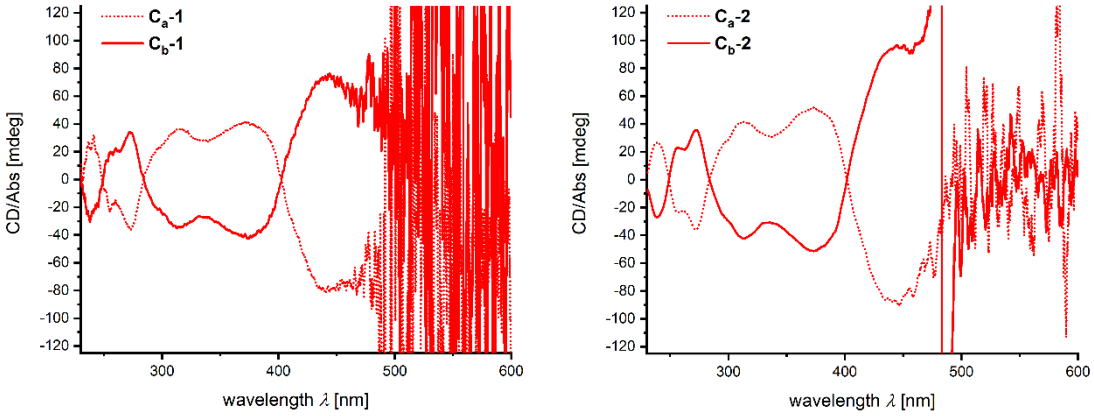

Figure 91 *g*-Factors for enantiomers of **C-1** in CH_2Cl_2 solution at 23 °C obtained by division of the CD in mdeg by the absorption of the sample. Subscript **a** and **b** denote the respective HPLC fraction (see Figure 85). *Adapted from the supporting information to ref.* [8].

3.10.2 ECD Photoisomerization Experiments

At this point, it is established that for both **1** and **2** a set of four stable (stereo)isomers (*R,Z*), (*S,Z*), (*R,E*) and (*S,E*) could be isolated. However, assignment of the absolute configuration is not obvious. To identify which HPLC fraction of **A-1** and **C-1** are of the same stereoconfiguration, a photoisomerization experiment was performed. A sample of **A$_a$-1** in CH_2Cl_2 was irradiated with 405 nm light while the change in ECD spectrum was monitored. This irradiation should result in the formation of the respective **C-1** isomer by double bond isomerization. Indeed, the spectral changes indicated formation of the **C$_b$-1** isomer. From this, it can be concluded that **A$_a$-1** and **C$_b$-1** must be of the same sulfoxide configuration (see Section 3.11 for assignments based on theoretical calculations).

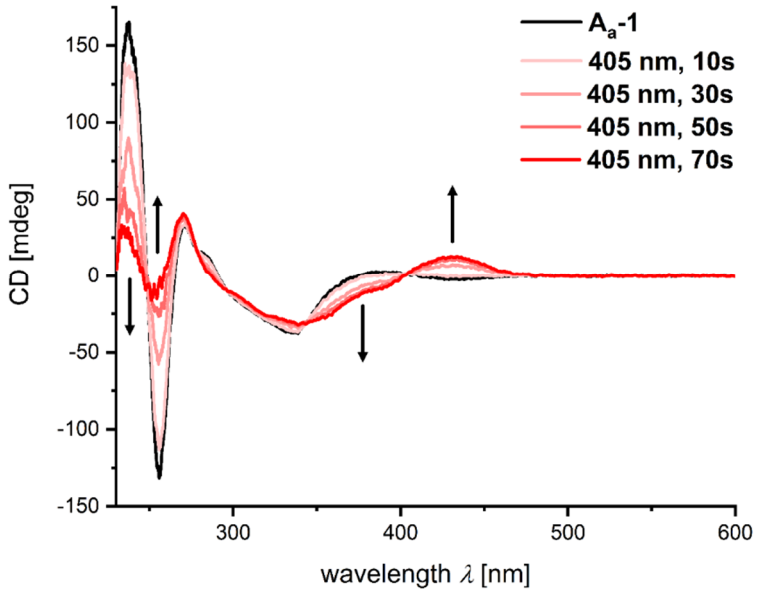

Figure 92 ECD spectra recorded during photoisomerization of enantiomerically pure **A$_a$-1** in CH_2Cl_2 solution at 25 °C (**a** denotes the HPLC fraction). Upon irradiation with 405 nm light at 25 °C, a mixture enriched in **C$_b$-1** was obtained. Therefore, **A$_a$-1** and **C$_b$-1** can be assigned to the same sulfoxide stereo configuration. *Adapted from the supporting information to ref.* [8].

As the **D-1** intermediate could be observed by low temperature ^{1}H NMR spectroscopy, additional low temperature ECD experiments were performed to probe the changes in molecular geometry during motor rotation. Analogously to the ^{1}H NMR experiment, a sample of **C$_b$-1** in CH_2Cl_2 was irradiated with 450 nm light at −80 °C, followed by annealing to 25 °C. The change in ECD spectra was monitored at −80 °C and is shown in Figure 93. A pronounced change in signal (sign inversion) around 340 nm was observed upon irradiation.

As supported by theoretical calculations (see Section 3.11), this coincides with a change in helical chirality (**C-1** to **D-1**). After warming of the sample to ambient temperature, another change in signal was observed in the same spectral region, matching a second helix inversion step (**D-1** to **A-1**).

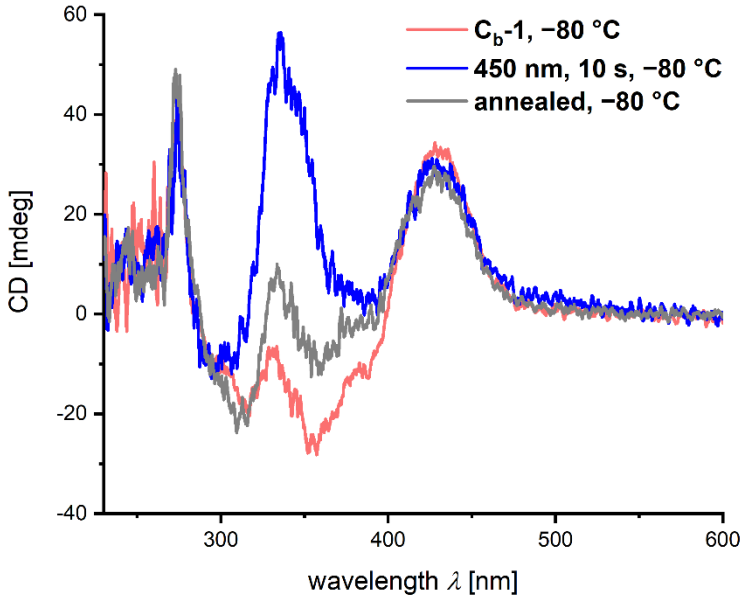

Figure 93 Low temperature ECD spectra recorded during photoisomerization of **Cb-1** in CH_2Cl_2 solution at −80 °C. A solution of enantiomerically pure **Cb-1** in CH_2Cl_2 (red spectrum) was irradiated with 450 nm light at −80 °C for 10 s (blue spectrum). The sample was annealed at 25 °C and another ECD spectrum was recorded at −80 °C (grey spectrum). Upon irradiation, there was a strong change in ECD signal around 340 nm which could thus be ascribed to the metastable **D-1** isomer with inverted helicity as compared to **Cb-1**. *Adapted from the supporting information to ref.* [8].

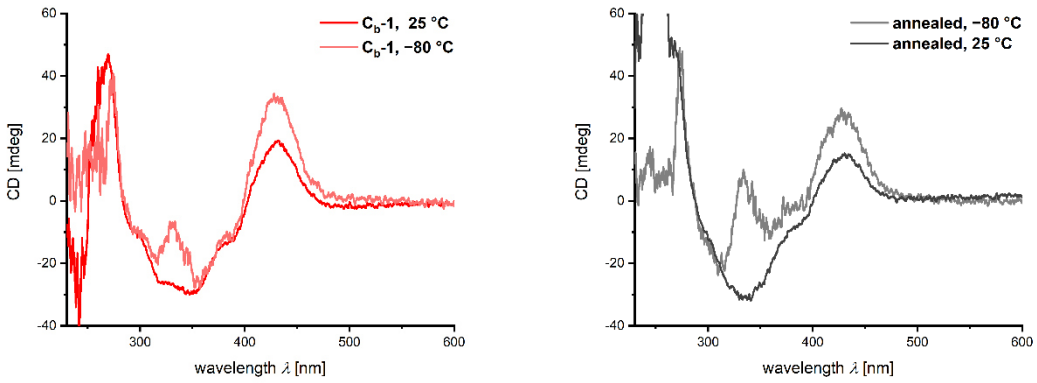

Figure 94 *left:* Comparison of ECD spectra of enantiomerically pure **C$_b$-1** in CH_2Cl_2 solution at 25 °C and −80 °C. *right:* Comparison of ECD spectra obtained after irradiation of **C$_b$-1** in CH_2Cl_2 solution with 450 nm light at −80 °C followed by thermal annealing at 25 °C. Spectra were measured at −80 °C and 25 °C, respectively. Changes in spectra indicate the partial formation of **A$_a$-1**. *Adapted from the supporting information to ref.* [8].

Inspection of the UV/Vis spectra recorded at ambient temperature before and after irradiation and subsequent annealing confirmed net conversion of **C$_b$-1** to **A$_a$-1** (see Figure 95).

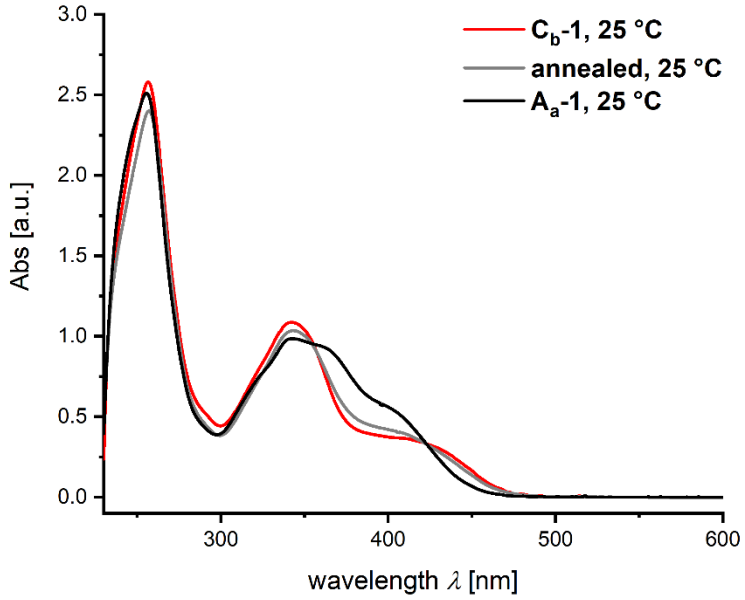

Figure 95 UV/Vis absorption spectra (recorded at 25 °C) corresponding to the low temperature ECD experiment described in Figure 94. The absorption spectrum of enantiomerically pure **A$_a$-1** was recorded separately and scaled to the isosbestic point at 423 nm. The absorption changes indicate a net conversion of **C$_b$-1** to **A$_a$-1** via transient **D-1**. *Adapted from the supporting information to ref.* [8].

An analogous photoisomerization experiment was conducted with compound **C$_b$-2**. A sample of **C$_b$-2** in CH_2Cl_2 was irradiated with 450 nm light at 25 °C and the change in ECD signal was monitored (see Figure 96). A pronounced change in signal (sign change) around 340 nm was observed upon irradiation. Again, this coincides with a change in helical chirality, as supported by theory ((*E*,*R*,*M*) to (*Z*,*R*,*P*) in this specific experiment). Furthermore, the UV/Vis spectrum of the mixture enriched in **D-2** was recorded, which confirmed accumulation of **D-2**. From this and the NMR experiments it can be concluded, that **C-1** and **C-2** undergo the same type of geometry changes upon isomerization to the respective **D**-isomer, namely (*E*,*S*,*P*) to (*Z*,*S*,*M*) or (*E*,*R*,*M*) to (*Z*,*R*,*P*) transformation. A compact comparison of the relevant ECD spectra of **1** and **2** and the respective **C**-to-**D** isomerization is shown in Figure 98.

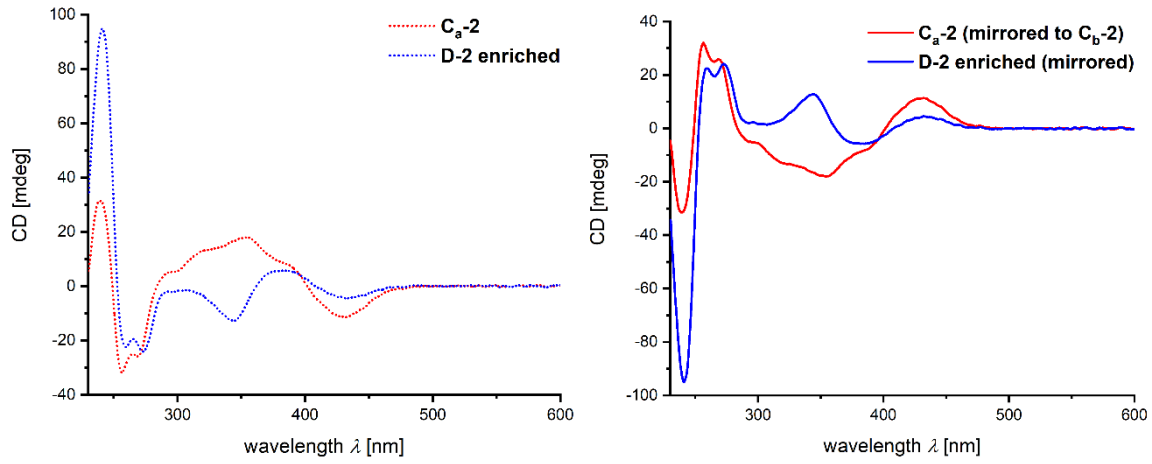

Figure 96 *left:* Experimental ECD spectra (recorded at 25 °C) of a solution of enantiomerically pure **C$_a$-2** in CH_2Cl_2 before (red spectrum) and after (blue spectrum) irradiation with 450 nm light at 25 °C. A significant change in ECD signal is observed around 340 nm, which could thus be attributed to the formation of the respective **D-2** isomer with inverted helicity as compared to **C$_b$-2**. *right:* The experimentally obtained ECD spectra shown on the left were mirrored by multiplication with −1 for direct comparison with other experiments as well as the theoretical description. *Adapted from the supporting information to ref.* [8].

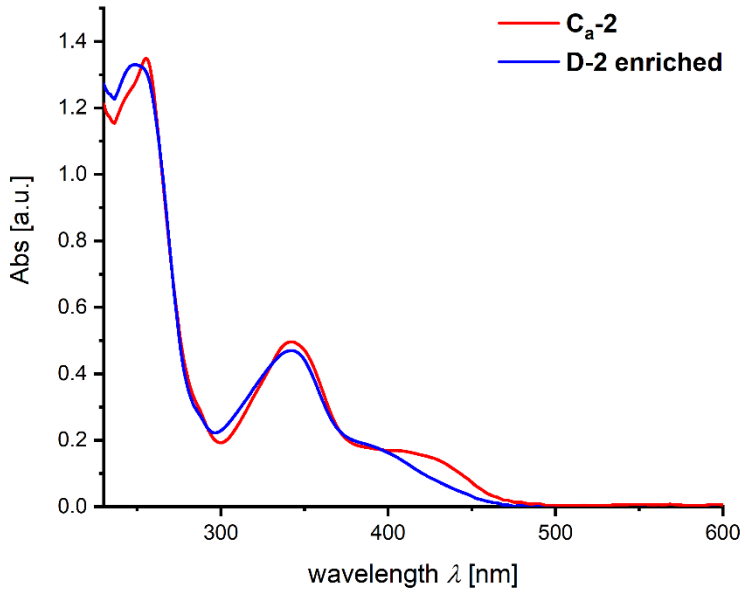

Figure 97 UV/Vis absorption spectra recorded at 25 °C corresponding to the photoisomerization experiment described in Figure 96. *Adapted from the supporting information to ref.* [8].

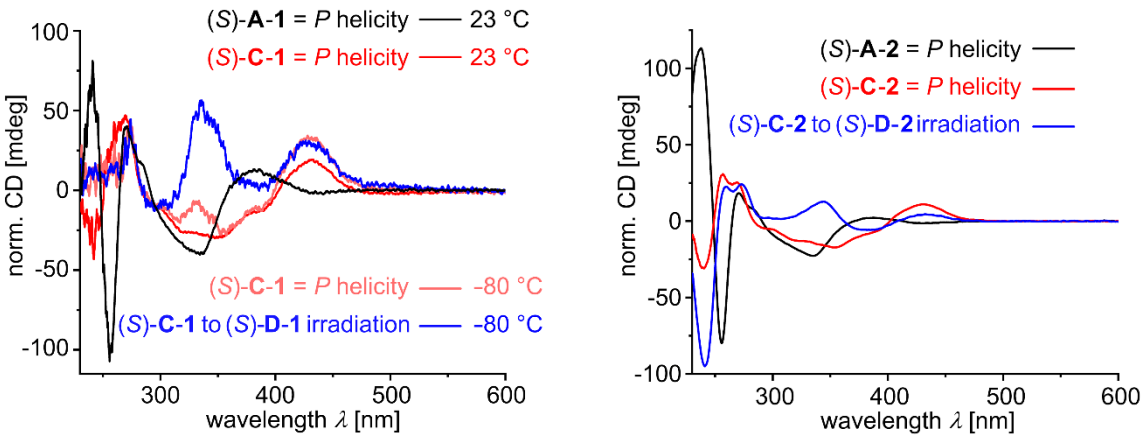

Figure 98 *left:* Comparison of experimental ECD spectra for (*S*,*P*)-configured isomers **A-1** and **C-1** measured in CH_2Cl_2 solution at the indicated temperatures. Upon irradiation of **C-1** with 450 nm light at low temperature, a characteristic change in ECD signal associated with the formation of (*S*,*M*)-configured **D-1** was observed. *right:* Comparison of experimental ECD spectra for (*S*,*P*)-configured isomers **A-2** and **C-2** measured in CH_2Cl_2 solution at 25 °C. Upon irradiation of **C-2** with 450 nm light at 25 °C, a characteristic change in ECD signal associated with the formation of (*S*,*M*)-configured **D-2** was observed. Spectra of isomers **C-2** and **D-2** were originally measured for the (*R*)-configured isomers and are mirrored to allow direct comparison with the spectra of **1**. Assignments of absolute configuration are based on theoretical results (see Section 3.11). *Adapted with formatting changes under terms of the CC BY 4.0*[138] *license from* N. N. Bach *et al.*, "Active Mechanical Threading by a Molecular Motor", *Angew. Chem. Int. Ed.* **2022**, *61*, e202201882. *© 2022, The Authors. Angew. Chem. Int. Ed. published by Wiley-VCH GmbH.*

3.11 Theoretical Description of Macrocyclic Motor 1

The molecular geometries of (*S*)-configured motor isomers **A-1** (*Z*,*S*,*P*), **B-1** (*E*,*S*,*M*), **C-1** (*E*,*S*,*P*) and **D-1** (*Z*,*S*,*M*), as well as the respective absorption and ECD spectra were explored using quantum chemical methods. Owing to the large size of molecule **1** and the high number of degrees of freedom associated with the flexible chains, an initial conformational search was performed in order to sample the conformational space. The individual conformers were then optimized at DFT B3LYP-D3BJ/6-311G(d,p) PCM (CH_2Cl_2) level, followed by TD-DFT calculation of electronic excitation spectra. The ECD spectra thus obtained could then be compared to the experimental ones (see Section 3.10). In the following section, the results from theoretical calculations will be discussed in more detail.

3.11.1 Ground State Geometries

First, a conformational search was conducted on all four isomers of (*S*)-configured macrocyclic motor **1** using the *MacroModel* software. A mixed torsional/low mode sampling employing the MMFF94 force field with $CHCl_3$ as solvent was carried out within an energy window of 40 kJ mol^{-1}. The starting structures for the individual isomers were manually generated from a crystal structure of **C-1** by rotation around the central double bond (see Section 3.4.1 for crystal structure). Without the use of constraints, only **A-1** and **C-1** type structures were obtained starting from **D-1** and **B-1**, respectively. Therefore, constraints were added on three dihedral angles around the central double bond in order to "freeze" (*M*)-helicity. For each isomer, the 25 structures of lowest energy were kept as starting structures for subsequent geometry optimizations at the B3LYP-D3BJ/6-31G(d) PCM (CH_2Cl_2) level of theory, followed by 'tight' optimization at the B3LYP-D3BJ/6-311G(d,p) PCM (CH_2Cl_2) level of theory. In a small number of cases the optimizations did not converge and the respective structures were not considered in the following. All structures were confirmed to be local minima, as frequency analysis at the same level found no imaginary vibrations. DFT and TD-DFT calculation were all performed with the *Gaussian16*[141] software package with an ultrafine integration grid.

In solution, the different conformers are populated according to the *Boltzmann* distribution based on their relative energies. Therefore, for each isomer only conformers within a relative energy window of approx. 3 kcal mol^{-1} were taken into consideration. Within this energy range approx. 99% of the total population is covered. In the following Figure 99–Figure 102,

superpositions of the significant theoretically obtained conformer geometries are shown. The lowest energy conformer is displayed with full opacity. When comparing the different conformer geometries for one isomer, the most pronounced differences are encountered in the orientation of the tetraethylene glycol chain as well as the aliphatic segment within the macrocycle. The HTI core structure, in contrast, appears to be rather rigid and there is only a small variation in the dihedral angle of the central double bond.

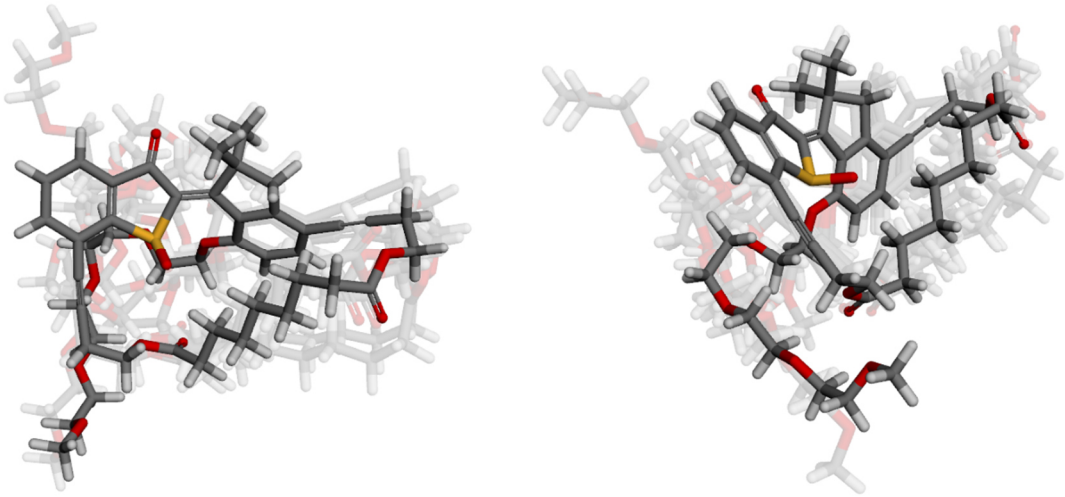

Figure 99 Superposition of significant minimum energy conformers obtained for (*S*)-**A-1** at the B3LYP-D3BJ/6-311G(d,p) PCM (CH_2Cl_2) level of theory, shown from two different viewing angles. The energy window is 0-2.63 kcal mol^{-1}. Each structure is aligned on the thioindigo fragment and the most stable conformer is depicted with full opacity. Note that there is no "pre-threading" observed in any of these structures, i.e. the tetraethylene glycol chain always resides outside of the macrocycle. *Adapted from the supporting information to ref.* [8].

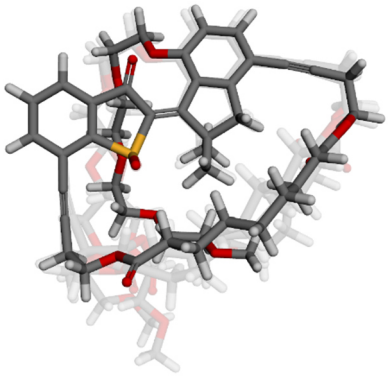

Figure 100 Superposition of significant minimum energy conformers obtained for (*S*)-**B-1** at the B3LYP-D3BJ/6-311G(d,p) PCM (CH_2Cl_2) level of theory. The energy window is 0-3.24 kcal mol^{-1}. Each structure is aligned on the thioindigo fragment and the most stable conformer is depicted with full opacity. Note that there is no "pre-threading" observed, i.e. the tetraethylene glycol chain always resides outside of the macrocycle. *Adapted from the supporting information to ref* [8].

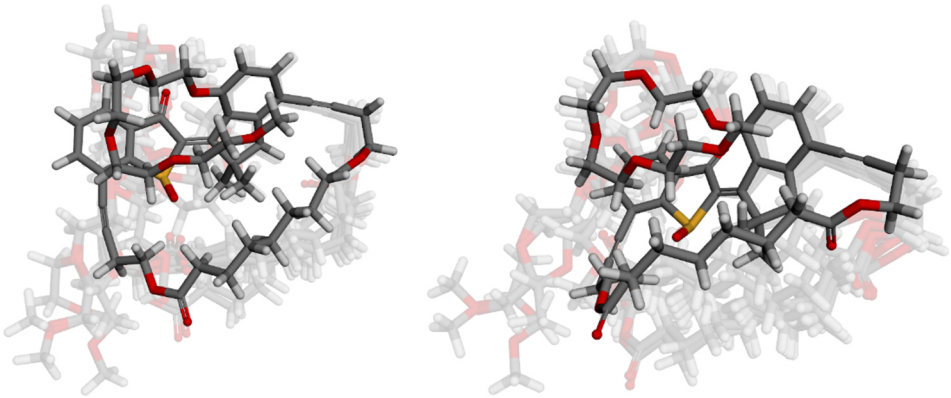

Figure 101 Superposition of significant minimum energy conformers obtained for (*S*)-**C-1** at the B3LYP-D3BJ/6-311G(d,p) PCM (CH_2Cl_2) level of theory, shown from two different viewing angles. The energy window is 0-3.26 kcal mol^{-1}. Each structure is aligned on the thioindigo fragment and the most stable conformer is depicted with full opacity. Note that there is no "pre-threading" observed, i.e. the tetraethylene glycol chain always resides outside of the macrocycle. *Adapted from the supporting information to ref.* [8].

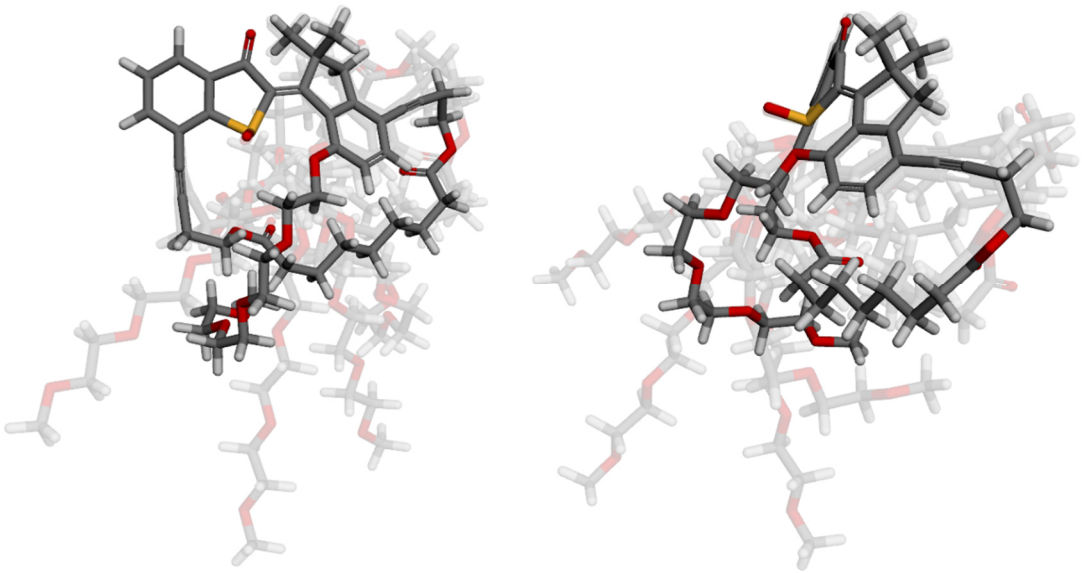

Figure 102 Superposition of significant minimum energy conformers obtained for (*S*)-**D-1** at the B3LYP-D3BJ/6-311G(d,p) PCM (CH_2Cl_2) level of theory, shown from two different viewing angles. The energy window is 0-3.18 kcal mol^{-1}. Each structure is aligned on the thioindigo fragment and the most stable conformer is depicted with full opacity. Note that there is no "pre-threading" observed in any of these structures, i.e. the tetraethylene glycol chain always resides outside of the macrocycle. *Adapted from the supporting information to ref.* [8].

3.11.2 Theoretically Obtained ECD Spectra

Electronic excitation spectra (UV/Vis and ECD) were calculated for each set of significant structures at the TD-B3LYP-D3BJ/6-311+G(d,p) PCM (CH_2Cl_2) level of theory, calculating 30 states for each conformer. The theoretically obtained spectra were then *Boltzmann*-averaged according to the *Gibbs* Free Energy difference and processed using *SpecDis* (V1.71).[142-143]

3.11.2.1 Comparison of Calculated and Experimental ECD Spectra

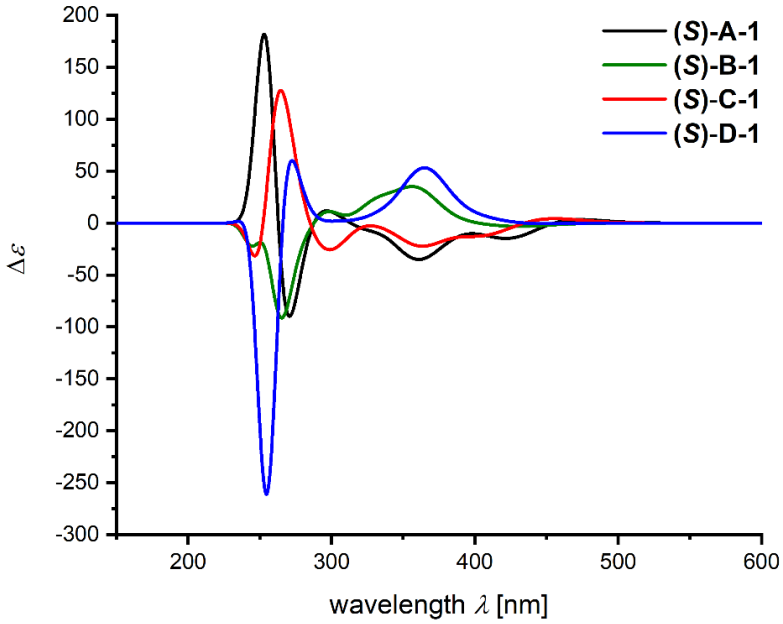

Figure 103 *Boltzmann*-weighted ECD spectra for (*S*)-configured motor **1** obtained on the TD-B3LYP-D3BJ/6-311+G(d,p) PCM (CH_2Cl_2) level of theory. Spectra were processed in *SpecDis* with a sigma value of 0.2 eV. *Adapted from the supporting information to ref.* [8].

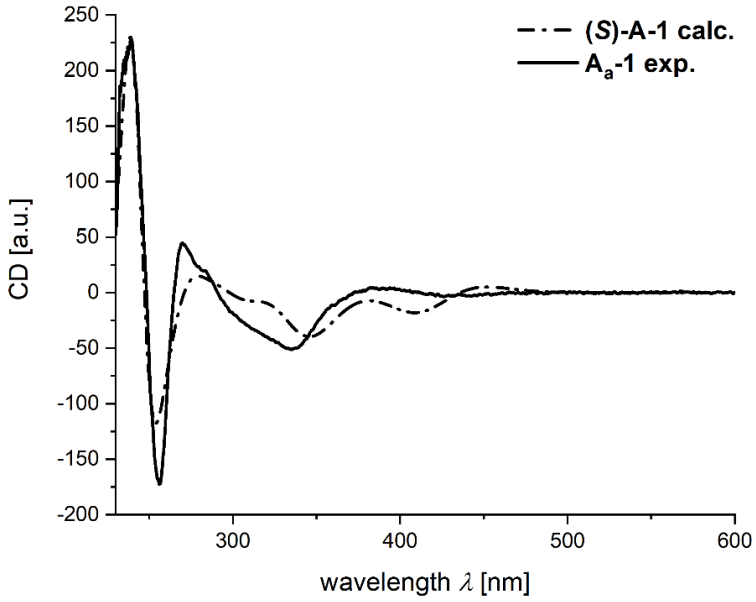

Figure 104 Comparison of experimental (solid line) and calculated (dotted line) ECD spectra of (*S*)-**A-1**. The subscript **a** denotes the respective HPLC fraction (see Figure 84). The theoretical spectrum was blue-shifted by 15 nm and a sigma value of 0.17 eV was used. Spectra were processed with *SpecDis* and scaled for better comparability. *Adapted from the supporting information to ref.* [8].

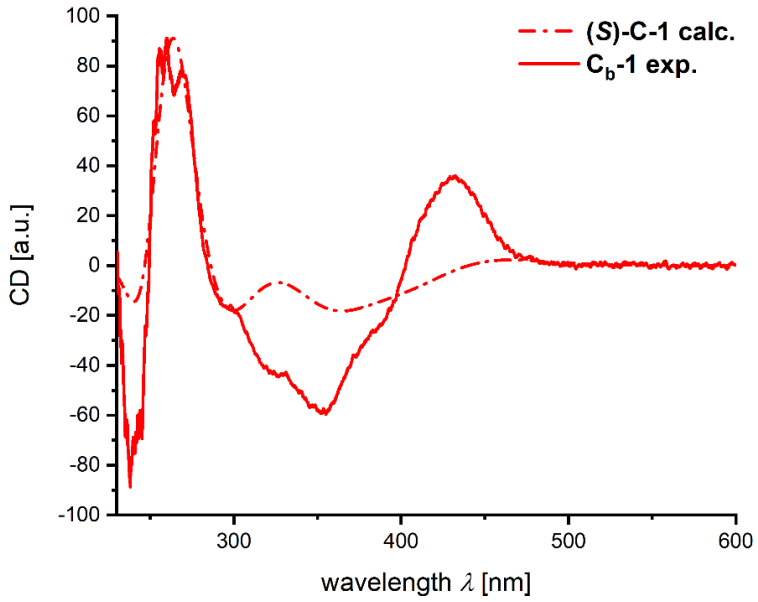

Figure 105 Comparison of experimental (solid line) and calculated (dotted line) ECD spectra of (*S*)-**C-1**. The subscript **b** denotes the respective HPLC fraction (see Figure 85). The theoretical spectrum was blue-shifted by 2 nm and a sigma value of 0.27 eV was used. Spectra were processed with *SpecDis* and scaled for better comparability. *Adapted from the supporting information to ref.* [8].

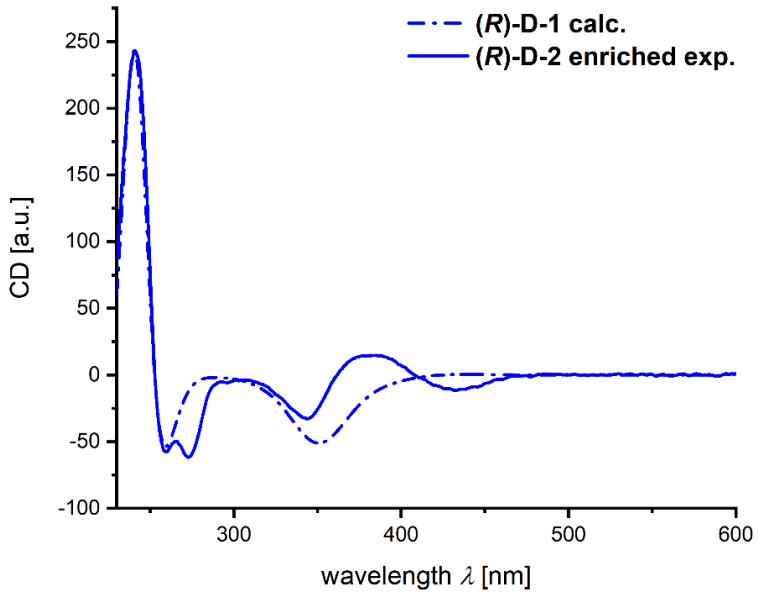

Figure 106 Comparison of the calculated (dotted line) ECD spectrum of (*R*)-**D-1** with the experimentally obtained spectrum of an (*R*)-configured mixture enriched in **D-2** (blue line). The theoretical spectrum was generated from the calculated enantiomeric spectrum of (*S*)-configured **D-1** by multiplication with −1 and was blue-shifted by 14 nm. A sigma value of 0.21 eV was used. For the experimental spectrum, a solution of enantiopure **C$_a$-2** ((*E*,*R*,*M*)-**2**) in CH_2Cl_2 was irradiated with 450 nm light for 30 s. Spectra were processed with *SpecDis* and scaled for better comparability. *Adapted from the supporting information to ref.* [8].

3.11.3 Pre-threaded Structure A'-1

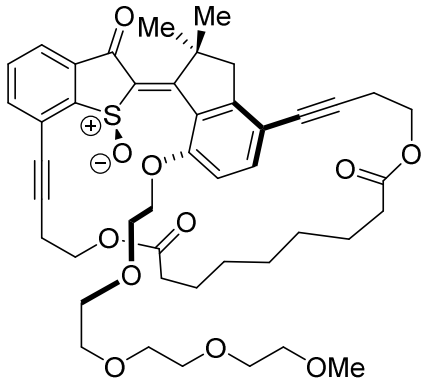

Figure 107 Threaded structure **A'-1** ((*Z,S,P*)-configuration). Unlike in structure **A-1**, the tetraethylene glycol chain is in a "threaded" state. *Adapted from the supporting information to ref.* [8].

As depicted in Figure 107, an alternative conformation for isomer **A-1** can be proposed, which is referred to as **A'-1** in the following. This hypothetical **A'-1** isomer has the same stereoconfiguration (*Z*,*S*,*P*/*Z*,*R*,*M*) but the tetraethylene glycol chain is in a "threaded" state, passing through the macrocycle. A threaded **A'-1** structure was modelled by manual modification of a **D-1** structure, followed by a minimization with the force field integrated in *Maestro*. In the following conformational search, only structures of **A-1**-type were found, even when constraints were added on the ethylene glycol chain. **A'-1** was also optimized at the B3LYP-D3BJ/6-311G(d,p) PCM (CH_2Cl_2) level of theory and the resulting geometry was confirmed as a local minimum by frequency analysis. The relative energy compared to the most stable **A-1** isomer was found to be +16.5 kcal mol^{-1}. These theoretical findings lead to the conclusion that "threaded" structures are energetically highly unfavorable. This is also supported by the experimental observation of a significantly increased activation barrier for thermal **D-1** to **A-1** helix inversion (16.4 kcal mol^{-1} vs 5.8 kcal mol^{-1} for the analogous process[9] for HTI motor **19**). Therefore, one plausible mechanism for **D-1** to **A-1** isomerization is *via* an **A'-1**-type structure and "threaded" structures might be close to a transition state on the energy potential surface.

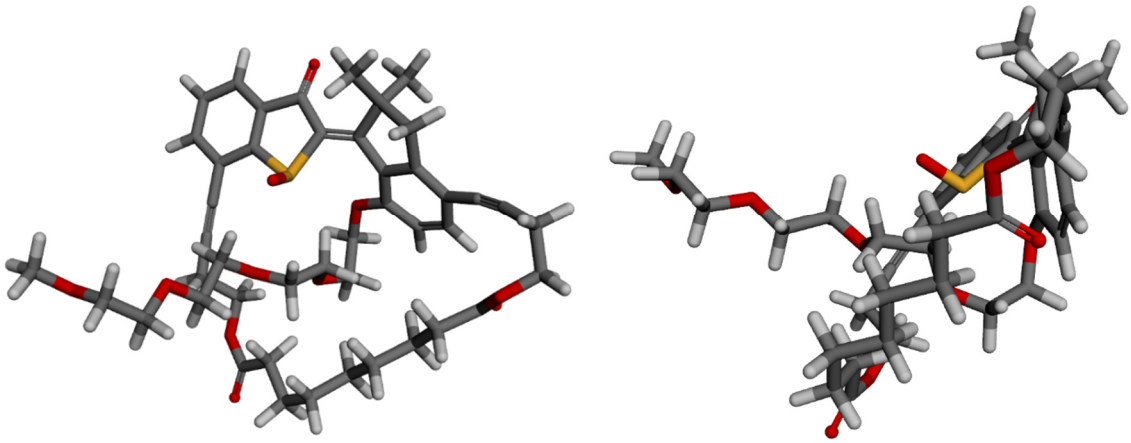

Figure 108 Ground state geometry obtained for **A'-1** at the B3LYP-D3BJ/6-311G(d,p) PCM (CH_2Cl_2) level of theory. Front and side view are shown to illustrate threading of the TEG chain. *Adapted from the supporting information to ref.* [8].

3.11.4 Calculated Thermochemical-Data

Table **9** Conformer numbering and respective energies obtained at the B3LYP-D3BJ/6-311G(d,p) PCM (CH_2Cl_2) level of theory. *Adapted from the supporting information to ref.* [8].

Isomer	Conformer	Energy Hartree	Rel. energy Hartree	Rel. energy kcal mol^{-1}
A-1	1	-2972.922507	0.002466	+1.55
	2	-2972.924973	0	0
	3	-2972.922966	0.002007	+1.26
	4	-2972.921515	0.003458	+2.17
	5	-2972.920779	0.004194	+2.63
	6	-2972.921723	0.00325	+2.04
	7	-2972.920778	0.004195	+2.63
	8	-2972.924462	0.000511	+0.32
	threaded	-2972.898754	0.026219	+16.45
B-1	1	-2972.923927	0	0
	2	-2972.920398	0.003529	+2.21
	3	-2972.918766	0.005161	+3.24
	4	-2972.922089	0.001838	+1.15
C-1	1	-2972.919637	0.000218	+0.14
	2	-2972.91795	0.001905	+1.2
	3	-2972.916543	0.003312	+2.08
	4	-2972.915907	0.003948	+2.48
	5	-2972.919432	0.000423	+0.27
	6	-2972.917951	0.001904	+1.19
	7	-2972.918253	0.001602	+1.01
	8	-2972.919855	0	0
	9	-2972.914663	0.005192	+3.26
	10	-2972.914794	0.005061	+3.18
	11	-2972.915191	0.004664	+2.93
D-1	1	-2972.905719	0.00507	+3.18
	2	-2972.90814	0.002649	+1.66
	3	-2972.910789	0	0
	4	-2972.908917	0.001872	+1.17
	5	-2972.908782	0.002007	+1.26

3.12 Proposed Mechanism of Operation for 1 and 2

Taking into account the analytical results presented in the previous chapters, a mode of operation for motor **1** and switch **2** can be proposed. Motor **1** basically follows the established HTI motor cycle.[9, 96] However, there are significant changes in the barriers for thermal helix inversion. The barrier for **B-1** (*E*,*S*,*M*/*E*,*R*,*P*) to **C-1** (*E*,*S*,*P*/*E*,*R*,*M*) isomerization is increased by 1.2 kcal mol^{-1} compared to motor **19**. For the **D-1** (*Z*,*S*,*M*/*Z*,*R*,*P*) to **A-1** (*Z*,*S*,*P*/*Z*,*R*,*M*) isomerization the difference is much larger, as the barrier is 10.6 kcal mol^{-1} higher than for original motor **19**. This is in part reflected in the theoretically obtained relative energy difference of 16.5 kcal mol^{-1} between the most stable **A-1** isomer and the "threaded" structure **A'-1**.

Table 10 Experimentally determined *Gibbs* energies of activation $\Delta G^{\ddagger}$ of thermal helix inversion steps for motors **1** and **19**.

THI	$\Delta G^{\ddagger}$, motor 1	$\Delta G^{\ddagger}$, motor 19[9]
(*Z*,*S*,*M*) to (*Z*,*S*,*P*)	16.4 kcal mol^{-1}	5.8 kcal mol^{-1}
(*E*,*S*,*M*) to (*E*,*S*,*P*)	14.1 kcal mol^{-1}	12.9 kcal mol^{-1}

HTI **2** on the other hand behaves like a three-state molecular switch. While the motor directionality is preserved in the switching (**A-2** → **C-2** → **D-2**), the cycle of motor operation is interrupted at the **D-2** stage. Due to the attachment of a bulky stopper group, THI directly to **A-2** is not possible as the chain is blocked from fully passing through the macrocycle. Furthermore, upon heating no isomerization to a "threaded" structure **A'-2** is observed. Instead, thermal "backwards" isomerization to **A-2** *via* **C-2** takes place at elevated temperatures, as was concluded from kinetic data analysis (see Figure 83).

From the results presented above it can be concluded, that THI from **D-1** to **A-1** is the "threading step" during which the tetraethylene glycol chain passes through the macrocycle. A "slipping" mechanism, in which the macrocyclic ring passes over the HTI core while "avoiding" a threading event could be excluded, as no direct **D-2** to **A-2** conversion was observed for the stoppered derivative. The mechanistic findings are summarized in Figure 109.

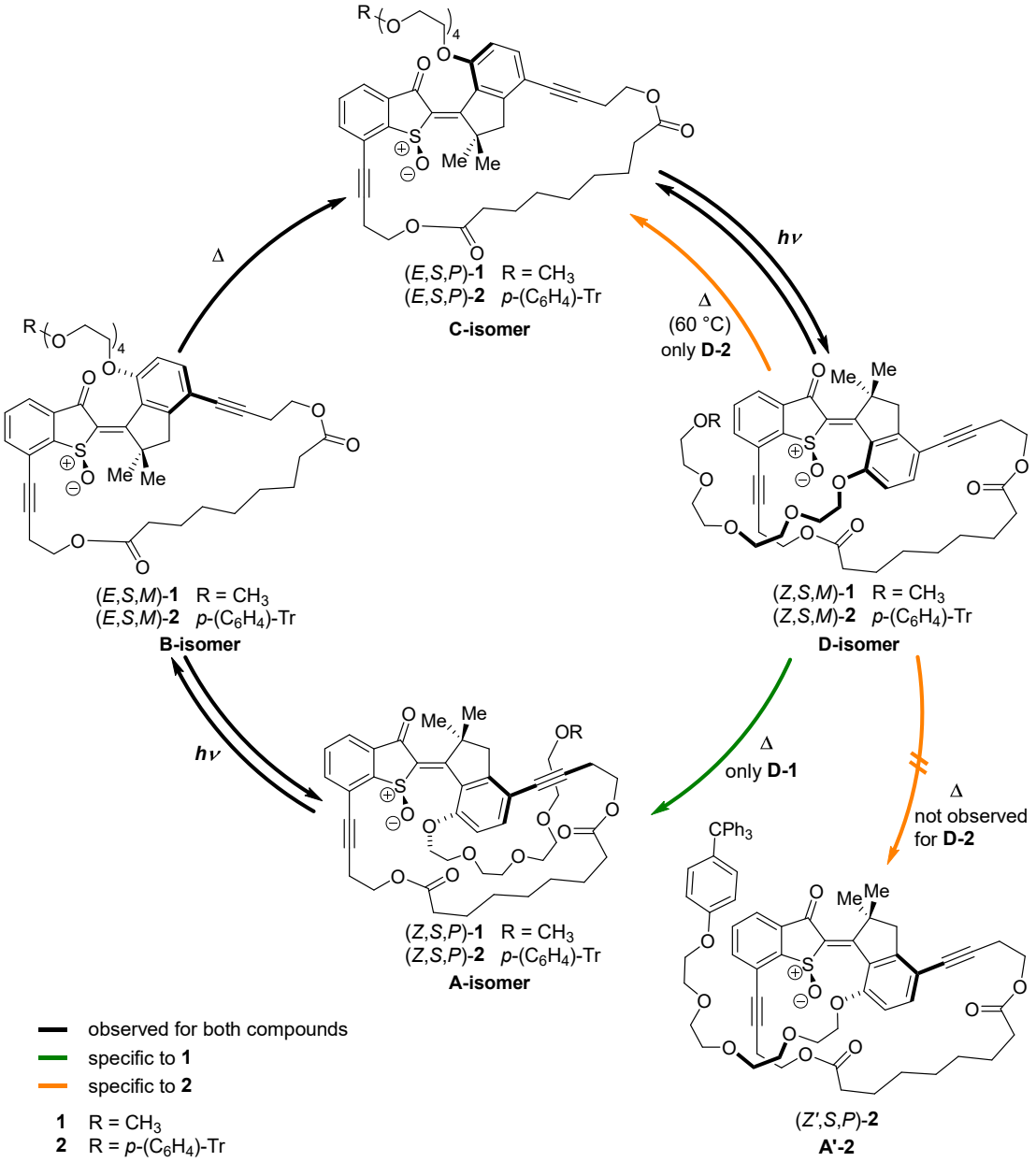

Figure 109 Schematic summary of the processes involved in motor or switch operation of compounds **1** and **2** respectively. For compound **1**, the typical four step HTI motor cycle could be observed. Starting from stable **A-1**, metastable **B-1** is generated upon irradiation with 405 nm light. **B-1** then undergoes a thermal helix inversion process to stable **C-1**. Irradiation with 450 nm light results in double-bond-isomerization to metastable **D-1**. In a second thermal helix inversion process, stable **A-1** is generated, completing 360° rotation. For compound **2**, irradiation of stable **A-2** with 405 nm light results in the formation of **C-2**. It was not possible to observe intermediate **B-2**, as there was no productive photochemistry at temperatures lower than −30 °C. However, it is assumed that isomerization proceeds *via* "fleeting" **B-2** at ambient temperatures. Irradiation of **C-2** with 450 nm light results in the formation of **D-2**. No thermal helix inversion to a "threaded" **A'-2** isomer was observed, even at elevated temperature. Instead, heating resulted in the formation of **A-2** *via* **C-2**, corresponding to reversion of motor rotation directionality.

3.13 Other Macrocyclic Motor Candidates

For some of the further motor candidates synthesized as part of this thesis (see Section 3.3.1), preliminary spectroscopic investigations into potential motor functionality were performed and are discussed in the following section.

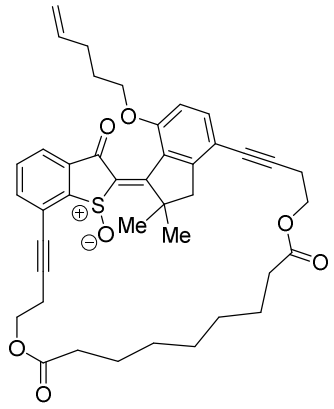

Figure 110 Molecular structure of **(*E*)-54**.

Macrocyclic HTI sulfoxide **54** is structurally very similar to **1** and **2**, with the only difference being the olefin chain instead of an ethylene glycol chain attached on the indanone fragment's oxygen.

After purification by column chromatography, two stable isomers of **54** could be isolated and were assigned *Z*- (**A**-) and *E*- (**C**-)configuration based on NMR and UV/Vis spectroscopy. The UV/Vis spectra in CH_2Cl_2 (see Figure 111) show the characteristic absorption profile of HTI sulfoxide molecular motors. Upon irradiation with 405 nm and 450 nm light, interconversion between the two isomers was observed. The *E*-isomer could be accumulated with 405 nm, whereas the *Z*-isomer could be accumulated with 450 nm light.

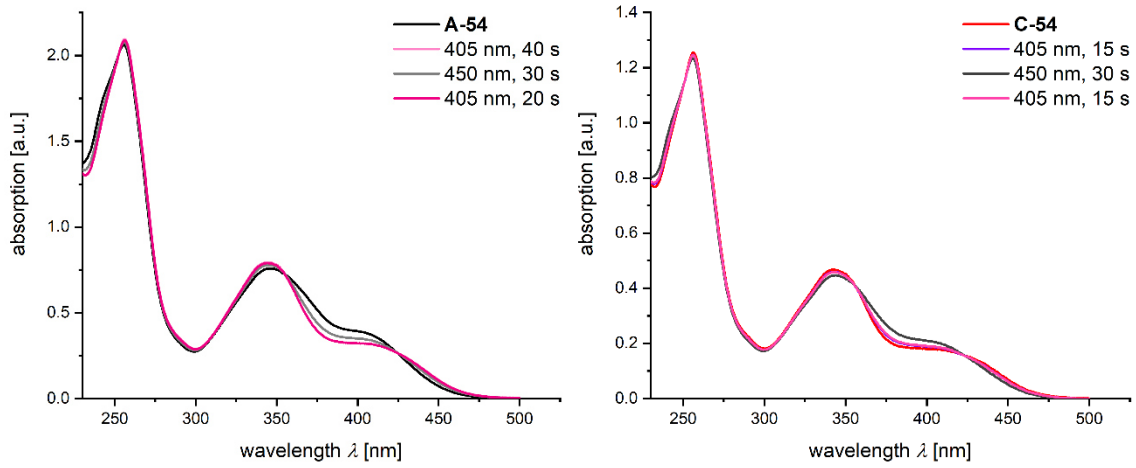

Figure 111 *left:* UV/Vis (CH_2Cl_2, 23 °C) absorption spectra recorded during photoisomerization experiments of **54**. A sample of pure racemic **A-54** (black spectrum) was irradiated with 405 nm light. The resulting spectrum (pink) shows characteristics of **C**-enrichment. Subsequent irradiation with 450 nm light resulted in partial formation of **A-54** (grey spectrum). The observed behavior is in agreement with interconversion of **A** to **C** and *vice versa* upon photoirradiation. No spectral characteristics of a **D**-type isomer were observed. *right:* UV/Vis (CH_2Cl_2, 23 °C) absorption spectra recorded during photoisomerization experiments of **54**. A sample of pure racemic **C-54** (red spectrum) was irradiated with 405 nm light. The resulting spectrum (violet) was very similar, indicating only little change in isomer composition. Subsequent irradiation with 450 nm light resulted in partial formation of **A-54** (grey spectrum). Upon irradiation with 405 nm light, the previous *pss* enriched in **C-54** was obtained. The observed behavior is in agreement with interconversion of **A** to **C** and *vice versa* upon photoirradiation. No spectral characteristics of a **D**-type isomer were observed.

In order to discern, whether the molecule behaves as a simple molecular switch or as molecular motor, low temperature ^{1}H NMR experiments were performed (see Figure 112–Figure 114). A sample of (*E*)-**54** in CD_2Cl_2 was kept at −60 °C inside an NMR spectrometer and was irradiated *in situ* with 405 nm or 450 nm light (see Figure 112). In the following, the characteristic region from approx. 6.60–6.80 ppm is discussed, as there is sufficient separation between the different isomer signals. Over the course of the experiment, only interconversion between **A**- and **C**-type isomers was observed. No metastable intermediate could be identified. The temperature was then lowered to −80 °C and irradiation was repeated (see Figure 113). Again, only **A** to **C**-interconversion was observed. As it is possible, that the barriers for thermal helix inversion are very low (i.e. below 13 kcal mol^{-1}),[95-96] the temperature was lowered even further. In a second experiment, a sample of **54** (*E*:*Z* approx. 1:1) in CD_2Cl_2:CS_2 (4:1) was kept at −105 °C in an NMR spectrometer. Upon *in situ* irradiation with 450 nm light, the build-up of a new signal,

tentatively assigned to a **D**-type isomer was observed. At the same time, the signal set assigned to **C** disappeared, indicating **C** to **D** conversion. Subsequent *in situ* irradiation with 405 nm light resulted in the generation of **C**-type isomer as well as possibly **B**-isomer. However, as there may be up to four species present in the mixture and the spectral resolution was unfortunately insufficient, no definite conclusion could be drawn at this point. Repeated *in situ* irradiation with 450 nm light resulted in a very similar spectrum as before, consisting of **A**-, **D**- and possibly **B**-type isomers. The tentative assignment of isomers is based on their observed order and mode of appearance. Upon annealing the sample at 23 °C, a mixture containing solely **A**- and **C**-type isomer was obtained. Additional shimming significantly improved the quality of the spectrum. When the sample was irradiated *in situ* with 450 nm light once more, the formation of a **D**-type isomer could clearly be observed. Additionally, there was a small change in shape of the **A**-signal at 6.75 ppm, that might be due to overlapping **B**-signal. Due to instrument constraints, the experiment had to be stopped at this point. In conclusion, the formation of a metastable isomer with **D**-characteristics is an indication, that **54** could be a molecular motor following the typical four-step isomerization cycle. Compared to motor **1**, the barriers for the assumed thermal helix inversion steps seem to be significantly lower. For a full characterization and investigations into possible motor functionality additional experiments, especially low temperature irradiation experiments with isolated isomers, are necessary.

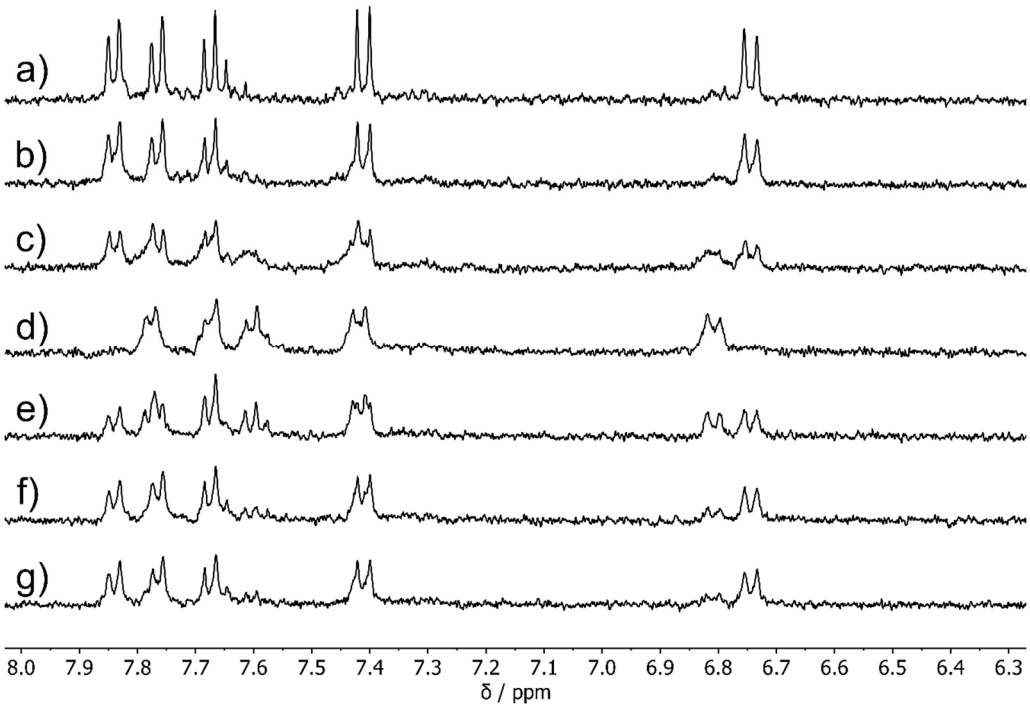

Figure 112 ^{1}H NMR (400 MHz, CD_2Cl_2, −60 °C) recorded during *in situ* photoirradiation of **54** at −60 °C. **a)** pure racemic **C-54 b,c)** during irradiation with 450 nm light **d)** after 10 min of irradiation with 450 nm light **e,f)** during irradiation with 405 nm light **g)** after 20 min of irradiation with 405 nm light.

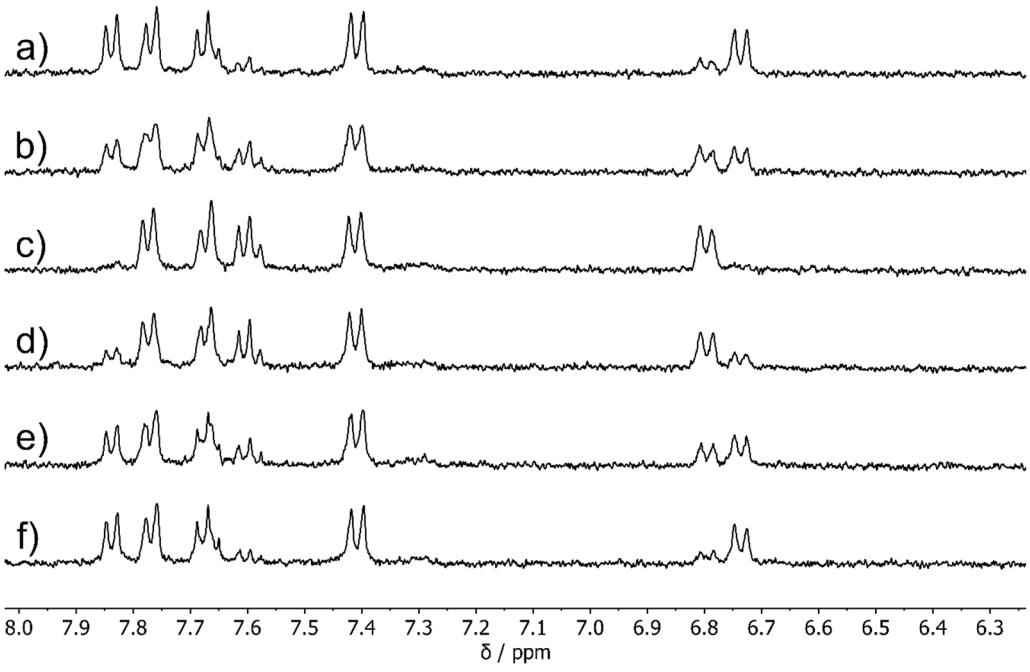

Figure 113 ^{1}H NMR (400 MHz, CD_2Cl_2, −80 °C) recorded during *in situ* photoirradiation of **54** at −80 °C. **a)** initial spectrum (mixture of racemic **A-54 and C-54 b)** during irradiation with 450 nm light **c)** after 10 min of irradiation with 450 nm light **d,e)** during irradiation with 405 nm light **g)** after 20 min of irradiation with 405 nm light.

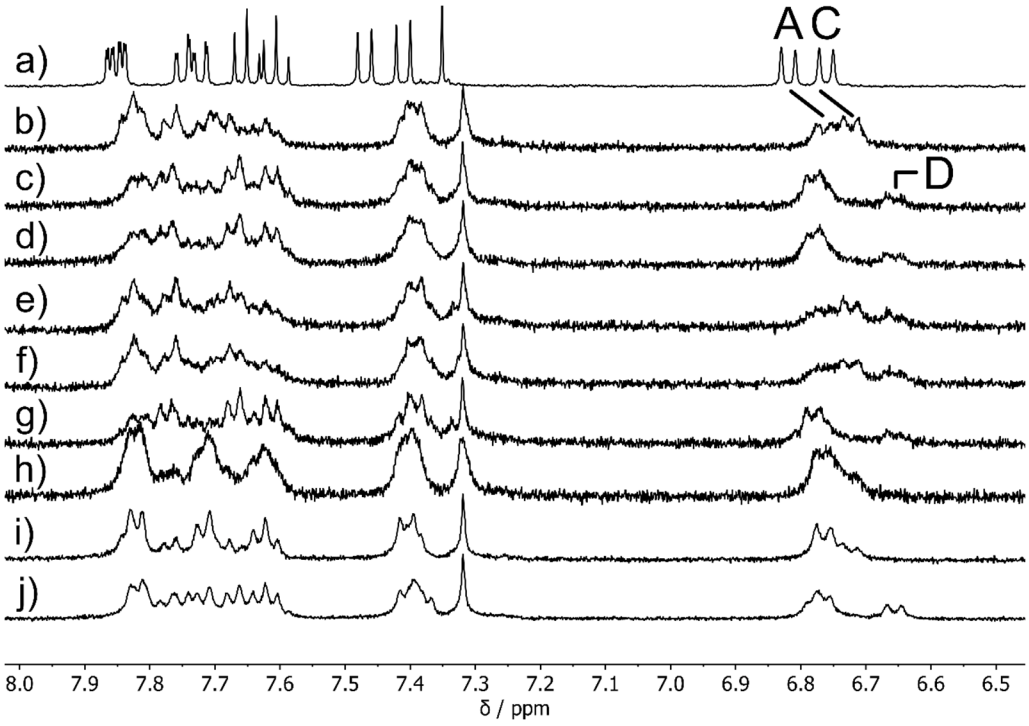

Figure 114 Aromatic region of ^{1}H NMR spectra (400 MHz, CD_2Cl_2:CS_2, 4:1) of an approx. 1:1 mixture (*E*:*Z*) of **54** recorded **a)** at 20 °C **b)** at −105 °C **c)** after irradiation with 450 nm light at −105 °C **d)** after keeping the sample in the dark at −105 °C for 15 min **e)** after irradiation with 405 nm light at −105 °C **f)** after keeping the sample in the dark at −105 °C for 7 min **g)** after irradiation with 450 nm light (again) at −105 °C **h)** after annealing the sample at 23 °C (spectrum measured at −105 °C) **i)** after shimming at −105 °C **j)** after irradiation with 450 nm light (again) at −105 °C. Due to initially inadequate shimming, spectra **b-h** have a low resolution.

Macrocycle **70** is an analogue of **2** with the aliphatic macrocyclic ring replaced by an oligo ethylene glycol chain. Macrocycle **75** has a similar structure but bears a longer ethylene glycol chain on the indanone fragment. Replacing the aliphatic macrocycle chain with an oligo ethylene glycol is expected to increase flexibility of the macrocycle as well as reduce unfavorable *gauche* interactions and torsional strain.[144-145] This might be beneficial for reducing the barrier of the **D**-to-**A**(**'**) helix inversion. Increasing the length of the chain bearing the stopper group is interesting with regard to the possible formation of an **A'**-type isomer. If the threading process is blocked due to the n = 4 chain being too short (i.e. thermal helix inversion not being feasible because the stopper group is already too close to the macrocycle), doubling the chain length might allow the **D**-to-**A'** threading step to proceed.

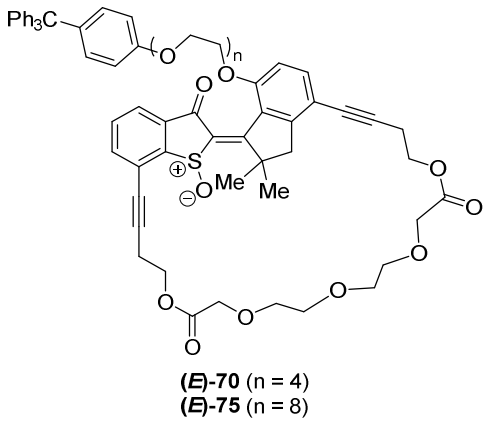

Figure 115 Molecular structures of (*E*)-**70** and *(E)*-**75**, which are structural analogues of macrocycle **2**. The aliphatic macrocyclic ring (of compound **2**) is replaced by an ethylene glycol chain. Compound **75** additionally bears a longer ethylene glycol chain on the indanone fragment.

For both derivatives, UV/Vis and ^{1}H NMR irradiation experiments were performed. The UV/Vis absorption spectrum of pure stable (*E*)-**70** in CH_2Cl_2 (Figure 116) shows the characteristics of a **C**-type isomer. Upon external irradiation with 405 nm light, only small spectral changes were observed. However, irradiation with 450 nm light resulted in a spectrum showing characteristic decrease in absorption around 425 nm, which is associated with **D**-isomer accumulation.

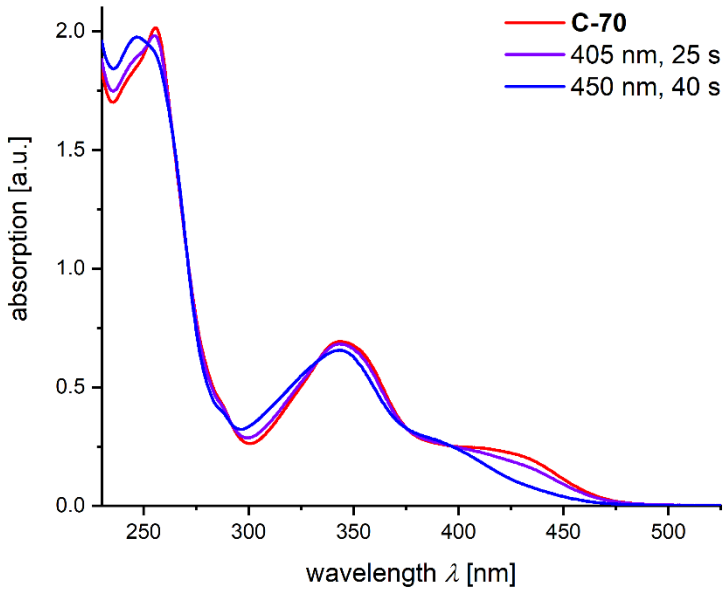

Figure 116 UV/Vis absorption spectra of a solution of (*E*)-**70** in CH_2Cl_2 at 23 °C (*red*: initial spectrum; *violet*: after irradiation with 405 nm light; *blue*: after irradiation with 450 nm light). The spectral changes upon irradiation with 450 nm light are characteristic for the accumulation of a **D**-type isomer.

In order to gain further insight into the structural changes upon photoirradiation, low temperature ^{1}H NMR experiments were performed. A sample of (*E*)-**70** in CD_2Cl_2 was irradiated *in situ* with 450 nm light at −80 °C (Figure 117). Over time, the **C**-type isomer was almost completely converted to a new isomer. Based on spectral similarity with **D-2**, this was tentatively assigned as **D**-type isomer. Upon annealing of the sample at 23 °C no change in (isomer) composition was observed, i.e. the **D**-type isomer was kinetically inert and did not undergo helix inversion at ambient temperatures. Upon irradiation with 405 nm light, the mixture could be enriched in **C**-isomer again.

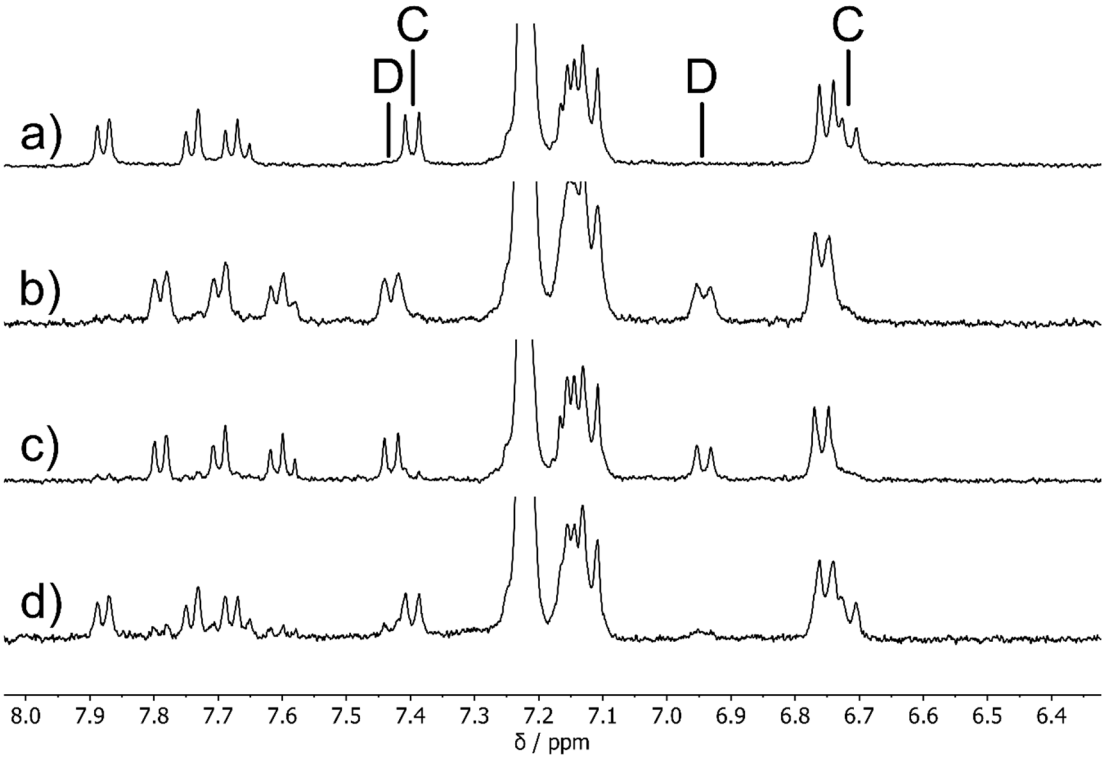

Figure 117 ^{1}H NMR (400 MHz, CD_2Cl_2, −80 °C) of a sample of **C-70**. **a)** initial spectrum of pure racemic **C-70 b)** after *in situ* irradiation with 450 nm light **c)** after annealing of the sample at 23 °C (spectrum measured at −80 °C) **d)** after *in situ* irradiation with 405 nm light. Characteristic signals are tentatively assigned to **C**- and **D**-type isomers based on spectral similarity to compound **2**.

An additional photoirradiation experiment was performed with the same sample at −30 °C (see Figure 118). Again, photoswitching between **C**- and **D**-type isomers was observed upon irradiation with 405 nm and 450 nm light.

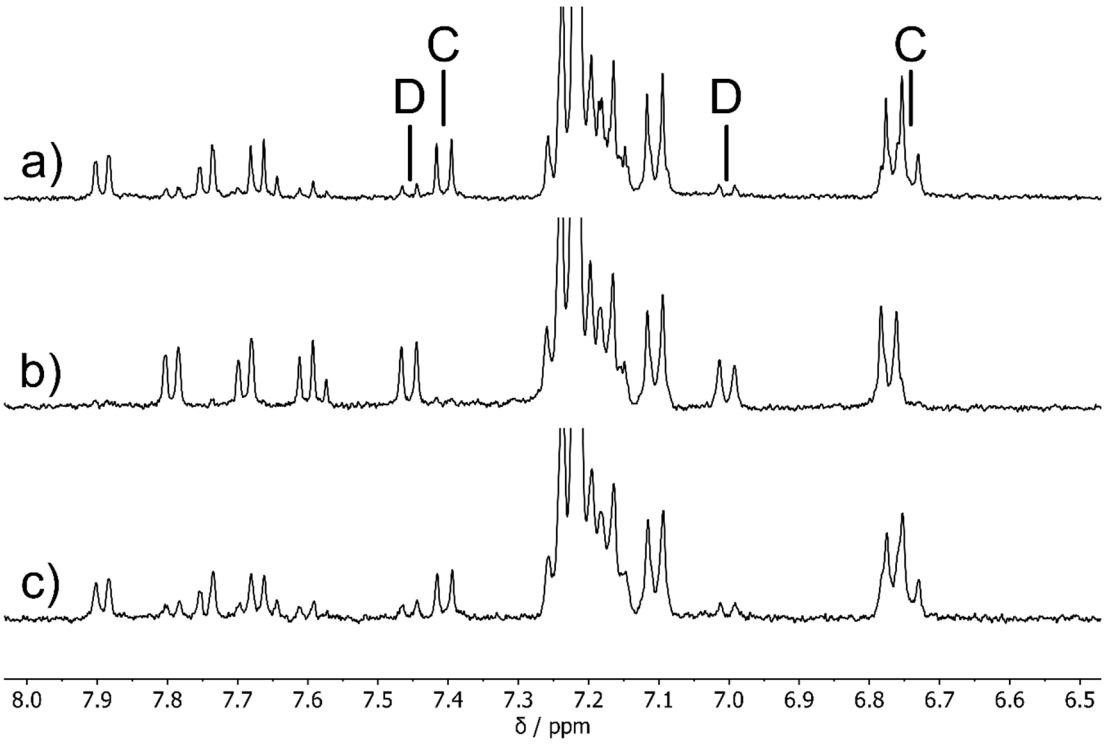

Figure 118 ^{1}H NMR (400 MHz, CD_2Cl_2, −30 °C) of a sample of (*E*/*Z*)-**70**. **a)** initial spectrum **b)** after *in situ* irradiation with 450 nm light **c)** after *in situ* irradiation with 405 nm light. Characteristic signals are tentatively assigned to **C**- and **D**-type isomers based on spectral similarity to compound **2**.

In order to probe a possible helix inversion step at elevated temperatures, a heating experiment was performed. To this end, after the low-temperature NMR experiments, the solvent was removed *in vacuo* and the sample was re-dissolved in $(CDCl_2)_2$. It was then kept at 100 °C in an oil bath and ^{1}H NMR spectra (at 25 °C) were recorded in irregular time intervals to monitor changes in isomer composition (see Figure 119). Over the course of approx. 2 h, the signal set assigned to a **D**-type disappeared and the formation of a signal set assigned to the **A**-type isomer was observed, resulting in a mixture containing both **A**- and **C**-type isomers. No new set of signals corresponding to a "threaded" **A'**-type isomer could be identified.

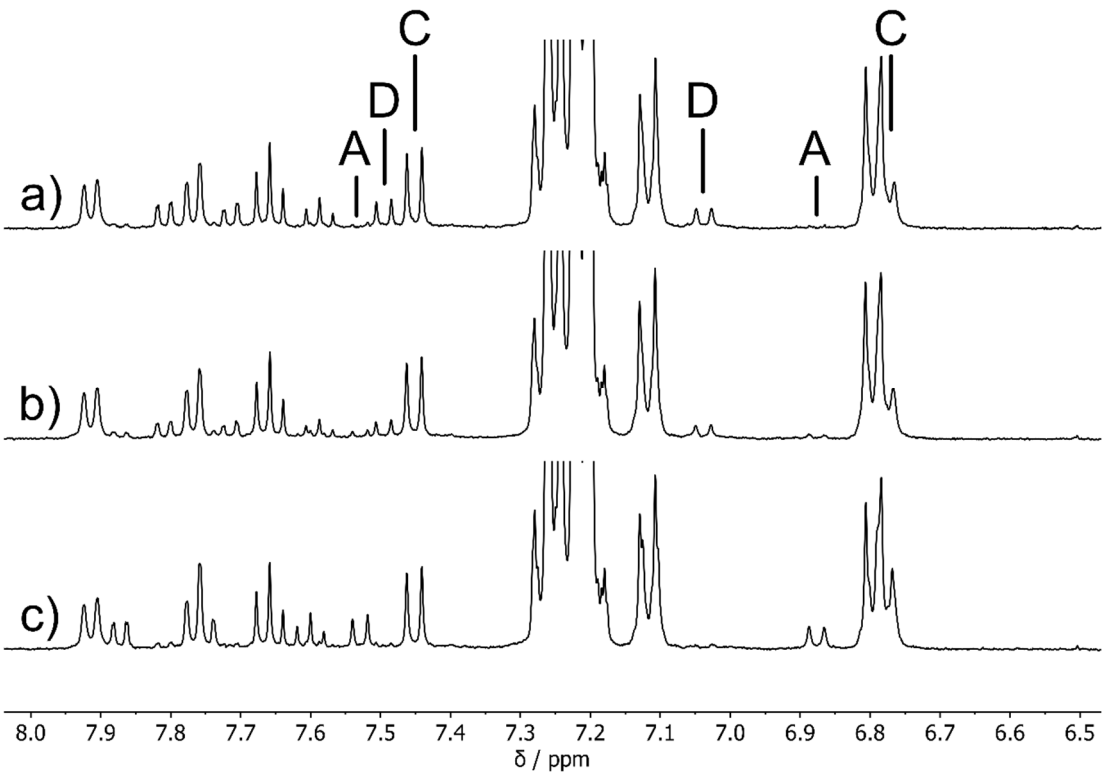

Figure 119 ^{1}H NMR (400 MHz, $(CDCl_2)_2$, 20 °C) spectra of an (*E*/*Z*)-mixture of **70**, obtained after the low-temperature experiments discussed above. **a)** initial spectrum **b)** after 27 min at 100 °C **c)** after a total of 127 min at 100 °C. Characteristic signals are tentatively assigned to **A-**, **C**- and **D**-type isomers based on spectral similarity to compound **2**. Upon heating, the disappearance of **D**-signals and the formation of **A**-signals is observed. Spectra are clipped vertically for clarity.

Similar experiments were performed for compound **75**. It should be noted, that **75** could not be fully characterized due to the small amount obtained, which was immediately used in irradiation experiments, and the structural assignment is tentatively based on HRMS and ^{1}H NMR, as well as spectral characteristics discussed in the following. When a UV/Vis sample of **75** in CH_2Cl_2 was irradiated with 405 nm or 450 nm light, the resulting spectra were characteristic for accumulation of **C**- or **D**-type isomers respectively (see Figure 120).

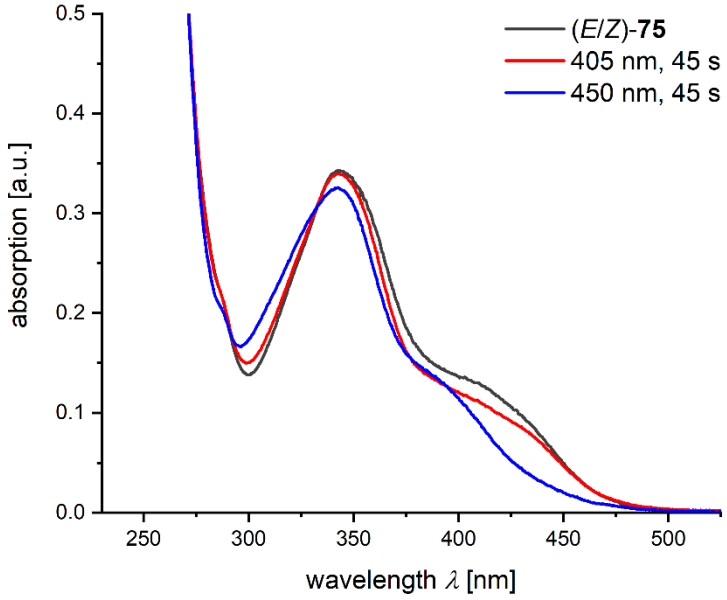

Figure 120 UV/Vis absorption spectra of an (*E*/*Z*)-mixture of **75** in CH_2Cl_2 at 23 °C (*grey*: initial spectrum; *red*: after irradiation with 405 nm light; *blue*: after irradiation with 450 nm light). The spectral changes upon irradiation with 450 nm light are characteristic for the accumulation of a **D**-type isomer.

In ^{1}H NMR experiments, a similar behavior was observed. When a sample of **75** in $(CDCl_2)_2$ was irradiated externally with 450 nm at 23 °C, the signal set assigned to the **A**-type isomer disappeared completely and the formation of a **D**-type isomer was observed (see Figure 121). This **D**-type isomer did not undergo noticeable thermal isomerization at ambient temperatures.

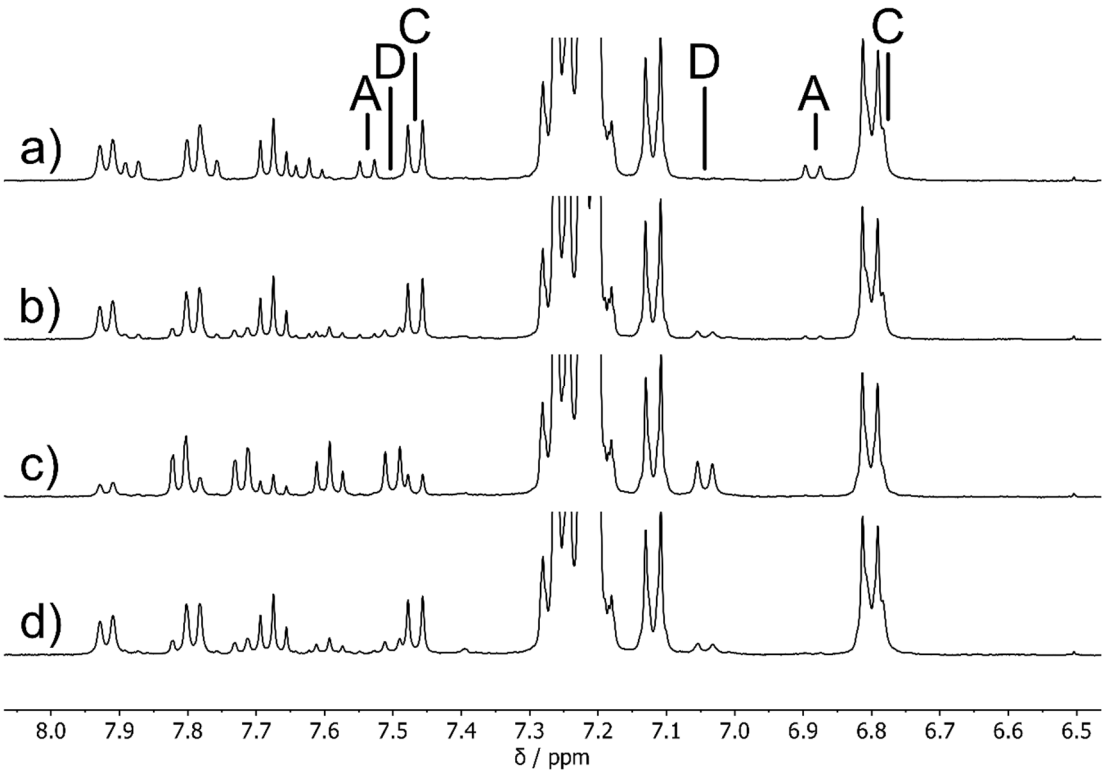

Figure 121 ^{1}H NMR (400 MHz, $(CDCl_2)_2$, 20 °C) spectra of **a)** a mixture of stable (*E*)- and (*Z*)-**75 b)** after external irradiation with 405 nm light **c)** after external irradiation with 450 nm light **d)** after external irradiation with (again) 405 nm light. Characteristic signals are tentatively assigned to **A**-, **C**- and **D**-type isomers based on spectral similarity to the respective isomers of **2**. Spectra are clipped vertically for clarity.

These observations strongly suggest that both compounds **70** and **75** follow the same directional switching mechanism that was found for compound **2**, with the bulky stopper group blocking the chain from passing through the macrocycle. Therefore, further modifications to the macrocyclic motor setup are necessary for achieving structures that are "locked" in a threaded state. Possibilities for future investigations include increasing the macrocyclic ring size, as well as the length of the stoppered chain. Another approach could be changing the attachment point of the stoppered chain on the indanone fragment, e.g. to the cyclopentyl ring.

4 A Prospective Hydrogen Bond Controlled Molecular Motor

An interesting aspect of molecular motor development is the control of motor motion by additional stimuli. Recent examples include cation-modulated rotary speed,[146] light-gated rotation,[147] chemical braking,[148] acid-base[149] and supramolecular[150] control of motor motion. In the following chapters, prospective HTI based motor **87** will be discussed. Molecule **87** incorporates a phenolic hydroxy group on the indanone fragment and is expected to form intramolecular hydrogen bonds, thus potentially changing original motor directionality by stabilization of previously metastable isomeric states, as well as potentially adding acid-base-responsiveness.

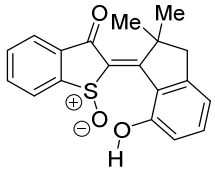

(*Z*)-**87**

Figure 122 Molecular structure of prospective motor **87**.

4.1 Synthesis of Prospective Motor 87

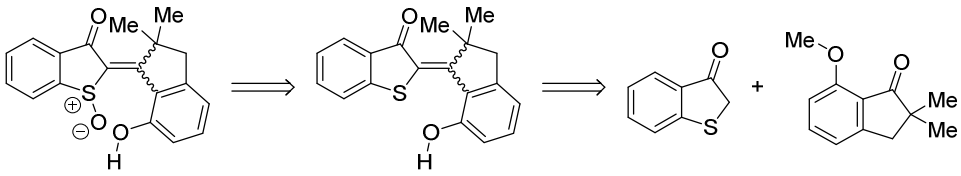

87

Scheme 44 Retrosynthetic approach towards potential hydroxy-HTI molecular motor **87**.

The synthesis strategy, as depicted in Scheme 44, was based on the well-established HTI synthesis by condensation of an indanone and a benzothiophenone followed by oxidation to the sulfoxide. In a first attempt, hydroxy-HTI **91** (see Scheme 45) was prepared and then subjected to oxidation with sodium perborate.

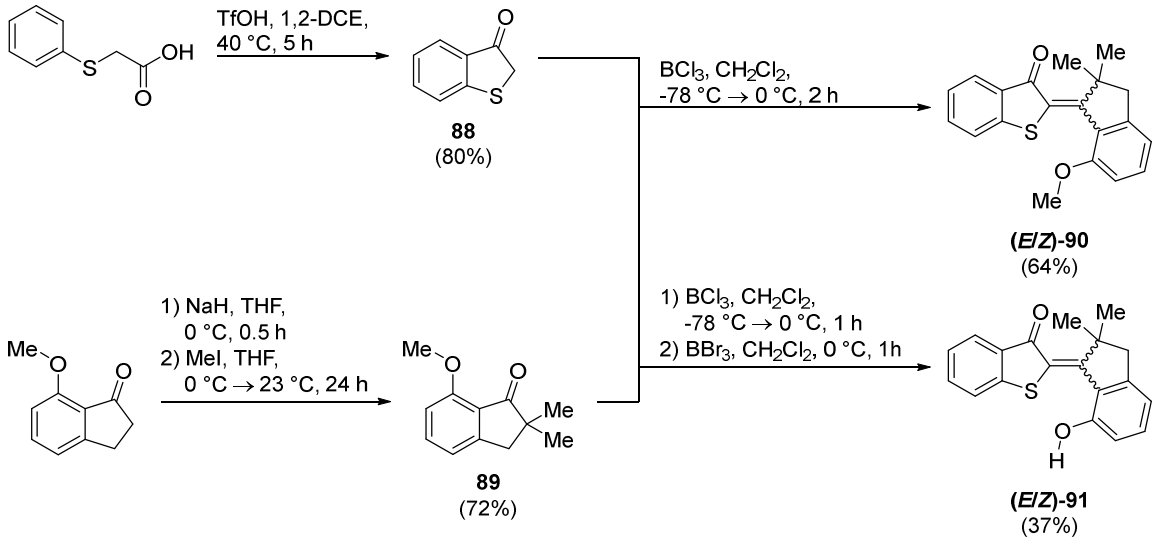

Scheme 45 Synthesis of HTI **90** by condensation of benzothiophenone **88** and indanone **89**. Phenol derivative **91** could be obtained by condensation of **88** and **89** and subsequent demethylation with BBr_3 in a one-pot procedure without the isolation of intermediate **90**.

HTI **90** could be obtained by BCl_3-mediated condensation of benzothiophenone **88** and indanone **89**. Demethylation of the phenol moiety with BBr_3 yielded HTI **91**. The condensation-demethylation sequence can also be performed in a one-pot type procedure (see Scheme 45). With hydroxy-HTI **91** at hand, oxidation to the sulfoxide was attempted using sodium perborate in acetic acid at 23 °C. However, as shown in Scheme 46, the desired product **87** could not be obtained. Instead, spirocyclic compound **92** could be isolated in 9% yield, the structure of which could be determined by X-ray crystallography (see Section 6.3 for crystal structure).

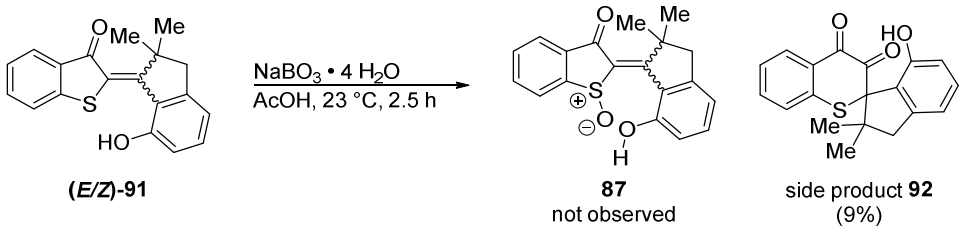

Scheme 46 Attempted synthesis of prospective motor **87** by oxidation of **91** with sodium perborate in acetic acid. No formation of the desired product was observed. Instead, spirocyclic compound **92** could be isolated and identified by X-ray crystallography.

In another synthesis attempt, depicted in Scheme 47, the order of demethylation and oxidation was reversed. HTI **90** was readily oxidized by sodium perborate in acetic acid, giving sulfoxide **93** in excellent yield (96%). Again, BBr_3 in CH_2Cl_2 was used for demethylation of the phenol moiety. The starting material was consumed after 40 min at

0 °C, as monitored by TLC. However, no formation of the desired demethylation product could be observed.

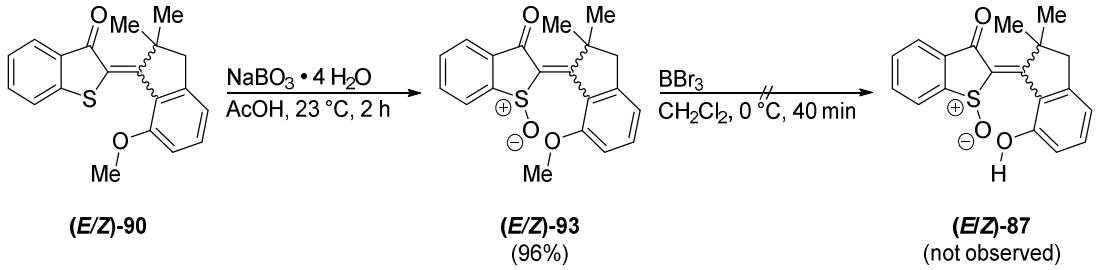

Scheme 47 Attempted synthesis of HTI **87** *via* oxidation of **90** followed by demethylation. No formation of the desired product could be observed upon treatment of sulfoxide **93** with BBr_3 in CH_2Cl_2.

Therefore, a protecting group strategy was applied (see Scheme 48). Sterically demanding silyl ethers, such as TBS, can be introduced and removed under mild conditions but should be reasonably stable to the conditions employed for oxidation to the sulfoxide (AcOH, sodium perborate, 23 °C). Silylated HTI **94** could be prepared from HTI **91**, using TBSCl and imidazole in DMF.[151] Again, oxidation to the sulfoxide was performed with sodium perborate in acetic acid, giving sulfoxide **95** in 32% yield over two steps. Finally, deprotection of the silyl ether with TBAF in THF gave the desired phenol derivative **87** in 80% yield.

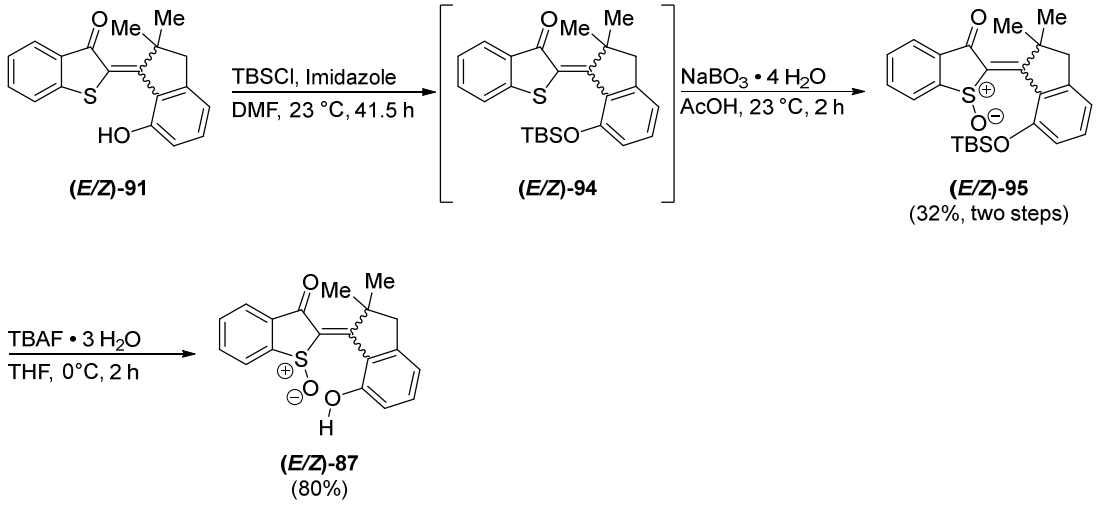

Scheme 48 Successful synthesis of phenol-type motor candidate **87** via silyl ether **94**

4.2 Theoretical Description of Prospective Motor 87

In the following, both neutral **87$_n$** and deprotonated (anionic) **87$_a$** will be discussed. Respective subscripts **n** (neutral) and **a** (anionic) are added for clarity. Geometry optimizations and subsequent frequency calculations were performed for both (*S*)-**87$_n$** and (*S*)-**87$_a$** at different levels of theory. For each compound, four minimum structures were found: isomers **A** (*Z*,*S*,*P*), **B** (*E*,*S*,*M*), **C** (*E*,*S*,*P*) and **D** (*Z*,*S*,*M*). A graphical comparison of the relative free energies found at different levels of theory is given in Figure 123 and Figure 124. In the case of **87$_a$**, the order of relative energies of each geometry was consistent for all the methods used. Isomer **A-87$_a$** was found to be the global minimum, while **B-87$_a$** and **D-87$_a$** were found as metastable isomers. In contrast, for neutral (*S*)-**87$_n$** significant differences were found depending on the choice of functional. With the initially investigated B3LYP functional, **C-87$_n$** was found as the global minimum and isomer **D-87$_n$** was 1.7 kcal mol^{-1} higher in energy (see Figure 124). In a comparative study by *Boese*, the Minnesota range of functionals from the *Truhlar* group were found to perform well for hydrogen bonded species.[152] Therefore, the M062X[153] functional was also used in the following. However, with the use of the M062X functional, the relative order of isomer energies was changed: **D-87$_n$** was found as the global minimum and isomer **C-87$_n$** was 0.6 kcal mol^{-1} higher in energy. The experimentally observed energy difference between neutral stable (*E*)- and (*Z*)-**87$_n$** in CD_2Cl_2 was 0.17 kcal mol^{-1} with (*Z*)-**87$_n$** being the more stable isomer, as determined by ^{1}H NMR from the isomeric ratio at 25 °C (see Section 4.3 for details). This experimental result is better reproduced by the M062X functional. Note that the inclusion of diffuse functions on hydrogen atoms or the addition of dispersive interactions had a negligible impact in comparison to the choice of functional.

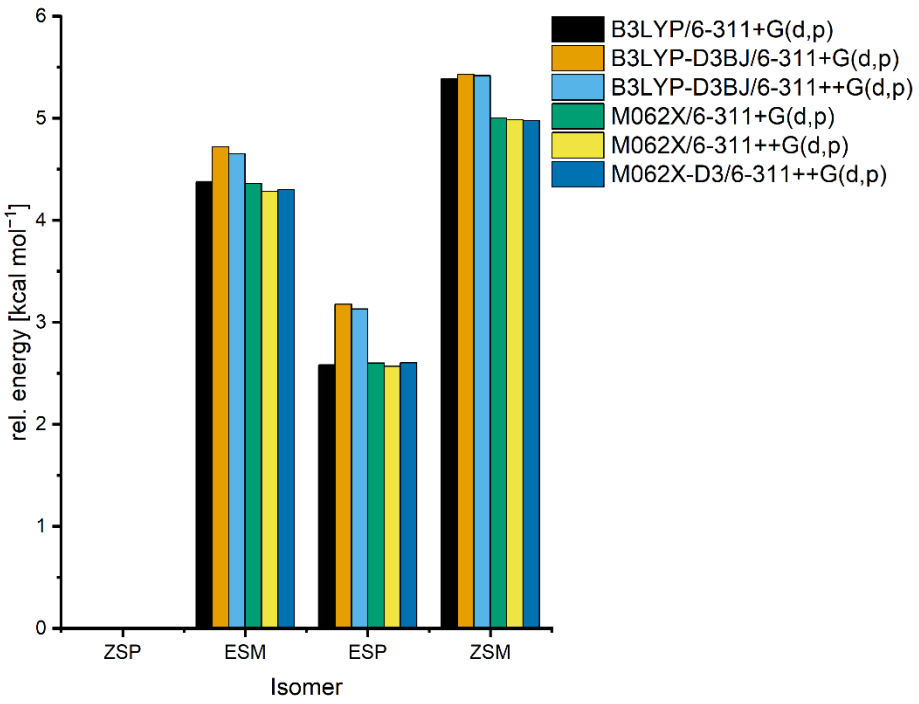

Figure 123 Relative Free Energies obtained for **87ₐ** at different levels of theory. No positively charged counter-ion was included in the calculations. A PCM (CH_2Cl_2) implicit solvent model was used in all cases. In all approaches, the (*Z*,*S*,*P*)-isomer (**A-87ₐ**) was found to be the global minimum.

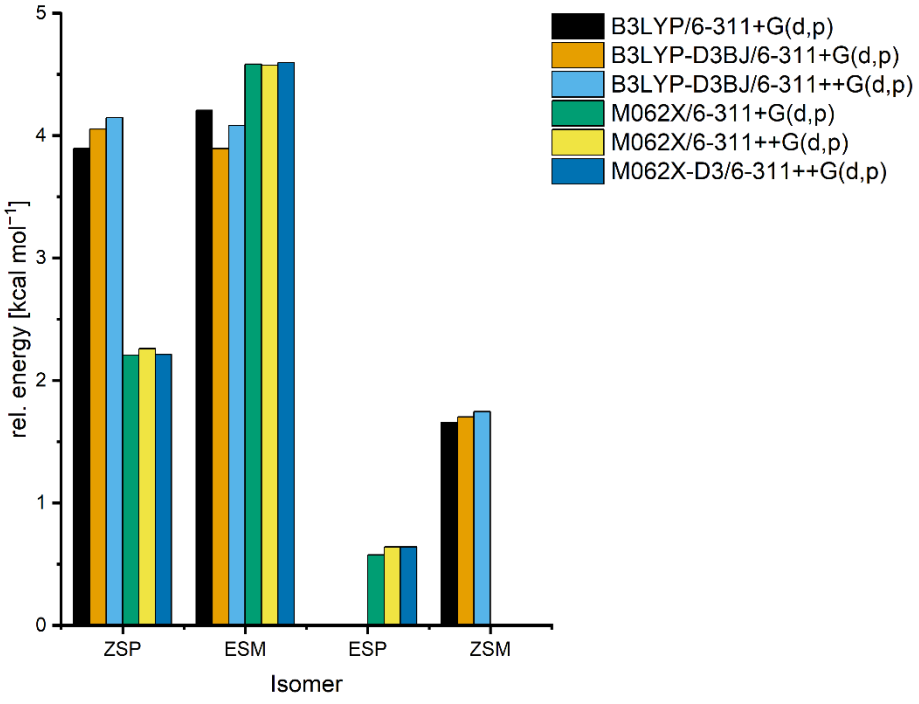

Figure 124 Relative Free Energies obtained for **87ₙ** at different levels of theory. A PCM (CH_2Cl_2) implicit solvent model was used in all cases. There are significant differences between the results produced by the B3LYP and the M062X functionals. With B3LYP, the (*E*,*S*,*P*)-isomer (**C-87ₙ**) was found to be the global minimum, whereas with M062X it was the (*Z*,*S*,*M*)-isomer (**D-87ₙ**).

The full energy profiles including transition states for hypothetical motor operation were then calculated at both the B3LYP-D3BJ/6-311+G(d,p) PCM (CH_2Cl_2) and M062X-D3/6-311++G(d,p) PCM (CH_2Cl_2) levels of theory (see Figure 127 and Figure 130 for energies). The minimum geometries found at the same levels of theory are shown in Figure 125 and Figure 126 for **87$_a$** and in Figure 128 and Figure 129 for **87$_n$**. Again, the profiles are very similar for **87$_a$**. The profile is in agreement with the established four-step ratcheting-type mechanism.[9] Stable **A-87$_a$** undergoes photoinduced double bond isomerization to metastable **B-87$_a$**. The following thermal helix inversion to stable **C-87$_a$** is characterized by an activation barrier of 19-20 kcal mol^{-1}, and hence should be observable by spectroscopic means at temperatures below −10 °C. Subsequent photoinduced double bond isomerization to metastable **D-87$_a$**, followed by a potentially ultrafast helix inversion step (activation barrier of 2-3 kcal mol^{-1}) to stable **A-87$_a$** completes the 360° motor rotation cycle.

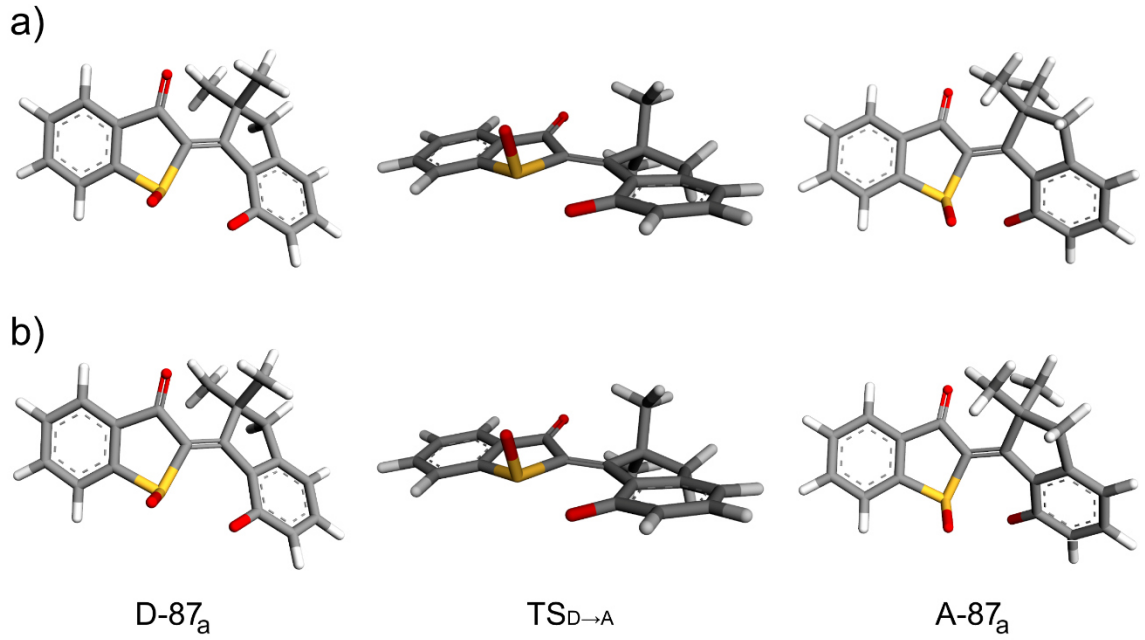

Figure 125 Theoretically obtained ground state geometries for (*Z*,*S*)-**87$_a$** at the **a)** B3LYP-D3BJ/6-311+G(d,p) PCM (CH_2Cl_2) and **b)** M062X-D3/6-311++G(d,p) PCM (CH_2Cl_2) level of theory. No positively charged counter-ion was included in the calculations. The respective geometries are virtually identical for both levels of theory.

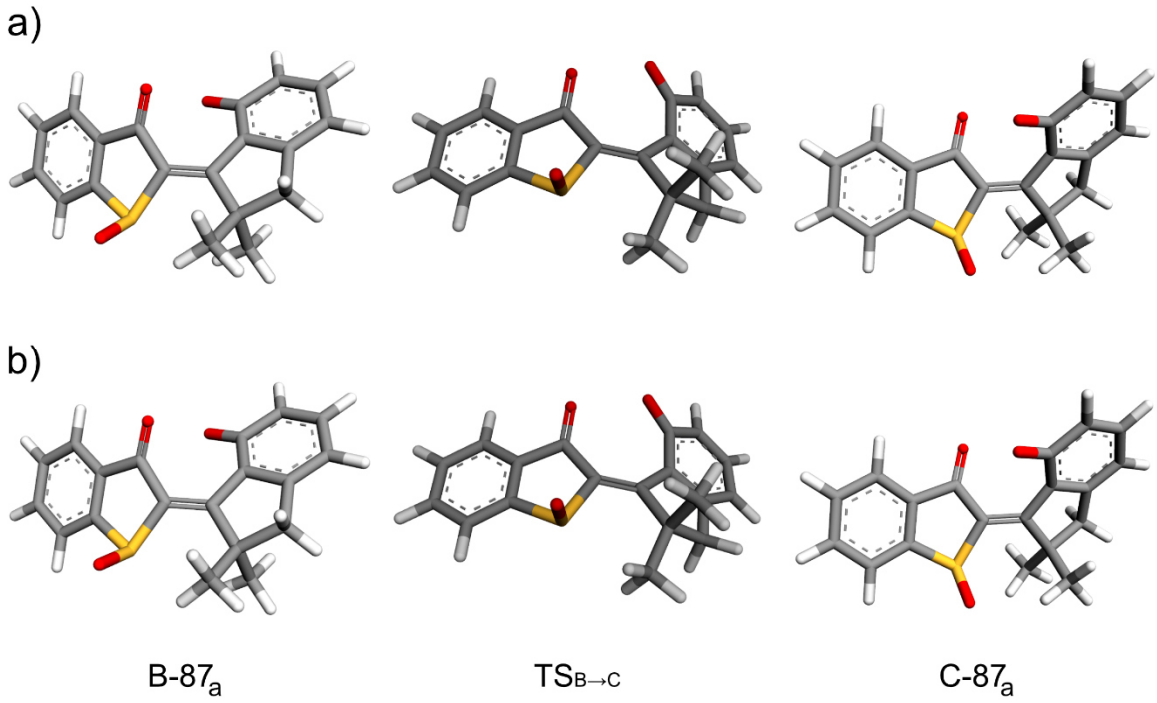

Figure 126 Theoretically obtained ground state geometries for (*E*,*S*)-**87**$_a$ at the **a)** B3LYP-D3BJ/6-311+G(d,p) PCM (CH_2Cl_2) and **b)** M062X-D3/6-311++G(d,p) PCM (CH_2Cl_2) levels of theory. No positively charged counter-ion was included in the calculations. The respective geometries are virtually identical for both levels of theory.

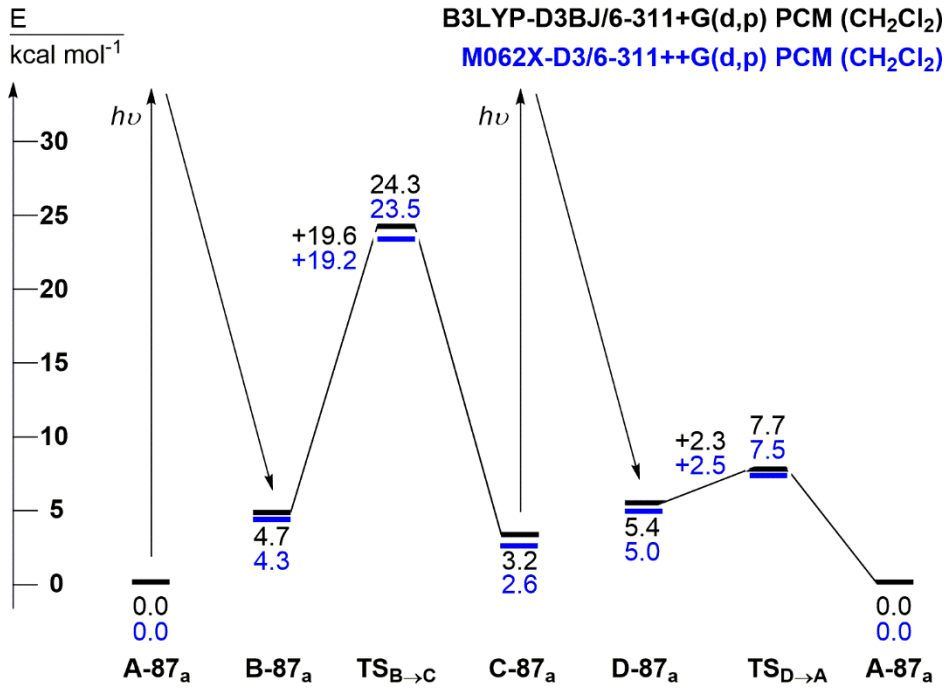

Figure 127 Theoretically obtained ground state energy profile for motor candidate **87**$_a$ at the B3LYP-D3BJ/6-311+G(d,p) PCM (CH_2Cl_2) (*black*) and M062X-D3/6-311++G(d,p) PCM (CH_2Cl_2) (*blue*) levels of theory.

The profile calculated for (*S*)-**87n** does not correspond to a four-step ratcheting mechanism. Instead, isomers **C-87n** and **D-87n** form a thermodynamic "sink", and neither forward nor backward motor operation is possible as both **A-87n** and **B-87n** are significantly higher in energy according to the theoretical results (Figure 130). Interestingly, two transition states were found for the helix inversion process of (*Z*)-**87n** (**D-87n** to **A-87n**). In TS1 the hydrogen bond between the phenolic hydroxy group and the sulfoxide remains, whereas it is broken in TS2 (see Figure 128 for geometries). It is thus plausible to assume that a sequence of the two transition states occurs during THI from **D-87n** to **A-87n**. As TS2 is significantly higher in energy than TS1 (approx. 5-6 kcal mol^{-1})[1], it constitutes the rate-limiting step of **D-87n** to **A-87n** isomerization. However, due to the large "uphill" energy difference between **D-87n** and **A-87n**, the THI process is not expected to be relevant.

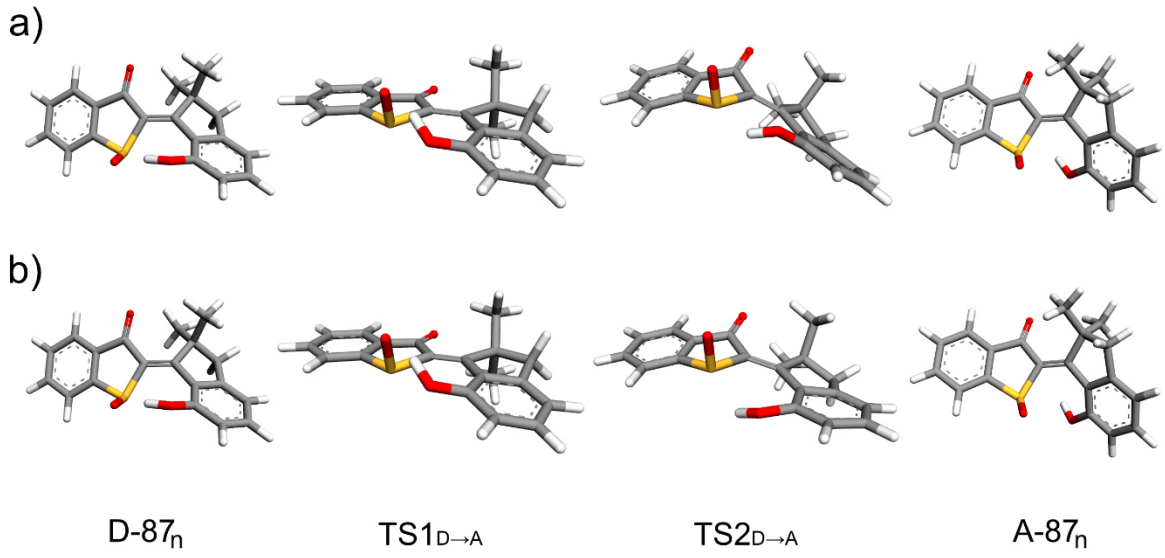

Figure 128 Theoretically obtained ground state geometries for (*Z*,*S*)-**87n** at the **a)** B3LYP-D3BJ/6-311+G(d,p) PCM (CH_2Cl_2) and **b)** M062X-D3/6-311++G(d,p) PCM (CH_2Cl_2) levels of theory. Two transition states were found for the helix inversion process. In TS1, the hydrogen bond between the phenolic hydroxy group and the sulfoxide is retained, whereas it is broken in TS2.

[1] Relative Free Energies (in kcal mol^{-1}): TS1: 8.4 (B3LYP-D3BJ/6-311+G(d,p) PCM (CH_2Cl_2)), 6.5 (M062X-D3/6-311++G(d,p) PCM (CH_2Cl_2)). TS2: 13.4 (B3LYP-D3BJ/6-311+G(d,p) PCM (CH_2Cl_2)), 12.5 (M062X-D3/6-311++G(d,p) PCM (CH_2Cl_2)).

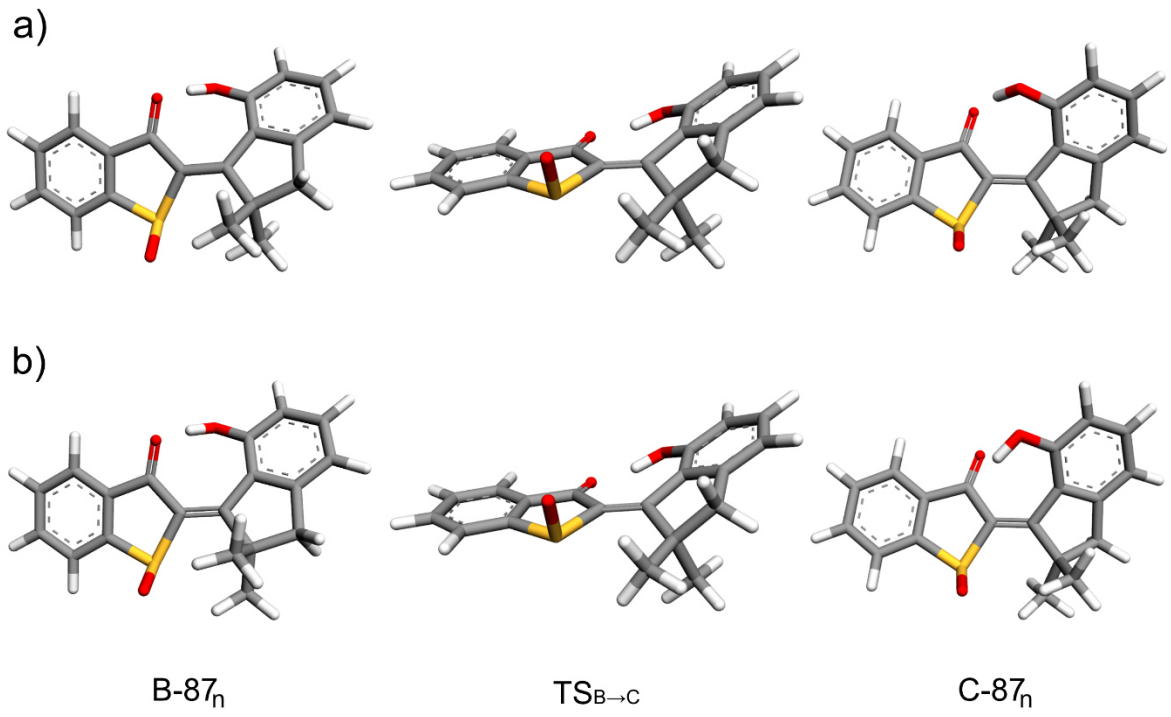

Figure 129 Theoretically obtained ground state geometries for (*E*,*S*)-**87ₙ** at the **a)** B3LYP-D3BJ/6-311+G(d,p) PCM (CH_2Cl_2) and **b)** M062X-D3/6-311++G(d,p) PCM (CH_2Cl_2) levels of theory. Hydrogen bonding between the carbonyl oxygen and the phenolic hydroxy group is found in both isomers for B3LYP compared to only in the **B**-isomer for M062X.

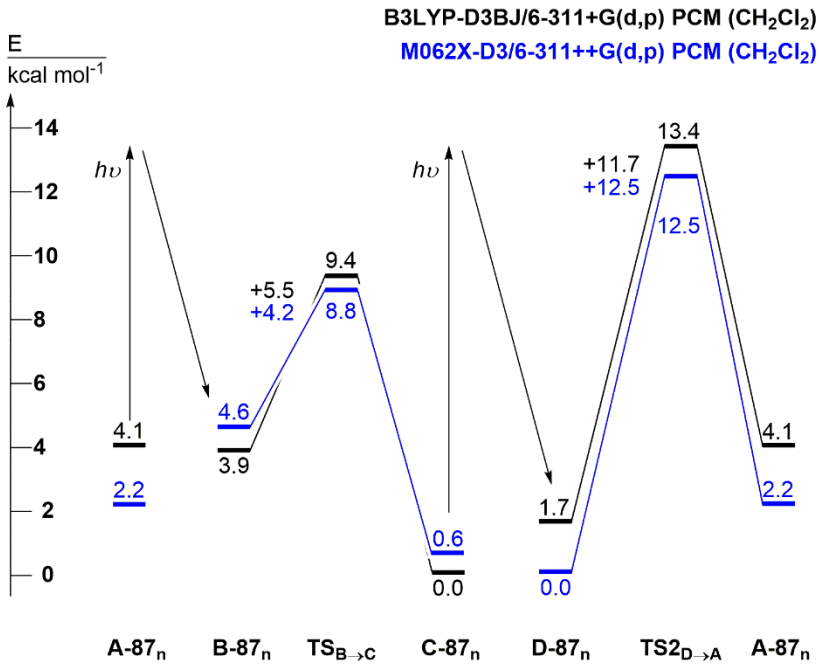

Figure 130 Theoretically obtained ground state energy profile for motor candidate **87ₙ** at the B3LYP-D3BJ/6-311+G(d,p) PCM (CH_2Cl_2) (*black*) and M062X-D3/6-311++G(d,p) PCM (CH_2Cl_2) (*blue*) levels of theory. Only TS2 is included in the energy scheme, as it corresponds to the rate-limiting step.

4.3 Conformational Analysis of Neutral **87**

A structural analysis was performed for potential motors neutral **87$_n$** and deprotonated **87$_a$** (with DBU) by solution NMR spectroscopy. ^{1}H NMR spectra and assignments of signals to the respective molecular structures are shown in the following. Due to the low barrier for double bond isomerization (see Section 4.5), stable (*E*)- and (*Z*)-**87$_n$** could not be separated by conventional HPLC or SFC methods. Therefore, NMR analysis was performed on mixtures of the two isomers. Interestingly, depending on the solvent (CD_2Cl_2 or DMF-d_7) different isomer ratios were established even though the samples were prepared from the same batch of solid **87$_n$**. This means that solvent polarity and / or hydrogen bonding capacity have a significant effect on the relative energies of stable isomers. In CD_2Cl_2, a *Z*:*E* ratio of 57:43 was established at 25 °C, corresponding to an energy difference of $\Delta G = 0.17$ kcal mol^{-1}. In DMF-d_7, the ratio was 66:34 (*Z*:*E*), corresponding to $\Delta G = 0.39$ kcal mol^{-1}. In both cases, the *Z*-isomer was the more stable one. This is in agreement with theoretical calculations on the M062X-D3/6-311++G(d,p) PCM (CH_2Cl_2) level of theory (see Section 4.2). Based on results from theory, (*Z*,*S*,*M*)/(*Z*,*R*,*P*)-**87$_n$** and (*E*,*S*,*P*)/(*E*,*R*,*M*)-**87$_n$** are expected to be the stable isomers, with (*Z*,*S*,*M*) being the most stable one. The free energy difference obtained from theory is $\Delta G = 0.64$ kcal mol^{-1}, corresponding to an isomeric ratio of 75:25 (*Z*:*E*).

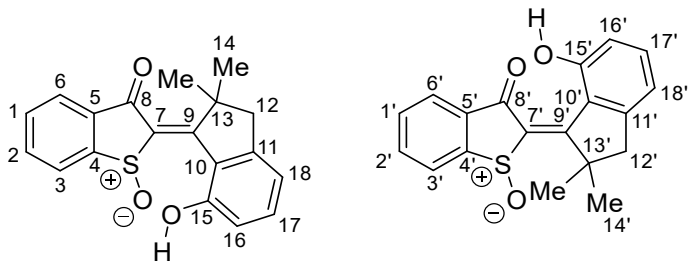

Figure 131 Molecular structures of (*Z*)-**87$_n$** (left) and (*E*)-**87$_n$** (right), as well as numbering used in the following.

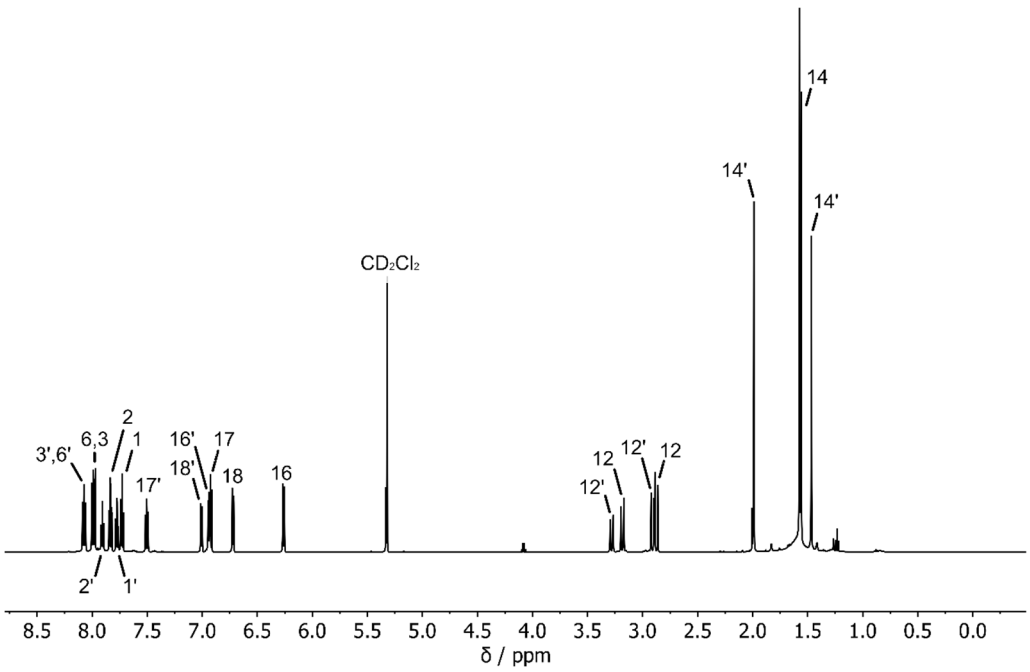

Figure 132 ^{1}H NMR (600 MHz, CD_2Cl_2, 25 °C) spectrum of **87$_n$** and assignments of signals to the respective protons. A *Z*:*E* ratio of 57:43 was established.

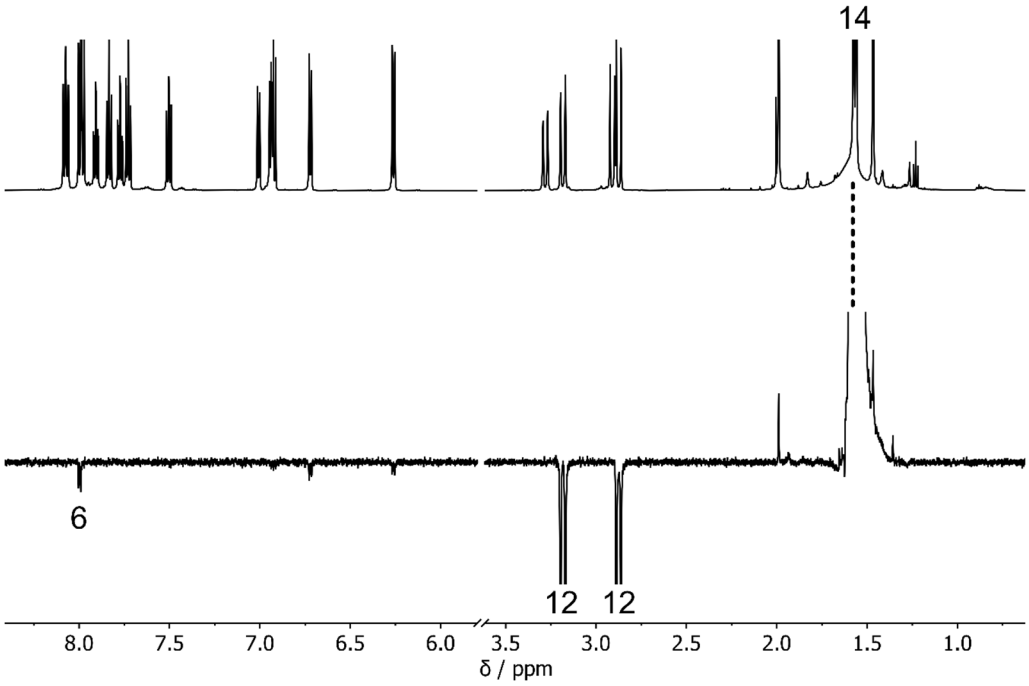

Figure 133 1D NOE (601 MHz, CD_2Cl_2, 25 °C) experiment for **87$_n$**. Methyl group protons 14 were irradiated in the NOE experiment (marked by a dotted line). The observed through space coupling with aromatic proton 6 on the thioindigo part confirms (*Z*)-configuration of the central double bond for the major isomer. Spectra are clipped vertically and only the region of interest is shown for clarity.

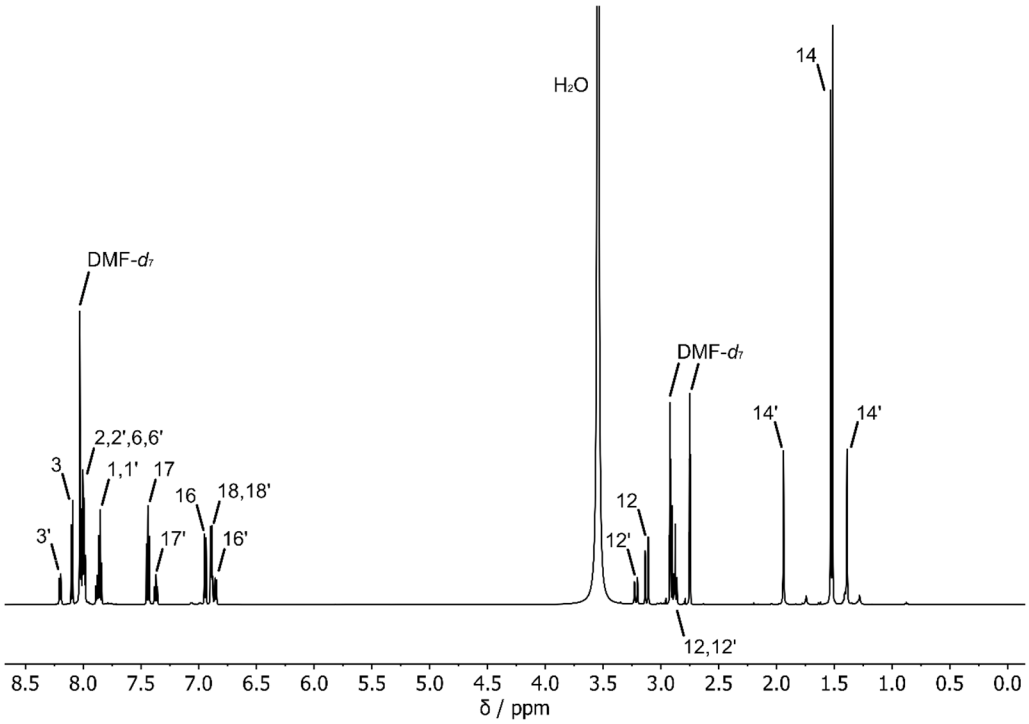

Figure 134 ^{1}H NMR (601 MHz, DMF-d_7, 25 °C) spectrum of **87$_n$**. A *Z*:*E* ratio of 66:34 was established.

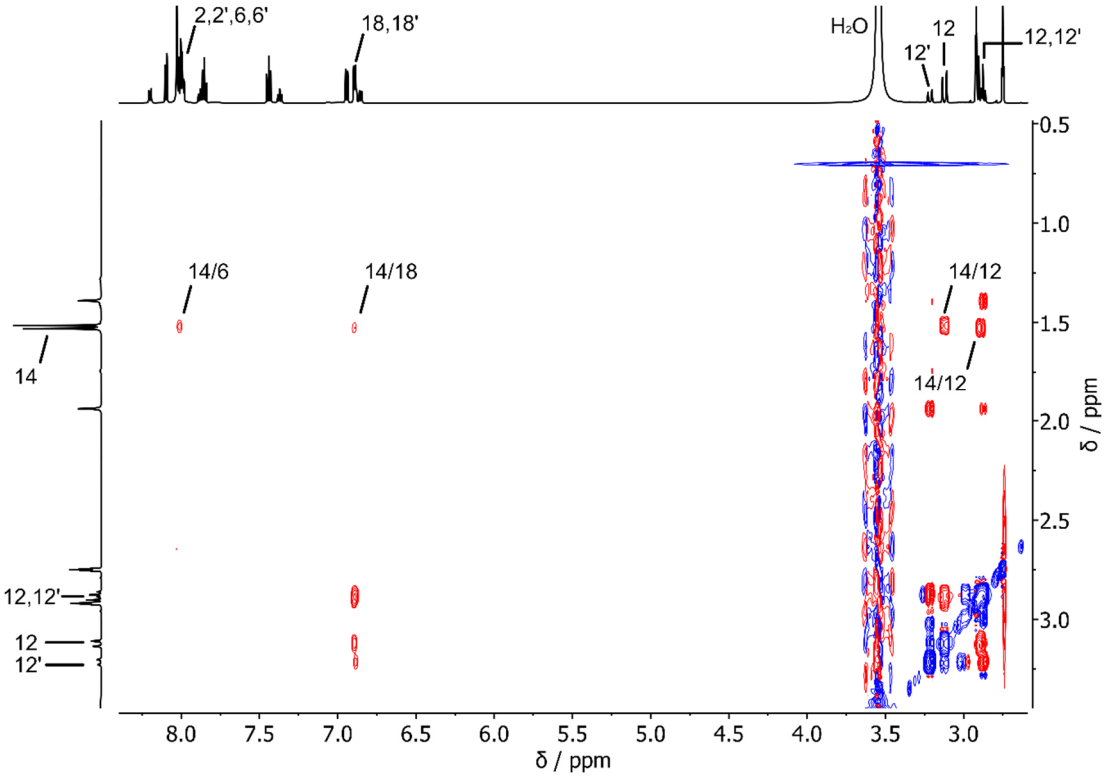

Figure 135 Excerpt of the NOESY (601 MHz, DMF-d_7, 25 °C) spectrum of **87$_n$**. (*Z*)-configuration of the major isomer is confirmed by the through space coupling between methyl group protons 14 on the indanone part with aromatic proton 6 on the thioindigo part.

4.4 Conformational Analysis of Deprotonated 87

In order to analyze the deprotonated form **87$_a$**, an appropriate base had to be chosen. Ideally, the base should be very strong and capable of quantitative deprotonation of **87**. Furthermore, it should be soluble in organic solvents and insensitive to ambient conditions (such as air and moisture). Finally, it should not show any absorption in the visible range of light. Based on these considerations, DBU (pK_{aH} = 24.31 in MeCN[154]) was chosen for the following investigations. When an equimolar amount of DBU was added to a solution of **87$_n$** in CD_2Cl_2, the color of the solution immediately changed from yellow to deep red. Despite starting from a *Z*/*E* mixture of **87$_n$**, only a single isomer was observed after deprotonation. Again, this is supported by theoretical results (see Section 4.2). Based on calculations on the M062X-D3/6-311++G(d,p) PCM (CH_2Cl_2) level of theory, (*Z*,*S*,*P*)/(*Z*,*R*,*M*)-**87$_a$** is expected to be the most stable isomer. The other isomers are 2.6–5.0 kcal mol^{-1} higher in energy and therefore not observable by NMR of an equilibrium mixture at ambient temperatures. Due to protons 3 and 6 being accidentally isochronous, (*Z*)-configuration of the central double bond could not be verified by NOE experiments. In additional NOESY experiments, through-space

couplings between $[DBU+H]^+$ and **87a** proton signals could be observed (see Figure 139), confirming the formation of an ion pair in CH_2Cl_2 solution.

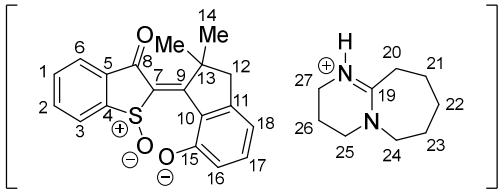

Figure 136 Molecular structure and atom numbering used in the following for a stoichiometric 1:1 complex of **87a** and $[DBU+H]^+$. The assignment of (*Z*)-configuration is based on theoretical calculations (see Section 4.2).

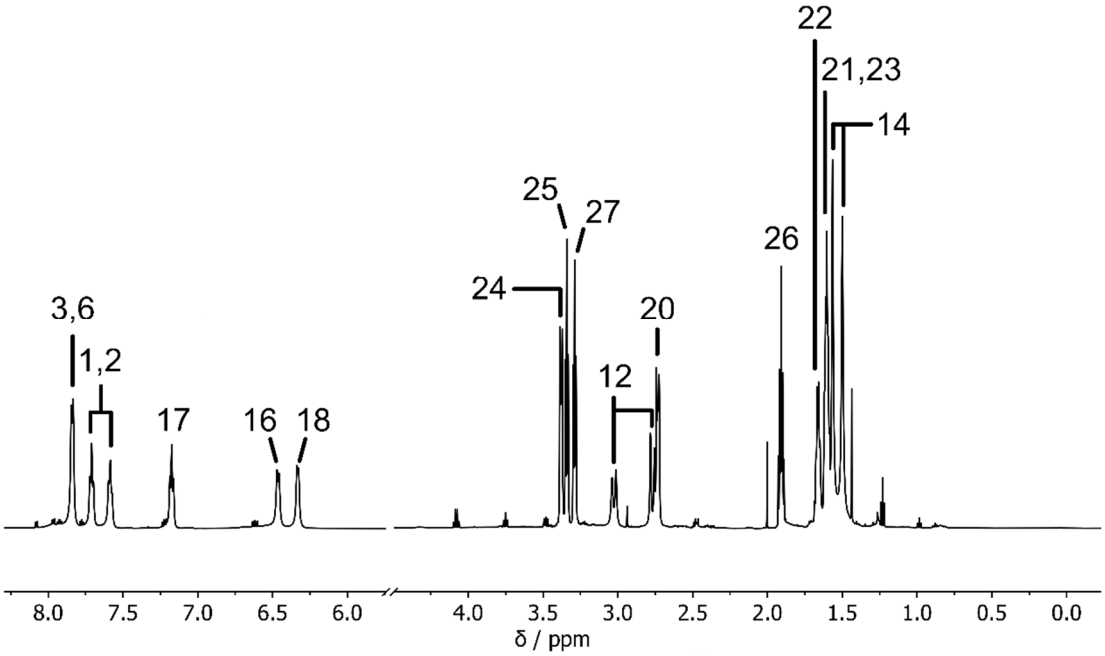

Figure 137 ^{1}H NMR (600 MHz, CD_2Cl_2, 25 °C) of the solution obtained by mixing equimolar amounts of **87$_n$** and DBU (approx. 2.4×10^{-2} M). Only one set of signals was observed in the mixture, corresponding to the organic salt.

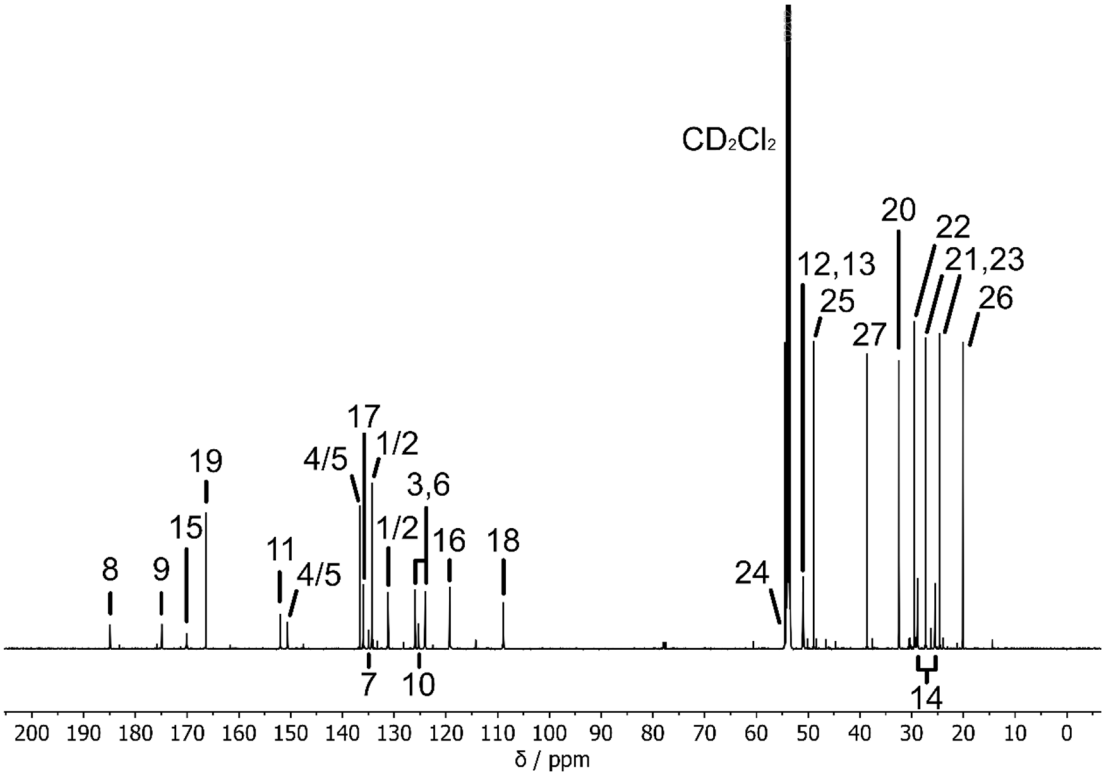

Figure 138 ^{13}C NMR (151 MHz, CD_2Cl_2, 25 °C) spectrum of the solution obtained by mixing equimolar amounts of **87$_n$** and DBU (approx. 2.4×10^{-2} M).

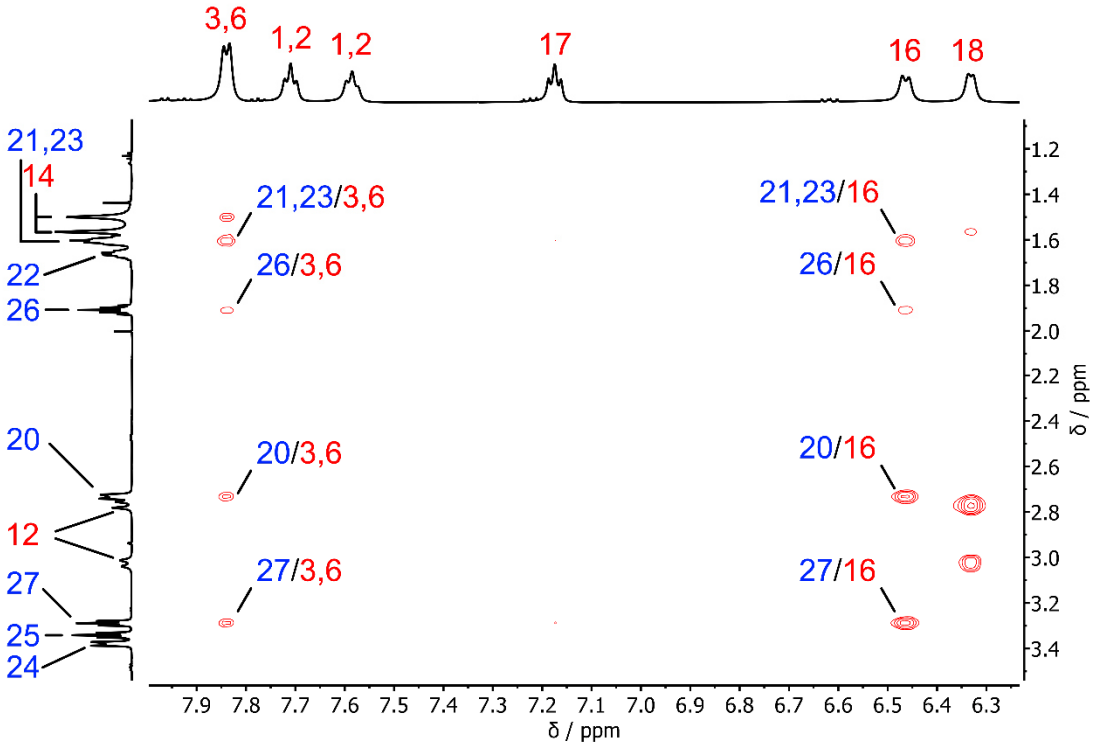

Figure 139 Excerpt from the NOESY (600 MHz, CD_2Cl_2, 25 °C) spectrum of the solution obtained by mixing equimolar amounts of **87$_n$** and DBU (approx. 2.4×10^{-2} M). Close proximity between $[DBU+H]^+$ and **87$_a$** is confirmed by the indicated cross signals between protons of the respective ions. *Note*: In the case of isochronous protons 3 and 6 as well as 21 and 23, it is not possible to tell which of the possible "pairs" is responsible for the signal. However, in all cases it is a through-space coupling between $[DBU+H]^+$ and **87$_a$** and therefore included herein. As protons 3 and 6 are isochronous, it is not possible to assign (*E*)- or (*Z*)-configuration based on NOE experiments. Signals are highlighted in blue ($[DBU+H]^+$) or red (**87$_a$**).

4.5 Deprotonation and Irradiation Experiments

Initial investigations into acid/base-response and potential photoswitching of **87** were performed by UV/Vis spectroscopy. When a solution of neutral **87$_n$** in spectroscopic grade DMF was prepared, a faint pink tint due to absorption around 550 nm was noticeable from the start. This is most likely caused by the presence of deprotonated form **87$_a$** because of basic contaminants (e.g. dimethylamine) or even the soda-lime-glass pipettes initially used for solvent transfer (when a small amount of **87$_n$** in DMF was kept in a glass pipette for some minutes, the solution significantly darkened towards a more purple color over time). Upon addition of an excess of DBU the solution turned purple and absorption at 550 nm was drastically increased. This is in agreement with the formation of phenolate **87$_a$** as the increased donor capacity of the phenolate is expected to result in a marked redshift of the absorption maximum. When the sample was irradiated with light of various wavelengths, no

absorption changes indicative of photoswitching were observed. However, when 565 nm or 450 nm light was used, there was a significant decrease in overall absorption, most likely due to photodegradation.

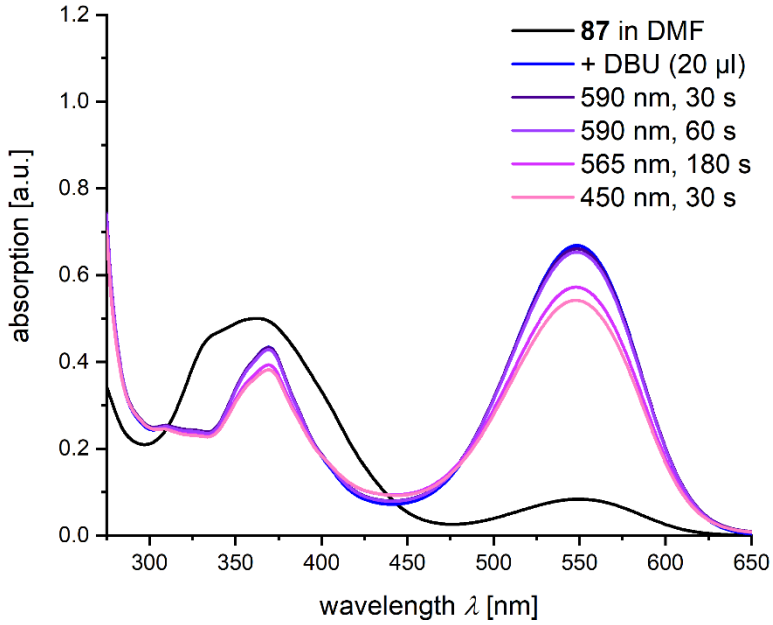

Figure 140 UV/Vis absorption spectra of **87**$_n$ in DMF (black), after addition of DBU (blue) and subsequent irradiation with light of different wavelengths (purple to pink). The initial absorption at 550 nm in the absorption spectrum of **87**$_n$ is most likely due to the presence of small amounts of **87**$_a$.

When an excess of TFA was added to acidify the sample, the color changed to a faint yellow and absorption at 550 nm was completely suppressed, whereas absorption in the 320-400 nm range was almost fully restored (see Figure 141). This suggests successful protonation to recover neutral **87**$_n$.

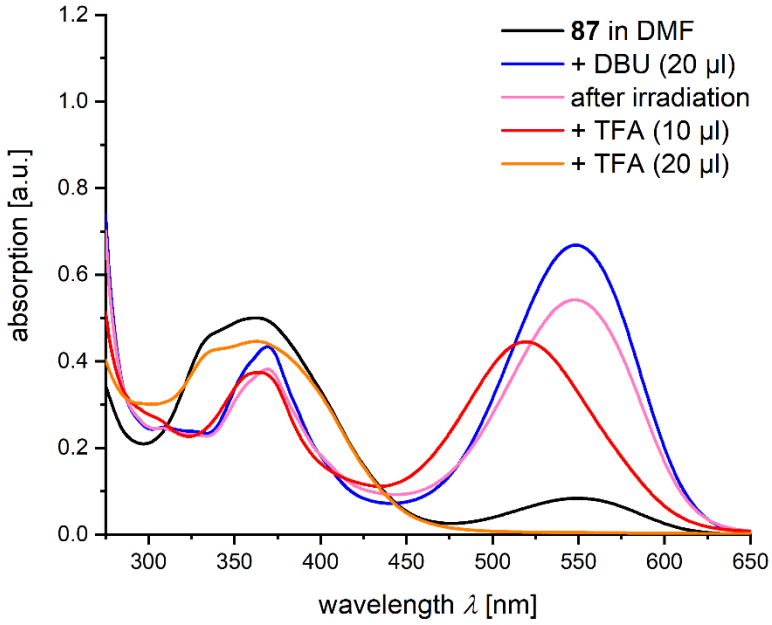

Figure 141 UV/Vis absorption spectra of **87**$_n$ in DMF (black), after addition of DBU (blue) and subsequent irradiation experiments (pink) followed by addition of TFA (red and orange).

Irradiation of this sample with 420 nm and 450 nm light resulted in reversible absorption changes around 375 nm, suggesting photoswitching between two isomeric forms.

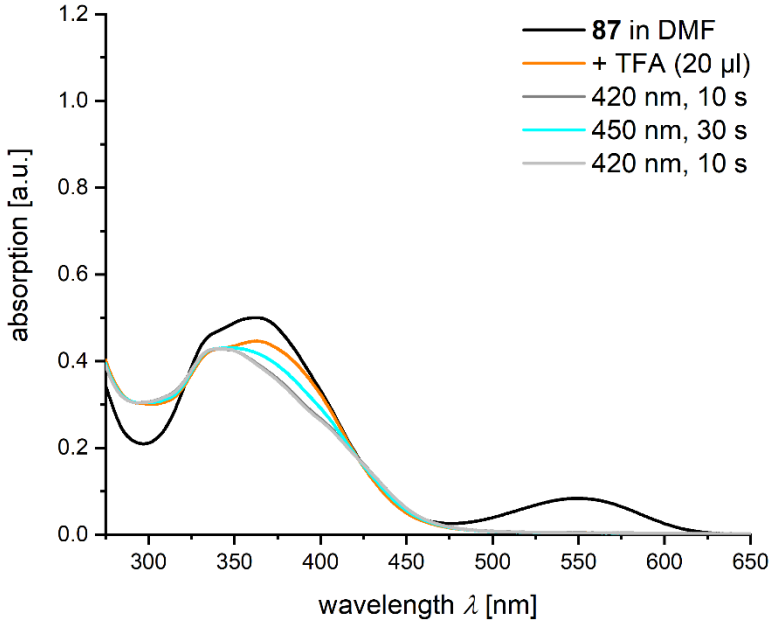

Figure 142 UV/Vis absorption spectra of **87**$_n$ in DMF (black), after the above experiments (orange) and irradiation with 420 nm (grey) and 450 nm (blue) light. A reversible change in absorption upon irradiation was observed.

To gain more insight into possible switching processes, ^{1}H NMR experiments were performed. When a sample of **87$_n$** in CD_2Cl_2 was irradiated *in situ* with 470 nm light at 0 °C, a change in isomer composition was observed (see Figure 143). Starting from an *Z*:*E* ratio of 56:44, a mixture enriched in (*Z*)-**87$_n$** was obtained (*Z*:*E* ratio of 82:18). During the irradiation process, no formation of intermediates was observed. The sample was then kept in the dark at 25 °C for 20 minutes, during which partial thermal back-isomerization occurred. Assuming a return to the previously determined equilibrium composition, an estimate of 22.1 kcal mol^{-1} can be given for the activation barrier at 25 °C (see Figure 144).

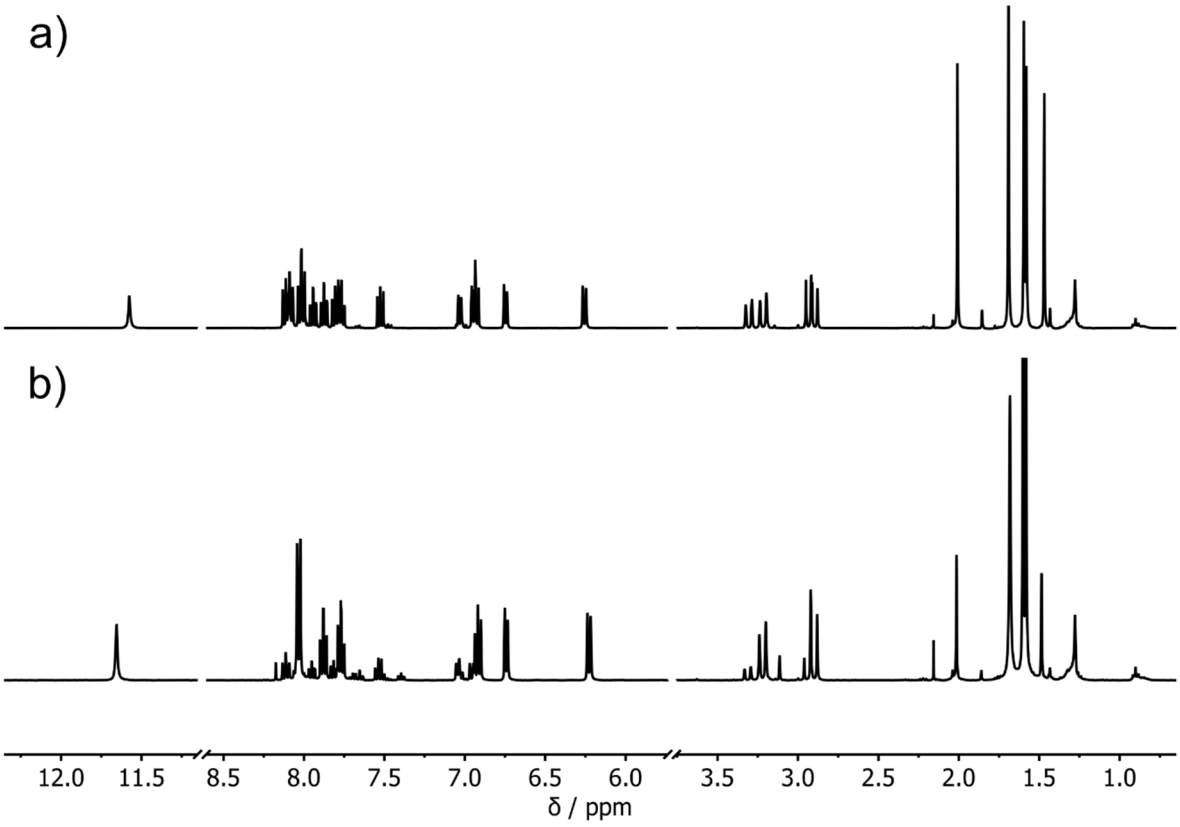

Figure 143 ^{1}H NMR (400 MHz, CD_2Cl_2, 0 °C) spectra of **87$_n$** before and after irradiation with 470 nm light. Photoirradiation of a sample of **87$_n$** in CD_2Cl_2 (**a)** *E*:*Z*, 44:56) resulted in accumulation of the (*Z*)-isomeric form (**b)** *E*:*Z*; 18:82). Irradiation was stopped due to the formation of a small amount of unidentified side product. Only regions of interest are shown and spectra are clipped vertically for clarity.

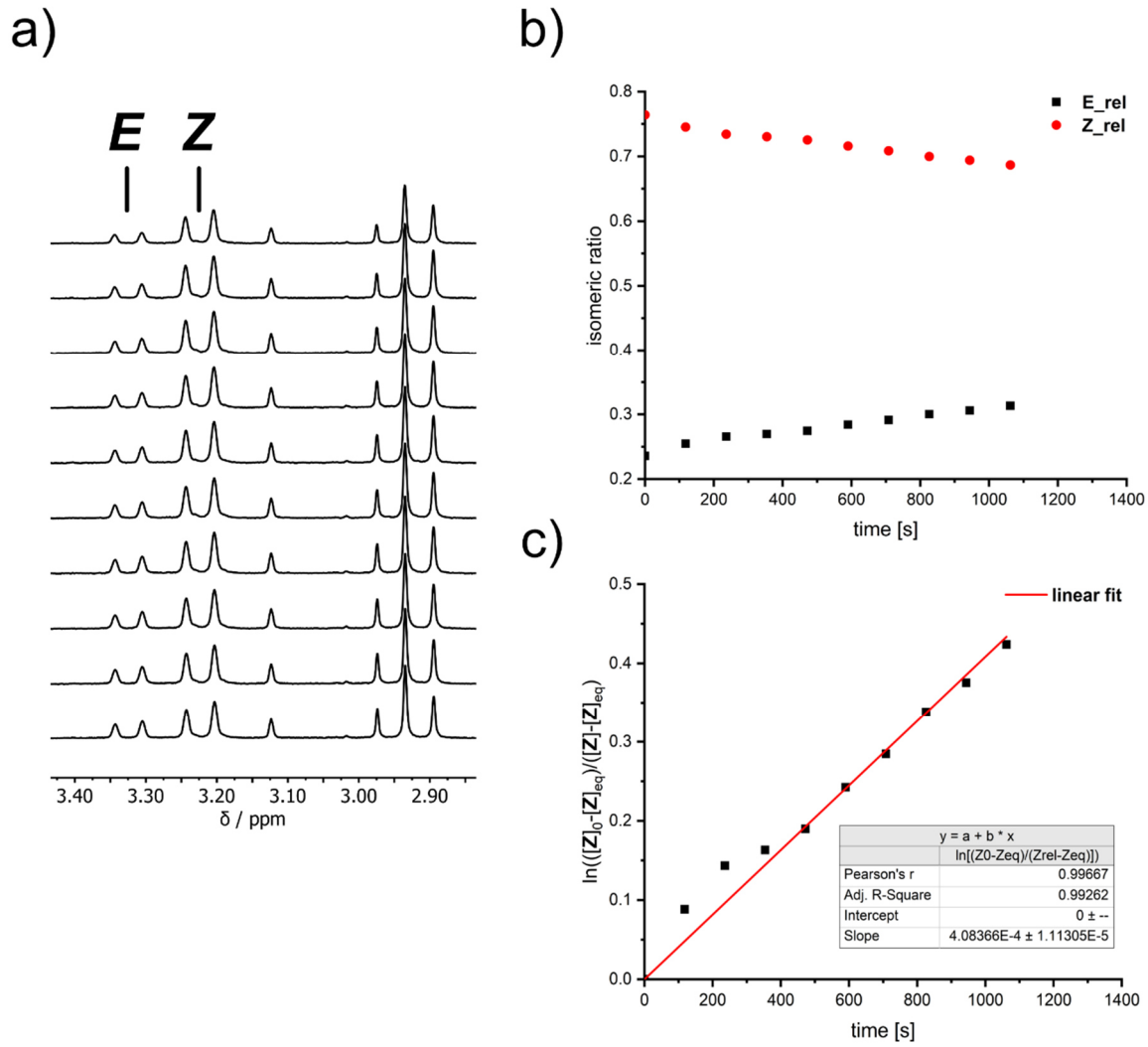

Figure 144 Kinetic analysis of the thermal *E*/*Z*-isomerization process of a sample enriched in (*Z*)-**87**$_n$. **a)** Indicative ^{1}H NMR (400 MHz, CD_2Cl_2, 25 °C) signals monitored over time. **b)** Isomeric ratio over time as obtained from integration of indicative ^{1}H NMR signals. **c)** ln plot of thermal decay of the *E*-isomer at 25 °C in the dark. An equilibrium ratio of 46% *E* and 54% *Z* is assumed (not reached, but known from the initial composition). The slope is 4.1×10^{-4} s^{-1}, which corresponds to a *Gibbs* energy of activation $\Delta G^{\ddagger} = 22.1$ kcal mol^{-1} at 25 °C.

An equimolar amount of DBU was then added to the sample to generate deprotonated form **87**$_a$, followed by *in situ* irradiation with 520 nm light. However, no change in spectra was observed, even at irradiation times of 40 min. This is most likely due to very high absorption of the sample (visual inspection of the sample confirmed insufficient light penetration of only approx. 2 mm). Two equiv. of TFA were then added to re-protonate **87**. The resulting spectrum was very similar to the initial spectrum of pure **87**$_n$, with the exception of a significant low-field shift for proton 16. At this point, chemical transformations cannot be

excluded. However, this signal shift could simply be caused by an increase in solvent polarity due to the addition of DBU-TFA salt.

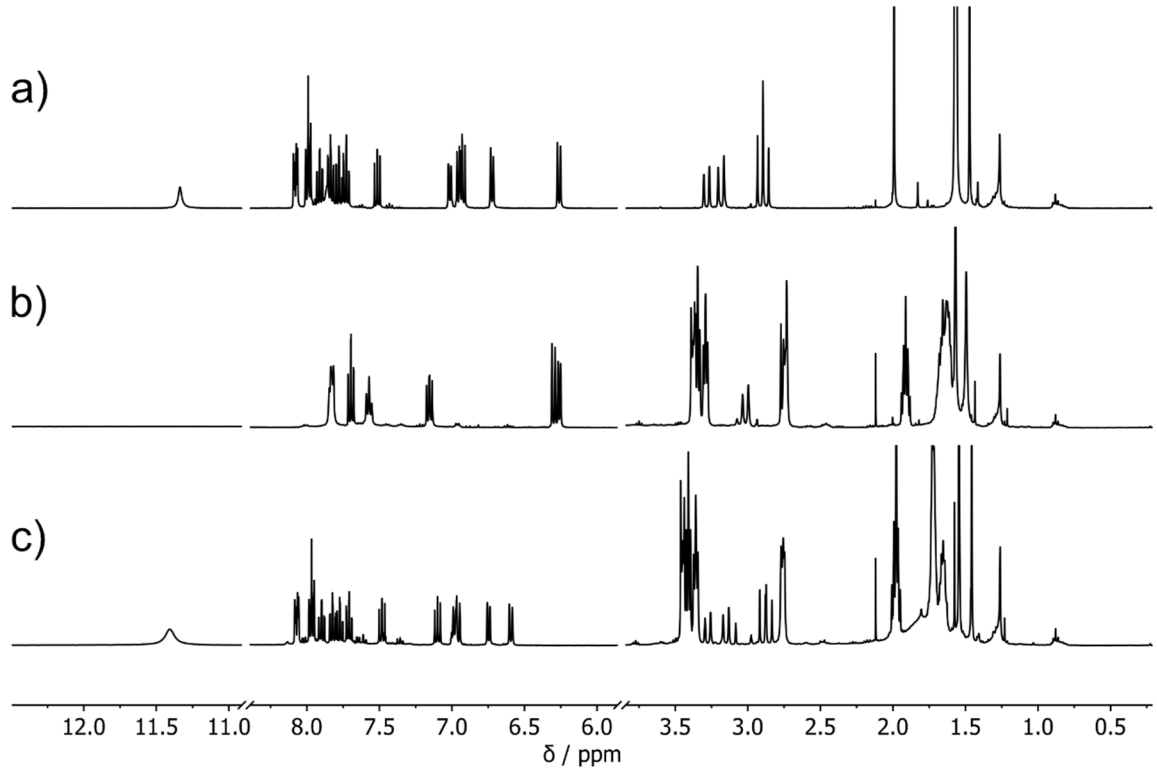

Figure 145 ^{1}H NMR (400 MHz, CD_2Cl_2, 25 °C) spectra of a sample of **a)** pure **87$_n$** in CD_2Cl_2 **b)** after addition of DBU (1 equiv.) to the sample **c)** after subsequent addition of TFA (2 equiv.). Only regions of interest are shown and spectra are clipped vertically for clarity.

Further ^{1}H NMR experiments were then performed with diluted samples of **87$_a$** (approx. 2 mM). In order to observe possible fleeting intermediates or photoproducts, samples were irradiated at lower temperatures (see Figure 146 for variable temperature NMR spectra). However, photoisomerization could neither be observed at −40 °C (520 nm, 625 nm) nor −80 °C (405 nm, 470 nm, 520 nm, 625 nm) upon irradiation with any of the wavelengths tested. A small amount of photodegradation could be noticed at −40 °C, which was not characterized further.

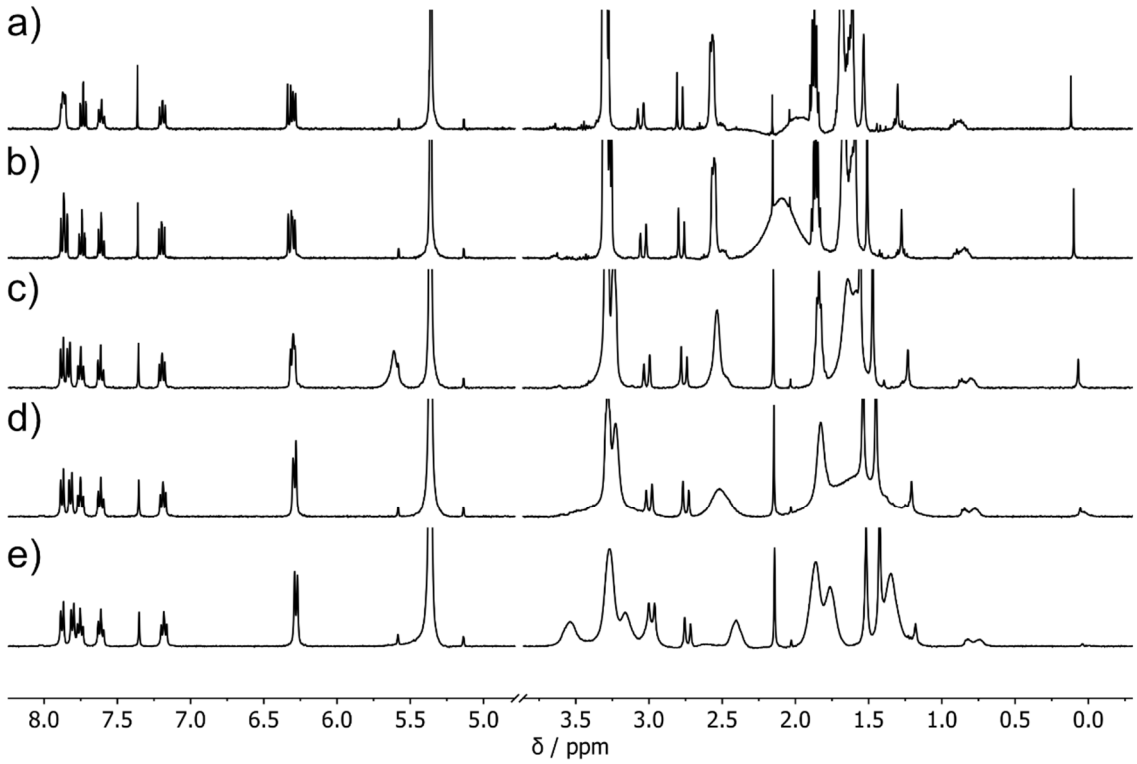

Figure 146 Variable temperature ^{1}H NMR (400 MHz, CD_2Cl_2) spectra of **87** with DBU (1:1, approx. 2 mM) in solution at **a)** 25 °C **b)** 0 °C **c)** −40 °C **d)** −60 °C **e)** −80 °C.

4.6 Summary

In conclusion, novel HTI sulfoxide **87** was successfully synthesized and characterized. Initial theoretical as well as experimental investigations suggest that neutral **87$_n$** is not a molecular motor, due to the changes in relative isomer energies compared to motor **19**. However, according to theoretical results, the typical motor profile is restored upon deprotonation. Furthermore, **87** could be an interesting candidate for multi-stimuli chiroptical applications, as depicted in Figure 147.

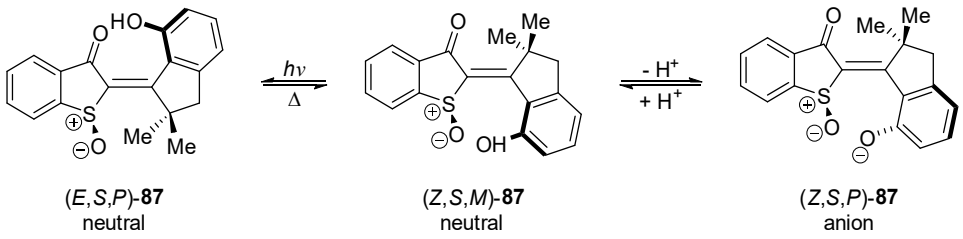

(*E*,*S*,*P*)-**87** neutral

(*Z*,*S*,*M*)-**87** neutral

(*Z*,*S*,*P*)-**87** anion

Figure 147 Potential switching of chiroptical properties of **87** based on theoretical and experimental results. Starting from stable (*Z*,*S*,*M*)-**87$_n$**, helicity could possibly be switched from *M* to *P* either by irradiation with light or by deprotonation with base, resulting in changes in ECD signal.

5 Synthesis of a Photochromic Ferrocenophane

In this section, the synthesis of a different macrocyclic photoswitch is discussed briefly. As shown in a schematic representation in Scheme 49, a ferrocene moiety was "constrained" in a macrocyclic system containing an HTI photoswitch with the goal of possibly switching ferrocene structure and reactivity with visible light. A structurally related system based on azobenzene was previously reported by *Aida* and coworkers.[155]

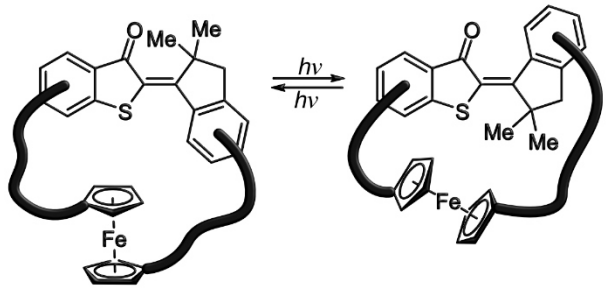

Scheme 49 Schematic representation of a macrocyclic system incorporating an HTI photoswitch and a ferrocene moiety. Both cyclopentadienyl units are part of the macrocycle, so switching between (*Z*)- and (*E*)-isomeric states is expected to result in structural changes and possibly strain on the ferrocene moiety.

The synthetic approach to ferrocenophane **96** is outlined in Scheme 50 and reduced to three simple building blocks: an established dibrominated HTI,[73] 1,1'-ferrocenedicarbonyl dichloride and 3-butyn-1-ol as linker between the two components.

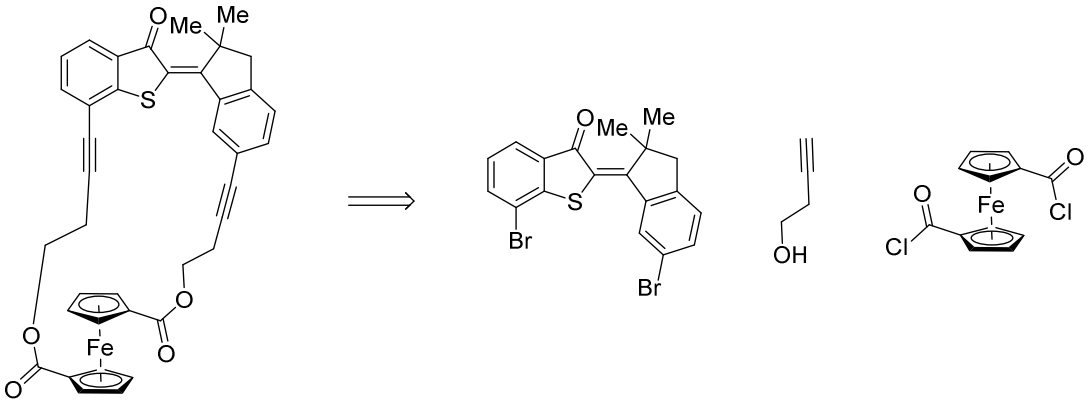

Scheme 50 Retrosynthetic analysis of macrocyclic photoswitchable ferrocene **97**.

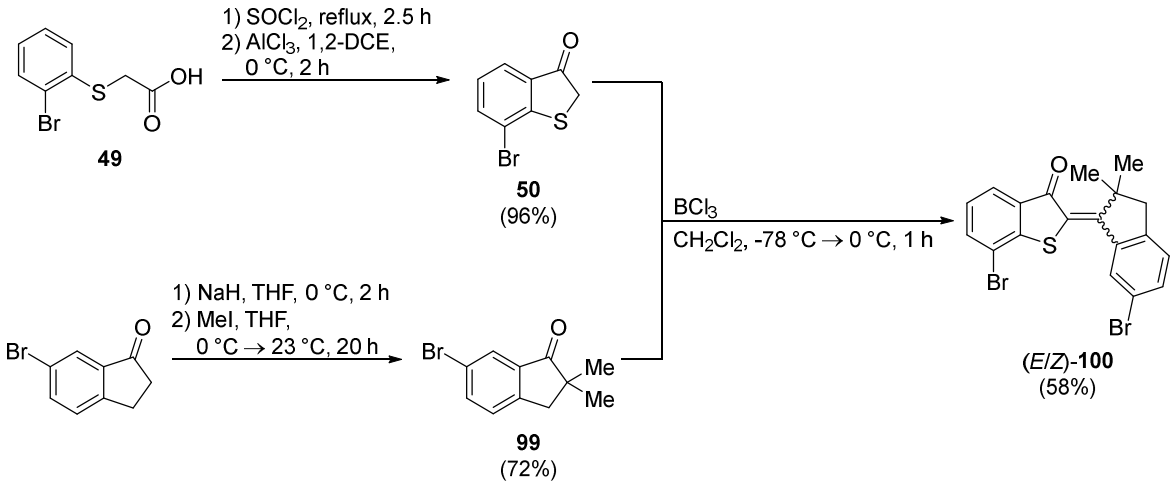

Scheme 51 Synthesis of dibrominated HTI **100** by BCl_3 mediated condensation of benzothiophenone **50** and indanone **99**.

HTI **100**[73] was prepared by BCl_3 mediated condensation of benzothiophenone **50** and indanone **99** in 58% yield. Subsequent SONOGASHIRA cross coupling with 3-butyn-1-ol to **101** proceeded with 76% yield. Finally, the macrocycle was closed by twofold esterification with acid chloride **102** under high dilution conditions, giving macrocycle (*Z*)-**96** in 40% yield.

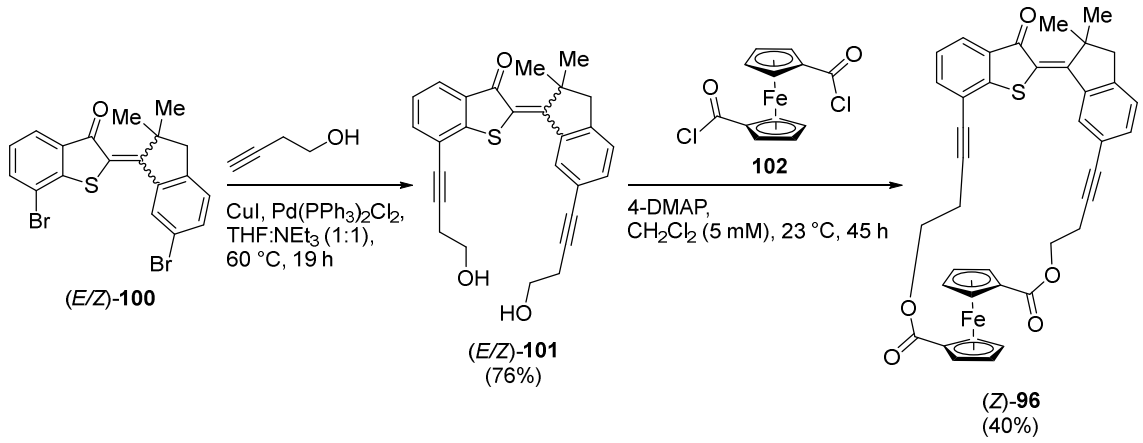

Scheme 52 SONOGASHIRA cross coupling of HTI **100** with 3-butyn-1-ol gave diol **101** in 76% yield. Subsequent esterification with dichloride **102** under high dilution conditions gave macrocyclic ferrocene derivative (*Z*)-**96**.

5.1 Structure in Solution

Macrocyclic ferrocene derivative **96** was obtained exclusively in *Z*-configuration, as evidenced by NMR spectroscopy (see Figure 149).

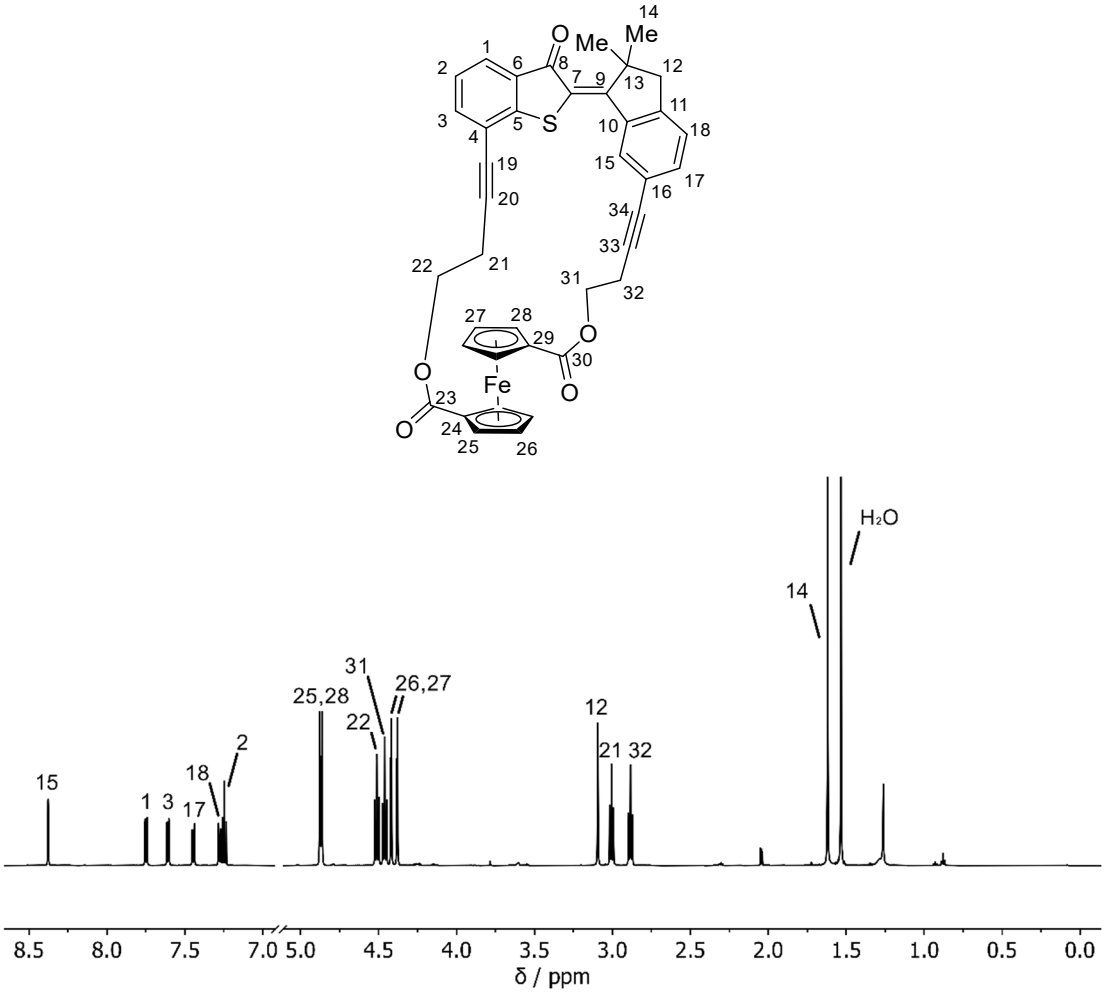

Figure 148 ^{1}H NMR (600 MHz, CD_2Cl_2, 25 °C) of (*Z*)-**96** with assignment of the signals to the molecular structure.

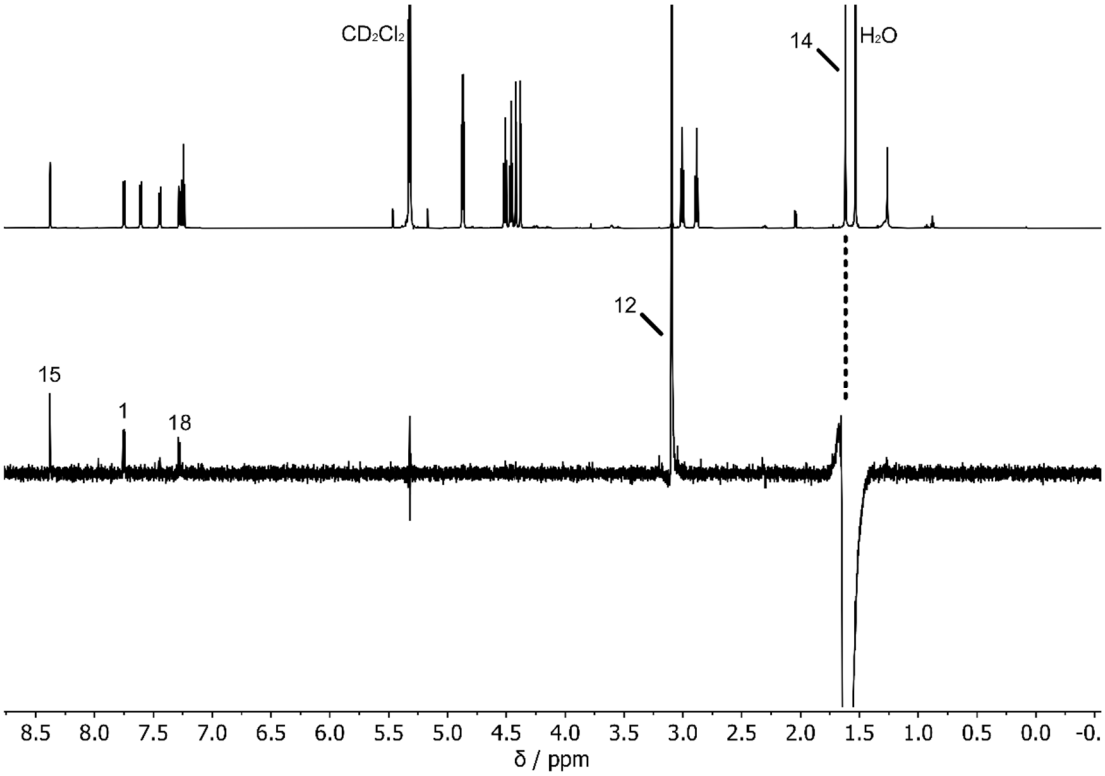

Figure 149 1D NOE (600 MHz, CD_2Cl_2, 25 °C) experiment on **96**. The dotted line indicates which proton signal was irradiated in the experiment. The observed through space coupling between methyl group protons 14 and aromatic proton 1 on the thioindigo fragment confirms *Z*-configuration of this isomer.

5.2 UV/Vis Spectroscopy

UV/Vis absorption spectra of pure (*Z*)-**96** were measured in CH_2Cl_2 and THF and are shown in Figure 150 and Figure 151 respectively. When the samples were irradiated with blue (405-435 nm) light, absorption changes presumably corresponding to reversible *E*/*Z*-photoisomerization were observed. The spectral changes could be reversed almost completely by irradiation with green (515-525 nm) light.

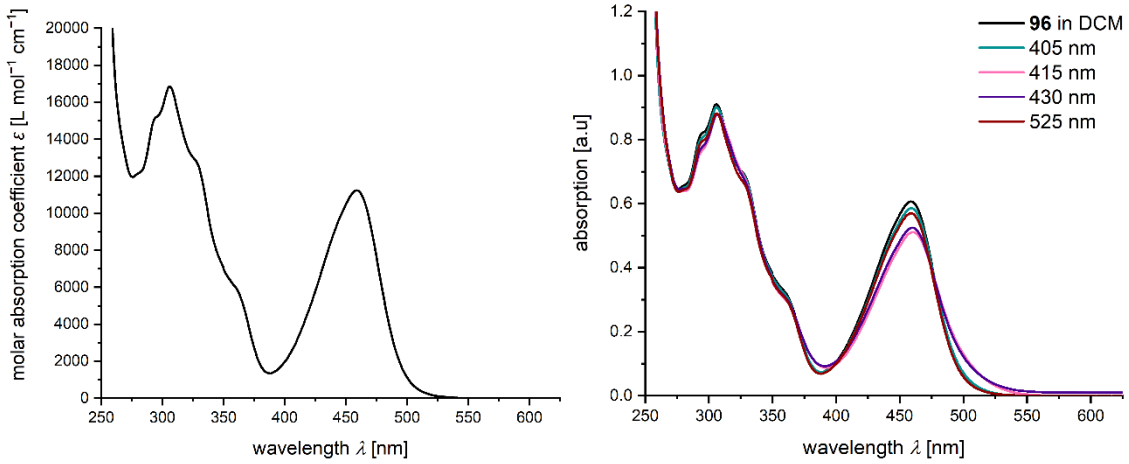

Figure 150 *left*: Molar absorption coefficient of (*Z*)-**96** in CH_2Cl_2 (23 °C). *right*: UV/Vis absorption spectra recorded during photoswitching experiments. A solution of pure (*Z*)-**96** in CH_2Cl_2 was irradiated with light of different wavelengths. Upon irradiation with short-wavelength (405-430 nm) light, a change in absorption was observed. While absorption at the maximum at 459 nm decreased, there was an absorption increase in the 500-550 nm region, with an isosbestic point at 477 nm. This could be reversed by irradiation with 535 nm light, which resulted in almost full recovery of the initial absorption spectrum. *Note*: Due to a fast thermal isomerization process, the *pss* spectra could not be determined accurately.

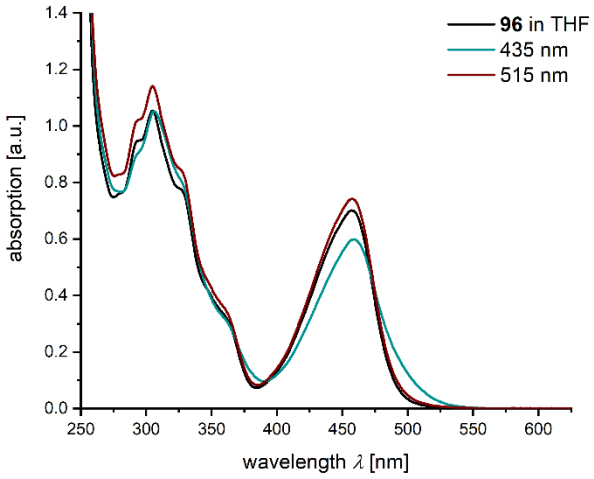

Figure 151 UV/Vis spectra of **96** recorded during photoswitching experiments. A solution of pure (*Z*)-**96** in THF was irradiated with light of different wavelengths. Upon irradiation with 435 nm light, a change in absorption was observed. While absorption at the maximum at 458 nm decreased, there was an absorption increase in the 500-550 nm region, with an isosbestic point at 472 nm. This could be reversed by irradiation with 515 nm light, which resulted in recovery of the initial spectrum. The observed increase in absorption is most likely due to the initial presence of undissolved material, which dissolved over the course of the experiment.

5.3 Photoswitching Experiments in ^{1}H NMR

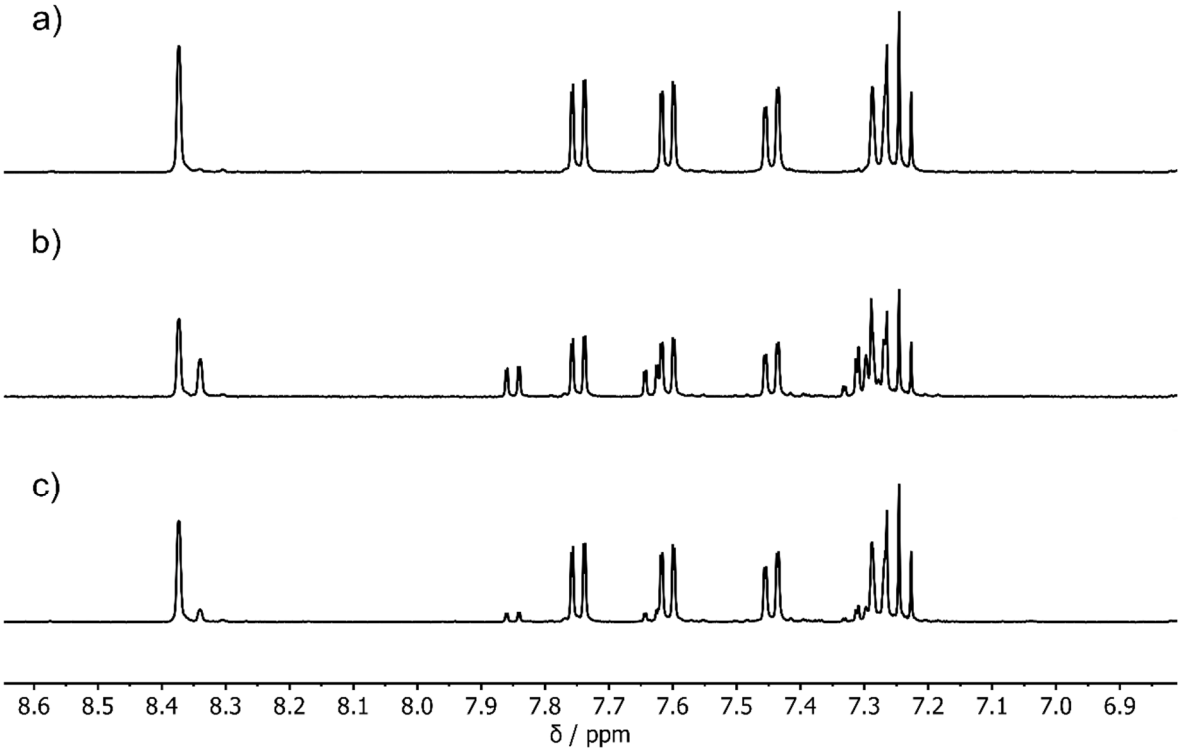

Figure 152 ^{1}H NMR spectra (400 MHz, CD_2Cl_2, 20 °C) of **96** recorded during photoirradiation experiments. **a)** pure (*Z*)-**96 b)** after external irradiation with 435 nm light emergence of a new set of signals was observed **c)** after subsequent external irradiation with 470 nm light the initial spectrum was almost completely restored. Only the aromatic region is shown for clarity. *Note*: Data were acquired by *Matthias Fischer*.

Additional irradiation experiments were performed in combination with ^{1}H NMR spectroscopy, to gain insight into structural changes upon light irradiation (see Figure 152). When a sample of pure (*Z*)-**96** in CD_2Cl_2 was irradiated with 435 nm light, the emergence of a second set of signals was observed, while there was a simultaneous proportional decrease in signals assigned to (*Z*)-**96**. Upon subsequent irradiation with 470 nm light, the initial spectrum was restored almost completely. This strongly suggests photoinduced double bond isomerization between *Z*- and *E*-configured **96**.

5.4 Cyclic Voltammetry Experiments

Cyclic voltammetry was used to probe possible changes in redox potential caused by structural changes upon photoirradiation. Data were recorded in THF with $TBAPF_6$ as supporting electrolyte and ferrocene was added as internal reference. However, no significant difference in redox potential *vs* Fc^+/Fc was found before (+0.45 V) and after (+0.46 V) irradiation of the sample with 435 nm light. Additional measurements by *Matthias Fischer* in CH_2Cl_2 with $TBABF_4$ as supporting electrolyte gave a redox potential of +0.48 V *vs* Fc^+/Fc for **96** at 0 °C. Again, no significant changes in redox potential were observed upon irradiation with 435 nm light. As the cyclic voltammetry measurements were performed on *E*/*Z*-mixtures of unspecified composition, the concentration of (*E*)-**96** might have been too low to have a noticeable effect on the measured redox potential. Attempts to isolate pure (*E*)-**96** were not successful. It is also a possibility that (*E*)- and (*Z*)-**96** do not differ significantly in redox potential. Furthermore, thermal isomerization or electrochemically triggered isomerization at the electrode surface might interfere with the measurement.

In summary, a ferrocenophane incorporating an HTI photoswitch unit was synthesized and characterized by spectroscopic methods. Initial investigations into the electrochemistry and possible photoswitching of electrochemical properties were performed.

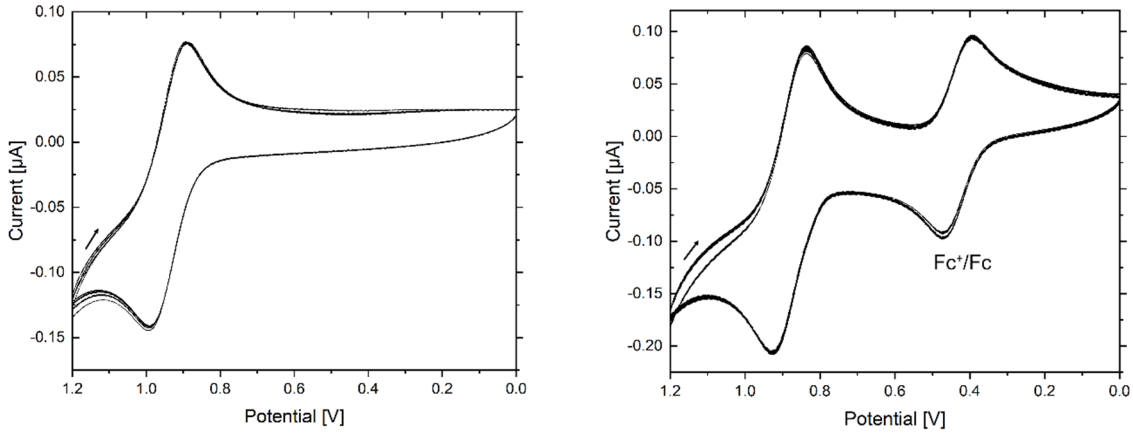

Figure 153 Cyclic voltammograms of **96** (recorded at 25 °C). *left*: **96** in THF (approx. 3.3×10^{-4} mol L^{-1}) with $TBAPF_6$ (approx. 0.1 M) as supporting electrolyte. *right*: **96** in THF (approx. 3.3×10^{-4} mol L^{-1}) with (approx. 0.1 M) as supporting electrolyte and ferrocene added as internal reference. The scan rate was 100 mV s^{-1}. The redox potential of **96** *vs* Fc^+/Fc was determined as +0.45 V.

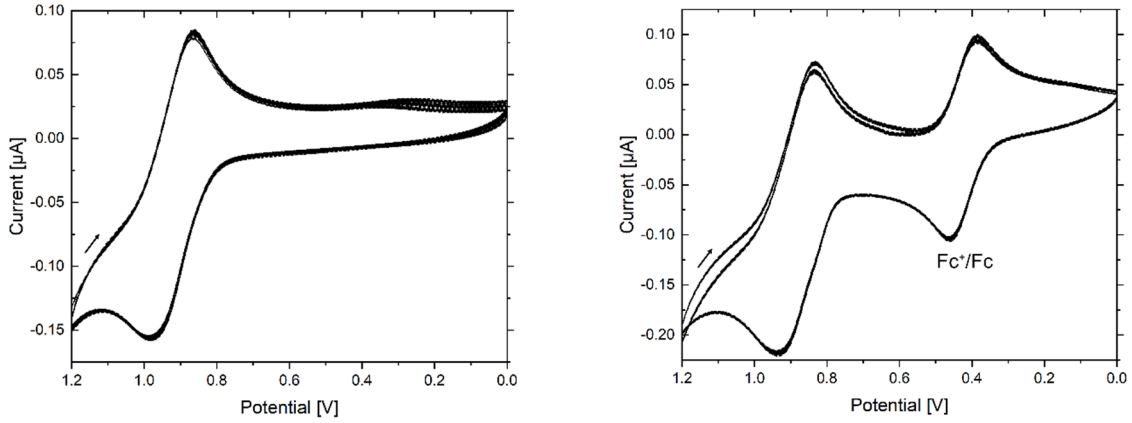

Figure 154 Cyclic voltammograms of **96** after irradiation with 435 nm light for 10 min, recorded at 25 °C. *left*: **96** in THF (approx. 3.3×10^{-4} mol L^{-1}) with $TBAPF_6$ (approx. 0.1 M) as supporting electrolyte. *right*: **96** in THF (approx. 3.3×10^{-4} mol L^{-1}) with (approx. 0.1 M) as supporting electrolyte and ferrocene added as internal reference. The scan rate was 100 mV s^{-1}. The redox potential of **96** *vs* Fc^+/Fc was determined as +0.46 V. No significant change in potential was observed.

6 Experimental

6.1 Materials and Methods

Reagents and solvents were obtained from *abcr, Acros, Iris Biotech, Fisher Scientific, Merck, Sigma-Aldrich* or *TCI* and used as received. Technical solvents were distilled on a rotary evaporator (*Heidolph Hei-VAP*) before use for column chromatography and extraction. Anhydrous solvents purchased from *Merck*, *Sigma-Aldrich* and *Acros* were used without further purification. Monitoring of reaction progress was done by thin-layer chromatography (TLC) using aluminum plates coated with SiO_2 (*Merck 60*, *F-254*). Detection was done by irradiation with UV light (254 nm or 366 nm) or staining with either $KMnO_4$ stain or vanillin stain in order to determine retardation factors (R_f). In the following procedures, "brine" is a saturated aqueous solution of NaCl.

Dry glassware was used where indicated. Glassware was dried with a hot air gun (600 °C) under vacuum, allowed to cool to ambient temperature and refilled with nitrogen or argon atmosphere. This procedure was typically performed a total of three times prior to use of the glassware for reactions.

Flash column chromatography was performed with silica gel 60 (*Merck*, particle size 0.063-0.200 mm; or *Macherey-Nagel*, particle size 0.04-0.063 mm). Automated flash column chromatography was performed on *Biotage Isolera One* or *Biotage Selekt* machines with pre-packed silica columns from *Biotage* or *Macherey-Nagel*.

High Performance Liquid Chromatography (HPLC) was performed on a *Shimadzu* HPLC system consisting of an *LC-20AP* solvent delivery module, a *CTO-20A* column oven, an *SPD-M20A* photodiode array UV/Vis detector, and a *CBM-20A* system controller using a semi-preparative CHIRALPAK® IC or ID column (particle size 5 µm) from *Daicel* and HPLC grade solvents from *Sigma-Aldrich, Honeywell, VWR*, or *ROTH*.

^{1}H-NMR and ^{13}C-NMR spectra were measured on a *Jeol ECX-400* (400 MHz), *Varian 400 MHz*, *Bruker Avance III HD 400 MHz*, *Bruker Avance Neo HD 400 MHz*, *Bruker Avance Neo HDX 500 MHz*, *Bruker Avance Neo HDX 600 MHz* with *cryo probe DCH-Z^{13}C/^{1}H*, *Varian 600 NMR* (600 MHz), or *Bruker Avance III HD 800 MHz* spectrometer. Chemical shifts (δ) are reported relative to residual solvent signals in the ^{1}H- and ^{13}C-NMR spectra, which were used as internal reference. Deuterated solvents were obtained from *Cambridge Isotope Laboratories* or *Eurisotop*, *Deutero GmbH*, and *Sigma-Aldrich*. For ^{1}H-NMR: $CDCl_3$ = 7.26 ppm, CD_2Cl_2 = 5.32 ppm, $(CDCl_2)_2$ = 6.00 ppm, $(CD_3)_2SO$ = 2.50 ppm. For ^{13}C-NMR: $CDCl_3$ = 77.16 ppm, CD_2Cl_2 = 54.00 ppm,

$(CD_3)_2SO$ = 39.52 ppm. Resonance multiplicity is indicated as *s* (singlet), *d* (doublet), *t* (triplet), *q* (quartet) and *m* (multiplet). Chemical shifts are given in parts per million (ppm). Coupling constant values (*J*) are given in *Hertz* (*Hz*). NMR spectra were evaluated using the *MestreNova* software package.

Electron Impact (EI) mass spectra were measured on a *Thermo Q Exactive GC Orbitrap* or *Finnigan MAT 95* mass spectrometer. **Electrospray ionization (ESI) mass spectra** were measured on a *Thermo Finnigan LTQ FT Ultra Fourier Transform Ion Cyclotron Resonance* mass spectrometer, a *Bruker Daltonics maXis 4G* or a *micrOTOF II* spectrometer. **Atmospheric pressure photoionization (APPI)** mass spectra were recorded on a *Bruker Daltonics maXis 4G* or a *micrOTOF II* spectrometer.

Infrared spectra (ATR) were recorded on a *Perkin Elmer Spectrum BX* spectrometer equipped with a *Smiths Detection DuraSamplIR II Diamond-ATR* unit or on a *Varian 660-IR* spectrometer with a spectral resolution of 4 cm^{-1}. Absorption bands are given as wavenumbers (cm^{-1}) and are qualitatively described as broad (br), very strong (vs), strong (s), medium (m), weak (w), and very weak (vw).

UV/Vis spectra were measured on a Varian Cary 5000 spectrophotometer. The spectra were recorded in a quartz cuvette (1 cm path length). CH_2Cl_2 for spectroscopy was obtained from VWR and filtered over basic alumina (activated, Brockmann I) prior to use.

Electronic circular dichroism (ECD) spectra were measured on a *Jasco J-810* or *Jasco J-815 CD Spectrometer*. For low temperature measurements, the samples were measured in fluorescence cuvettes and were placed inside an *Oxford Optistat DN 1704* cryostat with *Oxford ITC-4* temperature controller. Liquid nitrogen was used as cryogen. A steady flow of nitrogen gas was attached in order to minimize condensation of water inside the sample chamber. The detector was removed from the spectrometer housing, so that the cryostat could be placed in the beam path. Cryostat, cuvette, and detector were aligned with the beam path and the components were affixed on an optical breadboard. Irradiation of the samples by UHP LED (450 nm) was performed either directly through the cryostat windows with the sample inside the cryostat, or outside the cryostat with the sample kept on dry ice (−78 °C).

Photoisomerization experiments: Continuous irradiations of the solutions were conducted either in NMR tubes in different deuterated solvents (CD_2Cl_2, CD_2Cl_2:CS_2 (4:1, v:v), $(CDCl_2)_2$ or DMF-d_7; CD_2Cl_2 and $(CDCl_2)_2$ were filtered over basic alumina (activated, Brockmann I) prior to use) or in quartz cuvettes (1 cm) in protonated solvents. Irradiations were conducted using a *Prizmatix* or *Mightex* UHP LED (405 nm, 450 nm, 470 nm, 520 nm, 625 nm) coupled to a 1500 µm quartz fiber that was inserted into the sample solution for *in*

situ irradiation NMR-experiments or using LEDs from *Roithner Lasertechnik* or *Thorlabs* for external irradiation experiments.

Thermal isomerization experiments at elevated temperatures were conducted in amberized NMR tubes or in NMR tubes wrapped in aluminum foil in order to exclude ambient light. The samples were dissolved in the indicated deuterated solvents and kept in an oil bath with the temperature control set to the respective temperature. After the indicated time interval, samples were cooled to 0 °C in an ice bath in order to halt the isomerization process and ^{1}H NMR spectra were recorded at 20–25 °C.

Melting points (m.p) were measured on a *Stuart SMP10* or *Büchi M-560* melting point apparatus in open capillaries and are not corrected.

Cyclic Voltammetry was measured on a *CH Instruments CHI630E electrochemical analyzer* under argon atmosphere with a Pt working electrode, a Pt counter electrode and an Ag pseudo reference electrode.

Quantum chemical calculations were performed using the *Gaussian16* (Revision B.01[141] or C.01[156]) software package. *GaussView6* was used for handling input and output files. Conformational analyses were performed with the *MacroModel* package included in *Schrödinger* (Version 2019-4 or 2020-3). Experimental and calculated ECD spectra were processed with *SpecDis Version 1.71*.[142-143] Molecular geometries from quantum chemical calculations were visualized with *Discovery Studio Visualizer 2020*.

X-Ray crystal structures were measured on a *Bruker D8 Venture TXS* or on a *SuperNova Dual Atlas* diffractometer. Crystal structures were visualized with the *Mercury 2020.2.0* software. Thermal ellipsoids were set to 50% probability.

6.2 Synthesis of Compounds

Compound 1 *reported in ref.*[8]

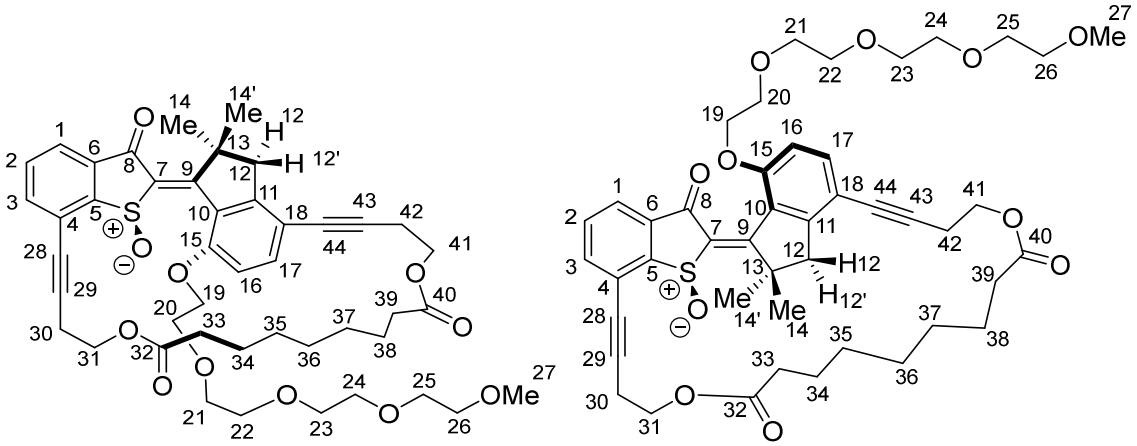

(*Z*)-isomer (*rac*) (*E*)-isomer (*rac*)

Note: Only the (*S*)-configured enantiomers are depicted for simplicity.

Compound **68** (35 mg, 44 µmol, 1.0 equiv.) was dissolved in acetic acid (1.5 mL). Sodium perborate tetrahydrate (26 mg, 0.17 mmol, 3.9 equiv.) was added and the reaction mixture was stirred at 23 °C in the dark for 2 h. The reaction was stopped by the slow addition of a saturated aqueous solution of $NaHCO_3$ (5 mL). H_2O (25 mL) and an additional 5 mL of a saturated aqueous solution of $NaHCO_3$ were added and the mixture was extracted with EtOAc (2 × 25 mL). The combined organic layers were dried over Na_2SO_4, filtered, and concentrated *in vacuo*. The residue was purified by flash column chromatography (SiO_2, MeOH:CH_2Cl_2, 2:98). Isomer **A-1** (24 mg, 30 µmol, 68%) and **C-1** (8 mg, 10 µmol, 23%) were obtained separately as yellow oils (combined yield: 91%).

(*Z*)-isomer (**A-1**)

R_f (MeOH:CH_2Cl_2, 2:98): 0.13.

^{1}H NMR (601 MHz, CD_2Cl_2): δ / ppm = 7.85 (dd, J = 7.7, 1.1 Hz, 1H, H-C(1)), 7.73 (dd, J = 7.6, 1.2 Hz, 1H, H-C(3)), 7.61 (t, J = 7.6 Hz, 1H, H-C(2)), 7.48 (d, J = 8.6 Hz, 1H, H-C(17)), 6.87 (d, J = 8.6 Hz, 1H, H-C(16)), 4.47 (dt, J = 10.4, 4.2 Hz, 1H, H_2-C(19)), 4.40 (ddd, J = 10.4, 7.8, 4.0 Hz, 1H, H_2-C(19)), 4.32–4.27 (m, 1H, H_2-C(31)), 4.27–4.22 (m, 2H, H_2-C(41)), 4.11–4.08 (m, 1H, H_2-C(20)), 4.08–4.04 (m, 1H, H_2-C(31)), 3.91 (dt, J = 10.9, 4.1 Hz, 1H, H_2-C(20)), 3.62–3.55 (m, 2H, H_2-C(21)), 3.52–3.47 (m, 6H, H_2-C(22 and 23 and 24)), 3.47–3.44 (m, 4H, H_2-C(25 and 26)), 3.30 (s, 3H, H_3-C(27)), 3.14 (d, J = 16.6 Hz, 1H, H'-C(12)), 2.97 (d, J = 16.7 Hz, 1H, H-C(12)), 2.89–2.81 (m, 2H, H_2-C(30)), 2.79–2.75 (m, 2H, H_2-C(42)), 2.35–2.23 (m, 2H, H_2-C(33)), 2.19–2.08 (m, 2H, H_2-C(36)), 1.59–1.55 (m,

2H, H_2-C(34)), 1.54 (s, 3H, H_3-C(14)), 1.50 (s, 3H, H_3-C(14‘)), 1.31–1.24 (m, 2H, H_2-C(34)), 1.23–1.15 (m, 2H, H_2-C(37)), 1.08–1.00 (m, 1H, H_2-C(36)), 0.95 (dd, J = 18.8, 9.1 Hz, 1H, H_2-C(36)), 0.83–0.75 (m, 1H, H_2-C(35)), 0.75–0.65 (m, 1H, H_2-C(35)).

^{13}C NMR (151 MHz, CD_2Cl_2): δ / ppm = 184.7 (C(8)), 174.8 (C(32)), 173.8, (C(40)), 170.9 (C(9)), 156.8 (C(15)), 153.7 (C(11)), 151.2 (C(5)), 143.3 (C(7)), 137.9 (C(3)), 137.9 (C(19)), 136.8 (C(6)), 132.1 (C(2)), 125.7 (C(10)), 124.0 (C(1)), 123.6 (C(4)), 113.1 (C(18)), 110.4 (C(16)), 96.8 (C(29)), 89.3 (C(43)), 78.9 (C(44)), 76.5 (C(28)), 72.1 (C(26)), 70.9 (C(21)), 70.7 (C(22)), 70.6 (C(24)), 70.6 (C(23)), 70.6 (C(25)), 69.3 (C(20)), 68.5 (C(19)), 62.2 (C(31)), 62.0 (C(41)), 58.9 (C(27)), 51.8 (C(13)), 50.4 (C(12)), 35.4 (C(39)), 33.8 (C(33)), 30.2 (C(36)), 29.9 (C(37)), 29.5 (C(35)), 28.2 (C(14‘)), 26.1 (C(38)), 25.5 (C(14)), 25.3 (C(34)), 20.5 (C(42)), 20.4 (C(30)).

HRMS (ESI): *m/z* calc. for $[C_{45}H_{54}O_{11}S+H]^+$: 803.3460; found: 803.3465 ($M+H^+$).

(*E*)-isomer (**C-1**)

R_f ($MeOH:CH_2Cl_2$, 2:98): 0.06.

^{1}H NMR (601 MHz, CD_2Cl_2): δ / ppm = 7.89 (dd, J = 7.6, 1.1 Hz, 1H, H-C(1)), 7.76 (dd, J = 7.6, 1.2 Hz, 1H, H-C(3)), 7.68 (t, J = 7.6 Hz, 1H, H-C(2)), 7.43 (d, J = 8.5 Hz, 1H, H-C(17)), 6.81 (d, J = 8.6 Hz, 1H, H-C(16)), 4.36–4.31 (m, 2H, H_2-C(31)), 4.31–4.26 (m, 2H, H_2-C(41)), 4.21 (ddd, J = 16.9, 10.0, 4.6 Hz, 2H, H_2-C(19)), 3.75–3.70 (m, 1H, H_2-C(20)), 3.65 (ddd, J = 10.9, 6.7, 4.7 Hz, 1H, H_2-C(20)), 3.56–3.51 (m, 4H, H_2-C(23 and 24 and 25)), 3.49–3.46 (m, 4H, H_2-C(23 and 24 and 26)), 3.40 (d, J = 1.8 Hz, 4H, H_2-C(21 and 22)), 3.32 (s, 3H, H_3-C(27)), 3.14 (d, J = 13.9 Hz, 1H, H-C(12)), 2.98 (d, J = 16.7 Hz, 1H, H’-C(12)), 2.96–2.90 (m, 1H, H_2-C(30)), 2.88–2.82 (m, 1H, H_2-C(30)), 2.77 (t, J = 5.5 Hz, 2H, H_2-C(42)), 2.50–2.46 (m, 2H, H_2-C(33)), 2.42–2.38 (m, 2H, H_2-C(39)), 2.01 (s, 3H, H_3-C(14’)), 1.74–1.63 (m, 4H, H_2-C(34 and 38)), 1.43 (s, 3H, H_3-C(14)), 1.39 (s, 6H, H_2-C(35 and 36 and 37)).

^{13}C NMR (DEPTq)(151 MHz, CD_2Cl_2): δ / ppm = 184.8 (C(8)), 174.1 (C(32)), 173.7(C(40)), 158.7 (C(15)), 154.0 (C(11)), 150.2 (C(5)), 137.4 (C(3)), 136.4 (C(4 or 6)), 135.6 (C(17)), 133.0 (C(2)), 127.7 (C(10)), 124.7 (C(1)), 124.1 (C(4 or 6)), 113.1 (C(18)), 110.9 (C(16)), 97.4 (C(29)), 90.4 (C(43)), 78.9 (C(44)), 76.5 (C(28)), 72.3 (C(26)), 71.1 (C(21 or 22)), 70.83 (C(23 or 24 or 25)), 70.81 (C(23 or 24 or 25)), 70.7 (C(23 or 24 or 25)), 70.6 (C(21 or 22)), 69.7 (C(20)), 68.1 (C(19)), 63.0 (C(41)), 62.5 (C(31)), 59.0 (C(27)), 52.4 (C(13)), 49.8 (C(12)), 34.8 (C(39)), 34.3 (C(33)), 30.2 (C(37)), 29.9 (C(35)), 29.4 (C(36)), 28.8 (C(14)), 27.5 (C(14’)), 25.2 (C(38)), 25.0 (C(34)), 20.7 (C(30)), 20.5 (C(42)).

IR: $\tilde{\nu}$ / cm^{-1} = 3055 (m), 3020 (m), 2931 (s), 2868 (m), 1734 (vs), 1682 (s), 1593 (s), 1554 (s), 1489 (m), 1466 (m), 1385 (m), 1363 (m), 1338 (m), 1284 (s), 1261 (s), 1171 (s), 1134 (s), 1099 (s), 1076 (s), 1065 (s), 1053 (m), 1036 (m), 818 (m), 810 (m), 762 (m), 750 (m), 727 (m), 634 (m), 573 (m), 555 (m), 505 (m), 457 (m).

HRMS (ESI): *m/z* calc. for $[C_{45}H_{54}O_{11}S+H]^+$: 803.3460; found: 803.3470 ($M+H^+$).

Compound 2 *reported in ref.*[8]

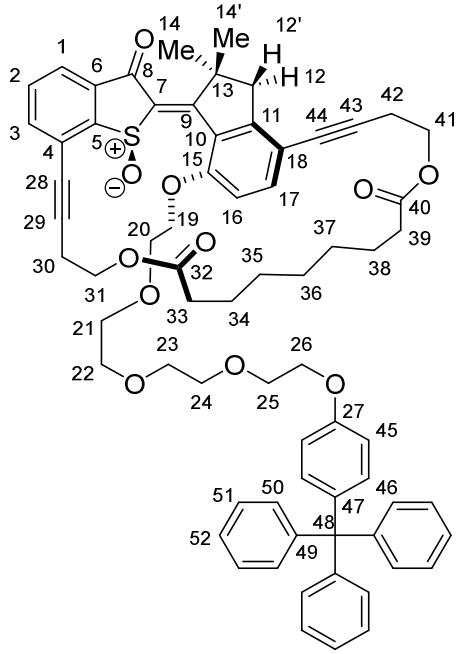

(*Z*)-isomer (*rac*)

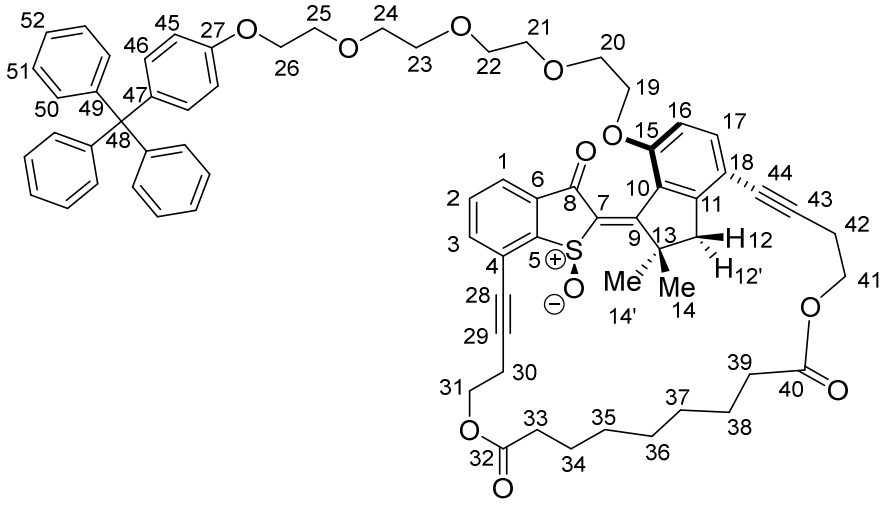

(*E*)-isomer (*rac*)

Note: Only the (*S*)-configured enantiomers are depicted for simplicity.

Compound **63** (mixture of (*E*)- and (*Z*)-isomers, 45 mg, 41 µmol, 1.0 equiv.) was dissolved in acetic acid (1.2 mL). Sodium perborate tetrahydrate (25 mg, 0.16 mmol, 3.9 equiv.) was added and the reaction mixture was stirred at 23 °C in the dark for 2.5 h. The reaction was stopped by the slow addition of a saturated aqueous solution of $NaHCO_3$ (5 mL). H_2O (25 mL) was added and the mixture was extracted with EtOAc (2 × 25 mL). The combined organic layers were dried over Na_2SO_4, filtered, and concentrated *in vacuo*. The residue was purified by flash column chromatography (SiO_2, EtOAc:*i*-Hex, 70:30). Fractions were concentrated *in vacuo*, subsequently dissolved in a H_2O-MeCN mixture and then lyophilized. Isomer **A-2** (19 mg, 17 µmol, 41%) and **C-2** (10 mg, 9 µmol, 22%) could be isolated in pure form as fine powdered yellow solids (combined yield: 63%).

(*Z*)-isomer (**A-2**)

R_f (EtOAc:*i*-Hex, 70:30): 0.53.

^{1}H NMR (800 MHz, CD_2Cl_2): δ / ppm = 7.85 (dd, J = 7.7, 1.1 Hz, 1H, H-C(1)), 7.71 (dd, J = 7.6, 1.1 Hz, 1H, H-C(3)), 7.58 (t, J = 7.6 Hz, 1H, H-C(2)), 7.47 (d, J = 8.5 Hz, 1H, H-C(17)), 7.26–7.23 (m, 6H, H-C(51)), 7.22 (dd, J = 8.5, 1.6 Hz, 6H, H-C(50)), 7.20–7.17 (m, 3H, H-C(52)), 7.12–7.10 (m, 2H, H-C(46)), 6.86 (d, J = 8.3 Hz, 1H, H-C(16)), 6.79–6.76 (m, 2H, H-C(45)), 4.47 (dt, J = 10.5, 4.3 Hz, 1H, H_2-C(19)), 4.39 (ddd, J = 10.4, 7.7, 4.0 Hz, 1H, H_2-C(19)), 4.31–4.28 (m, 1H, H_2-C(31)), 4.28–4.24 (m, 2H, H_2-C(41)), 4.09–4.07 (m, 1H, H_2-C(20)), 4.07–4.05 (m, 1H, H_2-C(31)), 4.05–4.03 (m, 2H, H_2-C(26)), 3.91 (dt, J = 11.0, 4.3 Hz, 1H, H_2-C(20)), 3.74–3.72 (m, 2H, H_2-C(25)), 3.61–3.57 (m, 2H, H_2-C(21)), 3.57–3.55 (m, 2H, H_2-C(24)), 3.52–3.48 (m, 4H, H_2-C(22 and 23)), 3.14 (d, J = 16.6 Hz, 1H, H'-C(12)), 2.97 (d, J = 16.6 Hz, 1H, H-C(12)), 2.84 (ddd, J = 17.6, 9.5, 3.6 Hz, 1H, H_2-C(30)), 2.81–2.78 (m, 1H, H_2-C(30)), 2.77 (t, J = 5.5 Hz, 2H, H_2-C(42), 2.33–2.29 (m, 1H, H_2-C(39)), 2.27 (ddd, J = 14.2, 7.8, 5.9 Hz, 1H, H_2-C(39)), 2.16–2.12 (m, 2H, H_2-C(33)), 1.55 (s, 3H, H_3-C(14')), 1.50 (s, 3H, H_3-C(14)), 1.32–1.25 (m, 2H, H_2-C(34)), 1.24–1.18 (m, 2H, H_2-C(35)), 1.07–0.91 (m, 2H, H_2-C(36)), 0.83–0.70 (m, 2H, H_2-C(37)).

^{13}C NMR (201 MHz, CD_2Cl_2): δ / ppm = 184.8 (C(8)), 174.8 (C(32)), 173.8 (C(40)), 171.0 (C(9)), 157.2 (C(27)), 156.9 (C(15)), 153.8 (C(11)), 151.5 (C(5)), 147.5 (C(49)), 143.7 (C(7)), 139.5 (C(47)), 138.0 (C(3)), 137.9 (C(17)), 137.0 (C(6)), 132.4 (C(46)), 132.1 (C(2)), 131.4 (C(50)), 127.9 (C(51)), 126.2 (C(52)), 126.0 (C(10)), 124.1 (C(1)), 123.8 (C(4)), 113.7 (C(45)), 113.3 (C(18)), 110.6 (C(16)), 96.9 (C(29)), 89.4 (C(43)), 79.1 (C(44)), 76.6 (C(28)), 71.0 (C(21)), 71.0 (C(22)), 70.8 (C(23)), 70.8 (C(24)), 70.0 (C(25)), 69.5 (C(20)), 68.6 (C(19)), 67.7 (C(26)), 64.7 (C(48)), 62.2 (C(31)), 62.1 (C(41)), 51.9 (C(13)), 50.6 (C(12)),

35.5 (C(39)), 34.0 (C(33)), 30.2 (C(36)), 29.9 (C(37)), 29.6 (C(35)), 28.3 (C(14)), 26.2 (C(38)), 25.6 (C(14‘)), 25.4 (C(34)), 20.6 (C(30)), 20.5 (C(42)).

IR: $\tilde{\nu}$ / cm^{-1} = 3020 (s), 2987 (s), 2929 (s), 2922 (s), 1732 (vs), 1670 (s), 1547 (s), 1489 (s), 1417 (s), 1369 (s), 1282 (s), 1257 (vs), 1174 (s), 1119 (s), 1095 (s), 1086 (s), 1068 (s), 856 (s), 823 (s), 810 (s), 785 (s), 762 (s), 750 (s), 702 (s), 642 (s), 604 (s), 509 (s), 463 (s).

HRMS (ESI): *m/z* calc. for $[C_{69}H_{70}O_{11}S+H]^+$: 1107.4712; found: 1107.4736 ($M+H^+$).

Enantiomers were separated on a Daicel Chiralpak IC semi-preparative column eluting with EtOAC:*n*-heptane 25:75 at 30 °C.

(*E*)-isomer (**C-2**)

R_f (EtOAc:*i*-Hex, 70:30): 0.14.

^{1}H NMR (800 MHz, CD_2Cl_2): δ / ppm = 7.88 (d, J = 6.3 Hz, 1H, H-C(1)), 7.73 (d, J = 7.6 Hz, 1H, H-C(3)), 7.66 (t, J = 7.5 Hz, 1H, H-C(2)), 7.41 (d, J = 8.5 Hz, 1H, H-C(17)), 7.26–7.23 (m, 6H, H-C(51)), 7.23–7.21 (m, 6H, H-C(50)), 7.20–7.17 (m, 3H, H-C(52)), 7.13–7.10 (m, 2H, H-C(46)), 6.79 (dd, J = 8.7, 3.4 Hz, 3H, H-C(16 and 45)), 4.34–4.30 (m, 2H, H_2-C(31)), 4.30–4.23 (m, 2H, H_2-C(41)), 4.23–4.17 (m, 2H, H_2-C(19)), 4.07–4.05 (m, 2H, H_2-C(26)), 3.78–3.74 (m, 2H, H_2-C(25)), 3.74–3.69 (m, 1H, H_2-C(20)), 3.66–3.62 (m, 1H, H_2-C(20)), 3.62–3.58 (m, 2H, H_2-C(24)), 3.53–3.48 (m, 2H, H_2-C(23)), 3.41 (d, J = 12.3 Hz, 4H, H_2-C(21 and 22)), 3.15 (d, J = 16.0 Hz, 1H, H-C(12) or H’-C(12)), 2.97 (d, J = 21.7 Hz, 1H, H-C(12) or H’-C(12)), 2.92 (ddd, J = 17.7, 7.5, 3.6 Hz, 1H, H_2-C(30)), 2.83 (ddd, J = 17.7, 7.0, 3.5 Hz, 1H, H_2-C(30)), 2.76 (t, J = 5.5 Hz, 2H, H_2-C(42)), 2.47 (t, J = 8.3 Hz, 2H, H_2-C(33)), 2.41–2.38 (m, 2H, H_2-C(39)), 2.01 (s, 3H, H_3-C(14 or 14‘), 1.74–1.63 (m, 4H, H_2-C(34 and 38)), 1.42 (s, 3H, H_3-C(14 or 14‘)), 1.39 (s, 6H, H_3-C(35 and 36 and 37)).

^{13}C NMR (201 MHz, CD_2Cl_2): δ / ppm = 182.6 (C(9)), 174.1 (C(32)), 173.7 (C(40)), 158.6 (C(15)), 157.2 (C(27)), 154.0 (C(11)), 150.1 (C(5)), 147.5 (C(49)), 139.5 (C(47)), 137.4 (C(3)), 136.4 (C(6)), 135.6 (C(17)), 133.0 (C(2)), 132.5 (C(46)), 131.4 (C(50)), 127.9 (C(51)), 126.2 (C(52)), 124.7 (C(1)), 124.4 (C(4)), 113.7 (C(45)), 113.0 (C(18)), 110.9 (C(16)), 97.4 (C(29)), 90.4 (C(43)), 78.9 (C(44)), 76.4 (C(28)), 70.0 (C(25)), 69.7 (C(20)), 68.1 (C(19)), 67.8 (C(26)), 64.7 (C(48)), 63.0 (C(41)), 62.5 (C(31)), 52.4 (C(13)), 49.8 (C(12)), 34.8 (C(39)), 34.3 (C(33)), 30.2 (C(35 or 36 or 37)), 29.9 (C(35 or 36 or 37)), 29.4 (C(35 or 36 or 37)), 28.7 (C(14 or 14‘), 27.5 (C(14 or 14‘)), 25.2 (C(34 or 38)), 25.0 (C(34 or 38)), 20.7(C(30)), 20.5(C(42)).

IR: $\tilde{\nu}$ / cm^{-1} = 3020 (m), 3008 (m), 2956 (s), 2929 (s), 2862 (s), 1734 (vs), 1682 (s), 1593 (s), 1550 (s), 1508 (s), 1489 (s), 1466 (s), 1446 (s), 1338 (m), 1284 (s), 1255 (s), 1182 (s), 1173 (s), 1130 (s), 1119 (s), 1095 (s), 1080 (s), 1066 (s), 1036 (s), 818 (m), 764 (s), 750 (s), 702 (s), 463 (s), 457 (m), 444 (s), 432 (m).
HRMS (ESI): *m/z* calc. for $[C_{69}H_{70}O_{11}S+H]^+$: 1107.4712; found: 1107.4747 ($M+H^+$).
Enantiomers were separated on a Daicel Chiralpak IC semi-preparative column eluting with EtOAc:*n*-heptane 50:50 at 30 °C.

Compound 30[104]

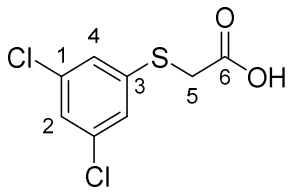

Bromoacetic acid (872 mg, 6.28 mmol, 1.1 equiv.) was dissolved in acetone (25 mL). K_2CO_3 (2.58 g, 18.7 mmol, 3.4 equiv.) was added at 25 °C. The suspension was cooled to 0 °C and 3,5-dichlorothiophenol (993 mg, 5.55 mmol, 1.0 equiv.) was added. The reaction mixture was allowed to warm to 25 °C and was stirred at that temperature for 17.5 h. The reaction was stopped by the addition of aq. HCl (2 M, 40 mL). H_2O (50 mL) was added and the mixture was extracted with EtOAc (3 × 100 mL). The combined organic layers were dried over Na_2SO_4, filtered, and concentrated *in vacuo*. The crude product was recrystallized from *n*-heptane to give acid **30** (1.04 g, 4.39 mmol, 79%) as colorless needles.

m.p.: 103 °C.
^{1}H NMR (400 MHz, CD_2Cl_2): δ / ppm = 7.29 (d, J = 1.8 Hz, 2H, H-C(4)), 7.24 (t, J = 1.8 Hz, 1H, H-C(2)), 3.74 (s, 2H, H-C(5)).
^{13}C NMR (101 MHz, CD_2Cl_2): δ / ppm = 175.2 (C(6)), 139.1 (C(3)), 135.9 (C(1)), 127.5 (C(2 or 4)), 127.5 (C(2 or 4)), 36.2 (C(5)).
IR: $\tilde{\nu}$ / cm^{-1} = 3100–2100 (w, br), 1686 (m), 1556 (s), 1397 (m), 1287 (m), 1199 (m), 1098 (m), 922 (m), 846 (m), 792 (s), 659 (s).
HRMS (EI): *m/z* calc. for $[C_8H_6Cl_2O_2S]^{\bullet+}$: 235.9460; found: 235.9459 ($M^{\bullet+}$).

Compound 31[104]

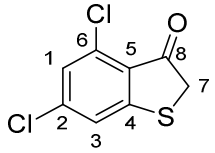

In a dried Schlenk flask under nitrogen atmosphere, compound **30** (862 mg, 3.64 mmol, 1.0 equiv.) was dissolved in dry CH_2Cl_2 (15 mL). At 0 °C, oxalyl chloride (0.36 mL, 4.3 mmol, 1.2 equiv.) and two drops of dry DMF were added. The reaction mixture was allowed to warm to 25 °C and was stirred at that temperature for 2 h. The volatiles were removed *in vacuo* and the residue was dissolved in 1,2-DCE (15 mL). At 0 °C, $AlCl_3$ (1.44 g, 10.8 mmol, 3.0 equiv.) was added, the mixture was allowed to warm to 25 °C and was stirred under nitrogen atmosphere for 40 min. The reaction was stopped by the addition of a saturated aqueous solution of $NaHCO_3$ (50 mL). H_2O (50 mL) was added and the mixture was extracted with CH_2Cl_2 (3 × 100 mL). The combined organic layers were washed with H_2O (1 × 200 mL) and brine (1 × 200 mL), dried over Na_2SO_4, filtered, and concentrated *in vacuo*. Benzothiophenone **31** (695 mg, 3.17 mmol, 87%) was obtained as a light-pink solid.

^{1}H NMR (400 MHz, CD_2Cl_2): δ / ppm = 7.34 (d, J = 1.7 Hz, 1H, H-C(3)), 7.18 (d, J = 1.7 Hz, 1H, H-C(1)), 3.86 (s, 2H, H_2-C(7)).
^{13}C NMR (101 MHz, CD_2Cl_2): δ / ppm = 196.0 (C(8)), 158.7 (C(4)), 142.2 (C(2)), 135.7 (C(6)), 127.5 (C(1)), 125.7 (C(5)), 123.6 (C(3)), 40.8 (C(7)).
HRMS (EI): *m*/*z* calc. for $[C_8H_4Cl_2OS]^{\bullet+}$: 217.9354; found: 217.9347 ($M^{\bullet+}$).

Compound 32

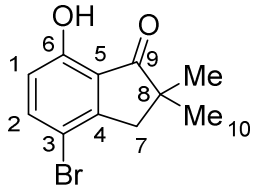

In a dried Schlenk flask under nitrogen atmosphere, a slurry of NaH (60% in mineral oil, 159 mg, 3.98 mmol, 3.0 equiv.) in dry THF (10 mL) was prepared. At 0 °C, 4-bromo-7-hydroxy-1-indanone (300 mg, 1.32 mmol, 1.0 equiv.) was added. The reaction mixture was stirred at 0 °C for 15 min. Iodomethane (0.21 mL, 3.4 mmol, 2.6 equiv.) was added dropwise and stirring was continued at 0 °C for 15 min, then at 50 °C for 3 h. The reaction mixture was allowed to cool to ambient temperature and the reaction was stopped by the addition of

H_2O (70 mL). The mixture was extracted with EtOAc (3 × 100 mL), the combined organic layers were dried over Na_2SO_4, filtered, and concentrated *in vacuo*. The crude product was purified by flash column chromatography (SiO_2, EtOAc:*i*-Hex, 2:98). Compound **32** was obtained as a colorless oil, which solidified to a faintly pink solid (105 mg, 0.41 mmol, 31%) upon storage in the fridge.

^{1}H NMR (400 MHz, $CDCl_3$): δ / ppm = 8.95 (s, 1H, -O*H*), 7.59 (d, J = 8.6 Hz, 1H, H-C(2)), 6.72 (d, J = 8.6 Hz, 1H, H-C(1)), 2.91 (s, 2H, H_2-C(7)), 1.28 (s, 6H, H_3-C(10)).
^{13}C NMR (101 MHz, $CDCl_3$): δ / ppm = 214.1 (C(9)), 157.3 (C(6)), 151.7 (C(4)), 140.2 (C(2)), 122.2 (C(5)), 116.3 (C(1)), 110.4 (C(3)), 46.1 (C(8)), 44.2 (C(7)), 25.1 (C(10)).
IR: $\tilde{\nu}$ / cm^{-1} = 3362 (w), 2962 (m), 1669 (vs), 1614 (s), 1464 (s), 1442 (s), 1336 (s), 1274 (vs), 1157 (s), 1106 (m), 1032 (m), 981 (m), 935 (m), 828 (s), 782 (m), 696 (s).
HRMS (EI): *m*/*z* calc. for $[C_{11}H_{11}BrO_2]^{\bullet+}$: 253.9937; found: 253.9928 ($M^{\bullet+}$).

Compound 33 *reported in ref.*[8]

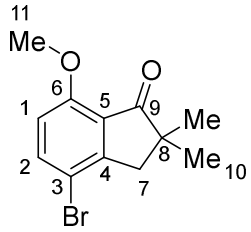

In a dried Schlenk flask, NaH (60% in mineral oil, 1.0 g, 25 mmol, 3.0 equiv.) was dispersed in dry THF (60 mL) under nitrogen atmosphere. At 0 °C, 4-bromo-7-methoxy-1-indanone (2.0 g, 8.3 mmol, 1.0 equiv.) was added and the reaction mixture was stirred at 0 °C for 30 min. Iodomethane (1.3 mL, 21 mmol, 2.5 equiv.) was added slowly and stirring was continued at 0 °C for 2.5 h, then the mixture was allowed to warm to 23 °C and subsequently stirred at that temperature for 18.5 h. The reaction was stopped by the addition of H_2O (100 mL) and the mixture was extracted with EtOAc (3 × 100 mL). The combined organic layers were dried over Na_2SO_4, filtered, and concentrated *in vacuo*. The crude product was purified by flash column chromatography (SiO_2, EtOAc:*i*-Hex, 30:70) to give compound **33** (1.5 g, 5.6 mmol, 67%) as a white solid.

R_f (EtOAc:*i*-Hex, 20:80): 0.37.
m.p: 112.3-114.5 °C.

^{1}H NMR (599 MHz, $CDCl_3$): δ / ppm = 7.64 (d, J = 8.7 Hz, 1H, H-C(2)), 6.72 (d, J = 8.7 Hz, 1H, H-C(1)), 3.92 (s, 3H, H-C(11)), 2.86 (s, 2H, H_2-C(7)), 1.22 (s, 6H, H_3-C(10)).
^{13}C NMR (151 MHz, $CDCl_3$): δ / ppm = 208.6 (C(9)), 157.9 (C(6)), 153.9 (C(4)), 138.8 (C(2)), 125.2 (C(5)), 112.0 (C(3)), 111.4 (C(1)), 56.2 (C(11)), 45.7 (C(8)), 43.8 (C(7)), 25.5 (C(10)).
IR: $\tilde{\nu}$ / cm^{-1} = 3081 (w), 2970 (m), 1715 (vs), 1564 (s), 1433 (m), 1380 (m), 1275 (s), 1180 (s), 1122 (s), 1080 (s), 998 (vs), 952 (s), 924 (m), 870 (m), 812 (vs), 779 (m), 687 (s).
HRMS (EI): *m/z* calc. for $[C_{12}H_{13}BrO_2]^{\bullet+}$: 268.0093; found: 268.0092 ($M^{\bullet+}$).

Compound (*E*/*Z*)-34

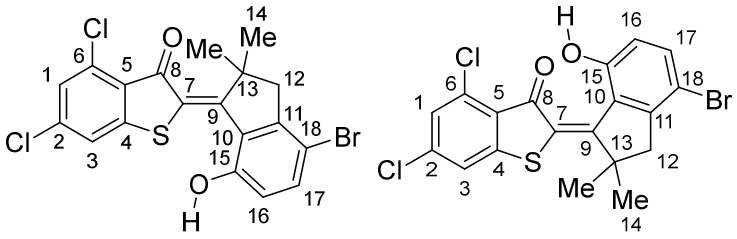

In a dried flask (A) under nitrogen atmosphere, compound **31** (48 mg, 0.22 mmol, 1.05 equiv.) was dissolved in dry CH_2Cl_2 (0.5 mL). In a separate dried flask (B) under nitrogen atmosphere, compound **33** (53 mg, 0.21 mmol, 1.0 equiv.) was dissolved in dry CH_2Cl_2 (0.5 mL). At −78 °C, BCl_3 (1.0 M in CH_2Cl_2, 0.22 mL, 0.22 mmol, 1.05 equiv.) was added to (A). The resulting mixture was immediately taken up by syringe (additional 0.25 mL of CH_2Cl_2 were added to rinse the flask) and added to (B) at −78 °C. The reaction mixture was then stirred at 0 °C for 5 min, before additional BCl_3 (1.0 M in CH_2Cl_2, 0.38 mL, 0.38 mmol, 1.8 equiv.) was added. Stirring was continued at 0 °C for 2.5 h. The reaction was stopped by the addition of a saturated aqueous solution of $NaHCO_3$ (5 mL). The mixture was diluted with H_2O (50 mL) and extracted with EtOAc (3 × 100 mL). The combined organic layers were washed with H_2O (1 × 200 mL) and brine (1 × 200 mL), dried over Na_2SO_4, filtered, and concentrated *in vacuo*. The crude product was purified by flash column chromatography (SiO_2, EtOAc:*i*-Hex, 5:95) followed by recrystallization from *n*-heptane to give compound **34** (mixture of (*E*)- and (*Z*)-isomers, 14 mg, 31 µmol, 14%) as a red solid.

Note: Analysis was performed on an *E*:*Z* mixture (approx. 60:40).
m.p.: 165 °C (decomposition).

R_f (EtOAc:*i*-Hex, 10:90): 0.56.

(*E*)-isomer

^{1}H NMR (601 MHz, CD_2Cl_2): δ / ppm = 7.61 (d, J = 8.7 Hz, 1H, H-C(17)), 7.55 (s, 1H, -OH), 7.51 (d, J = 1.7 Hz, 1H, H-C(3)), 7.33 (d, J = 1.7 Hz, 1H, H-C(1)), 6.95 (d, J = 8.7 Hz, 1H, H-C(16)), 3.09 (s, 2H, H_2-C(12)), 1.58 (s, 6H, H_3-C(14)).

^{13}C NMR (151 MHz, CD_2Cl_2): δ / ppm = 188.3 (C(8)), 166.1 (C(9)), 160.0 (C(15)), 150.3 (C(11)), 148.7*, 144.7*, 141.3 (C(5)), 140.2*, 137.5 (C(17)), 136.5 (C(6)), 130.9 (C(10)), 127.9 (C(1)), 126.4*, 126.1 (C(2)), 122.1 (C(16)), 121.9 (C(3)), 119.1*, 110.9 (C(18)), 52.2 (C(13)), 51.4 (C(12)), 27.5 (C(14)).

(*Z*)-isomer

^{1}H NMR (601 MHz, CD_2Cl_2): δ / ppm = 7.74 (d, J = 1.7 Hz, 1H, H-C(3)), 7.48 (d, J = 8.7 Hz, 1H, H-C(17)), 7.45 (d, J = 1.8 Hz, 1H, H-C(1)), 7.06 (dd, J = 8.7, 0.8 Hz, 1H, H-C(16)), 3.36 (d, J = 15.5 Hz, 1H, H_2-C(12)), 2.65 (d, J = 15.5 Hz, 1H, H_2-C(12)), 1.56 (s, 3H, H_3-C(14)), 0.94 (s, 3H, H_3-C(14)).

^{13}C NMR (151 MHz, CD_2Cl_2): δ / ppm = 149.5 (C(15)), 148.7*, 145.0 (C(11)), 144.7*, 140.2*, 133.4 (C(17)), 132.1 (C(5)), 129.2 (C(6)), 129.1 (C(10)), 127.2 (C(1)), 126.4*, 125.8 (C(2)), 121.9 (C(3)), 119.1*, 116.0 (C(16)), 114.0 (C(18)), 77.2 (C(9)), 50.7 (C(13)), 47.3 (C(12)), 26.0 (C(14)), 21.7 (C(14)).

*could not be assigned unambiguously

HRMS (EI): *m/z* calc. for $[C_{19}H_{13}BrCl_2O_2S]^{\bullet+}$: 453.9191; found: 453.9187 ($M^{\bullet+}$).

Compound (*E*/*Z*)-35

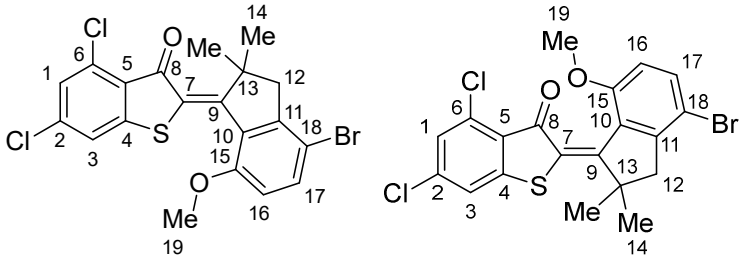

In a dried Schlenk flask (A) under nitrogen atmosphere, compound **31** (196 mg, 0.895 mmol, 1.1 equiv.) was dissolved in dry CH_2Cl_2 (1.9 mL). In a separate dried Schlenk flask (B) under nitrogen atmosphere, compound **33** (222 mg, 0.825 mmol, 1.0 equiv.) was dissolved in dry CH_2Cl_2 (0.9 mL). At −78 °C, BCl_3 (1.0 M in CH_2Cl_2, 0.90 mL, 0.90 mmol, 1.1 equiv.) was added to (A). The resulting mixture was immediately taken up by syringe and added to (B) at 0 °C. The reaction mixture was stirred at 0 °C for 50 min. The reaction was stopped by the addition of H_2O (5 mL). The mixture was diluted with H_2O (50 mL) and extracted with EtOAc (3 × 50 mL). The combined organic layers were washed with H_2O (1 × 100 mL) and brine (1 × 100 mL), dried over Na_2SO_4, filtered, and concentrated *in vacuo*. The crude product was purified by flash column chromatography (SiO_2, EtOAc:*i*-Hex, 5:95) followed by recrystallization from *n*-heptane to give compound **35** (mixture of (*E*)- and (*Z*)-isomers, 222 mg, 0.472 mmol, 57%) as an orange solid.

Note: Analysis was performed on an *E*:*Z* mixture (approx. 1.2:1.0)
R_f (EtOAc:*i*-Hex, 10:90): 0.47 and 0.60.

(*Z*)-isomer
^{1}H NMR (500 MHz, CD_2Cl_2): δ / ppm = 7.55 (d, J = 8.9 Hz, 1H, H-C(17)), 7.29 (d, J = 1.6 Hz, 1H, H-C(3)), 7.18 (d, J = 1.7 Hz, 1H, H-C(1)), 6.76 (d, J = 8.7 Hz, 1H, H-C(16)) 3.95 (s, 3H, H_3-C(19)), 2.96 (s, 2H, H_2-C(12)), 1.53 (s, 6H, H_3-C(14)).
^{13}C NMR (126 MHz, CD_2Cl_2): δ / ppm = 186.0 or 184.1 (C(8)), 162.3 (C(9)), 155.8 (C(15)), 150.1*, 149.7 (C(11)), 147.8*, 140.2 (C(2)), 136.1 (C(17)), 134.5 (C(6)), 129.1 (two signals, C(10) and *), 126.9 (C(1)), 126.4*, 126.3*, 126.1*, 121.7 (C(3)), 111.9 (C(16)), 111.0 (C(18)), 55.3 (C(19)), 52.6 (C(12)), 51.1 (C(13)), 26.7 (C(14)).

(*E*)-isomer

^{1}H NMR (500 MHz, CD_2Cl_2): δ / ppm = 7.47 (d, J = 8.7 Hz, 1H, H-C(17)), 7.39 (d, J = 1.7 Hz, 1H, H-C(1 or 3)), 7.24 (d, J = 1.6 Hz, 1H, H-C(1 or 3)), 6.73 (d, J = 8.9 Hz, 1H, H-C(16)), 3.84 (s, 3H, H_3-C(19)), 3.12 (d, J = 16.4 Hz, 1H, H_2-C(12)), 2.84 (d, J = 15.7 Hz, 1H, H_2-C(12)), 1.67 (s, 3H, H_3-C(14)), 1.21 (s, 3H, H_3-C(14)).

^{13}C NMR (126 MHz, CD_2Cl_2): δ / ppm = 186.0 or 184.1 (C(8)), 157.9 (C(15)), 156.4 (C(9)), 150.1*, 148.4 (C(11)), 147.8*, 139.8 (C(2)), 134.7 (C(6)), 134.6 (C(17)), 129.5 (C(10)), 129.1*, 127.2 (C(1 or 3)), 126.4*, 126.3*, 126.1*, 122.3 (C(1 or 3)), 111.6 (C(16)), 110.2 (C(18)), 55.7 (C(19)), 50.7 (C(12)), 49.9 (C(13)), 26.5 (C(14)), 26.0 (C(14)).

*could not be assigned unambiguously

IR: $\tilde{\nu}$ / cm^{-1} = 2942 (w, br), 1662 (s), 1570 (s), 1508 (s), 1466 (s), 1372 (m), 1280 (s), 1226 (m), 1171 (m), 1075 (s), 1051 (s), 977 (s), 936 (m), 847 (s), 818 (s), 798 (vs), 678 (m).

HRMS (EI): m/z calc. for $[C_{20}H_{15}BrCl_2O_2S]^{\bullet+}$: 467.9348; found: 467.9353 ($M^{\bullet+}$).

Compound 36

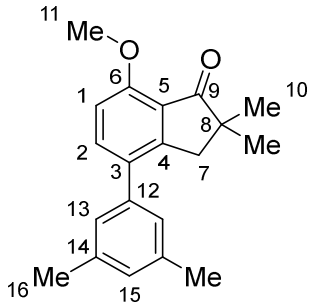

Compound **33** (153 mg, 0.57 mmol, 1.0 equiv.), (3,5-dimethylphenyl)boronic acid (168 mg, 1.12 mmol, 2.0 equiv.), K_2CO_3 (231 mg, 1.67 mmol, 2.9 equiv.) and $Pd(PPh_3)_4$ (66 mg, 57 µmol, 0.1 equiv.) were added to a round bottom flask in this order. The flask was evacuated and refilled with dry N_2 three times. 1,4-Dioxan (4.8 mL) and H_2O (1.2 mL) were added and the flask was carefully evacuated and refilled with nitrogen five times under vigorous stirring. The reaction mixture was stirred at 65 °C for 8 h, then at 23 °C for 16.5 h. The reaction was stopped by the addition of a saturated aqueous solution of NH_4Cl (50 mL). The mixture was diluted with H_2O (50 mL) and extracted with EtOAc (2 × 50 mL). The combined organic layers were dried over Na_2SO_4, filtered, and concentrated *in vacuo*. The crude product was purified by flash column chromatography (SiO_2, EtOAc:*i*-Hex, 20:80) to give compound **36** (159 mg, 0.54 mmol, 95%) as a yellow foam.

R_f (EtOAc:*i*-Hex, 20:80): 0.33.

^{1}H NMR (400 MHz, $CDCl_3$): δ / ppm = 7.52 (d, J = 8.4 Hz, 1H, H-C(2)), 7.01 (s, 3H, H-C(13 and 15)), 6.88 (d, J = 8.5 Hz, 1H, H-C(1)), 3.98 (s, 3H, H_3-C(11)), 2.97 (s, 2H, H_2-C(7)), 2.38 (s, 6H, H_3-C(16)), 1.21 (s, 6H, H_3-C(10)).

^{13}C NMR (101 MHz, $CDCl_3$): δ / ppm = 209.4 (C(9)), 157.8 (C(6)), 152.0 (C(4)), 139.1 (C(12)), 138.1 (C(14)), 136.6 (C(2)), 132.5 (C(3)), 128.9 (C(15)), 126.5 (C(13)), 123.3 (C(5)), 109.5 (C(1)), 55.9 (C(11)), 45.7 (C(8)), 42.6 (C(7)), 25.5 (C(10)), 21.5 (C(16)).

IR: $\tilde{\nu}$ / cm^{-1} = 2958 (w, br), 1706 (vs), 1601 (s), 1577(s), 1496 (s), 1461 (m), 1437 (m), 1378 (m), 1277 (vs), 1239 (m), 1218 (m), 1165 (m), 1081 (s), 1017 (s), 923 (m), 852 (m), 815 (s), 730 (m), 705 (m).

HRMS (EI): *m*/*z* calc. for $[C_{20}H_{22}O_2]^{\bullet+}$: 294.1614; found: 294.1614 ($M^{\bullet+}$).

Compound (*E*/*Z*)-37

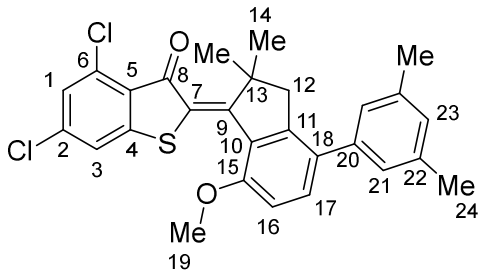

(*Z*)-isomer

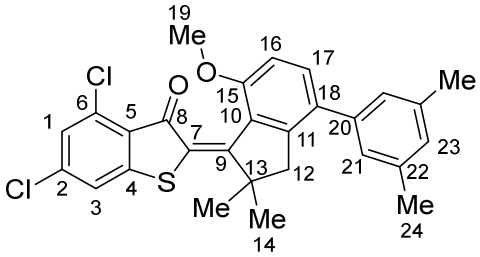

(*E*)-isomer

In a dried Schlenk flask (A) under nitrogen atmosphere, compound **31** (86 mg, 0.39 mmol, 1.1 equiv.) was dissolved in dry CH_2Cl_2 (1.2 mL). In a separate dried Schlenk flask (B) under nitrogen atmosphere, compound **36** (100 mg, 0.340 mmol, 1.0 equiv.) was suspended in dry CH_2Cl_2 (0.82 mL). At −78 °C, BCl_3 (1.0 M in CH_2Cl_2, 0.37 mL, 0.37 mmol, 1.1 equiv.) was added to (A). The resulting mixture was immediately taken up by syringe and added to (B) at 0 °C. The reaction mixture was stirred at 0 °C for 45 min. The reaction was stopped by the addition of H_2O (10 mL). The mixture was diluted with H_2O (50 mL) and extracted with EtOAc (3 × 50 mL). The combined organic layers were dried over Na_2SO_4, filtered, and concentrated *in vacuo*. The crude product was purified by flash column chromatography (SiO_2, EtOAc:*i*-Hex, 10:90) to give compound **37** (mixture of (*E*)- and (*Z*)-isomers, 67 mg, 0.14 mmol, 36%) as an orange solid.

Note: Analysis was performed on an *E*:*Z* mixture (approx. 3:2).

R_f (EtOAc:*i*-Hex, 10:90): 0.55 and 0.61.

(*Z*)-isomer

^{1}H NMR (400 MHz, CD_2Cl_2): δ / ppm = 7.45 (d, J = 8.5 Hz, 1H, H-C(17)), 7.31 (d, J = 1.7 Hz, 1H, H-C(1 or 3)), 7.18 (d, J = 1.7 Hz, 1H, H-C(1 or 3)), 7.01 (s, 2H, H-C(21)), 6.99 (s, 1H, H-C(23)), 6.92 (d, J = 8.6 Hz, 1H, H-C(17)), 3.99 (s, 3H, H_3-C(19)), 3.03 (s, 2H, H_2-C(12)), 2.36 (s, 6H, H_3-C(24)), 1.48 (s, 6H, H_3-C(14)).

^{13}C NMR (101 MHz, CD_2Cl_2): δ / ppm = 185.9 (C(8)), 163.4 (C(9)), 155.8 (C(15)), 150.4*, 147.9 (two signals, C(11) and *), 140.0 (C(20)), 139.9 (C(4)), 138.4 (C(22)), 134.3 (C(17)), 132.1 (C(18)), 129.0 (C(23)), 128.1*, 128.0 (C(10)), 126.7 (C(21) and C(1 or 3)), 126.5 (C(5)), 124.9*, 121.7 (C(1 or 3)), 110.3 (C(16)), 55.1 (C(19)), 52.1 (C(13)), 51.6 (C(12)), 26.7 (C(14)), 21.5 (C(24)).

(*E*)-isomer

^{1}H NMR (400 MHz, CD_2Cl_2): δ / ppm = 7.40 (d, J = 1.7 Hz, 1H, H-C(1 or 3)), 7.40 (d, J = 8.5 Hz, 1H, H-C(17)), 7.24 (d, J = 1.7 Hz, 1H, H-C(1 or 3)), 7.04 (s, 2H, H-C(21)), 6.99 (s, 1H, H-C(23)), 6.88 (d, J = 8.6 Hz, 1H, H-C(16)), 3.88 (s, 3H, H_3-C(19)), 3.37 (d, J = 15.6 Hz, 1H, H_2-C(12)), 2.73 (d, J = 15.7 Hz, 1H, H_2-C(12)), 2.36 (s, 6H, H_3-C(24)), 1.66 (s, 3H, H_3-C(14)), 1.13 (s, 3H, H_3-C(14)).

^{13}C NMR (101 MHz, CD_2Cl_2): δ / ppm = 184.3 (C(8)), 157.8 (C(15)), 157.4 (C(9)), 150.4*, 147.9*, 146.7 (C(11)), 140.2 (C(20)), 139.5 (C(4)), 138.4 (C(22)), 134.6*, 134.4*, 132.7 (C(17)), 131.6 (C(18)), 128.8 (C(23)), 128.5 (C(10)), 128.1*, 127.1 (C(1 or 3)), 126.7 (C(21)), 126.6 (C(5)), 124.9*, 122.3 (C(1 or 3)), 110.1 (C(16)), 55.4 (C(19)), 50.8 (C(13)), 49.9 (C(12)), 26.7 (C(14)), 25.9 (C(14)), 21.5 (C(24)).

*could not be assigned unambiguously

IR: $\tilde{\nu}$ / cm^{-1} = 2918 (w, br), 1681 (m), 1667 (m), 1572 (vs), 1530 (s), 1493 (m), 1372 (m), 1277 (vs), 1214 (m), 1078 (s), 1056 (s), 831 (vs), 810 (vs), 708 (s), 662 (s).

HRMS (EI): *m*/*z* calc. for $[C_{28}H_{24}Cl_2O_2S]^{\bullet+}$: 494.0869; found: 494.0862 ($M^{\bullet+}$).

Compound 38

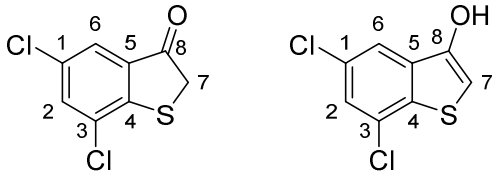

Compound **40** (1.02 g, 4.30 mmol, 1.00 equiv.) in $SOCl_2$ (2.8 mL, 38.4 mmol, 8.93 equiv.) was stirred at 80 °C for 2 h. Excess $SOCl_2$ was removed *in vacuo* and the residue was dissolved in 1,2-DCE (18 mL). At 0 °C, $AlCl_3$ (1.71 g, 12.8 mmol, 2.98 equiv.) was added and the reaction mixture was stirred at 0 °C for 2.5 h, then at 23 °C for 2 h. The reaction mixture was poured into ice water (200 mL), followed by extraction with CH_2Cl_2 (3 × 100 mL). The combined organic layers were dried over Na_2SO_4, filtered, and concentrated *in vacuo* to give compound **38** (884 mg, 4.04 mmol, 94%) as a brown solid.

^{1}H NMR (400 MHz, CD_2Cl_2): δ / ppm = 7.64 (d, J = 1.9 Hz, 1H, H-C(2 or 6)), 7.59 (d, J = 1.9 Hz, 1H, H-C(2 or 6)), 3.89 (s, 2H, H_2-C(7)).
^{1}H NMR (400 MHz, $(CD_3)_2SO$): δ / ppm = 10.50 (s, 1H, -O*H*), 7.74 (d, J = 1.8 Hz, 1H, H-C(2)), 7.62 (dd, J = 1.8, 0.7 Hz, 1H, H-C(6)), 6.72 (d, J = 0.6 Hz, 1H, H-C(7)).
^{13}C NMR (101 MHz, $(CD_3)_2SO$): δ / ppm = 148.2 (C(4)), 134.8 (C(1 or 8)), 134.6 (C(1 or 8)), 129.4 (C(3)), 127.9 (C(5)), 124.0 (C(6)), 119.3 (C(2)), 101.7 (C(7)).
HRMS (EI): *m*/*z* calc. for $[C_8H_4Cl_2OS]^{\bullet+}$: 217.9354; found: 217.9354 ($M^{\bullet+}$).

Compound (*E*/*Z*)-39

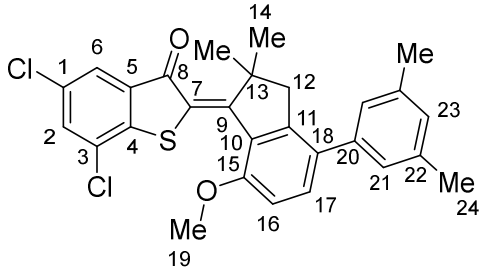

(*Z*)-isomer

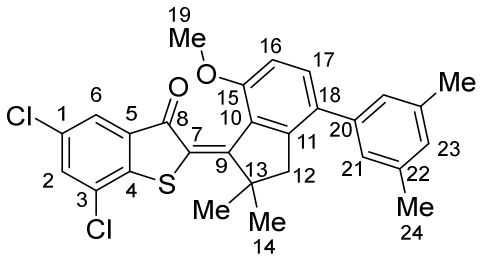

(*E*)-isomer

In a dried Schlenk flask (A) under nitrogen atmosphere, compound **38** (191 mg, 0.872 mmol, 1.1 equiv.) was dissolved in dry CH_2Cl_2 (1.6 mL). A separate dried Schlenk flask (B) under nitrogen atmosphere was prepared, containing a solution of compound **36** (1.0 M in CH_2Cl_2, 0.8 ml, 0.80 mmol, 1.0 equiv.). At −78 °C, BCl_3 (1.0 M in CH_2Cl_2, 0.88 mL, 0.88 mmol, 1.1 equiv.) was added to (A). The resulting mixture was immediately taken up by syringe and added to (B) at 0 °C. The reaction mixture was stirred at 0 °C for 1 h. The reaction was stopped by the addition of H_2O (10 mL). The mixture was diluted with H_2O (50 mL) and extracted with EtOAc (3 × 50 mL). The combined organic layers were washed with H_2O (1 × 100 mL) and brine (1 × 100 mL), dried over Na_2SO_4, filtered, and concentrated *in vacuo*. The crude product was purified by flash column chromatography (SiO_2, EtOAc:*i*-Hex, 10:90) to give compound **39** (mixture of (*E*)- and (*Z*)-isomers, 217 mg, 0.438 mmol, 55%) as a red solid.

Note: Analysis was performed on an *E*:*Z* mixture (approx. 2:1).

R_f (EtOAc:*i*-Hex, 10:90): 0.58 and 0.66.

(*Z*)-isomer

^{1}H NMR (400 MHz, CD_2Cl_2): δ / ppm = 7.67 (d, J = 1.9 Hz, 1H, H-C(6)), 7.53 (d, J = 1.9 Hz, 1H, H-C(2)), 7.47 (d, J = 8.4 Hz, 1H, H-C(17)), 7.01 (s, 2H, H-C(21)), 6.99 (s, 1H, H-C(23)), 6.94 (d, J = 8.4 Hz, 1H, H-C(16)), 4.02 (s, 3H, H_3-C(19)), 3.05 (s, 2H, H_2-C(12)), 2.38–2.35 (m, 6H, H_3-C(24)), 1.49 (s, 6H, H_3-C(14)).

(*E*)-isomer

^{1}H NMR (400 MHz, CD_2Cl_2): δ / ppm = 7.78 (d, J = 1.9 Hz, 1H, H-C(6)), 7.57 (d, J = 1.9 Hz, 1H, H-C(2)), 7.43 (d, J = 8.5 Hz, 1H, H-C(17)), 7.04 (s, 2H, H-C(21)), 6.99 (s, 1H, H-C(23)), 6.89 (d, J = 8.6 Hz, 1H, H-C(16)), 3.86 (s, 3H, H_3-C(19)), 3.38 (d,

J = 15.7 Hz, 1H, H_2-C(12)), 2.76 (d, *J* = 15.3 Hz, 1H, H_2-C(12)), 2.38–2.35 (m, 6H, H_3-C(24)), 1.72 (s, 3H, H_3-C(14)), 1.18 (s, 3H, H_3-C(14)).

IR: $\tilde{\nu}$ / cm^{-1} = 2954 (w, br), 1668 (m), 1535 (s), 1431 (s), 1275 (s), 1077 (s), 850 (vs), 616 (vs).
HRMS (APPI): *m*/*z* calc. for $[C_{28}H_{24}Cl_2O_2S+H]^+$: 495.0947; found: 495.0948 ($M+H^+$).

Compound 40

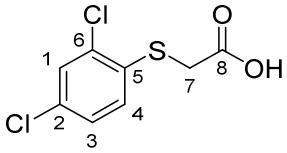

2-Bromoacetic acid (863 mg, 6.21 mmol,1.1 equiv.) was dissolved in acetone (25 mL). At 0 °C, K_2CO_3 (2.29 g, 16.6 mmol, 3.0 equiv.) and 2,4-dichloro thiophenol (0.71 mL, 5.6 mmol, 1.0 equiv.) were added. The reaction mixture was stirred at 0 °C for 20 min, then additional acetone (25 mL) was added and stirring was continued at 23 °C for 31 h. The reaction was stopped by the addition of aq. HCl (2 M, 100 mL) and the mixture was extracted with EtOAc (3 × 100 mL). The combined organic layers were dried over Na_2SO_4, filtered, and concentrated *in vacuo* to give compound **40** (1.29 g, 5.44 mmol, 97%) as a colorless solid.

m.p.: 122 °C.
^{1}H NMR (400 MHz, $(CD_3)_2SO$): δ / ppm = 12.95 (br, 1H, -CO_2H), 7.62 (d, *J* = 2.2 Hz, 1H, H-C(1)), 7.42 (dd, *J* = 8.6, 2.2 Hz, 1H, H-C(3)), 7.35 (d, *J* = 8.6 Hz, 1H, H-C(4)), 3.93 (s, 2H, H_2-C(7)).
^{13}C NMR (101 MHz, $(CD_3)_2SO$): δ / ppm = 169.9 (C(8)), 134.6 (C(5)), 131.4 (C(2 or 6)), 130.3 (C(2 or 6)), 128.8 (C(1)), 128.4 (C(4)), 127.8 (C(3)), 33.8 (C(7)).
IR: $\tilde{\nu}$ / cm^{-1} = 3533 (w, br), 3100–2300 (w, br), 1703 (s), 1456 (m), 1429 (m), 1382 (m), 1308 (s), 1260 (m), 1199 (s), 1154 (m), 1104 (m), 1032 (s), 895 (s), 866 (vs), 803 (vs), 682 (s), 662 (s).
HRMS (EI): *m*/*z* calc. for $[C_8H_6Cl_2O_2S]^{\bullet+}$: 235.9460; found: 235.9455 ($M^{\bullet+}$).

Compound 42[122]

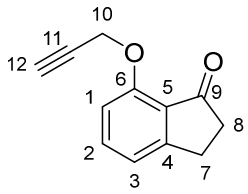

Propargyl bromide (80% in PhMe, 1.08 g, 7.26 mmol, 0.98 equiv.) and K_2CO_3 (4.16 g, 30.1 mmol, 4.1 equiv.) were added to a solution of 7-hydroxy-1-indanone (1.10 g, 7.42 mmol, 1.0 equiv.) in DMF (50 mL). The reaction mixture was stirred at 70 °C for 3 h, then at 23 °C for 23 h. H_2O (100 mL) was added and the mixture was extracted with EtOAc (3 × 100 mL). The combined organic layers were washed with aq. LiCl (10%, 1 × 150 mL), H_2O (2 × 150 mL) and brine (1 × 200 mL), dried over Na_2SO_4, filtered, and concentrated *in vacuo*. Indanone **42** (1.23 g, 6.61 mmol, 89%) was obtained as an off-white solid.

R_f (EtOAc:*i*-Hex, 20:80): 0.17.

^{1}H NMR (400 MHz, $CDCl_3$): δ / ppm = 7.52 (t, J = 7.8 Hz, 1H, H-C(2)), 7.06 (dq, J = 7.6, 0.9 Hz, 1H, H-C(3)), 6.95 (d, J = 8.3 Hz, 1H, H-C(1)), 4.86 (d, J = 2.5 Hz, 2H, H_2-C(10)), 3.10–3.05 (m, 2H, H_2-C(7)), 2.69–2.63 (m, 2H, H_2-C(8)), 2.52 (t, J = 2.4 Hz, 1H, H-C(12)).

^{13}C NMR (101 MHz, $CDCl_3$): δ / ppm = 204.6 (C(9)), 158.1 (C(4)), 155.9 (C(6)), 136.2 (C(2)), 125.9 (C(5)), 119.6 (C(3)), 111.0 (C(1)), 78.1 (C(11)), 76.5 (C(12)), 56.3 (C(10)), 36.9 (C(8)), 25.7 (C(7)).

HRMS (EI): m/z calc. for $[C_{12}H_{10}O_2]^{\bullet+}$: 186.0675; found: 186.0673 ($M^{\bullet+}$).

Compound 43[122]

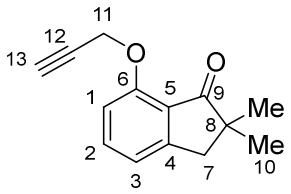

In a dried Schlenk flask under nitrogen atmosphere, a slurry of NaH (60% in mineral oil, 650 mg, 16.3 mmol, 3.1 equiv.) in dry THF (36 mL) was prepared. At 0 °C, compound **42** (973 mg, 5.22 mmol, 1.0 equiv.) was added. The reaction mixture was stirred at 0 °C for 1 h, then iodomethane (0.84 mL, 13 mmol, 2.5 equiv.) was added. The reaction mixture was allowed to warm to 23 °C and stirring was continued at this temperature for 2 h. H_2O (50 mL) was added and the mixture was extracted with EtOAc (3 × 75 mL). The combined organic layers were washed with H_2O (1 × 200 mL) and brine (1 × 200 mL), dried over Na_2SO_4, filtered, and concentrated *in vacuo*. The crude product was purified by flash column chromatography (SiO_2, EtOAc:*i*-Hex, 15:85) to give compound **43** (868 mg, 4.05 mmol, 78%) as an off-white solid.

^{1}H NMR (400 MHz, CD_2Cl_2): δ / ppm = 7.54 (t, J = 7.8 Hz, 1H, H-C(2)), 7.04 (dq, J = 7.6, 1.0 Hz, 1H, H-C(1 or 3)), 6.92 (d, J = 8.2 Hz, 1H, H-C(1 or 3)), 4.84 (d, J = 2.3 Hz, 2H, H_2-C(11)), 2.94 (s, 2H, H_2-C(7)), 2.62 (t, J = 2.4 Hz, 1H, H-C(13)), 1.18 (s, 6H, H3-C(10)).
^{13}C NMR (101 MHz, CD_2Cl_2): δ / ppm = 208.6 (C(9)), 156.4 (C(6)), 155.3 (C(4)), 136.4 (C(2)), 124.3 (C(5)), 119.9 (C(1 or 3)), 111.2 (C(1 or 3)), 78.4 (C(12)), 76.4 (C(12)), 56.6 (C(11)), 45.8 (C(8)), 42.8 (C(7)), 25.5 (C(10)).
HRMS (EI): m/z calc. for $[C_{14}H_{14}O_2]^{\bullet+}$: 214.0988; found: 214.0989 ($M^{\bullet+}$).

Compound (*E*/*Z*)-44

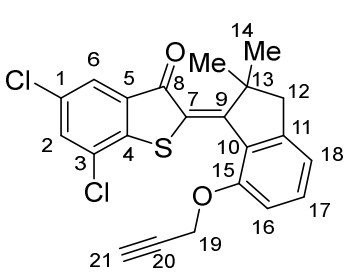

In a dried Schlenk flask (A) under nitrogen atmosphere, compound **38** (680 mg, 3.10 mmol, 1.1 equiv.) was dissolved in dry CH_2Cl_2 (5.0 mL). In a separate dried Schlenk flask (B) under nitrogen atmosphere, compound **43** (594 mg, 2.77 mmol, 1.0 equiv.) was dissolved in dry CH_2Cl_2 (3.0 mL). At −78 °C, BCl_3 (1.0 M in CH_2Cl_2, 3.0 mL, 3.0 mmol, 1.1 equiv.) was added to (A). The resulting mixture was immediately taken up by syringe and added to (B) at 0 °C. The reaction mixture was stirred at 0 °C for 20 min. The ice bath was removed and the reaction was stopped by the addition of H_2O (15 mL). The mixture was extracted with EtOAc (2 × 25 mL). The combined organic layers were washed with H_2O (1 × 25 mL) and brine (1 × 25 mL), dried over Na_2SO_4, filtered, and concentrated *in vacuo*. The crude product was purified by flash column chromatography (SiO_2, EtOAc:*i*-Hex, 5:95) to give compound **44** (mixture of (*E*)- and (*Z*)-isomers, 605 mg, 1.46 mmol, 53%) as an orange foam.

Single crystals suitable for X-Ray crystallography could be obtained by crystallization from CH_2Cl_2/*n*-heptane.

Note: Analysis was performed on an *E*:*Z*-mixture (approx. 3:1).

R_f (EtOAc:*i*-Hex, 10:90): 0.43 and 0.54.

(*E*)-isomer

^{1}H NMR (601 MHz, CD_2Cl_2): δ / ppm = 7.78 (d, J = 1.9 Hz, 1H, H-C(6)), 7.56 (d, J = 1.9 Hz, 1H, H-C(2)), 7.38 (dd, J = 7.5 Hz, 1H, H-C(17)), 6.99–6.95 (m, 1H, H-C(18)), 6.86 (d, J = 8.3 Hz, 1H, H-C(16)), 4.73 (d, J = 2.4 Hz, 2H, H_2-C(19)), 3.20 (d, J = 16.0 Hz, 1H, H_2-C(12)), 2.81 (d, J = 15.4 Hz, 1H, H_2-C(12)), 2.48 (t, J = 2.4 Hz, 1H, H-C(21)), 1.72 (s, 3H, H_3-C(14)), 1.24 (s, 3H, H_3-C(14)).

^{13}C NMR (DEPTq, 151 MHz, CD_2Cl_2): δ / ppm = 185.3 (C(8)), 159.3 (C(9)), 157.2 (C(15)), 150.3 (C(11)), 141.7 (C(1 or 4)), 135.2 (C(5)), 133.1 (C(2)), 132.9 (C(17)), 131.6 (C(1 or 4)), 129.4 (C(3)), 128.6 (C(10)), 125.7 (C(7)), 124.7 (C(6)), 118.2 (C(18)), 110.5 (C(16)),

79.0 (C(20)), 75.7 (C(21)), 56.4 (C(19)), 51.2 (C(13)), 49.5 (C(12)), 26.7 (C(14)), 26.2 (C(14)).

(*Z*)-isomer

^{1}H NMR (601 MHz, CD_2Cl_2): δ / ppm = 7.67 (d, J = 2.0 Hz, 1H, H-C(6)), 7.52 (d, J = 2.0 Hz, 1H, H-C(2)), 7.46 (t, J = 7.9 Hz, 1H, H-C(17)), 6.99–6.95 (m, 2H, H-C(16 and 18)), 4.93 (d, J = 2.5 Hz, 2H, H_2-C(19)), 3.00 (s, 2H, H_2-C(12)), 2.63 (t, J = 2.4 Hz, 1H, H-C(21)), 1.52 (s, 6H, H_3-C(14)).

^{13}C NMR (DEPTq, 151 MHz, CD_2Cl_2): δ / ppm = 187.2 (C(8)), 165.1 (C(9)), 154.7 (C(15)), 151.5 (C(11)), 143.6 (C(1 or 4)), 135.0 (C(5)), 134.3 (C(17)), 133.4 (C(2)), 131.2 (C(1 or 4)), 129.0 (C(3)), 128.5 (C(7)), 128.3 (C(10)), 124.2 (C(6)), 118.7 (C(18)), 111.3 (C(16)), 78.1 (C(20)), 76.5 (C(21)), 55.8 (C(19)), 52.2 (C(13)), 51.4 (C(12)), 26.4 (C(14)).

IR: $\tilde{\nu}$ / cm^{-1} = 3298 (m), 2957 (m), 2123 (w), 1665 (s), 1528 (s), 1432 (m), 1287 (s), 1063 (s), 769 (s).

HRMS (EI): *m*/*z* calc. for $[C_{22}H_{16}Cl_2O_2S]^{\bullet+}$: 414.0243; found: 414.0242 ($M^{\bullet+}$).

Compound (*E*/*Z*)-46

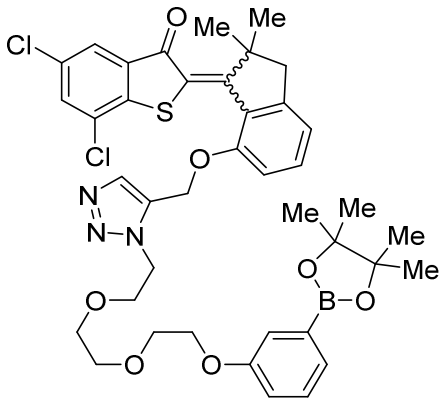

To a solution of azide **45**[122] (275 mg, 0.729 mmol, 1.0 equiv.) in DMF (3.6 mL), HTI **44** (291 mg, 0.701 mmol, 1.0 equiv.), sodium (L)-ascorbate (14 mg, 0.071 mmol, 0.1 equiv.) and $CuSO_4 \cdot 5\ H_2O$ (4 mg, 0.02 mmol, 0.03 equiv.) were added. The reaction mixture was stirred at 23 °C for a total of 2 d. (Note: After 19 h, additional $CuSO_4 \cdot 5\ H_2O$ (3 mg) and sodium (L)-ascorbate (9 mg) were added, and 23 h after that more $CuSO_4 \cdot 5\ H_2O$ (6 mg) and sodium (L)-ascorbate (9 mg) were added to the reaction.) The reaction mixture was poured into a saturated aqueous solution of NH_4Cl (50 mL). H_2O (25 mL) was added and

the mixture was extracted with EtOAc (3 × 50 mL). The combined organic layers were washed with H_2O (2 × 75 mL) and brine (2 × 75 mL), dried over Na_2SO_4, filtered, and concentrated *in vacuo*. The crude product was purified by flash column chromatography (SiO_2, MeOH:CH_2Cl_2, 0:100→5:95) to give triazole **46** (417 mg, mixture of products, most likely *E*/*Z* isomers and free boronic acid) as a red oil. The product mixture was used in attempted cross coupling reactions without further purification.

HRMS (ESI): *m*/*z* calc. for $[C_{40}H_{44}BCl_2N_3O_7S+H]^+$: 792.2443; found: 792.2435 ($M+H^+$).

Compound 47

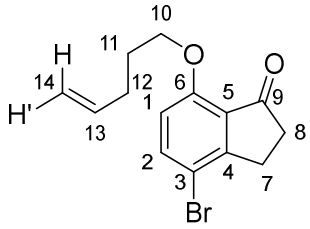

To a solution of 4-bromo-7-hydroxy-1-indanone (981 mg, 4.34 mmol, 1.0 eq) in DMF (30 mL), K_2CO_3 (2.43 g, 16.3 mmol, 3.8 equiv.) and 5-bromo-1-pentene (0.63 mL, 5.3 mmol, 1.2 equiv.) were added. The reaction mixture was stirred at 80 °C for 27 h, then it was allowed to cool to ambient temperature and H_2O (100 mL) was added. The mixture was extracted with EtOAc (3 × 100 mL). The combined organic layers were washed with H_2O (2 × 200 mL) and brine (3 × 200 mL), dried over Na_2SO_4, filtered, and concentrated *in vacuo*. The residue was purified by flash column chromatography (SiO_2, EtOAc:*i*-Hex, 20:80) to give compound **47** as a yellow solid (1.20 g, 4.07 mmol, 94%).

R_f (EtOAc:*i*-Hex, 20:80): 0.53.

^{1}H NMR (400 MHz, $CDCl_3$): δ / ppm = 7.59 (d, J = 8.7 Hz, 1 H, H-C(2)), 6.69 (d, J = 8.7 Hz, 1H, H-C(1)), 5.84 (ddt, J = 16.9, 10.2, 6.7 Hz, 1H, H-C(13)), 5.05 (dq, J = 17.1, 1.6 Hz, 1H, H-C(14)), 4.98 (ddt, J = 10.2, 2.1, 1.2 Hz, 1H, H'-C(14)), 4.07 (t, J = 6.6 Hz, 2H, H-C(10)), 3.00–2.94 (m, 2H, H-C(7)), 2.69–2.63 (m, 2H, H-C(8)), 2.27 (q, J = 6.8 Hz, 2H, H-C(12)), 1.96 (p, J = 6.7 Hz, 2H, H-C(11)).

^{13}C NMR (101 MHz, $CDCl_3$): δ / ppm = 203.6 (C(9)), 157.0 (C(4 or 6)), 156.7 (C(4 or 6)), 138.6 (C(2)), 137.7 (C(13)), 127.3 (C(5)), 115.5 (C(14)), 112.3 (C(1)), 111.6 (C(3)), 68.2 (C(10)), 36.7 (C(8)), 30.0 (C(12)), 28.0 (C(11)), 26.9 (C(7)).

IR: $\tilde{\nu}$ / cm^{-1} = 2942 (w, br), 1707 (vs), 1581 (s), 1477 (s), 1458 (s), 1290 (vs), 1220 (s), 1187 (s), 1128 (s), 1071 (s), 1032 (s), 1019 (s), 980 (s), 905 (s), 822 (m), 808 (vs), 710 (m).
HRMS (EI): *m/z* calc. for $[C_{14}H_{15}BrO_2]^{\bullet+}$: 294.0250, found: 294.0247 ($M^{\bullet+}$).

Compound 48

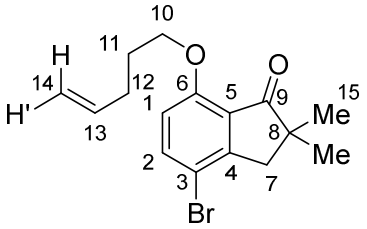

In a dried Schlenk flask under nitrogen atmosphere, a slurry of NaH (396 mg, 60% in mineral oil, 9.90 mmol, 2.9 equiv.) in dry THF (22 mL) was prepared. At 0 °C, compound **47** (1.00 g, 3.39 mmol, 1.0 equiv.) was added. The reaction mixture was stirred at 0 °C for 40 min. Iodomethane (0.53 mL, 8.5 mmol, 2.5 equiv.) was added and stirring was continued at 0 °C for 40 min, then at 23 °C for 19.5 h. The reaction was stopped by the addition of H_2O (50 mL). The mixture was diluted with additional H_2O (50 mL) and extracted with EtOAc (3 × 100 mL). The combined organic layers were dried over Na_2SO_4, filtered, and concentrated *in vacuo*. The residue was purified by flash column chromatography (SiO_2, EtOAc:*i*-Hex, 10:90) to give compound **48** (684 mg, 2.12 mmol, 63%) as a light-pink oil.

R_f (EtOAc:*i*-Hex, 10:90): 0.54.
^{1}H NMR (400 MHz, $CDCl_3$): δ / 7.60 (d, J = 8.7 Hz, 1H, H-C(2)), 6.70 (d, J = 8.7 Hz, 1H, H-C(1)), 5.83 (ddt, J = 16.9, 10.2, 6.6 Hz, 1H, H-C(13)), 5.04 (dq, J = 17.1, 1.6 Hz, 1H, H-C(14)), 4.97 (ddt, J = 10.2, 2.1, 1.2 Hz, 1H, H'-C(14)), 4.06 (t, J = 6.5 Hz, 2H, H-C(10)), 2.85 (s, 2H, H-C(7)), 2.32–2.25 (m, 2H, H-C(12)), 1.96 (p, J = 6.7 Hz, 2H, H-C(11)), 1.21 (s, 6H, H-C(15)).
^{13}C NMR (101 MHz, $CDCl_3$): δ / ppm = 208.2 (C(9)), 157.4 (C(6)), 153.8 (C(4)), 138.7 (C(2)), 137.7 (C(13)), 125.4 (C(5)), 115.5 (C(14)), 112.4 (C(1)), 111.7 (C(3)), 68.2 (C(10)), 45.7 (C(8)), 43.8 (C(7)), 29.9 (C(12)), 28.0 (C(11)), 25.5 (C(15)).
IR: $\tilde{\nu}$ / cm^{-1} = 2958 (m), 2926 (m), 1711 (vs), 1640 (w), 1583 (s), 1459 (s), 1380 (m), 1283 (vs), 1189 (s), 1127 (s), 1074 (s), 991 (s), 935 (s), 910 (s), 808 (s), 710 (m).
HRMS (EI): *m/z* calc. for $[C_{16}H_{19}BrO_2]^{\bullet+}$: 322.0563; found: 322.0563 ($M^{\bullet+}$).

Compound 49[73] *reported in ref.*[8]

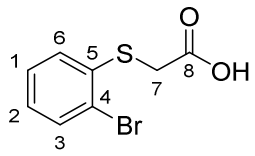

To a solution of 2-bromo acetic acid (2.5 g, 18 mmol, 1.1 equiv.) in acetone (170 mL), K_2CO_3 (7.0 g, 51 mmol, 3.0 equiv.) and 2-bromo thiophenol (2.0 mL, 17 mmol, 1.0 equiv.) were added at 0 °C. The suspension was allowed to warm to 25 °C overnight and was stirred for a total of 116 h (after 27 h additional 100 mL of acetone were added). The reaction was stopped by the addition of aq. HCl (2 M, 200 mL). Acetone was removed *in vacuo* and the resulting precipitate was separated by filtration, washed with H_2O and dried under high vacuum. Compound **49** (3.6 g, 15 mmol, 88%) was obtained as colorless microcrystalline solid.

m.p.: 118 °C.

^{1}H NMR (400 MHz, $(CD_3)_2SO$): δ / ppm = 12.93 (s, 1H, -CO_2H), 7.60 (dd, J = 8.0, 1.3 Hz, 1H, H-C(3)), 7.37 (ddd, J = 8.5, 7.3, 1.4 Hz, 1H, H-C(1)), 7.30 (dd, J = 8.0, 1.6 Hz, 1H, H-C(6)), 7.10 (ddd, J = 7.9, 7.2, 1.6 Hz, 1H, H-C(2)), 3.90 (s, 2H, H_2-C(7)).

^{13}C NMR (101 MHz, $(CD_3)_2SO$): δ / ppm = 170.1 (C(8)), 137.2 (C(5)), 132.6 (C(3)), 128.3 (C(1)), 126.7 (C(2/6)), 126.6 (C(2/6)), 120.8 (C(4)), 34.2 (C(7)).

IR: $\tilde{\nu}$ / cm^{-1} = 3000–2500 (w, br), 1701 (m), 1427 (m), 1384 (w), 1316 (m), 1199 (s), 1022 (w), 892 (m), 749 (s), 671 (m).

HRMS (EI): *m*/*z* calc. for $[C_8H_7BrO_2S]^{\bullet+}$: 245.9345; found: 245.9344 ($M^{\bullet+}$).

Compound 50[73] *reported in ref.*[8]

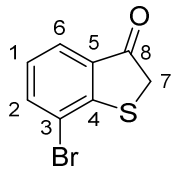

Compound **49** (3.6 g, 15 mmol, 1.0 equiv.) was refluxed in $SOCl_2$ (9.0 mL, 0.12 mol, 8.0 equiv.) for 2.5 h. Excess $SOCl_2$ was removed *in vacuo* and the residue was dissolved in 1,2-DCE (60 mL). At 0 °C, $AlCl_3$ (3.7 g, 28 mmol, 1.9 equiv.) was added and the mixture was stirred under nitrogen atmosphere at 0 °C for 2 h. The reaction mixture was poured into ice water (300 mL) and the resulting mixture was extracted with CH_2Cl_2 (2 × 200 mL). The

combined organic phases were dried over Na_2SO_4, filtered, and concentrated *in vacuo* to give compound **50** (3.2 g, 14 mmol, 93%) as a pink solid, which was used without further purification.

^{1}H NMR (400 MHz, $CDCl_3$): δ / ppm = 7.74 (dd, J = 6.1, 1.2 Hz, 1H, H-C(6)), 7.72 (dd, J = 6.1, 1.0 Hz, 1H, H-C(2)), 7.13 (t, J = 7.7 Hz, 1H, H-C(1)), 3.84 (s, 2H, H_2-C(7)).
^{13}C NMR (101 MHz, $CDCl_3$): δ / ppm = 199.6 (C(8)), 155.5 (C(4)), 138.2 (C(2)), 133.1 (C(5)), 126.3 (C(1)), 125.4 (C(6)), 118.9 (C(3)), 40.3 (C(7)).
HRMS (EI): *m*/*z* calc. for $[C_8H_5BrOS]^{\bullet+}$: 227.9239; found: 227.9238 ($M^{\bullet+}$).

Compound (*E*/*Z*)-51

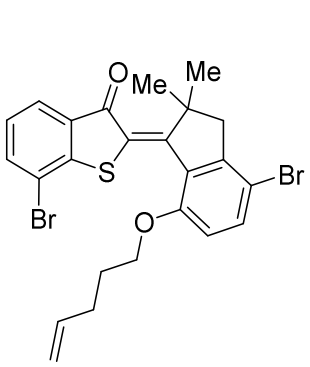

(*Z*)-isomer

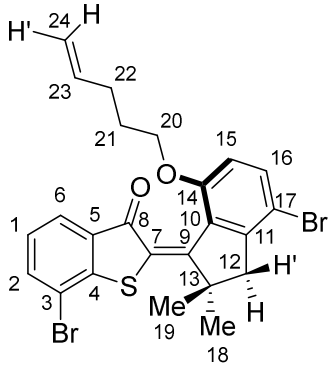

(*E*)-isomer (*rac*)

In a dried Schlenk flask under nitrogen atmosphere, a solution of benzothiophenone **50** (195 mg, 0.851 mmol, 1.2 equiv.) in dry CH_2Cl_2 (1.60 mL) was prepared (flask A). In a second dried Schlenk flask under nitrogen atmosphere, a solution of indanone **48** (223 mg, 0.689 mmol, 1.0 eq) in dry CH_2Cl_2 (0.8 mL) was prepared (flask B). At −78 °C, BCl_3 (1.0 M in CH_2Cl_2, 0.85 mL, 0.85 mmol, 1.2 eq) was added to flask A under stirring. The reaction mixture was then immediately taken up by syringe (an additional 0.8 mL of CH_2Cl_2 was added to rinse the flask) and transferred to flask B, which was kept at 0 °C. The reaction mixture was stirred at 0 °C under nitrogen atmosphere for 0.5 h. The reaction was stopped by the addition of H_2O (5 mL). The mixture was diluted with H_2O (50 mL) and extracted with EtOAc (3 × 50 mL). The combined organic layers were dried over Na_2SO_4, filtered, and concentrated *in vacuo*. The crude product was purified by flash column chromatography (SiO_2, EtOAc:*i*-Hex, 4:96) and a red oil was obtained. EtOAc (2.0 mL) was added, the mixture was sonicated, followed by removal of the solvent *in vacuo*, to give compound **51** (mixture of (*E*)- and (*Z*)-isomers, 158 mg, 0.296 mmol, 43%) as an orange solid.

Crystals of the (*E*)-isomer suitable for X-ray crystallography could be obtained.

(*E*)-isomer

R_f (EtOAc:*i*-Hex, 10:90): 0.42.

^{1}H NMR (599 MHz, CD_2Cl_2): δ / ppm = 7.78 (dd, J = 7.6, 0.9 Hz, 1H, H-C(6)), 7.71 (dd, J = 7.7, 1.0 Hz, 1H, H-C(2)), 7.46 (d, J = 8.8 Hz, 1H, H-C(16)), 7.20 (t, J = 7.7 Hz, 1H, H-C(1)), 6.71 (d, J = 8.8 Hz, 1H, H-C(15)), 5.63 (ddt, J = 16.9, 10.2, 6.7 Hz, 1H, H-C(23)), 4.85–4.81 (m, 1H, H'-C(24)), 4.79 (dd, J = 17.1, 1.6 Hz, 1H, H-C(24)), 4.12 (dt, J = 8.7, 6.2 Hz, 1H, H-C(20)), 3.93–3.87 (m, 1H, H-C(20)), 3.13 (d, J = 15.9 Hz, 1H, H-C(12)), 2.86 (d, J = 15.9 Hz, 1H, H'-C(12)), 1.96 (q, J = 7.5 Hz, 2H, H-C(22)), 1.74 (s, 3H, H-C(18)), 1.69 (p, J = 7.3 Hz, 2H, H-C(21)), 1.27 (s, 3H, H-C(19)).

^{13}C NMR (151 MHz, CD_2Cl_2): δ / ppm = 186.8 (C(8)), 157.8 (C(14)), 157.8 (C(9)), 148.9 (C(11)), 145.7 (C(4)), 138.2 (C(23)), 136.9 (C(2)), 134.8 (C(16)), 134.6 (C(3 or 5)), 130.1 (C(10)), 127.3 (C(7)), 126.8 (C(1)), 125.2 (C(6)), 117.9 (C(3 or 5)), 115.2 (C(24)), 112.3 (C(15)), 110.1 (C(17)), 68.3 (C(20)), 51.0 (C(12)), 50.6 (C(13)), 30.6 (C(22)), 28.9 (C(21)), 26.8 (C(18)), 26.4 (C(19)).

IR: $\tilde{\nu}$ / cm^{-1} = 2952 (w, br), 1666 (s), 1581 (m), 1538 (m), 1452 (m), 1406 (m), 1268 (s), 1105 (m), 1056 (s), 1044 (s), 910 (m), 797 (s), 739 (s), 662 (m).

HRMS (EI): *m/z* calc. for $[C_{24}H_{22}Br_2O_2S]^{\bullet+}$: 531.9702, found: 531.9702 ($M^{\bullet+}$).

Compound (*E*/*Z*)-52

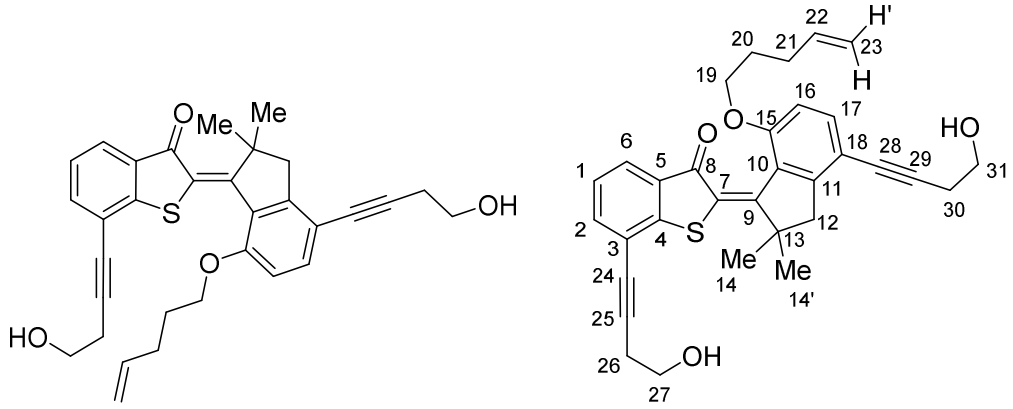

Copper(I) iodide (6 mg, 0.03 mmol, 0.07 equiv.), XPhos Pd G2 (37 mg, 47 µmol, 0.1 equiv.) and compound **51** (0.24 g, 0.45 mmol, 1.0 equiv.) were added to a round bottom flask. The flask was evacuated and refilled with nitrogen for a total of three times. 1,4-Dioxane (2.4 mL) and DIPA (2.4 mL) were added and the flask was carefully evacuated and refilled with nitrogen for a total of three times under stirring. 3-Butyn-1-ol (85 µL, 1.1 mmol, 2.4 equiv.) was added and the mixture was stirred at 65 °C under nitrogen atmosphere for 2.5 h. The reaction was stopped by the addition of a saturated aqueous solution of NH_4Cl (10 mL). The mixture was diluted with H_2O (50 mL) and extracted with CH_2Cl_2 (3 × 50 mL). The combined organic layers were dried over Na_2SO_4, filtered, and concentrated *in vacuo*. The residue was purified by flash column chromatography (SiO_2, MeOH:CH_2Cl_2, 5:95) to give compound **52** (mixture of (*E*)- and (*Z*)-isomers, 0.17 g, 0.33 mmol, 73%) as a red oil.

Note: NMR analysis was performed on an *E*:*Z* mixture (approx. 4:1).

(*E*)-isomer

^{1}H NMR (599 MHz, CD_2Cl_2): δ / ppm = 7.74 (dd, J = 7.7, 1.3 Hz, 1H, H-C(6)), 7.58 (dd, J = 7.4, 1.3 Hz, 1H, H-C(2)), 7.38 (d, J = 8.6 Hz, 1H, H-C(17)), 7.22 (t, J = 7.6 Hz, 1H, H-C(1)), 6.73 (d, J = 8.6 Hz, 1H, H-C(16)), 5.62 (ddt, J = 17.0, 10.3, 6.7 Hz, 1H, H-C(22)), 4.82 (ddt, J = 10.3, 2.5, 1.2 Hz, 1H, H‘-C(23)), 4.78 (dq, J = 17.0, 1.7 Hz, 1H, H-C(23)), 4.16–4.11 (m, 1H, H_2-C(19)), 3.94–3.88 (m, 1H, H_2-C(19)), 3.86 (q, J = 6.3 Hz, 2H, H_2-C(27)), 3.78 (q, J = 6.3 Hz, 3H, H_2-C(31)), 3.15 (d, J = 15.9 Hz, 1H, H_2-C(12)), 2.93 (d, J = 15.9 Hz, 1H, H_2-C(12)), 2.79 (t, J = 6.3 Hz, 2H, H_2-C(26)), 2.69 (t, J = 6.3 Hz, 2H, H_2-C(30)), 2.00–1.93 (m, 3H, H_2-C(21)), 1.73 (s, 3H, H_3-C(14 or 14‘)), 1.69 (p, J = 7.4, 7.0 Hz, 2H, H_2-C(20)), 1.25 (s, 3H, H_3-C(14 or 14‘)).

^{13}C NMR (151 MHz, CD_2Cl_2): δ / ppm = 186.9 (C(8)), 158.0 (C(15)), 157.3 (C(9)), 151.9 (C(11)), 147.0 (C(4)), 138.1 (C(22)), 136.5 (C(2)), 135.2 (C(17)), 132.6 (C(5)), 128.5 (C(10)), 126.3 (C(7)), 125.6 (C(6)), 125.2 (C(1)), 119.1 (C(3)), 115.0 (C(23)), 112.2 (C(18)), 110.4 (C(16)), 94.4 (C(25)), 88.8 (C(29)), 80.0 (C(28)), 78.4 (C(24)), 68.0 (C(19)), 61.6 (C(31)), 61.4 (C(27)), 50.7 (C(13)), 49.4 (C(12)), 30.4 (C(21)), 28.7 (C(20)), 26.8 (C(14 or 14')), 26.3 (C(14 or 14')), 24.4 (C(26)), 24.3 (C(30)).

HRMS (ESI): *m/z* calc. for $[C_{32}H_{32}O_4S+H]^+$: 513.2094; found: 513.2094 ($M+H^+$).

Compound (*E*/*Z*)-53

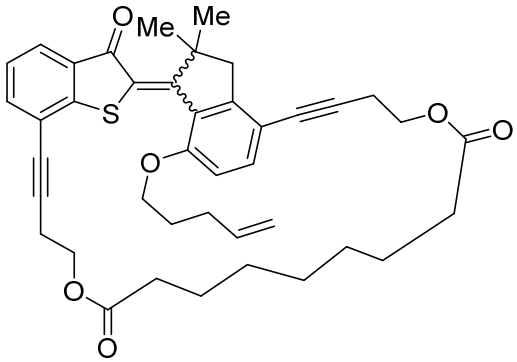

1) Azelaoyl chloride preparation

Azelaic acid (94 mg, 0.50 mmol, 1.0 equiv.) was refluxed in thionyl chloride (1.0 mL, 14 mmol, 18 equiv.) for 3.75 h. Excess thionyl chloride was removed *in vacuo* and the residue was dissolved in dry CH_2Cl_2 (0.5 mL), giving a 1.0 M solution of azelaoyl chloride which was used in the following step.

2) Macrocyclization

In a dried Schlenk flask under nitrogen atmosphere, azelaoyl chloride (1.0 M in CH_2Cl_2, 0.11 mL, 0.11 mmol, 1.0 equiv.) was added to a solution of 4-dimethylaminopyridine (27 mg, 0.22 mmol, 2.0 equiv.) in dry CH_2Cl_2 (110 mL). Compound **52** (55 mg in 1.0 mL of dry CH_2Cl_2, 0.11 mmol, 1.0 equiv.) was added and the reaction mixture was stirred at 23 °C for 6 d. The solvent was removed *in vacuo* and the residue was purified by flash column chromatography (SiO_2, MeOH:CH_2Cl_2, 1:99). Compound **53** (mixture of (*E*) and (*Z*)-isomers, 38 mg, 0.057 mmol, 52%) was obtained as an orange oil. The compound was used in the next synthetic step without full characterization.

HRMS (EI): *m/z* calc. for $[C_{41}H_{44}O_6S]^{\bullet+}$: 664.2853; found: 664.2862 ($M^{\bullet+}$).

Compound (*E*/*Z*)-54

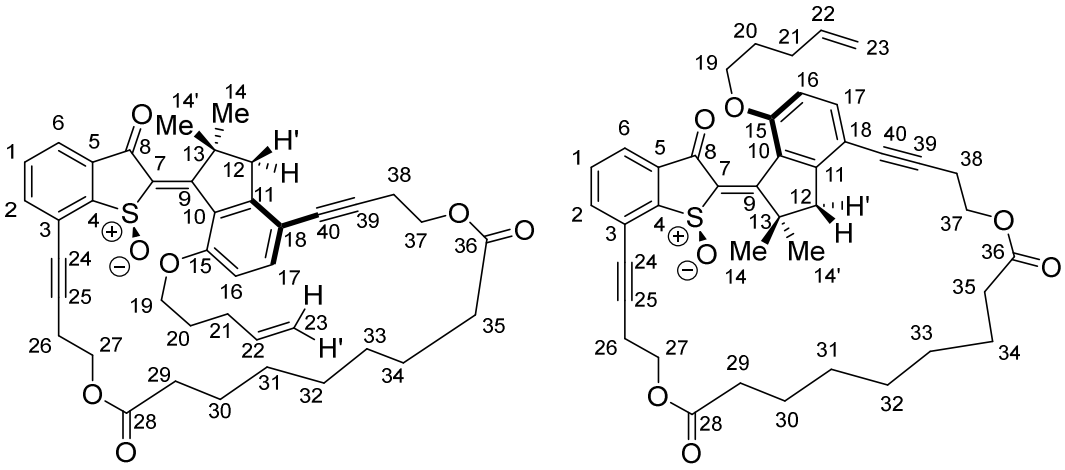

(*Z*)-isomer (*rac*) (*E*)-isomer (*rac*)

Note: Only the (S)-configured enantiomers are depicted for clarity.

Compound **53** (18 mg, 0.027 mmol, 1.0 equiv.) was dissolved in acetic acid (0.9 mL). $NaBO_3 \bullet 4\ H_2O$ (16 mg, 0.10 mmol, 3.7 equiv.) was added and the mixture was stirred at 23 °C for 2.5 h. The reaction was stopped by the addition of a saturated aqueous solution of $NaHCO_3$ (12 mL). The mixture was diluted with H_2O (25 mL) and extracted with EtOAc (3 × 25 mL). The combined organic layers were dried over Na_2SO_4, filtered, and concentrated *in vacuo*. The crude product was purified by flash column chromatography (SiO_2, EtOAc:*i*-Hex, 40:60) to give (*Z*)-**54** (8 mg, 0.012 mmol) and (*E*)-**54** (5 mg, 0.007 mmol) as yellow oils (combined yield: 13 mg, 0.019 mmol, 70%).

(*Z*)-isomer:

R_f (SiO_2, EtOAc:*i*-Hex, 40:60): 0.51.

^{1}H NMR (599 MHz, CD_2Cl_2): δ / ppm = 7.86 (dd, *J* = 7.7, 1.2 Hz, 1H, H-C(6)), 7.72 (dd, *J* = 7.6, 1.1 Hz, 1H, H-C(2)), 7.60 (t, *J* = 7.6 Hz, 1H, H-C(1)), 7.48 (d, *J* = 8.6 Hz, 1H, H-C(17)), 6.83 (d, *J* = 8.6 Hz, 1H, H-C(16)), 5.83 (ddt, *J* = 17.0, 10.2, 6.7 Hz, 1H, H-C(22)), 5.00 (dq, *J* = 17.1, 1.6 Hz, 1H, H-C(23)), 4.94 (ddt, *J* = 10.1, 2.3, 1.2 Hz, 1H, H'-C(23)), 4.37 (dt, *J* = 9.3, 6.5 Hz, 1H, H_2-C(19)), 4.29–4.22 (m, 3H, H_2-C(27) and H_2-C(37)), 4.18 (dt, *J* = 9.3, 7.3 Hz, 1H, H_2-C(19)), 4.13–4.08 (m, 1H, H_2-C(37)), 3.15 (d, *J* = 16.6 Hz, 1H, H-C(12) or H'-C(12)), 2.97 (d, *J* = 16.5 Hz, 1H, H-C(12) or H'-C(12)), 2.85–2.80 (m, 2H, H_2-C(26)), 2.79–2.76 (m, 2H, H_2-C(38)), 2.32–2.26 (m, 2H, H_2-C(35)), 2.26–2.20 (m, 2H, H_2-C(21)), 2.20–2.15 (m, 2H, H_2-C(29)), 2.07 (pd, *J* = 7.3, 1.7 Hz, 2H, H_2-C(20)), 1.56 (s, 3H, H_3-C(14 or 14')), 1.55–1.53 (m, 2H, H_2-C(34)), 1.50 (s, 3H, H_3-C(14 or 14')), 1.35–

1.28 (m, 2H, H_2-C(30)), 1.24–1.19 (m, 2H, H_2-C(33)), 1.09–0.94 (m, 2H, H_2-C(32)), 0.83–0.69 (m, 2H, H_2-C(31)).

^{13}C NMR (151 MHz, CD_2Cl_2): δ / ppm = 184.9 (C(8)), 174.8 (C(28)), 173.8 (C(36)), 171.2 (C(9)), 157.2 (C(15)), 153.8 (C(11)), 151.7 (C(4)), 143.7 (C(7)), 138.3 (C(22)), 137.99 (C(2 or 17)), 137.98 (C(2 or 17)), 137.0 (C(5)), 132.1 (C(1)), 126.0 (C(10)), 124.1 (C(6)), 123.9 (C(3)), 115.3 (C(23)), 113.0 (C(18)), 110.4 (C(16)), 96.8 (C(25)), 89.3 (C(39)), 79.2 (C(40)), 76.6 (C(24)), 69.1 (C(19)), 62.16 (C(27 or 37)), 62.06 (C(27 or 37)), 52.0 (C(13)), 50.7 (C(12)), 35.5 (C(35)), 34.0 (C(29)), 30.7 (C(21)), 30.2 (C(32)), 30.0 (C(33)), 29.7 (C(31)), 28.5 (C(20)), 28.2 (C(14 or 14‘)), 26.2 (C(34)), 25.6 (C(14 or 14‘)), 25.4 (C(30)), 20.66 (C(38)), 20.55 (C(26)).

HRMS (EI): *m/z* calc. for $[C_{41}H_{44}O_7S]^{\bullet+}$: 680.2802; found: 680.2816 ($M^{\bullet+}$).

(*E*)-isomer:

R_f (SiO_2, EtOAc:*i*-Hex, 40:60): 0.31.

^{1}H NMR (599 MHz, CD_2Cl_2): *δ* / ppm = 7.85 (dd, *J* = 7.6, 1.1 Hz, 1H, H-C(6)), 7.75 (dd, *J* = 7.6, 1.2 Hz, 1H, H-C(2)), 7.65 (t, *J* = 7.6 Hz, 1H, H-C(1)), 7.42 (d, *J* = 8.6 Hz, 1H, H-C(17)), 6.77 (d, *J* = 8.4 Hz, 1H, H-C(16)), 5.72–5.64 (m, 1H, H-C(22)), 4.89–4.87 (m, 1H, H_2-C(23)), 4.86 (dq, *J* = 2.9, 1.4 Hz, 1H, H_2-C(23)), 4.35–4.31 (m, 2H, H_2-C(27)), 4.31–4.23 (m, 2H, H_2-C(37)), 4.20–4.08 (m, 1H, H_2-C(19)), 3.98 (q, *J* = 6.7 Hz, 1H, H_2-C(19)), 3.15 (d, *J* = 12.5 Hz, 1H, H-C(12) or H’-C(12)), 2.97 (d, *J* = 17.6 Hz, 1H, H-C(12) or H’-C(12)), 2.95–2.90 (m, 1H, H/H’H_2-C(26)), 2.85 (ddd, *J* = 17.8, 6.5, 4.0 Hz, 1H, H/H’H_2-C(26)), 2.77 (t, *J* = 5.5 Hz, 2H, H_2-C(38)), 2.50–2.46 (m, 2H, H_2-C(29)), 2.42–2.38 (m, 2H, H_2-C(35)), 2.03 (br, 5H, H_2-C(21) and H_3-C(14 or 14’)), 1.80–1.73 (m, 2H, H_2-C(20)), 1.68 (m, 4H, H_2-C(30) and H_2-C(34)), 1.44–1.37 (m, 8H, H_3-C(14 or 14’) and H_2-C(31) and H_2-C(33).

^{13}C NMR (151 MHz, CD_2Cl_2): *δ* / ppm = 174.1 (C(28)), 173.7 (C(36)), 154.1 (C(11)), 138.0 (C(22)), 137.3 (C(2)), 135.6 (C(17)), 132.9 (C(1)), 124.7 (C(6)), 115.2 (C(23)), 112.7 (C(18)), 110.7 (C(16)), 90.3 (C(39)), 79.0 (C(40)), 76.5 (C(24)), 68.3 (C(19)), 63.0 (C(37)), 62.5 (C(27)), 52.5 (C(13)), 49.9 (C(12)), 34.9 (C(35)), 34.3 (C(29)), 30.4 (C(21)), 30.2 (C(31 or 33)), 29.9 (C(31 or 33)), 29.4 (C(32)), 28.8 (br, C(14 or 14’)), 28.6 (C(20)), 27.5 (br, C(14 or 14’)), 25.2 (C(30 or 34)), 25.1 (C(30 or 34)), 20.7 (C(26)), 20.5 (C(38)).

Note: Some carbon signals could not be observed due to low signal intensity.

HRMS (EI): *m/z* calc. for $[C_{41}H_{44}O_7S]^{\bullet+}$: 680.2802; found: 680.2791.

Compound 55[133] *reported in ref.*[8]

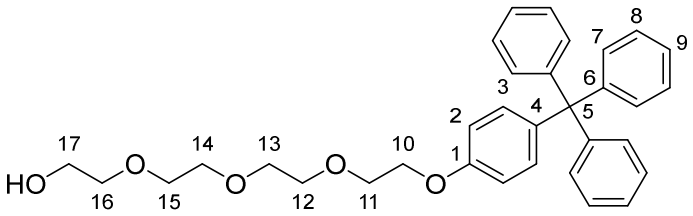

To a solution of tetraethylene glycol monotosylate (**106**) (4.1 g, 12 mmol, 2.0 equiv.) in MeCN (100 mL), 4-tritylphenol (2.0 g, 5.9 mmol, 1.0 equiv.) and K_2CO_3 (1.0 g, 7.1 mmol, 1.2 equiv.) were added and the mixture was refluxed for 6 h, then stirring was continued at 60 °C for 18 h. The solvent was removed *in vacuo* and the residue was distributed between H_2O (100 mL) and $CHCl_3$ (100 mL). The organic phase was separated, washed with brine (100 mL), dried over Na_2SO_4, filtered, and concentrated *in vacuo*. The crude product was purified by flash column chromatography (SiO_2, CH_2Cl_2:EtOAc, 50:50) to give compound **55** (2.1 g, 4.1 mmol, 69%) as a white solid.

R_f (CH_2Cl_2:EtOAC, 50:50): 0.16.

m.p: 89.7-90.3 °C.

^{1}H NMR (400 MHz, CD_2Cl_2): δ / ppm = 7.29–7.17 (m, 15H, H-C(7 and 8 and 9)), 7.16–7.11 (m, 2H, H-C(3)), 6.84–6.79 (m, 2H, H-C(2)), 4.12–4.08 (m, 2H, H-C(10)), 3.83–3.79 (m, 2H, H-C(11)), 3.70–3.61* (m, 10H), 3.58–3.55* (m, 2H).

*TEG-chain H_2-C(12 and 13 and 14 and 15 and 16 and 17).

^{13}C NMR (101 MHz, CD_2Cl_2): δ / ppm = 157.2 (C(1)), 147.6 (C(6)), 139.6 (C(4)), 132.5 (C(3)), 131.4 (C(7/8)), 127.9 (C(7/8)), 126.2 (C(9)), 113.7 (C(2)), 72.8*, 71.1*, 71.0*, 70.9*, 70.7*, 70.1 (C(11)), 67.8 (C(10)), 64.7 (C(5)), 62.0*.

*TEG-chain C(12 or 13 or 14 or 15 or 16 or 17).

IR: $\tilde{\nu}$ / cm^{-1} = 3469 (w, br), 2874 (m), 1606 (w), 1508 (m), 1481 (m), 1442 (m), 1249 (s), 1182 (m), 1096 (s, br), 1035 (s), 938 (m), 884 (w), 818 (m), 750 (s), 700 (vs).

HRMS (ESI): *m/z* calc. for $[C_{33}H_{36}O_5+Na]^+$: 535.2455; found: 535.2456 ($M+Na^+$).

Compound 56

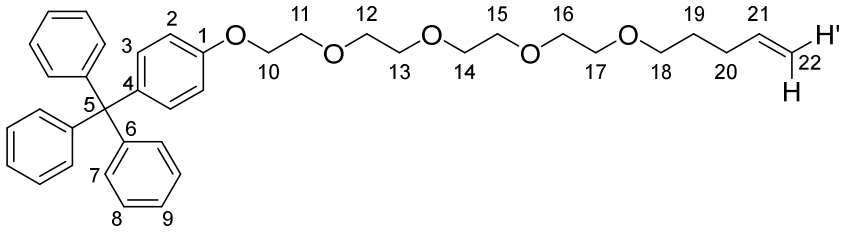

In a dried Schlenk flask under nitrogen atmosphere, a slurry of NaH (60% in mineral oil, 31 mg, 0.78 mmol, 1.6 equiv.) in dry THF (2.5 mL) was prepared. Compound **55** (0.25 g, 0.49 mmol, 1.0 equiv.) was added at 0 °C, the mixture was stirred at 0 °C for five minutes, then 5-bromo-1-pentene (65 µL, 0.55 mmol, 1.1 equiv.) was added and stirring was continued at the same temperature for 1 h. The reaction mixture was then allowed to warm to 23 °C and stirring was continued for 24 h. The reaction was stopped by the addition of H_2O (5 mL). The mixture was diluted with H_2O (20 mL) and extracted with CH_2Cl_2 (3 × 25 mL). The combined organic layers were dried over Na_2SO_4, filtered, and concentrated *in vacuo*. The crude product was purified by flash column chromatography (SiO_2, EtOAc:*i*-Hex, 50:50) to give compound **56** (0.14 g, 0.24 mmol, 49%.) as a colorless oil that solidified over time.

^{1}H NMR (601 MHz, CD_2Cl_2): δ / ppm = 7.28–7.22 (m, 12H, H-C(7 and 8)), 7.21–7.17 (m, 3H, H-C(9)), 7.15–7.11 (m, 2H, H-C(3)), 6.83–6.79 (m, 2H, H-C(2)), 5.84 (ddt, J = 17.0, 10.2, 6.7 Hz, 1H, H-C(21)), 5.05–5.00 (m, 1H, H'-C(22)), 4.95 (ddd, J = 10.2, 2.2, 1.1 Hz, 1H, H-C(22)), 4.10 (t, J = 4.7 Hz, 2H, H_2-C(10)), 3.81 (t, J = 5.0, 4.5 Hz, 2H, H_2-C(11)), 3.68 (dd, J = 6.1, 3.3 Hz, 2H, H_2-C(12)), 3.65–3.57 (m, 8H, H_2-C(13 and 14 and 15 and 16)), 3.56–3.53 (m, 2H, H_2-C(17)), 3.44 (t, J = 6.6 Hz, 2H, H_2-C(18)), 2.11 (q, J = 8.1 Hz, 2H, H_2-C(20)), 1.66 (p, J = 7.1 Hz, 2H, H_2-C(19)).

^{13}C NMR (151 MHz, CD_2Cl_2): δ / ppm = 157.2 (C(1)), 147.5 (C(6)), 139.5 (C(4)), 138.9 (C(21)), 132.5 (C(3)), 131.4 (C(7 or 8)), 127.9 (C(7 or 8)), 126.2 (C(9)), 114.7 (C(22)), 113.7 (C(2)), 71.1 (C(12)), 71.0*, 70.95*, 70.94*, 70.92*, 70.5 (C(17)), 70.0 (C(11)), 67.8 (C(10)), 64.7 (C(5)), 30.7 (C(20)), 29.3 (C(19)).

*(C(13 or 14 or 15 or 16))

HRMS (EI): *m/z* calc. for $[C_{38}H_{44}O_5]^{\bullet+}$: 580.3183; found: 580.3186 ($M^{\bullet+}$).

Compound (*E*/*Z*)-58

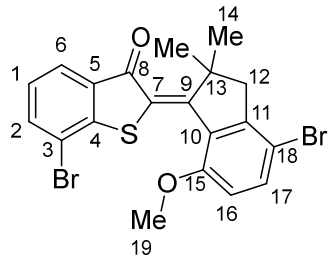

(*Z*)-isomer

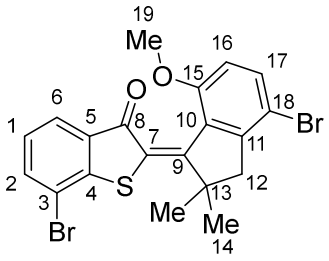

(*E*)-isomer

In a dried Schlenk flask (A) under argon atmosphere, compound **50** (557 mg, 2.43 mmol, 1.1 equiv.) was dissolved in dry CH_2Cl_2 (6 mL). In a separate dried Schlenk flask (B) under argon atmosphere, compound **33** (596 mg, 2.21 mmol, 1.0 equiv.) was dissolved in dry CH_2Cl_2 (4 mL). At −78 °C, BCl_3 (1.0 M in CH_2Cl_2, 2.4 mL, 2.4 mmol, 1.1 equiv.) was added to (A). The resulting mixture was immediately transferred *via* double-ended cannula and added to (B) at −78 °C. The reaction mixture was stirred at −78 °C for 15 min, then at 0 °C for 2 h. The reaction was stopped by the addition of H_2O (20 mL). The mixture was diluted with H_2O (50 mL) and extracted with EtOAc (3 × 50 mL). The combined organic layers were dried over Na_2SO_4, filtered, and concentrated *in vacuo*. The crude product was purified by automated flash column chromatography (SiO_2, EtOAc:*i*-Hex, 1:99→6:94) to give compound **58** (mixture of (*E*)- and (*Z*)-isomers, 680 mg, 1.42 mmol, 64%) as an orange solid.

R_f (EtOAc:*i*-Hex, 10:90): 0.24 and 0.53.

(*Z*)-isomer:

^{1}H NMR (601 MHz, $CDCl_3$): δ / ppm = 7.74 (dd, J = 7.6, 1.1 Hz, 1H, H-C(6)), 7.65 (dd, J = 7.7, 1.1 Hz, 1H, H-C(2)), 7.53 (d, J = 8.8 Hz, 1H, H-C(17)), 7.12 (t, J = 7.7 Hz, 1H, H-C(1)), 6.75 (d, J = 8.8 Hz, 1H, H-C(16)), 4.00 (s, 3H, H_3-C(19)), 2.97 (s, 2H, H_2-C(11)), 1.56 (s, 6H, H_3-C(14)).

^{13}C NMR (151 MHz, $CDCl_3$): δ / ppm = 188.7 (C(8)), 163.1 (C(9)), 155.7 (C(15)), 149.6 (C(11)), 147.0 (C(4)), 136.9 (C(2)), 136.0 (C(17)), 134.15 (C(5)), 129.7 (C(7)), 129.1 (C(10)), 125.9 (C(1)), 124.6 (C(6)), 116.9 (C(3)), 111.6 (C(16)), 110.8 (C(18)), 55.0 (C(19)), 52.5 (C(12)), 51.0 (C(13)), 26.5 (C(14)).

IR: $\tilde{\nu}$ / cm^{-1} = 2935 (w, br), 1662 (s), 1583 (m), 1514 (s), 1467 (s), 1408 (s), 1381 (m), 1273 (s), 1055 (s), 979 (m), 755 (s), 637 (w).

(*E*)-isomer:

^{1}H NMR (601 MHz, $CDCl_3$): δ / ppm = 7.83 (dd, J = 7.6, 1.1 Hz, 1H, H-C(6)), 7.69 (dd, J = 7.7, 1.1 Hz, 1H, H-C(2)), 7.46 (d, J = 8.8 Hz, 1H, H-C(17)), 7.17 (t, J = 7.7 Hz, 1H, H-C(1)), 6.70 (d, J = 8.8 Hz, 1H, H-C(16)), 3.83 (s, 3H, H_3-C(19)), 3.12 (d, J = 16.0 Hz, 1H, H_2-C(12)), 2.85 (d, J = 15.9 Hz, 1H, H_2-C(12)), 1.74 (s, 3H, H_3-C(14)), 1.28 (s, 3H, H_3-C(14)).

^{13}C NMR (151 MHz, $CDCl_3$): δ / ppm = 186.6 (C(8)), 158.0 (C(15)), 157.4 (C(9)), 148.4 (C(11)), 145.4 (C(4)), 136.5 (C(2)), 134.6 (C(17)), 134.24 (C(5)), 129.6 (C(10)), 126.9 (C(7)), 126.3 (C(1)), 124.8 (C(6)), 117.6 (C(3)), 111.3 (C(16)), 110.1 (C(18)), 55.5 (C(19)), 50.6 (C(12)), 50.1 (C(13)), 26.6 (C(14)), 26.3 (C(14)).

IR: $\tilde{\nu}$ / cm^{-1} = 2923 (w, br), 1659 (s), 1576 (m), 1529 (s), 1404 (m), 1284 (s), 1039 (s), 737 (vs).

HRMS (APPI): *m/z* calc. for $[C_{20}H_{16}Br_2O_2S+H]^+$: 478.9311; found: 478.9320 ($M+H^+$).

Compound (*E*/*Z*)-59 *reported in ref.[8]*

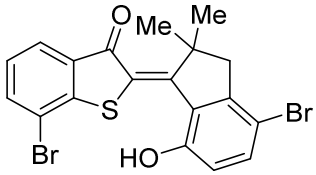

(*Z*)-isomer

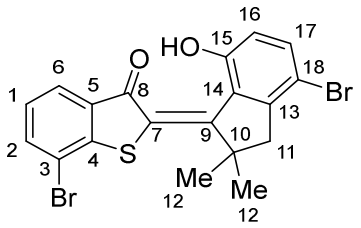

(*E*)-isomer

In a dried Schlenk flask a solution of compound **50** (276 mg, 1.20 mmol, 1.1 equiv.) in dry CH_2Cl_2 (3.0 mL) was cooled to −78 °C under nitrogen atmosphere. Subsequently, BCl_3 (1.0 M in CH_2Cl_2, 1.2 mL, 1.2 mmol, 1.1 equiv.) was added. The mixture was immediately taken up by syringe (an additional 2.0 mL of dry CH_2Cl_2 were added to rinse the flask) and added to a second Schlenk flask containing a solution of compound **33** (301 mg, 1.12 mmol, 1.0 equiv.) in dry CH_2Cl_2 (1.5 mL) at 0 °C. The reaction mixture was stirred at 0 °C for 45 min. BBr_3 (1.0 M in CH_2Cl_2, 1.1 mL, 1.1 mmol, 1.0 equiv.) was added and stirring was continued at 0 °C for 45 min. The reaction was stopped by the addition of H_2O (5 mL). The mixture was diluted with H_2O (50 mL) and extracted with EtOAc (3 × 50 mL). The combined organic layers were dried over Na_2SO_4, filtered, and concentrated *in vacuo*. The crude product was purified by flash column chromatography (SiO_2, EtOAc:*i*-Hex, 10:90) to

give compound **59** (mixture of (*E*)- and (*Z*)-isomers, 411 mg, 0.882 mmol, 79%) as a red foam.

Single crystals of the (*E*)-isomer for structure determination by X-ray diffraction could be obtained by recrystallization from *n*-heptane.

R_f (EtOAc:*i*-Hex, 10:90): 0.63 and 0.69 (heat is necessary to colorize the second spot).
m.p: 148.0-150.0 °C.

(*E*)-isomer
^{1}H NMR (400 MHz, CD_2Cl_2): δ / ppm = 8.01 (dd, J = 7.8, 1.1 Hz, 1H, H-C(6)), 7.86 (s, 1H, -OH), 7.83 (dd, J = 7.8, 1.1 Hz, 1H, H-C(2)), 7.62 (d, J = 8.8 Hz, 1H, H-C(17)), 7.29 (t, J = 7.7 Hz, 1H, H-C(1)), 6.96 (dt, J = 8.8, 0.8 Hz, 1H, H-C(16)), 3.11 (s, 2H, H_2-C(11)), 1.64 (s, 6H, H_3-C(12)).
^{13}C NMR (101 MHz, CD_2Cl_2): δ / ppm = 191.1 (C(8)), 167.1 (C(9)), 160.2 (C(15), 150.5 (C(13)), 146.5 (C(4)), 138.1 (C(2)), 137.6 (C(17)), 134.1 (C(5)), 131.0 (C(14)), 127.0 (C(7)), 126.9 (C(1)), 126.4 (C(6)), 122.2 (C(16)), 117.1 (C(3)), 110.9 (C(18)), 52.3 (C(10)), 51.5 (C(11)), 27.7 (C(12)).
IR: $\tilde{\nu}$ / cm^{-1} = 3059 (w), 2956 (w), 2924 (m), 1577 (m), 1560 (m), 1498 (s), 1493 (s), 1464 (s), 1454 (s), 1431 (m), 1423 (m), 1408 (s), 1387 (m), 1369 (m), 1361 (m), 1263 (s), 1215 (m), 1176 (m), 1159 (s), 1132 (m), 1103 (s), 1057 (s), 1039 (s), 1009 (m), 883 (m), 872 (m), 816 (m), 800 (vs), 775 (s), 758 (s), 741 (vs), 735 (vs), 702 (s), 683 (m), 660 (s), 648 (m), 561 (s), 540 (m), 521 (m), 496 (m), 474 (m), 461 (m), 449 (s).
HRMS (EI): *m/z* calc. for $[C_{19}H_{14}Br_2O_2S]^{\bullet+}$: 463.9076; found: 463.9079 ($M^{\bullet+}$).

Compound 60[133] *reported in ref.[8]*

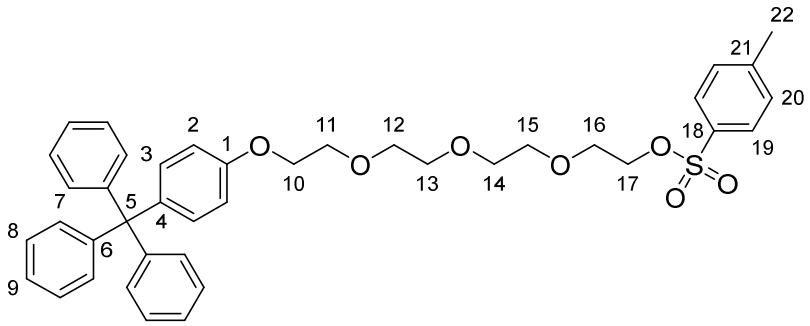

Compound **55** (978 mg, 1.91 mmol, 1.0 equiv.), NEt_3 (1.3 mL, 9.5 mmol, 5.0 equiv.) and 4-dimethylaminopyridine (12 mg, 0.098 mmol, 0.05 equiv.) were dissolved in CH_2Cl_2 (20 mL) and cooled to 0 °C. A solution of *p*-TsCl (915 mg in 7.0 mL CH_2Cl_2, 4.80 mmol, 2.5 equiv.) was slowly added at 0 °C. The reaction mixture was stirred for 14 h while slowly warming to 23 °C. The reaction was stopped by the addition of aq. HCl (2 M, 70 mL). The aqueous layer was separated and extracted with CH_2Cl_2 (100 mL). The combined organic phases were washed with H_2O (100 mL) and brine (100 mL), dried over Na_2SO_4, filtered, and concentrated *in vacuo*. The residue was purified by flash column chromatography (SiO_2, EtOAc:CH_2Cl_2, 10:90) to yield tosylate **60** (1.1 g, 1.6 mmol, 84%) as a colorless viscous oil.

R_f (EtOAc:CH_2Cl_2, 10:90): 0.76.

^{1}H NMR (400 MHz, CD_2Cl_2): δ / ppm = 7.78 (d, J = 8.3 Hz, 2H, H-C(19)), 7.36 (d, J = 8.1 Hz, 2H, H-C(20)), 7.30–7.16 (m, 15H, H-C(7 and 8 and 9)), 7.13 (d, J = 8.8 Hz, 2H, H-C(3)), 6.80 (d, J = 8.9 Hz, 2H, H-C(2)), 4.14–4.10 (m, 2H, H_2-C(17)), 4.10–4.06 (m, 2H, H_2-C(10)), 3.82–3.76 (m, 2H, H_2-C(11)), 3.68–3.62 (m, 4H, H_2-C(16 and 12)), 3.62–3.57 (m, 2H, H_2-C(13)), 3.55 (s, 4H, H_2-C(14 and 15)), 2.43 (s, 3H, H_3-C(22)).

^{13}C NMR (101 MHz, CD_2Cl_2): δ / ppm = 157.4 (C(1)), 147.7 (C(6)), 145.6 (C(21)), 139.7 (C(4)), 133.5 (C(18)), 132.6 (C(3)), 131.5 (C(7/8)), 130.4 (C(20)), 128.4 (C(19)), 128.0 (C(7/8)), 126.4 (C(9)), 113.9 (C(2)), 71.3*, 71.2*, 71.1*, 71.0*, 70.2*, 70.1*, 69.1*, 68.0 (C(10)), 64.9 (C(5)), 21.9 (C(22)).

*TEG chain C(11 or 12 or 13 or 14 or 15 or 16 or 17)

IR: $\tilde{\nu}$ / cm^{-1} = 2874 (w), 1597 (w), 1508 (m), 1490 (m), 1442 (m), 1292 (w), 1248 (s), 1175 (vs), 1120 (s), 1097 (s), 1012 (s), 914 (s), 818 (s), 749 (vs), 700 (vs), 663 (s).

HRMS (EI): *m/z* calc. for $[C_{40}H_{42}O_7S]^{\bullet+}$: 666.2646; found: 666.2638 ($M^{\bullet+}$).

Compound (*E*/*Z*)-61 *reported in ref.*[8]

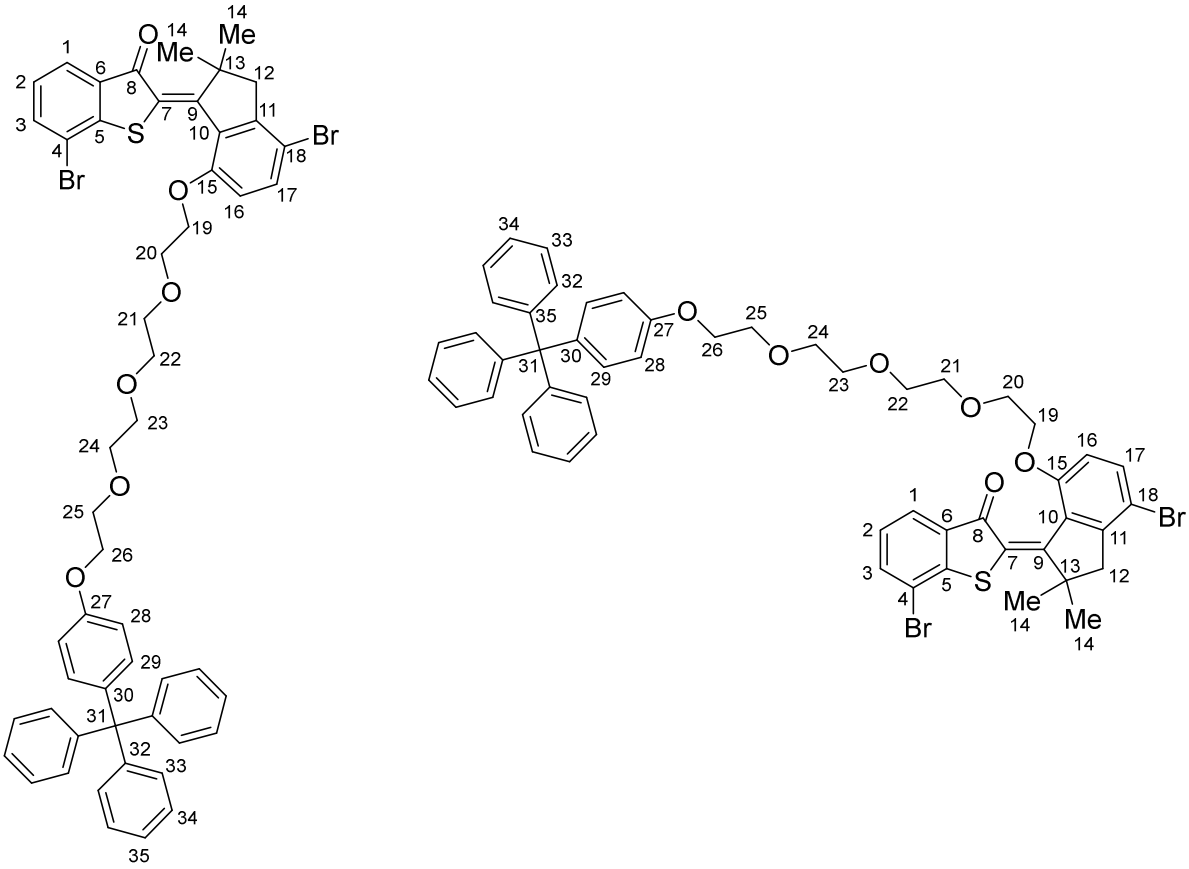

(*Z*)-isomer (*E*)-isomer

Compound **60** (716 mg, 1.07 mmol, 0.9 equiv.) was dissolved in DMF (13 mL). Compound **59** (559 mg, 1.20 mmol, 1.0 equiv.), K_2CO_3 (739 mg, 5.35 mmol, 4.5 equiv.) and NaI (44 mg, 0.29 mmol, 0.24 equiv.) were added and the reaction mixture was stirred at 90 °C for 21 h. The reaction mixture was poured into H_2O (150 mL) and extracted with EtOAc (3 × 100 mL, small amounts of brine were added for better phase separation). The combined organic phases were washed with H_2O (1 × 200 mL, 1 × 300 mL) and brine (4 × 200 mL), dried over Na_2SO_4, filtered, and concentrated *in vacuo*. The crude product was purified by flash column chromatography (SiO_2, EtOAc:*i*-Hex, 40:60) to give isomer (*Z*)-**61** (156 mg, 0.162 mmol, 14%) as an orange oil and isomer (*E*)-**61** (403 mg, 0.419 mmol, 35%) as an orange foam. *Note*: 189 mg of starting material **59** were recovered (total yield based on recovered starting material: 73%).

(*Z*)-isomer

R_f (EtOAc:*i*-Hex, 50:50): 0.65.

^{1}H NMR (400 MHz, CD_2Cl_2): δ / ppm = 7.72 (dd, J = 7.6, 1.1 Hz, 1H, H-C(1)), 7.66 (dd, J = 7.7, 1.1 Hz, 1H, H-C(3)), 7.52 (d, J = 8.8 Hz, 1H, H-C(17)), 7.27–7.17 (m, 16H, H-C(2 and 33 and 34 and 35)), 7.12–7.09 (m, 2H, H-C(29)), 6.81 (d, J = 8.8 Hz, 1H, H-C(16)), 6.78 (d, J = 8.9 Hz, 2H, H-C(28)), 4.32 (t, J = 5.1 Hz, 2H)*, 4.07–4.02 (m, 2H)*, 3.98 (t, J = 5.1 Hz, 2H)*, 3.76–3.72 (m, 2H)*, 3.62–3.55 (m, 4H)*, 3.52 (m, 4H)*, 2.97 (s, 2H, H_2-C(12)), 1.53 (s, 6H, H_3-C(14)).

*TEG-chain H_2-C(19 or 20 or 21 or 22 or 23 or 24 or 25 or 26).

HRMS (EI): *m/z* calc. for $[C_{52}H_{48}Br_2O_6S]^{\bullet+}$: 958.1533; found: 958.1545 ($M^{\bullet+}$).

(*E*)-isomer

R_f (EtOAc:*i*-Hex, 50:50): 0.29.

^{1}H NMR (601 MHz, CD_2Cl_2): δ / ppm = 7.80 (dd, J = 7.6, 1.1 Hz, 1H, H-C(1)), 7.70 (dd, J = 7.7, 1.1 Hz, 1H, H-C(3)), 7.45 (d, J = 8.8 Hz, 1H, H-C(17)), 7.27–7.16 (m, 16H, H_2-C(2 and 32 and 33 and 34)), 7.11 (d, J = 9.1 Hz, 2H, H-C(29)), 6.78 (d, J = 9.1 Hz, 2H, H-C(28)), 6.72 (d, J = 8.8 Hz, 1H, H-C(16)), 4.17 (d, J = 4.2 Hz, 1H, H_2-C(19)), 4.16–4.10 (m, 1H, H_2-C(19)), 4.07–4.02 (m, 2H, H_2-C(26)), 3.77–3.72 (m, 2H, H_2-C(25)), 3.69–3.64 (m, 1H, H_2-C(24)), 3.58 (d, J = 9.4 Hz, 3H, H_2-C(20 and 24)), 3.47 (d, J = 4.4 Hz, 2H, H_2-C(23)), 3.37–3.30 (m, 3H, H_2-C(21 and 22)), 3.27 (dd, J = 7.3, 3.9 Hz, 1H, H_2-C(21)), 3.12 (d, J = 16.0 Hz, 1H, H_2-C(12)), 2.86 (d, J = 16.0 Hz, 1H, H_2-C(12)), 1.73 (s, 3H, H_3-C(14)), 1.26 (s, 3H, H_3-C(14)).

^{13}C NMR (151 MHz, CD_2Cl_2): δ / ppm = 186.6 (C(8)), 157.7 (C(9)), 157.4 (C(15)), 157.2 (C(27)), 145.6 (C(35)), 139.5 (C(5)), 136.8 (C(3)), 134.7 (C(17)), 134.4 (C(6)), 132.4 (C(29)), 131.3 (C(32)), 129.9 (C(10)), 127.8 (C(33)), 127.2 (C(7)), 126.7 (C(2)), 126.2 (C(34)), 125.0 (C(1)), 117.7 (C(4)), 113.7 (C(28)), 112.4 (C(16)), 110.3 (C(18)), 71.0 (C(24)), 71.0 (C(21)), 70.8 (C(23)), 70.6 (C(22)), 70.0 (C(25)), 69.7 (C(20)), 68.2 (C(19)), 67.7 (C(26)), 64.7 (C(31)), 50.6 (C(12)), 50.4 (C(13)), 26.6 (C(14)), 26.2 (C(14)).

IR: $\tilde{\nu}$ / cm^{-1} = 3469 (w, br), 2874 (m), 1606 (w), 1508 (m), 1489 (m), 1442 (m), 1249 (s), 1182 (m), 1096 (s, br), 1035 (s), 938 (m), 819 (m), 750 (s), 700 (vs).

HRMS (EI): *m/z* calc. for $[C_{52}H_{48}Br_2O_6S]^{\bullet+}$: 958.1533; found: 958.1576 ($M^{\bullet+}$).

Compound (*E*/*Z*)-62 *reported in ref.*[8]

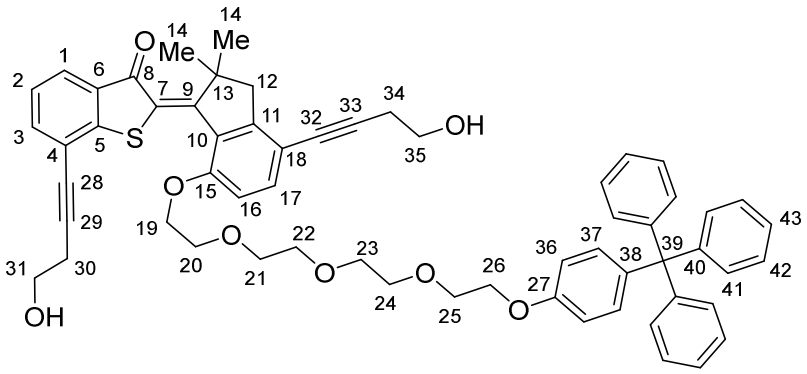

(*Z*)-isomer

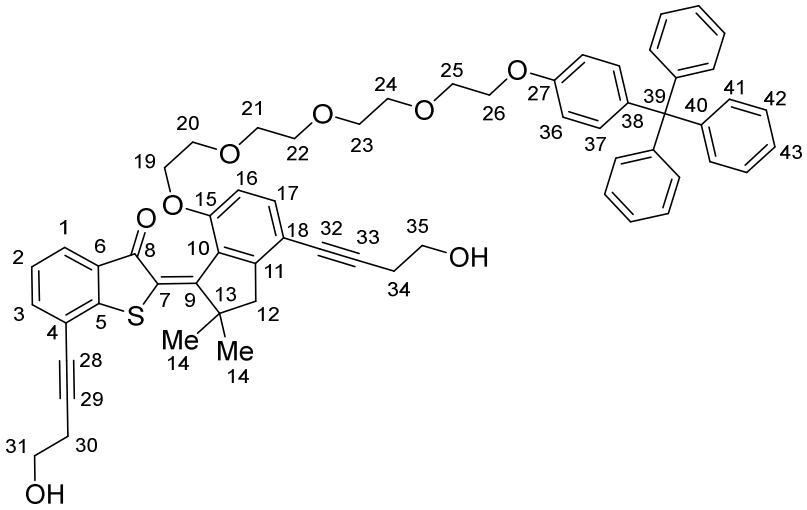

(*E*)-isomer

Compound **61** (mixture of (*E*)- and (*Z*)-isomers) (380 mg, 0.395 mmol, 1.0 equiv.), CuI (6 mg, 0.03 mmol, 0.08 equiv.) and XPhos Pd G2 (29 mg, 0.037 mmol, 0.09 equiv.) were added to a Schlenk flask equipped with a magnetic stirring bar and a septum. The flask was evacuated and refilled with dry nitrogen three times. Dry 1,4-dioxan (2.0 mL) and dry DIPA (2.0 mL) were added and the flask was evacuated and refilled with dry nitrogen five times while stirring vigorously. 3-Butyn-1-ol (75 µl, 1.0 mmol, 2.5 equiv.) was added and the reaction mixture was stirred at 65 °C for 5 h. The reaction was stopped by the addition of a saturated aqueous solution of NH_4Cl (15 mL). The mixture was diluted with H_2O (75 mL) and extracted with CH_2Cl_2 (2 × 100 mL). The combined organic layers were dried over Na_2SO_4, filtered, and concentrated *in vacuo*. The residue was purified by flash column chromatography (SiO_2, MeOH:CH_2Cl_2, 5:95) to give compound **62** (mixture of (*E*)- and (*Z*)-isomers, 277 mg, 0.295 mmol, 75%) as an orange foam.

R_f (MeOH:CH_2Cl_2, 5:95): 0.44.

HRMS (ESI): *m/z* calc. for $[C_{60}H_{58}O_8S+H]^+$: 939.3925; found: 939.3944 ($M+H^+$).

Note: NMR analysis was performed on an *E*:*Z* mixture (approx. 2:1).

(*Z*)-isomer

^{1}H NMR (400 MHz, CD_2Cl_2): δ / ppm = 7.67 (dd, *J* = 7.7, 1.3 Hz, 1H, H-C(1), 7.51 (dd, *J* = 7.5, 1.3 Hz, 1H, H-C(3)), 7.43 (d, *J* = 8.6 Hz, 1H, H-C(17)), 7.29–7.17 (m, 15H, H-C(41 and 42 and 43), 7.15 (s, 1H, H-C(2)), 7.14–7.09 (m, 2H, H-C(37)), 6.83 (d, *J* = 8.6 Hz, 1H, H-C(16)), 6.81–6.77 (m, 2H, H-C(36)), 4.32 (t, *J* = 5.5 Hz, 2H, H_2-C(19)), 4.00 (t, *J* = 5.4 Hz, 2H, H_2-C(20)), 3.81–3.77 (m, 4H, H_2C-(31 and 35)), 3.70–3.64 (m)*, 3.63–3.60 (m)*, 3.60–3.56 (m)*, 3.56–3.51 (m)*, 3.45 (dd, *J* = 5.7, 4.0 Hz)*, 3.36–3.24 (m)*, 3.02 (s, 2H, H_2C-(12)), 2.69 (tt, *J* = 6.3, 2.2 Hz, 4H, H_2C-(30 and 34)), 1.53 (s, 6H, H_3C-(14)).

*Due to signal overlap of (*E*)- and (*Z*)-isomers, the tetraethylene glycol chain signals could not be fully assigned.

^{13}C NMR (101 MHz, CD_2Cl_2): δ / ppm = 189.0 (C(8)), 162.9 (C(9)), 157.2 (C(27)), 155.6‡, 153.2‡, 149.2 (C(5)), 147.5 (C(40)), 136.6 (C(3)), 136.4 (C(17)), 132.6‡, 132.5‡, 131.4 (C(41 or 42)), 128.5‡, 127.9 (C(41 or 42)), 126.4‡, 126.2 (C(43)), 125.2 (C(1)), 124.7 (C(2)), 118.6 (C(4)), 113.7 (C(36)), 111.3 (C(16)), 94.8 (C(29 or 33)), 89.7 (C(29 or 33)), 79.5 (C(28 or 32)), 78.1 (C(28 or 32)), 71.2*, 71.0*, 71.0*, 71.0*, 70.9*, 70.8*, 70.7*, 70.5*, 69.5 (C(20)), 68.2 (C(19)), 67.7‡, 64.7 (C(39)), 61.6 (C(31 or 35)), 61.3 (C(31 or 35)), 51.3 (C(12 or 13)), 51.2 (C(12 or 13)), 26.6 (C(14)), 24.34 (C(30 or 34)), 24.28 (C(30 or 34)).

‡Could not be assigned unambiguously.

*Due to signal overlap of the (*E*)- and (*Z*)-isomer the tetraethylene glycol chain signals could not be fully assigned.

(*E*)-isomer

^{1}H NMR (400 MHz, CD_2Cl_2): δ / ppm = 7.76 (dd, *J* = 7.7, 1.3 Hz, 1H, H-C(1)), 7.57 (dd, *J* = 7.5, 1.3 Hz, 1H, H-C(3)), 7.38 (d, *J* = 8.5 Hz, 1H, H-C(17)), 7.29–7.17 (m, 16H, H-C(2 and 41 and 42 and 43)), 7.14–7.09 (m, 2H, H-C(37)), 6.81–6.77 (m, 2H, H-C(36)), 6.74 (d, *J* = 8.6 Hz, 1H, H-C(16)), 4.22–4.14 (m, 2H, H_2-C(19)), 4.07–4.04 (m, 2H, H_2-C(26)), 3.84 (s, 2H, H_2-C(31)), 3.81–3.77 (m, 2H, H_2-C(35)), 3.78–3.72 (m, 2H, H_2-C(25)), 3.70–3.64 (m, 1H, H_2-C(20)), 3.63–3.56 (m, 3H, H_2-C(20 and 24)), 3.56–3.51 (m)*, 3.45 (dd, *J* = 5.7, 4.0 Hz)*, 3.36–3.24 (m)*, 3.15 (d, *J* = 16.9 Hz, 1H, H_2-C(12)), 2.93 (d, *J* = 16.0 Hz, 1H, H_2-

C(12)), 2.77 (t, J = 6.3 Hz, 2H, H_2-C(30)), 2.69 (tt, J = 6.3, 2.2 Hz, 2H, H_2-C(34)), 1.73 (s, 3H, H_3-C(14)), 1.25 (s, 3H, H_3-C(14)).

*Due to signal overlap of the (*E*)- and the (*Z*)-isomer the tetraethylene glycol chain signals could not be fully assigned.

^{13}C NMR (101 MHz, CD_2Cl_2): δ / ppm = 187.0 (C(8)), 157.8 (C(10 or 15)), 157.4 (C(10 or 15)), 157.18 (C(27)), 157.16‡, 155.6‡, 153.2‡, 152.0 (C(11)), 147.5 (C(40)), 147.1 (C(5)), 139.6 (C(38)), 136.6 (C(3)), 135.2 (C(17)), 132.6‡,132.57‡, 132.54 (C(37)), 131.4 (C(41 or 42)), 128.5‡, 127.9 (C(41 or 42)), 126.4‡, 126.2 (C(43)), 125.5 (C(1)), 125.2 (C(2)), 119.2 (C(4)), 113.7 (C(36)), 112.6 (C(18)), 110.6 (C(16)), 94.6 (C(29)), 89.0 (C(33)), 79.8 (C(32)), 78.3 (C(28)), 71.2*, 71.0*, 71.0*, 71.0*, 70.9*, 70.8*, 70.7*, 70.5*, 70.0 (C(25)), 69.8 (C(20)), 68.0 (C(19)), 67.8 (C(26)), 67.7‡, 64.7 (C(39)), 61.61 (C(35)), 61.4 (C(31)), 50.7 (C(13)), 49.4 (C(12)), 26.8 (C(14)), 26.3 (C(14)), 24.4 (C(30)), 24.31 (C(34)).

‡Could not be assigned unambiguously.

*Due to signal overlap of the (*E*)- and (*Z*)-isomer the tetraethylene glycol chain signals could not be fully assigned.

Compound (*E*/*Z*)-63 *reported in ref.*[8]

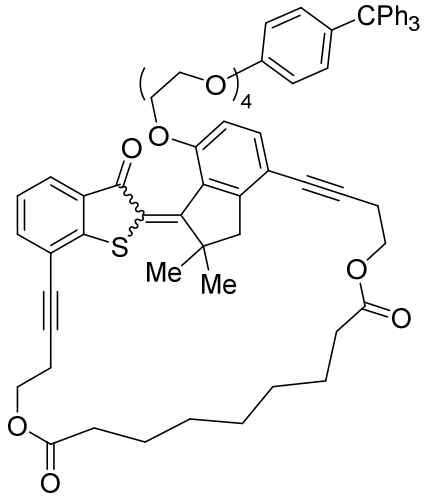

1) Azelaoyl chloride preparation

Azelaic acid (95 mg, 0.50 mmol, 1.0 eq) was refluxed in $SOCl_2$ (1.0 mL, 14 mmol, 28 equiv.) for 1.5 h. Excess $SOCl_2$ was removed *in vacuo* and the residue was dissolved in dry CH_2Cl_2 (1.0 mL) to give a 0.5 M solution of azelaoyl chloride, which was used without further purification.

2) Macrocyclization

In a dried Schlenk flask under nitrogen atmosphere azelaoyl chloride (0.5 M in CH_2Cl_2, 0.1 mL, 0.05 mmol, 1.1 equiv.) was added to a solution of 4-dimethylaminopyridine (14 mg, 0.11 mmol, 2.3 equiv.) in dry CH_2Cl_2 (50 mL). The reaction mixture was stirred at 23 °C for 5 min, then compound **62** (mixture of (*E*)- and (*Z*)-isomers, 44 mg in 5.0 mL dry CH_2Cl_2, 0.047 mmol, 1.0 equiv.) was added and stirring was continued for 6 d. The volatiles were removed *in vacuo* and the residue was purified by flash column chromatography (SiO_2, MeOH:CH_2Cl_2, 1:99). Compound **63** (mixture of (*E*)- and (*Z*)-isomers, 25 mg, 0.023 mmol, 49%) was obtained as an orange oil. The compound was used for the next synthetic step without full characterization.

HRMS (ESI): *m/z* calc. for $[C_{69}H_{70}O_{10}S+NH_4]^+$: 1108.5028; found: 1108.5050 ($M+NH4^+$).

Compound 65[157] *reported in ref.[8]*

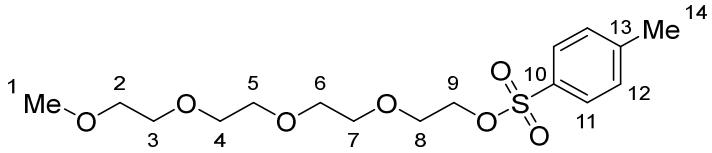

To a solution of tetraethylene glycol monomethyl ether (3.0 g, 14 mmol, 1.0 equiv.) in THF (30 mL) a solution of NaOH (0.85 g in 5 mL of H_2O, 22 mmol, 1.6 equiv.) was added at 0 °C. Then, a solution of *p*-TsCl (3.0 g in 10 mL THF, 16 mmol, 1.1 equiv.) was added dropwise at 0 °C over the course of 30 min. After complete addition, stirring was continued at 0 °C for 2 h. The reaction mixture was poured into ice-water (200 mL) and extracted with CH_2Cl_2 (3 × 100 mL). The combined organic layers were washed with H_2O (2 × 200 mL) and brine (100 mL), dried over Na_2SO_4, filtered, and concentrated *in vacuo* to give tosylate **65** (3.68 g, 10.2 mmol, 73%) as a faint yellow oil.

^{1}H NMR (400 MHz, $CDCl_3$): δ / ppm = 7.80–7.75 (m, 2H, H-C(11)), 7.32 (d, J = 7.9 Hz, 2H, H-C(12)), 4.16–4.11 (m, 2H, H_2-C(9)), 3.68–3.65 (m, 2H, H_2-C(8)), 3.63–3.60 (m, 6H, H_2-C(3) and either H_2-C(4 and 5) or H2-C(6 and 7)), 3.56 (s, 4H, either H_2-C(4 and 5) or H_2-C(6 and 7)), 3.52 (dd, J = 6.0, 3.0 Hz, 2H, H_2-C(2)), 3.35 (s, 3H, H_3-C(1)), 2.43 (s, 3H, H_3-C(14)).

^{13}C NMR (101 MHz, $CDCl_3$): δ / ppm = 144.9 (C(13)), 133.1 (C(10)), 129.9 (C(12)), 128.0 (C(11)), 72.0 (C(2)), 70.8*, 70.7*, 70.7*, 70.6*, 70.6*, 69.3 (C(9)), 68.7 (C(8)), 59.1 (C(1)), 21.7 (C(14)).

*(C(3 or 4 or 5 or 6 or 7)).

IR: $\tilde{\nu}$ / cm^{-1} = 2871 (w), 1597 (w), 1495 (vw), 1450 (w), 1398 (w), 1352 (s), 1306 (w), 1292 (w), 1248 (w), 1188 (m), 1174 (vs), 1095 (s), 1016 (m), 916 (s), 849 (m), 816 (s), 773 (s), 706 (w), 690 (w), 661 (s), 634 (w), 575 (m), 553 (vs), 530 (m), 501 (m), 467 (w), 428 (w), 422 (w), 413 (w), 405 (w).

HRMS (ESI): *m/z* calc. for $[C_{16}H_{26}O_7S+K]^+$: 401.1031; found: 401.1036 ($M+K^+$).

Compound (*E*/*Z*)-66 *reported in ref.[8]*

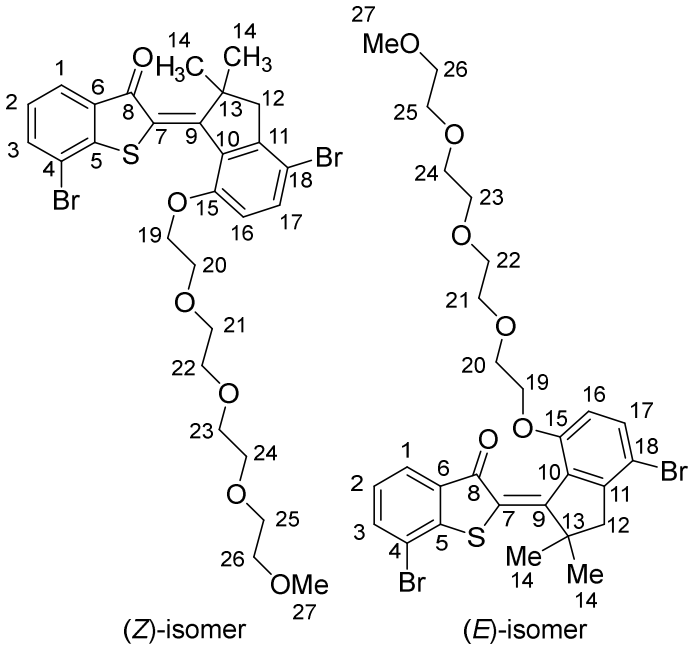

Compound **59** (mixture of (*E*)- and (*Z*)-isomers, 220 mg, 0.472 mmol, 1.0 equiv.), NaI (80 mg, 0.53 mmol, 1.1 equiv.) and K_2CO_3 (196 mg, 1.41 mmol, 3.0 equiv.) were added to a two-neck round bottom flask equipped with a magnetic stirring bar, a septum and a reflux condenser. The flask was evacuated and refilled with dry nitrogen once. Dry butanone (5 mL) was added, followed by the addition of tosylate **65** (206 mg, 0.568 mmol, 1.2 eq). The reaction mixture was refluxed under nitrogen atmosphere for a total of 4 h (after a period of 2.75 h additional 3 mL of butanone were added). The reaction mixture was poured into H_2O (100 mL) and extracted with EtOAc (2 × 100 mL). The combined organic phases were washed with H_2O (200 mL, a small amount of 10% aq. LiCl was added for better phase separation) and brine (2 × 200 mL), dried over Na_2SO_4, filtered, and concentrated *in vacuo*.

The residue was purified by flash column chromatography (SiO_2, EtOAc:*i*-Hex, 60:40). Isomer (*Z*)-**66** (140 mg of an inseparable mixture with 37% TEG-iodide as judged by ^{1}H NMR spectroscopy, 0.17 mmol, 36%) and isomer (*E*)-**66** (84 mg of an inseparable mixture with 34% tosylate **65** as judged by ^{1}H NMR spectroscopy, 0.10 mmol, 21%) were obtained as orange oils. The obtained compounds were used in the next synthetic step without further purification.

(*Z*)-isomer

R_f (EtOAc:*i*-Hex, 50:50): 0.22.

^{1}H NMR (400 MHz, CD_2Cl_2): δ / ppm = 7.73 (dd, J = 7.6, 1.1 Hz, 1H, H-C(1)), 7.68 (dd, J = 7.7, 1.1 Hz, 1H, H-C(3)), 7.54 (d, J = 8.8 Hz, 1H, H-C(17)), 7.15 (t, J = 7.7 Hz, 1H, H-C(2)), 6.84 (d, J = 8.8 Hz, 1H, H-C(16)), 4.36–4.31 (m, 2H, H_2-C(19)), 4.02–3.97 (m, 2H, H_2-C(20)), 3.73 (t, J = 6.7 Hz, 1H, H_2-C(26)), 3.65–3.56 (m, 4H, H_2-C(21 and 24)), 3.55–3.44 (m, 4H, H_2-C(22 and 23)), 3.31 (s, 3H, H_3-C(27)), 2.97 (s, 2H, H_2-C(12)), 1.54 (s, 6H, H_3-C(14)).

^{13}C NMR (101 MHz, CD_2Cl_2): δ / ppm = 188.7 (C(8)), 163.2 (C(9)), 155.5 (C(15)), 150.0 (C(11)), 147.3 (C(5)), 137.1 (C(3)), 136.1 (C(17)), 134.4 (C(6)), 129.8 (C(10)), 129.5 (C(7)), 126.3 (C(2)), 124.8 (C(1)), 117.0 (C(4)), 113.3 (C(16)), 111.1 (C(18)), 72.3 (C(25)), 72.3 (C(26)), 71.0 (C(22)), 70.9 (C(23)), 70.8 (C(21)), 70.6 (C(24)), 69.5 (C(20)), 68.8 (C(19)), 59.0 (C(27)), 52.7 (C(12)), 51.2 (C(13)), 26.5 (C(14)).

HRMS (EI): *m/z* calc. for $[C_{28}H_{32}Br_2O_6S]^{\bullet+}$: 654.0281; found 654.0282 ($M^{\bullet+}$).

(*E*)-isomer

R_f (EtOAc:*i*-Hex, 50:50): 0.07.

^{1}H NMR (400 MHz, CD_2Cl_2): δ / ppm = 7.81 (dd, J = 7.6, 1.1 Hz, 1H, H-C(1)), 7.73 (dd, J = 7.8, 1.1 Hz, 1H, H-C(3)), 7.47 (d, J = 8.8 Hz, 1H, H-C(17)), 7.22 (t, J = 7.7 Hz, 1H, H-C(2)), 6.74 (d, J = 8.9 Hz, 1H, H-C(16)), 4.22–4.10 (m, 4H, H_2-C(19 and 20)), 3.71–3.63 (m, 2H, H_2-C(21)), 3.62–3.42 (m, 10H, H-C(22 and 23 and 24 and 25 and 26)), 3.31 (s, 3H, H_3-C(27)), 3.13 (d, J = 16.0 Hz, 1H, H_2-C(12)), 2.86 (d, J = 16.0 Hz, 1H, H_2-C(12)), 1.74 (s, 3H, H_3-C(14)), 1.28 (s, 3H, H_3-C(14)).

^{13}C NMR (101 MHz, CD_2Cl_2): δ / ppm = 186.6 (C(8)), 171.2 (C(9)), 157.7 (C(15)), 148.8 (C(11)), 145.5 (C(5)), 136.8 (C(3)), 134.7 (C(17)), 134.4 (C(6)), 130.3(C(7)), 130.0 (C(10)), 126.7 (C(2)), 125.0 (C(1)), 117.8 (C(4)), 112.5 (C(16)), 110.3 (C(18)), 72.3 (C(26)), 72.3(C(25)), 70.8 (C(22)), 70.6 (C(23)), 69.9 (C(21)), 69.8 (C(24)), 69.0 (C(20)), 68.2 (C(19)), 59.0 (C(27)), 50.8 (C(12)), 26.6 (C(14)), 26.5 (C(14)), 26.3 (C(13)).
HRMS (EI): *m/z* calc. for $[C_{28}H_{32}Br_2O_6S]^{\bullet+}$: 654.0281; found 654.0272 ($M^{\bullet+}$).

Compound (*E*/*Z*)-67 *reported in ref.[8]*

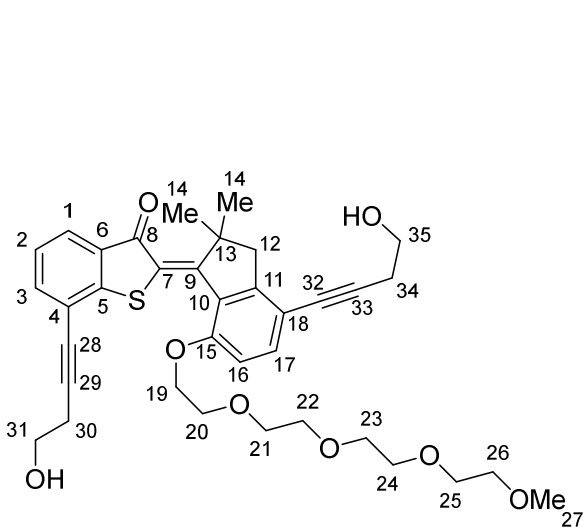

(*Z*)-isomer

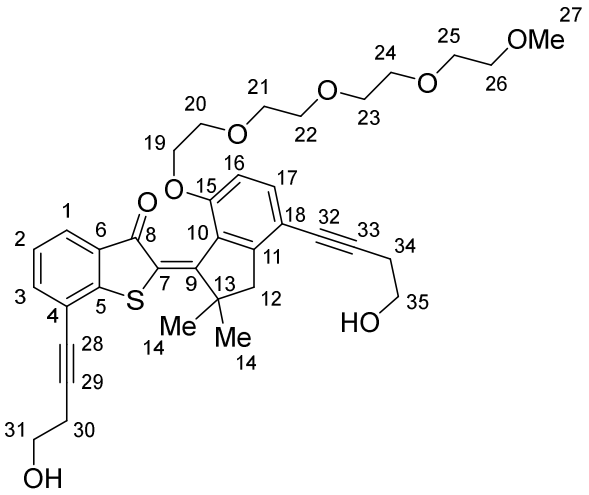

(*E*)-isomer

Compound **66** (289 mg of a mixture with TEG-tosylate and TEG-iodide, total content of **66** as judged by ^{1}H NMR spectroscopy: 0.33 mmol, 1.0 equiv.), CuI (9 mg, 0.05 mmol, 0.15 equiv.) and XPhos Pd G2 (31 mg, 0.039 mmol, 0.12 equiv.) were added to a Schlenk flask equipped with a septum and a magnetic stirring bar. The flask was evacuated and refilled with nitrogen three times. Dry 1,4-dioxane (2.0 mL) and dry DIPA (2.0 mL) were added and the flask was evacuated and refilled with nitrogen three times under vigorous stirring. 3-Butyn-1-ol (78 µL, 1.0 mmol, 3.0 equiv.) was added and the reaction mixture was stirred at 65 °C under nitrogen for 4.5 h. The reaction was stopped by the addition of a saturated aqueous solution of NH_4Cl (10 mL). H_2O (50 mL) was added and the mixture was extracted with CH_2Cl_2 (2 × 50 mL). The combined organic phases were dried over Na_2SO_4, filtered, and concentrated *in vacuo*. The crude product was purified by flash column chromatography (SiO_2, MeOH:CH_2Cl_2, 5:95) to give compound **67** (mixture of (*E*)- and (*Z*)-isomers, 172 mg, 0.271 mmol, 82%) as a red oil.

R_f (MeOH:CH_2Cl_2, 5:95): 0.32.

HRMS (ESI): *m/z* calc. for $[C_{36}H_{42}O_8S+H]^+$: 635.2673; found: 635.2688 ($M+H^+$).

Note: NMR analysis was performed on an *E*:*Z* mixture (approx. 2:1).

(*E*)-isomer

^{1}H NMR (800 MHz, CD_2Cl_2): δ / ppm = 7.76 (dd, *J* = 7.6, 1.3 Hz, 1H, H-C(1)), 7.59 (dd, *J* = 7.4, 1.3 Hz, 1H, H-C(3)), 7.39 (d, *J* = 8.5 Hz, 1H, H-C(17)), 7.25 (t, *J* = 7.6 Hz, 1H, H-C(2)), 6.76 (d, *J* = 8.5 Hz, 1H, H-C(16)), 4.20 (dt, *J* = 10.0, 4.1 Hz, 1H, H_2-C(19)), 4.18–4.14 (m, 1H, H_2-C(19)), 3.85 (t, *J* = 6.3 Hz, 2H, H_2-C(31)), 3.78 (t, *J* = 5.4 Hz, 2H, H_2-C(35)), 3.68 (dt, *J* = 10.9, 4.0 Hz, 1H, H_2-C(20)), 3.60–3.57 (m, 1H, H_2-C(20)), 3.55–3.51 (m)*, 3.51–3.49 (m)*, 3.49–3.46 (m)*, 3.43–3.41 (m)*, 3.32 (s, 3H, H_3-C(27)), 3.30–3.24 (m, 2H, H_2-C(21)), 3.15 (d, *J* = 16.0 Hz, 1H, H_2-C(12)), 2.93 (d, *J* = 15.9 Hz, 1H, H_2-C(12)), 2.79 (t, *J* = 6.3 Hz, 2H, H_2-C(30)), 2.69 (t, *J* = 6.0 Hz, 2H, H_2-C(34)), 1.73 (s, 3H, H_3-C(14)), 1.25 (s, 3H, H_3-C(14)).

^{13}C NMR (201 MHz, CD_2Cl_2): δ / ppm = 187.0 (C(8)), 157.8 (C(9)), 157.4 (C(15)), 152.0 (C(18)), 147.1 (C(5)), 136.6 (C(3)), 135.2 (C(17)), 132.5 (C(4)), 128.5 (C(10)), 126.4 (C(7)), 125.4 (C(1)), 125.2 (C(2)), 119.2 (C(6)), 112.6 (C(11)), 110.6 (C(16)), 94.6 (C(29)), 89.0 (C(33)), 79.8 (C(32)), 78.3 (C(28)), 72.3*, 72.2*, 71.0*, 70.8*, 70.7*, 70.5*, 69.8 (C(20)), 68.0 (C(19)), 61.6 (C(35)), 61.4 (C(31)), 59.0 (C(27)), 50.7 (C(13)), 49.3 (C(12)), 26.7 (C(14)), 26.3 (C(14)), 24.4 (C(30)), 24.3 (C(34)).

*Due to signal overlap, full assignment of the tetraethylene glycol chain signals was not possible.

(*Z*)-isomer

^{1}H NMR (800 MHz, CD_2Cl_2): δ / ppm = 7.68 (dd, *J* = 7.7, 1.2 Hz, 1H, H-C(1)), 7.53 (dd, *J* = 7.5, 1.2 Hz, 1H, H-C(3)), 7.45 (d, *J* = 8.5 Hz, 1H, H-C(17)), 7.17 (t, *J* = 7.6 Hz, 1H, H-C(2)), 6.85 (d, *J* = 8.6 Hz, 1H, H-C(16)), 4.34 (t, *J* = 5.5 Hz, 2H, H_2-C(19)), 4.01 (t, *J* = 5.5 Hz, 2H, H_2-C(20)), 3.78 (t, *J* = 5.4 Hz, 4H, H_2-C(31 and 35)), 3.64–3.61 (m, 2H, H_2-C(21)), 3.55–3.51 (m)*, 3.51–3.49 (m)*, 3.49–3.46 (m)*, 3.43–3.41 (m)*, 3.32 (s, 3H, H_3-C(27)), 3.02 (s, 2H, H_2-C(12)), 2.71 (t, *J* = 6.3 Hz, 2H, H_2-C(30)), 2.69 (t, *J* = 5.9 Hz, 2H, H_2-C(34)), 1.53 (s, 6H, H_3-C(14)).

^{13}C NMR (201 MHz, CD_2Cl_2): δ / ppm = 189.0 (C(8)), 162.8 (C(9)), 155.6 (C(15)), 153.2 (C(18)), 149.2 (C(5)), 136.6 (C(3)), 136.4 (C(17)), 132.5 (C(4)), 129.1 (C(7)), 128.0 (C(10)), 125.2 (C(1)), 124.7 (C(2)), 118.6 (C(6)), 113.2 (C(11)), 111.2 (C(16)), 94.8 (C(29)), 89.7

(C(33)), 79.5 (C(32)), 78.1 (C(28)), 72.3*, 72.2*, 71.2 (C(21)), 71.0*, 70.8*, 70.7*, 70.5*, 69.5 (C(20)), 68.2 (C(19)), 61.6 (C(31 or 35)), 61.3 (C(31 or 35)), 59.0 (C(27)), 51.3 (C(13)), 51.2 (C(12)), 26.6 (C(14)), 24.4, 24.32 (C(30 or 34)), 24.26 (C(30 or 34)).

*Due to signal overlap, full assignment of the tetraethylene glycol chain signals was not possible.

Compound (*E*/*Z*)-68 *reported in ref.*[8]

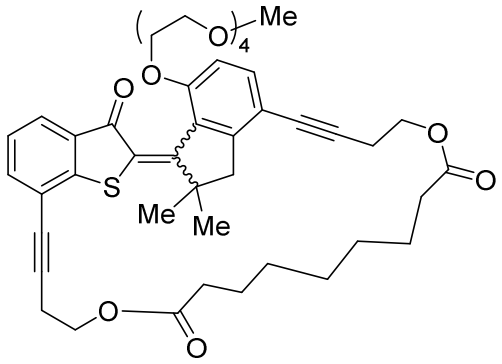

1) Azelaoyl chloride preparation

Azelaic acid (191 mg, 1.01 mmol, 1.0 equiv.) was refluxed in $SOCl_2$ (1.3 mL, 18 mmol, 18 eq) for 3.75 h. Excess $SOCl_2$ was removed *in vacuo* and the residue was dissolved in dry CH_2Cl_2 (2.0 mL) to give a 0.5 M solution of azelaoyl chloride, which was used without further purification.

2) Macrocyclization

In a dried Schlenk flask under nitrogen atmosphere azelaoyl chloride (0.5 M in CH_2Cl_2, 0.28 mL, 0.14 mmol, 1.0 eq) was added to a solution of 4-dimethylaminopyridine (33 mg, 0.27 mmol, 1.9 eq) in dry CH_2Cl_2 (120 mL). The reaction mixture was stirred at 23 °C for 5 min, then compound **67** (90 mg in 3.4 mL dry CH_2Cl_2, 0.14 mmol, 1.0 eq) was added and stirring was continued for 7 d. The volatiles were removed *in vacuo* and the residue was purified by flash column chromatography (SiO_2, MeOH:CH_2Cl_2, 2:98). Compound **68** (mixture of (*E*)- and (*Z*)-isomers, 40 mg, 51 µmol, 36%) was obtained as an orange oil. The compound was used in the next synthetic step without full characterization.

HRMS (ESI): *m/z* calc. for $[C_{45}H_{54}O_{10}S+NH_4]^+$: 804.3776; found: 804.3771 ($M+NH_4^+$).

Compound 70

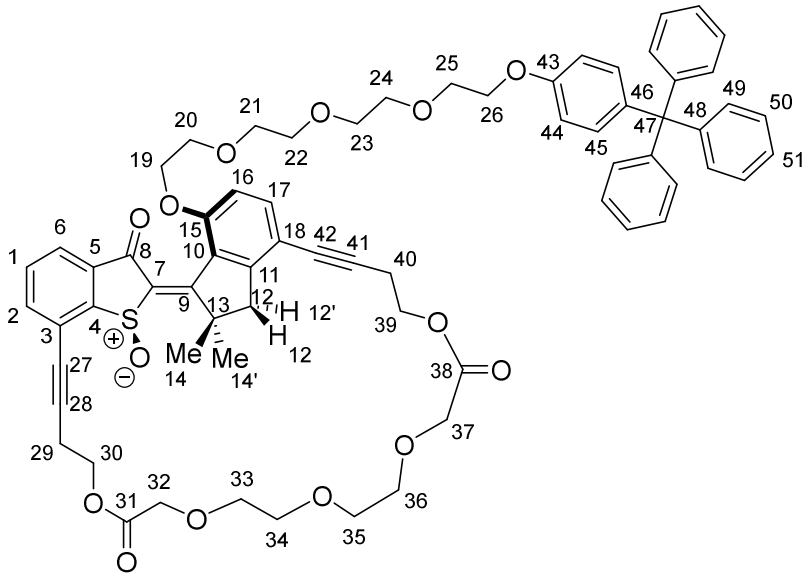

1) Acid chloride preparation

In a dried flask, 3,6,9-trioxaundecanedioic acid (0.17 mL, 0.99 mmol, 1.0 equiv.) was dissolved in dry CH_2Cl_2 (3.0 mL) under nitrogen atmosphere. Oxalyl chloride (0.68 mL, 8.0 mmol, 8.1 equiv.) was added under stirring at 29 °C. After the gas evolution had ceased, two drops of dry DMF were added and stirring was continued at 29 °C for 45 min. The volatiles were removed *in vacuo* and the residue was taken up in dry CH_2Cl_2 (2.0 mL, 0.5 M solution of acid chloride).

2) Macrocyclization

In a dried flask under nitrogen atmosphere, 4-DMAP (28 mg, 0.23 mmol, 2.1 equiv.) and compound **62** (103 mg, 0.110 mmol, 1.0 equiv.) were dissolved in dry CH_2Cl_2 (100 mL). 3,6,9-Trioxaundecanedioic acid dichloride (0.5 M in CH_2Cl_2, 0.22 mL, 0.11 mmol, 1.00 equiv.) was added dropwise and the reaction mixture was stirred at 30 °C for 92 h. The volatiles were removed under reduced pressure and the residue was purified by flash column chromatography (SiO_2, MeOH:CH_2Cl_2, 2.5:97.5). Macrocyclic product **69** (43 mg, 38 µmol, 35%) was obtained as an orange oil.

3) Oxidation

To a solution of compound **69** (36 mg, 32 µmol, 1.0 equiv.) in acetic acid (1.1 mL), $NaBO_3 \cdot 4\ H_2O$ (21 mg, 0.14 mmol, 4.4 equiv.) was added and the reaction mixture was stirred at 25 °C in the dark for 2 h. The reaction was stopped by the addition of a saturated aqueous solution of $NaHCO_3$ (12 mL). H_2O (50 mL) was added and the mixture was extracted with EtOAc (2 × 50 mL). The combined organic layers were dried over Na_2SO_4,

filtered, and concentrated *in vacuo*. The crude product was purified by flash column chromatography (SiO_2, 100% EtOAc). The yield was not determined.

^{1}H NMR (800 MHz, CD_2Cl_2): δ / ppm = 7.90 (dd, J = 7.6, 1.0 Hz, 1H, H-C(6)), 7.74 (dd, J = 7.5, 1.2 Hz, 1H, H-C(2)), 7.65 (t, J = 7.6 Hz, 1H, H-C(1)), 7.41 (d, J = 8.6 Hz, 1H, H-C(17)), 7.26–7.21 (m, 12H, H-C(49 and 50)), 7.20–7.17 (m, 3H, H-C(51)), 7.12–7.10 (m, 2H, H-C(45)), 6.80–6.78 (m, 2H, H-C(44)), 6.78–6.76 (m, 1H, H-C(16)), 4.52 (d, J = 16.8 Hz, 1H, H_2-C(32)), 4.44 (ddd, J = 10.5, 8.2, 3.5 Hz, 1H, H_2-C(30)), 4.42–4.36 (m, 2H, H_2-C(39)), 4.32–4.28 (m, 2H, H_2-C(30) and H_2-C(32)), 4.21 (d, J = 2.0 Hz, 3H, H_2-C(19) and H_2-C(37), 4.15 (ddd, J = 10.0, 7.0, 4.4 Hz, 1H, H_2-C(19)), 4.07–4.04 (m, 2H, H_2-C(26)), 3.78-3.73 (m, 6H, H_2-C(25) and –CH_2O–), 3.71–3.63 (m, 5H, –CH_2O–), 3.62–3.58 (m, 3H, H_2-C(20) and –CH_2O–), 3.51–3.49 (m, 2H, –CH_2O–), 3.41–3.31 (m, 4H, –CH_2O–), 3.15 (d, J = 15.5 Hz, 1H, H-C(12) or H'-C(12)), 2.92 (ddd, J = 17.6, 8.3, 3.7 Hz, 2H, H_2-C(29) and H-C(12) or H'-C(12)), 2.87 (ddd, J = 17.6, 6.6, 3.4 Hz, 1H, H_2-C(29)), 2.81–2.78 (m, 2H, H_2-C(40)), 2.00 (s, 3H, H_3-C(14 or 14'))**, 1.42 (s, 3H, H_3-C(14 or 14')).

**overlapping with residual EtOAc signal

^{13}C NMR (201 MHz, CD_2Cl_2): δ / ppm = 182.6 (C(8)), 170.9 (C(31)), 170.4 (C(38)), 170.1 (C(9)), 158.5 (C(15)), 157.2 (C(43)), 154.0 (C(11)), 150.1 (C(4)), 147.5 (C(48)), 139.62**, 139.54 (C(46)), 137.9 (C(2)), 136.5**, 136.2 (C(17)), 132.8 (C(1)), 132.4 (C(45)), 131.3 (C(49 or 50)), 127.94**, 127.85 (C(49 or 50)), 126.2 (C(51)), 124.7 (C(6)), 124.1 (C(3)), 113.7 (C(44)), 112.9 (C(18)), 110.8 (C(16)), 96.5 (C(28 or 41)), 89.2 (C(28 or 41)), 79.2 (C(27 or 42)), 76.8 (C(27 or 42)), 71.8*, 71.4*, 71.07*, 71.03*, 70.8*, 70.6*, 70.0*, 69.7*, 69.0 (C(37)), 68.7 (C(32)), 68.1 (C(19)), 67.8 (C(26)), 64.7 (C(47)), 62.5 (C(30 or 39)), 62.4 (C(30 or 39)), 52.8 (C(13)), 49.8 (C(12)), 28.5 (C(14 or 14')), 26.7 (C(14 or 14')), 20.7 (C(29 or 40)), 20.6 (C(29 or 40)).

*ethylene glycol chain

**could not be assigned unambiguously

HRMS (ESI): *m/z* calc. for $[C_{68}H_{68}O_{14}S+NH_4]^+$: 1158.4668; found: 1158.4695 ($M+NH_4^+$).

Compound 71

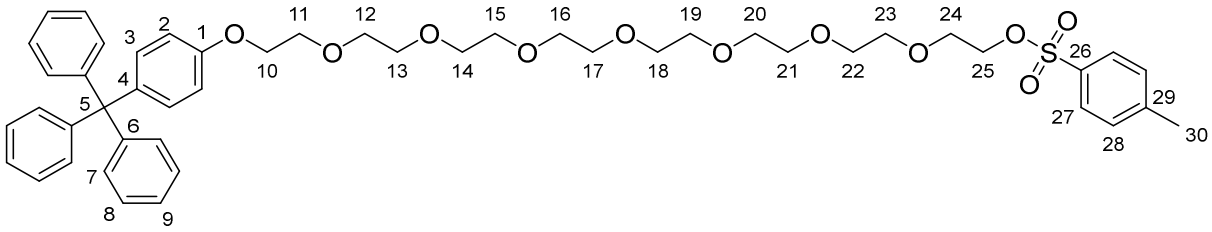

To a solution of compound **105** (402 mg, 0.584 mmol, 1.0 equiv.) in CH_2Cl_2 (6.0 mL) at 0 °C, 4-DMAP (8 mg, 0.07 mmol, 0.1 equiv.) and NEt_3 (0.40 mL, 2.9 mmol, 5.0 equiv.) were added, followed by the dropwise addition of *p*-TsCl (311 mg, 1.63 mmol, 2.8 equiv., dissolved in 2.0 mL CH_2Cl_2). The reaction mixture was stirred for 22.5 h while slowly warming to 23 °C. The reaction was stopped by the addition of aq. HCl (2 m, 50 mL). The mixture was extracted with CH_2Cl_2, the combined organic layers were washed with H_2O (2 × 100 mL) and brine (1 × 150 mL), dried over Na_2SO_4, filtered, and concentrated *in vacuo*. The crude product was purified by flash column chromatography (SiO_2, MeOH:CH_2Cl_2, 2:98) to give the tosylation product **71** (436 mg, 0.517 mmol, 89%) as brownish oil.

^{1}H NMR (400 MHz, CD_2Cl_2): δ / ppm = 7.80–7.76 (m, 2H, H-C(27)), 7.37 (d, J = 7.9 Hz, 2H, H-C(28)), 7.28–7.16 (m, 15H, H-C(7 and 8 and 9)), 7.14–7.09 (m, 2H, H-C(3)), 6.83–6.78 (m, 2H, H-C(2)), 4.15–4.10 (m, 2H, H_2-C(25)), 4.09 (dd, J = 5.6, 4.0 Hz, 2H, H_2-C(10)), 3.82–3.78 (m, 2H, H_2-C(11)), 3.69–3.61 (m, 6H, H_2-C(24) and –CH_2O–), 3.61–3.56 (m, 16H, –CH_2O–), 3.54 (s, 4H, –CH_2O–), 2.44 (s, 3H, H_3-C(20)).

^{13}C NMR (101 MHz, CD_2Cl_2): δ / ppm = 157.2 (C(1)), 147.6 (C(6)), 145.5 (C(29)), 139.5 (C(4)), 133.3 (C(26)), 132.5 (C(3)), 131.4 (C(7 or 8)), 130.3 (C(28)), 128.3 (C(27)), 127.9 (C(7 or 8)), 126.2 (C(9)), 113.7 (C(2)), 71.13*, 71.05*, 70.9 (m)*, 70.8*, 70.0 (C(11 or 25)), 69.9 (C(11 or 25)), 69.0 (C(24)), 67.8 (C(10)), 64.7 (C(5)), 21.8 (C(30)).

*ethylene glycol chain (C(12 to 23))

HRMS (ESI): *m/z* calc. for $[C_{48}H_{58}O_{11}S+NH_4]^+$: 806.4038; found: 860.4038 ($M+NH_4^+$).

Compound 72

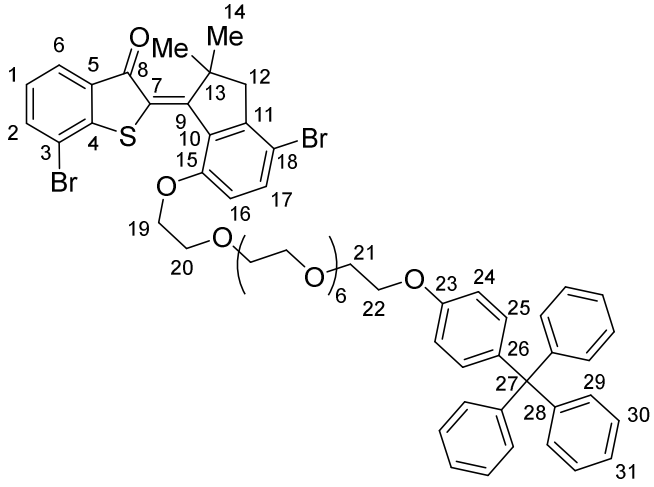

(*Z*)-isomer

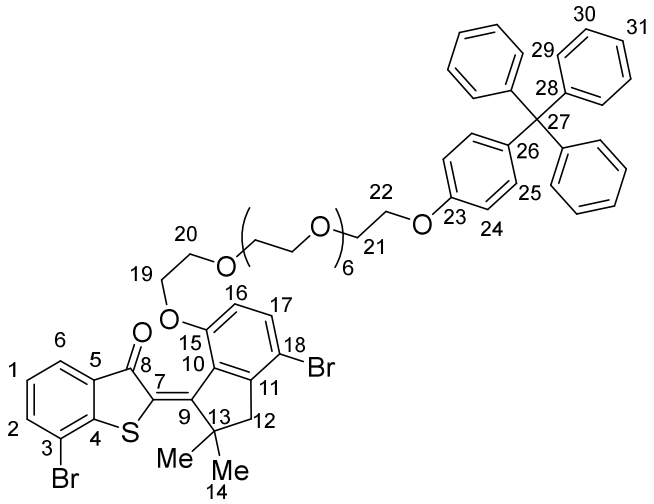

(*E*)-isomer

Compound **71** (395 mg, 0.469 mmol, 1.0 equiv.) was dissolved in dry DMF (5.0 mL) and TBAI (43 mg, 0.12 mmol, 0.26 equiv.), compound **59** (263 mg, 0.564 mmol, 1.2 eq) and K_2CO_3 (320 mg, 2.31 mmol, 4.9 equiv.) were added in this order. The reaction mixture was stirred at 90 °C for 16 h. The reaction was stopped by the addition of H_2O (50 mL) and the mixture was extracted with EtOAc (3 × 50 mL, 1 × 25 mL). The combined organic layers were washed with H_2O (3 × 100 mL) and brine (2 × 100 mL), dried over Na_2SO_4, filtered, and concentrated *in vacuo*. The crude product was purified by flash column chromatography (SiO_2, MeOH:CH_2Cl_2, 2:98) to give compound **72** (293 mg, mixture with residual linker) as a red oil, which was used in the next step without full characterization.

HRMS (ESI): *m/z* calc. for $[C_{60}H_{64}Br_2O_{10}S+NH_4]^+$: 1152.2925; found: 1152.2957 ($M+NH_4^+$).

Compound 73

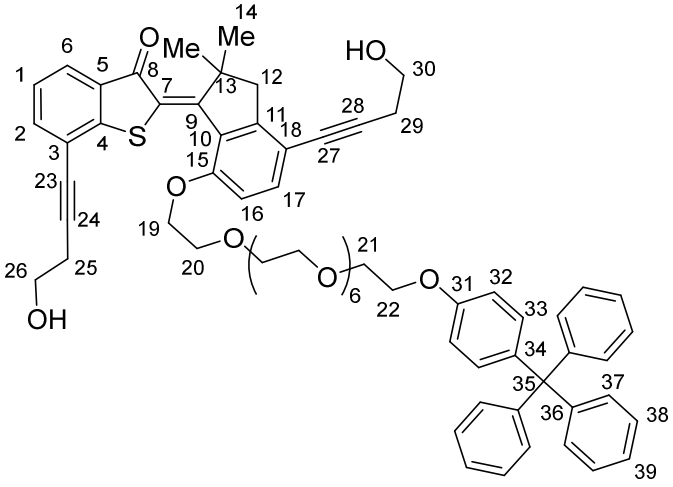

(*Z*)-isomer

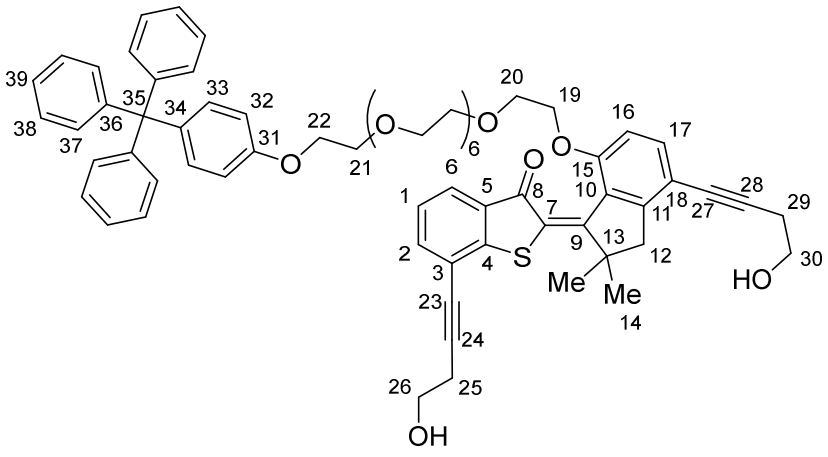

(*E*)-isomer

Compound **72** (285 mg, mixture with residual linker, see previous step), CuI (4 mg, 0.02 mmol) and XPhos Pd G2 (20 mg, 25 µmol) were added to a round bottom flask and the flask was sealed with a rubber septum. The flask was evacuated and refilled with dry nitrogen three times. Dry 1,4-dioxan (1.3 mL) and dry diisopropylamine (1.3 mL) were added and the flask was again carefully evacuated and refilled with dry nitrogen three times under vigorous stirring. 3-Butyn-1-ol (45 µL, 0.60 mmol) was added and the reaction mixture was stirred at 65 °C under nitrogen atmosphere for 6.5 h. The reaction mixture was allowed to cool to 23 °C and stirring was continued for 15 h. The reaction was stopped by the addition of a saturated aqueous solution of NH_4Cl (10 mL). H_2O (50 mL) was added and the mixture was extracted with CH_2Cl_2 (3 × 50 mL). The combined organic layers were dried over Na_2SO_4, filtered, and concentrated *in vacuo*. The crude product was purified by flash column chromatography (SiO_2, MeOH:CH_2Cl_2, 5:95) to give compound **73** (157 mg, 0.141 mmol, 30% over two steps) as an orange foam.

Note: Analysis was performed on an *E*:*Z* mixture (approx. 3:1).

(*E*)-isomer

^{1}H NMR (800 MHz, CD_2Cl_2): δ / ppm = 7.76 (dd, J = 7.7, 1.3 Hz, 1H, H-C(6)), 7.59 (dd, J = 7.5, 1.2 Hz, 1H, H-C(2)), 7.38 (d, J = 8.5 Hz, 1H, H-C(17)), 7.27–7.21 (m, 13H, H-C(1 and 37 and 38)), 7.20–7.14 (m, 3H, H-C(39)), 7.11 (dt, J = 8.7, 1.7 Hz, 2H, H-C(33)), 6.81–6.78 (m, 2H, H-C(32)), 6.75 (d, J = 8.5 Hz, 1H, H-C(16)), 4.21–4.13 (m, 2H, H_2-C(19)), 4.10–4.07 (m, 3H, H_2-C(22)), 3.85 (q, J = 6.2 Hz, 2H, H_2-C(26)), 3.81–3.76 (m, 4H, H_2-C(30 and 21)), 3.69–3.65 (m)*, 3.64–3.54 (m)*, 3.54–3.51 (m)*, 3.50 (dd, J = 5.6, 3.9 Hz)*, 3.43–3.40 (m)*, 3.35–3.23 (m)*, 3.15 (d, J = 16.0 Hz, 1H, H_2-C(12)), 2.93 (d, J = 15.9 Hz, 1H, H_2-C(12)), 2.78 (t, J = 6.3 Hz, 1H, H_2-C(25)), 2.69 (t, J = 6.4 Hz, 1H, H_2-C(29)), 1.73 (s, 3H, H_3-C(14)), 1.25 (s, 3H, H_3-C(14)).

^{13}C NMR (201 MHz, CD_2Cl_2): δ / ppm = 187.0 (C(8)), 157.8 (C(15)), 157.4 (C(9)), 157.2 (C(31)), 152.0 (C(11)), 147.5 (C(36)), 147.1 (C(4)), 139.5 (C(34)), 136.7 (C(2)), 135.2 (C(17)), 132.6 (C(5 or 7)), 132.4 (C(33)), 131.3 (C(37 or 38)), 128.5 (C(10)), 127.8 (C(37 or 38)), 126.4 (C(5 or 7)), 126.2 (C(39)), 125.4 (C(6)), 125.2 (C(1)), 119.2 (C(3)), 113.7 (C(32)), 112.6 (C(18)), 110.6 (C(16)), 94.7 (C(24)), 89.0 (C(28)), 79.8 (C(27)), 78.3 (C(23)), 71.2*, 71.1*, 70.9 (m)*, 70.8 (m)*, 70.7*, 70.5*, 70.0*, 69.7*, 68.0 (C(19)), 67.8 (C(22)), 64.7 (C(35)), 61.6 (C(30)), 61.4 (C(26)), 50.7 (C(13)), 49.3 (C(12)), 26.8 (C(14)), 26.3 (C(14)), 24.4 (C(25 or 29)), 24.3 (C(25 or 29)).

*octaethylene glycol chain (unambiguous assignment was not possible due to signal overlap of both isomers)

(*Z*)-isomer

^{1}H NMR (800 MHz, CD_2Cl_2): δ / ppm = 7.67 (dd, J = 7.7, 1.2 Hz, 1H, H-C(6)), 7.52 (dd, J = 7.4, 1.3 Hz, 1H, H-C(2)), 7.44 (d, J = 8.5 Hz, 1H, H-C(17)), 7.27–7.21 (m, 12H, H-C(37 and 38), 7.20–7.14 (m, 4H, H-C(1 and 39)), 7.11 (dt, J = 8.7, 1.7 Hz, 2H, H-C(33)), 6.85 (d, J = 8.7 Hz, 1H, H-C(16)), 6.81–6.78 (m, 2H, H-C(32)), 4.34 (t, J = 5.5 Hz, 2H, H2-C(19)), 4.01 (t, J = 5.5 Hz, 2H, H_2-C(20)), 3.81–3.76 (m, 4H, H_2-C(26 and 30)), 3.69–3.65 (m)*, 3.64–3.54 (m)*, 3.54–3.51 (m)*, 3.50 (dd, J = 5.6, 3.9 Hz)*, 3.43–3.40 (m)*, 3.35–3.23 (m)*, 3.02 (s, 2H, H_2-C(12)), 2.71 (t, J = 6.3 Hz, 2H, H_2-C(25)), 2.68–2.67 (m, overlapping with isomer, 2H, H_2-C(29)), 1.53 (s, 6H, H_3-C(14)).

^{13}C NMR (201 MHz, CD_2Cl_2): δ / ppm = 189.0 (C(8)), 162.8 (C(9)), 155.6 (C(15)), 153.2 (C(11)), 149.2 (C(4)), 147.5 (C(36)), 136.6 (C(2)), 136.4 (C(17)), 132.5 (C(5 or 7)), 132.4 (C(33)), 131.3 (C(37 or 38)), 129.2 (C(5 or 7)), 128.0 (C(11)), 127.8 (C(37 or 38)), 126.2 (C(39)), 125.2 (C(6)), 124.7 (C(1)), 118.6 (C(3)), 113.7 (C(32)), 113.2 (C(18)), 111.3 (C(16)), 94.9 (C(24)), 89.7 (C(28)), 79.5 (C(27)), 78.1 (C(23)), 71.2*, 71.1*, 70.9 (m)*, 70.8 (m)*, 70.7*, 70.5*, 70.0*, 69.7*, 69.5 (C(20)), 68.2 (C(19)), 67.8 (C(22)), 64.7 (C(35)), 61.6 (C(26 or 30)), 61.3 (C(26 or 30)), 51.3 (C(13)), 51.2 (C(12)), 26.6 (C(14)), 24.33 (C(25 or 29)), 24.27 (C(25 or 29)).

*octaethylene glycol chain (unambiguous assignment was not possible due to signal overlap of both isomers)

HRMS (ESI): *m/z* calc. for $[C_{68}H_{74}O_{12}S+NH_4]^+$: 1132.5239; found: 1132.5257 ($M+NH_4^+$).

Compound 76[158]

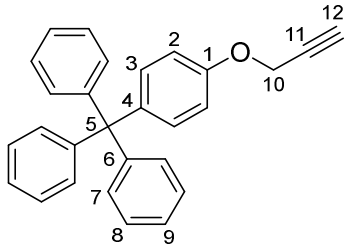

Tritylphenol (2.0 g, 5.9 mmol, 1.0 equiv.) was dissolved in acetone (85 mL). Propargyl bromide (1.3 g, 8.7 mmol, 1.5 equiv.) and K_2CO_3 (8.2 g, 59 mmol, 10 equiv.) were added and the mixture was stirred at 23 °C for 25 h. Acetone was removed under reduced pressure and the solid residue was distributed between $CHCl_3$ (100 mL) and H_2O (100 mL). The aqueous layer was separated and extracted with $CHCl_3$ (1 × 100 mL). The combined organic layers were dried over Na_2SO_4, filtered, and concentrated *in vacuo*. The crude product was purified by flash column chromatography (SiO_2, EtOAc:*i*-Hex, 2:98) to give compound **76** (1.4 g, 3.7 mmol, 63%) as a white solid.

R_f (EtOAc:*i*-Hex, 10:90): 0.63.

^{1}H NMR (500 MHz, CD_2Cl_2): δ / ppm = 7.29–7.22 (m, 12H, H-C(7 and 8)), 7.22–7.18 (m, 3H, H-C(9)), 7.18–7.15 (m, 2H, H-C(3)), 6.89–6.84 (m, 2H, H-C(2)), 4.68 (d, J = 2.5 Hz, 2H, H_2-C(10)), 2.58 (t, J = 2.4 Hz, 1H, H-C(12)).

^{13}C NMR (126 MHz, CD_2Cl_2): δ / ppm = 156.0 (C(1)), 147.5 (C(6)), 140.4 (C(4)), 132.5 (C(3)), 131.4 (C(7 or 8)), 127.9 (C(7 or 8)), 126.3 (C(9)), 114.0 (C(2)), 79.1 (C(11)), 75.6 (C(12)), 64.8 (C(5)), 56.2 (C(10)).

IR: $\tilde{\nu}$ / cm^{-1} = 3304 (w), 3029 (w, br), 1603 (w), 1504 (m), 1489 (m), 1442 (m), 1300 (w), 1223 (m), 1181 (m), 1029 (m), 699 (s), 671 (m).

HRMS (EI) *m/z*: calc. for $[C_{28}H_{22}O]^{\bullet+}$: 374.1665; found: 374.1665 ($M^{\bullet+}$).

Compound 77[159]

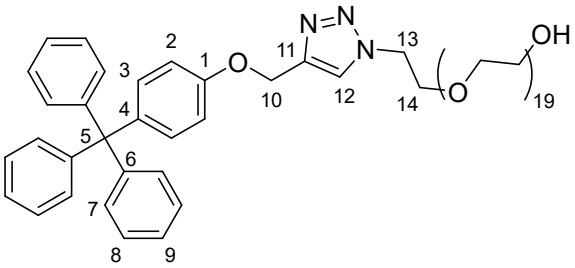

$Cu(MeCN)_4PF_6$ (6 mg, 0.02 mmol, 0.15 equiv.) and N_3-PEG_{20}-OH (125 mg, 0.135 mmol, 1.0 equiv.) were added to a Schlenk flask and the flask was evacuated and refilled with dry nitrogen. Dry MeCN (2.8 mL), dry CH_2Cl_2 (2.8 mL) and 2,6-lutidine (0.05 mL, 0.4 mmol, 3.0 equiv.) were added, followed by the addition of alkyne **76** (154 mg, 0.411 mmol, 3.0 equiv.). The reaction mixture was stirred under nitrogen atmosphere at 23 °C in the dark for 47 h. The volatiles were removed under reduced pressure and the solid residue was purified by flash column chromatography (SiO_2, MeOH:CH_2Cl_2, 5:95→10:90). Triazole **77** (0.16 g, 0.12 mmol, 86%) was obtained as a colorless oil.

^{1}H NMR (601 MHz, CD_2Cl_2): δ / ppm = 7.85 (s, 1H, H-C(12)), 7.27–7.21 (m, 12H, H-C(7 and 8)), 7.20–7.17 (m, 3H, H-C(9)), 7.16–7.13 (m, 2H, H-C(3)), 6.91–6.88 (m, 2H, H-C(2)), 5.14 (s, 2H, H_2-C(10)), 4.56–4.52 (m, 2H, H_2-C(13)), 3.89–3.85 (m, 2H, H_2-C(14)), 3.68–3.65 (m, 2H, –CH_2O–), 3.62–3.55 (m, 74H, –CH_2O–).

^{13}C NMR (151 MHz, CD_2Cl_2): δ / ppm = 156.9 (C(1)), 147.5 (C(6)), 144.0 (C(11)), 139.8 (C(4)), 132.5 (C(3)), 131.3 (C(7 or 8)), 127.9 (C(7 or 8)), 126.2 (C(9)), 124.5 (C(12)), 113.9 (C(2)), 72.9*, 70.9 (m)*, 70.8*, 70.7*, 69.8 (C(14)), 64.7 (C(5)), 62.2 (C(10)), 62.0*, 50.7 (C(13)).

*ethylene glycol chain

HRMS (ESI): *m/z* calc. for $[C_{68}H_{103}N_3O_{21}+H+NH_4]^{2+}$: 658.3748; found: 658.3750 ($M+H^+ +NH_4^+$).

Compound 78

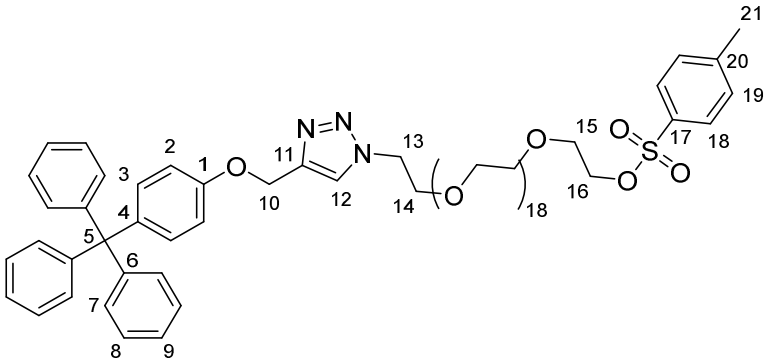

To a solution of compound **77** (370 mg, 0.28 mmol, 1.0 equiv.) in CH_2Cl_2 (3.0 mL) at 0 °C, 4-DMAP (10 mg, 0.08 mmol, 0.3 equiv.) and NEt_3 (0.20 mL, 1.4 mmol, 5.0 eq) were added, followed by the addition of *p*-TsCl (139 mg, 0.729 mmol, 2.6 eq). The reaction mixture was stirred at 0 °C for 90 min, then at 23 °C for 46 h. The volatiles were removed under removed pressure and the residue was purified by automated flash column chromatography (SiO_2, MeOH:CH_2Cl_2, 2:98→15:85). The tosylation product **78** was obtained as a light-yellow oil (373 mg, 0.26 mmol, 93%).

^{1}H NMR (600 MHz, CD_2Cl_2): δ / ppm = 7.85 (s, 1H, H-C(12)), 7.78 (d, J = 8.4 Hz, 2H, H-C(18)), 7.37 (d, J = 8.1 Hz, 2H, H-C(19)), 7.27–7.21 (m, 12H, H-C(7 and 8)), 7.21–7.17 (m, 3H, H-C(9)), 7.16–7.12 (m, 2H, H-C(3)), 6.91–6.88 (m, 2H, H-C(2)), 5.14 (s, 2H, H_2-C(10)), 4.54 (t, J = 5.1 Hz, 2H, H_2-C(13)), 4.14–4.11 (m, 2H, H_2-C(16)), 3.87 (t, J = 5.1 Hz, 2H, H_2-C(14)), 3.66–3.63 (m, 2H, H_2-C(15)), 3.60–3.58 (m, 50H, –CH_2O–), 3.58–3.55 (m, 18H, –CH_2O–), 3.54 (s, 4H, –CH_2O–), 2.45 (s, 3H, H_3-C(21)).

^{13}C NMR (151 MHz, CD_2Cl_2): δ / ppm = 156.9 (C(1)), 147.5 (C(6)), 145.5 (C(20)), 144.0 (C(11)), 139.9 (C(4)), 133.3 (C(17)), 132.5 (C(3)), 131.3 (C(7 or 8)), 130.3 (C(19)), 128.3 (C(18)), 127.9 (C(7 or 8)), 126.2 (C(9)), 124.5 (C(12)), 114.0 (C(2)), 71.0*, 70.9 (br, m)*, 70.79*, 70.77*, 69.9 (C(16)), 69.8 (C(14)), 69.0 (C(15)), 64.7 (C(5)), 62.3 (C(10)), 50.7 (C(13)), 21.8 (C(21)).

*ethylene glycol chain

HRMS (ESI): *m/z* calc. for $[C_{75}H_{109}N_3O_{23}S+H+NH_4]^{2+}$: 735.3792; found: 735.3799 ($M+H^+ +NH_4^+$).

Compound (*E*/*Z*)-81

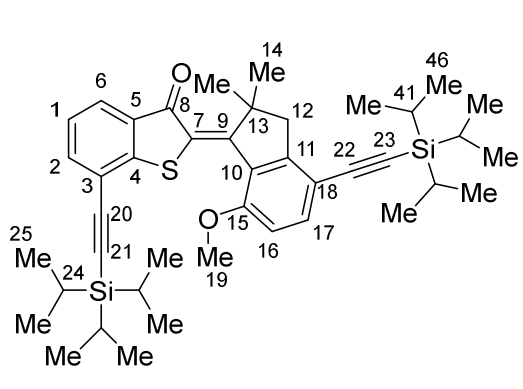

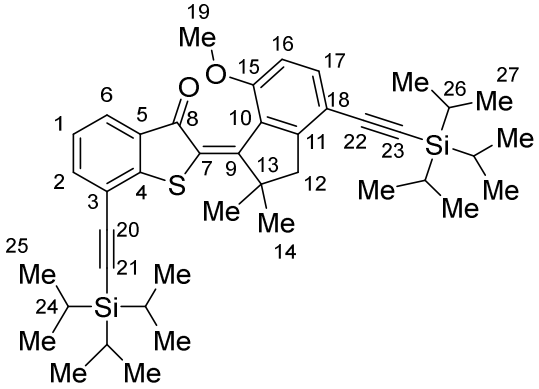

Compound **58** (196 mg, 0.408 mmol, 1.0 eq), CuI (9 mg, 0.05 mmol, 0.1 equiv.) and XPhos Pd G2 (34 mg, 0.043 mmol, 0.1 equiv.) were added to a round bottom flask equipped with a septum and magnetic stir bar. The flask was evacuated and refilled with argon three times. Dry 1,4-dioxane (2 mL) and diisopropylamine (2 mL) were added. The mixture was stirred at 23 °C for 10 min before TIPS-acetylene (0.23 mL, 1.0 mmol, 2.5 eq) was added. The reaction mixture was stirred at 65 °C for 51 h, then at 23 °C for 18 h. The reaction was stopped by the addition of a saturated aqueous solution of NH_4Cl (10 mL). H_2O was added and the mixture was extracted with CH_2Cl_2 (3 × 50 mL). The combined organic layers were dried over Na_2SO_4, filtered, and concentrated *in vacuo*. The crude product was purified by automated flash column chromatography (SiO_2, EtOAc:*i*-Hex, 1:99→10:90) to give compound **81** (mixture of (*E*)- and (*Z*)-isomers, 211 mg, 0.309 mmol, 76%) as a red oil.

Note: NMR-analysis was performed on an *E*:*Z* mixture (approx. 2:1).

(*Z*)-isomer:

^{1}H NMR (601 MHz, $CDCl_3$): δ / ppm = 7.72 (dd, J = 7.7, 1.2 Hz, 1H, H-C(6)), 7.60 (dd, J = 7.4, 1.2 Hz, 1H, H-C(2)), 7.53 (d, J = 8.6 Hz, 1H, H-C(17)), 7.17 (dd, J = 8.0, 7.2 Hz, 1H, H-C(1)), 6.76 (d, J = 8.6 Hz, 1H, H-C(16)), 3.95 (s, 3H, H_3-C(19)), 3.04 (s, 2H, H_2-C(12)), 1.56 (s, 6H, H_3-C(14)), 1.18 (s, 42H, H_3-C(25 and 27) and H-C(24 and 26)).

^{13}C NMR (151 MHz, $CDCl_3$): δ / ppm = 188.9 (C(8)), 162.9 (C(9)), 156.3 (C(15)), 153.5 (C(11)), 149.5 (C(4)), 137.1 (C(2)), 136.7 (C(17)), 132.4 (C(3)), 129.2 (C(7)), 127.8 (C(18)), 125.6 (C(6)), 124.3 (C(1)), 118.3 (C(5)), 113.0 (C(10)), 109.4 (C(16)), 104.2 (C(22)), 102.48 (C(20)), 97.8 (C(21 or 23)), 93.2 (C(21 or 23)), 54.8 (C(19)), 51.3 (C(12 and 13)), 26.6 (C(14)), 18.9*, 18.8*, 11.5*, 11.4*.

*Due to signal overlap between both isomers, the *i*-Pr signals could not be assigned unambiguously.

(*E*)-isomer:

^{1}H NMR (601 MHz, $CDCl_3$): δ / ppm = 7.80 (dd, J = 7.6, 1.2 Hz, 1H, H-C(6)), 7.62 (dd, J = 7.5, 1.2 Hz, 1H, H-C(2)), 7.46 (d, J = 8.5 Hz, 1H, H-C(17)), 7.22 (dd, J = 7.9, 7.1 Hz, 1H, H-C(1)), 6.73 (d, J = 8.5 Hz, 1H, H-C(16)), 3.84 (s, 3H, H_3-C(19)), 3.17 (d, J = 16.1 Hz, 1H, H_2-C(12)), 2.92 (d, J = 16.0 Hz, 1H, H_2-C(12)), 1.70 (s, 3H, H_3-C(14)), 1.26 (s, 3H, H_3-C(14)), 1.14–1.11 (m, 42H, H_3-C(25 and 27) and H-C(24 and 26)).

^{13}C NMR (151 MHz, $CDCl_3$): δ / ppm = 186.9 (C(8)), 158.7 (C(15)), 157.0 (C(9)), 152.1 (C(11)), 148.0 (C(4)), 136.1 (C(2)), 135.6 (C(17)), 132.4 (C(3)), 128.2 (C(18)), 126.4 (C(7)), 125.7 (C(6)), 124.6 (C(1)), 119.0 (C(5)), 112.4 (C(10)), 109.5 (C(16)), 104.7 (C(22)), 102.52 (C(20)), 98.5 (C(21 or 23)), 92.4 (C(21 or 23)), 55.4 (C(19)), 50.4 (C(13)), 49.3 (C(12)), 26.6 (C(14)), 26.3 (C(14)), 18.9*, 18.8*, 11.5*, 11.4*.

*Due to signal overlap between both isomers, the *i*-Pr signals could not be assigned unambiguously.

HRMS (APPI): *m/z* calc. for $[C_{42}H_{58}O_2SSi_2+H]^+$: 683.3769; found: 683.3787 ($M+H^+$).

Compound (*E*/*Z*)-82

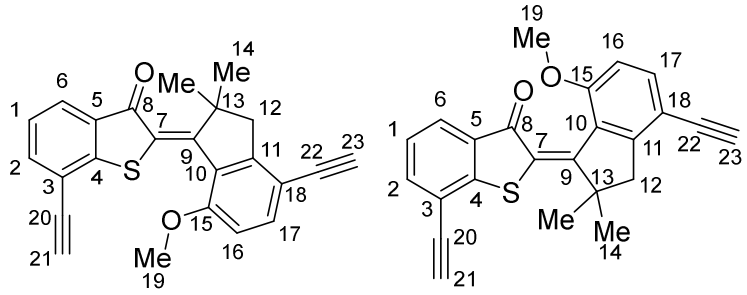

To a solution of compound **81** (97 mg, 0.14 mmol, 1.0 equiv.) in THF (3 mL), TBAF • 3 H_2O (132 mg, 0.418 mmol, 3.0 equiv.) was added at 0 °C. The reaction mixture was stirred at 0 °C for 3.5 h, then the reaction was stopped by the addition of a saturated aqueous solution of NH_4Cl (50 mL). The mixture was extracted with EtOAc (2 × 50 mL). The combined organic layers were washed with H_2O (2 × 50 mL) and brine (1 × 50 mL), dried over Na_2SO_4, filtered, and concentrated *in vacuo*. The crude product was purified by automated flash column chromatography (SiO_2, EtOAc:*i*-Hex, 1:99→25:75) to give (*Z*)-**82** (17 mg, 0.046 mmol) and (*E*)-**82** (35 mg, 0.094 mmol) separately as yellow oils (combined yield: 52 mg, 0.14 mmol, quant.).

Note: NMR-analysis was performed on an *E*:*Z* mixture (approx. 3:1).

(*Z*)-isomer:

^{1}H NMR (601 MHz, $CDCl_3$): δ / ppm = 7.76 (dd, J = 7.7, 1.2 Hz, 1H, H-C(6)), 7.62 (dd, J = 7.5, 1.2 Hz, 1H, H-C(2)), 7.54 (d, J = 8.5 Hz, 1H, H-C(17)), 7.18 (t, J = 7.6 Hz, 1H, H-C(1)), 6.79 (d, J = 8.5 Hz, 1H, H-C(16)), 4.01 (s, 3H, H_3-C(19)), 3.43 (s, 1H, H-C(21)), 3.18 (s, 1H, H-C(23)), 3.07 (s, 2H, H_2-C(12)), 1.56 (s, 6H, H3-C(14)).

^{13}C NMR (151 MHz, $CDCl_3$): δ / ppm = 188.7 (C(8)), 162.8 (C(9)), 156.6 (C(15)), 153.7 (C(11)), 149.3 (C(4)), 137.5 (C(2)), 136.9 (C(17)), 132.5 (C(5)), 129.0 (C(7)), 127.8 (C(10)), 126.1 (C(6)), 124.5 (C(1)), 116.9 (C(3)), 111.4 (C(18)), 109.9 (C(16)), 83.6 (C(21)), 81.1 (C(22)), 79.6 (C(23)), 79.5 (C(20)), 54.9 (C(19)), 51.4 (C(13)), 51.0 (C(12)), 26.7 (C(14)), 26.3 (C(14)).

(*E*)-isomer:

^{1}H NMR (601 MHz, $CDCl_3$): δ / ppm = 7.85 (dd, J = 7.7, 1.2 Hz, 1H, H-C(6)), 7.65 (dd, J = 7.4, 1.2 Hz, 1H, H-C(2)), 7.48 (d, J = 8.5 Hz, 1H, H-C(17)), 7.24 (t, J = 7.6 Hz, 1H, H-C(1)), 6.76 (d, J = 8.6 Hz, 1H, H-C(16)), 3.86 (s, 3H, H_3-C(19)), 3.51 (s, 1H, H-C(21)), 3.18 (d, J = 14.9 Hz, 1H, H_2-C(12)), 3.15 (s, 1H, H-C(23)), 2.96 (d, J = 15.4 Hz, 1H, H_2-C(12)), 1.74 (s, 3H, H_3-C(14)), 1.29–1.24 (m, 3H, H_3-C(14)).

^{13}C NMR (151 MHz, $CDCl_3$): δ / ppm = 186.7 (C(8)), 159.0 (C(15)), 157.1 (C(9)), 152.4 (C(11)), 147.4 (C(4)), 137.0 (C(2)), 135.8 (C(17)), 132.5 (C(5)), 128.3 (C(10)), 126.3 (C(6)), 126.0 (C(7)), 124.8 (C(1)), 117.5 (C(3)), 110.7 (C(18)), 109.7 (C(16)), 83.8 (C(21)), 81.6 (C(22)), 79.7 (C(20)), 79.1 (C(23)), 55.4 (C(19)), 50.6 (C(13)), 49.1 (C(12)), 26.7 (C(14)), 26.3 (C(14)).

HRMS (APPI): *m/z* calc. for $[C_{24}H_{18}O_2S+H]^+$: 371.1100; found: 371.1123 ($M+H^+$).

Compound 83[160]

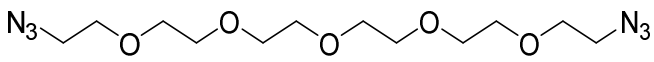

In a dried Schlenk flask under argon atmosphere, hexaethylene glycol (1.3 mL, 5.2 mmol, 1.0 equiv.) was dissolved in dry CH_2Cl_2 (10 mL). At 0 °C, triethylamine (2.3 mL, 17 mmol, 3.3 equiv.) and mesyl chloride (0.95 mL, 12 mmol, 2.3 equiv.) were added. The mixture was allowed to warm to 23 °C and was stirred at this temperature for 24 h. The reaction was

stopped by the addition of aq. HCl (0.5 M, 50 mL). The mixture was extracted with CH_2Cl_2 (2 × 50 mL). The combined organic layers were washed with a saturated aqueous solution of $NaHCO_3$ (1 × 100 mL), H_2O (1 × 100 mL) and brine (1 × 100 mL), dried over Na_2SO_4, filtered, and concentrated *in vacuo*. The residue was dissolved in dry DMF (12 mL). Sodium azide (860 mg, 13.2 mmol, 2.5 equiv.) was added and the reaction mixture was stirred at 65 °C under nitrogen atmosphere for 30 min, more DMF (8 mL) was added and stirring was continued for 19 h. The mixture was allowed to cool to ambient temperature and Et_2O (50 mL) was added. The precipitate was removed by filtration and the filtrate was washed with H_2O (3 × 50 mL) and brine (3 × 50 mL). The organic layer was dried over Na_2SO_4, filtered, and concentrated *in vacuo*. Diazide **83** was obtained as a light-yellow oil (518 mg, 1.56 mmol, 30%).

^{1}H NMR (400 MHz, $CDCl_3$): δ / ppm = 3.69–3.64 (m, 20H), 3.38 (t, J = 5.1 Hz, 4H).

Compound (*Z*)-84

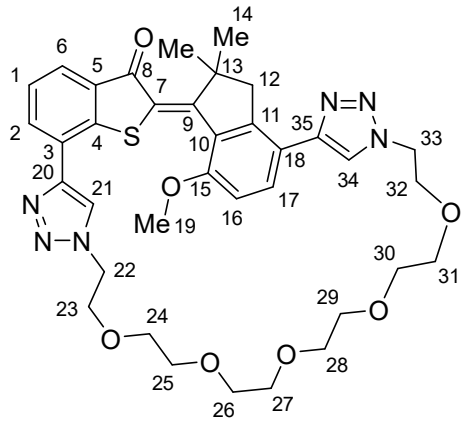

Compound **82** (70 mg, 0.19 mmol, 1.0 equiv.), TBTA (51 mg, 0.10 mmol, 0.5 equiv.) and $CuSO_4$ • 5 H_2O (8 mg, 0.03 mmol, 0.2 equiv.) were added to a round bottom flask. The flask was evacuated and refilled with nitrogen a total of three times. DMF (9 mL) was added and compound **83** (67 mg dissolved in 0.5 mL DMF, 0.20 mmol, 1.05 equiv.) was added to the mixture. The reaction mixture was stirred under nitrogen atmosphere at 23 °C in the dark for 3 d. A saturated aqueous solution of NH_4Cl (50 mL) was added and the mixture was extracted with EtOAc (2 × 50 mL) and CH_2Cl_2 (2 × 50 mL). The combined organic layers were washed with H_2O (2 × 200 mL) and brine (2 × 200 mL), dried over Na_2SO_4, filtered, and concentrated *in vacuo*. After purification by automated flash column chromatography (SiO_2, MeOH:CH_2Cl_2, 1:99→10:90) followed by supercritical fluid chromatography (SiO_2,

MeOH:CO_2, 10:90→40:60), compound (*Z*)-**84** (4 mg, 0.006 mmol, 3%) was obtained as a yellow oil.

^{1}H NMR (601 MHz, CD_2Cl_2): δ / ppm = 8.33 (dd, *J* = 7.6, 1.3 Hz, 1H, H-C(2)), 8.26 (s, 1H, H-C(21)), 8.06 (d, *J* = 8.6 Hz, 1H, H-C(17)), 8.01 (s, 1H, H-C(34)), 7.78 (dd, *J* = 7.6, 1.3 Hz, 1H, H-C(6)), 7.37 (t, *J* = 7.6 Hz, 1H, H-C(1)), 7.01 (d, *J* = 8.7 Hz, 1H, H-C(16)), 4.64–4.61 (m, 2H, H_2-C(22)), 4.61–4.58 (m, 2H, H_2-C(33)), 4.00 (s, 3H, H_3-C(19)), 3.86–3.83 (m, 2H, H_2-C(32)), 3.83–3.80 (m, 2H, H_2-C(23)), 3.60–3.56 (m, 2H, H_2-C(31)), 3.54–3.49 (m, 4H, H_2-C(24 and 30)), 3.38–3.33 (m, 4H, H_2-C(25) and H_2-C(26 or 27 or 28 or 29)), 3.22–3.19 (m, 2H, H_2-C(26 or 27 or 28 or 29)), 3.19 (s, 2H, H_2-C(12)), 3.06 (ddd, *J* = 5.9, 4.8, 1.2 Hz, 2H, H_2-C(26 or 27 or 28 or 29)), 3.01 (ddd, *J* = 5.9, 4.8, 1.2 Hz, 2H, H_2-C(26 or 27 or 28 or 29)), 1.57 (s, 6H, H_3-C(14)).

^{13}C NMR (151 MHz, CD_2Cl_2): δ / ppm = 188.8 (C(8)), 162.9 (C(9)), 156.4 (C(15)), 147.5 (C(11)), 145.6 (C(35)), 144.3 (C(20)), 142.9 (C(4)), 133.4 (C(3 or 5)), 132.6 (C(2 or 17)), 132.5 (C(2 or 17)), 128.8 (C(7 or 10 or 18)), 128.6 (C(7 or 10 or 18)), 126.2 (C(3 or 5)), 125.4 (C(1 or 6)), 125.2 (C(1 or 6)), 123.4 (C(21)), 123.0 (C(34)), 121.3 (C(10 or 18)), 110.8 (C(16)), 71.1*, 70.9*, 70.8*, 70.7*, 70.5*, 70.4*,**, 70.3*, 69.8 (C(23 or 32)), 69.5 (C(23 or 32)), 55.2 (C(19)), 51.92 (C(13)), 51.87 (C(12)), 50.9 (C(22)), 50.7 (C(33)), 26.6 (C(14)).

*C(24 or 25 or 26 or 27 or 28 or 29 or 30 or 31)

**two carbon atoms (judging by signal intensity)

HRMS (APPI): *m/z* calc. for $[C_{36}H_{42}N_6O_7S+H]^+$: 703.2908; found: 703.2915 ($M+H^+$).

Compound (*E*/*Z*)-87

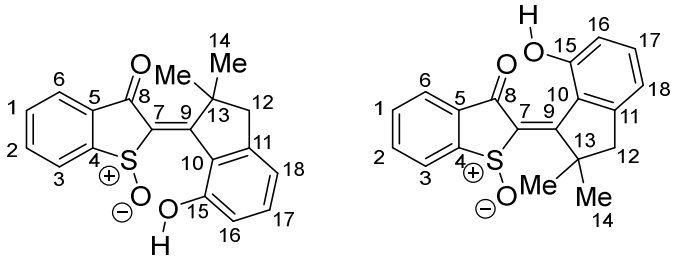

(*Z*)-isomer (*E*)-isomer

At 0 °C, TBAF • 3 H_2O (210 mg, 0.666 mmol, 2.5 equiv.) was added to a solution of compound **95** (119 mg, 0.271 mmol, 1.0 equiv.) in THF. The reaction mixture was stirred at 0 °C for 2 h and the reaction was stopped by the addition of a saturated aqueous solution of NH_4Cl (25 mL). The mixture was extracted with EtOAc (3 × 25 mL). The combined organic layers were dried over Na_2SO_4, filtered, and concentrated *in vacuo*. The crude product was purified by automated flash column chromatography (SiO_2, MeOH:CH_2Cl_2, 1:99→5:95). Compound **87** (mixture of (*E*)- and (*Z*)-isomers, 70 mg, 0.22 mmol, 81%) was obtained as a yellow solid.

Note: Analysis was performed on an *E:Z* mixture (approx. 1:1).

R_f (MeOH:CH_2Cl_2, 2:98): 0.18.

(*Z*)-isomer

^{1}H NMR (601 MHz, CD_2Cl_2): δ / ppm = 8.00 (dt, J = 7.6, 1.1 Hz, 1H, H-C(6)), 7.98 (dt, J = 7.7, 0.9 Hz, 1H, H-C(3)), 7.83 (td, J = 7.4, 1.2 Hz, 1H, H-C(2)), 7.73 (td, J = 7.4, 1.1 Hz, 1H, H-C(1)), 6.92 (dd, J = 8.3, 7.2 Hz, 1H, H-C(17)), 6.72 (d, J = 7.2 Hz, 1H, H-C(18)), 6.26 (d, J = 8.2 Hz, 1H, H-C(16)), 3.18 (d, J = 15.8 Hz, 1H, H_2-C(12)), 2.87 (d, J = 15.8 Hz, 1H, H_2-C(12)), 1.57 (s, 3H, H_3-C(14)), 1.56 (s, 3H, H_3-C(14)).

^{13}C NMR (151 MHz, CD_2Cl_2): δ / ppm = 184.7 (C(8)), 173.2 (C(9)), 156.8 (C(15)), 151.2 (C(11)), 148.6 (C(4)), 137.9 (C(7)), 136.2 (C(5)), 135.52 (C(17)), 135.50 (C(2)), 132.5 (C(1)), 126.56 (C(3)), 125.0 (C(6)), 123.3 (C(10)), 116.0 (C(18)), 115.5 (C(16)), 52.4 (C(13)), 50.9 (C(12)), 28.4 (C(14)), 25.6 (C(14)).

(*E*)-isomer

^{1}H NMR (601 MHz, CD_2Cl_2): δ / ppm = 8.08 (d, J = 7.6 Hz, 1H, H-C(3)), 8.07 (d, J = 7.5 Hz, 1H, H-C(6)), 7.91 (td, J = 7.5, 1.2 Hz, 1H, H-C(2)), 7.77 (td, J = 7.5, 1.1 Hz, 1H, H-C(1)), 7.50 (t, J = 7.8, 7.4 Hz, 1H, H-C(17)), 7.01 (d, J = 7.2 Hz, 1H, H-C(18)), 6.94 (d, J = 8.2 Hz, 1H, H-C(16)), 3.28 (d, J = 15.1 Hz, 1H, H_2-C(12)), 2.91 (d, J = 15.3 Hz, 1H, H_2-C(12)), 1.99 (s, 3H, H_3-C(14)), 1.47 (s, 3H, H_3-C(14)).

^{13}C NMR (151 MHz, CD_2Cl_2): δ / ppm = 189.7 (C(8)), 176.4 (C(9)), 160.0 (C(15)), 152.7 (C(11)), 148.9 (C(4)), 137.2 (C(7)), 136.6 (C(17)), 136.5 (C(2)), 135.4 (C(5)), 133.2 (C(1)), 129.5 (C(10)), 127.2 (C(3)), 126.64 (C(6)), 119.3 (C(16)), 118.0 (C(18)), 54.7 (C(13)), 50.5 (C(12)), 29.3 (C(14)), 27.9 (C(14)).

IR: $\tilde{\nu}$ / cm^{-1} = 3100–2200 (m, br), 1684 (m), 1588 (s), 1544 (s), 1455 (s), 1279 (s), 1158 (m), 1078 (m), 998 (s), 831 (m), 775 (s), 745 (s).

HRMS (APPI): *m/z* calc. for $[C_{19}H_{16}O_3S]^+$: 324.0820; found: 324.0811 (M^+).

Deprotonation of Compound 87

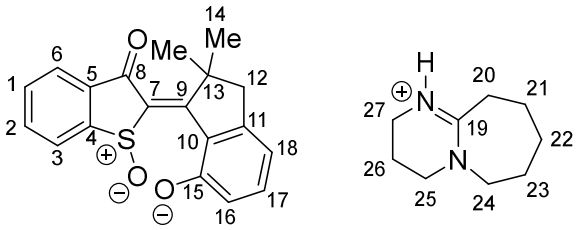

To a solution of compound **87** (5 mg, 15 µmol, 1.0 equiv.) in CD_2Cl_2 (0.6 mL), DBU (0.5 M in CD_2Cl_2, 31 µL, 16 mmol, 1.1 equiv.) was added to give a deep red solution of the organic salt.

^{1}H NMR (601 MHz, CD_2Cl_2): δ / ppm = 7.84 (d, J = 7.8 Hz, 2H, H-C(3 and 6)), 7.71 (t, J = 7.4 Hz, 1H, H-C(1 or 2)), 7.59 (d, J = 7.5 Hz, 1H, H-C(1 or 2)), 7.17 (t, J = 7.7 Hz, 1H, H-C(17)), 6.46 (d, J = 8.8 Hz, 1H, H-C(16)), 6.33 (d, J = 7.3 Hz, 1H, H-C(18)), 3.40–3.36 (m, 2H, H_2-C(24)), 3.34 (t, J = 5.9 Hz, 2H, H_2-C(25)), 3.29 (t, J = 5.8 Hz, 2H, H_2-C(27)), 3.03 (d, J = 15.5 Hz, 1H, H_2-C(12)), 2.77 (d, J = 15.6 Hz, 1H, H_2-C(12)), 2.75–2.71 (m, 2H, H_2-C(20)), 1.91 (p, J = 5.9 Hz, 2H, H_2-C(26)), 1.69–1.64 (m, 2H, H_2-C(22)), 1.61 (q, J = 5.4 Hz, 4H, H_2-C(21 and 23)), 1.57 (s, 3H, H_3-C(14)), 1.50 (s, 3H, H_3-C(14)).

^{13}C NMR (151 MHz, CD_2Cl_2): δ / ppm = 184.9 (C(8)), 174.9 (C(9)), 170.1 (C(15)), 166.4 (C(19)), 152.0 (C(11)), 150.6 (C(4 or 5)), 136.7 (C(4 or 5)), 136.0 (C(17)), 134.9 (C(7)), 134.3 (C(1 or 2)), 131.2 (C(1 or 2)), 125.9 (C(3 or 6)), 125.3 (C(10)), 124.0 (C(3 or 6)), 119.3 (C(16)), 108.9 (C(18)), 54.5 (C(24)), 51.0 (C(13)), 50.9 (C(12)), 48.9 (C(25)), 38.6 (C(27)), 32.5 (C(20)), 29.5 (C(22)), 28.9 (C(14)), 27.3 (C(21 or 23)), 25.5 (C(14)), 24.6 (C(21 or 23)), 20.1 (C(26)).

Compound 88[64]

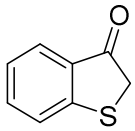

In a dried flask under argon atmosphere, triflic acid (6.0 mL, 68 mmol, 4.6 equiv.) was added to a solution of (phenylthio)acetic acid (2.49 g, 14.8 mmol, 1.0 equiv.) in dry 1,2-DCE (22 mL). The reaction mixture was stirred at 23 °C for 10 min and then at 40 °C for 5 h. The reaction mixture was poured into ice water (300 mL) followed by extraction with CH_2Cl_2 (3 × 100 mL). The combined organic layers were washed with a saturated aqueous solution of $NaHCO_3$ (1 × 300 mL) and brine (1 × 300 mL), dried over Na_2SO_4, filtered, and concentrated *in vacuo*. Benzothiophenone **88** (1.77 g, 11.8 mmol, 80%) was obtained as a light-brown solid.

^{1}H NMR (400 MHz, $CDCl_3$): δ / ppm = 7.78 (ddd, J = 7.8, 1.4, 0.8 Hz, 1H), 7.55 (ddd, J = 8.5, 7.1, 1.4 Hz, 1H), 7.43 (dt, J = 8.0, 0.9 Hz, 1H), 7.22 (ddd, J = 8.0, 7.1, 1.0 Hz, 1H), 3.79 (s, 2H).
^{13}C NMR (101 MHz, $CDCl_3$): δ / ppm = 200.2, 154.4, 135.8, 131.1, 126.8, 124.7, 39.4.
HRMS (APPI): *m/z* calc. for $[C_8H_6OS+H]^+$: 151.0212; found: 151.0231 ($M+H^+$).

Compound 89

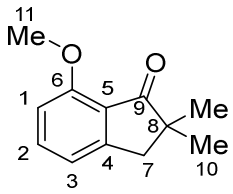

In a dried flask under nitrogen atmosphere, a slurry of NaH (60% in mineral oil, 645 mg, 16.1 mmol, 2.3 equiv.) in dry 2-Me-THF (40 mL) was prepared. 7-Methoxy-1-indanone (1.13 g, 6.97 mmol, 1.0 equiv.) was added at 0 °C and the reaction mixture was stirred at 0 °C for 1 h. Iodomethane (0.85 mL, 14 mmol, 2.0 equiv.) was added and stirring was continued at 0 °C for 2 h. The mixture was allowed to warm to 22 °C and stirred at this temperature for 21 h. The reaction was stopped by the addition of H_2O (1 × 100 mL). The mixture was extracted with EtOAc (3 × 100 mL), the combined organic layers were dried over Na_2SO_4, filtered, and concentrated *in vacuo*. The crude product was purified by automated flash column chromatography (SiO_2, EtOAc:*i*-Hex, 2:98→20:80). Compound **89** was obtained as an off-white solid (1.13 g, 5.94 mmol, 85%).

R_f (EtOAc:*i*-Hex, 10:90): 0.15.

^{1}H NMR (500 MHz, $CDCl_3$): δ / ppm = 7.51 (t, J = 7.9 Hz, 1H, H-C(2)), 6.96 (dd, J = 7.5, 0.9 Hz, 1H, H-C(3)), 6.78 (d, J = 8.7 Hz, 1H, H-C(1)), 3.94 (s, 3H, H_3-C(11)), 2.94 (s, 2H, H_2-C(7)), 1.21 (s, 6H, H_3-C(10)).

^{13}C NMR (126 MHz, $CDCl_3$): δ / ppm = 209.3 (C(9)), 158.6 (C(6)), 154.9 (C(4)), 136.5 (C(2)), 123.5 (C(5)), 118.5 (C(3)), 109.0 (C(1)), 55.9 (C(11)), 45.7 (C(8)), 42.7 (C(7)), 25.6 (C(10)).

IR: $\tilde{\nu}$ / cm^{-1} = 2920 (w, br), 1701 (m), 1590 (m), 1484 (m), 1280 (m), 1195 (s), 1063 (m), 981 (m), 776 (m).

HRMS (APPI): *m/z* calc. for $[C_{12}H_{14}O_2+H]^+$: 191.1067; found: 191.1078 ($M+H^+$).

Compound (*E*/*Z*)-90

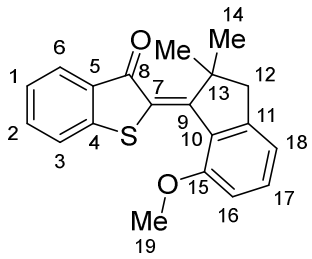

(*Z*)-isomer

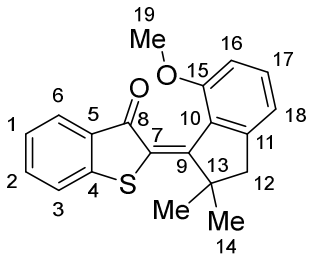

(*E*)-isomer

In a dried Schlenk flask under argon atmosphere, a solution of benzothiophenone **88** (161 mg, 1.07 mmol, 1.1 equiv.) in dry CH_2Cl_2 (3.0 mL) was prepared (flask A). In a second dried Schlenk flask under argon atmosphere, a solution of indanone **89** (185 mg, 0.972 mmol, 1.0 eq) in dry CH_2Cl_2 (2.0 mL) was prepared (flask B). At −78 °C, BCl_3 (1.0 M in CH_2Cl_2, 1.1 mL, 1.1 mmol, 1.1 eq) was added to flask A under stirring. The reaction mixture was then immediately taken up by syringe and added to flask B at −78 °C. The reaction mixture was stirred at −78 °C for 2 min, then at 0 °C for 75 min. The reaction was stopped by the addition of H_2O (5 mL). The mixture was diluted with H_2O (50 mL) and extracted with EtOAc (3 × 50 mL). The combined organic layers were dried over Na_2SO_4, filtered, and concentrated *in vacuo*. The crude product was purified by automated flash column chromatography (SiO_2, EtOAc:*i*-Hex, 1:99→12:88). Compound **90** was obtained as an orange solid (mixture of (*E*)- and (*Z*)-isomers, 187 mg, 0.580 mmol, 60%). The product was used in the next synthetic step without full characterization.

Crystals of the (*E*)-isomer suitable for X-ray crystallography could be obtained by slow evaporation from EtOAc/*i*-Hex.

HRMS (APPI): *m/z* calc. for $[C_{20}H_{18}O_2S+H]^+$: 323.1100; found: 323.1142 ($M+H^+$).

Compound (*E*/*Z*)-91

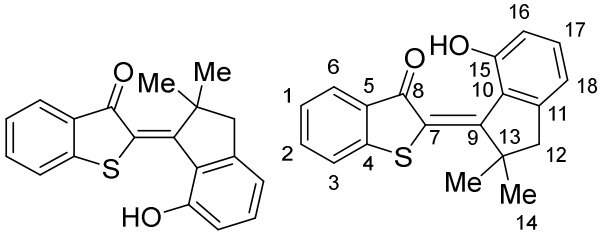

In a dried Schlenk flask under argon atmosphere, a solution of compound **88** (262 mg, 1.74 mmol, 1.1 equiv.) in dry CH_2Cl_2 (4 mL) was prepared (flask A). In a second dried Schlenk flask under argon atmosphere, a solution of compound **89** (306 mg, 1.61 mmol, 1.0 eq) in dry CH_2Cl_2 (3 mL) was prepared (flask B). At −78 °C, BCl_3 (1 M in CH_2Cl_2, 1.70 mL, 1.70 mmol, 1.1 eq) was added to flask A under stirring. The reaction mixture was then immediately transferred *via* transfer cannula to flask B, which was kept at 0 °C. The reaction mixture was stirred at 0 °C under argon atmosphere for 1 h, then BBr_3 (1 M in CH_2Cl_2, 1.60 mL, 1.60 mmol, 1.0 eq) was added and stirring was continued at 0 °C for 1 h. The reaction was stopped by the addition of H_2O (10 mL). The mixture was diluted with H_2O (100 mL) and extracted with EtOAc (3 × 100 mL). The combined organic layers were dried over Na_2SO_4, filtered, and concentrated *in vacuo*. The crude product was purified by automated flash column chromatography (SiO_2, EtOAc:*i*-Hex, 1:99→10:90). Compound **91** was obtained as a red foam (mixture of *E*- and *Z*-isomers, 185 mg, 0.600 mmol, 37%).

R_f (EtOAc:*i*-Hex, 20:80): 0.72.

(*E*)-Isomer

^{1}H NMR (601 MHz, CD_2Cl_2) δ / ppm = 8.13 (s, 1H, -O*H*), 8.02 (ddd, J = 7.9, 1.4, 0.7 Hz, 1H, H-C(6)), 7.65 (ddd, J = 8.3, 7.1, 1.3 Hz, 1H, H-C(2)), 7.60 (dt, J = 8.0, 1.0 Hz, 1H, H-C(3)), 7.48 (dd, J = 8.1, 7.2 Hz, 1H, H-C(17)), 7.36 (ddd, J = 7.9, 7.0, 1.0 Hz, 1H, H-C(1)), 7.01–7.00 (m, 1H, H-C(16 or 18)), 6.99 (t, J = 1.0 Hz, 1H, H-C(16 or 18)), 3.08 (s, 2H, H_2-C(12)), 1.58 (s, 6H, H_3-C(14)).

^{13}C NMR (151 MHz, CD_2Cl_2) δ / ppm = 191.1 (C(8)), 166.6 (C(9)), 160.8 (C(15)), 151.9 (C(11)), 145.2 (C(4)), 135.4 (C(2)), 134.9 (C(17)), 132.5 (C(5)), 129.9 (C(10)), 127.5 (C(6)), 125.6 (C(7)), 125.3 (C(1)), 123.3 (C(3)), 119.8 (C(16)), 117.6 (C(18)), 53.1 (C(13)), 50.2 (C(12)), 27.6 (C(14)).

HRMS (APPI): *m/z* calc. for $[C_{19}H_{16}O_2S+H]^+$: 309.0944; found: 309.0950 ($M+H^+$).

Compound 92

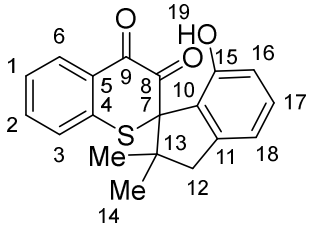

Compound **91** (110 mg, 0.357 mmol, 1.0 equiv.) was dissolved in AcOH (10 mL). $NaBO_3 \bullet 4\ H_2O$ (223 mg, 1.45 mmol, 4.1 equiv.) was added and the reaction mixture was stirred at 23 °C in the dark for 2.5 h. The reaction was stopped by the addition of a saturated aqueous solution of $NaHCO_3$ (100 mL). The mixture was extracted with EtOAc (2 × 50 mL). The combined organic layers were dried over Na_2SO_4, filtered, and concentrated *in vacuo*. The crude product was purified by automated flash column chromatography (SiO_2, EtOAc:*i*-Hex, 2:98→20:80). Compound **92** (10 mg, 31 µmol, 9%) was obtained as a yellow solid that crystallized from CD_2Cl_2 solution. The structure was determined by X-ray diffraction.

^{1}H NMR (400 MHz, CD_2Cl_2): δ / ppm = 8.00 (dd, J = 7.9, 1.8 Hz, 1H, Ar-H), 7.58–7.51 (m, 1H, Ar-H), 7.35–7.24 (m, 3H, Ar-H), 6.87–6.80 (m, 2H, Ar-H), 6.61 (s, 1H, -OH), 3.21 (d, J = 16.9 Hz, 1H, H_2-C(12)), 2.68 (d, J = 15.9 Hz, 1H, H_2-C(12)), 1.31 (s, 3H, H_3-C(14)), 1.07 (s, 3H, H_3-C(14)).

HRMS (APPI): *m/z* calc. for $[C_{19}H_{16}O_3S+H]^+$: 325.0893; found: 325.0901 ($M+H^+$).

Compound (*E*/*Z*)-93

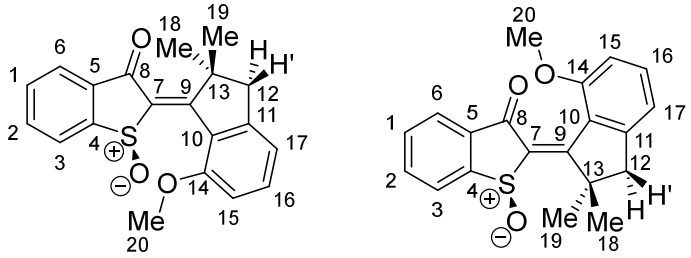

(*Z*)-isomer (*rac*) (*E*)-isomer (*rac*)

Compound **90** (91 mg, 0.28 mmol, 1.0 equiv.) was dissolved in AcOH (10 mL). $NaBO_3 \bullet 4\ H_2O$ (182 mg, 1.18 mmol, 4.2 equiv.) was added and the reaction mixture was stirred at 23 °C in the dark for 2 h. The reaction was stopped by the slow addition of a saturated aqueous solution of $NaHCO_3$ (50 mL). The mixture was extracted with EtOAc

(2 × 50 mL). The combined organic layers were dried over Na_2SO_4, filtered, and concentrated *in vacuo*. The crude product was purified by automated flash column chromatography (SiO_2, EtOAc:*i*-Hex, 20:80→80:20). (*E*)-**93** (38 mg, 0.11 mmol) and (*Z*)-**93** (53 mg, 0.16 mmol) were obtained separately as yellow solids (combined yield: 91 mg, 0.27 mmol, 96%).

(*E*)-isomer

^{1}H NMR (601 MHz, CD_2Cl_2): δ / ppm = 8.06 (d, J = 7.7 Hz, 1H, H-C(3)), 7.99 (ddd, J = 7.5, 1.2, 0.7 Hz, 1H, H-C(6)), 7.85 (td, J = 7.5, 1.2 Hz, 1H, H-C(2)), 7.74 (td, J = 7.5, 1.0 Hz, 1H, H-C(1)), 7.45 (dd, J = 8.4, 7.3 Hz, 1H, H-C(16)), 6.96 (ddt, J = 7.4, 1.4, 0.8 Hz, 1H, H-C(17)), 6.81 (d, J = 8.3 Hz, 1H, H-C(15)), 3.82 (s, 3H, H_3-C(20)), 3.26 (d, J = 15.3 Hz, 1H, H-C(12) or H'-C(12)), 2.83 (d, J = 15.3 Hz, 1H, H-C(12) or H'-C(12)), 1.95 (s, 3H, H_3-C(18 or 19)), 1.38 (s, 3H, H_3-C(18 or 19)).

^{13}C NMR (151 MHz, CD_2Cl_2): δ / ppm = 183.2 (C(8)), 169.6 (C(9)), 159.5 (C(14)), 150.8 (C(11)), 149.5 (C(4)), 139.9 (C(7)), 136.0 (C(5)), 135.1 (C(2)), 134.6 (C(16)), 132.7 (C(1)), 128.0 (C(10)), 127.2 (C(3)), 125.2 (C(6)), 117.4 (C(17)), 109.4 (C(15)), 55.4 (C(20)), 52.8 (C(13)), 50.0 (C(12)), 28.3 (C(18 or 19)), 26.2 (C(18 or 19)).

HRMS (APPI): *m/z* calc. for $[C_{20}H_{18}O_3S+H]^+$: 339.1049; found: 339.1079 ($M+H^+$).

(*Z*)-isomer

^{1}H NMR (601 MHz, CD_2Cl_2): δ / ppm = 8.00 (dt, J = 7.7, 0.9 Hz, 1H, H-C(3)), 7.96 (ddd, J = 7.7, 1.2, 0.7 Hz, 1H, H-C(6)), 7.83 (td, J = 7.5, 1.2 Hz, 1H, H-C(2)), 7.71–7.67 (m, 1H, H-C(1)), 7.52 (dd, J = 8.3, 7.3 Hz, 1H, H-C(16)), 6.97 (ddt, J = 7.4, 1.5, 0.8 Hz, 1H, H-C(17)), 6.90 (d, J = 8.3 Hz, 1H, H-C(15)), 4.09 (s, 3H, H_3-C(20)), 3.18 (d, J = 16.0 Hz, 1H, H'-C(12) or H-C(12)), 2.86 (d, J = 15.9 Hz, 1H, H'-C(12) or H-C(12)), 1.53 (s, 3H, H_3-C(18 or 19)), 1.52 (s, 3H, H_3-C(18 or 19)).

^{13}C NMR (151 MHz, CD_2Cl_2): δ / ppm = 185.2 (C(8)), 170.3 (C(9)), 157.9 (C(14)), 151.8 (C(11)), 150.8 (C(4)), 143.5 (C(7)), 136.2 (C(5)), 135.5 (C(2 or 16)), 135.4 (C(2 or 16)), 132.1 (C(1)), 126.6 (C(3)), 125.6 (C(10)), 124.8 (C(6)), 117.9 (C(17)), 109.3 (C(15)), 55.2 (C(20)), 52.2 (C(13)), 50.8 (C(12)), 28.3 (C(18 or 19)), 25.5 (C(18 or 19)).

HRMS (APPI): *m/z* calc. for $[C_{20}H_{18}O_3S+H]^+$: 339.1049; found: 339.1089 ($M+H^+$).

Compound (*E*/*Z*)-95

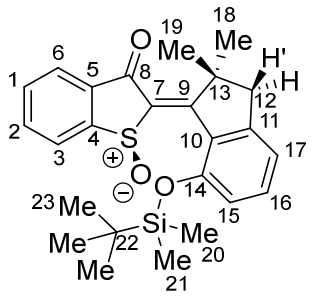

(*Z*)-isomer (*rac*) (*E*)-isomer (*rac*)

Note: Only the (*S*)-configured enantiomers are shown for clarity.

1) Silylation

To a solution of compound **91** (285 mg, 0.924 mmol, 1.0 eq) in DMF (4 mL), TBSCl (182 mg, 1.21 mmol, 1.3 equiv.) and 1*H*-imidazole (175 mg, 2.57 mmol, 2.8 equiv.) were added. The reaction mixture was stirred at 22 °C in the dark for 41.5 h. The reaction mixture was diluted with H_2O (50 mL) and extracted with EtOAc (3 × 50 mL). The combined organic layers were washed with H_2O (3 × 100 mL) and brine (1 × 100 mL), dried over Na_2SO_4, filtered, and concentrated *in vacuo*. After automated flash column chromatography (SiO_2, EtOAc:*i*-Hex, 1:99→10:90), compound **94** was obtained in a red oil (238 mg), which also contained residual starting material. The product was used in the next step without further purification.

HRMS (APPI): *m/z* calc. for $[C_{25}H_{30}O_2SSi+H]^+$: 423.1809; found: 423.1808 ($M+H^+$).

2) Oxidation

Compound **94** (mixture with compound **91**) (238 mg) was dissolved in acetic acid (20 mL) and $NaBO_3$ • 4 H_2O (328 mg, 2.13 mmol) was added. The reaction mixture was stirred at 23 °C in the dark for 2 h. The reaction was stopped by the addition of a saturated aqueous solution of $NaHCO_3$ (120 mL). The mixture was extracted with EtOAc (2 × 120 mL), washed with H_2O (2 × 200 mL) and brine (1 × 200 mL), dried over Na_2SO_4, filtered, and concentrated *in vacuo*. The crude product was purified by automated flash column chromatography (SiO_2, EtOAc:*i*-Hex, 5:95→50:50). (*E*)-**95** was obtained as a yellow solid (87 mg, 0.198 mmol) and (*Z*)-**95** was obtained as a viscous orange oil (42 mg, 0.096 mmol) (combined yield of 129 mg, 0.294 mmol, 32% over two steps).

(*E*)-isomer

^{1}H NMR (601 MHz, CD_2Cl_2) δ / ppm = 8.06 (dt, J = 7.7, 0.9 Hz, 1H, H-C(3)), 7.98–7.95 (m, 1H, H-C(6)), 7.84 (ddd, J = 7.7, 7.3, 1.2 Hz, 1H, H-C(2)), 7.72 (td, J = 7.4, 1.0 Hz, 1H, H-C(1)), 7.35 (dd, J = 8.3, 7.2 Hz, 1H, H-C(16)), 6.97 (d, J = 7.3 Hz, 1H, H-C(17)), 6.76 (d, J = 8.2 Hz, 1H, H-C(15)), 3.26 (d, J = 15.1 Hz, 1H, H-C(12) or H'-C(12)), 2.82 (d, J = 15.2 Hz, 1H, H-C(12) or H'-C(12)), 1.96 (s, 3H, H_3-C(18 or 19)), 1.38 (s, 3H, H_3-C(18 or 19)), 0.71 (s, 9H, H_3-C(23)), -0.01 (s, 3H, H_3-C(20 or 21)), -0.05 (s, 3H, H_3-C(20 or 21)).

^{13}C NMR (151 MHz, CD_2Cl_2) δ / ppm = 182.5 (C(8)), 170.5 (C(9)), 156.3 (C(14)), 150.4 (C(11)), 149.4 (C(4)), 139.3 (C(7)), 135.8 (C(5)), 135.2 (C(2)), 133.9 (C(16)), 132.4 (C(1)), 131.2 (C(10)), 127.2 (C(3)), 125.8 (C(6)), 118.9 (C(15)), 118.2 (C(17)), 52.9 (C(13)), 50.1 (C(12)), 28.2 (C(18 or 19)), 26.4 (C(18 or 19)), 25.9 (C(23)), 18.6 (C(22)), -3.5 (C(20 or 21)), -4.0 (C(20 or 21)).

HRMS (APPI): *m/z* calc. for $[C_{25}H_{30}O_3SSi+H]^+$: 439.1758; found: 439.1770 ($M+H^+$).

(*Z*)-isomer

^{1}H NMR (601 MHz, CD_2Cl_2): δ / ppm = 8.01 (dt, J = 7.7, 0.9 Hz, 1H, H-C(3)), 7.97 (ddd, J = 7.7, 1.2, 0.7 Hz, 1H, H-C(6)), 7.83 (td, J = 7.5, 1.2 Hz, 1H, H-C(2)), 7.72–7.68 (m, 1H, H-C(1)), 7.41 (dd, J = 8.2, 7.3 Hz, 1H, H-C(16)), 6.98 (d, J = 7.3 Hz, 1H, H-C(17)), 6.86 (d, J = 8.2 Hz, 1H, H-C(15)), 3.18 (d, J = 15.8 Hz, 1H, H_2-C(12)), 2.84 (d, J = 15.8 Hz, 1H, H_2-C(12)), 1.53 (s, 3H, H_3-C(18) or H_3-C(19)), 1.50 (s, 3H, H_3-C(18) or H_3-C(19)), 0.87 (s, 9H, H_3-C(23)), 0.20 (s, 3H, H_3-C(20) or H_3-C(21)), 0.19 (s, 3H, H_3-C(20) or H_3-C(21)).

^{13}C NMR (151 MHz, CD_2Cl_2): δ / ppm = 184.7 (C(8)), 171.2 (C(9)), 154.6 (C(14)), 151.4 (C(11)), 150.9 (C(4)), 143.6 (C(7)), 136.2 (C(5)), 135.5 (C(2)), 134.8 (C(16)), 132.2 (C(1)), 129.0 (C(10)), 126.9 (C(3)), 124.9 (C(6)), 119.1 (C(15)), 118.8 (C(17)), 52.5 (C(13)), 50.8 (C(12)), 27.8 (C(18 or 19)), 26.1 (C(23)), 25.6 (C(18 or 19)), 19.0 (C(22)), -3.1 (C(20 or 21)), -3.9 (C(20 or 21)).

HRMS (APPI): *m/z* calc. for $[C_{25}H_{30}O_3SSi+H]^+$: 439.1758; found: 439.1774 ($M+H^+$).

Compound (*Z*)-96

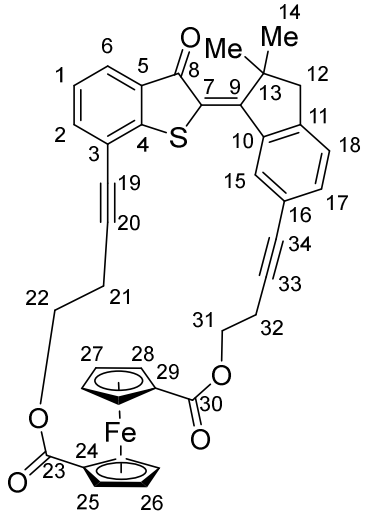

In a dried Schlenk flask under nitrogen atmosphere, compound **102** (0.13 g, 0.42 mmol, 1.0 equiv.) was dissolved in dry CH_2Cl_2 (90 mL). 4-DMAP (0.10 g,0.82 mmol, 2.0 equiv.) was added and the mixture was stirred at 23 °C for five minutes. Compound **101** (0.18 g,0.42 mmol, 1.0 equiv.) was added and the reaction mixture was stirred at 23 °C in the dark for 45 h. The volatiles were removed *in vacuo* and the residue was purified by flash column chromatography (SiO_2, MeOH:CH_2Cl_2, 1:99), followed by a second flash column chromatography step (SiO_2, CH_2Cl_2) to give compound (*Z*)-**96** (0.11 g, 0.17 mmol, 40%) as an orange solid.

R_f (MeOH:CH_2Cl_2, 2:98): 0.91.

^{1}H NMR (601 MHz, CD_2Cl_2): δ / ppm = 8.38 (s, 1H, H-C(15)), 7.75 (dd, J = 7.7, 1.2 Hz, 1H, H-C(6)), 7.61 (dd, J = 7.5, 1.2 Hz, 1H, H-C(2)), 7.45 (dd, J = 7.8, 1.4 Hz, 1H, 17), 7.28 (dq, J = 7.7, 1.1 Hz, 1H, H-C(18)), 7.25 (t, J = 7.6 Hz, 1H, H-C(1)), 4.88 (t, J = 2.0 Hz, 2H, H_2-C(25 or 28)), 4.86 (t, J = 2.0 Hz, 2H, H_2-C(25 or 28)), 4.51 (t, J = 7.6 Hz, 2H, H_2-C(22)), 4.46 (t, J = 7.3 Hz, 2H, H_2-C(31)), 4.42 (t, J = 2.0 Hz, 2H, H_2-C(26 or 27)), 4.38 (t, J = 2.0 Hz, 2H, H_2-C(26 or 27)), 3.09 (s, 2H, H_2-C(12)), 3.01 (t, J = 7.6 Hz, 2H, H_2-C(21)), 2.88 (t, J = 7.3 Hz, 2H, H_2-C(32)), 1.62 (s, 6H, H_3-C(14)).

^{13}C NMR (151 MHz, CD_2Cl_2): δ / ppm = 187.8 (C(8)), 169.8 (C(23)), 169.7 (C(30)), 163.3 (C(9)), 150.2 (C(11)), 147.7 (C(4)), 140.5 (C(10)), 137.2 (C(2)), 133.7 (C(17)), 132.6 (C(15)), 132.4 (C(5)), 126.7 (C(7)), 126.0 (C(6)), 125.7 (C(18)), 125.5 (C(1)), 122.8 (C(16)), 119.0 (C(3)), 93.2 (C(20)), 86.3 (C(33)), 82.3 (C(34)), 77.8 (C(21)), 74.0 (C(24 or 29)), 73.8 (C(24 or 29)), 72.52 (C(26 or 27)), 72.45 (C(26 or 27)), 71.99 (C(25 or 28)), 71.98 (C(25 or

28)), 62.8 (C(31)), 62.2 (C(22)), 51.6 (C(12)), 48.6 (C(13)), 25.4 (C(14)), 20.7 (C(21)), 20.3 (C(32)).

IR: $\tilde{\nu}$ / cm^{-1} = 2914 (w, br), 1709 (s), 1656 (m), 1515 (m), 1465 (m), 1266 (s), 1131 (s), 968 (m), 898 (m), 756 (s), 734 (m).

HRMS (APPI): *m/z* calc. for $[C_{39}H_{30}FeO_5S+H]^+$: 667.1236; found: 667.1247 ($M+H^+$).

Compound 99[73]

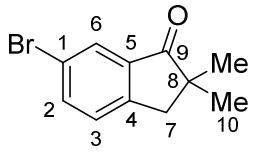

In a dried Schlenk flask under nitrogen atmosphere, a slurry of NaH (60% in mineral oil, 190 mg, 4.75 mmol, 2.7 equiv.) in dry THF (10 mL) was prepared. At 0 °C, 6-bromo-1-indanone (369 mg, 1.74 mmol, 1.0 equiv.) was added and the reaction mixture was stirred at 0 °C for 2 h. Iodomethane (0.24 mL, 3.9 mmol, 2.2 equiv.) was added dropwise and stirring was continued at 0 °C for 1 h, then at 23 °C for 20 h. The reaction was stopped by the addition of H_2O (10 mL). The mixture was extracted with EtOAc (3 × 100 mL). The combined organic layers were dried over Na_2SO_4, filtered, and concentrated *in vacuo*. The crude product was purified by flash column chromatography (SiO_2, EtOAc:*i*-Hex, 15:85). Compound **99** (298 mg, 1.25 mmol, 72%) was obtained as a pale yellow solid.

R_f (SiO_2, EtOAc:*i*-Hex, 20:80): 0.71.

^{1}H NMR (400 MHz, $CDCl_3$): δ / ppm = 7.86 (d, J = 2.0 Hz, 1H, H-C(6)), 7.67 (dd, J = 8.1, 2.0 Hz, 1H, H-C(2)), 7.31 (dd, J = 8.1, 0.8 Hz, 1H, H-C(3)), 2.93 (s, 2H, H_2-C(7)), 1.22 (s, 6H, H_3-C(10)).

^{13}C NMR (101 MHz, $CDCl_3$): δ / ppm = 210.0 (C(9)), 150.8 (C(4)), 137.7 (C(2)), 137.4 (C(5)), 128.4 (C(3)), 127.5 (C(6)), 121.7 (C(1)), 46.2 (C(8)), 42.6 (C(7)), 25.3 (C(10)).

IR: $\tilde{\nu}$ / cm^{-1} = 2956 (m), 2923 (m), 1712 (s), 1596 (m), 1466 (m), 1435 (s), 1414 (m), 1288 (m), 1254 (s), 1189 (s), 1172 (s), 1116 (s), 1051 (m), 1002 (m), 913 (w), 886 (m), 862 (m), 818 (vs), 768 (s), 727 (m).

HRMS (EI): *m/z* calc. for $[C_{11}H_{11}BrO]^+$: 237.9988; found: 237.9986 (M^+).

Compound (*E*/*Z*)-100[73]

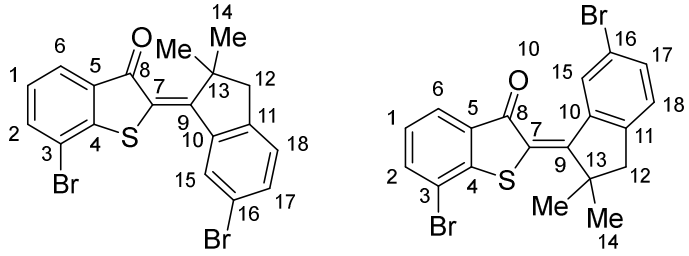

In a dried Schlenk flask (A) under nitrogen atmosphere, compound **50** (636 mg, 2.78 mmol, 1.1 equiv.) was dissolved in dry CH_2Cl_2 (5 mL). In a separate dried Schlenk flask (B) under nitrogen atmosphere, compound **99** (592 mg, 2.48 mmol, 1.0 equiv.) was dissolved in dry CH_2Cl_2 (2.5 mL). At −78 °C, BCl_3 (1.0 M in CH_2Cl_2, 2.8 mL, 2.8 mmol, 1.1 equiv.) was added to (A). The resulting mixture was immediately taken up by syringe and added to (B) at 0 °C. The reaction mixture was stirred at 0 °C for 1 h. The reaction was stopped by the addition of H_2O (20 mL). More H_2O (50 mL) was added and the mixture was extracted with EtOAc (3 × 100 mL). The combined organic layers were dried over Na_2SO_4, filtered, and concentrated *in vacuo*. The crude product was purified by flash column chromatography (SiO_2, EtOAc:*i*-Hex, 1:99) followed by recrystallization from *n*-heptane. Compound **100** (mixture of (*E*)- and (*Z*)-isomers, 652 mg, 1.45 mmol, 58%) was obtained as thin orange needles.

Note: Analysis was performed on an *E*:*Z* mixture (approx. 1:1).

(*Z*)-isomer

^{1}H NMR (400 MHz, $CDCl_3$): δ / ppm = 8.31 (d, J = 1.9 Hz, 1H, H-C(15)), 7.82 (dd, J = 7.7, 1.1 Hz, 1H, H-C(6)), 7.71 (dt, J = 7.7, 1.4 Hz, 1H, H-C(2)), 7.52 (dd, J = 12.9, 1.8 Hz, 1H, H-C(17)), 7.22–7.14 (m, 2H, H-C(1 and 18)), 3.03 (s, 2H, H_2-C(12)), 1.63 (s, 6H, H3-C(14)).

^{13}C NMR (101 MHz, $CDCl_3$): δ / ppm = 187.4 (C(8)), 163.6 (C(9)), 148.8 (C(11)), 146.1 (C(4)), 142.0 (C(7)), 137.1 (C(2)), 134.4 (C(17)), 133.9 (C(5)), 130.9 (C(15)), 127.0 (C(16)), 126.7 (C(1 or 18)), 126.3 (C(1 or 18)), 125.4 (C(6)), 121.1 (C(10)), 117.5 (C(3)), 51.0 (C(12)), 49.3 (C(13)), 25.4 (C(14)).

(*E*)-isomer

^{1}H NMR (400 MHz, $CDCl_3$): δ / ppm = 9.23 (d, J = 2.0 Hz, 1H, H-C(15)), 7.88 (dd, J = 7.7, 1.1 Hz, 1H, H-C(6)), 7.71 (dt, J = 7.7, 1.4 Hz, 1H, H-C(2)), 7.50 (dd, J = 12.8, 1.8 Hz, 1H, H-C(17)), 7.22–7.14 (m, 2H, H-C(1 and 18)), 2.96 (s, 2H, H_2-C(12)), 1.57 (s, 6H, H_3-C(14)).

^{13}C NMR (101 MHz, $CDCl_3$): δ / ppm = 187.5 (C(8)), 163.0 (C(9)), 147.2 (C(11)), 145.5 (C(4)), 139.9 (C(9)), 137.2 (C(2)), 134.7 (C(17)), 134.1 (C(5)), 131.7 (C(15)), 128.1 (C(16)), 126.9 (C(1 or 18)), 126.4 (C(1 or 18)), 125.7 (C(6)), 120.2 (C(10)), 117.2 (C(3)), 49.5 (C(13)), 49.0 (C(12)), 26.9 (C(14)).

HRMS (EI): *m/z* calc. for $[C_{19}H_{14}Br_2OS]^{\bullet+}$: 447.9127; found: 447.9129 ($M^{\bullet+}$).

Compound (*E*/*Z*)-101

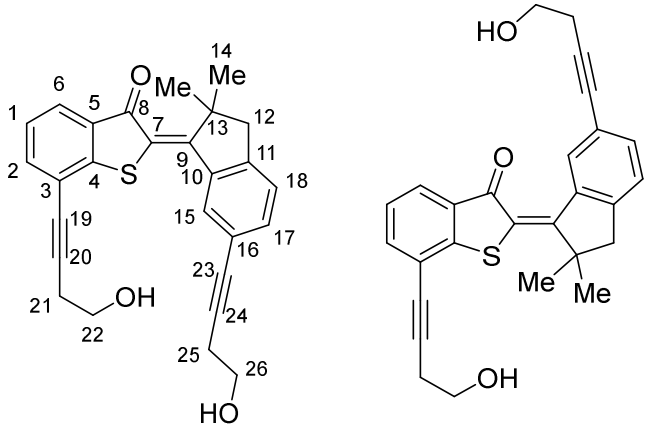

(*Z*)-isomer (*E*)-isomer

Copper(I) iodide (11 mg, 58 µmol, 0.1 equiv.), $Pd(PPh_3)_2Cl_2$ (35 mg, 50 µmol, 0.1 equiv.) and compound **100** (0.248 g, 0.551 mmol, 1.0 equiv.) were added to a round bottom flask. The flask was evacuated and refilled with nitrogen for a total of three times. THF (2.8 mL) and NEt_3 (2.8 mL) were added and the reaction mixture was purged with nitrogen for 5 min. 3-Butyn-1-ol (0.10 mL, 1.32 mmol, 2.4 equiv.) was added and the mixture was stirred at 60 °C under nitrogen atmosphere for 18.5 h. The reaction mixture was poured into a saturated aqueous solution of NH_4Cl (125 mL) and extracted with CH_2Cl_2 (3 × 125 mL). The combined organic layers were washed with brine (1 × 125 mL), dried over Na_2SO_4, filtered, and concentrated *in vacuo*. The residue was purified by flash column chromatography (SiO_2, CH_2Cl_2 → MeOH:CH_2Cl_2, 2:98) to give compound **101** (mixture of (*E*)- and (*Z*)-isomers, 0.179 g, 0.418 mmol, 76%) as an orange solid.
Crystals of the (*E*)-isomer could be obtained by slow evaporation from CH_2Cl_2 solution.

Note: NMR-analysis was performed on an *E*:*Z*-mixture (approx. 1:3).

(*Z*)-isomer

^{1}H NMR (400 MHz, CD_2Cl_2): δ / ppm = 8.26 (s, 1H, H-C(15)), 7.75 (dd, J = 7.7, 1.1 Hz, 1H, H-C(6)), 7.58 (dd, J = 7.6, 1.1 Hz, 1H, H-C(2)), 7.45 (dd, J = 7.9, 1.2 Hz, 1H, H-C(17)), 7.27 (d, J = 8.8 Hz, 1H, H-C(18)), 7.24 (t, J = 7.6 Hz, 1H, H-C(1)), 3.90 (t, J = 6.4 Hz, 2H, H_2-C(22)), 3.82 (t, J = 5.9 Hz, 2H, H_2-C(26)), 3.09 (s, 2H, H_2-C(12)), 2.81 (t, J = 6.4 Hz, 2H, H_2-C(21)), 2.71 (t, J = 5.9 Hz, 2H, H_2-C(25)), 1.62 (s, 6H, H_3-C(14)).

^{13}C NMR (101 MHz, CD_2Cl_2): δ / ppm = 187.8 (C(8)), 163.6 (C(9)), 150.2 (C(11)), 148.1 (C(4)), 140.5 (C(10)), 136.6 (C(2)), 134.6 (C(17)), 131.6 (C(15)), 125.9 (C(1 or 6 or 18)), 125.7 (C(1 or 6 or 18)), 125.6 (C(1 or 6 or 18)), 122.8 (C(16)), 119.2 (C(3)), 95.2 (C(20)), 87.6 (C(24)), 82.1 (C(23)), 78.2 (C(19)), 61.44 (C(22 or 26)), 61.36 (C(22 or 26)), 51.6 (C(12)), 48.8 (C(13)), 25.5 (C(14)), 24.4 (C(21 or 24)), 24.3 (C(21 or 24)).

Note: Carbon atoms C(5) and C(7) could not be assigned unambiguously from the isomeric mixture.

Compound 102[161]

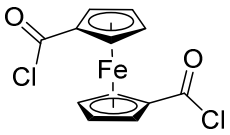

In a dried Schlenk flask under nitrogen atmosphere, a slurry of 1,1'-ferrocenedicarboxylic acid (2.3 g, 10 mmol, 1.0 equiv.) in dry CH_2Cl_2 (40 mL) was prepared. At 0 °C in the dark, dry pyridine (0.81 mL, 10 mmol, 1.0 equiv.) was added, followed by the slow addition of oxalyl chloride (1.7 mL, 20 mmol, 2.0 equiv.). The reaction mixture was stirred at 0 °C for 30 min, then at 25 °C for 40 h (Note: After 38 h more oxalyl chloride (0.85 mL, 10 mmol, 1.0 equiv.) was added). The volatiles were removed *in vacuo* and the solid residue was extracted with boiling *n*-heptane (3 × 50 mL). The combined organic layers were concentrated *in vacuo* and the residue was recrystallized from *n*-heptane. Compound **102** (1.04 g, 3.34 mmol, 33%) was obtained as red microcrystalline solid.

^{1}H NMR (400 MHz, $CDCl_3$): δ / ppm = 5.04 (t, J = 2.0 Hz, 4H), 4.76 (t, J = 2.0 Hz, 4H).

^{13}C NMR (101 MHz, $CDCl_3$): δ / ppm = 168.8, 76.3, 74.3.

Compound 103[122]

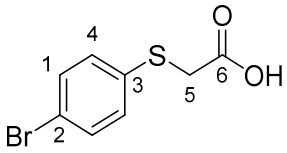

2-Bromoacetic acid (1.19 g, 8.61 mmol, 1.1 equiv.) was dissolved in acetone (80 mL). At 0 °C, K_2CO_3 (3.35 g, 24.2 mmol, 3.1 equiv.) and 4-bromo thiophenol (1.49 g, 7.88 mmol, 1.0 equiv.) were added. The reaction mixture was stirred at 0 °C for 2 h, then at 23 °C for 22.5 h. The reaction was stopped by the addition of aq. HCl (2 M, 125 mL) and the mixture was extracted with EtOAc (3 × 80 mL). The combined organic layers were dried over Na_2SO_4, filtered, and concentrated *in vacuo* to give compound **103** (1.87 g, 7.57 mmol, 96%) as a colorless solid.

^{1}H NMR (400 MHz, $(CD_3)_2SO$): δ / ppm = 12.81 (s, 1H, -CO_2H), 7.50 (dt, J = 8.7, 2.8, 2.1 Hz, 2H, H-C(1 or 4)), 7.29 (dt, J = 8.5, 2.9, 2.0 Hz, 2H, H-C(1 or 4)), 3.82 (s, 2H, H-C(5)).
^{13}C NMR (101 MHz, $(CD_3)_2SO$): δ / ppm = 170.4 (C(6)), 135.5 (C(3)), 131.8 (C(1 or 4)), 129.7 (C(1 or 4)), 118.8 (C(2)), 34.8 (C(5)).
HRMS (EI): *m*/*z* calc. for $[C_8H_7BrO_2S]^{\bullet+}$: 245.9345; found: 245.9345 ($M^{\bullet+}$).

Compound 104[122]

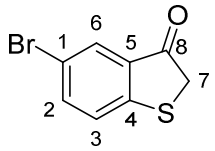

Compound **103** (1.50 g, 6.07 mmol, 1.0 equiv.) in $SOCl_2$ (4.0 mL, 55 mmol, 9.1 equiv.) was stirred at 80 °C for 2 h. Excess $SOCl_2$ was removed *in vacuo* and the residue was dissolved in 1,2-DCE (25 mL). At 0 °C, $AlCl_3$ (1.63 g,12.2 mmol, 2.0 equiv.) was added and the reaction mixture was stirred at 0 °C for 3 h. The reaction mixture was poured into ice water (200 mL), followed by extraction with CH_2Cl_2 (3 × 100 mL). The combined organic layers were dried over Na_2SO_4, filtered, and concentrated *in vacuo* to give compound **104** (1.33 g, 5.81 mmol, 96%) as a brown solid.

^{1}H NMR (400 MHz, CD_2Cl_2): δ / ppm = 7.85 (dd, J = 2.0, 0.6 Hz, 1H, H-C(6)), 7.65 (dd, J = 8.4, 2.1 Hz, 1H, H-C(2)), 7.34 (dd, J = 8.5, 0.6 Hz, 1H, H-C(3)), 3.83 (s, 2H, H_2-C(7)).
^{13}C NMR (101 MHz, CD_2Cl_2): δ / ppm = 198.8 (C(8)), 153.4 (C(4)), 138.6 (C(2)), 133.2 (C(5)), 129.4 (C(6)), 126.4 (C(3)), 118.6 (C(1)), 40.3 (C(7)).
HRMS (EI): *m/z* calc. for $[C_8H_5BrOS]^{\bullet+}$: 227.9239; found: 227.9239 ($M^{\bullet+}$).

Compound 105

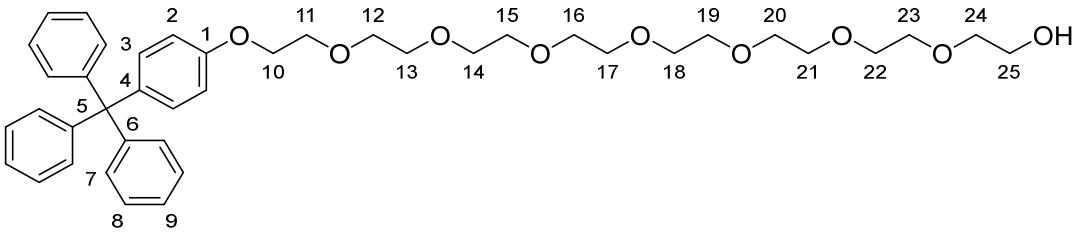

To a solution of octaethylene glycol monotosylate (**107**) (473 mg, 0.902 mmol, 0.8 equiv.) in DMF (10 mL), KI (72 mg, 0.43 mmol, 0.4 equiv.), 4-tritylphenol (370 mg, 1.10 mmol, 1.0 equiv.) and K_2CO_3 (616 mg, 4.46 mmol, 4.1 equiv.) were added. The reaction mixture was stirred at 90 °C for 16.5 h. The temperature was increased to 130 °C and stirring was continued for 6 h. TBAI (160 mg, 0.433 mmol, 0.4 equiv.) was added and stirring was continued for 17 h. Monitoring by TLC showed only little conversion. The temperature was reduced to 70 °C, acetone (10 mL) was added and stirring was continued at 70 °C for 6 h. The reaction was stopped by the addition of H_2O (150 mL). The mixture was extracted with EtOAc (3 × 100 mL). The combined organic layers were washed with H_2O (3 × 200 mL) and brine (1 × 200 mL), dried over Na_2SO_4, filtered, and concentrated *in vacuo*. The oily residue was purified by flash column chromatography (SiO_2, MeOH:CH_2Cl_2, 4:96) to give compound **105** (427 mg, 0.620 mmol, 69%) as a brown oil.

^{1}H NMR (400 MHz, CD_2Cl_2): δ / ppm = 7.28–7.16 (m, 15H, H-C(7 and 8 and 9)), 7.14–7.10 (m, 2H, H-C(3)), 6.82–6.78 (m, 2H, H-C(2)), 4.11–4.07 (m, 2H, H_2-C(10)), 3.82–3.78 (m, 2H, H_2-C(11)), 3.69–3.64 (m, 4H, -CH_2O-), 3.64–3.58 (m, 22H, -CH_2O-), 3.57–3.54 (m, 2H, -CH_2O-).
^{13}C NMR (101 MHz, CD_2Cl_2): δ / ppm = 157.2 (C(1)), 147.6 (C(6)), 139.6 (C(4)), 132.5 (C(3)), 131.4 (C(7 or 8)), 127.9 (C(7 or 8)), 126.2 (C(9)), 113.7 (C(2)), 72.9*, 71.1*, 70.9 (m)*, 70.7*, 70.0 (C(11)), 67.8 (C(10)), 64.7 (C(5)), 62.0*.
*ethylene glycol chain (C(12 to 25))
HRMS (ESI): *m/z* calc. for $[C_{41}H_{52}O_9+NH_4]^+$: 706.3950; found: 706.3959 ($M+NH_4^+$).

Tetraethylene glycol monotosylate (106)[162] *reported in ref.*[8]

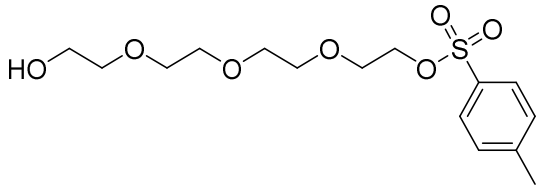

Tetraethylene glycol (37.1 g, 191 mmol, 11 equiv.) was dissolved in THF (7.0 mL). Aq. NaOH (1.4 g NaOH in 7.0 mL of water, 35 mmol, 1.9 equiv.) was added at 0 °C, followed by the slow addition of *p*-TsCl (3.5 g in 20 mL THF, 18 mmol, 1.0 equiv.) over the course of 30 min. The reaction mixture was stirred at 0 °C for 6.5 h, then it was poured into ice water (250 mL). The mixture was extracted with CH_2Cl_2 (2 × 200 mL) and the combined organic phases were washed with H_2O (4 × 200 mL), dried over Na_2SO_4, filtered, and concentrated *in vacuo* to give compound tetraethylene glycol monotosylate (5.1 g, 15 mmol, 83%) as a faintly yellow oil.

^{1}H NMR (400 MHz, $CDCl_3$): δ / ppm = 7.79–7.74 (m, 2H), 7.34–7.29 (m, 2H), 4.15–4.11 (m, 2H), 3.69–3.64 (m, 4H), 3.61 (dt, J = 5.3, 2.4 Hz, 4H), 3.57 (d, J = 4.1 Hz, 6H), 2.42 (s, 3H).
^{13}C NMR (101 MHz, $CDCl_3$): δ / ppm = 144.9, 133.0, 129.9, 128.0, 72.5, 70.8, 70.7, 70.5, 70.4, 69.3, 68.7, 61.7, 21.7.
IR: $\tilde{\nu}$ / cm^{-1} = 2870 (w), 1597 (w), 1452 (w), 1350 (s), 1306 (w), 1292 (w), 1248 (w), 1188 (m), 1174 (vs), 1120 (s), 1095 (s), 1066 (m), 1011 (m), 916 (s), 816 (s), 773 (s), 706 (w), 690 (w), 661 (s), 634 (w), 582 (m), 552 (vs), 501 (m), 467 (m), 434 (m), 418 (w), 409 (w).
HRMS (ESI): *m/z* calc. for $[C_{15}H_{24}O_7S+H]^+$: 349.1316; found: 349.1318 ($M+H^+$).

Octaethylene glycol monotosylate (107)[163]

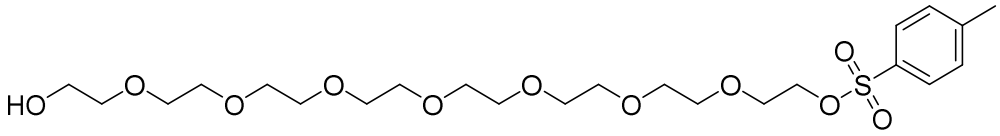

In a dried Schlenk flask under nitrogen atmosphere, octaethylene glycol (0.60 g, 1.6 mmol, 1.0 equiv.) was dissolved in dry CH_2Cl_2 (8.0 mL). At 0 °C, Ag_2O (0.57 g, 2.5 mmol, 1.6 equiv.), KI (98 mg, 0.59 mmol, 0.4 equiv.) and *p*-TsCl (0.31 g, 1.6 mmol, 1.0 equiv.) were added. The mixture was stirred for 3.5 h, while slowly warming to 23 °C. The reaction mixture was filtered over a short plug of silica and the plug was rinsed with MeOH:CH_2Cl_2 (1:5). The filtrate was concentrated *in vacuo* and the crude product was then purified by column chromatography (SiO_2, MeOH:CH_2Cl_2, 5:95). Octaethylene glycol monotosylate (0.47 g, 0.90 mmol, 56%) was obtained as a slightly yellow oil.

^{1}H NMR (400 MHz, $CDCl_3$): δ / ppm = 7.81–7.77 (m, 2H), 7.36–7.31 (m, 2H), 4.17–4.13 (m, 2H), 3.73–3.58 (m, 26H), 3.57 (s, 4H), 2.44 (s, 3H).
HRMS (ESI): *m/z* calc. for $[C_{23}H_{40}O_{11}S+NH_4]^+$: 542.2630; found: 542.2638 ($M+NH_4^+$).

6.3 Crystal Structure Data

Crystal Structure Data of (*rac*)-*(E)*-59 *reported in ref.* [8][$]

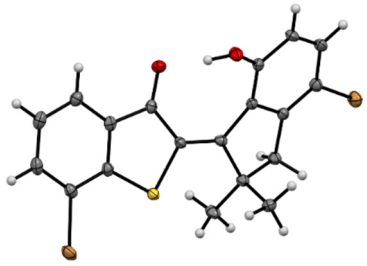

Compound	**(*E*)-59 (xv390)** CCDC 2123711
net formula	$C_{19}H_{14}Br_2O_2S$
M_r/g mol^{-1}	466.18
crystal size/mm	0.100 × 0.070 × 0.020
T/K	106.(2)
radiation	MoKα
diffractometer	'Bruker D8 Venture TXS'
crystal system	triclinic
space group	'P -1'
a/Å	8.2363(5)
b/Å	8.3643(5)
c/Å	12.1540(8)
α/°	93.051(2)
β/°	93.362(2)
γ/°	95.150(2)
V/Å^3	831.04(9)
Z	2
calc. density/g cm^{-3}	1.863
μ/mm^{-1}	5.012
absorption correction	Multi-Scan
transmission factor range	0.74–0.91
refls. measured	14942
R_{int}	0.0425
mean σ(*I*)/*I*	0.0411
θ range	2.888–28.279
observed refls.	3535
x, y (weighting scheme)	0.0148, 0.6424
hydrogen refinement	H(C) constr, H(O) refall
refls in refinement	4086
parameters	223
restraints	0
$R(F_{obs})$	0.0263
$R_w(F^2)$	0.0632
S	1.033
shift/error$_{max}$	0.001
max electron density/e Å^{-3}	0.431
min electron density/e Å^{-3}	−0.325

Crystal Structure Data of (*rac*)-(*E*)-34[$]

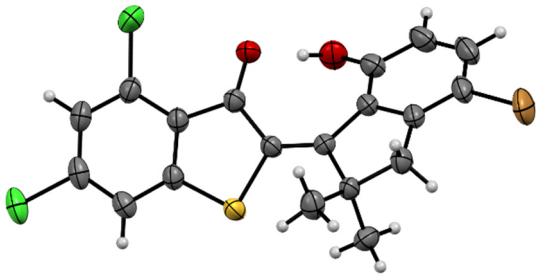

Compound	**(*E*)-34 (wv322)**
net formula	$C_{19}H_{13}BrCl_2O_2S$
M_r/g mol^{-1}	456.16
crystal size/mm	0.090 × 0.050 × 0.040
T/K	300.(2)
radiation	MoKα
diffractometer	'Bruker D8 Venture TXS'
crystal system	triclinic
space group	'P -1'
a/Å	8.2743(5)
b/Å	9.3113(6)
c/Å	12.1425(8)
α/°	83.201(2)
β/°	78.645(2)
γ/°	80.116(2)
V/Å^3	900.12(10)
Z	2
calc. density/g cm^{-3}	1.683
μ/mm^{-1}	2.706
absorption correction	Multi-Scan
transmission factor range	0.84–0.90
refls. measured	9180
R_{int}	0.0216
mean σ(*I*)/*I*	0.0313
θ range	3.114–27.077
observed refls.	3055
x, y (weighting scheme)	0.0572, 0.4498
hydrogen refinement	H(C) constr, H(O) refall
refls in refinement	3930
parameters	232
restraints	0
$R(F_{obs})$	0.0376
$R_w(F^2)$	0.1109
S	1.051
shift/error$_{max}$	0.001
max electron density/e Å^{-3}	0.832
min electron density/e Å^{-3}	−0.692

Crystal Structure Data of (*Z*)-35[$]

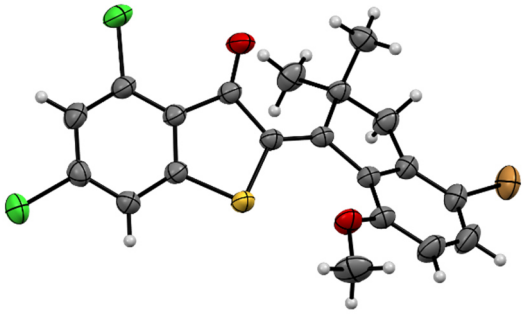

Compound	**(*Z*)-35 (wv331)**
net formula	$C_{20}H_{15}BrCl_2O_2S$
M_r/g mol^{-1}	470.19
crystal size/mm	0.080 × 0.070 × 0.020
T/K	299.(2)
radiation	MoKα
diffractometer	'Bruker D8 Venture TXS'
crystal system	monoclinic
space group	'P 1 21/n 1'
a/Å	9.6541(4)
b/Å	7.7924(3)
c/Å	25.5323(9)
α/°	90
β/°	97.9510(10)
γ/°	90
V/Å^3	1902.29(13)
Z	4
calc. density/g cm^{-3}	1.642
μ/mm^{-1}	2.564
absorption correction	Multi-Scan
transmission factor range	0.85–0.95
refls. measured	19070
R_{int}	0.0276
mean σ(*I*)/*I*	0.0243
θ range	2.992–26.369
observed refls.	3216
x, *y* (weighting scheme)	0.0327, 1.4520
hydrogen refinement	constr
refls in refinement	3885
parameters	238
restraints	0
$R(F_{obs})$	0.0316
$R_w(F^2)$	0.0801
S	1.029
shift/error$_{max}$	0.003
max electron density/e Å^{-3}	0.408
min electron density/e Å^{-3}	−0.509

Crystal Structure Data of (*rac*)-(*E*)-44[§]

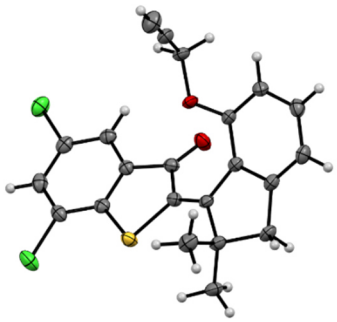

Compound	**(*E*)-44 (22DUB_NB01)**
Formula	$C_{22}H_{16}Cl_2O_2S$
$D_{calc.}$/ g cm^{-3}	1.435
μ/mm^{-1}	4.172
Formula Weight	415.31
Color	clear light orange
Shape	block-shaped
Size/mm^3	0.30×0.20×0.10
T/K	157(7)
Crystal System	triclinic
Space Group	P-1
a/Å	9.4682(5)
b/Å	10.9017(8)
c/Å	11.6449(7)
α/°	102.432(6)
β/°	108.205(5)
γ/°	113.784(6)
V/Å^3	960.96(11)
Z	2
Z'	1
Wavelength/Å	1.54184
Radiation type	Cu K$_\alpha$
Diffractometer	SuperNova Dual Atlas
Θ_{min}/°	4.346
Θ_{max}/°	71.431
Measured Refl's.	6251
Indep't Refl's	3598
Refl's I≥2 σ(I)	3349
R_{int}	0.0189
Parameters	246
Restraints	0
Largest Peak	0.289
Deepest Hole	-0.299
GooF	1.047
wR_2 (all data)	0.0852
wR_2	0.0833
R_1 (all data)	0.0334
R_1	0.0314

Crystal Structure Data of (*rac*)-(*E*)-51[$]

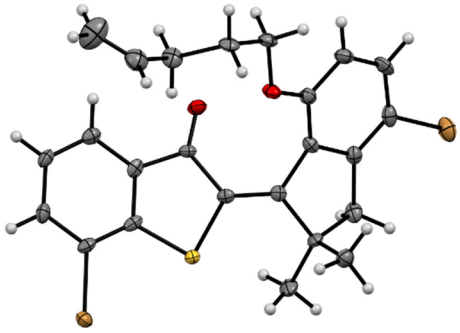

Compound	**(*E*)-51 (xv103)**
net formula	$C_{24}H_{22}Br_2O_2S$
M_r/g mol^{-1}	534.29
crystal size/mm	0.070 × 0.060 × 0.020
T/K	111.(2)
radiation	MoKα
diffractometer	'Bruker D8 Venture TXS'
crystal system	monoclinic
space group	'P 1 21/c 1'
a/Å	9.0862(3)
b/Å	23.0080(6)
c/Å	20.9085(7)
α/°	90
β/°	94.1830(10)
γ/°	90
V/Å^3	4359.4(2)
Z	8
calc. density/g cm^{-3}	1.628
μ/mm^{-1}	3.833
absorption correction	Multi-Scan
transmission factor range	0.81–0.93
refls. measured	9013
R_{int}	0.0592
mean σ(*I*)/*I*	0.0453
θ range	2.830–26.371
observed refls.	7816
x, *y* (weighting scheme)	0.0262, 6.8627
hydrogen refinement	constr
refls in refinement	9013
parameters	528
restraints	0
$R(F_{obs})$	0.0403
$R_w(F^2)$	0.0776
S	1.058
shift/error$_{max}$	0.001
max electron density/e Å^{-3}	0.813
min electron density/e Å^{-3}	−0.540

Crystal Structure Data of 92[§]

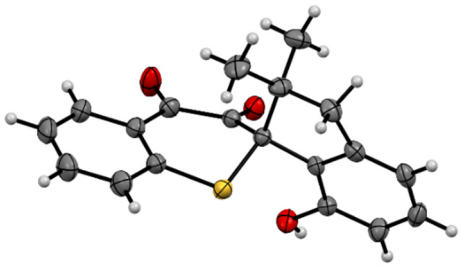

Compound	**92 (21DUB_NB02)**
Formula	$C_{19}H_{16}O_3S$
$D_{calc.}$/ g cm^{-3}	1.362
μ/mm^{-1}	1.923
Formula Weight	324.38
Color	clear light orange
Shape	block
Size/mm^3	0.23×0.14×0.13
T/K	153(1)
Crystal System	monoclinic
Flack Parameter	-0.03(2)
Hooft Parameter	-0.014(13)
Space Group	$P2_1$
a/Å	9.5385(5)
b/Å	8.6468(4)
c/Å	10.4500(6)
α/°	90
β/°	113.453(7)
γ/°	90
V/Å^3	790.69(8)
Z	2
Z'	1
Wavelength/Å	1.54184
Radiation type	Cu Kα
Diffractometer	SuperNova Dual Atlas
Θ_{min}/°	4.612
Θ_{max}/°	69.440
Measured Refl's.	4637
Indep't Refl's	2821
Refl's I≥2 σ(I)	2621
R_{int}	0.0331
Parameters	211
Restraints	1
Largest Peak	0.149
Deepest Hole	-0.306
GooF	1.071
wR_2 (all data)	0.1016
wR_2	0.0968
R_1 (all data)	0.0442
R_1	0.0398

Crystal Structure Data of (*rac*)-(*E*)-90[§]

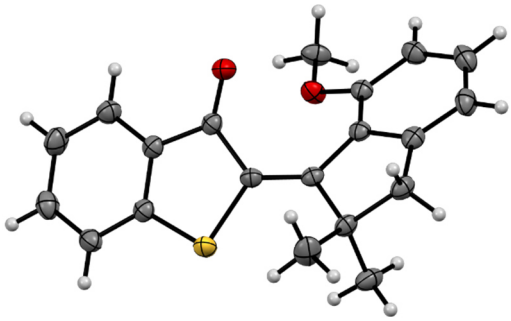

Compound	**(*E*)-90 (21DUB_NB01)**
Formula	$C_{20}H_{18}O_2S$
$D_{calc.}$/ g cm^{-3}	1.334
μ/mm^{-1}	1.842
Formula Weight	322.40
Color	clear light yellow
Shape	block
Size/mm^3	0.36×0.24×0.23
T/K	153(2)
Crystal System	monoclinic
Space Group	$C2/c$
a/Å	27.5568(6)
b/Å	10.7540(3)
c/Å	10.8714(2)
α/°	90
β/°	94.998(2)
γ/°	90
V/Å^3	3209.44(13)
Z	8
Z'	1
Wavelength/Å	1.54184
Radiation type	Cu K$_\alpha$
Diffractometer	SuperNova Dual Atlas
Θ_{min}/°	3.220
Θ_{max}/°	67.381
Measured Refl's.	8899
Indep't Refl's	2818
Refl's I≥2 σ(I)	2555
R_{int}	0.0172
Parameters	212
Restraints	0
Largest Peak	0.237
Deepest Hole	-0.221
GooF	1.037
wR_2 (all data)	0.0879
wR_2	0.0848
R_1 (all data)	0.0377
R_1	0.0339

Crystal Structure Data of (*E*/*Z*)-100[$]

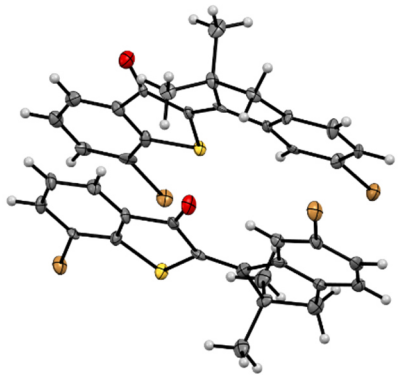

Compound	**(*E*/*Z*)-100 (vv795)**
net formula	$C_{19}H_{14}Br_2OS$
M_r/g mol^{-1}	450.18
crystal size/mm	0.100 × 0.020 × 0.010
T/K	103.(2)
radiation	MoKα
diffractometer	'Bruker D8 Venture TXS'
crystal system	monoclinic
space group	'P 1 21/c 1'
a/Å	7.0404(4)
b/Å	21.8167(12)
c/Å	21.1695(13)
α/°	90
β/°	95.177(2)
γ/°	90
V/Å^3	3238.3(3)
Z	8
calc. density/g cm^{-3}	1.847
μ/mm^{-1}	5.136
absorption correction	Multi-Scan
transmission factor range	0.73–0.95
refls. measured	15798
R_{int}	0.0883
mean σ(*I*)/*I*	0.1455
θ range	3.279–26.371
observed refls.	3821
x, *y* (weighting scheme)	0.0430, 6.7185
hydrogen refinement	constr
refls in refinement	6540
parameters	419
restraints	12
$R(F_{obs})$	0.0665
$R_w(F^2)$	0.1394
S	1.009
shift/error$_{max}$	0.001
max electron density/e Å^{-3}	0.894
min electron density/e Å^{-3}	−1.619

Crystal Structure Data of (*Z*)-101[$]

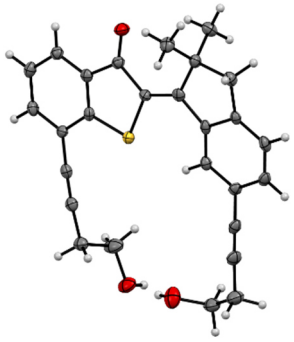

Compound	**(*Z*)-101 (wv019)**
net formula	$C_{27}H_{24}O_3S$
M_r/g mol^{-1}	428.52
crystal size/mm	0.100 × 0.070 × 0.020
T/K	103.(2)
radiation	MoKα
diffractometer	'Bruker D8 Venture TXS'
crystal system	monoclinic
space group	'P 1 21/n 1'
a/Å	6.9849(2)
b/Å	24.3612(8)
c/Å	25.2771(10)
α/°	90
β/°	96.160(2)
γ/°	90
V/Å^3	4276.3(3)
Z	8
calc. density/g cm^{-3}	1.331
μ/mm^{-1}	0.179
absorption correction	Multi-Scan
transmission factor range	0.92–1.00
refls. measured	45409
R_{int}	0.1175
mean σ(*I*)/*I*	0.0884
θ range	3.236–25.019
observed refls.	4707
x, y (weighting scheme)	0.0411, 2.9358
hydrogen refinement	H(C) constr, H(O) restr
refls in refinement	7475
parameters	579
restraints	6
$R(F_{obs})$	0.0558
$R_w(F^2)$	0.1327
S	1.011
shift/error$_{max}$	0.001
max electron density/e Å^{-3}	0.282
min electron density/e Å^{-3}	−0.336

H(O) refined with SADI.

Crystal Structure Data of (*Z*)-37[$]

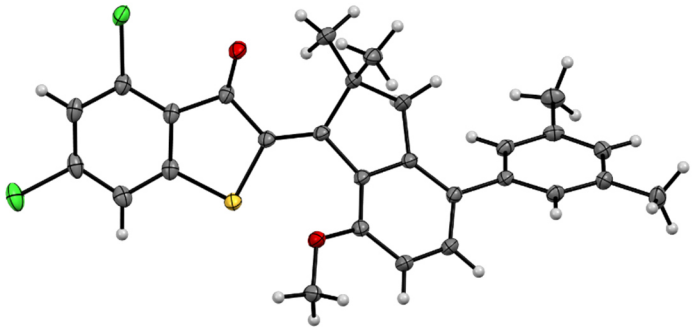

Compound	**(*Z*)-37 (xv218)**
net formula	$C_{28}H_{24}Cl_2O_2S$
M_r/g mol^{-1}	495.43
crystal size/mm	0.100 × 0.040 × 0.030
T/K	111.(2)
radiation	MoKα
diffractometer	'Bruker D8 Venture TXS'
crystal system	triclinic
space group	'P -1'
a/Å	7.9155(4)
b/Å	8.2602(4)
c/Å	20.0716(10)
α/°	86.805(2)
β/°	81.312(2)
γ/°	66.991(2)
V/Å^3	1194.08(10)
Z	2
calc. density/g cm^{-3}	1.378
μ/mm^{-1}	0.384
absorption correction	Multi-Scan
transmission factor range	0.94–0.99
refls. measured	21155
R_{int}	0.0271
mean σ(*I*)/*I*	0.0262
θ range	3.048–27.483
observed refls.	4902
x, y (weighting scheme)	0.0455, 0.6503
hydrogen refinement	constr
refls in refinement	5484
parameters	303
restraints	0
$R(F_{obs})$	0.0341
$R_w(F^2)$	0.0975
S	1.082
shift/error$_{max}$	0.002
max electron density/e Å^{-3}	0.347
min electron density/e Å^{-3}	−0.303

7 References

[1] E. Schrödinger, *What is Life?: With Mind and Matter and Autobiographical Sketches*, Cambridge University Press, Cambridge, **2012**.

[2] R. P. Feynman, *Eng. Sci.* **1960**, *23*, 22-36.

[3] J.-P. Sauvage, *Angew. Chem. Int. Ed.* **2017**, *56*, 11080-11093.

[4] J. F. Stoddart, *Angew. Chem. Int. Ed.* **2017**, *56*, 11094-11125.

[5] B. L. Feringa, *Angew. Chem. Int. Ed.* **2017**, *56*, 11060-11078.

[6] Nobel Prize Outreach AB, *The Nobel Prize in Chemistry 2016*, can be found under https://www.nobelprize.org/prizes/chemistry/2016/summary/, **2023** (accessed 26.01.2023).

[7] A. Coskun, M. Banaszak, R. D. Astumian, J. F. Stoddart, B. A. Grzybowski, *Chem. Soc. Rev.* **2012**, *41*, 19-30.

[8] N. N. Bach, V. Josef, H. Maid, H. Dube, *Angew. Chem. Int. Ed.* **2022**, *61*, e202201882.

[9] R. Wilcken, M. Schildhauer, F. Rott, L. A. Huber, M. Guentner, S. Thumser, K. Hoffmann, S. Oesterling, R. de Vivie-Riedle, E. Riedle, H. Dube, *J. Am. Chem. Soc.* **2018**, *140*, 5311-5318.

[10] S. Erbas-Cakmak, D. A. Leigh, C. T. McTernan, A. L. Nussbaumer, *Chem. Rev.* **2015**, *115*, 10081-10206.

[11] W. R. Browne, B. L. Feringa, *Nat. Nanotechnol.* **2006**, *1*, 25-35.

[12] E. R. Kay, D. A. Leigh, F. Zerbetto, *Angew. Chem. Int. Ed.* **2007**, *46*, 72-191.

[13] S. Kassem, T. van Leeuwen, A. S. Lubbe, M. R. Wilson, B. L. Feringa, D. A. Leigh, *Chem. Soc. Rev.* **2017**, *46*, 2592-2621.

[14] K. Kinbara, T. Aida, *Chem. Rev.* **2005**, *105*, 1377-1400.

[15] G. Saper, H. Hess, *Chem. Rev.* **2020**, *120*, 288-309.

[16] H. Noji, R. Yasuda, M. Yoshida, K. Kinosita, *Nature* **1997**, *386*, 299-302.

[17] J. Gelles, R. Landick, *Cell* **1998**, *93*, 13-16.

[18] R. D. Vale, R. A. Milligan, *Science* **2000**, *288*, 88-95.

[19] IUPAC, *Compendium of Chemical Terminology, 2nd ed. (the "Gold Book") compiled by A. D. McNaught and A. Wilkinson, Online version created by S. J. Chalk*, can be found under https://doi.org/10.1351/goldbook, **2019** (accessed 24.01.2023).

[20] M. Fritzsche, *C. R. Hebd. Seances Acad. Sci.* **1867**, *64*, 1035-1037.

[21] K. Nakatani, J. Piard, P. Yu, R. Métivier, in *Photochromic Materials*, **2016**, pp. 1-45.

[22] H. Bouas-Laurent, H. Dürr, *Pure Appl. Chem.* **2001**, *73*, 639-665.

[23] M. Kathan, S. Hecht, *Chem. Soc. Rev.* **2017**, *46*, 5536-5550.

[24] D. Villarón, S. J. Wezenberg, *Angew. Chem. Int. Ed.* **2020**, *59*, 13192-13202.

[25] G. S. Hartley, *Nature* **1937**, *140*, 281-281.

[26] A. A. Beharry, G. A. Woolley, *Chem. Soc. Rev.* **2011**, *40*, 4422-4437.

[27] R. Siewertsen, H. Neumann, B. Buchheim-Stehn, R. Herges, C. Näther, F. Renth, F. Temps, *J. Am. Chem. Soc.* **2009**, *131*, 15594-15595.

[28] M. N. Chaur, D. Collado, J.-M. Lehn, *Chem. - Eur. J.* **2011**, *17*, 248-258.

[29] E. Fischer, Y. Hirshberg, *J. Chem. Soc.* **1952**, 4522.

[30] G. Berkovic, V. Krongauz, V. Weiss, *Chem. Rev.* **2000**, *100*, 1741-1754.

[31] L. Wimberger, S. K. K. Prasad, M. D. Peeks, J. Andréasson, T. W. Schmidt, J. E. Beves, *J. Am. Chem. Soc.* **2021**, *143*, 20758-20768.

[32] M. Irie, T. Fukaminato, K. Matsuda, S. Kobatake, *Chem. Rev.* **2014**, *114*, 12174-12277.

[33] M. Irie, *Chem. Rev.* **2000**, *100*, 1685-1716.

[34] G. S. Hammond, N. J. Turro, A. Fischer, *J. Am. Chem. Soc.* **1961**, *83*, 4674-4675.

[35] W. G. Dauben, R. L. Cargill, *Tetrahedron* **1961**, *15*, 197-201.

[36] J. Orrego-Hernández, A. Dreos, K. Moth-Poulsen, *Acc. Chem. Res.* **2020**, *53*, 1478-1487.

[37] S. Helmy, F. A. Leibfarth, S. Oh, J. E. Poelma, C. J. Hawker, J. Read de Alaniz, *J. Am. Chem. Soc.* **2014**, *136*, 8169-8172.

[38] M. M. Lerch, S. J. Wezenberg, W. Szymanski, B. L. Feringa, *J. Am. Chem. Soc.* **2016**, *138*, 6344-6347.

[39] A.-L. Leistner, Z. L. Pianowski, *Eur. J. Org. Chem.* **2022**, e202101271.

[40] C. Petermayer, H. Dube, *Acc. Chem. Res.* **2018**, *51*, 1153-1163.

[41] E. D. Głowacki, G. Voss, L. Leonat, M. Irimia-Vladu, S. Bauer, N. S. Sariciftci, *Isr. J. Chem.* **2012**, *52*, 540-551.

[42] A. Baeyer, *Ber. Dtsch. Chem. Ges.* **1883**, *16*, 2188-2204.

[43] Nobel Prize Outreach AB, *The Nobel Prize in Chemistry 1905*, can be found under https://www.nobelprize.org/prizes/chemistry/1905/summary/, **2023** (accessed 25.01.2023).

[44] J. Pina, D. Sarmento, M. Accoto, P. L. Gentili, L. Vaccaro, A. Galvão, J. S. Seixas de Melo, *J. Phys. Chem. B* **2017**, *121*, 2308-2318.

[45] C.-Y. Huang, A. Bonasera, L. Hristov, Y. Garmshausen, B. M. Schmidt, D. Jacquemin, S. Hecht, *J. Am. Chem. Soc.* **2017**, *139*, 15205-15211.

[46] L. A. Huber, P. Mayer, H. Dube, *ChemPhotoChem* **2018**, *2*, 458-464.

[47] C. Petermayer, S. Thumser, F. Kink, P. Mayer, H. Dube, *J. Am. Chem. Soc.* **2017**, *139*, 15060-15067.

[48] C. Petermayer, H. Dube, *J. Am. Chem. Soc.* **2018**, *140*, 13558-13561.

[49] D. V. Berdnikova, *Chem. Commun.* **2019**, *55*, 8402-8405.

[50] D. V. Berdnikova, *Beilstein J. Org. Chem.* **2019**, *15*, 2822-2829.

[51] M. Sacherer, F. Hampel, H. Dube, *Nat. Commun.* **2023**, *14*, 4382.

[52] S. Thumser, L. Köttner, N. Hoffmann, P. Mayer, H. Dube, *J. Am. Chem. Soc.* **2021**, *143*, 18251-18260.

[53] S. Wiedbrauk, H. Dube, *Tetrahedron Lett.* **2015**, *56*, 4266-4274.

[54] P. Friedländer, *Ber. Dtsch. Chem. Ges.* **1906**, *39*, 1060-1066.

[55] V. A. Izmail'skii, M. A. Mostoslavskii, *Ukr. Khem. Zh.* **1961**, *27*, 234.

[56] A. Gerwien, T. Reinhardt, P. Mayer, H. Dube, *Org. Lett.* **2018**, *20*, 232-235.

[57] P. Soundarya, G. Sekar, *Org. Biomol. Chem.* **2022**, *20*, 7405-7409.

[58] A. Nakamura, F. Rao, K. Ukiya, R. Matsunaga, S.-i. Ohira, T. Maegawa, *Org. Biomol. Chem.* **2023**.

[59] T. B. Nguyen, P. Retailleau, *Org. Lett.* **2018**, *20*, 186-189.

[60] B. Maerz, S. Wiedbrauk, S. Oesterling, E. Samoylova, A. Nenov, P. Mayer, R. de Vivie-Riedle, W. Zinth, H. Dube, *Chem. - Eur. J.* **2014**, *20*, 13984-13992.

[61] S. Wiedbrauk, B. Maerz, E. Samoylova, P. Mayer, W. Zinth, H. Dube, *J. Phys. Chem. Lett.* **2017**, *8*, 1585-1592.

[62] T. Cordes, T. Schadendorf, K. Rück-Braun, W. Zinth, *Chem. Phys. Lett.* **2008**, *455*, 197-201.

[63] T. Cordes, T. Schadendorf, B. Priewisch, K. Rück-Braun, W. Zinth, *J. Phys. Chem. A* **2008**, *112*, 581-588.

[64] J. E. Zweig, T. R. Newhouse, *J. Am. Chem. Soc.* **2017**, *139*, 10956-10959.

[65] V. Josef, F. Hampel, H. Dube, *Angew. Chem. Int. Ed.* **2022**, *61*, e202210855.

[66] A. Gerwien, B. Jehle, M. Irmler, P. Mayer, H. Dube, *J. Am. Chem. Soc.* **2022**, *144*, 3029-3038.

[67] S. Crespi, N. Simeth, M. Di Donato, S. Doria, C. N. Stindt, M. F. Hilbers, F. L. Kiss, R. Toyoda, S. Wesseling, W. J. Buma, B. L. Feringa, W. Szymanski, *Angew. Chem. Int. Ed.* **2021**, *60*, 25290–25295.

[68] A. Sailer, F. Ermer, Y. Kraus, F. H. Lutter, C. Donau, M. Bremerich, J. Ahlfeld, O. Thorn-Seshold, *ChemBioChem* **2019**, *20*, 1305-1314.

[69] A. Sailer, J. C. M. Meiring, C. Heise, L. N. Pettersson, A. Akhmanova, J. Thorn-Seshold, O. Thorn-Seshold, *Angew. Chem. Int. Ed.* **2021**, *60*, 23695-23704.

[70] T. Lougheed, V. Borisenko, T. Hennig, K. Rück-Braun, G. A. Woolley, *Org. Biomol. Chem.* **2004**, *2*, 2798-2801.

[71] S. Herre, T. Schadendorf, I. Ivanov, C. Herrberger, W. Steinle, K. Rück-Braun, R. Preissner, H. Kuhn, *ChemBioChem* **2006**, *7*, 1089-1095.

[72] T. Cordes, B. Heinz , N. Regner, C. Hoppmann, T. E. Schrader, W. Summerer, K. Rück-Braun, W. Zinth, *ChemPhysChem* **2007**, *8*, 1713-1721.

[73] S. Wiedbrauk, T. Bartelmann, S. Thumser, P. Mayer, H. Dube, *Nat. Commun.* **2018**, *9*, 1456.

[74] T. Bartelmann, F. Gnannt, M. Zitzmann, P. Mayer, H. Dube, *Chem. Sci.* **2021**, *12*, 3651-3659.

[75] M. Guentner, E. Uhl, P. Mayer, H. Dube, *Chem. - Eur. J.* **2016**, *22*, 16433-16436.

[76] H. Dube, J. Rebek, *Angew. Chem. Int. Ed.* **2012**, *51*, 3207-3210.

[77] T. R. Kelly, H. De Silva, R. A. Silva, *Nature* **1999**, *401*, 150-152.

[78] S. Borsley, D. A. Leigh, B. M. W. Roberts, *Nat. Chem.* **2022**, *14*, 728-738.

[79] Y. Zhang, Z. Chang, H. Zhao, S. Crespi, B. L. Feringa, D. Zhao, *Chem* **2020**, *6*, 2420-2429.

[80] K. Mo, Y. Zhang, Z. Dong, Y. Yang, X. Ma, B. L. Feringa, D. Zhao, *Nature* **2022**, *609*, 293-298.

[81] M. R. Wilson, J. Solà, A. Carlone, S. M. Goldup, N. Lebrasseur, D. A. Leigh, *Nature* **2016**, *534*, 235-240.

[82] V. Serreli, C.-F. Lee, E. R. Kay, D. A. Leigh, *Nature* **2007**, *445*, 523-527.

[83] S. Borsley, D. A. Leigh, B. M. W. Roberts, *J. Am. Chem. Soc.* **2021**, *143*, 4414-4420.

[84] S. Amano, M. Esposito, E. Kreidt, D. A. Leigh, E. Penocchio, B. M. W. Roberts, *Nat. Chem.* **2022**.

[85] V. García-López, D. Liu, J. M. Tour, *Chem. Rev.* **2020**, *120*, 79-124.

[86] M. Baroncini, S. Silvi, A. Credi, *Chem. Rev.* **2020**, *120*, 200-268.

[87] D. R. S. Pooler, A. S. Lubbe, S. Crespi, B. L. Feringa, *Chem. Sci.* **2021**.

[88] N. Koumura, R. W. J. Zijlstra, R. A. van Delden, N. Harada, B. L. Feringa, *Nature* **1999**, *401*, 152-155.

[89] N. Koumura, E. M. Geertsema, M. B. van Gelder, A. Meetsma, B. L. Feringa, *J. Am. Chem. Soc.* **2002**, *124*, 5037-5051.

[90] J. C. M. Kistemaker, P. Štacko, D. Roke, A. T. Wolters, G. H. Heideman, M.-C. Chang, P. van der Meulen, J. Visser, E. Otten, B. L. Feringa, *J. Am. Chem. Soc.* **2017**, *139*, 9650-9661.

[91] L. Greb, J.-M. Lehn, *J. Am. Chem. Soc.* **2014**, *136*, 13114-13117.

[92] A. Cnossen, L. Hou, M. M. Pollard, P. V. Wesenhagen, W. R. Browne, B. L. Feringa, *J. Am. Chem. Soc.* **2012**, *134*, 17613-17619.

[93] L. Pfeifer, M. Scherübl, M. Fellert, W. Danowski, J. Cheng, J. Pol, B. L. Feringa, *Chem. Sci.* **2019**, *10*, 8768-8773.

[94] R. A. van Delden, N. Koumura, A. Schoevaars, A. Meetsma, B. L. Feringa, *Org. Biomol. Chem.* **2003**, *1*, 33-35.

[95] M. Guentner, M. Schildhauer, S. Thumser, P. Mayer, D. Stephenson, P. J. Mayer, H. Dube, *Nat. Commun.* **2015**, *6*, 8406.

[96] L. A. Huber, K. Hoffmann, S. Thumser, N. Böcher, P. Mayer, H. Dube, *Angew. Chem. Int. Ed.* **2017**, *56*, 14536-14539.

[97] L. A. Huber, S. Thumser, K. Grill, D. Voßiek, N. N. Bach, P. Mayer, H. Dube, *Chem. - Eur. J.* **2021**, *27*, 10758-10765.

[98] A. Gerwien, P. Mayer, H. Dube, *Nat. Commun.* **2019**, *10*, 4449.

[99] A. Gerwien, P. Mayer, H. Dube, *J. Am. Chem. Soc.* **2018**, *140*, 16442-16445.

[100] M. Schildhauer, F. Rott, S. Thumser, P. Mayer, R. de Vivie-Riedle, H. Dube, *ChemPhotoChem* **2019**, *3*, 365-371.

[101] S. Corra, M. Curcio, M. Baroncini, S. Silvi, A. Credi, *Adv. Mater.* **2020**, *32*, 1906064.

[102] J. Vachon, G. T. Carroll, M. M. Pollard, E. M. Mes, A. M. Brouwer, B. L. Feringa, *Photochem. Photobiol. Sci.* **2014**, *13*, 241-246.

[103] J. Kaleta, J. Chen, G. Bastien, M. Dračínský, M. Mašát, C. T. Rogers, B. L. Feringa, J. Michl, *J. Am. Chem. Soc.* **2017**, *139*, 10486-10498.

[104] K. Hoffmann, P. Mayer, H. Dube, *Org. Biomol. Chem.* **2019**, *17*, 1979-1983.

[105] K.-Y. Chen, O. Ivashenko, G. T. Carroll, J. Robertus, J. C. M. Kistemaker, G. London, W. R. Browne, P. Rudolf, B. L. Feringa, *J. Am. Chem. Soc.* **2014**, *136*, 3219-3224.

[106] Q. Li, G. Fuks, E. Moulin, M. Maaloum, M. Rawiso, I. Kulic, J. T. Foy, N. Giuseppone, *Nat. Nanotechnol.* **2015**, *10*, 161-165.

[107] J. Foy, Q. Li, A. Goujon, J.-R. Colard-Itté, G. Fuks, E. Moulin, O. Schiffmann, D. Dattler, D. Funeriu, N. Giuseppone, *Nat. Nanotechnol.* **2017**, *12*, 540-545.

[108] W. Danowski, T. van Leeuwen, S. Abdolahzadeh, D. Roke, W. R. Browne, S. J. Wezenberg, B. L. Feringa, *Nat. Nanotechnol.* **2019**, *14*, 488-494.

[109] C. Stähler, L. Grunenberg, M. W. Terban, W. R. Browne, D. Doellerer, M. Kathan, M. Etter, B. V. Lotsch, B. L. Feringa, S. Krause, *Chem. Sci.* **2022**.

[110] R. Eelkema, M. M. Pollard, J. Vicario, N. Katsonis, B. S. Ramon, C. W. M. Bastiaansen, D. J. Broer, B. L. Feringa, *Nature* **2006**, *440*, 163-163.

[111] J. Chen, F. K.-C. Leung, M. C. A. Stuart, T. Kajitani, T. Fukushima, E. van der Giessen, B. L. Feringa, *Nat. Chem.* **2018**, *10*, 132-138.

[112] S. Chen, L. Yang, F. K.-C. Leung, T. Kajitani, M. C. A. Stuart, T. Fukushima, P. van Rijn, B. L. Feringa, *J. Am. Chem. Soc.* **2022**, *144*, 3543-3553.

[113] D. Dattler, G. Fuks, J. Heiser, E. Moulin, A. Perrot, X. Yao, N. Giuseppone, *Chem. Rev.* **2020**, *120*, 310-433.

[114] R. Costil, M. Holzheimer, S. Crespi, N. A. Simeth, B. L. Feringa, *Chem. Rev.* **2021**.

[115] A. Gerwien, F. Gnannt, P. Mayer, H. Dube, *Nat. Chem.* **2022**, *14*, 670-676.

[116] G. S. Kottas, L. I. Clarke, D. Horinek, J. Michl, *Chem. Rev.* **2005**, *105*, 1281-1376.

[117] M. Baroncini, A. Credi, S. Silvi, in *Out‐of‐Equilibrium (Supra)molecular Systems and Materials*, **2021**, pp. 305-336.

[118] Y. Wang, Y. Tian, Y.-Z. Chen, L.-Y. Niu, L.-Z. Wu, C.-H. Tung, Q.-Z. Yang, R. Boulatov, *Chem. Commun.* **2018**, *54*, 7991-7994.

[119] G. Ragazzon, M. Baroncini, S. Silvi, M. Venturi, A. Credi, *Nat. Nanotechnol.* **2015**, *10*, 70-75.

[120] D.-H. Qu, B. L. Feringa, *Angew. Chem. Int. Ed.* **2010**, *49*, 1107-1110.

[121] J.-J. Yu, L.-Y. Zhao, Z.-T. Shi, Q. Zhang, G. London, W.-J. Liang, C. Gao, M.-M. Li, X.-M. Cao, H. Tian, B. L. Feringa, D.-H. Qu, *J. Org. Chem.* **2019**, *84*, 5790-5802.

[122] E. Uhl, S. Thumser, P. Mayer, H. Dube, *Angew. Chem. Int. Ed.* **2018**, *57*, 11064-11068.

[123] E. Uhl, P. Mayer, H. Dube, *Angew. Chem. Int. Ed.* **2020**, *59*, 5730-5737.

[124] C. Gao, A. Vargas Jentzsch, E. Moulin, N. Giuseppone, *J. Am. Chem. Soc.* **2022**, *144*, 9845-9852.

[125] M. Kathan, S. Crespi, N. O. Thiel, D. L. Stares, D. Morsa, J. de Boer, G. Pacella, T. van den Enk, P. Kobauri, G. Portale, C. A. Schalley, B. L. Feringa, *Nat. Nanotechnol.* **2022**, *17*, 159-165.

[126] M. Kathan, S. Crespi, N. O. Thiel, D. L. Stares, D. Morsa, J. de Boer, G. Pacella, T. van den Enk, P. Kobauri, G. Portale, C. A. Schalley, B. L. Feringa, *Nat. Nanotechnol.* **2021**.

[127] P. Štacko, J. C. M. Kistemaker, T. van Leeuwen, M.-C. Chang, E. Otten, B. L. Feringa, *Science* **2017**, *356*, 964-968.

[128] Y. Liu, Q. Zhang, S. Crespi, S. Chen, X.-K. Zhang, T.-Y. Xu, C.-S. Ma, S.-W. Zhou, Z.-T. Shi, H. Tian, B. L. Feringa, D.-H. Qu, *Angew. Chem. Int. Ed.* **2021**, *60*, 16129-16138.

[129] C. Stähler, D. R. S. Pooler, R. Costil, D. Sudan, P. van der Meulen, R. Toyoda, B. L. Feringa, *J. Org. Chem.* **2022**.

[130] L. Pfeifer, C. N. Stindt, B. L. Feringa, *J. Am. Chem. Soc.* **2023**.

[131] F. L. Benton, T. E. Dillon, *J. Am. Chem. Soc.* **1942**, *64*, 1128-1129.

[132] T. M. Kosak, H. A. Conrad, A. L. Korich, R. L. Lord, *Eur. J. Org. Chem.* **2015**, *2015*, 7460-7467.

[133] V. Balzani, J. Becher, A. Credi, M. B. Nielsen, F. M. Raymo, J. F. Stoddart, A. M. Talarico, M. Venturi, *J. Org. Chem.* **2000**, *65*, 1947-1956.

[134] S. T. Diver, A. J. Giessert, *Chem. Rev.* **2004**, *104*, 1317-1382.

[135] Nobel Prize Outreach AB, *Morten Meldal - Facts - 2022*, can be found under https://www.nobelprize.org/prizes/chemistry/2022/meldal/facts/, **2023** (accessed 30.01.2023).

[136] Nobel Prize Outreach AB, *K. Barry Sharpless - Facts - 2022*, can be found under https://www.nobelprize.org/prizes/chemistry/2022/sharpless/facts/, **2023** (accessed 30.01.2023).

[137] J. E. Hein, V. V. Fokin, *Chem. Soc. Rev.* **2010**, *39*, 1302-1315.

[138] *Creative Commons Attribution 4.0 International Public License*, can be found under https://creativecommons.org/licenses/by/4.0/, (accessed 05.12.2023).

[139] C. Laurence, P. Nicolet, M. Lucon, T. Dalati, C. Reichardt, *J. Chem. Soc., Perkin Trans. 2* **1989**, 873-876.

[140] S. Hoops, S. Sahle, R. Gauges, C. Lee, J. Pahle, N. Simus, M. Singhal, L. Xu, P. Mendes, U. Kummer, *Bioinformatics* **2006**, *22*, 3067-3074.

[141] *Gaussian 16 Rev. B.01*, M. J. Frisch, G. W. Trucks, H. B. Schlegel, G. E. Scuseria, M. A. Robb, J. R. Cheeseman, G. Scalmani, V. Barone, G. A. Petersson, H. Nakatsuji, X. Li, M. Caricato, A. V. Marenich, J. Bloino, B. G. Janesko, R. Gomperts, B. Mennucci, H. P. Hratchian, J. V. Ortiz, A. F. Izmaylov, J. L. Sonnenberg, D. Williams-Young, F. Ding, F. Lipparini, F. Egidi, J. Goings, B. Peng, A. Petrone, T. Henderson, D. Ranasinghe, V. G. Zakrzewski, J. Gao, N. Rega, G. Zheng, W. Liang, M. Hada, M. Ehara, K. Toyota, R. Fukuda, J. Hasegawa, M. Ishida, T. Nakajima, Y. Honda, O. Kitao, H. Nakai, T. Vreven, K. Throssell, J. A. Montgomery Jr., J. E. Peralta, F. Ogliaro, M. J. Bearpark, J. J. Heyd, E. N. Brothers, K. N. Kudin, V. N. Staroverov, T. A. Keith, R. Kobayashi, J. Normand, K. Raghavachari, A. P. Rendell, J. C. Burant, S. S. Iyengar, J. Tomasi, M. Cossi, J. M. Millam, M. Klene, C. Adamo, R. Cammi, J. W. Ochterski, R. L. Martin, K. Morokuma, O. Farkas, J. B. Foresman, D. J. Fox, Gaussian, Inc., Wallingford, CT, **2016**.

[142] T. Bruhn, A. Schaumlöffel, Y. Hemberger, G. Bringmann, *Chirality* **2013**, *25*, 243-249.

[143] *SpecDis V1.71*, T. Bruhn, A. Schaumlöffel, Y. Hemberger, G. Pescitelli, Berlin, Germany, **2017**.

[144] K. B. Wiberg, *Angew. Chem., Int. Ed. Engl.* **1986**, *25*, 312-322.

[145] A. Abe, J. E. Mark, *J. Am. Chem. Soc.* **1976**, *98*, 6468-6476.

[146] R. Dorel, C. Miró, Y. Wei, S. J. Wezenberg, B. L. Feringa, *Org. Lett.* **2018**, *20*, 3715-3718.

[147] D. Roke, C. Stuckhardt, W. Danowski, S. J. Wezenberg, B. L. Feringa, *Angew. Chem. Int. Ed.* **2018**, *57*, 10515-10519.

[148] T. van Leeuwen, W. Danowski, S. F. Pizzolato, P. Štacko, S. J. Wezenberg, B. L. Feringa, *Chem. - Eur. J.* **2018**, *24*, 81-84.

[149] L. Pfeifer, S. Crespi, P. van der Meulen, J. Kemmink, R. M. Scheek, M. F. Hilbers, W. J. Buma, B. L. Feringa, *Nat. Commun.* **2022**, *13*, 2124.

[150] S. J. Wezenberg, B. L. Feringa, *Nat. Commun.* **2018**, *9*, 1984.

[151] E. J. Corey, A. Venkateswarlu, *J. Am. Chem. Soc.* **1972**, *94*, 6190-6191.

[152] A. D. Boese, *ChemPhysChem* **2015**, *16*, 978-985.

[153] Y. Zhao, D. G. Truhlar, *Theor. Chem. Acc.* **2008**, *120*, 215-241.

[154] S. Tshepelevitsh, A. Kütt, M. Lõkov, I. Kaljurand, J. Saame, A. Heering, P. G. Plieger, R. Vianello, I. Leito, *Eur. J. Org. Chem.* **2019**, *2019*, 6735-6748.

[155] T. Muraoka, K. Kinbara, T. Aida, *Chem. Commun.* **2007**, 1441-1443.

[156] *Gaussian 16 Rev. C.01*, M. J. Frisch, G. W. Trucks, H. B. Schlegel, G. E. Scuseria, M. A. Robb, J. R. Cheeseman, G. Scalmani, V. Barone, G. A. Petersson, H. Nakatsuji, X. Li, M. Caricato, A. V. Marenich, J. Bloino, B. G. Janesko, R. Gomperts, B. Mennucci, H. P. Hratchian, J. V. Ortiz, A. F. Izmaylov, J. L. Sonnenberg, Williams, F. Ding, F. Lipparini, F. Egidi, J. Goings, B. Peng, A. Petrone, T. Henderson, D. Ranasinghe, V. G. Zakrzewski, J. Gao, N. Rega, G. Zheng, W. Liang, M. Hada, M. Ehara, K. Toyota, R. Fukuda, J. Hasegawa, M. Ishida, T. Nakajima, Y. Honda, O. Kitao, H. Nakai, T. Vreven, K. Throssell, J. A. Montgomery Jr., J. E. Peralta, F. Ogliaro, M. J. Bearpark, J. J. Heyd, E. N. Brothers, K. N. Kudin, V. N. Staroverov, T. A. Keith, R. Kobayashi, J. Normand, K. Raghavachari, A. P. Rendell, J. C. Burant, S. S. Iyengar, J. Tomasi, M. Cossi, J. M. Millam, M. Klene, C. Adamo, R. Cammi, J. W. Ochterski, R. L. Martin, K. Morokuma, O. Farkas, J. B. Foresman, D. J. Fox, Gaussian, Inc., Wallingford, CT, **2016**.

[157] M. D. Tzirakis, M. N. Alberti, H. Weissman, B. Rybtchinski, F. Diederich, *Chem. - Eur. J.* **2014**, *20*, 16070-16073.

[158] M. V. Skorobogatyi, A. A. Pchelintseva, A. L. Petrunina, I. A. Stepanova, V. L. Andronova, G. A. Galegov, A. D. Malakhov, V. A. Korshun, *Tetrahedron* **2006**, *62*, 1279-1287.

[159] G. H. Clever, M. Shionoya, *Chem. - Eur. J.* **2010**, *16*, 11792-11796.

[160] A. Kohata, P. K. Hashim, K. Okuro, T. Aida, *J. Am. Chem. Soc.* **2019**, *141*, 2862-2866.

[161] L. Tao, Y. Bingqin, G. Bo, *Z. Naturforsch., B: J. Chem. Sci.* **2007**, *62*, 605-609.

[162] P. Tegeder, M. Freitag, K. M. Chepiga, S. Muratsugu, N. Möller, S. Lamping, M. Tada, F. Glorius, B. J. Ravoo, *Chem. - Eur. J.* **2018**, *24*, 18682-18688.

[163] A. Bouzide, G. Sauvé, *Org. Lett.* **2002**, *4*, 2329-2332.